UNITED STATES
DEPARTMENT OF THE INTERIOR
BUREAU OF RECLAMATION

BOULDER CANYON PROJECT

FINAL REPORTS

PART V—TECHNICAL INVESTIGATIONS

Bulletin 3

MODEL TESTS OF BOULDER DAM

UNITED STATES
DEPARTMENT OF THE INTERIOR
HAROLD L. ICKES, Secretary

BUREAU OF RECLAMATION
JOHN C. PAGE, Commissioner
R. F. WALTER, Chief Engineer

BOULDER CANYON PROJECT

FINAL REPORTS

PART V—TECHNICAL INVESTIGATIONS

Bulletin 3

MODEL TESTS OF BOULDER DAM

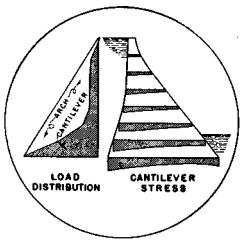

DENVER, COLORADO
1939

This bulletin is one of a series prepared to record the history of the Boulder Canyon Project, the results of technical studies and experimental investigations, and the more unusual features of design and construction. A list of the bulletins available and tentatively proposed for publication is given at the back of this report.

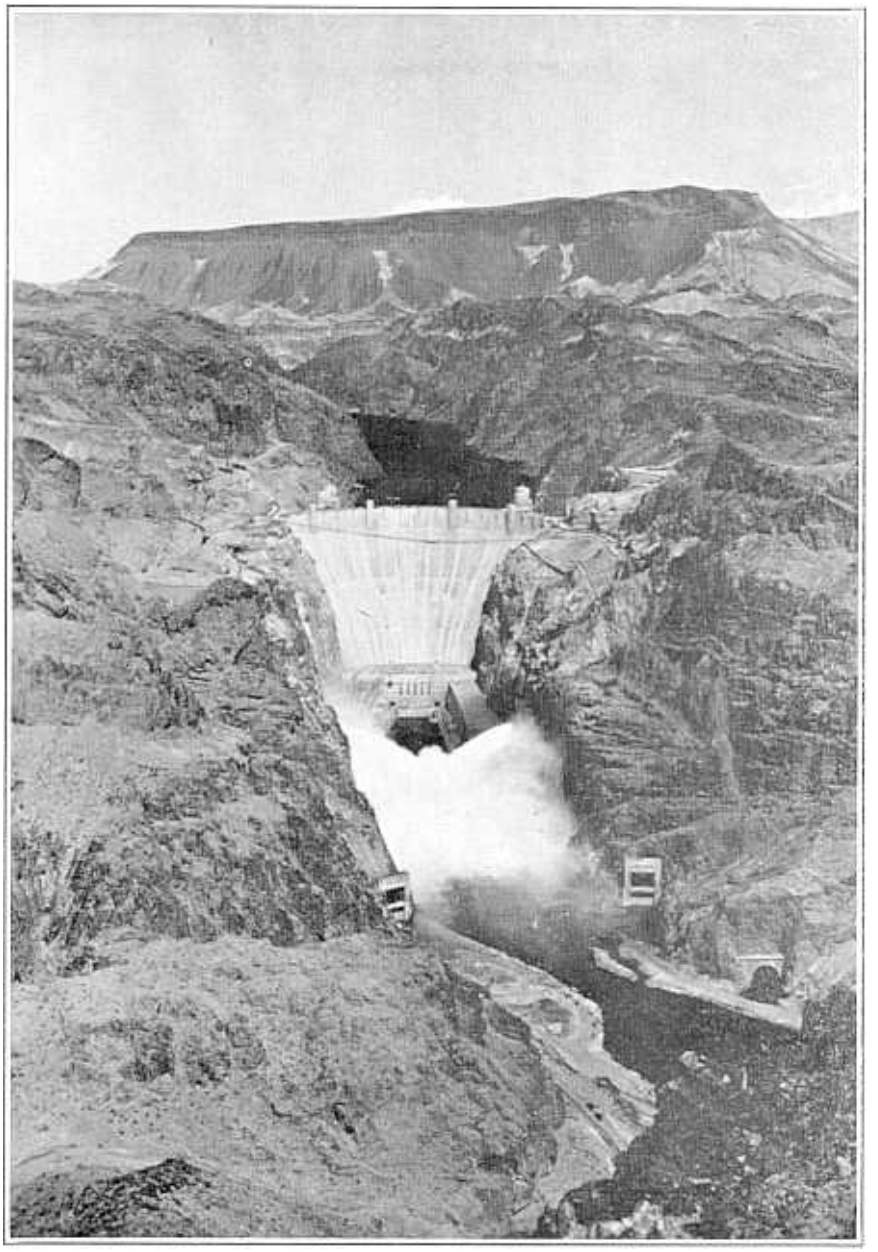

FRONTISPIECE—BOULDER DAM

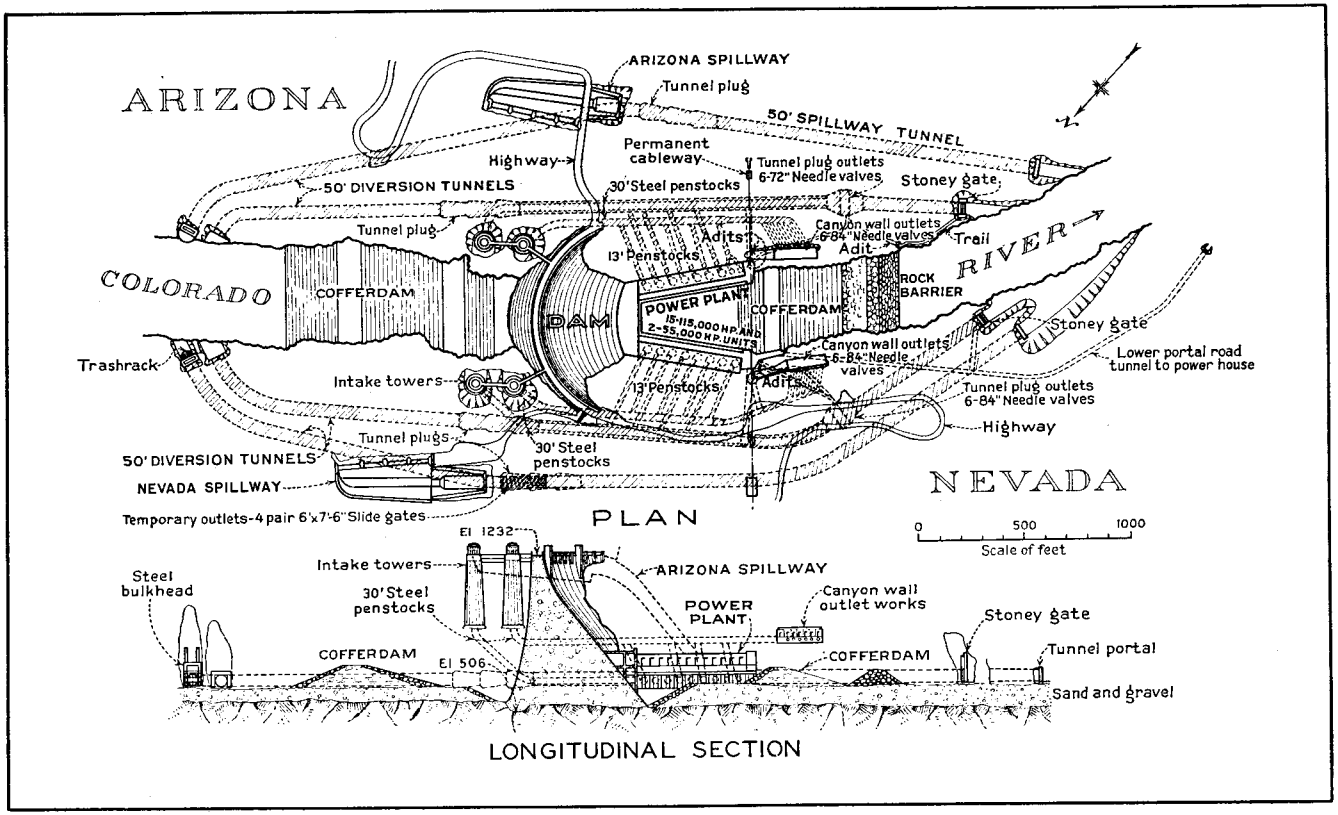

BOULDER DAM AND APPURTENANT WORKS

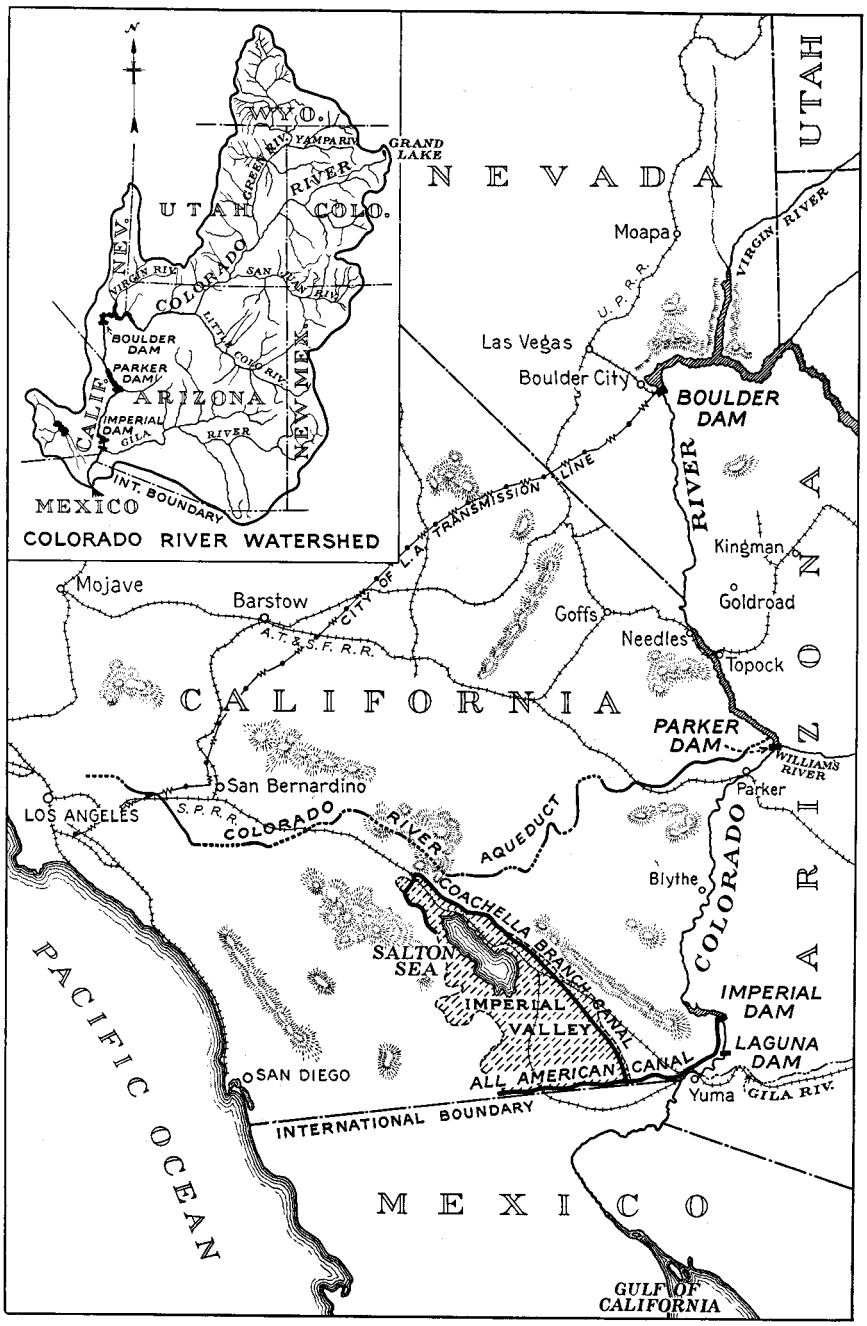

BOULDER CANYON PROJECT—LOCATION MAP

BOULDER CANYON PROJECT

ENGINEERING ORGANIZATION DURING CONSTRUCTION

ADMINISTRATIVE OFFICE, WASHINGTON, D. C.

Elwood Mead* — Commissioner of Reclamation

ENGINEERING AND EXECUTIVE OFFICE, DENVER, COLORADO

Raymond F. Walter — Chief Engineer
Sinclair O. Harper — Assistant Chief Engineer
John L. Savage — Chief Designing Engineer
Leslie N. McClellan — Chief Electrical Engineer
William H. Nalder — Assistant Chief Designing Engineer
Byram W. Steele — Civil Engineer-Dams
Erdman B. Debler — Hydraulic Engineer
Charles M. Day* — Mechanical Engineer
Ivan E. Houk — Senior Engineer-Technical Studies
Harry R. McBirney — Civil Engineer-Canals
Kenneth B. Keener — Assistant Civil Engineer-Dams
Harvey F. McPhail — Electrical Engineer
Robert A. Monroe — Structural Engineer
Porter J. Preston — Senior Engineer-Investigations
Howard C. Stetson — Senior Engineer-Specifications

PROJECT OFFICE, BOULDER CITY, NEVADA

Walker R. Young — Construction Engineer
Ralph Lowry — Field Engineer
John C. Page — Office Engineer

CONSULTANTS

Colorado River Board: — William L. Sibert,* Chairman
Charles P. Berkey — Warren J. Mead
Daniel W. Mead — Robert Ridgway*
Boulder Dam Board: — Andrew J. Wiley,* Chairman
William F. Durand — Arthur P. Davis*
David C. Henny* — Louis C. Hill*
Concrete Research Board: — Phaon H. Bates, Chairman
Franklin R. McMillan — Raymond E. Davis
Herbert J. Gilkey — William K. Hatt

Special Consultants:
Harald M. Westergaard — Mechanics
Frederick L. Ransome* — Geology
Gordon B. Kaufmann — Architectural Features

PRINCIPAL CONTRACTORS

General Contractors — Six Companies, Inc., San Francisco
Penstock & Outlet Pipe — The Babcock & Wilcox Co., New York

*Deceased.

FOREWORD

Colorado River, originating in the melting snows of the Wyoming and Colorado Rockies and augmented by rapid run-off from spasmodic rains and cloudbursts over a vast arid region, has menaced life and property in its descent to the Gulf of California since the days of the first covered wagon.

With increased population along the lower reaches of the river the problem of controlling the Colorado became more important. During recent years millions of dollars have been spent in mitigating the evils of silt deposition and in protecting the highly cultivated Imperial Valley lands from annual threats of inundation.

The need for a comprehensive plan of development to check the ravages of Colorado River, to regulate its flow, and to utilize a part of its enormous energy led, first, to investigations by the Reclamation Service of all water storage possibilities; next, to the Colorado River Compact, a mutual agreement for the protection of the seven basin states; and, finally, to the adoption of the Boulder Canyon Project, as the initial development.

The Boulder Canyon Project Act, approved December 21, 1928, authorized a total appropriation of $165,000,000 for the various features involved. These include Boulder Dam and appurtenant works, the power plant, the reservoir, and the All-American Canal System. The purposes of the project are: (1) flood and silt control for protection of lands along the lower river; (2) improvement of navigation; (3) river regulation and storage of water for irrigation and municipal use; and (4) development of electric power for domestic and industrial purposes. The project is self-liquidating, largely through contracts for disposal of electrical energy. It was constructed and is being operated under the supervision of the Bureau of Reclamation, United States Department of the Interior.

Boulder Dam is located on the Nevada-Arizona boundary near Las Vegas, Nevada, at a place where Colorado River has carved a deep gorge between towering rock cliffs, known as Black Canyon. The dam is a concrete arch gravity structure with a maximum height of 726 feet above foundation rock, a maximum base thickness of 660 feet, and a crest length of 1,244 feet. The dam and appurtenant works contain 4,400,000 cubic yards of concrete, of which 3,250,000 cubic yards were required in the dam.

During construction the river was diverted through four 50-foot diameter, concrete-lined tunnels, two on each side of the river. These tunnels were subsequently plugged near the upstream ends. The spillways, each of 200,000 second-feet capacity, are connected through inclined shafts to the two outer tunnels. A 30-foot diameter steel power penstock is installed in each of the inner tunnels. Discharge from the reservoir is controlled by cylinder gates in four intake towers, founded on the canyon walls near the upstream face of the dam. Four 30-foot steel penstocks, connected to the bases of the intake towers, conduct water to the power plant and to the outlet valves for release of flood, irrigation, and domestic water supply when the power plant discharge is insufficient for such purposes. The reservoir above the dam is 115 miles long and has a capacity of 30,500,000 acre-feet, the equivalent of two years' normal river flow.

The power plant is in a U-shaped, reinforced concrete structure, over 200 feet high and 1,500 feet long, located immediately downstream from the dam. The plant is designed for an ultimate installation of fifteen 115,000 and two 55,000 horsepower units, making a total installed capacity of 1,835,000 horsepower.

The All-American Canal, located near the Mexican border, will carry water to irrigate lands in the Imperial and Coachella Valleys. The canal proper, with a diversion capacity of 15,000 second-feet, is the largest ever constructed for irrigation purposes in America.

The entire Boulder Canyon Project is characterized by the extraordinary. The height and base thickness of the dam, the size of the power units, the dimensions of the fusion-welded, plate-steel pipes, the novel system of artificially cooling the concrete, the speed and coordination of construction, and other major features of the project are without precedent. The magnitude of the undertaking introduced many new problems and intensified many usual ones, requiring investigations of an extensive and diversified character to insure structures representing the utmost in efficiency, safety, and economy of construction and operation.

The major credit for the conception of the project and the initiation of investigations leading to its adoption must be given to the late Arthur P. Davis, former Director of the Reclamation Service. Dr. Elwood Mead, Commissioner of Reclamation during the greater part of the construction period, passed away January 26, 1936, four months after the dedication of Boulder Dam. In commemoration of his untiring services on the Boulder Canyon Project, the reservoir created by the construction of the dam has been officially named "Lake Mead".

CONTENTS

PRELIMINARY EXPERIMENTS

COMMERCIAL BUILDING PLASTERS

TESTS OF RECOMMENDED MIX

CHAPTER III—PLASTER-CELITE MODEL AND MATERIALS TESTS

CONSTRUCTION OF SUPPLEMENTAL BASE

FORMS FOR MODEL

CASTING THE MODEL

PROPERTIES OF MODEL MATERIAL

SUBSEQUENT INVESTIGATIONS

CHAPTER IV—PRELIMINARY TESTS OF PLASTER-CELITE MODEL

TESTING PROCEDURE

RESULTS OF STRAIN MEASUREMENTS

STRESSES COMPUTED FROM STRAINS

CHAPTER VI—MISCELLANEOUS TESTS

SPECIAL DEFLECTION TESTS

FLOW TEST

TEMPERATURE TESTS

TENSION AT DOWNSTREAM FACE

CHAPTER VII—TRIAL LOAD ANALYSIS OF MODEL

INTRODUCTION

RADIAL ADJUSTMENT

TANGENTIAL ADJUSTMENT

TWIST ADJUSTMENT

RESULTS OF ANALYSES

CHAPTER VIII—INVESTIGATION OF RUBBER-LITHARGE MATERIAL

STRESS-STRAIN RELATIONS

ELASTICITY TESTS

ELASTICITY DATA

THERMAL EXPANSION

CHAPTER IX—CONSTRUCTION OF RUBBER-LITHARGE MODEL

MODEL BASE

CONSTRUCTION OF MODEL

CHAPTER X—DEFLECTION MEASUREMENTS

RADIAL DEFLECTION TESTS

TANGENTIAL DEFLECTION TESTS

SLOPE DEFLECTION TESTS

VERTICAL DEFLECTION TESTS

CANYON MOVEMENTS

CHAPTER XI—STRAINS AND STRESSES

APPARATUS

WATER LOAD CONDITIONS

DEAD LOAD CONDITIONS

COMBINED LOAD CONDITIONS

CHAPTER XII—FLOW AND TEMPERATURE TESTS

FLOW TEST

TEMPERATURE TEST

CHAPTER XIII—TRIAL LOAD ANALYSIS OF RUBBER-LITHARGE MODEL

PROCEDURE

ADJUSTMENTS

RESULTS OF ANALYSIS

LIST OF FIGURES

LIST OF TABLES

CHAPTER I—INTRODUCTION

1. General.—The preparation of plans for Boulder Dam involved the development of many new methods of theoretical analysis and masonry dam design, as well as the application of many existing theories to problems of greater magnitude than those for which they had been developed. In verifying the fundamental accuracy of new and existing theories the use of models took an important part, in both hydraulic and structural problems. In contrast to the hydraulic models, which provided direct empirical data, the principal function of the structural models was to furnish a check on analytical methods of design. Although considerable information which could not be readily obtained by analytical methods was derived from the arch dam model tests, this was only incidental to their use in determining the adequacy of the trial load method of analysis.[1] From this viewpoint, the method of applying results of structural model tests of dams by the Bureau of Reclamation differs somewhat from the use of other types of structural models.

2. Scope of Bulletin.—The program of structural model tests included materials investigations and tests on two complete models, representing two designs for Boulder Dam, together with comparisons of results with mathematical analyses. The first model was constructed of a mixture of plaster and diatomaceous earth developed in the investigations of materials. The second model, incorporating design changes, was constructed of a rubber-litharge compound. Detailed studies were also made on cross-sectional models of the crown cantilever and a thick arch, and are described in a separate bulletin on "Model Tests of Arch and Cantilever Elements."

In this bulletin are described the results of the tests on the two complete models. Since the materials investigations and tests on each model were performed in a separate program, the same order is followed in presenting the results in this bulletin. The materials

[1] "Trial Load Method of Analyzing Arch Dams," Bull. 1, Part V—Technical Investigations, Boulder Canyon Project Final Reports, 1938.

investigations, leading to the development of the plaster and diatomaceous earth compound, and the plaster model tests are described in chapters II to VII, inclusive. Descriptions of the rubber-litharge material and the rubber model tests are presented in chapters VIII to XIII, inclusive.

MODEL THEORY

3. Model Requirements.—To obtain similarity between a model and its prototype, there are certain theoretical requirements which must be fulfilled. Also, there are many physical requirements which must be met in order that the experiments may be performed by practical laboratory procedures. The following list presents the more important requirements.

1. The model must be a true scalar representation of the prototype.

2. The loading of the model must be proportional to the loading of the prototype.

3. Upon application of load, resulting strains and deflections must be susceptible of measurement with available laboratory equipment. Since the model must necessarily be constructed to a small scale, it ordinarily requires a higher specific gravity of loading, or a greatly reduced stiffness compared to the prototype.

4. In a massive structure where the stress distribution is influenced by volume strains, Poisson's ratio should be the same for the model and prototype.

5. The model material must be homogeneous, isotropic, and obey Hooke's law within the working stress limits, since these are the conditions assumed to exist in a concrete dam.

6. Foundations and abutments must be sufficiently extensive to allow freedom for the model to deform in a manner similar to the prototype.

7. If effects of both live load and gravity forces are to be investigated, the ratio of dead weight to live load should be the same in both model and prototype. If the effects of live load only are to be investigated, the results are not affected by the specific gravity of the model, providing Hooke's law is obeyed and no cracking occurs.

Requirement 3 largely determines the scale of the model. With

the specific gravity of live load and the modulus of elasticity of the model material determined, magnitudes of strains and deflections depend upon the size of the model. With measuring apparatus of a known sensitivity, the necessary size of model can be easily determined.

4. Similarity Relations.—If all similarity requirements are fulfilled, the relations between model and prototype may be expressed in simple terms. To express these relations mathematically, the following notation is used:

n = scale ratio of prototype to model.

G = ratio of specific gravity of live load on model to live load on prototype.

E_m = modulus of elasticity of model material.

E_d = modulus of elasticity of prototype material.

S = stress at a point on the prototype.

s = stress at corresponding point on model.

D = deflection of a point on prototype.

d = deflection of corresponding point on model.

With the model loaded corresponding to the water load on the dam, the relation between unit pressures at corresponding points, and also unit stresses is $S = (n/G)\, s$. The relation of the unit strains is the unit stresses multiplied by the ratio of the moduli of elasticity, or $\frac{n}{G} \times \frac{E_m}{E_d}$. These strains are acting over lengths on the dam n times the corresponding lengths on the model. The deformation of the dam represents the total effect of the unit strains; therefore the deflection of the dam, $D = \frac{n^2 E_m}{G E_d} \times d$.

The foregoing relations apply when all similarity requirements are fulfilled, which is not always possible in model tests of masonry dams. However, since the purpose of the tests conducted by the Bureau of Reclamation was to obtain data for verifying methods of theoretical analyses, variations from true similarity could be considered. Therefore, such deficiencies in similarity as were unavoidable did not detract greatly from the value of the tests.

EARLY MODEL TESTS

5. Stevenson Creek Model.—Although the relations between prototype and model are simple when proper similarity is obtained, there is seldom an opportunity to check model measurements against similar measurements on the prototype. Such an opportunity did exist when the investigations of the Stevenson Creek Test Dam were completed.[2] The Stevenson Creek Test Dam is a thin concrete arch, 60 feet high, built to permit accurate observations of arch dam action under actual service conditions.

In cooperation with the Engineering Foundation Arch Dam Committee and the University of Colorado, the Bureau of Reclamation conducted a series of arch dam model experiments on the Stevenson Creek and Gibson dams.[3] The Stevenson Creek model was constructed to a one-twelfth scale, making a model 5 feet high, 2 inches thick at the top, 7½ inches thick at the bottom, and 11 feet 8 inches long at the crest. Concrete, mixed from the same aggregate as in the dam, was used in the model. The model was loaded with a film of mercury, contained in a rubber bag which fitted the upstream face and was held in place by a steel plate, rigidly braced against the walls of the testing pit. Measurements of deflections and strains were made at the downstream face. These measurements checked closely with measurements made on the prototype and also with the deflections calculated by the trial load method.

The principal conclusions from this investigation were:

1. A properly constructed small scale model can be relied upon to produce strains and deformations similar to its prototype.
2. Mercury is a satisfactory medium for producing model-testing loads.
3. The trial load method of analysis gives accurate results for a thin arch dam.

6. Gibson Model Tests.—The next step in the program was to build a model of an arch dam in which a considerable portion of the load is carried by gravity action. The Gibson Dam is an excellent example of this type. The model was built on a scale of 1 to 68 and

---

[2]"Arch Dam Investigation, Report by Committee," Vol. I, Engineering Foundation, Nov., 1927; also Procs. Am. Soc. C. E., May, 1928, Part 3.

[3]"Arch Dam Investigation, Report by Committee," Vol. II, Engineering Foundation, May, 1934.

was 2 feet 10½ inches high, 2⅝ inches thick at the top, 15⅜ inches thick at the base, and 13 feet 6 inches long at the crest. It was constructed of concrete and loaded with mercury in the same manner as the model of the Stevenson Creek Dam. The procedure of testing was also the same as in the first model. However, the Gibson model investigations included a temperature test as well as live load mercury tests.

In the temperature test of the Gibson model, the temperature of the model was first raised by running hot water over the faces. When a fairly uniform high temperature was obtained the model was allowed to cool, after which the temperature was further lowered by running ice water over the faces. Continuous observations of radial deflection and temperature were taken throughout the temperature cycle.

The behavior of the Gibson model was entirely satisfactory and the agreement of the measured deflections with those calculated by the trial load method was excellent. In the analysis of the model, a number of refinements were introduced to include effects of tangential shear and twist. The fact that good agreement was obtained gave further proof of the accuracy of the trial load method of analyzing arch dams.

INVESTIGATION OF MATERIALS

7. **Preliminary Tests.**—It was evident from the tests on the Gibson model that a concrete model of Boulder Dam, with its thick cantilevers and relatively short arches, would be much too rigid to provide measurable deflections under a mercury load. Consequently, it was necessary to develop a model material with a low modulus of elasticity, but possessing other qualities necessary to insure similarity with the prototype.

The first studies were made on a number of plastic materials mixed with various ingredients. After being molded into specimens these materials still remained plastic and were therefore unfit for the purpose. Various materials were mixed with Portland cement in order to lower its strength and stiffness; but these proved to be either too hard or lacking in strength. Plaster, having an initial strength and stiffness lower than cement, offered greater possibilities. After testing specimens of plaster mixed with various inert materials, it was found that a mixture of commercial building plaster and diatomaceous earth, "Celite", had most of the required properties.

8. Plaster-Celite Materials.—After the preliminary tests indicated the possibilities of plaster-celite materials, a thorough study was made of mixtures of various brands of plaster with different proportions of celite, together with various admixtures. Some of the mixtures set too fast; others were not workable. Some were mixed with lead shot to increase the weight. Mixtures having satisfactory workability were tested for elastic properties and physical characteristics such as bond, shrinkage, and rate of drying.

The mixture, as finally developed, had the following desirable properties:

1. Workable consistency, easily poured in any type of form likely to be used.
2. Set in 20 to 30 minutes at virtually constant volume.
3. Poisson's ratio about the same as concrete.
4. Straight line stress-strain relation and a relatively low modulus of elasticity.
5. Easily shaped with hand tools after casting.
6. Bonded satisfactorily with previously cast material when the latter was coated with shellac and varnish.
7. Almost the same ratio of compressive and tensile strengths as concrete.
8. Ingredients were inexpensive and readily available.

The material also had the following undesirable properties which increased the difficulties of the work but did not affect the essential functions of the model:

1. Slow rate of drying, the material remaining plastic until dry. This necessitated construction of models in thin layers, allowing each layer to dry before casting the succeeding layer. The model, when completed, had to be protected from moisture throughout the tests.
2. Lack of uniformity in commercial plasters. In order to obtain a certain modulus of elasticity, trial mixes were necessary for each shipment of material.
3. Subject to damage by moisture. This prevented the use of water as a live load, or as a temperature control medium in direct contact with the model.

The preliminary investigation of materials indicated that usual laboratory equipment would not be satisfactory for testing plaster-celite specimens, due to the comparatively low stresses used in testing.

Special equipment, using direct loads, was therefore developed and used for most of the tests. Also, light-weight apparatus for attaching gages to the specimens was developed.

During the construction of the model, specimens were cast from the material of each layer and used in establishing a complete record of the elastic properties of the model. The laboratory measurements on the specimens included tests for modulus of elasticity and ultimate strength in tension, compression, and shear, and Poisson's ratio in compression. In addition, auxiliary tests were made to determine the rate of plastic flow in tension, compression, and torsion, and the coefficient of thermal expansion. At the conclusion of the model tests, some questions arose concerning the degree of isotropy in a model built up in layers. Consequently, when the model was dismantled, several large specimens comprising several layers of the material were cut out for further laboratory tests. These were shaped into cubes and loaded in the direction of the three principal axes, in a special compressed-air testing machine. These tests showed that the built-up material was satisfactorily isotropic.

9. Rubber and Litharge Material.—During the testing of the plaster-celite model, the Aluminum Corporation of America developed a rubber and litharge compound which they used for a model of the Calderwood Dam.[4] Since the tests on the plaster-celite model of Boulder Dam, together with further analytical studies, indicated that some changes in design were desirable, it was decided that another model, incorporating these changes, should be built. The rubber and litharge material was selected for this purpose.

The rubber-litharge material had certain advantages over plaster-celite, principally in having a lower modulus of elasticity and a unit weight equal to that of concrete. Water load could be applied directly, giving the same proportion of live load and dead load as in the prototype. Furthermore, apparatus made to work under water permitted measurements to be made on the upstream face.

A shipment of 40,000 pounds of rubber-litharge was obtained from the Republic Rubber Company, Youngstown, Ohio, for building the model. Preliminary tests on specimens, made with available equipment, indicated that the material had pronounced directional properties and a high Poisson's ratio. Consequently, mathematical

---

[4]Karpov, A. V., and R. L. Templin, "Model of Calderwood Dam," Trans. Am. Soc. C. E., 1935, pp. 185-262.

studies were made of the stress-strain relations for an anisotropic material, in order to interpret properly the results of the materials tests. Also, apparatus, specimen shapes, and testing procedures were developed to meet the testing requirements of this type of material.

To determine the modulus of elasticity, volume modulus, and Poisson's ratio, prism-shaped specimens were used to facilitate measurements along three axes. From specimens fabricated of squares of material, cut from a single sheet of rubber and assembled with the same relative direction of axes, it was found that the modulus of elasticity was different for each axis, with a different Poisson's ratio for each of the two axes normal to the loaded axis. Thus the material had three different moduli of elasticity and six possible Poisson's ratios. It was found that there was very little total volume change, although Poisson's ratios in excess of 0.50 on certain axes were observed. It has been found that some compounds show an actual increase in volume under load.[5]

Although the rubber-litharge material had a number of advantages, it is evident that the similarity requirements in regard to elastic properties were violated. The effect of this violation will be further discussed.

BOULDER DAM TESTS

10. Plaster Model Tests.—Construction of the plaster model of Boulder Dam was begun in December, 1930, at the University of Colorado. The model was located in the same testing pit that was used for the previous models of Stevenson Creek and Gibson dams. The model, with foundation and abutments, was cast in layers to form a monolith so that the dam, with foundation and abutments, formed a continuous elastic body, representing the condition in the prototype with all joints grouted. The scale selected was 1 to 240, or one inch on the model represented 20 feet on the prototype.

The program of tests included measurements of radial, tangential, and slope deflections, and strains on the downstream face, for partial, normal, and overload conditions. Mercury was used as the loading medium. Measurements were made of effects of plastic flow under constant load, and of radial deflections due to temperature changes. Also a number of tests for special effects were conducted.

---

[5]Ariano, R., "The Resistance of Rubber to Compression." The India Rubber Journal, August 11, 1928, p. 8.

With respect to effects of live load, requirements for similarity were almost completely obeyed in the plaster-celite model. The model material, having a Poisson's ratio very nearly the same as concrete, had a similar distribution of strain and stress, and consequently, similar deflections. Using the elastic constants determined for the model, a trial load analysis was made. The agreement between computed and observed data was satisfactory.

In addition to the check on the trial load analysis, the plaster-celite model indicated stress concentrations near the top of the dam at the abutments, where there was a rapid change in the length of the arches. This effect was remedied in the later design by providing fillets at the ends of the upper arches, thus increasing the thickness of the arches near the abutments.

11. Rubber Model Tests.—The rubber-litharge material was furnished in 6-inch, 12-inch, and 24-inch squares, 1-inch thick. The model was built up in layers, using vulcanizing rubber cement at all joints, applied without heating. This provided joints of ample strength and facilitated dismantling, since the unvulcanized rubber cement was readily soluble in benzol. The scale selected for the model was 1 to 180, or one inch on the model represented 15 feet on the prototype. A larger proportion of depth and length of canyon was included in this model than in the previous one, in order to allow greater foundation deformation.

Water, maintained at the same temperature as the rubber, was used as a loading medium. In general, the same measurements were made on the rubber model as on the plaster model, except for measurements of strain on the upstream face and a different manner of conducting temperature tests. Also the type of testing apparatus was considerably different.

At the conclusion of the investigations of the rubber-litharge material, it was evident that similarity between the rubber model and the prototype would not be obtained. The rubber model, deforming at constant volume under load, had large vertical movements as well as horizontal movements. Due to this condition there was no direct mathematical relation between the rubber model and the concrete dam. In making the analysis of the model, the observed elastic constants were used and additional calculations to consider the vertical movements were included. The fact that an agreement between the model results and the theoretical analysis for the model was obtained,

gave further proof of the versatility of the trial load method of arch dam analysis.

12. Acknowledgments. — The model investigations were conducted under the immediate supervision of Engineer A. W. Simonds. Other engineers who assisted in the laboratory investigations were Eldred D. Smith, J. A. Stubbs, E. W. Ryland, C. W. Fletcher, F. M. Russell, George C. Rouse, D. B. Holford, and F. C. Knoth. A large part of the office work was done by L. T. French, W. E. Green, J. G. Ross, and N. J. Castellan. R. W. Whinnerah contributed the analyses of the models by the trial load method.

Acknowledgment is also due the University of Colorado for placing its testing laboratories, equipment, and shops at the disposal of the Bureau of Reclamation personnel. Much assistance and cooperation were received from members of the Civil Engineering faculty, particularly from Professor C. L. Eckel, Head of the Department, from Professors F. R. Dungan and L. B. Sutherland who assisted in the tests, and from Professor E. O. Bergman who contributed the mathematical stress-strain relations of anisotropic materials. A large part of the equipment and special apparatus for testing was built in the University machine shop by M. M. Eaton.

BIBLIOGRAPHY

The following bibliography includes the principal articles on structural model tests of dams which have been published in engineering literature up to the present time. A few early tests are described in publication 8, in addition to the one cited.

1. Engineering Foundation.
   Report by Committee, Arch Dam Investigation, Vol. I, Nov., 1927; also Proc. Am. Soc. C. E., Part 3, May, 1928.
2. Houk, Ivan E.
   Experimental Work on Small Scale Models of Arch Dams, Reclamation Era, Oct., 1927, pp. 152-154.
3. Karpov, A. V., and R. L. Templin.
   Building and Testing an Arch Dam Model, Civil Engineering, Jan., 1932.
4. Savage, J. L., Ivan E. Houk, H. J. Gilkey, and Frederick Vogt.
   Arch Dam Investigation, Vol. II, Engineering Foundation, May, 1934.
5. Savage, J. L., and Ivan E. Houk.
   Model Tests Confirm Design of Hoover Dam (now Boulder Dam), Eng. News-Rec., April 7, 1932.

6. Savage, J. L.
Dam Stresses and Strains Studied by Slice Models, Eng. News-Rec., Dec. 6, 1934.

7. Smith, Eldred D.
Structural Model Testing of Dams, Dams and Control Works, 2nd Ed. 1938, U. S. Department of the Interior, Bureau of Reclamation.

8. Wilson, John Sigismund, and William Gore.
Stresses in Dams: An Experimental Investigation by Means of India-Rubber Models, Proc. Inst. C. E., London, Paper No. 3705, 1907-08, pp. 107-129.

CHAPTER II—INVESTIGATION OF MATERIALS

INTRODUCTION

13. Purpose of Tests.—The early tests on concrete models of arch dams, briefly discussed in chapter I, showed that a model of the proportions of Boulder Dam could not be successfully investigated if built of concrete. The tests discussed in this chapter were made in an effort to discover or develop a material suitable for use in constructing models of thick arch dams. After considering theoretical and practical requirements, the following tentative specifications for a suitable material were prepared:

1. The material should be uniformly elastic in all directions, for all working stresses.

2. It should have a Poisson's ratio about the same as concrete.

3. It should have a modulus of elasticity sufficiently low to allow measurable deformations under a mercury load, yet have sufficient strength to resist damage in handling.

4. The ratios of tensile and shearing strengths to compressive strength should be about the same as for concrete.

5. It should not flow excessively under continuous load.

6. There should be very little or no shrinkage after setting.

7. It should possess a workability which would permit it to be cast easily into shapes suitable for testing, as well as to allow mixing and placing of large masses in building the model.

8. It should be possible to repair the model in case of accidental damage.

14. Specimens.—In the early tests small beams and cylinders were used. Flexural tests were made with ½ by 1 by 8-inch beams, and compression tests with 2 by 4-inch cylinders. It was soon recognized that the small quantities of material used in making such specimens did not offer an opportunity to judge the workability of the mixes. Therefore a practice of using ten to forty pounds of dry

material and casting larger specimens was adopted. In the adopted practice, test specimens usually included 3 by 3 by 40-inch beams, 3 by 6-inch cylinders, and 2 by 4-inch cylinders.

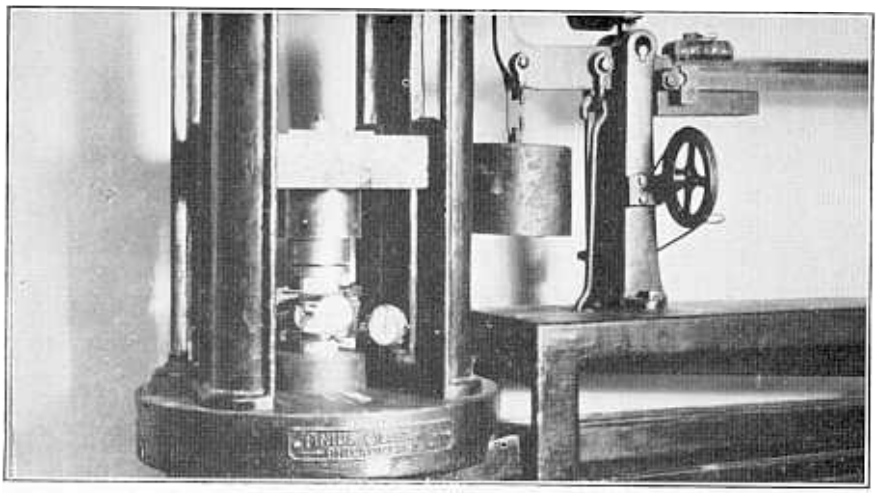

FIGURE 1—PLASTER SPECIMEN READY FOR TESTING

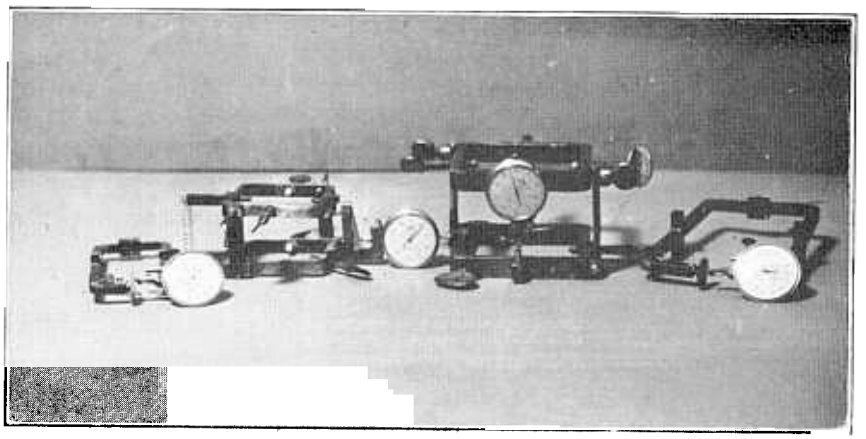

FIGURE 2—INSTRUMENTS FOR MEASURING DEFORMATIONS OF COMPRESSION SPECIMENS

15. Testing Apparatus.—In all compression tests described in this chapter, a hand-operated, 20,000-pound testing machine was used. A 2 by 4-inch plaster specimen in the testing machine is shown in

figure 1. Longitudinal and lateral deformations were measured with the compressometers and extensometers shown in figure 2. These instruments for measuring deformations of cylinders were used in tests for determining the modulus of elasticity and Poisson's ratio of all materials studied in the preliminary investigations. The compressometers and extensometers were designed for testing concrete cylinders. In using them on other materials, it was soon recognized that their steel frames were too heavy for making satisfactory measurements on light specimens of plaster compounds. The points of the set screws which clamped the apparatus to the specimen would damage the plaster. The compressometer for the 3 by 6-inch cylinders was excessively heavy; consequently results of tests on cylinders of

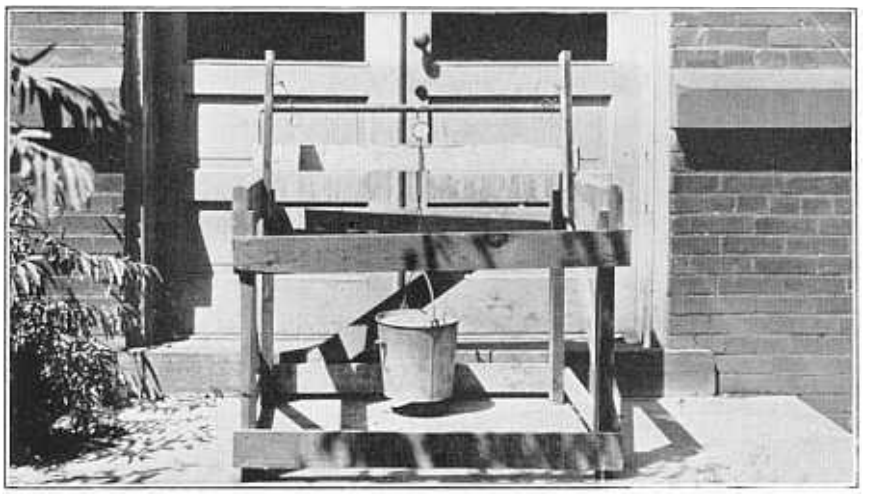

FIGURE 3—APPARATUS FOR FLEXURAL TESTS ON BEAMS

this size are not believed to be as reliable as those obtained on the smaller cylinders.

After construction of the plaster-celite model was started and extensive tests on the plaster-celite material were begun, machines for testing low-strength materials were designed and built. Compressometers and extensometers of aluminum were made for measuring deformations of the specimens. Tests made with the redesigned light-weight equipment yielded satisfactory results in determining the modulus of elasticity and Poisson's ratio.

Flexural tests were made with an improvised apparatus which supported the beam at the ends and allowed a concentrated load to be

applied at the center. The concentrated load was imposed by suspending a bucket of sand or shot from the center of the beam. The apparatus, with a dial gage for measuring center deflections of a 3 by 3 by 40-inch beam, is shown in figure 3. Tensile strength was not considered an essential property for the model material. Consequently, no tensile tests were made during the preliminary investigations.

16. Scope of Investigation.—The investigation included a wide range of combinations of materials which had been considered as possibilities for fulfilling the requirements set forth in section 13. Tests on some of the mixtures were rather limited due to early discoveries of failure to meet one or more of the tentative specifications. Tests of plaster mixes were comprehensive. Plaster was recognized as possessing the desired qualities and extensive studies were made to discover the most suitable brand and proportions for the final product.

PRELIMINARY EXPERIMENTS

17. Tar, Pitch, and Resin.—Several tar, pitch, and resin combinations were tested and found to be unsatisfactory. A product composed of one part pitch, one part resin, and one part plaster of Paris was plastic and began to melt at about 90 degrees Fahrenheit. If more plaster of Paris was added the mixture was stiffer, but still plastic. A combination of 3 parts linseed oil, 4 parts tar, and 16 parts resin, was decidedly plastic. These mixes were inclined to be sticky and could not be removed from the forms without damaging the specimens.

A mixture of 4 parts iron filings, 2 parts loam, 1 part powdered sandstone, and salt water produced a material similar to adobe. This material was not suitable for use in a testing pit where there is a possibility of damage by water.

18. Sulphur and Celite.—Several compositions using sulphur as the cementing agent were investigated. Commercial powdered sulphur was very thin when melted and required a watertight form to hold it. It crystallized on cooling and formed a material which was not uniform. When celite was added to sulphur a very inflammable mixture resulted. It was imperative to pour the celite into the melted sulphur as the mixture ignited readily when the two substances were mixed dry and heated. This mixture was rather gummy and not suitable for model construction.

19. Linseed-Oil Mixtures.—A number of beams were made of neat cement using linseed oil in the mixing water. Specimens containing more than 3 per cent of oil had insufficient strength to carry any load whatever, while those containing smaller percentages of oil had moduli of elasticity higher than the desired value. Mixtures of plaster of Paris, water, and lubricating oil showed higher moduli of elasticity at an age of 34 days, than if no oil were used. Therefore, tests of such combinations of materials were discontinued.

20. Under-Sanded Concrete.—It was thought that a weak, porous concrete might have a modulus of elasticity low enough for model purposes. Some pea gravel containing a small amount of sand was available from the aggregates used in the model of Gibson Dam. This was mixed with cement in the proportion of 1 to 6⅔ by weight, water being added to produce a water-cement ratio of 0.67 by volume. The product was a porous concrete having an ultimate strength in flexure of 250 pounds per square inch when 21 days old, and a modulus of elasticity of 1,700,000 and 1,800,000 pounds per square inch, respectively, for wet and dry curing.

In measuring deflections of the model under load, it was proposed to use small metal inserts, embedded in the downstream face. Due to the difficulty involved in securing inserts in the porous material, as well as the relatively high modulus, this mixture was rejected.

21. Cement-Asbestos Sheets.—A beam, cut from sheets made by compressing cement and asbestos, gave a fairly straight stress-strain diagram up to stresses of 175 pounds per square inch. However, the modulus of elasticity of 3,500,000 pounds per square inch was entirely too high.

22. Rubber-Aggregate Concrete. — Concrete mixed with finely ground automobile-tire rubber in place of coarse aggregate, to lower the modulus of elasticity, was investigated and discarded. The resulting mix was unsuitable for testing. Expansion of the rubber particles when wet by the mixing water cracked the entire mass into small pieces.

23. Hard Rubber. — Modulus of elasticity tests on two small beams of hard rubber showed values of 390,000 and 480,000 pounds per square inch. The stress-strain diagrams were fairly straight up to stresses of 140 pounds per square inch, but curved downward in proportion to the load when the stresses were further increased. One

of the beams was subjected to a flow test by imposing a maximum stress of 200 pounds per square inch for a period of 21 hours. The total flow during this period was 23 per cent of the initial elastic deformation. Upon release of load, a recovery of 71 per cent of the total deformation took place, increasing to 84 per cent during the succeeding 24 hours. The results of the tests, together with the difficulty of casting homogeneous thick sections and the lack of a satisfactory hard rubber cement, showed that the construction and testing of a hard rubber model of Boulder Dam would not be advisable.

24. **Cement and Plaster of Paris.**—Both cement and plaster of Paris have been considered as binding materials for mixes to be used in model construction. Plaster of Paris has the advantage that its modulus of elasticity is only one-half that of cement. Therefore, products having lower moduli of elasticity are more easily made with plaster as the binding material than with cement. Furthermore, all plaster products have a workable quality after hardening which is not found in cement products. For instance, the thickness of the model can easily be dressed down to the correct amount, joints and keyways can be cut in the model sections after casting, and slots can be made to represent cracks in the dam. The disadvantage of plaster products compared with concrete, is that they must be protected from water. If such materials are used, the testing pit must be kept dry and the model protected with shellac or varnish.

25. **Cement or Mortar and Asbestos.**—Specimens made with a mix of cement and asbestos, or mortar and asbestos, were so soft and fragile that they broke before being tested. An undesirable shrinkage of from three to four per cent was noticed in the cylinders. The tests showed that, by using asbestos as an admixture with cement, the modulus of elasticity could be reduced to about 500,000 pounds per square inch. Adding asbestos in an effort to lower the modulus beyond this value rapidly reduced the strength and the elastic range, and caused the deformation to become largely plastic.

26. **Cement and Celite.**—With the assumption that an appreciable amount of celite had to be added to cement to cause a substantial reduction in the modulus of elasticity, a mix was first made from one part cement and one-half part celite by weight. In order to obtain satisfactory workability it was necessary to add 1.9 parts of water. This combination remained decidedly plastic for a long time. Meas-

urements on 2 by 4-inch cylinders, after hardening, showed a settlement of five per cent.

A mix of 1.0 part cement to 0.25 parts celite to 1.17 parts water was unsatisfactory. The average settlement of 2 by 4-inch cylinders was 4.5 per cent. All of the small beams were broken by early shrinkage.

One 3 by 3 by 40-inch beam was made using 1 part cement to 2 parts sand to 0.2 parts celite to 0.57 parts water. Another was made with the same formula, with the exception that the celite content was reduced and 1.0 part water used. With the reduced content of celite a product of better consistency was obtained. However, the modulus of elasticity at 28 days was 1,800,000 pounds per square inch. These beams were cured under water. After a two-week period they had expanded 0.017 per cent. An equal time in air produced a shrinkage of 0.08 per cent.

The high strength and modulus of elasticity of cement and celite mixes, having small amounts of celite, suggested adding sugar to the mixing water. The sugar satisfactorily checked the hardening of the cement; but after setting had taken place the material crumbled easily. On becoming wet, it showed a tendency to disintegrate. From the standpoint of handling and durability it was altogether unsatisfactory. Mixes were made with hydrated lime and cement, but with little success, as these materials did not combine very well. The combination hardened slowly, and like the mixtures of cement and celite, it had a tendency to crack due to excessive shrinkage.

27. **Cement, Asbestos, and Celite.**—Beams containing both asbestos and celite were made, some with neat cement and some with mortar. All specimens were hard and strong, but those having low moduli of elasticity also had low limits within which the stress-strain curves were straight. When additional load was applied the deformations of the beams became plastic.

28. **Plaster of Paris and Asbestos.**—A number of beams were made using different mixes of plaster, asbestos, and water. Tests showed that the beams had moduli of elasticity ranging from 300,000 to 590,000 pounds per square inch, at stresses from 40 to 120 pounds per square inch. Mixes having the lower moduli of elasticity were those containing the greater amounts of asbestos. The beams, when stressed beyond 40 pounds per square inch, were definitely plastic in deformation.

29. Plaster of Paris and Celite.—Early tests with plaster of Paris as a binding material established its superiority over cement in one important respect; namely, there was no tendency for shrinkage cracks to form during setting, and there was very little shrinkage after setting. The most satisfactory admixtures tested were asbestos and celite. In using these materials, relatively large proportions of mixing water had to be added to produce workable mixes. When the specimens were dried in air the greater part of the mixing water evaporated, leaving a porous material which had a low strength and a low modulus of elasticity. The physical properties were largely dependent upon the amount of moisture retained in the mixture. The most satisfactory product seemed to be one in which the moisture content was reduced to a minimum. In order to preserve uniform physical properties it was necessary to cover the material with a waterproof coating. Hot paraffin, shellac, varnish, and paints were tried with varying degrees of success. The most suitable waterproofing consisted of two coats of orange shellac and one coat of ship varnish. After extended tests with asbestos and celite admixtures, the latter was considered the better of the two, due to tendencies of asbestos to produce a softer mixture which showed plastic deformations under relatively low stresses.

By using plaster of Paris as a binder and celite as an admixture, a material was produced which more closely approached the desired product than any which had previously been developed. With this combination it was possible to obtain a material having a modulus of elasticity as low as 100,000 pounds per square inch without possessing undesirable shrinkage characteristics. Furthermore, the material was highly elastic under ordinary stress conditions.

In order to obtain a workable mix, which would completely fill the forms, it was necessary to use an amount of water equal to the weight of the dry materials. The most satisfactory proportion of the plaster of Paris and celite ingredients was 2 to 1, by weight. An increase in the amount of celite produced a mix which remained plastic for a long time. Equal parts of plaster and celite produced a product which remained highly plastic, even after a period of 24 hours. A plain mix of plaster and water hardened after about one and one-half hours. Settlement in the form during this period amounted to about two per cent. Using a 2 to 1 mixture of plaster of Paris and celite, hardening took place within half an hour, with no appreciable settlement in the form. After hardening, an increase in temperature due to the chemical reaction of the plaster and the mixing water was

noticed. This temperature change caused a slight increase in the volume of the material.

When removed from the forms, the weight of specimens made of plain plaster of Paris with 50 per cent water was about 105 pounds per cubic foot. For a mixture of two parts plaster of Paris, one part celite, and three parts water, the weight was about 80 pounds per cubic foot. After exposure to air for several days, the greater part of the water evaporated, leaving the plaster of Paris with a weight of 92 pounds per cubic foot and the plaster and celite mix with about 48 pounds per cubic foot.

Tests were made on plaster of Paris and celite beams to determine the modulus of elasticity in flexure. For plain mixes of plaster and water, tested at ages of 4 to 30 days, the modulus of elasticity varied between 1,550,000 and 1,650,000 pounds per square inch. Plaster of Paris and celite mixes had moduli of elasticity ranging from 140,000 to 840,000 pounds per square inch. The higher values occurred in mixes low in celite and the lower values occurred in mixes having 1 part celite to 2 parts plaster of Paris. Flexural specimens were made in both the ½ by 1 by 8-inch and 3 by 3 by 40-inch sizes. They were tested to maximum stresses of 31 to 37 pounds per square inch at 28 days. A 3 by 3 by 40-inch beam made from a mix of 1 part plaster of Paris, ½ part celite, and 1½ parts water, tested at an age of 28 days to a maximum stress of 37 pounds per square inch, had the lowest modulus of this group of specimens.

A 2 by 4-inch cylinder, made from a mix of 1 part plaster of Paris, ½ part celite, and 2 parts water, was tested at an age of 28 days to determine the value of Poisson's ratio. The results showed a value of 0.35 which was fairly constant over a wide range of stress. The modulus of elasticity for the same specimen was 170,000 pounds per square inch, which checked closely with the values found in the tests on beams. The ultimate compressive strength of the material was about 180 pounds per square inch.

A flow test was made on a beam containing 1 part plaster of Paris to ¼ part celite to 1 part water. A flow of 8 per cent of the initial deformation was measured after a stress of 50 pounds per square inch had been imposed on the specimen for a period of 24 hours. Flow tests of other beams, some of which contained more moisture, showed considerably more flow. In some cases, flows in excess of 100 per cent of the initial deformation were observed. These tests again emphasized the necessity for complete control of moisture content if the material were to be used successfully for model construction.

COMMERCIAL BUILDING PLASTERS

30. Characteristics.—The preliminary experiments showed that a mixture of plaster of Paris and celite would more nearly meet the requirements for a model material than any other product tested. It was believed that some of the commercial building plasters might be even more satisfactory than plaster of Paris.

The following excerpts from a book by Edwin C. Eckel[6] may serve to explain the relation between plaster of Paris and commercial building plasters, known as cement plasters:

> "A theoretically pure plaster of Paris, being a definite chemical compound ($Ca\ SO_4 + \frac{1}{2}\ H_2\ O$), would have the composition: lime sulphate, 93.8 per cent; water, 6.2 per cent. This composition is approached quite closely in plasters made from pure rock gypsum.
>
> "Cement plasters can be made in two different ways which give two different products as far as composition is concerned. (1) Cement plasters may be made by adding retarders to a pure plaster of Paris. As the retarder is organic matter and rarely amounts to over one per cent of the total mass, the resulting product will on analysis differ very little from the plaster of Paris of which it is made. (2) Cement plaster may also be made by burning an impure gypsum, with or without the addition of a retarder. In this case analysis would show the presence of a large per cent of clayey matter, etc., and a cement plaster of this type will therefore have a composition very different from pure plaster of Paris."

The term "cement plasters" refers to slow-setting building plasters which are generally used in structural work. It has no relation to Portland or natural cement.

Investigations were conducted on the following commercial building plasters, which were obtainable at Boulder, Colorado:

Plaster of Paris:

- Certainteed plaster of Paris.
- Red Top quick-set plaster.

---

[6]Eckel, Edwin C., "Cements, Limes and Plasters," 2nd Ed., 1922, p. 63, John Wiley & Sons, Inc.

Cement plasters:

Red Top slow-set plaster.
Sunflower molding plaster.
Ideal finishing plaster.
Acme finishing plaster.

It should be noted that the Certainteed and Red Top quick-set plasters, being commercial products, cannot be considered as chemically pure plaster of Paris materials. Although the four products listed as cement-plasters are similar in general, they have individual characteristics, and, when combined with celite, have somewhat different properties. The differences between these plasters and commercial plaster of Paris suggested that they be classified as cement-plasters. Chemical analyses of the brands were not available to serve as a definite basis for classification.

31. Certainteed Plaster of Paris.—Certainteed plaster of Paris, normally a quick-setting plaster, did not prove satisfactory for mixing with celite. The addition of celite decreased the time of set to such an extent that 36 pounds of dry material could not be mixed with 36 pounds of water before hardening took place. Consequently, it was necessary to mix the plaster and celite together dry. When water was added, the mixture became sticky; so that tough balls, from one to three inches in diameter, formed as the material was worked with a hoe. On account of the poor workability, experimenting was discontinued on this brand of plaster of Paris.

32. Red Top Quick-Set Plaster.—The action of Red Top quick-set plaster resembled that of Certainteed plaster of Paris when combined with celite. The resulting product set quickly and was altogether unsatisfactory for building models.

33. Red Top Slow-Set Plaster.—Adding celite to Red Top slow-set plaster shortened its normal time of set 10 to 15 minutes. As the mix was exceedingly gummy and sticky when water was added, it required some time to work a batch of 35 to 40 pounds of dry material to a uniform consistency. Consequently there was no time to lose in pouring the material into the forms. The 3 by 3 by 40-inch beam forms could be filled easily, but the 2 by 4-inch cylinder molds required more time and the mix was apt to start setting before they could be filled. Stress-strain diagrams for compression tests on 2 by 4-inch, Red Top slow-set cylinders are shown on figure 4. The desig-

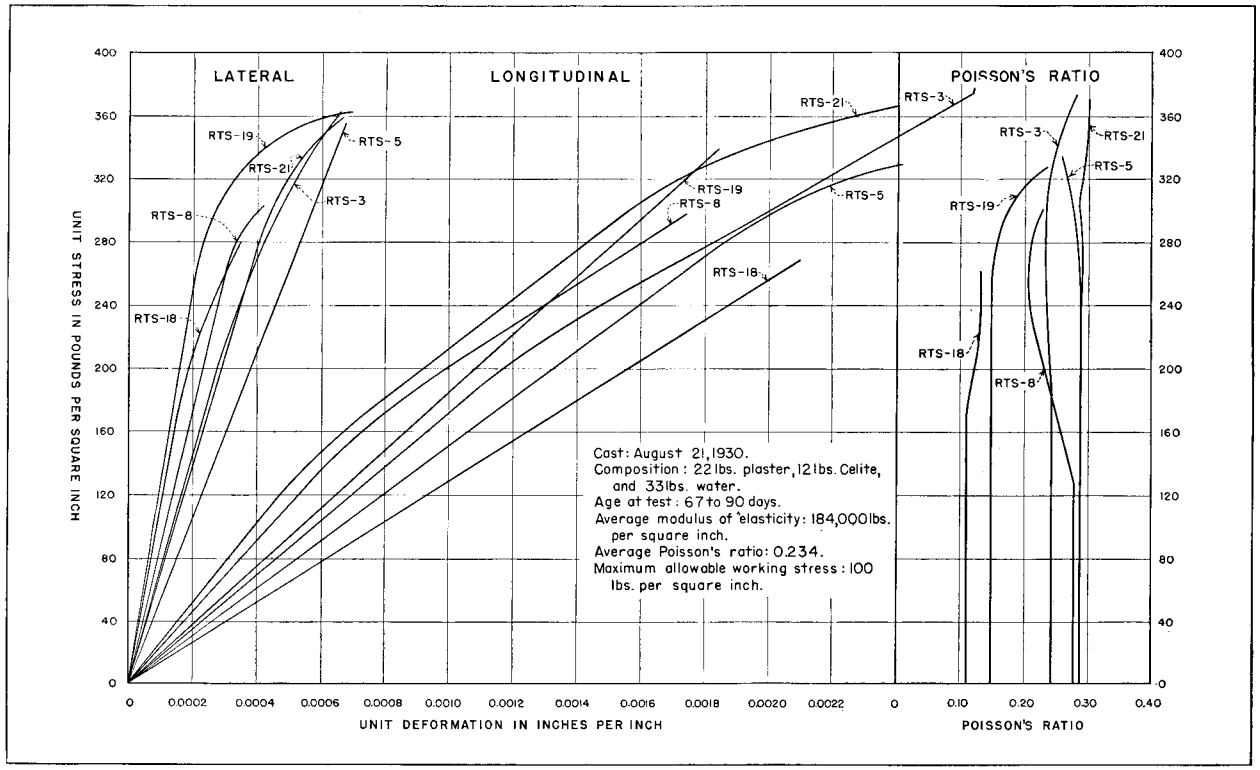

FIGURE 4—STRESS-STRAIN DIAGRAMS FOR COMPRESSION TESTS

2 by 4-inch Cylinders Made With Red Top Slow-Set Plaster

nations on the curves refer to the specimen numbers selected as representative of the entire group.

The customary procedure in making plaster and celite specimens was to mix and pour a batch one day, and remove the forms the following day. As soon as the forms were removed the cylinders were capped with plaster of Paris. The high relative humidity of the concrete laboratory retarded the drying of the specimens. Therefore, on

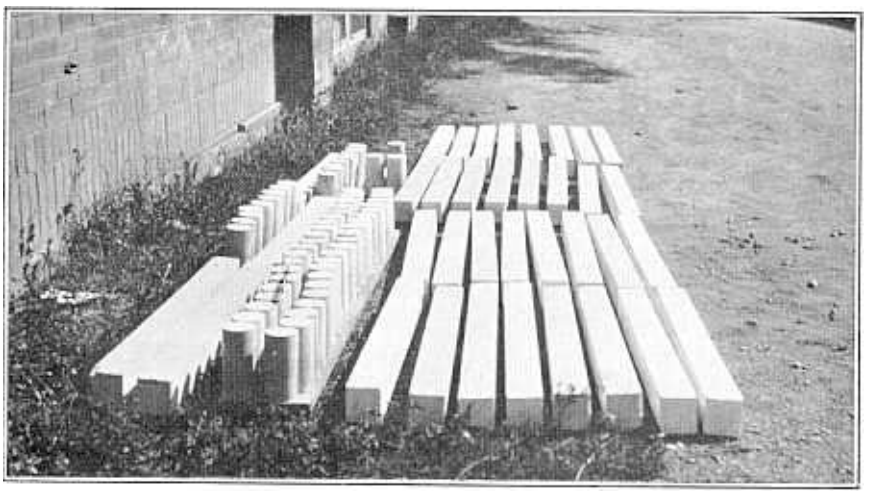

FIGURE 5—PLASTER CYLINDERS AND BEAMS DRYING IN THE SUNSHINE

fair days they were placed outside the building to dry in the sunshine. Figure 5 shows 3 by 6-inch cylinders and 3 by 3 by 40-inch beams drying out-of-doors. During the late fall and winter months the specimens were dried over a steam radiator inside the building.

Tests were made on 3 by 3 by 40-inch beams to determine the modulus of elasticity in flexure. The beams were supported at the ends and 2-pound increments of load successively applied at the center. As each increment of load was added, the deflection was observed by reading the dial gage mounted at the center of the beam. The apparatus used in these tests is shown in figure 3. The modulus of elasticity was calculated from the formula for the deflection at the center of a simple beam. Wooden forms for the 3 by 3 by 40-inch beams had cross-sectional dimensions varying from 2.85 to 3.15 inches. In calculations for moment of inertia exact dimensions were used. The

modulus of elasticity in flexure was found to be 228,000 to 270,000 pounds per square inch for two beams tested.

Twenty-one 2 by 4-inch cylinders were cast from the batch represented on figure 4, which shows test data for selected typical specimens. Two cylinders were defective. Some shrinkage of the specimens in the forms was noticed. The average modulus of elasticity in compression was 184,000 pounds per square inch, the average value of Poisson's ratio was 0.234, and the average ultimate strength was 293 pounds per square inch.

34. Retarders.—As the experiments with mixes of commercial building plaster and celite progressed, two essential requirements became apparent. First, the mix must be of a thin consistency to prevent formation of honeycombed places in the specimens due to entrapped air; and, second, a retarder must be added to prevent the mix from setting too rapidly. At the suggestion of W. G. Banks, chemist for the Colorado Portland Cement Company, ground bentonite, trade name "Aquagel," was added to the mix as a retarder, with the result that the setting time could easily be controlled. Later it was discovered that cold water was also an effective retarder. Both retarders were used with equally satisfactory results.

35. Sunflower Molding Plaster. — Sunflower molding plaster, combined with celite, produced mixtures with satisfactory workability. In a few specimens small air pockets were found, but the majority of the specimens were smooth, sound, and wholly satisfactory. The modulus of elasticity varied from 80,000 to 217,000 pounds per square inch for different mixes. Poisson's ratio remained about the same as for concrete, or approximately 0.175. Typical stress-strain relations for 2 by 4-inch specimens, made from a mix of 22 pounds of Sunflower molding plaster, 12 pounds of celite, and 41.6 pounds of water, are shown in figure 6. Specimens were tested at ages of 24 to 111 days. The results of all tests on this mixture were as follows:

Specimens	Size, inches	Average E lb. per sq. in.	Poisson's ratio
Three beams	3 x 3 x 40	213,000	- - -
Three cylinders	3 x 6	138,000	0.232
Twelve cylinders	2 x 4	134,000	0.175

Since considerable time was required to cast a number of 2 by 4-inch cylinders, several 3 by 6-inch cylinders were also made. The larger molds could be filled more rapidly than the smaller molds.

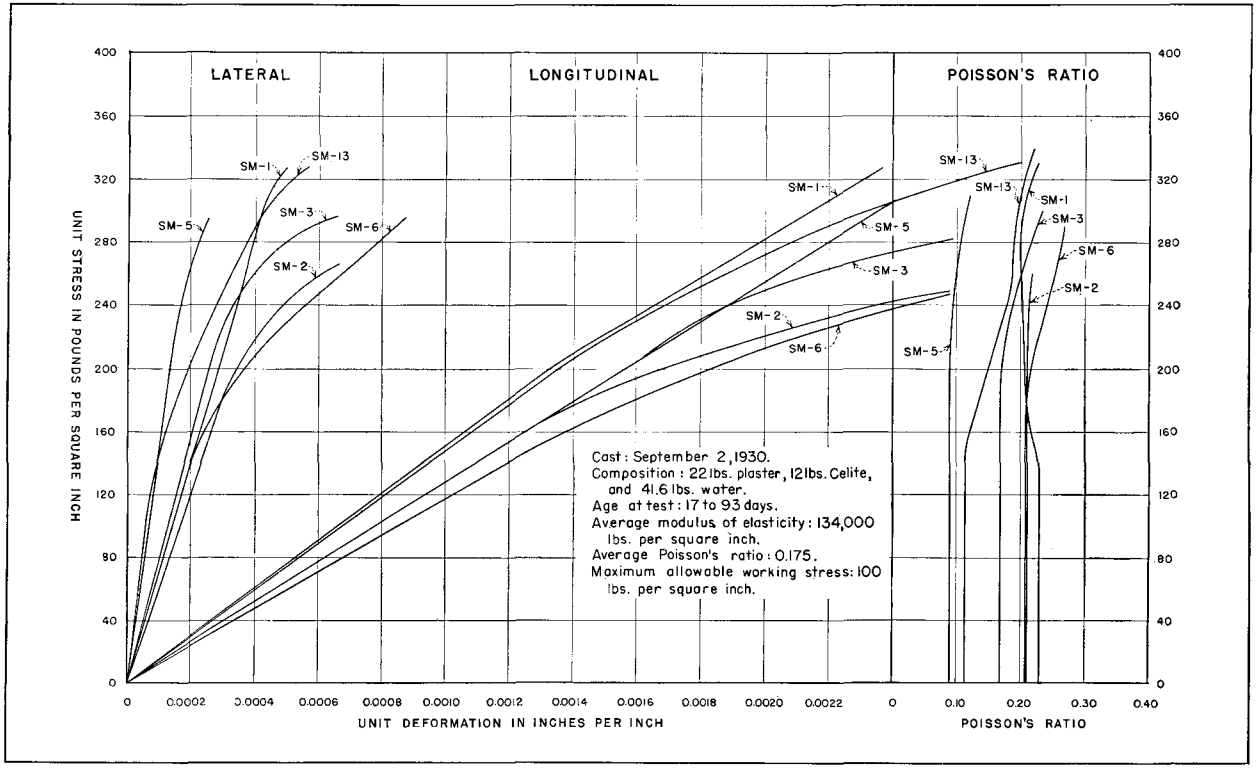

FIGURE 6—STRESS-STRAIN DIAGRAMS FOR COMPRESSION TESTS

2 by 4-inch Cylinders Made With Sunflower Molding Plaster

However, apparatus for measuring lateral and longitudinal deformations of 3 by 6-inch cylinders was not satisfactory, owing to its excessive weight as mentioned previously. Consequently the results of the tests on the larger cylinders are not believed to be as reliable as those on the smaller cylinders.

Tests were made to determine the effect of aquagel on the elastic properties of specimens made with Sunflower molding plaster and celite. Test specimens were made from a mix having no aquagel as well as from mixtures of the same proportions containing varying amounts of aquagel. The average modulus of elasticity in compression for 12 to 14 specimens, cast from a 36-pound batch, was as follows: no aquagel, 135,000 pounds per square inch; one teaspoon of aquagel, 129,000 pounds per square inch; two teaspoons of aquagel, 100,000 pounds per square inch; three teaspoons of aquagel, 80,000 pounds per square inch. Although aquagel is an excellent retarder for this type of work, its water retaining property, which produces specimens of lower strength and modulus of elasticity, made its use undesirable.

36. Ideal Finishing Plaster.—Some combinations of Ideal finishing plaster and celite were satisfactory, while others set too quickly. The first batch set so rapidly that most of the 2 by 4-inch cylinders were defective. Fairly satisfactory results were obtained with specimens made of 22 pounds of plaster, 10 pounds of celite, and 37 pounds of water. This mixture had an average modulus of elasticity of 164,000 pounds per square inch in compression, an average Poisson's ratio of 0.167, and an average ultimate strength of 304 pounds per square inch. Stress-strain curves for typical 2 by 4-inch specimens are shown in figure 7. Specimens tested at ages of 31 to 120 days gave the following results:

Specimens	Size, inches	Average E lb. per sq. in.	Poisson's ratio	Ult. strength lb. per sq. in.
3 beams	3 x 3 x 40	233,000	- - -	- -
3 cylinders	3 x 6	144,000	0.182	231
13 cylinders	2 x 4	164,000	0.167	304

Leaner mixes using Ideal finishing plaster showed results which were not very uniform, due in part to using excess water. To make a homogeneous material, free from air pockets, it was customary to use as much water as possible without causing segregation. However, at times some segregation occurred unintentionally, thereby producing erratic specimens. Leaner mixes shrank considerably after

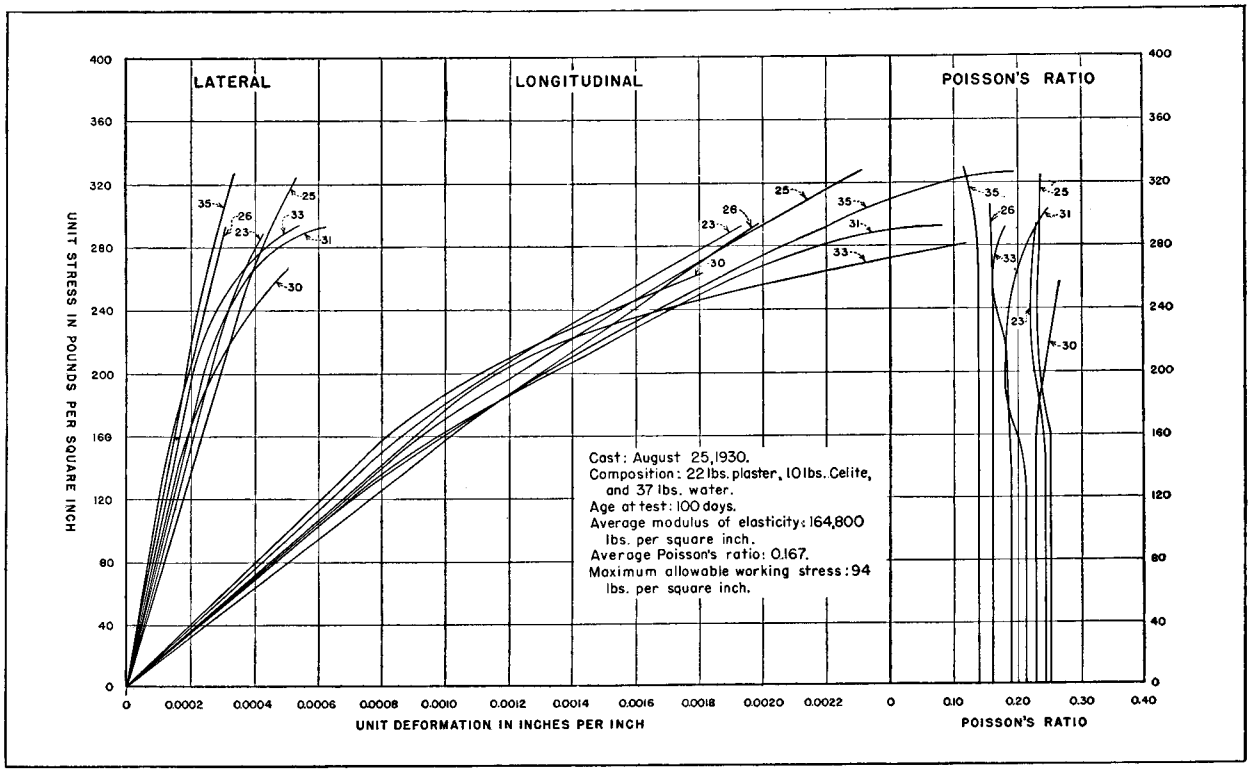

FIGURE 7—STRESS-STRAIN DIAGRAMS FOR COMPRESSION TESTS

2 by 4-inch Cylinders Made With Ideal Finishing Plaster

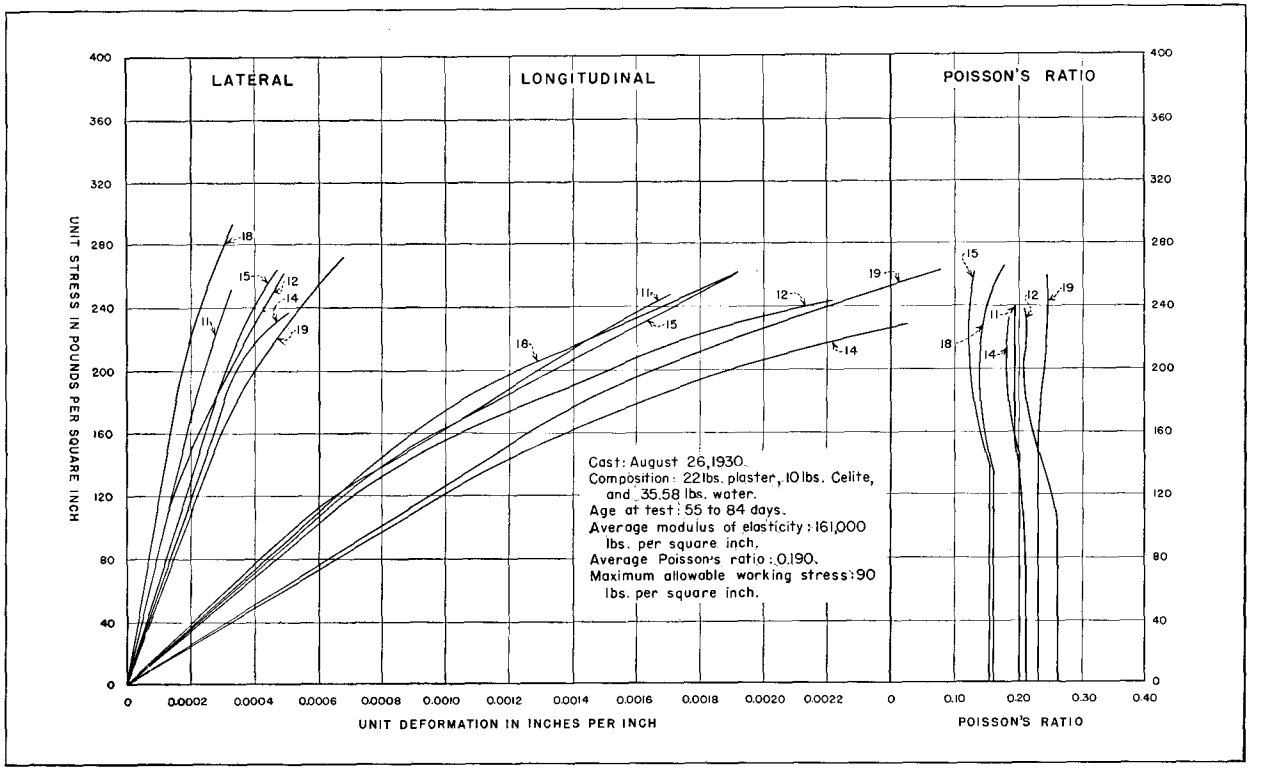

FIGURE 8—STRESS-STRAIN DIAGRAMS FOR COMPRESSION TESTS

2 by 4-inch Cylinder Made With Acme Finishing Plaster

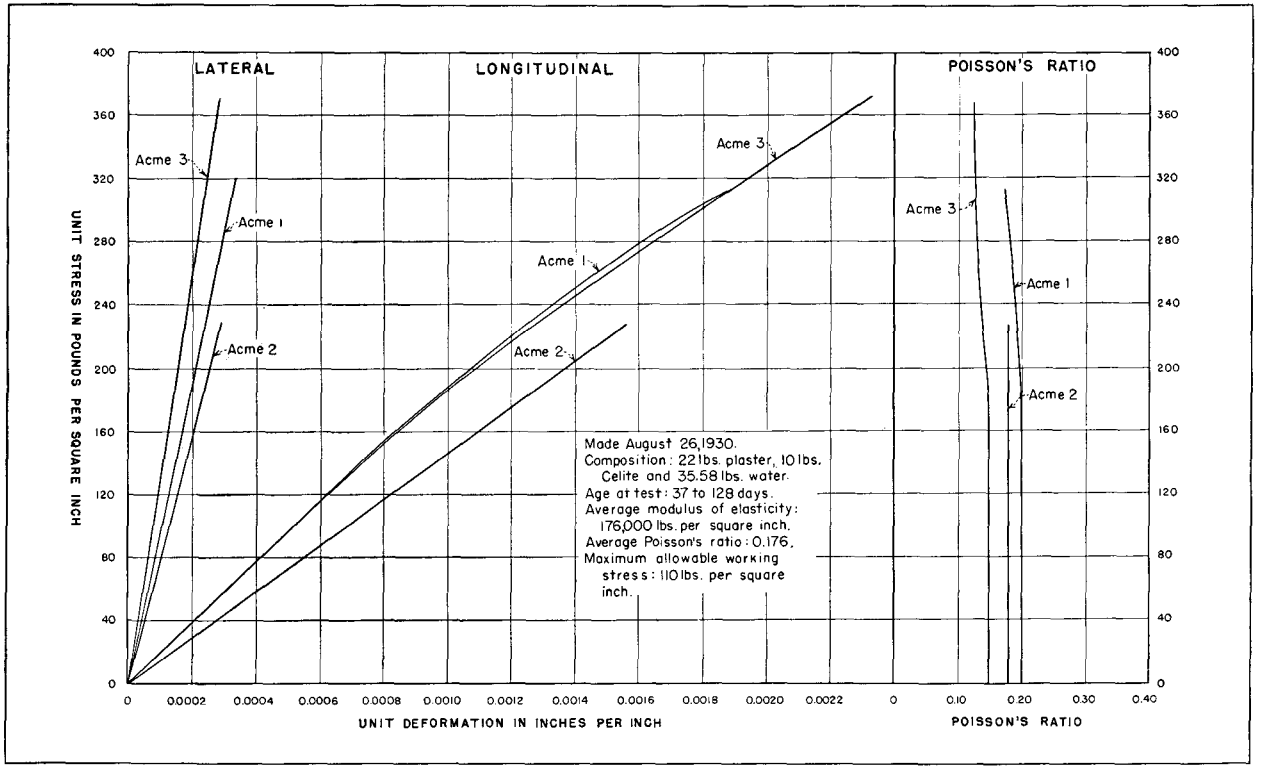

FIGURE 9—STRESS-STRAIN DIAGRAMS FOR COMPRESSION TESTS

3 by 6-inch Cylinders Made With Acme Finishing Plaster

hardening. A batch of 16 pounds of plaster, 12 pounds of celite, 42 pounds of water, and 5 teaspoons of aquagel was about as lean as could be made without excessive shrinkage.

In casting 3 by 3 by 40-inch beams, the forms were placed on a sheet of building paper on a concrete floor, filled with the plaster mixture, and then removed in about 24 hours. After removing the forms the beams were placed on three 1 by 4-inch cleats to dry, thus allowing air to circulate underneath them. Frequently, beams of the leaner mixes sagged between the cleats during the period of plasticity before they were entirely dry. As soon as sagging was noticed all 3 by 3 by 40-inch beams were allowed to dry either on the floor or on a flat plank.

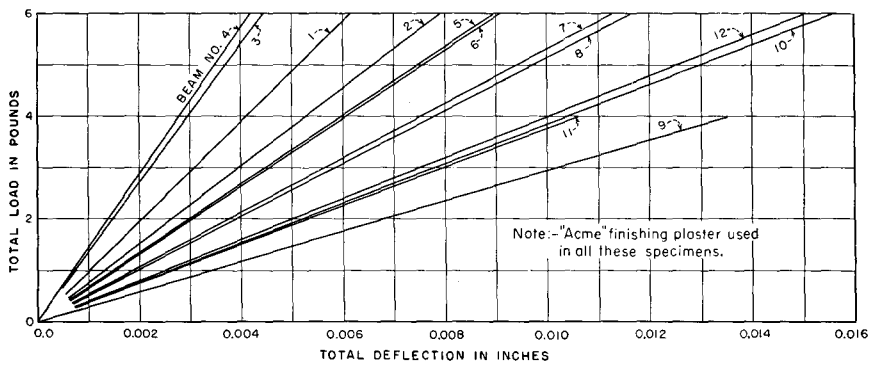

BEAM NO.	DATE MADE	DATE OF TEST	AGE IN DAYS	COMPOSITION				MODULUS OF ELASTICITY	WT. PER CU. FT. (LBS.)
				PLASTER (LBS.)	CELITE (LBS.)	WATER (LBS.)	AQUAGEL (TSP.)		
1	8-20-30	9-24-30	35	22	11	25.86	None	157,000	40.4
2	8-20-30	12-5-30	106	22	11	25.86	None	122,000	38.1
3	8-26-30	9-24-30	29	22	10	35.58	None	216,000	44.9
4	8-26-30	12-5-30	101	22	10	35.58	None	226,000	44.3
5	9-5-30	9-24-30	19	18	12	42.00	4	106,000	38.9
6	9-5-30	12-5-30	31	18	12	42.00	4	109,000	37.2
7	9-9-30	9-25-30	16	8	6	21.00	2	82,000	36.4
8	9-9-30	12-5-30	87	8	6	21.00	2	92,000	35.4
9	9-8-30	9-25-30	17	12	12	42.00	5	47,000	31.0
10	9-15-30	12-6-30	82	4	4	14.00	2	64,000	31.7
11	9-9-30	9-25-30	16	14	12	42.00	4	59,000	33.9
12	9-9-30	12-6-30	88	14	12	42.00	4	65,000	32.9

FIGURE 10—LOAD-DEFLECTION DIAGRAMS FOR ACME BEAMS

37. Acme Finishing Plaster.—Acme finishing plaster proved to be the most satisfactory of all brands of plaster used in combination with celite. The workability was satisfactory, and very few specimens were defective due to entrapped air or premature setting. In setting there was a slight swelling, which was preferred to the shrinkage encountered in some of the other brands of plaster. If the mixing water had a temperature of 60 degrees Fahrenheit, or less, there was

no danger of too rapid setting; but when warmer water was used it was necessary to add a small amount of aquagel as a retarder. This was particularly true in the case of the leaner mixes.

Typical stress-strain diagrams for cylinders cast from a mix of 22 pounds of Acme finishing plaster, 10 pounds of celite, and 35.58 pounds of water are shown in figures 8 and 9. Figure 8 shows data for 2 by 4-inch cylinders and figure 9 shows data for 3 by 6-inch cylinders. Results of flexural tests on 3 by 3 by 40-inch beams of several different mixes are shown in figure 10. The results of tests of the richer mixes show greater consistency than those of the leaner mixes, due in part to the difficulty in preventing segregation of material in the leaner mixes. The spread of the curves for a relatively rich mix is fairly narrow, as shown in figure 8.

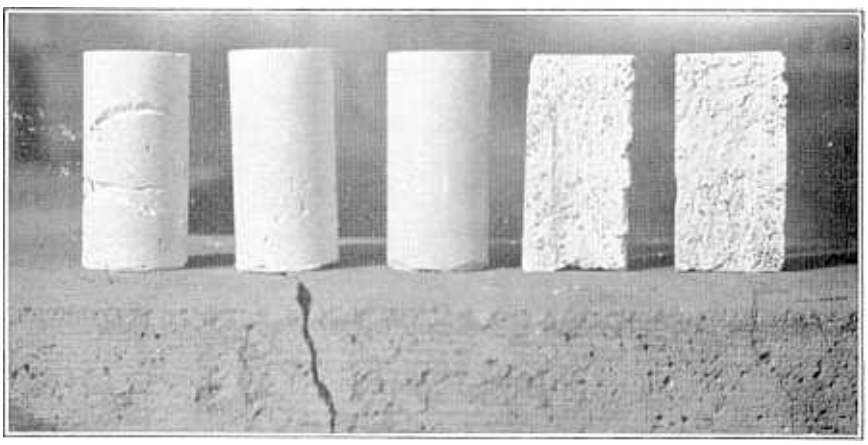

FIGURE 11—TYPICAL SHOT-LOADED CYLINDERS
Acme Finishing Plaster, Celite, and Lead Shot

38. Acme Plaster, Celite, and Lead.—The unit weight of plaster and celite is relatively low compared with that of most building materials. It was thought that an advantage might be derived from constructing the model of Boulder Dam of a material of the same unit weight as concrete. Therefore, some experimenting was done in an effort to increase the unit weight of plaster and celite mixes. It was found that the unit weight of plaster mixes could easily be controlled by the addition of small lead shot. Typical appearances of 2 by 4-inch shot-loaded cylinders are shown in figure 11. The cylinder which had been cut in half showed an apparent nonuniform distribution of shot.

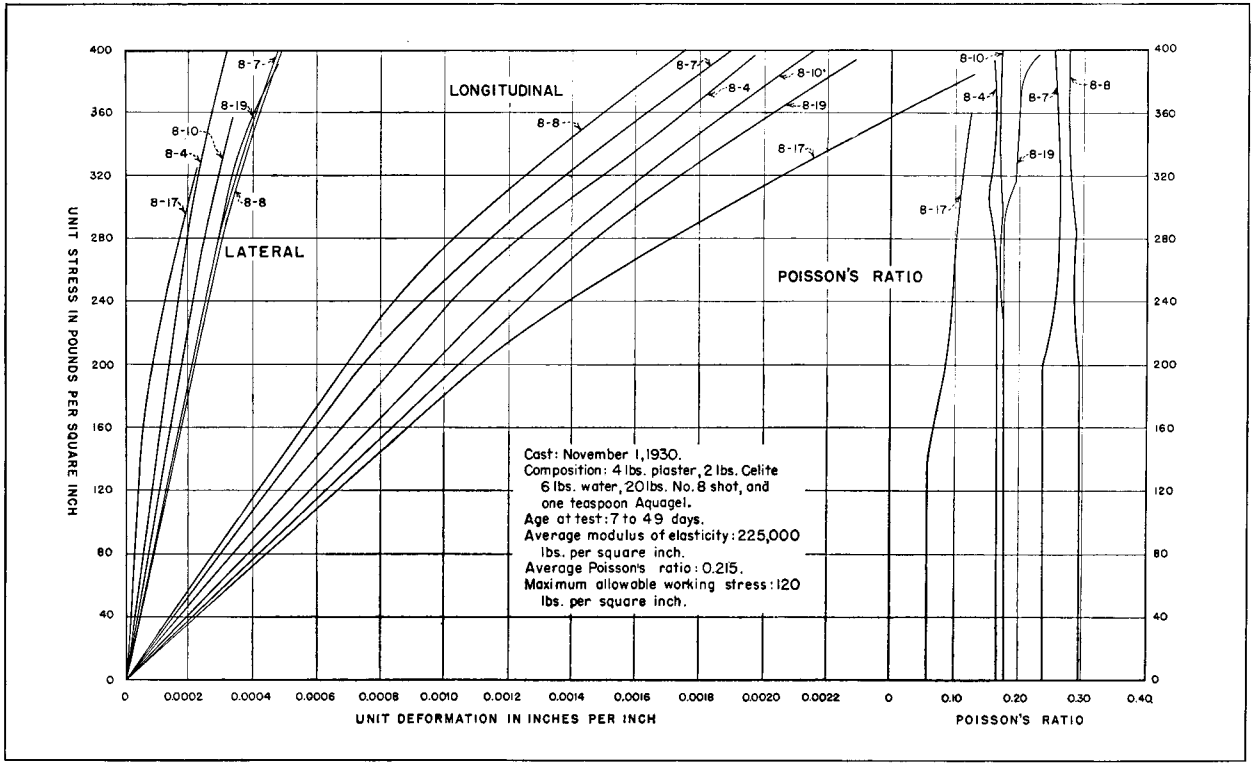

FIGURE 12—STRESS-STRAIN DIAGRAMS FOR SHOT-LOADED SPECIMENS

Compression Tests on 2 by 4-inch Acme Plaster and Celite Cylinders

This was incorrect because many of the shot were torn out by the saw in cutting the cylinder.

The addition of shot tended to increase the strength of the plaster product, with a resulting increase in the modulus of elasticity. It was difficult to secure uniform distribution of shot in the larger mixes, since the shot had a tendency to segregate at the bottom of the mixing pan. The plaster and celite mixtures were too thin to hold the shot in suspension. Several sizes of shot were used in the experiments. Number 5 was the largest, and number 10 the smallest. Within this range no effect of differences in size could be detected. Unit weights of specimens containing shot varied from 130 to 180 pounds per cubic foot.

The modulus of elasticity of shot-loaded specimens varied from 68,600 to 235,000 pounds per square inch, depending on the proportions of the ingredients. Poisson's ratio was about 0.20, nearly the same as for concrete. Stress-strain curves for a shot-loaded Acme plaster and celite mix are shown in figure 12. No flexural tests were made as there was insufficient shot available for casting 3 by 3 by 40-inch beams.

TESTS OF RECOMMENDED MIX

39. Recommended Mix.—The most satisfactory material found for models of thick arch dams was a mixture of 24 pounds of Acme finishing plaster, 12 pounds of celite, and 45 pounds of water. If the temperature of the water was above 60 degrees Fahrenheit, one to four teaspoons of aquagel were needed as a retarder, depending on the water temperature. This amount of material made a batch of convenient size, which could be handled by one or two men.

The recommended mix had a unit weight of 41.5 pounds per cubic foot, an average modulus of elasticity of 122,000 pounds per square inch in compression, and 165,000 pounds per square inch in flexure, a Poisson's ratio of 0.214, and a maximum allowable working stress of 80 pounds per square inch in compression. Typical stress-strain diagrams are shown in figure 13. Load deflection curves for 3 by 3 by 40-inch beams are shown in figure 14. In all tests the modulus of elasticity in flexure was greater than in compression. This was probably due to the fact that the flexural tests were made with simply supported beams in which only the outside fibers were stressed to a maximum. Also, some of the difference may have been caused by the apparatus used in the compression tests.

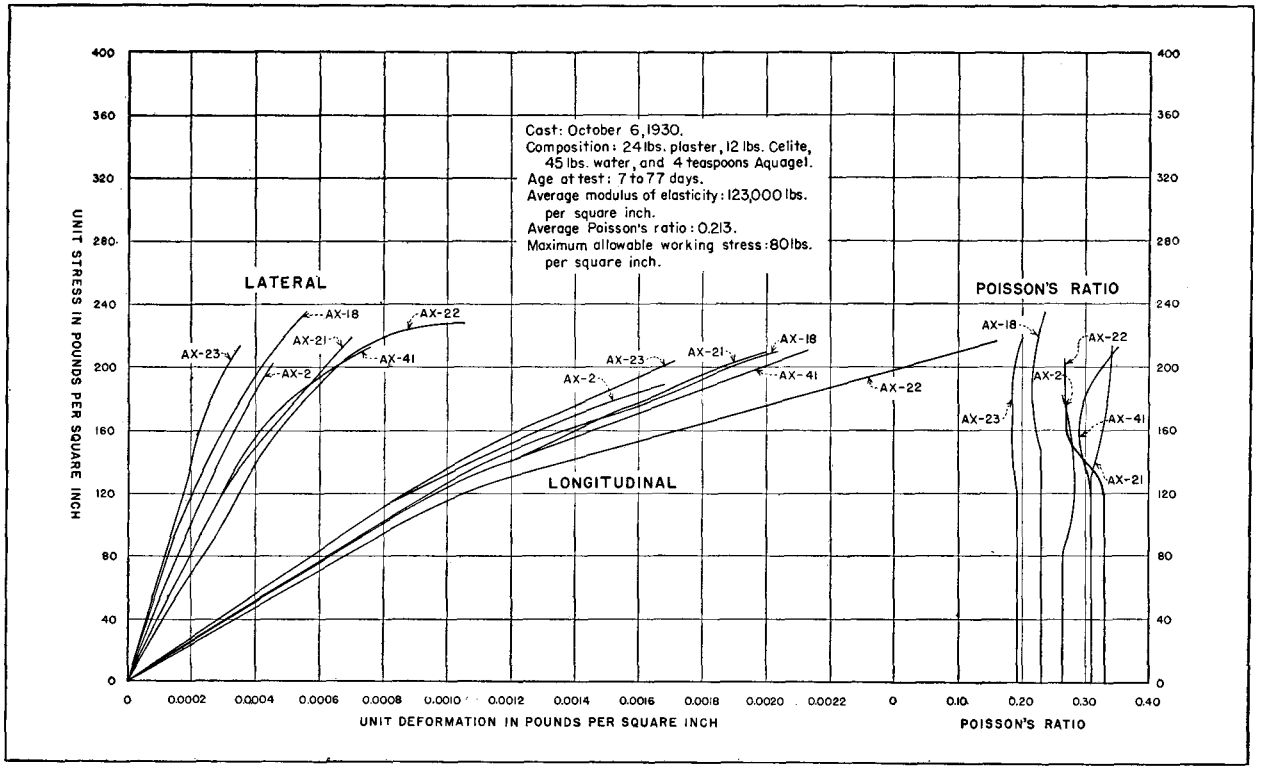

FIGURE 13—STRESS-STRAIN DIAGRAMS FOR RECOMMENDED MIX

Compression Tests on 2 by 4-inch Acme Plaster Cylinders

It was found that plaster compounds did not increase in strength with age after they were about seven days old. This fact is brought out by E. C. Eckel,[7] who stated: "Cement plasters and stuccos attain almost their full strength at the end of one week, showing little further gain at three months." In investigating this property, several 2 by 4-inch cylinders and some 3 by 3 by 40-inch beams were tested, with

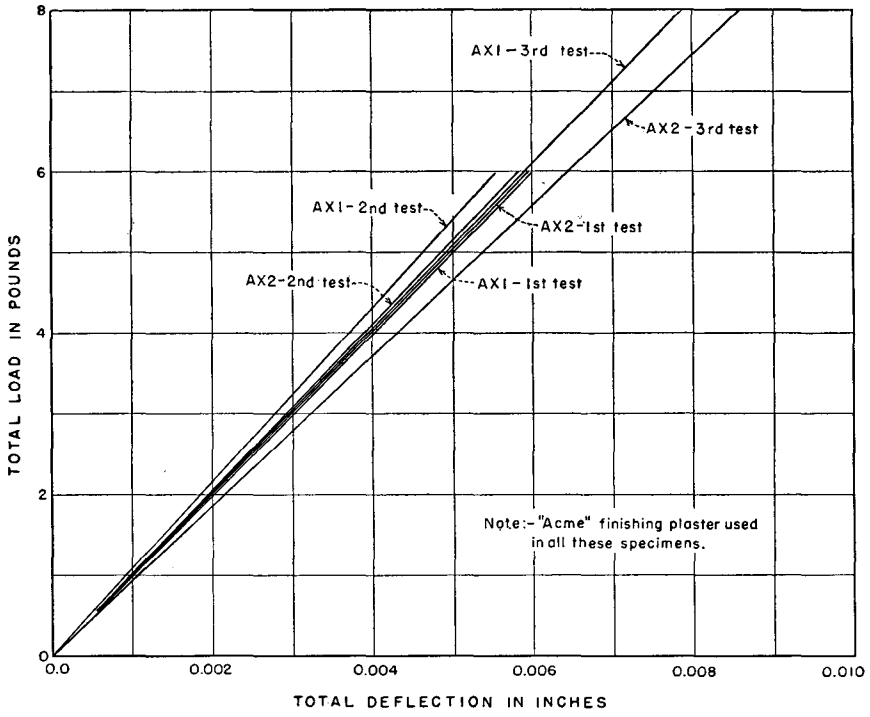

BEAM NO.	DATE MADE	DATE OF TEST	AGE IN DAYS	COMPOSITION				MODULUS OF ELASTICITY	WT. PER CU. FT. (LB.)
				PLASTER (LBS.)	CELITE (LBS.)	WATER (LBS.)	AQUAGEL (TSP.)		
AX1	10-5-30	10-29-30	24	24	12	45	4	160,000	41.7
AX2	10-5-30	10-29-30	24	24	12	45	4	167,000	41.7
AX1	10-5-30	11-4-30	30	24	12	45	4	173,000	41.4
AX2	10-5-30	11-4-30	30	24	12	45	4	169,000	41.4
AX1	10-5-30	12-4-30	60	24	12	45	4	168,000	41.3
AX2	10-5-30	12-4-30	60	24	12	45	4	160,000	41.6

Note:-This mix is the same as used in the 3'x 3'x 3' block and 6"x 8" shrinkage beam

FIGURE 14—LOAD-DEFLECTION DIAGRAMS FOR RECOMMENDED MIX

Flexural Tests on 3 by 3 by 40-inch Beams

[7]Eckel, Edwin C., "Cements, Limes and Plasters," 2nd Ed., 1922, p. 67, John Wiley & Sons, Inc.

TABLE 1—EFFECT OF AGE ON RECOMMENDED MIX

Composition: 24 lb. plaster, 12 lb. celite, 45 lb. water, and 4 teaspoons aquagel.

Number of Specimens Tested	Age in Days	Average Modulus of Elasticity*	Average Poisson's Ratio
4	7	129,000	0.213
4	14	120,000	0.175
4	21	115,000	0.203
4	28	130,000	0.249
3	35	116,000	0.202

*In pounds per square inch.

results as shown in table 1 and figure 14. The conclusion drawn from the tests was that, after the material had set and dried, age did not affect the strength or elastic properties.

The recommended mix contained as much water as could be used without segregation occurring in the mixing pan. If less water was used the strength and modulus of elasticity were materially increased. This fact can be seen by comparing the compressive tests shown in figures 13, 15, and 16, and by studying the flexural tests shown in figure 17. Tests to determine effects of varying the water content were made by keeping the proportions of dry materials the same and using 45, 40, and 35 pounds of water. The results are given below.

Amount of water per batch, lb.	Modulus of elasticity, lb. per sq. in.	Maximum working stress, lb. per sq. in.
45	122,000	80
40	136,000	80
35	193,000	102

40. Shrinkage of Recommended Mix.—Some apprehension was felt over the possibility of shrinkage of the model dam and abutments which might cause the formation of cracks along the areas of contact. In order to study the shrinkage of the recommended mix, a 6 by 8-inch beam was cast on two sheets of rubber, with the ends of the beam terminating in 8 by 16 by 20-inch blocks which were securely anchored to concrete. Plugs for making strain-gage observations were set in the top of the beam and readings were taken regularly for three months. No cracks developed and no movements were indicated by the strain gage. The beam is shown in the foreground of figure 18.

41. Workability of Recommended Mix.—The usual batch of the recommended mix contained 36 pounds of dry materials and 45 pounds

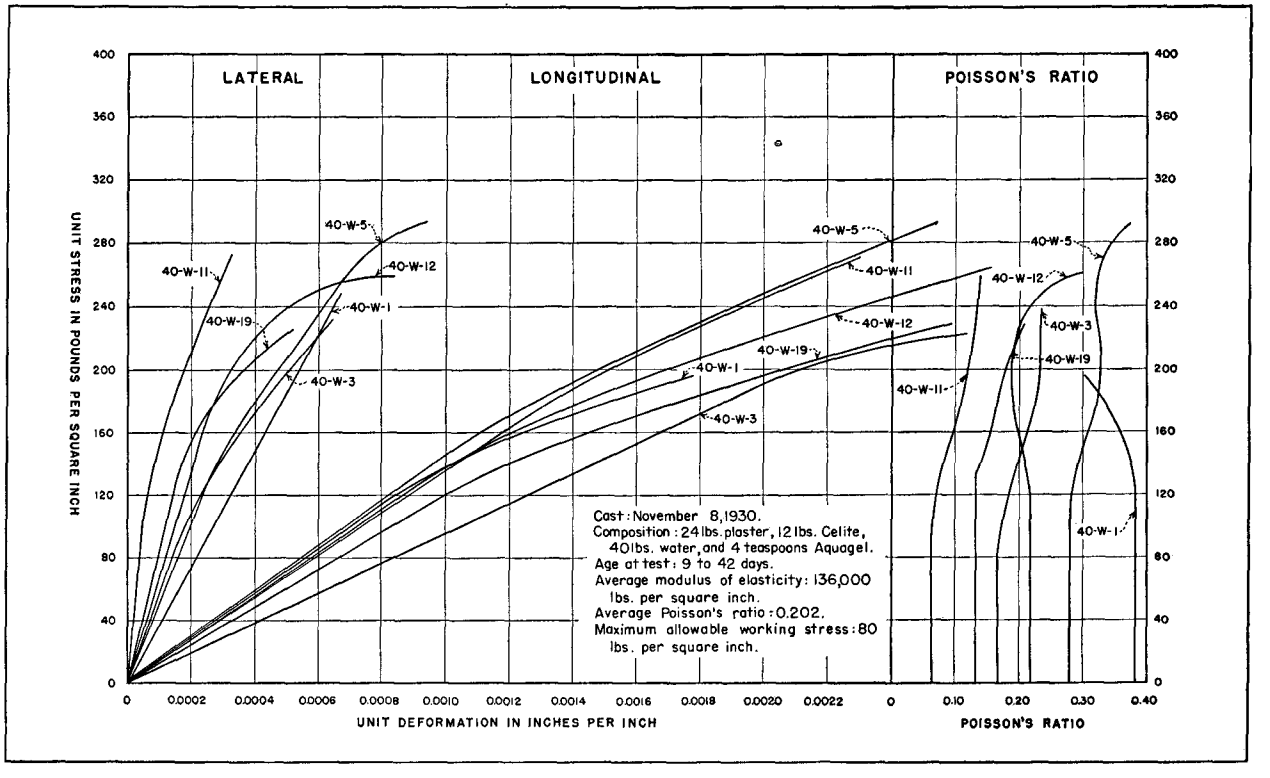

FIGURE 15—STRESS-STRAIN DIAGRAMS, REDUCED MIXING WATER

Compression Tests on 2 by 4-inch Acme Plaster Cylinders

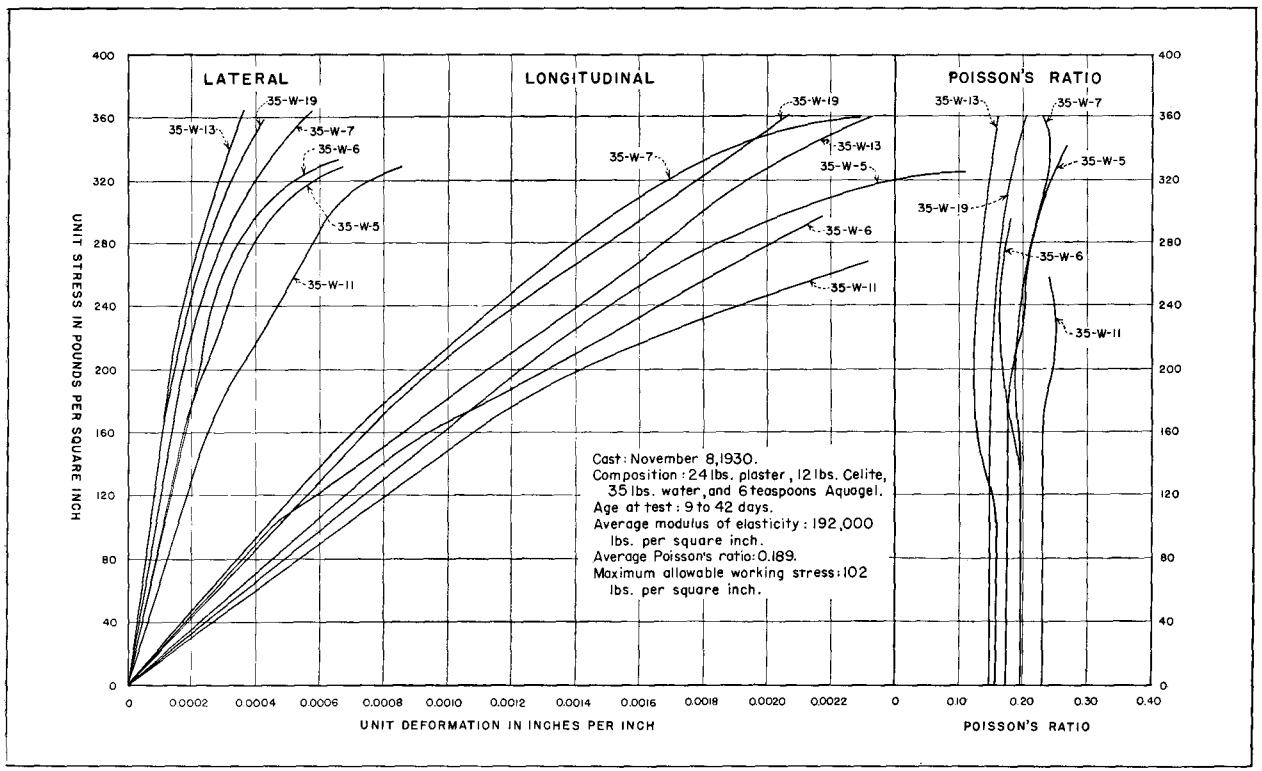

FIGURE 16—STRESS-STRAIN DIAGRAMS, REDUCED MIXING WATER

Compression Tests on 2 by 4-inch Acme Plaster Cylinders

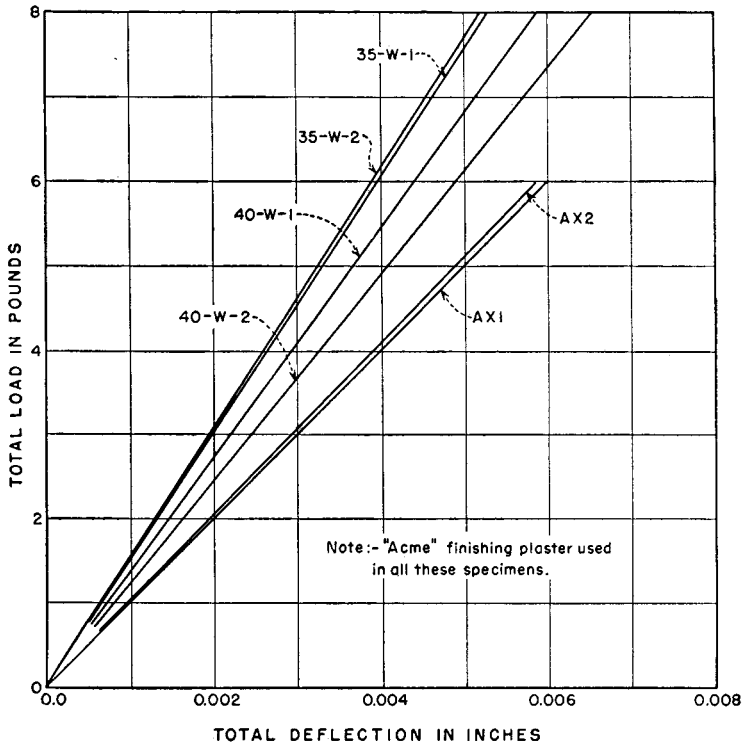

BEAM NO.	DATE MADE	DATE OF TEST	AGE IN DAYS	COMPOSITION				MODULUS OF ELASTICITY	WT. PER CU. FT. (LBS.)
				PLASTER (LBS.)	CELITE (LBS.)	WATER (LBS.)	AQUAGEL (TSP.)		
35-W-1	11-8-30	12-4-30	26	24	12	35	6	249,000	48.6
35-W-2	11-8-30	12-4-30	26	24	12	35	6	251,000	47.8
40-W-1	11-8-30	12-4-30	26	24	12	40	4	211,000	44.1
40-W-2	11-8-30	12-4-30	26	24	12	40	4	201,000	44.4
AX1 *	10-5-30	10-29-30	24	24	12	45	4	160,000	41.7
AX2 *	10-5-30	10-29-30	24	24	12	45	4	167,000	41.7

* First test.

FIGURE 17—LOAD-DEFLECTION DIAGRAMS, VARIABLE MIXING WATER

Flexural Tests on 3 by 3 by 40-inch Acme Plaster Beams

of water. Since all test specimens were relatively small compared to the proposed model, it was decided to cast a three-foot cube so that the problems involved in mixing and placing larger masses of the material could be studied. It was not feasible to mix sufficient quantities of material to pour the block at one time, owing to the possibility of initial set occurring before the pour was completed. The block was therefore cast in three-inch layers, a layer being poured each morning and afternoon until the desired height was reached. The

bond between the layers proved to be satisfactory. The finished block is shown in the background of figure 18.

The greatest difficulty involved in building and curing the block was the length of time required for the material to dry. As a possible means of hastening the time of drying of the proposed model, it was decided to try pouring a layer from three to four inches thick, allowing it to dry, then pouring a succeeding layer on top of the dried material. Experiments were made with 4 by 6 by 38-inch beams, cast in two stages, to observe whether a fresh layer would bond to

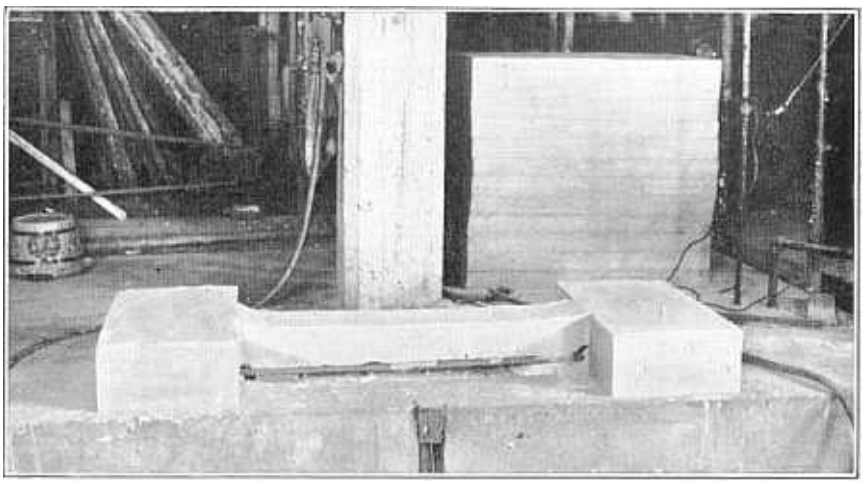

FIGURE 18—SHRINKAGE BEAM AND 3-FOOT CUBICAL BLOCK

a dry one. When the lower half of the beam was poured, greased wooden plugs were set in the top, to form keyways for bonding the two halves together. However, as the lower half of the beam dried, cracks appeared at the corners of the keyways.

Another set of beams was made in which keyways were cut with a saw and chisel as soon as the first layers were sufficiently dry, see figures 19 and 20. When thoroughly dry the first layers were placed in the forms again, and second layers cast. Typical results are shown in figure 21. The dry base drew water out of the upper part by capillary action so rapidly that shrinkage cracks developed. The difference in drying conditions between the two halves produced an upper portion which did not bear any resemblance to the lower portion.

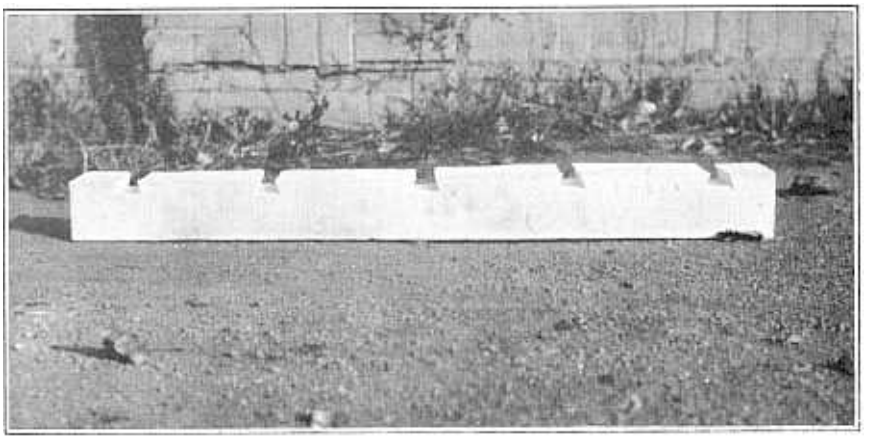

FIGURE 19—KEYWAYS IN LOWER HALF OF PLASTER-CELITE BEAM

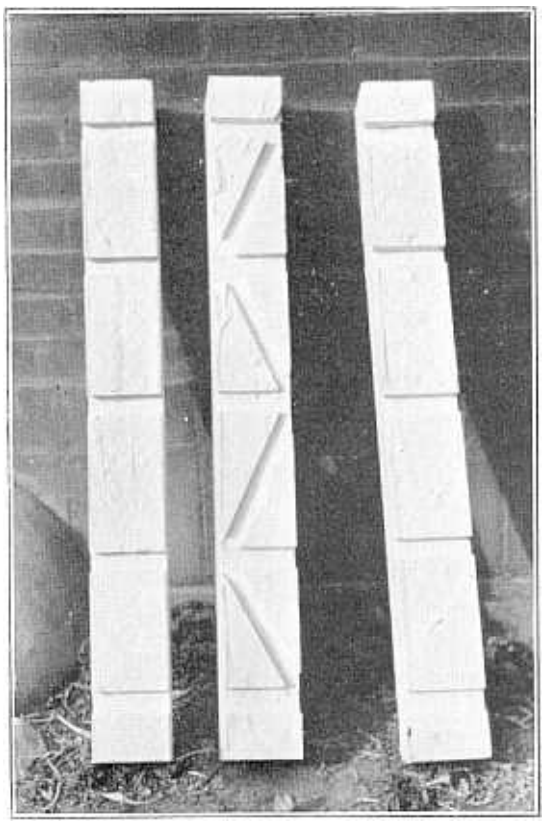

FIGURE 20—KEYWAYS IN PLASTER-CELITE BEAMS

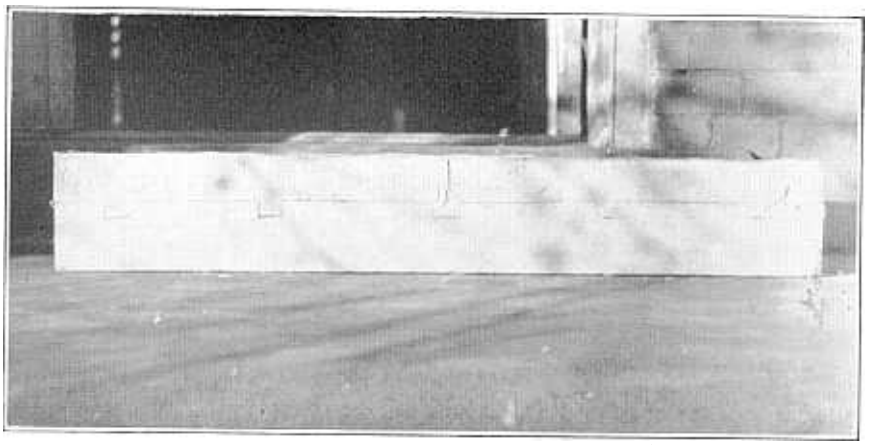

FIGURE 21—TYPICAL FAILURE OF PLASTER-CELITE BEAM
Upper Layer Poured on Keyed Lower Layer Shown in Figure 20, Without Shellacking Dried Surface

A third set of beams was made with keyways of about equal length as shown in figure 22. To prevent moisture being drawn from the second layer into the first, the first layer of one beam was painted with two coats of orange shellac before the second layer was poured. In this beam the bond between the old and new layers was satisfactory, as may be seen in figure 23. In beams where the first layers were not shellacked, the two halves failed to bond satisfactorily. One of these beams is shown in figure 24.

42. Bond at Metal Inserts.—In order to make deflection measurements of the Stevenson Creek and Gibson models, small metal inserts were embedded in the concrete at the downstream faces of the models. Rods which actuated measuring dials were attached to the inserts. As it was desired to use the same system in measuring movements of the Boulder model, tests were made to determine the bond of plaster materials to the metal inserts. Several 2 by 4-inch cylinders of the recommended mix and also of the shot mixes were made with deflection anchors cast in one end. A section through one of the anchors is shown in figure 37. The method used in testing the specimens is shown in figure 25, a hook for supporting the load being attached to the insert as shown in the figure. The specimens were tested by placing them on a support with a slot under the insert, and gradually adding shot to a bucket suspended from the hook until failure occurred. Cylinders before and after being tested are shown in figure 26.

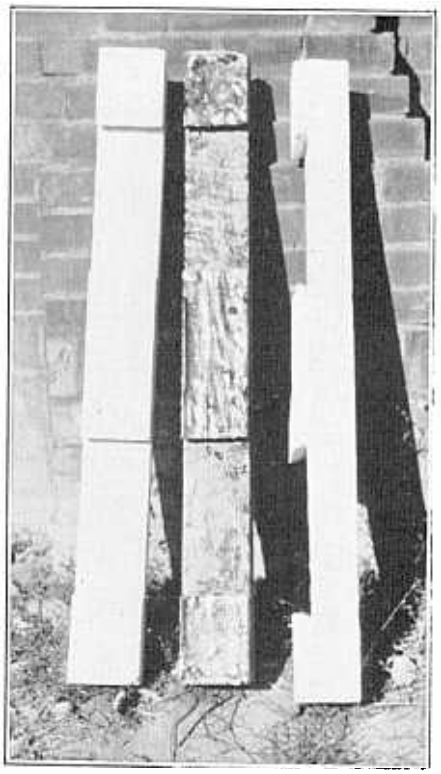

FIGURE 22—KEYWAYS IN PLASTER-CELITE BEAMS
Second Series of Tests. Center Beam Painted With Two Coats of Orange Shellac

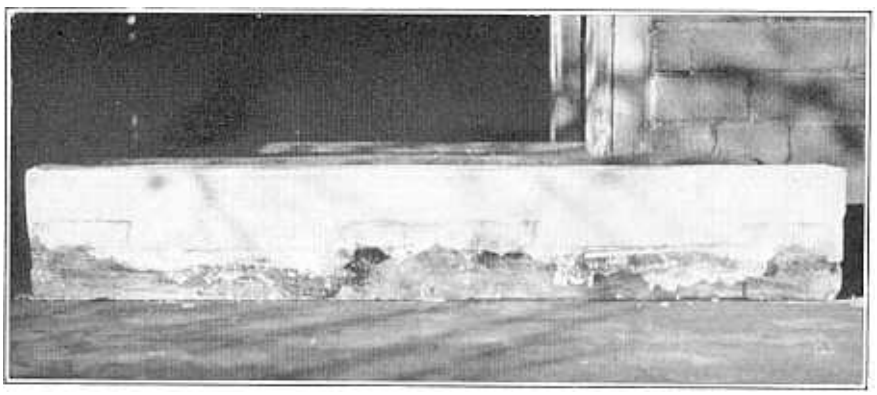

FIGURE 23—BEAM SHOWING SATISFACTORY BOND BETWEEN LAYERS
Surface of First Layer Painted with Shellac Before Pouring Second Layer

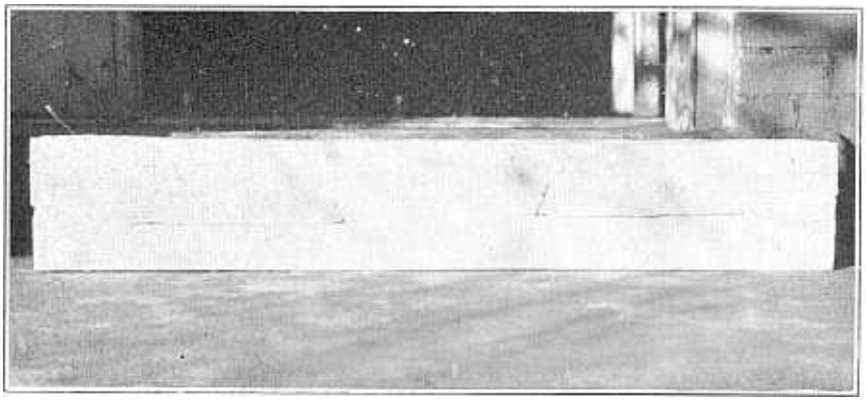

FIGURE 24—FAILURE OF PLASTER-CELITE BEAM
Surface of First Layer Not Painted with Shellac Before Pouring Second Layer

The strength developed in bond to the metal inserts was remarkable. For shot-loaded cylinders the average load required to pull out the inserts was 119 pounds. For cylinders cast from the recommended mix, an average of 64 pounds was required to pull out inserts with plain ends, and 94 pounds for inserts with a wire loop around the ends of the anchor screws.

43. Evaporation Rates.—An investigation was made of the rate of evaporation of the recommended mix under different storage conditions and using different sizes of specimens. A set of evaporation test specimens consisted of one 4 by 6 by 38-inch beam, one 3 by 3 by 40-inch beam, one 6 by 8 by 18-inch block, one 6 by 12-inch cylinder, two 3 by 6-inch cylinders, and seven 2 by 4-inch cylinders. A group of evaporation specimens is shown in figure 27. Results of evaporation tests, for various storage and drying conditions, are shown on figure 28.

The specimens were poured and allowed to remain undisturbed until the end of the second day when the forms were removed. The specimens were then weighed and placed in storage. At this time the weights of all specimens, except the 2 by 4-inch cylinders, were from 150 to 180 per cent of the dry weights.

Curves showing the ratio of evaporation for representative specimens under different storage conditions are given in figure 28. The larger specimens, such as the 4 by 6 by 38-inch beams and the 6 by 8 by 18-inch blocks, gave an indication of the rate of evaporation to be expected in the two to three-inch layers to be used in constructing

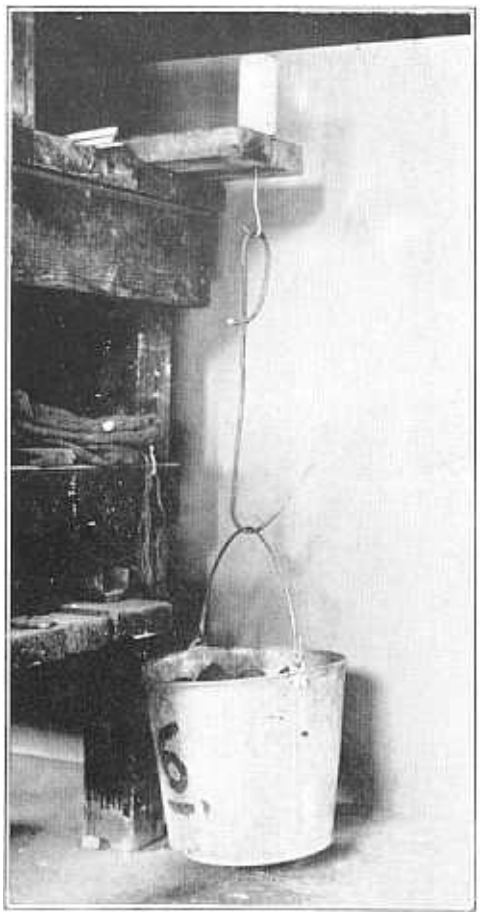

FIGURE 25—TESTING BOND BETWEEN PLASTER AND INSERTS

the model. Under ordinary conditions in the model testing pit, such layers would require from 15 to 20 days to dry; but by blowing warm air over them, the time could be reduced to about 7 to 10 days. For the model, evaporation took place almost entirely through the top of the layer, except near the top of the model where evaporation also took place at the sides. For such conditions, rates of evaporation naturally were lower than for specimens which were exposed on at least three faces.

The 3 by 3 by 3-foot experimental block which was built in the concrete laboratory near the testing pit was watched with considerable interest. Although electric fans and heaters were used to increase

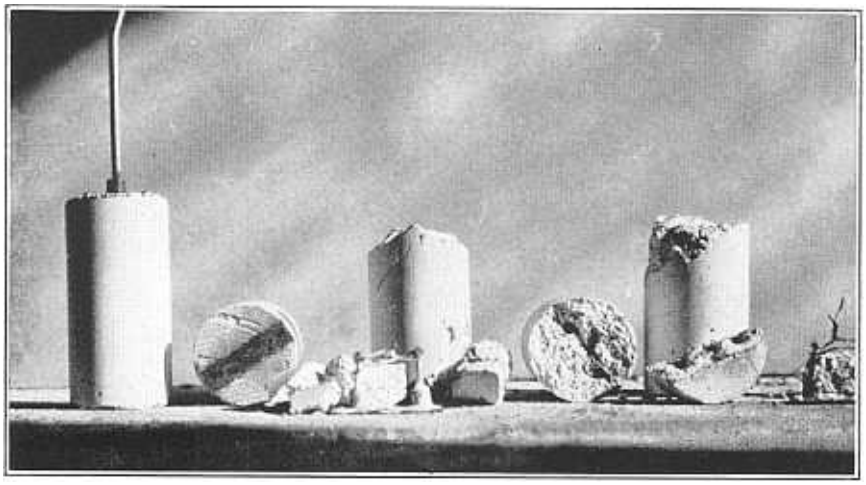

FIGURE 26—SPECIMENS BEFORE AND AFTER TESTING BOND AT INSERTS

Specimen at Left Ready for Test. Specimens at Right Show Characteristic Failure

evaporation rates, the interior of the block required considerable time to dry. Borings were made at intervals to determine the moisture content of the interior. Six months after the block was finished a moisture content of eight per cent was found in the material removed from the center of the block. This was still too high to obtain satisfactory elastic conditions.

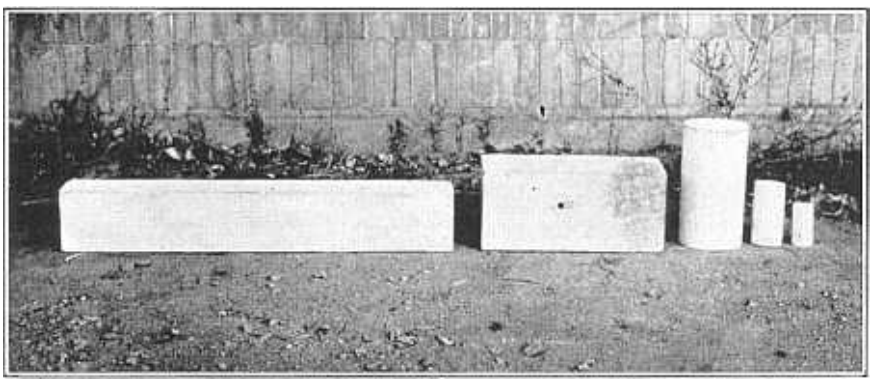

FIGURE 27—SET OF EVAPORATION TEST SPECIMENS

4 by 6 by 38-inch Beam, 6 by 8 by 18-inch Block, 6 by 12-inch Cylinder, 3 by 6-inch Cylinder, and 2 by 4-inch Cylinder

44. Plotting Test Data.—The compression tests discussed in this chapter were made with the 20,000-pound, hand-operated testing machine shown in figure 1, using the strain meters shown in figure 2. The testing was done by the increment method; that is, the poise

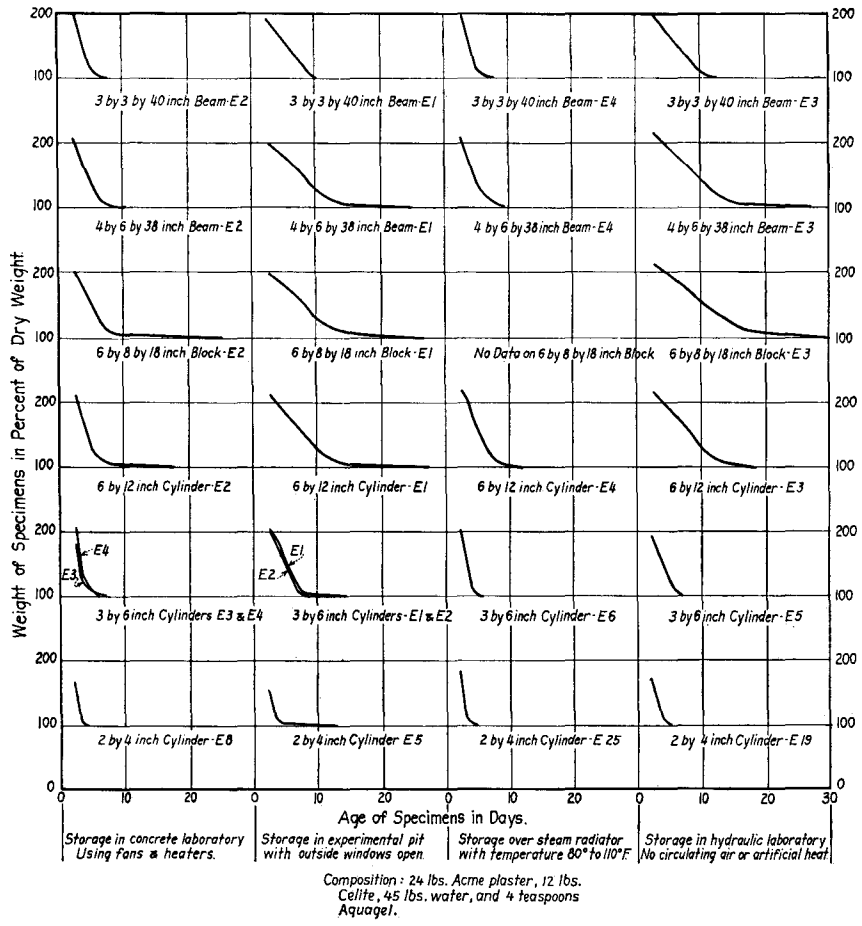

FIGURE 28—EVAPORATION RATES OF PLASTER-CELITE SPECIMENS

was set at some predetermined figure on the scale beam and the load applied until the beam balanced. At this time the dial gages of the strain meters were read. The poise was then moved ahead another increment and the load applied as before until the beam balanced, when the dials were again read.

A table containing observed and reduced data for a typical test is shown in figure 29. In this test, 50-pound increments were used in loading the specimen. The columns headed "Lat. Def." and "Long. Def." give dial readings of the strain meters, the former being for the lateral extensometer and the latter for the longitudinal compressometer. In reducing the data the unit stress was obtained by dividing the total load by the area of the cross section of the specimen tested. The molds for the 2 by 4-inch cylinders had a diameter of 1.98 inches and a cross-sectional area of 3.079 square inches. The area of the cross section of the 3 by 6-inch cylinders was 7.065 square inches. The unit lateral deformation was obtained by multiplying the observed lateral gage reading by the factor 0.000,025,2 for the 2 by 4-inch cylinders, and by 0.000,016,7 for the 3 by 6-inch cylinders. These factors were computed from the design and dimensions of the extensometers. The unit longitudinal deformation was obtained by multiplying the observed longitudinal gage reading by the factor 0.000,140 for the 2 by 4-inch cylinders, and by 0.000,120,7 for the 3 by 6-inch cylinders. These factors were obtained by calibrating the compressometers against a standard dial gage.

Curves for lateral and longitudinal deformation were next plotted. Since some slack existed in the assembled apparatus, the deformation curves rarely passed through the origin of coordinates, as may be

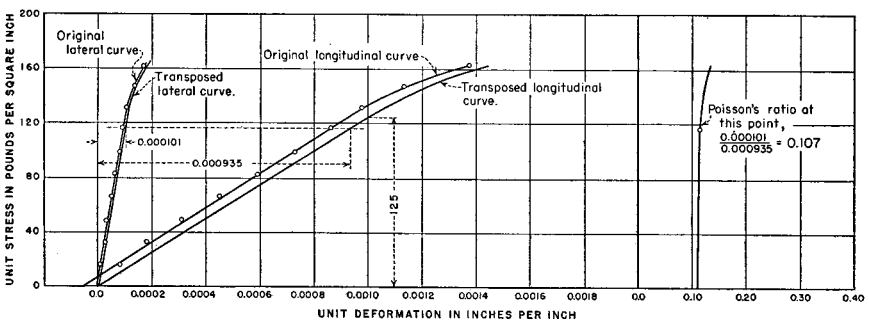

This method was used in all tests of the 2-inch by 4-inch and 3-inch by 6-inch cylinders.
Curves shown above are for 2-inch by 4-inch cylinder AX40.
Deformation curves, when plotted, rarely pass through the origin of coordinates. Therefore, they are transposed horizontally until they intersect the origin.
The modulus of elasticity is the tangent modulus for the lower stresses where the deformation curves are straight.
In this example,

$$\text{Modulus} = \frac{\text{STRESS}}{\text{STRAIN}} = \frac{125}{0.0010} =$$

125,000 lbs. per square inch.

Longitudinal gage factor = 0.000,140.
Lateral gage factor = 0.000,025,2.

TOTAL LOAD	OBSERVED DATA		REDUCED DATA			
	LAT. DEF. 0.0001"	LONG. DEF. 0.001"	UNIT STRESS	UNIT LAT. DEF.	UNIT LONG. DEF.	POISSON'S RATIO
0	0.0	0.0	0.0	0.00000	0.00000	0.107
50	0.4	0.6	16.2	0.00001	0.00008	0.107
100	1.0	1.3	32.5	0.00003	0.00018	0.107
150	1.1	2.2	48.7	0.00003	0.00031	0.107
200	1.8	3.2	65.0	0.00005	0.00045	0.107
250	2.2	4.2	81.2	0.00006	0.00059	0.107
300	3.0	5.2	92.5	0.00008	0.00073	0.107
350	3.5	6.1	113.7	0.00009	0.00086	0.107
400	4.3	7.0	130.0	0.00011	0.00098	0.108
450	5.6	9.4	146.2	0.00014	0.00131	0.117
500	6.9	9.8	162.5	0.00017	0.00137	0.124
550	FAILED					

FIGURE 29—METHOD OF PLOTTING COMPRESSION TEST DATA

seen in figure 29. In order to place all stress-strain curves on the same basis, the curves were transposed parallel to their original positions, so that they would pass through the origin. This simplified the computations of the modulus of elasticity and Poisson's ratio.

Values of the modulus of elasticity given in this bulletin are "tangent moduli" for the parts of the curves which lie below the elastic limit. As the plaster compounds were very elastic, the stress-strain diagrams for the lower unit stresses were found to be straight in nearly all of the tests. To find the modulus of elasticity it was only necessary to produce the initial slope of the longitudinal curve until it intersected the 0.0010 deformation line. By reading the stress at this point and dividing by 0.0010, the modulus was obtained. Poisson's ratio was found by dividing the abscissa of the lateral curve by the abscissa of the longitudinal curve.

Flexural tests were made with the apparatus shown in figure 3. A typical set of test data and resulting curves are shown in figure 30. The beams were tested four or more times and the average results used in plotting. A little slack in the apparatus was responsible for the fact that the loading and unloading curves do not coincide.

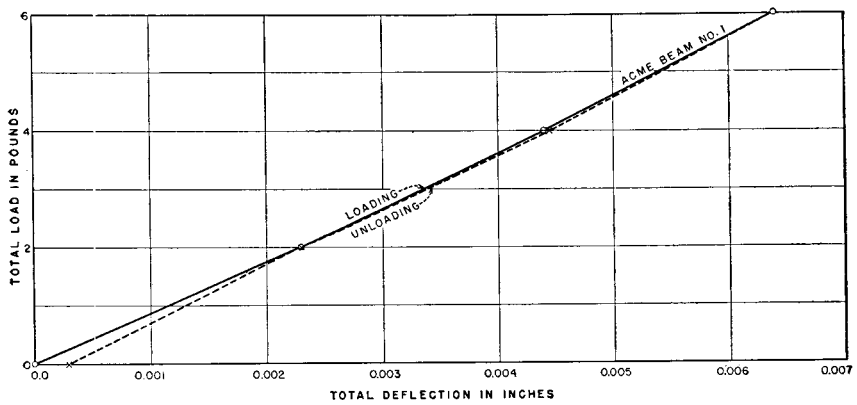

Deflection observations for each beam were repeated several times and the average value of the observed deflection was used in plotting.

As the exact dimensions of the beams varied somewhat from the nominal dimensions, the exact dimensions were used in calculating the moments of inertia.

For the above beam, breadth = 3.06"; depth = 3.04"; and moment of inertia = 7.16.

Modulus of elasticity =

$$\frac{1}{48} \times \frac{Pl^3}{ID} = \frac{1}{48} \times \frac{6 \times 38^3}{7.16 \times 0.0064} = \left\{\begin{array}{l}149{,}000 \text{ pounds per} \\ \text{square inch.}\end{array}\right.$$

LOAD IN LBS.	OBSERVED DATA Gage readings in ten-thousandths of an inch					
	TEST 1	2	3	4	5	AV. DEF.
0	0	0	0	0	0	0
2	24	23	23	24	23	23
4	45	43	44	47	44	44
6	64	64	64	69	64	64
4	46	44	45	49	44	45
2	25	24	23	28	20	23
0	3	2	3	6	0	3

FIGURE 30—METHOD OF PLOTTING FLEXURAL TEST DATA

CHAPTER III—PLASTER-CELITE MODEL AND MATERIALS TESTS

45. Design of Model.—The plaster-celite model of Boulder Dam was designed from the plan and section shown on figure 31. This was a tentative design, based on technical study 32-B, which was revised before construction. The design finally adopted for the dam is shown on page iv. The principal change made in preparing final plans was the straightening of the downstream face near the base of the dam. The design shown in figure 31 had constant radius arches and variable cantilever slopes at the downstream face, in the lower portion of the dam. By use of constant radius arches, each arch element had a constant thickness from abutment to abutment. The scale selected for the model was 1 to 240, or 1 inch on the model represented 20 feet on the dam. This gave a model 36⅞ inches high, with a top thickness of 2¼ inches and a maximum base thickness of 32 inches.

The same pit that was used for testing the previous models of arch dams was used for the model of Boulder Dam. The concrete base and the reference pier which were used for the Gibson model were left in the pit, but it was necessary to remove a portion of the base to make room for the new concrete base for the Boulder model. The old reference pier, however, served as a support for the bracing required to hold the mercury loading apparatus.

In order to adapt the testing pit to the Boulder model, concrete abutments containing 2½ cubic yards each, and conforming approximately to the shape of the cross section at Boulder Canyon, were constructed in the testing pit. Since the model would have a much lower strength and stiffness than concrete, it was necessary to provide a supplemental plaster-celite base to provide for foundation movements. Such movements could not be obtained with the model cast directly against concrete. Figure 32 shows the position of the model in the testing pit with the concrete base, supplemental plaster base, and reference base for deflection instruments. A minimum thickness of 12 inches, corresponding to a depth of 240 feet in the canyon rock, was specified for the supplemental plaster base.

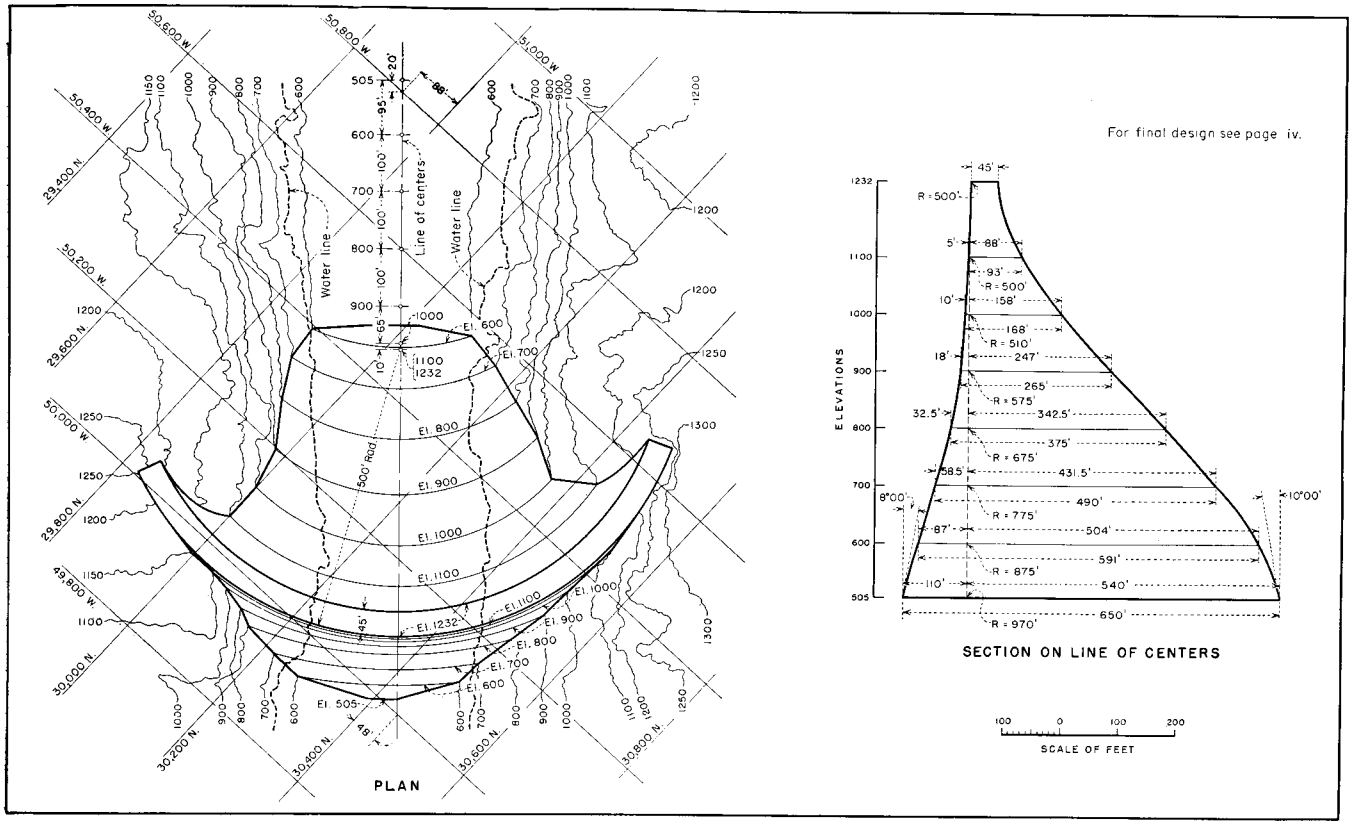

FIGURE 31—BOULDER DAM, PLAN AND MAXIMUM SECTION, STUDY 32-B

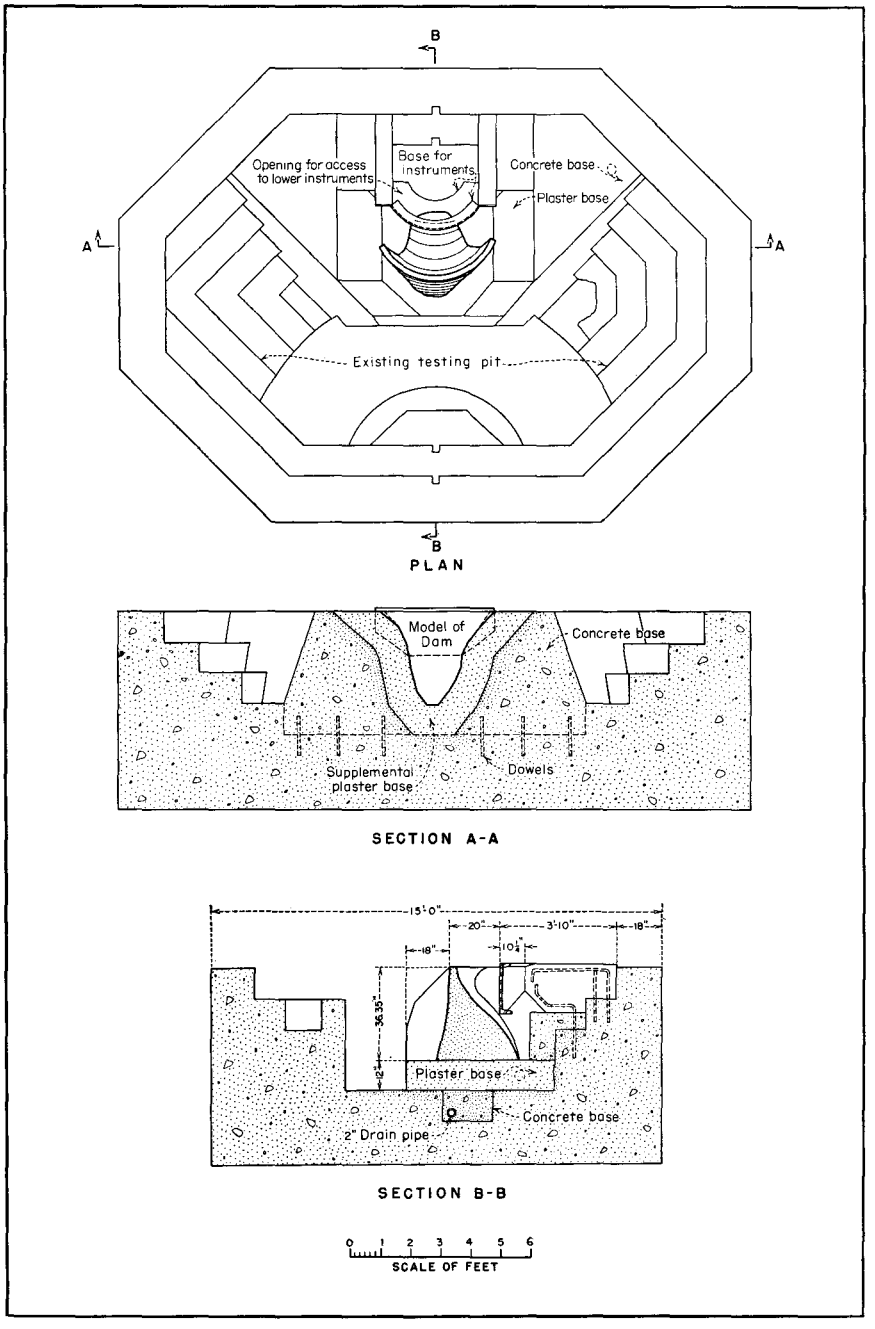

FIGURE 32—LOCATION OF MODEL IN TESTING PIT

CONSTRUCTION OF SUPPLEMENTAL BASE

46. Method of Construction.—The plaster-celite mixture set in about an hour in cool weather, and more rapidly in warm weather. The resulting product held water for a considerable time after setting. In order to dry the base thoroughly it was cast in layers three inches thick, and warm air blown over each layer from 10 to 15 days until dry. Samples of the material in each layer, obtained by boring with a carpenter's auger, were accurately weighed and carefully dried at a temperature not greater than 100 degrees Fahrenheit to determine

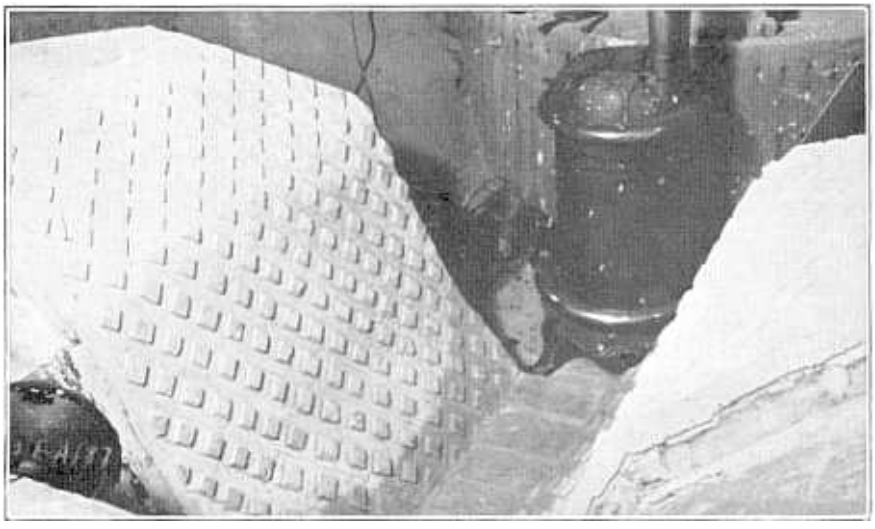

FIGURE 33—KEYWAYS BETWEEN LAYERS OF SUPPLEMENTAL BASE

the moisture content. The drying was carefully controlled, since exposure of plaster to excessive heat causes dehydration. When the moisture content was less than 4 per cent by weight, the test holes were plugged and the surface of each layer painted with two coats of orange shellac and one coat of waterproof ship varnish. The next layer was then cast. To insure a good bond between adjacent layers, it was customary to cut a series of keyways, intersecting perpendicularly across the face of each layer, before the succeeding layer was cast, as shown in figure 33.

47. Form for Casting Canyon Walls.—Since it was desired to duplicate the topography of the canyon as closely as possible, the

final layer of the base required a special form. A topographical map of the canyon was made on wallboard to a scale of 1 to 240. Each contour was traced and transferred to another sheet of wallboard. These contours were then sawed out with a scroll saw and nailed to blocks of wood having the scale height of the contour interval, so that the air space of the canyon was duplicated to scale. The form was next covered with a one-inch diamond-mesh wire netting and plastered over smoothly. After the form was thoroughly dry, it

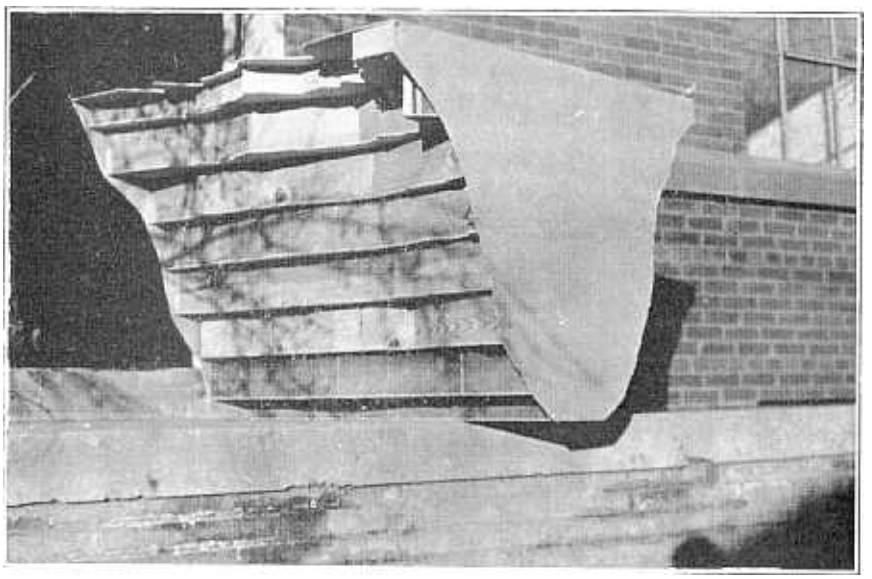

FIGURE 34—FORM FOR CASTING CANYON WALLS
View Taken Before Covering with Wire Netting and Plaster

was sanded smooth, painted with shellac, and carefully greased with cup grease. The form was then lowered into place and the final layer of the canyon poured. Figure 34 shows the form under construction, and figure 35 shows it being lowered into place.

FORMS FOR MODEL

48. Necessity for Wooden Forms.—Since it was not possible to develop the surfaces of the model of Boulder Dam from flat plates, steel forms could not be used. The curved portions of both forms were made of sugar pine which was carefully shaped to exact dimensions.

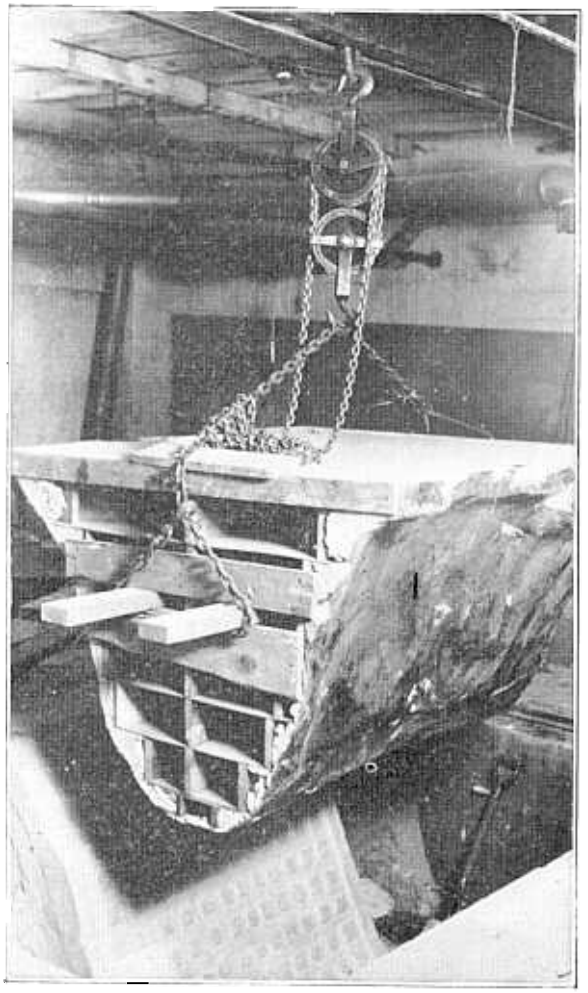

FIGURE 35—LOWERING FORM FOR CANYON WALLS

View Taken Prior to Pouring Final Layer of Supplemental Base

The upstream form served for casting the model and, later, for supporting the mercury loading bag against the upstream face. This was the same general arrangement for applying load as was used in the previous models, mercury being forced into the rubber bag between the upstream face of the model and the upstream form. It was imperative that the upstream form be sufficiently rigid to take the reaction of the mercury load. As the wooden form was not strong enough

to support this pressure, it was reinforced with a flat steel plate, one-quarter of an inch thick, attached with screws to the back of the form. It was necessary to trim off a few irregulartities of the canyon topography upstream from the model to allow the upstream form to be set properly.

The downstream form was made in sections, 2½ inches thick, which were held together with bolts. The bolts were arranged so that the form could be assembled one piece at a time in order to allow space for pouring and drying the model. The upstream form was assembled complete in one piece. Both forms were set in position and lines of contact with the canyon walls marked on the walls. The contact zone was then excavated according to the plans for the construction of Boulder Dam. Figure 36 shows the downstream form in place before excavating the model abutments.

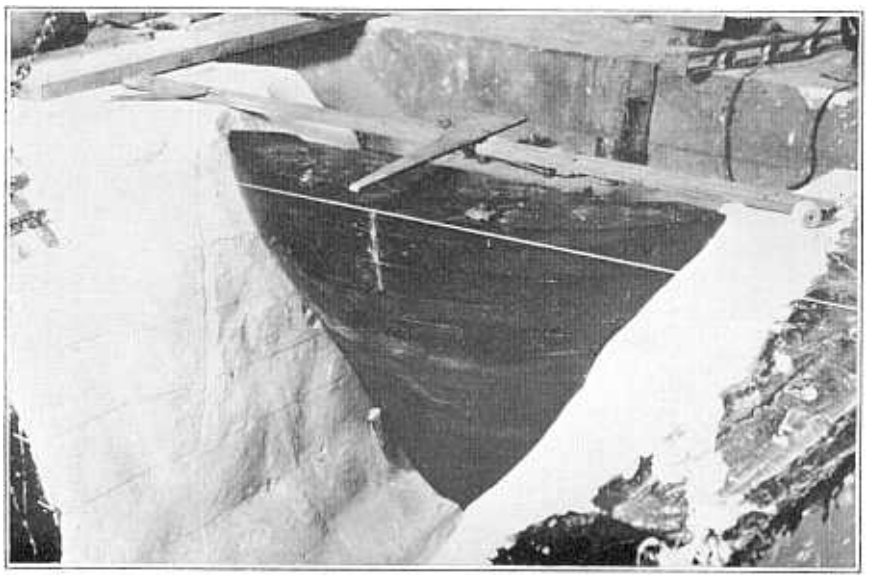

FIGURE 36—DOWNSTREAM FORM IN PLACE BEFORE EXCAVATING ABUTMENTS

49. Anchors for Deflection Rods.—Anchors to which invar steel rods could be fastened for measuring radial deflections of the model were attached to the downstream form with small tacks. The arrangement of the anchors is shown in figure 37. In stripping the forms from the model, the tacks pulled out of the wood readily, leaving the anchors firmly embedded in the plaster.

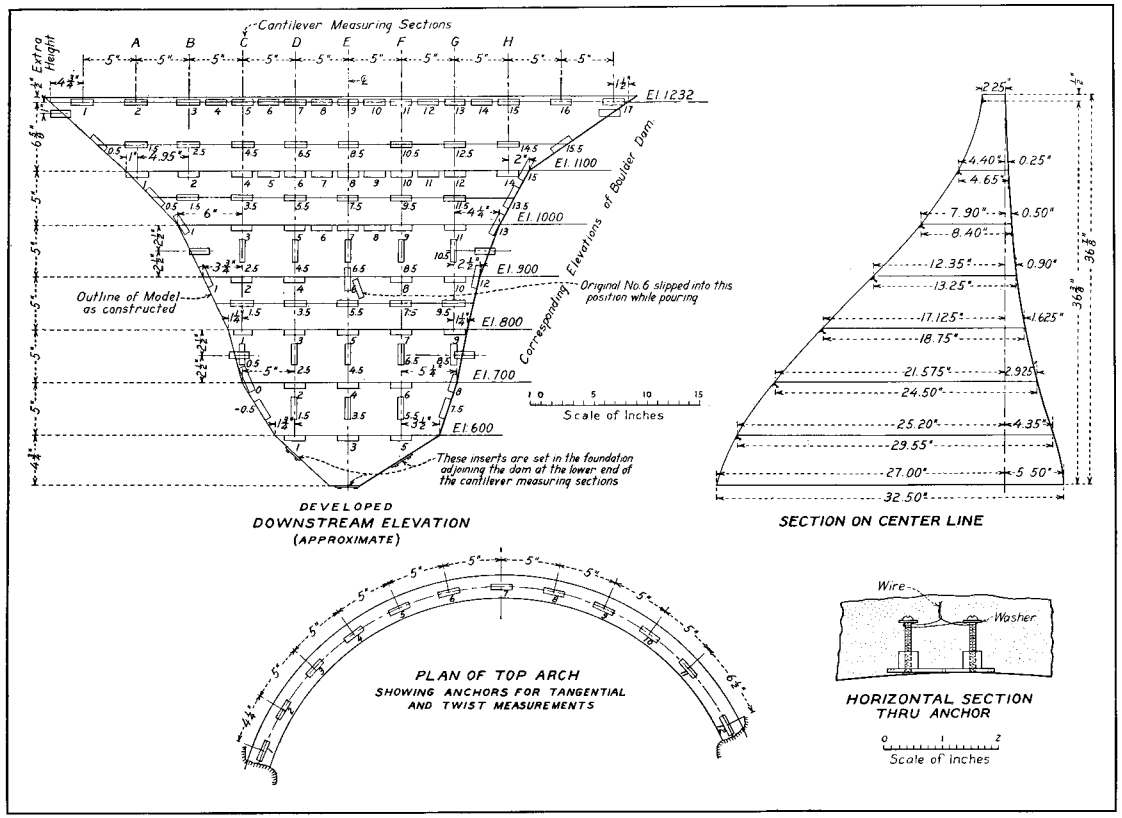

FIGURE 37—LOCATIONS OF ANCHORS FOR DEFLECTION MEASUREMENTS

CASTING THE MODEL

50. General Procedure.—The procedure followed in casting the model was the same as in casting the supplemental base. The thickness of the layers, however, was reduced to 2½ inches, since such layers could be easily dried in seven to ten days. The entire upstream form and a few of the lower sections of the downstream form were fastened in place with quick-setting plaster, and the bottom of the canyon painted with shellac and varnish. The canyon with the forms in place, prior to pouring the first layer of the model, is shown in

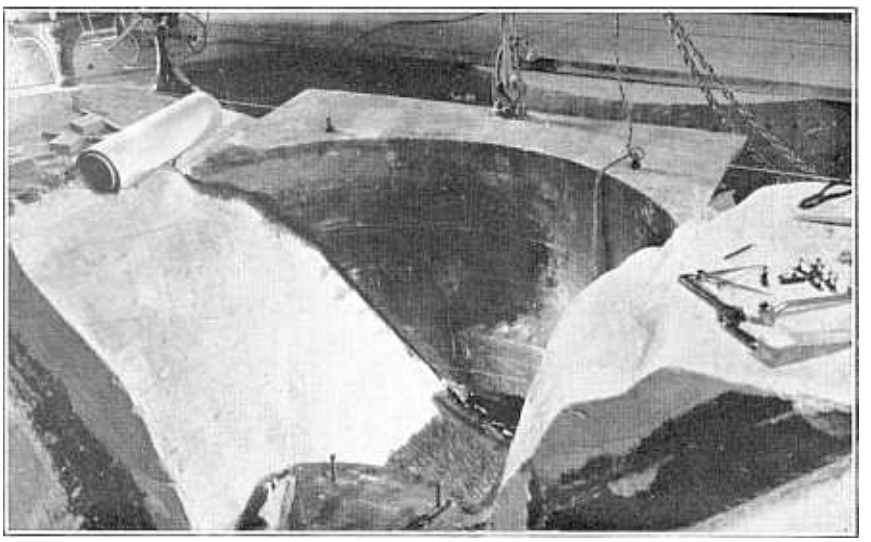

FIGURE 38—FORMS IN PLACE PRIOR TO POURING FIRST LAYER OF MODEL

figure 38. A portion of the roughened abutments and the upstream cut-off wall can be seen between the forms.

As soon as each layer had set, grooves were cut in the top of the layer, one-half inch deep and one inch wide, to increase the bond between layers. The model poured to elevation 950 is shown in figure 39. The bonding grooves can be seen in the top of the last layer cast.

51. Installation of Thermocouples.—A temperature test was included in the proposed testing program; therefore, thermocouples were embedded in the interior of the model for measuring tempera-

tures. The thermocouples were m le of two pie wire, one of copper, the other constantan, each about six fee The ends were soldered together and one conr ction was eml iodel at the point where the measurement of temperatur The wires were pl
wires from th

52. Completion of the Model.—When the iode was poured to elevation 1050, the section was sufficiently thin y readily from both faces after the forms were stripped. The remainder of the model

FIGURE 39—MODEL POURED TO ELEVATION 950

was poured in two parts to prevent undue segregation of materials The first part was cast and allowed to set for about an hour. The usual grooves were then cut in the upper surface, the surface shellacked, and the second part poured. Four days after the top of the model was cast, the forms were stripped and drying was begun on both faces. Three deflection-rod anchors were accidentally loosened while removing the forms. These were grouted in place
setting plaster, so that they could be used during the test program.

The plaster-celite mixture used in making the model swelled ghtly in setting. Although this was expected t was not feasible allow for the expansion in setting the forms. he result was that

the model was slightly thicker than originally intended. Dimensions of the model as constructed are shown in figure 40. The model was so near the design dimensions that it was not considered necessary to dress down the excess portions with sandpaper. The model was built one-half an inch higher than shown in the plans to protect the top row of anchors. This increase in height did not add enough material to affect the stiffness of the model appreciably.

From the time the first layer of the plaster base was poured, five months and ten days were required to complete the casting of the model. Altogether, 21 layers were cast, taking an average of about 9 days to dry each layer. The drying periods for the base layers were slightly longer than for the dam layers.

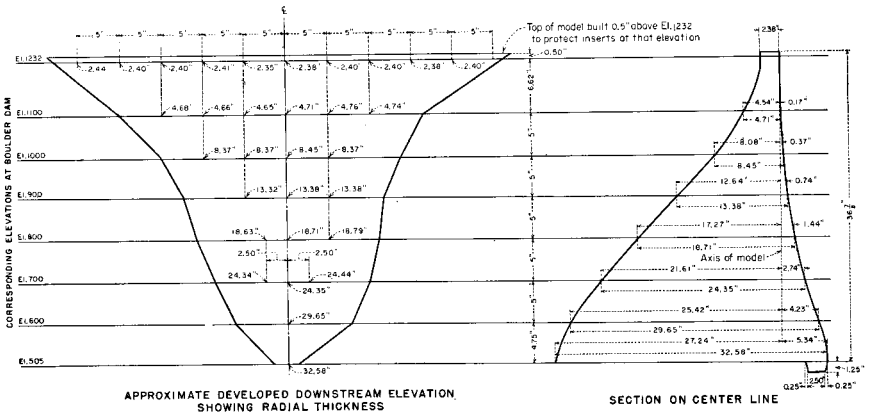

FIGURE 40—DIMENSIONS OF MODEL AS CONSTRUCTED

PROPERTIES OF MODEL MATERIAL

53. Concrete Base.—The concrete abutments on which the plaster-celite supplemental base rested were made of 1:2½:4 proportions by volume. No record was kept of the water-cement ratio, as a concrete of high strength was unnecessary, the maximum stress due to load being about 30 pounds per square inch. The average slump was 6 inches. Considerable care was taken to obtain a concrete of uniform density which would be free from rock pockets. Several 6 by 12-inch test cylinders were made from the new concrete. The 28-day strength of standard cured specimens averaged 3,450 pounds per square inch. Average values of the modulus of elasticity and

Poisson's ratio at the same age were 2,290,000 pounds per square inch and 0.14, respectively.

54. Special Testing Apparatus.—The preliminary investigations of contemplated model materials, including plaster-celite mixtures, comprised a large number of tests. In all the preliminary work standard apparatus for concrete testing was used. Since the plaster-celite material, when dry, had about one-twentieth the ultimate strength and modulus of elasticity of concrete, some difficulty was encountered in conducting tests with apparatus designed for concrete specimens. The weight of the apparatus and the sluggish action of the hand-operated testing machine of 20,000 pounds capacity often caused erratic results.

It was desired to make a complete record of the physical properties of the plaster-celite material used in the model. In view of the difficulties encountered in testing plaster specimens with the equipment used in testing concrete specimens, it was decided to design special machines for applying load to the specimens, and to develop strain meters which would be sufficiently sensitive to record deformations caused by small increments of load.

55. Compressometers.—The compressometers used by the Materials Testing Laboratory at the University of Colorado were similar to those developed in the Lewis Institute, Chicago. The design of the apparatus was modified to make it suitable for testing plaster-celite specimens. Compressometers shown in figures 41 and 42 were made from the new designs. The parts of the new instruments were made of aluminum whenever possible, the size of the members being kept to a minimum. The apparatus is essentially the same as that previously described.[8] The essential features of the redesigned compressometers are:

1. The bottom yoke is attached to the cylinder by three set screws which bear against small blocks. This insures proper stability and prevents the points of the set screws from damaging the specimen.

2. The upper yoke is attached to the cylinder by two set screws which bear against small blocks with the same advantage as above.

---

[8]Walker, Stanton, "The Modulus of Elasticity of Concrete." Proc. Am. Soc. Test. Mats., Vol. 19, 1919, Part II, p. 520.

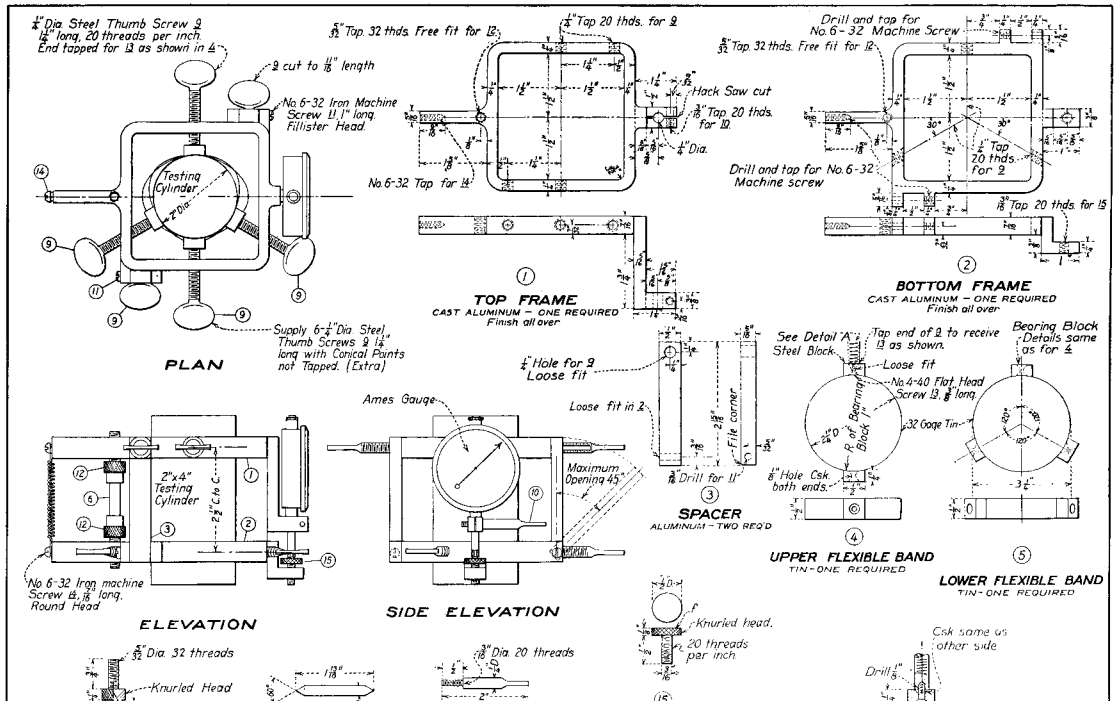

FIGURE 41—COMPRESSOMETER FOR 2 BY 4-INCH CYLINDERS

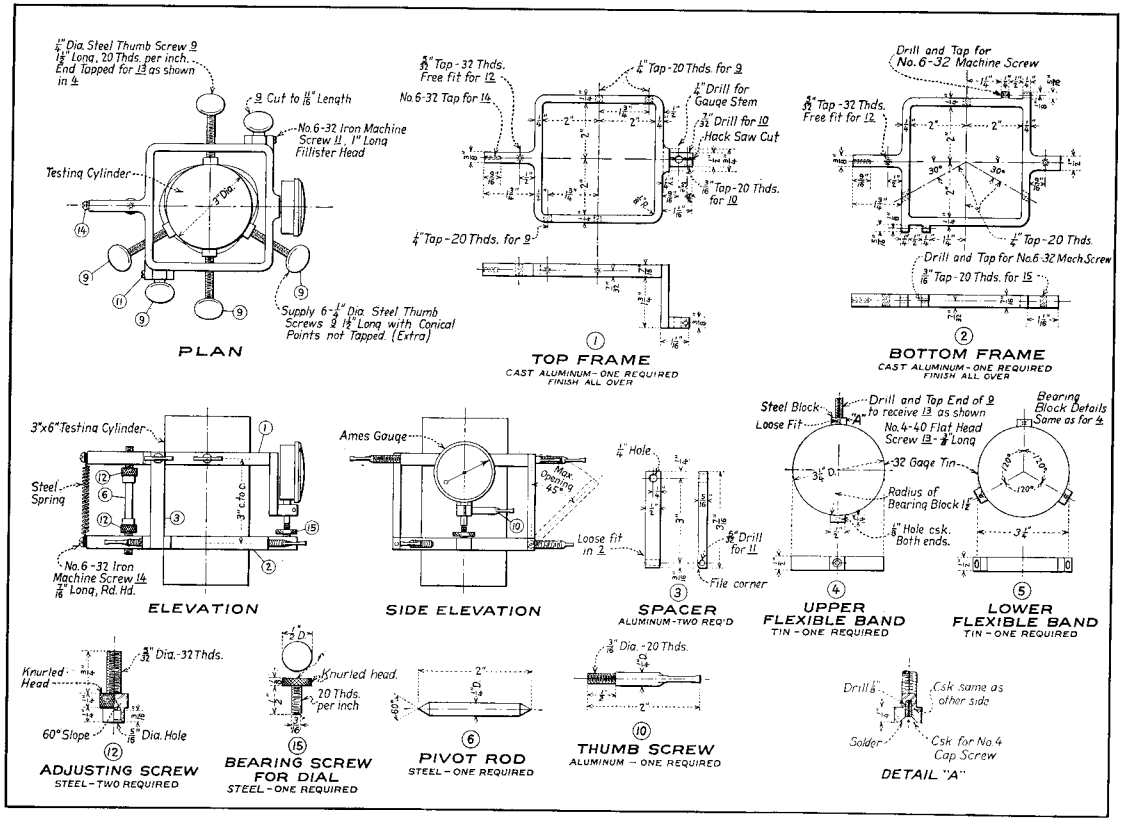

FIGURE 42—COMPRESSOMETER FOR 3 BY 6-INCH CYLINDERS

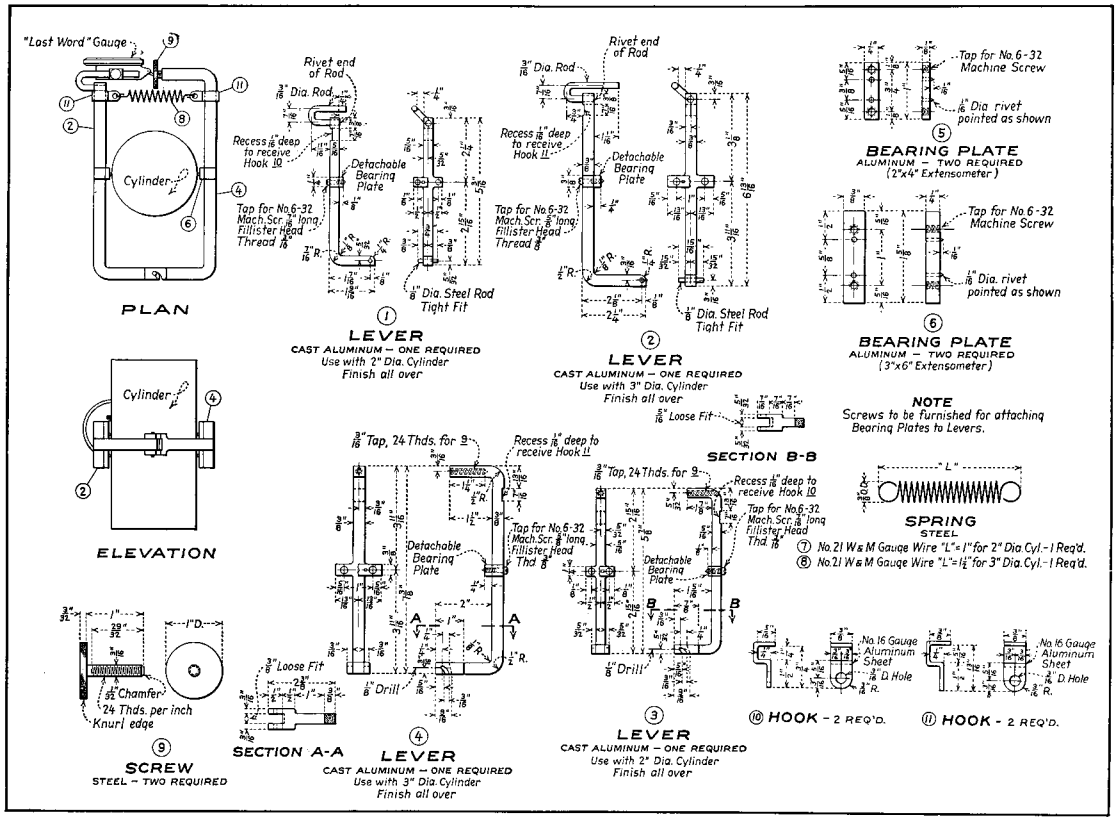

FIGURE 43—LATERAL EXTENSOMETERS FOR 2 BY 4-INCH AND 3 BY 6-INCH CYLINDERS

3. To aid in centering the specimen and to aline the bearing blocks, a flexible tin band is soldered to the faces of the bearing blocks.

4. The deformation is measured with a dial gage reading to 0.0001 of an inch.

5. The average deformation of the cylinder is measured on a single gage.

6. The gage is easily removable from the apparatus.

7. The deformation is transmitted to the gage by a knurled-head steel screw, which allows adjustment of the gage reading when attaching the compressometer.

56. Lateral Extensometers.—The extensometers used in measuring the lateral deformations are shown in figure 43. They were modified from the type developed by Professor H. J. Gilkey and Doctor Fredrik Vogt.[9] The essential features of these instruments are:

1. The extensometer consists of two aluminum legs, hinged at the rear and held together with a spring at the front.

2. The legs bear against the specimen through small aluminum blocks in which two small needle points are fastened. The tension of the spring and the four needle points keep the apparatus properly alined.

3. The deformation is measured with a light-weight dial gage reading to 0.0001 of an inch.

4. Final adjustment of the gage can be made with the knurled-head steel screw which the gage bears against.

In using the lateral extensometers, two objectionable features were experienced. The first was the uncertainty as to the exact location of the point of revolution of the hinge of the two legs. This caused relatively small errors, however, as they amounted to only about one per cent in the 2 by 4-inch extensometer, and less in the 3 by 6-inch extensometer. The second was that the dial gage registered negative movements which caused occasional erratic lateral deformations due to slack or improper bearing of the instrument.

57. Testing Machines.—The direct-load apparatus developed for use in testing the plaster-celite material is shown in figure 44. The

[9]Proc. Am. Soc. Test. Mats., Vol. 30, 1930, Part I, p. 632.

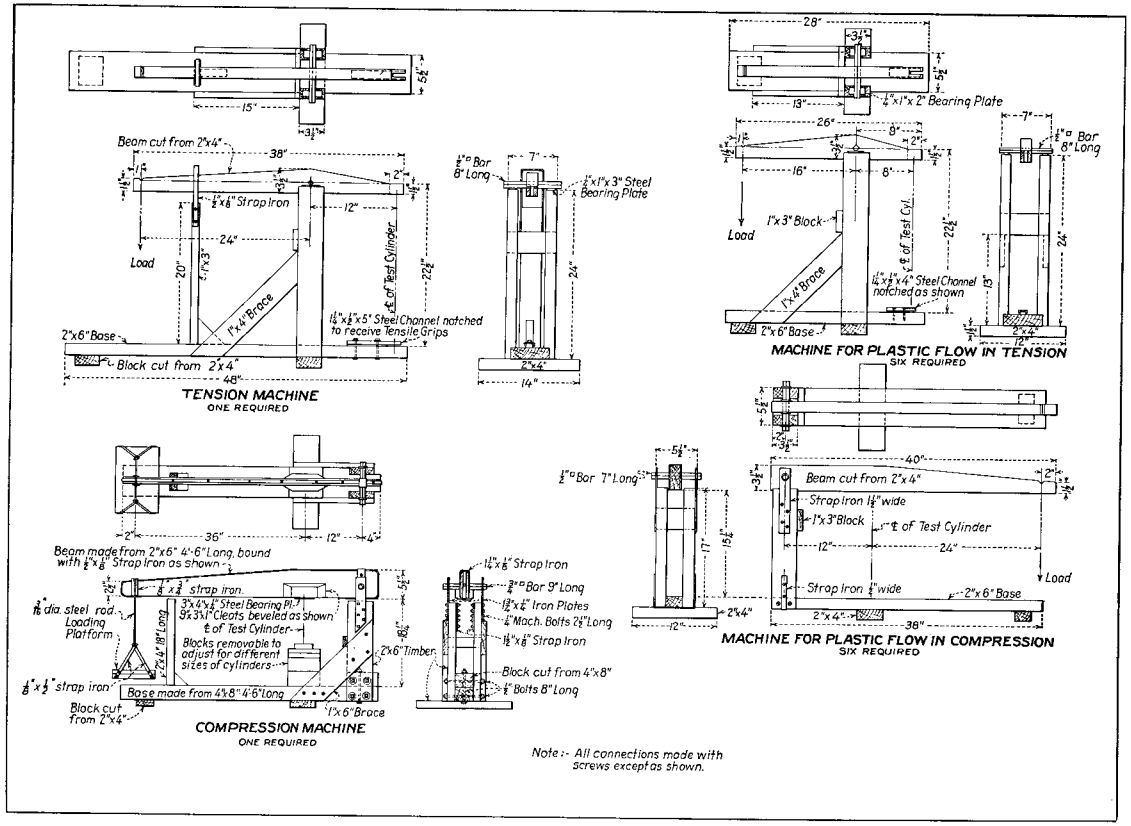

FIGURE 44—DIRECT-LOAD APPARATUS USED IN MATERIALS TESTS

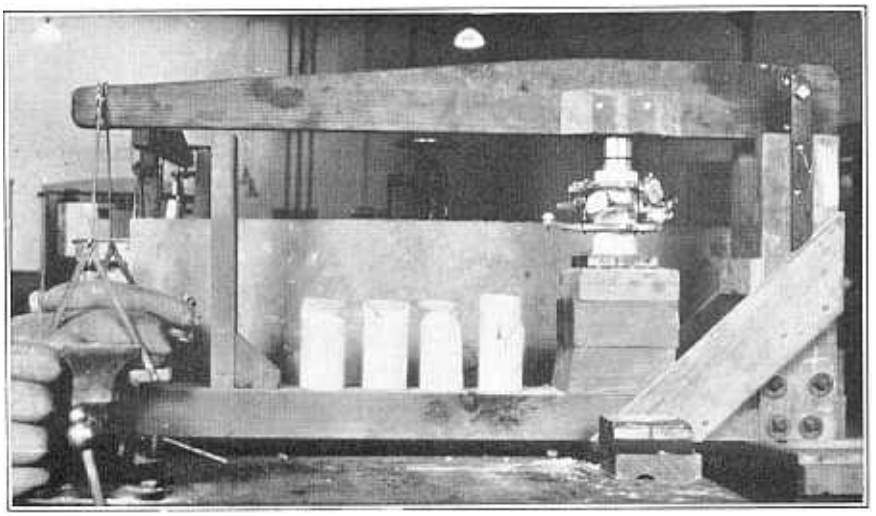

FIGURE 45—COMPRESSION MACHINE TESTING A 3 BY 6-INCH CYLINDER

Note the Characteristic Cone-shaped Failure of the Broken Cylinders

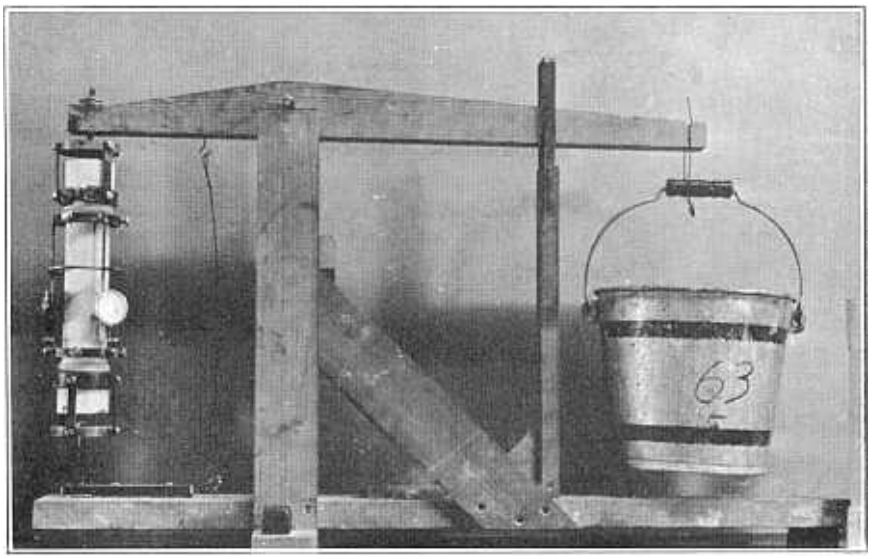

FIGURE 46- TENSION TESTING MACHINE IN OPERATION

compression-testing machine, shown in figure 45, and the tension-testing machine, shown in figure 46, were built for making routine tests of specimens. These machines were designed for testing 2½ by 12-inch cylinders in tension and 2 by 4-inch, 3 by 6-inch, 3 by 12 inch, or 6 by 12-inch cylinders in compression. The design of the machines was based on the principle of the lever and fulcrum. In the tension tests, the load was applied to the specimen by placing bags of lead shot in a bucket suspended on the end of the tension machine. In the compression tests, the load was applied by placing small bags of lead shot on the platform suspended from the end of the lever. Test loads were applied to specimens through spherical blocks, bearing against a greased steel plate. This prevented the rotation of the lever, caused by strain in the specimen, from producing bending or shear in the specimen.

Six smaller machines of each type shown in figure 44 were built for making plastic flow tests under sustained loads. The compressive-flow testing machine is shown in figure 47. As the loads applied in

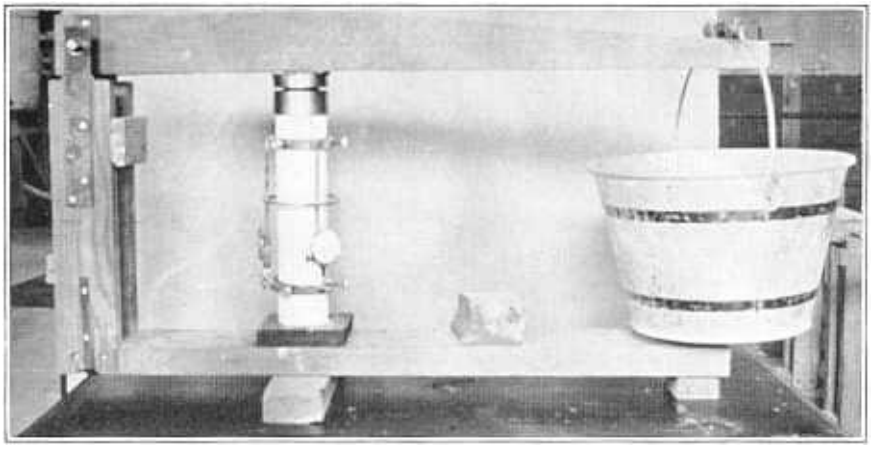

FIGURE 47—COMPRESSIVE-FLOW TESTING MACHINE

the flow tests were much smaller than the maximum for which the tension and compression machines were designed, the machines for making the flow tests were of much lighter construction. These machines were designed for testing 2½ by 12-inch specimens in tension and 3 by 12-inch cylinders in compression.

58. Grips and Strain Meters.—Tensile tests of 3 by 12-inch concrete cylinders had been made in the Materials Testing Laboratory of the University of Colorado for some time prior to the Boulder model tests. The apparatus consisted of a pair of grips and a strain meter on which three dial gages, measuring to 0.0001 of an inch, were mounted. Since this apparatus was too heavy for making satisfactory tests of plaster specimens, the grips and strain meter shown in figure 48 were developed. The essential features of the redesigned grips are:

1. The rubber liner in the tension collar prevents the grip from bearing directly on the specimen and damaging it.
2. The grips are self-alining so that no bending can occur in the specimen.

The tension collar was attached to a circular steel plate with three loosely connected steel straps 120 degrees apart. The test load was applied to the circular steel plates through bolts with spherical heads. These features permitted the grips to automatically aline themselves with the load, producing uniform stress in the specimen.

The strain meter for tensile tests consisted of two steel collars attached to the specimen with knurled-head screws. In order to prevent damage to the plaster, a flexible brass band encircled the specimen for the points of the screws to bear against. Fastened to one collar were three invar steel rods, 120 degrees apart, on which dial gages were mounted. On the other collar were three flat-head screws which were used in adjusting dial-gage settings when mounting the strain meter on the specimen. This type of strain meter was used in measuring longitudinal deformations in all tension tests and in the compressive flow tests.

It was originally planned to use 3 by 12-inch cylinders in testing the material in tension. The available forms for casting the 3 by 12-inch cylinders were not exactly circular. Consequently, specimens cast in these forms were placed in a lathe and turned to a diameter of 2½ inches for a distance of 9½ inches in the center portion. The ends were left approximately three inches in diameter but were turned to a true circle.

59. Apparatus for Torsion Tests.—In making auxiliary tests of the materials used in the Stevenson Creek and Gibson models, a torsion machine for testing 3 by 12-inch concrete cylinders was devised.[10] This

[10]"Arch Dam Investigation, Report by Committee," Vol. II, Engineering Foundation, May, 1934, pp. 454 and 455.

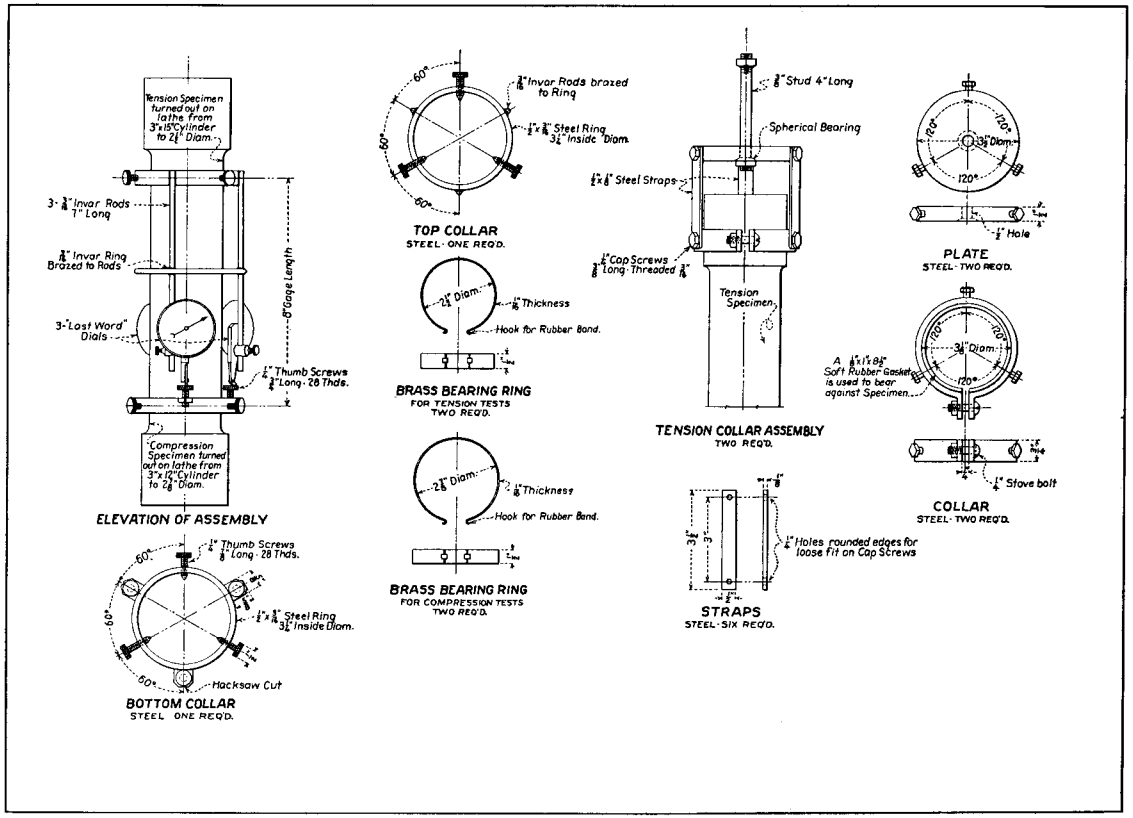

FIGURE 48—TENSION GRIPS AND 8-INCH STRAIN METER

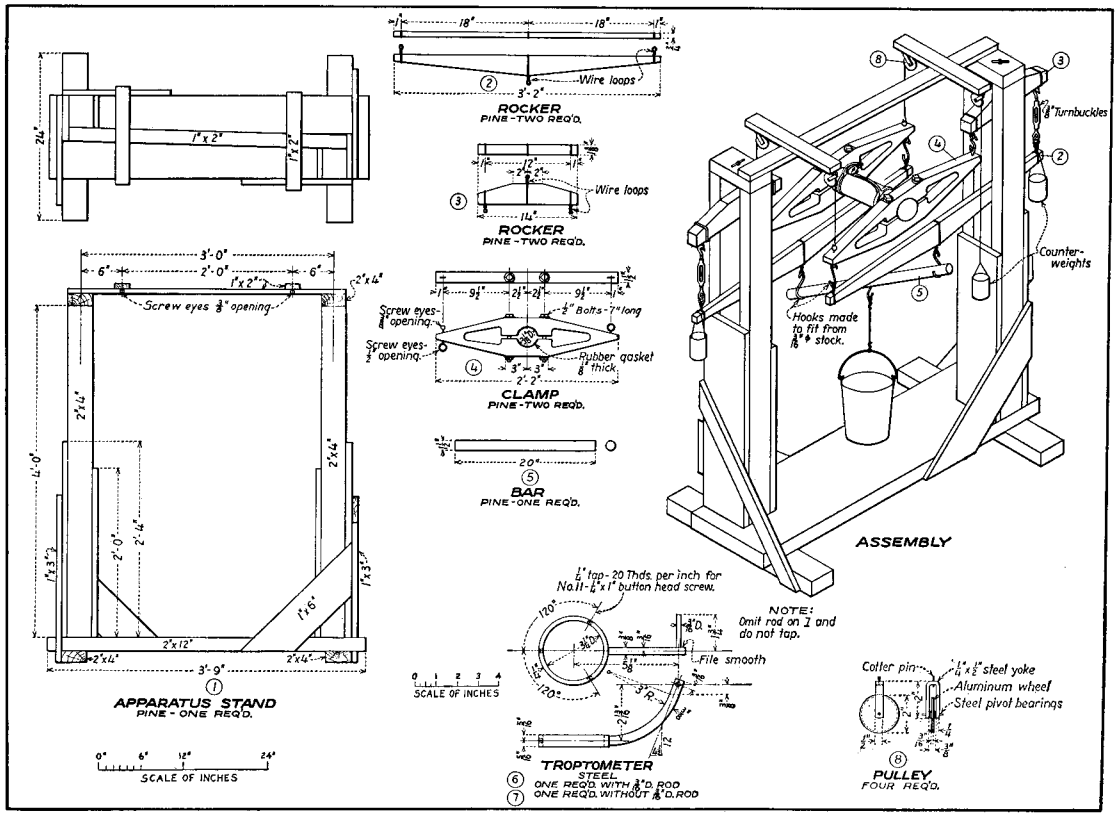

FIGURE 49—DESIGN OF TORSION MACHINE

machine operated satisfactorily when testing concrete cylinders, but was too heavy for testing plaster-celite specimens. The apparatus was redesigned, using lighter members and counterweights, and arranged for direct loading. Figures 49 and 50 illustrate the design and operation of the torsion machine. Although the machine was of rather crude appearance, its operation was satisfactory and the results of the torsion tests were consistent. The essential feature of the machine was the system of rockers and clamps which supported the specimen. By applying a load in the bucket a torque was exerted on the specimen.

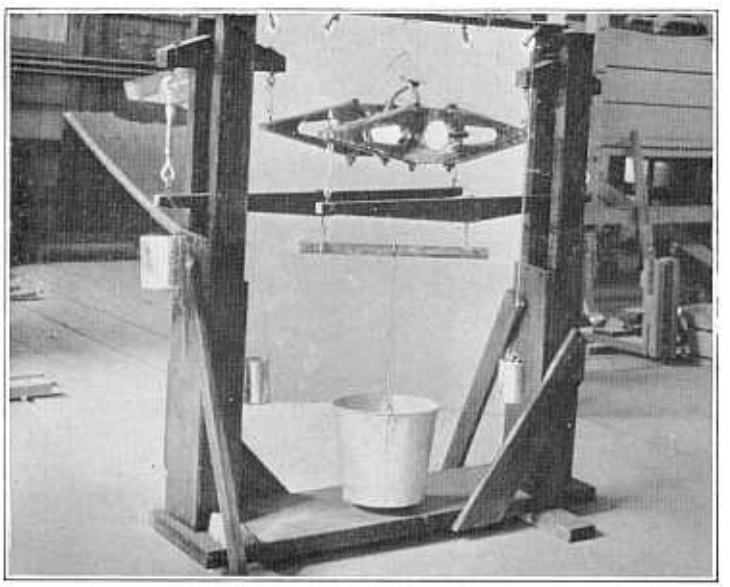

FIGURE 50—TORSION TESTING MACHINE IN OPERATION

The deformation was measured by the troptometer on which a dial gage, reading to 0.0001 of an inch, was mounted. The troptometer was fastened to the specimen by screws, bearing against flexible brass bands placed around the specimen.

60. Apparatus for Flexural Tests.—Flexural tests were made on 3 by 3 by 40-inch beams, simply supported over a span of 38 inches. A concentrated load was applied at the center and the deflection measured with the apparatus shown in figure 51. The modulus of elasticity was computed from the deflection at the center of the span. Flexural tests of beams under sustained loads are shown in figure 52.

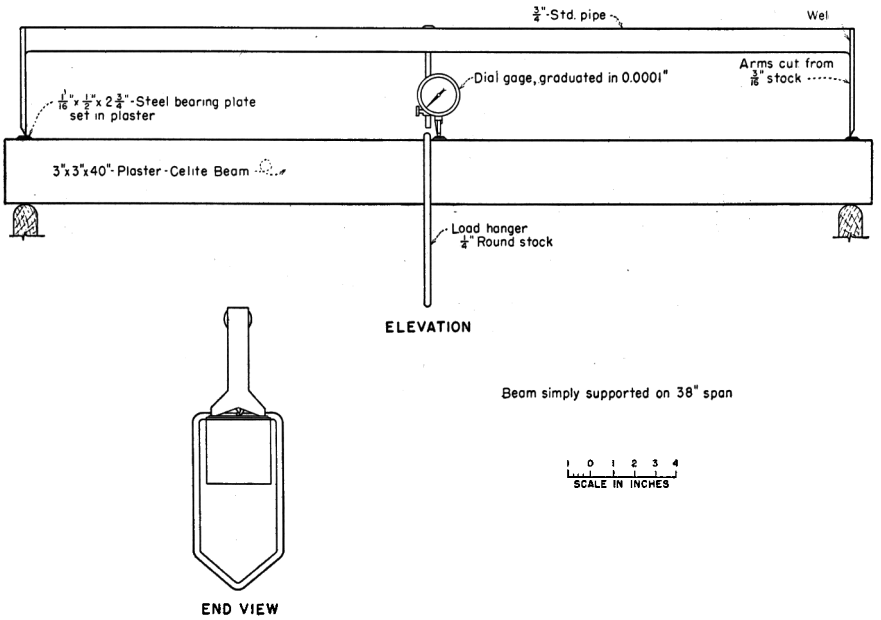

FIGURE 51—APPARATUS FOR BEAM TESTS

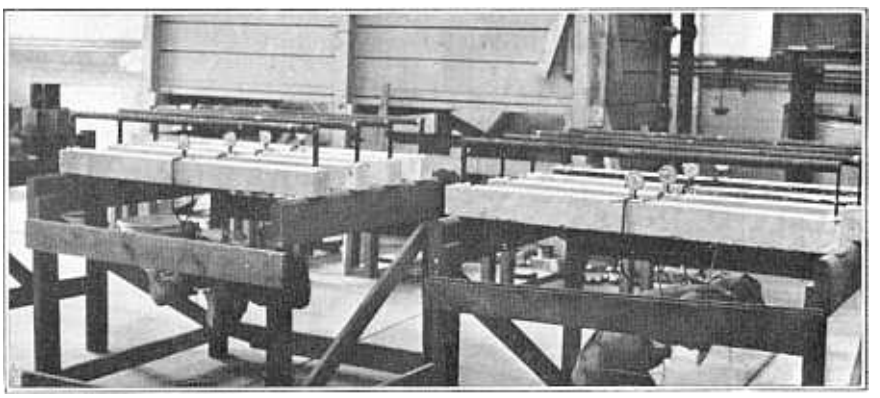

FIGURE 52—FLEXURAL FLOW TESTS ON BEAMS

61. **Methods of Plotting.**—Figures 29 and 30, chapter II, illustrate the method used in plotting results of compression and flexure tests. Except for calibration factors and different means of applying load, the data from the compression and flexure tests on the model material were recorded and reduced in the same manner as in the pre-

liminary investigations. Similar methods of plotting results were followed in the torsion and tension tests, but the original curves usually passed through the origin, making it unnecessary to transpose the curve. In all cases, the slope of the tangent to the lower portion of the curve was used to calculate the modulus of elasticity.

62. Compression Tests.—A typical stress-strain curve for a 3 by 6-inch plaster-celite cylinder, showing the method of plotting results of compression tests, is given in figure 53. In using the direct-load

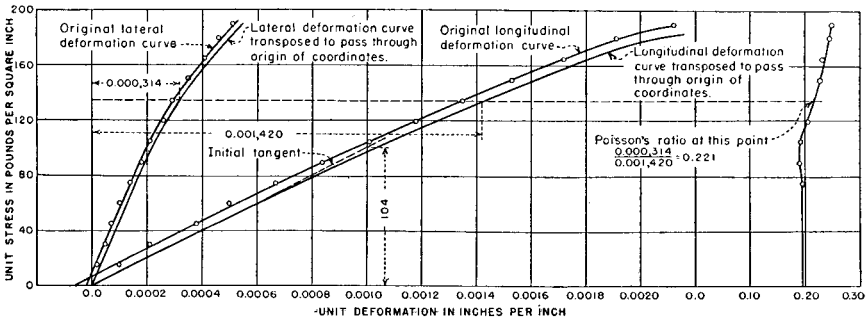

Curves shown above are for 3" x 6" cylinder No. 90 - 5.
Deformation curves, when plotted, rarely pass through the origin of coordinates. They are therefore transposed horizontally until they intersect the origin.
The modulus of elasticity is the tangent modulus for the lower stresses where the deformation curves are straight.
In this example,

$$\text{Modulus} = \frac{\text{STRESS}}{\text{STRAIN}} = \frac{104}{0.0010} = \begin{cases} 104{,}000 \text{ pounds} \\ \text{per square inch.} \end{cases}$$

Longitudinal gage factor = 0.000,017,3
Lateral gage factor = 0.000,016,3

UNIT LOAD	OBSERVED DATA		REDUCED DATA		
	LAT. DEF. 0.0001"	LONG. DEF. 0.0001"	UNIT LAT. DEF.	UNIT LONG. DEF.	POISSON'S RATIO
0	0.0	0.0	0.00000	0.00000	
15	1.4	5.5	0.00002	0.00010	0.198
30	3.0	12.0	0.00005	0.00021	0.198
45	4.5	22.0	0.00007	0.00038	0.198
60	6.3	29.0	0.00010	0.00050	0.198
75	8.5	38.5	0.00014	0.00067	0.198
90	11.0	48.5	0.00018	0.00084	0.191
105	13.1	58.5	0.00021	0.00101	0.193
120	16.0	68.5	0.00026	0.00118	0.204
135	18.2	78.0	0.00029	0.00135	0.212
150	21.3	88.5	0.00035	0.00153	0.228
165	25.0	99.5	0.00041	0.00172	0.233
180	28.2	110.5	0.00046	0.00191	0.244
190	31.0	123.0	0.00051	0.00212	0.249
190+	FAILED				

FIGURE 53—METHOD OF PLOTTING RESULTS OF COMPRESSION TESTS

testing machine, sacks of lead shot were prepared to give load increments of 15 pounds per square inch. These loads were recorded in the column, "Unit Load." Observed data were actual gage readings, and reduced data were obtained by multiplying observed readings by calibration factors. Calibration factors, for the 3 by 6-inch apparatus, were 0.000,017,3 for the longitudinal gage and 0.000,016,3 for the lateral gage. Calibration factors for the 2 by 4-inch apparatus were 0.000,018,8 and 0.000,023,8, respectively. The decimal points in the calibration factors were placed so that the factors were applicable to gage readings expressed in ten-thousandths of an inch, as recorded in the table in figure 53. Factors for lateral gages were calculated from the geo-

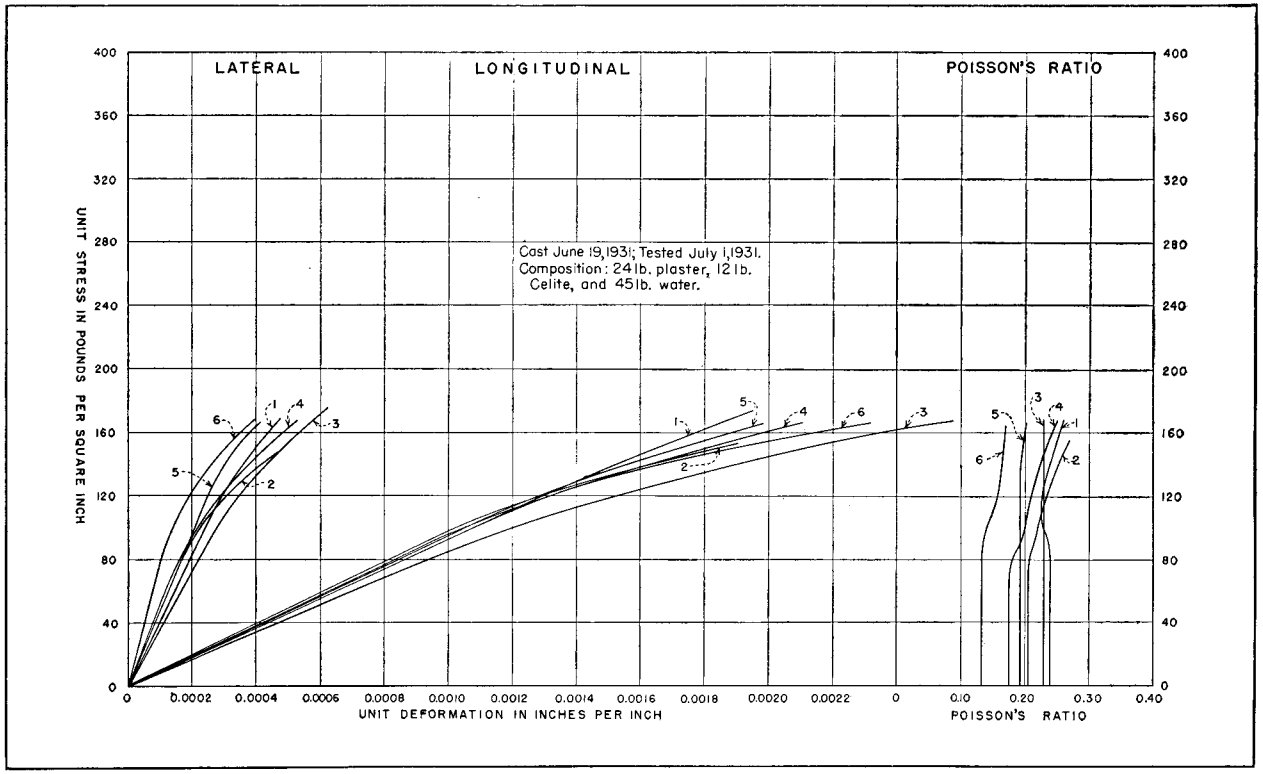

FIGURE 54—STRESS-STRAIN DIAGRAMS FOR COMPRESSION TESTS

metrical relation between the hinge, point of contact on the specimen, and point of bearing of the gage. The compressometers were calibrated by the universal calibrator used in the tests of the Stevenson Creek and Gibson models.[11]

The typical stress-strain curve in figure 53 shows that the new equipment gave consistent results. The plotted points follow the curves closely throughout the entire range of stress. More consistent results were obtained with the 3 by 6-inch equipment than with the 2 by 4-inch equipment, due to the longer gage lengths, larger gage readings, and larger areas. The larger quantities, together with the improved mechanical operation of the light-weight apparatus, reduced the proportion of errors considerably. Figure 54 shows typical results of compression tests of 3 by 6-inch cylinders.

63. Tension Tests.—Tension specimens were tested with two pounds per square inch stress increments, using the direct-load ma-

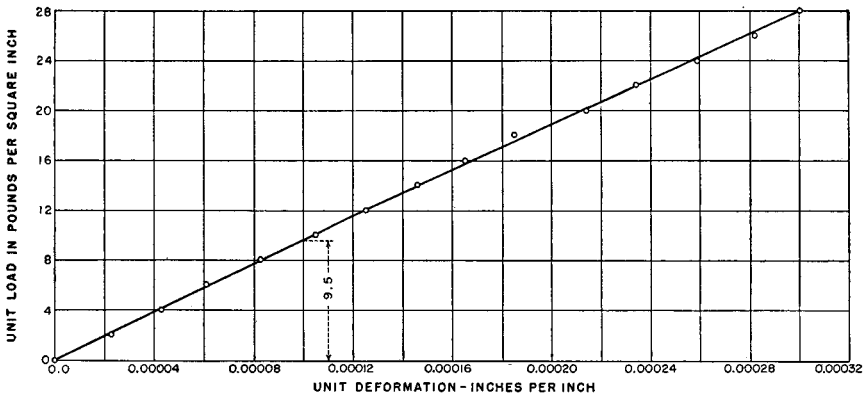

Curve shown above is for $2\frac{1}{2}$"x 12" cylinder No. 120-2.
The unit deformation is obtained by dividing the average observed deformation by the gage length of eight inches.
Unit deformation for unit load of 20 pounds per square inch equals $\frac{0.00171}{8} = \{0.000214$ inches per inch.
Modulus of elasticity, $E = \frac{\text{STRESS}}{\text{STRAIN}} = \frac{9.5}{0.00010} = \{95\,000$ pounds per square inch.

UNIT LOAD	OBSERVED DATA* DEFORMATION DIAL 1	DIAL 2	DIAL 3	REDUCED DATA AVERAGE* DEFORM.	UNIT DEF.-INCHES
0	0.0	0.0	0.0	0.0	0.000000
2	2.0	1.3	2.0	1.8	0.000023
4	4.2	2.2	3.8	3.4	0.000043
6	6.2	3.8	5.3	4.9	0.000061
8	8.5	4.2	7.0	6.6	0.000083
10	11.5	5.4	8.2	8.4	0.000105
12	13.8	6.3	10.0	10.0	0.000125
14	16.0	7.2	11.8	11.7	0.000146
16	18.2	8.2	13.2	13.2	0.000165
18	21.0	9.1	15.0	15.0	0.000185
20	23.8	10.5	17.0	17.1	0.000214
22	26.4	11.0	18.8	18.7	0.000234
24	29.3	12.0	20.7	20.7	0.000259
26	32.2	12.8	22.8	22.6	0.000282
28	35.7	13.5	24.8	24.7	0.000304

*Gage reading in ten-thousandths of an inch

FIGURE 55—METHOD OF PLOTTING RESULTS OF TENSION TESTS

[11]Loc. cit., pp. 470, 471.

chine shown on figure 46. The method of plotting stress-strain diagrams is shown on figure 55. With three dial gages mounted 120 degrees part, the average reading represented the total deformation, regardless of the distribution of the readings. The gage length of eight inches made the readings sufficiently large to insure accuracy. The tension graphs usually passed through the origin and were always straight lines since failure occurred at the yield point. The average ultimate strength in tension was 30 pounds per square inch. Figure 58-A shows typical results of tension tests. Numbers on the curves represent elevations of the model from which the material was cast, and specimen numbers. For example, 85-2 represents specimen 2, from material poured between elevations 800 and 850. The same designation was followed for all types of specimens.

64. Torsion Tests.—Torsion test specimens were cast 12 inches long by 3 inches in diameter. After drying, they were turned in a lathe to true circular cylinders of 2⅞-inch diameter. The procedure used in setting up the apparatus for a test was as follows:

1. The troptometer with dial gage was mounted on the specimen.

2. The ends of the specimens were inserted in the rubber-lined clamps and the assembly placed on a table or other flat surface. The clamps were then tightened and the dial adjusted to zero reading.

3. The clamp and specimen assembly was connected to the rocker arms of the testing machine.

4. Counterweights were used to eliminate initial torsion in the specimen, caused by dead weight. The amount of weight was adjusted to return the dial reading to zero.

5. Loads were then applied to the loading bar of the machine and dial readings recorded for all increments of load.

From the dimensions of the machine, it was determined that one pound of load on the loading bar produced 6 inch-pounds of torque on the specimen. With 5-pound load increments, a shearing stress of 6.43 pounds per square inch in the extreme fiber was produced for each load increment. Figure 56 shows the method of plotting results of torsion tests and the formulas used in calculating unit stresses and unit strains. The modulus of elasticity was calculated by dividing the unit stress by the unit strain. Typical stress-strain graphs for torsion are shown on figure 58-C.

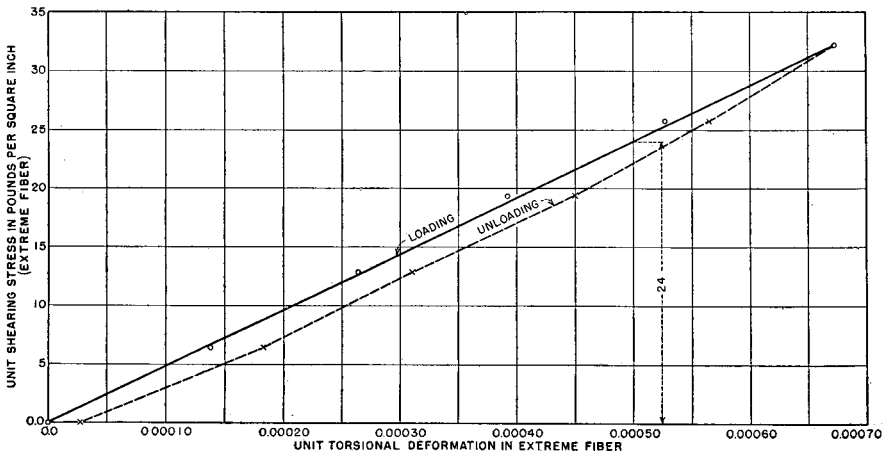

Curve shown above is for $2\frac{7}{8}$" x 12" cylinder No. 100-5.
The measured gage length of the troptometer was 5.84".
Distance from bearing point of "Last Word" dial to radius of cylinder was 3.90".
Each 5-pound load increment applied a torque of 30 inch-pounds on the specimen.
Shearing stress in extreme fiber for a 5-pound load increment,

$$S = \frac{Tc}{J} = \frac{30 \times 1.4375}{\left[\frac{3.14159 \times (1.4375)^4}{2}\right]} = \left\{\begin{array}{l}6.43 \text{ pounds per} \\ \text{square inch.}\end{array}\right.$$

Unit deformation for a 20-pound load,

$$\Delta s = \frac{r\theta}{l} = \frac{1.4375\left(\frac{0.01148}{1.4375 + 3.90}\right)}{5.84} = 0.000527.$$

Modulus of elasticity,

$$E = \frac{\text{STRESS}}{\text{STRAIN}} = \frac{24}{0.00050} = 48{,}000 \text{ pounds per square inch.}$$

UNIT LOAD	OBSERVED DATA	REDUCED DATA	
	DEFORM.	UNIT STRESS	UNIT DEFORM.
0	0.0	0.00	0.000000
5	30.0	6.43	0.000138
10	56.9	12.86	0.000264
15	85.2	19.29	0.000392
20	114.8	25.72	0.000527
25	146.2	32.15	0.000673
20	122.6	25.72	0.000564
15	98.0	19.29	0.000450
10	67.8	12.86	0.000311
5	39.8	6.43	0.000183
0	6.0	0.00	0.000028

FIGURE 56—METHOD OF PLOTTING RESULTS OF TORSION TESTS

65. Flexural Tests.—Flexural tests were made on 3 by 3 by 40-inch beams, simply supported on 38-inch spans. The load was applied at the center and the deflection of the dial gage observed at the center. Three readings were taken with the beam in one position, after which the beam was inverted and three additional readings taken. The mean of the six readings was used to calculate the modulus of elasticity in flexure.

The stress in the outside fiber was calculated by the usual formula, $S = \frac{Mc}{I}$. The modulus of elasticity was obtained from the formula for deflection of elastic beams at the center,

$$E = \frac{1}{48}\frac{PL^3}{Iy},$$

where y is the observed deflection at the center. In order that results of the flexural tests might be shown as stress-strain diagrams, unit

stresses and unit strains at extreme fibers were calculated in the following manner:

$$\frac{\text{Unit stress}}{\text{Unit strain}} = E = \frac{1}{48}\,\frac{P\,L^3}{I\,y}$$

$$\text{or unit strain} = \frac{48\,I\,y}{P\,L^3} \times \text{unit stress.}$$

For a simply supported beam with a concentrated load at the center, the unit stress,

$$S = \frac{M\,c}{I} = \frac{P\,L}{4} \times \frac{c}{I}.$$

Combining,

$$S = \frac{48\,I\,y}{P\,L^3} \times \frac{P\,L}{4} \times \frac{c}{I} = \frac{12\,c\,y}{L^2}.$$

The modulus of elasticity was obtained by dividing the unit stress by the unit strain. Figure 57 shows an example of calculations for modulus of elasticity. Figure 58-B shows a typical set of stress-strain graphs for flexural tests.

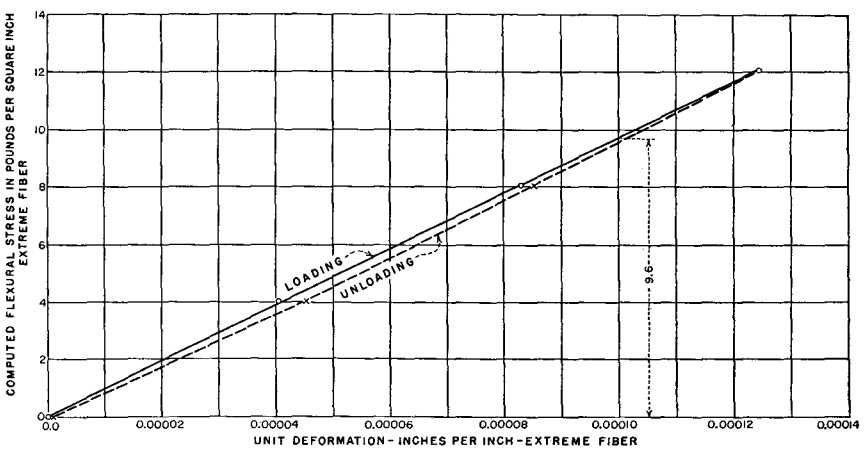

Curve shown above is for 3"x 3"x 40" beam No.120-3.
The beam was simply supported on a 38" span, concentrated load applied at center.
For a concentrated load of 2 pounds on beam, stress in extreme fiber,
$\frac{Mc}{I} = \frac{19 \times 1.53}{7.23} = 4.02$ (Exact depth = 3.06 in.)
Unit deformation of extreme fiber,
$\frac{12cy}{l^2} = \frac{12 \times 1.47 \times 0.003323}{38 \times 38} = 0.0000405$ in.
Modulus of elasticity,
$E = \frac{\text{STRESS}}{\text{STRAIN}} = \frac{9.6}{0.00010} =$ {96,000 pounds per square inch.

TOTAL LOAD ON BEAM	OBSERVED DATA* BEAM NORMAL 1	2	3	BEAM INVERTED 1	2	3	REDUCED DATA AVERAGE*	UNIT STRESS	UNIT DEFORM-INCHES
0	0.0	0.0	0.0	0.0	0.0	0.0	0.00	0.00	0.0000000
2	33.0	33.0	33.6	33.5	33.2	33.9	33.23	4.02	0.0000405
4	68.0	67.0	70.3	69.0	67.2	67.2	69.15	8.05	0.0000831
6	106.5	99.4	102.0	106.0	102.5	101.5	102.15	12.06	0.0001246
4	70.3	68.2	71.5	73.6	68.6	68.2	69.98	8.05	0.0000853
2	37.1	38.4	39.0	39.6	35.0	34.0	37.02	4.02	0.0000452
0	3.8	4.5	4.2	5.5	0.8	0.5	2.22	0.00	0.0000039

*Gage readings in ten-thousandths of an inch.

FIGURE 57—METHOD OF PLOTTING RESULTS OF FLEXURAL TESTS

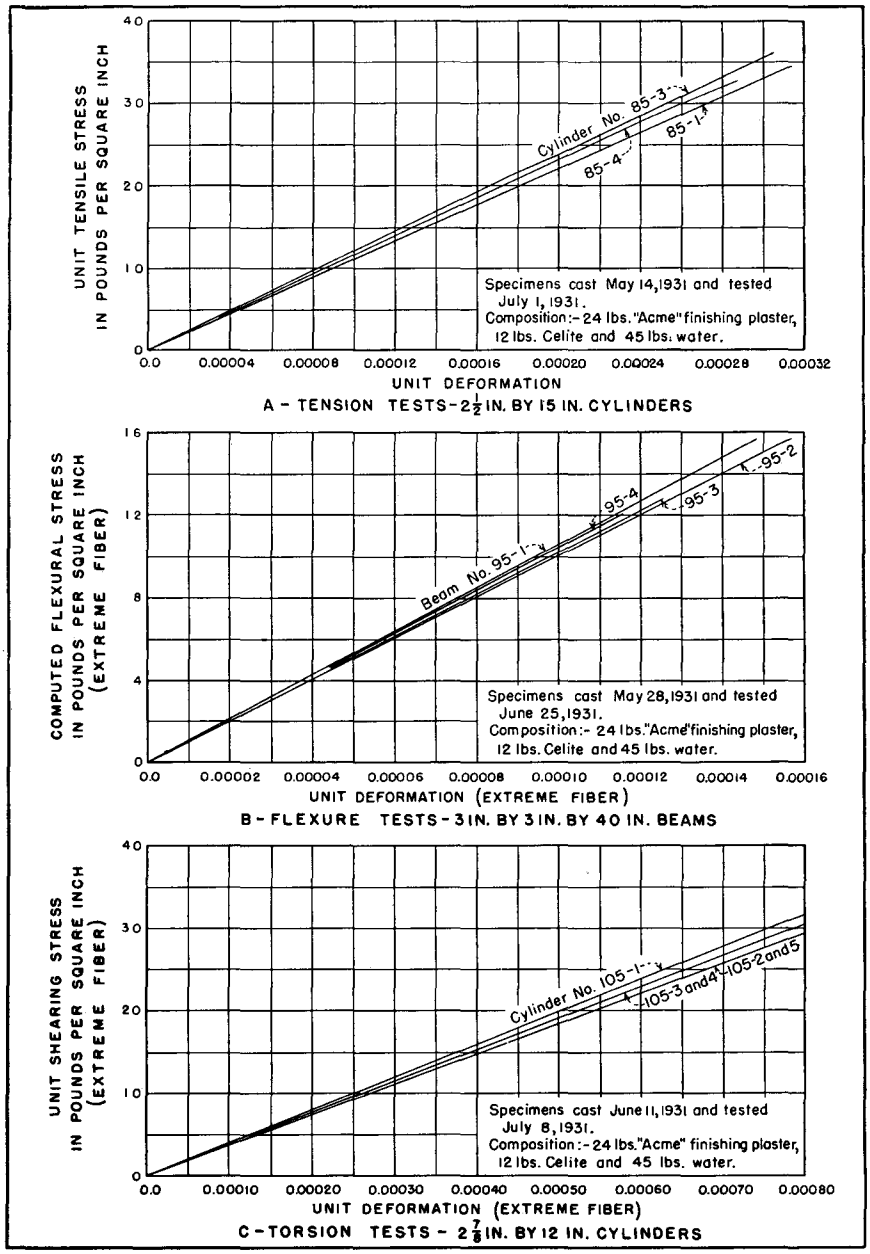

FIGURE 58—TYPICAL RESULTS OF TENSION, FLEXURE, AND TORSION TESTS

66. Plastic Flow Tests.—In the preliminary investigations of materials, some plastic flow tests were made on beams. Also, flow tests of concrete specimens under sustained tensile, compressive, and flexural loads had been made in connection with the auxiliary tests of materials used in models of the Stevenson Creek and Gibson dams, previously cited. With the new testing equipment, constructed for testing light-weight materials, plastic flow tests for plaster-celite specimens were undertaken.

The equipment for conducting plastic flow tests was the same as the equipment used in the tests for elastic properties, except that smaller direct load apparatus, shown in figure 44, was used for the compression and tension tests. Tension specimens were the same as those used in the elastic properties tests, but the compression specimens were cast 3 by 12 inches in size and turned in a lathe to true circular cylinders 2⅞ by 12 inches in size. The strain meter with 8-inch gage length, using three dial gages, was used on both tension and compression specimens, since the longer gage length recorded small changes due to flow more accurately than the compressometer used in the compression tests for elastic properties. No change was made in the equipment for flexural and torsion flow tests.

Flow tests on compression specimens were made with stresses of 20 and 40 pounds per square inch, tension and flexural tests with 20 pounds per square inch, and torsion tests with shear stresses of approximately 20 pounds per square inch. Variations in dimensions of beams caused small variations in unit stresses. Loads applied to the torsion specimens produced stresses slightly below 20 pounds per square inch. The 20-pound compressive flow tests gave rather erratic results due to the small amount of plastic flow. The general trend was evident, but satisfactory curves were not obtained.

Flow tests were conducted during periods of 20 to 24 days. The specimens were all exposed to fluctuations of temperature in the laboratory, and considerable variations in observed gage readings were expected. However, a sufficient number of observations were made on each specimen so that an average curve could be drawn. A large part of the plastic flow occurred within the first few hours of the test, during which temperature changes were small. The rate of flow was so slow at the end of 20 days that a longer period of testing was not considered necessary.

Figure 59 shows a typical plastic flow curve for compression, and figure 60 shows comparisons of test data for several specimens.

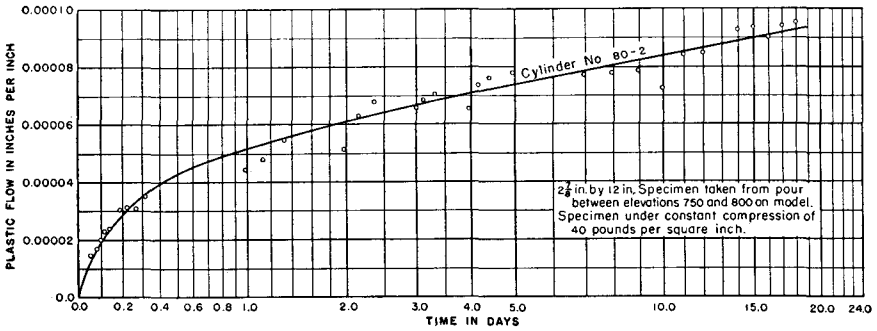

FIGURE 59—TYPICAL PLASTIC FLOW IN COMPRESSION

All curves were plotted on a logarithmic time scale and a linear scale for strain. The amount of plastic flow plotted on all curves indicates the increase in strain beyond the initial elastic strain. Specimen 75-1, figure 60, which showed the highest rate of flow of any test, probably was affected by an air pocket or improper casting. The principal

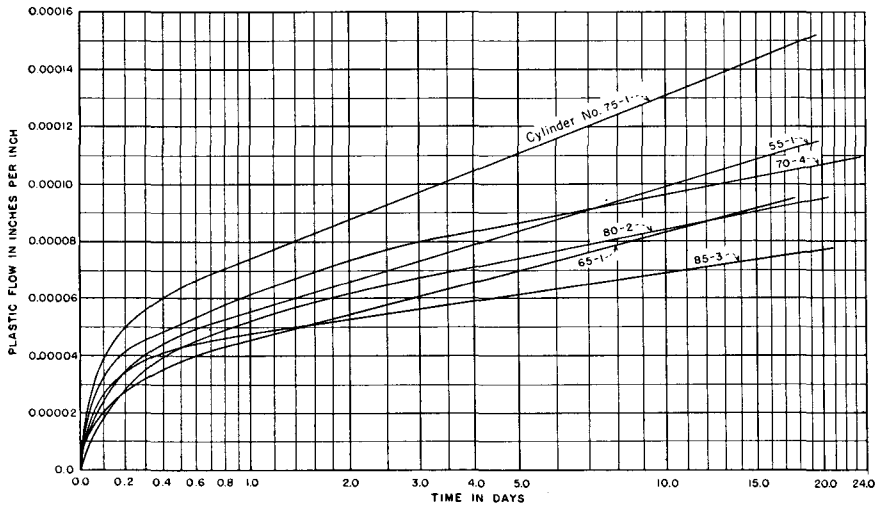

Cylinder specimens for compressive tests are 2⅞ in. by 12 in., finished size; 8-inch gage length. Specimens under constant compression of 40 pounds per square inch.

SPECIMEN NUMBER	FROM POUR BETWEEN ELEVATIONS		UNIT* STRESS
55-1	500 and	550	40
65-1	600	650	40
70-4	650	700	40
75-1	700	750	40
80-2	750	800	40
85-3	800	850	40

*Pounds per square inch.

FIGURE 60—COMPARISON OF PLASTIC FLOW DATA, COMPRESSION TESTS

characteristic of the compression tests was that approximately one-quarter of the 20-day flow occurred during the first hour, and about one-half during the first day. The average plastic flow in 20 days at 40 pounds per square inch stress was 0.000,10 inches per inch which was 25 per cent of the initial elastic deformation. The average 20-day

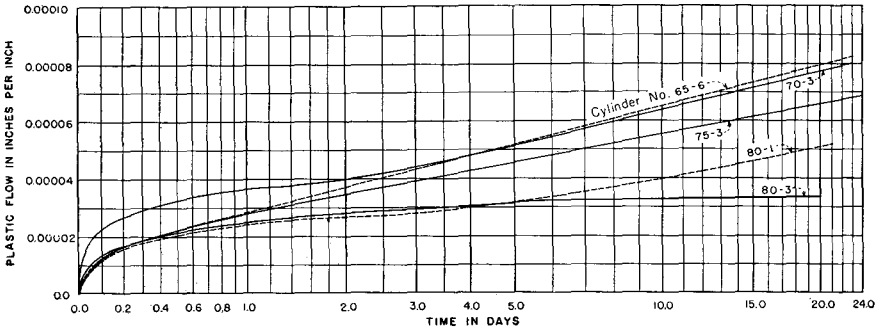

Cylinder specimens for tension tests are $2\frac{1}{2}$ in. by 12 in., finished size; 8-inch gage length.
Specimens under constant tension of 20 pounds per square inch.

SPECIMEN NUMBER	FROM POUR BETWEEN ELEVATIONS		UNIT * STRESS
65-6	600 and	650	20
70-3	650	700	20
75-3	700	750	20
80-1	750	800	20
80-3	750	800	20

*Pounds per square inch.

FIGURE 61—COMPARISON OF PLASTIC FLOW DATA, TENSION TESTS

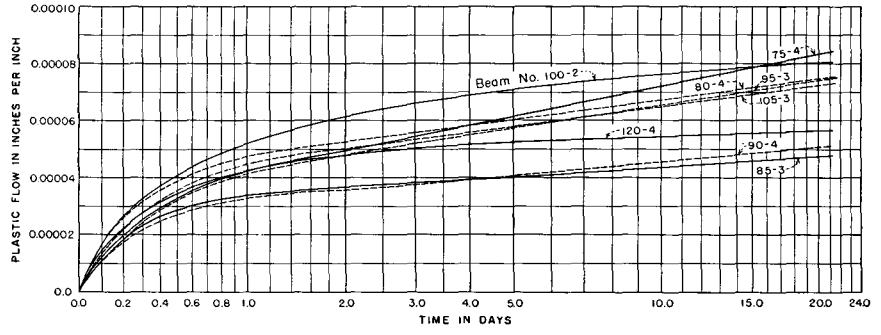

Beam specimens - 3 in. by 3 in. by 40 in., nominal size.
Each specimen under constant flexural stress as shown in table.

SPECIMEN NUMBER	FROM POUR BETWEEN ELEVATIONS		UNIT * STRESS
75-4	700 and	750	19.1
80-4	750	800	21.1
85-3	800	850	20.8
90-4	850	900	19.7
95-3	900	950	21.5
100-2	950	1000	21.1
105-3	1000	1050	21.1
120-4	1050	1242	19.4

*Pounds per square inch (Extreme fiber)

FIGURE 62—COMPARISON OF PLASTIC FLOW DATA, FLEXURAL TESTS

plastic flow for compression specimens loaded to 20 pounds per square inch was only 5 per cent of the initial elastic deformation.

Figure 61 shows comparisons of plastic flow data for specimens loaded to 20 pounds per square inch in tension. Rates of flow for tension were greater than for similar loads in compression, probably due to the fact that the applied stress was a greater proportion of the maximum strength in the case of the tension tests. However, the initial rate of flow was smaller in tension than in compression. Flow in flexural specimens, shown in figure 62, was approximately the average of the flow in tension and compression.

Figure 63 shows a typical plastic flow curve for torsion. In the test illustrated, approximately 70 per cent of the 20-day flow occurred during the first day. Upon removal of load the recovery was rapid for the first three days, then it slowed down until about 60 per cent of the 20-day flow remained as permanent set.

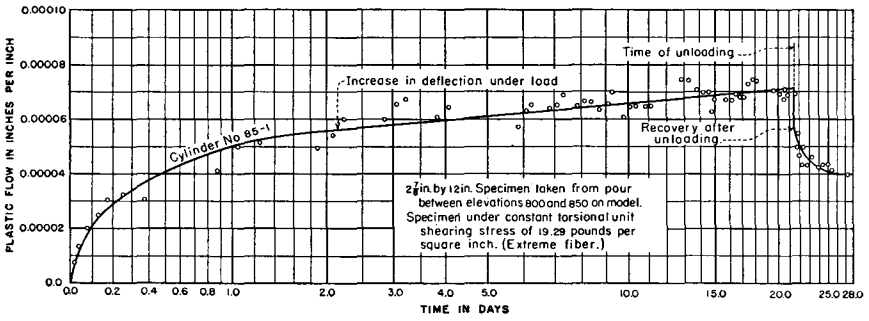

FIGURE 63—TYPICAL PLASTIC FLOW IN TORSION

The results of the flow tests indicated that, in order to reduce such effects in the model, the model tests should be run with as short a loading time as possible.

67. Coefficient of Expansion.—The proposed program of tests on the model included a temperature test. Consequently, a test to determine the thermal coefficient of expansion of plaster-celite was made. Four 3 by 3 by 40-inch beams were selected for the tests. Figures 64 and 65 show apparatus used for measuring changes in length and controlling temperatures. Tests were conducted in the following manner. The beam was allowed to attain the uniform temperature of the air in the testing room. The mild steel reference bar, which had

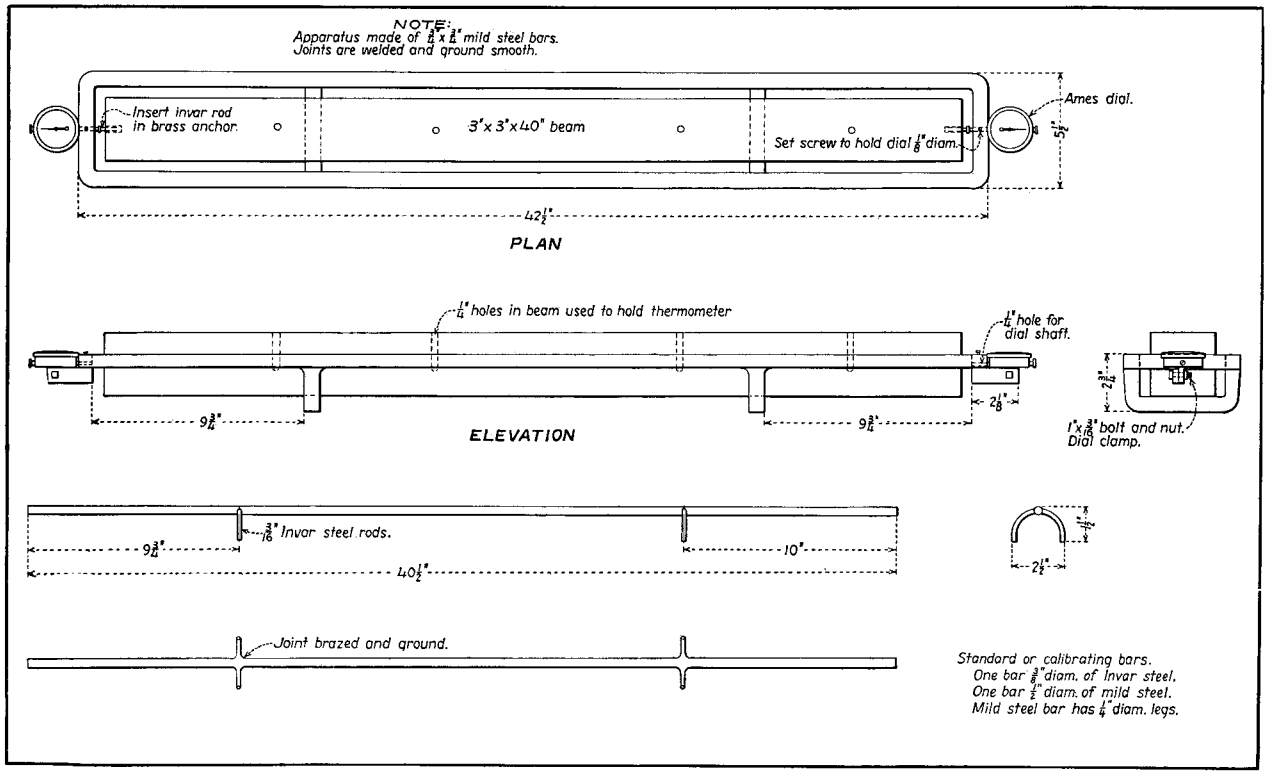

FIGURE 64—APPARATUS FOR MEASURING THERMAL EXPANSION

been calibrated against the invar steel reference bar for changes in length due to temperature variation, was placed in the yoke shown in figure 64 for a reference reading. The plaster-celite beam was next placed in the yoke and an initial reading made. The beam was then placed in the smaller of the two galvanized-iron boxes shown in figure 65 and covered tightly. This box was placed in the larger box, and water having a temperature different from the initial temperature of the beam was circulated around the inner box until the beam had a uniform change in temperature. The beam was placed in the yoke

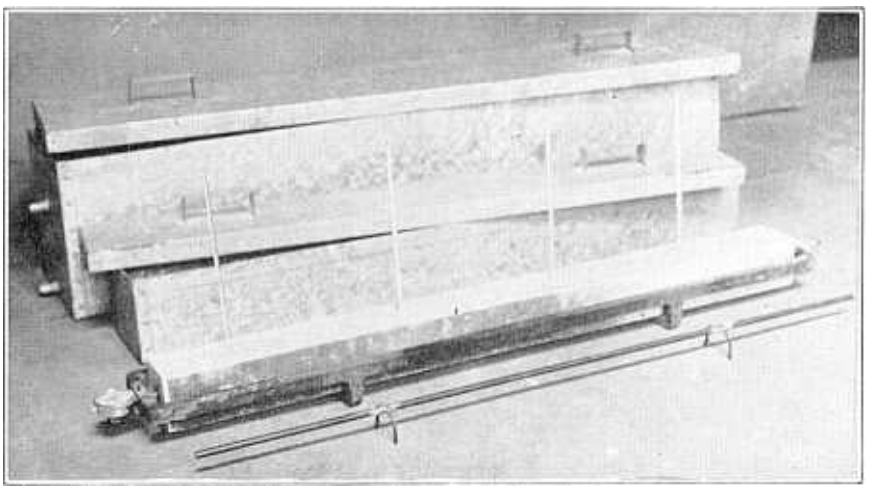

FIGURE 65—THERMAL-EXPANSION TEST OF PLASTER-CELITE BEAM

again and another set of observations made which was compared with the mild steel reference bar. The coefficient of expansion was computed from the change in length and temperature of the beam.

Several tests were made through different ranges of temperature. During the heating tests the temperature varied from 78 to 130 degrees Fahrenheit. During the cooling tests the temperature varied from 83 to 25 degrees. The coefficient of expansion was found by dividing the net change in length of the beam by the product of the length of the beam and the change in temperature. It was found to vary from 0.000,010,7 to 0.000,011,6 inches per inch per degree Fahrenheit, for the different beams. The average coefficient of expansion was 0.000,011 inches per inch per degree Fahrenheit. The tests showed that the expansion of the material was a linear function of the temperature.

68. Unit Weight.—The unit weight of the material used in building the model and the supplemental base was determined from measurements and weights of the 3 by 3 by 40-inch beams used in the flexural tests. As the other test specimens were usually capped with quick-setting plaster before their removal from the forms, they could not be used in determining unit weights. The dimensions of the beams were carefully measured at a number of sections. The average breadth, depth, and length of each beam was used in computing the volume. Twenty-seven beams were used in determining the unit weight. The average weight per cubic foot of all beams, when thoroughly dry, was 41.8 pounds per cubic foot. The variation in weight was small, the maximum weight being 43.1 pounds per cubic foot and the minimum 41.1 pounds per cubic foot.

69. Average Results.—Nearly 400 specimens were made from the material used in the model. As each layer was poured, the unused portion of the batch was cast into compression, tension, torsion, and flexural specimens, so that a complete record of elastic properties of each layer was obtained. The average results of the tests were:

Modulus of elasticity in compression, 87,000 lbs. per sq. in.
Modulus of elasticity in tension, 102,400 lbs. per sq. in.
Modulus of elasticity in flexure, 107,000 lbs. per sq. in.
Modulus of elasticity in torsion, 45,000 lbs. per sq. in.
Poisson's ratio for 2 by 4-inch cylinders, 0.177.
Poisson's ratio for 3 by 6-inch cylinders, 0.195.

Due to longer gage lengths and larger deflections, 3 by 6-inch specimens gave more reliable results than 2 by 4-inch specimens. The values for the 3 by 6-inch specimens are therefore considered more reliable.

70. Effect of Age on Plaster.—The length of time that plaster had been in storage affected the strength and modulus of elasticity of the resulting product when combined with celite. In making the preliminary tests for a suitable material for the model of Boulder Dam, a relatively small quantity of plaster was obtained and mixed a few days later. In building the model, considerable time was taken in drying each layer. As a result the plaster was held in storage for some time. As soon as any deterioration was noticed, the supply was discarded and a fresh supply obtained.

The plaster was usually purchased in lots of five sacks. The total amount was immediately poured into a large metal pan and stirred until thoroughly blended. The plaster was then stored in paper-lined, galvanized-iron cans with tight-fitting tops. Even in such storage the plaster deteriorated to some extent if kept longer than two months.

SUBSEQUENT INVESTIGATIONS

71. General.—Plaster-celite mixtures were used in a number of model tests after the completion of tests for Boulder Dam. Considerable additional data on characteristics of plaster-celite mixtures were obtained in the later tests, and important conclusions derived therefrom are included in this report to complete the discussion. Also, certain questions arose concerning the degree of isotropy obtained in a model built up in layers. Consequently, when the Boulder model was dismantled, specimens were cut out of the interior and tested for such properties.

72. Segregation.—In later investigations, the same brand of plaster, mixed with the same proportion of celite used in the Boulder model, was found to have considerably different characteristics. It was believed that these differences were due to changes in the constituents of the plaster, probably caused by variations in the material at its source. Although these variations would have no effect on the commercial uses of the plaster, they had pronounced effects on the plaster-celite mixtures. Contrasted to the mixture used on the Boulder model, which had a time of set of about 20 minutes, and expanded slightly in setting; mixtures of the same brand of materials and proportions, three years later, had a time of set of about one hour and a slight shrinkage during setting. Furthermore, segregation occurred in the later mixtures, making the bottom of a layer harder than the top. It was found that the segregation was caused by the longer time of set, which allowed the mixing water to rise and the heavier material to settle. This situation was remedied by blending Sunflower molding plaster with the Acme finishing plaster, the former being faster setting. By this process it was possible to obtain a time of set of 20 minutes which was sufficient to prevent segregation.

73. Recommended Procedure.—Due to the variations which may occur in commercial building plasters, the following program was finally adopted in order to obtain uniformity in plaster-celite models.

1. At the beginning of each program of tests, samples of plasters were obtained; and, using the results of the preliminary studies as a guide, trial mixes were made to check the modulus of elasticity, time of set, and shrinkage or expansion.

2. If the original proportions did not give a satisfactory mixture, the proportions were varied or the plaster blended until a satisfactory product was obtained. This did not involve more than two or three trial mixes.

3. With the proper proportions determined, a fairly large supply of material was obtained, sufficient to last about two months. A trial mix was made from each shipment of material to check on variations.

This procedure was followed on a model project using 3,000 pounds of material, and very uniform elastic properties were obtained. In making up later mixtures, the moisture content of the celite was measured and proper allowance made in the weight. Moisture content appeared to be the only variable quantity in celite.

74. Isotropy.—When the tests on the Boulder model were completed, the model was removed intact from the testing pit and stored in the laboratory. Before disposing of the model, a large block of material was cut out of the interior, for testing to determine isotropic properties and, incidentally, the effect of age. Cylinder specimens, 3 by 6 inches in size, were cut out in vertical and horizontal planes with respect to the model. Typical results of the cylinder tests are shown on figure 66. These results were practically identical with the tests made while the model was under construction. Also there was

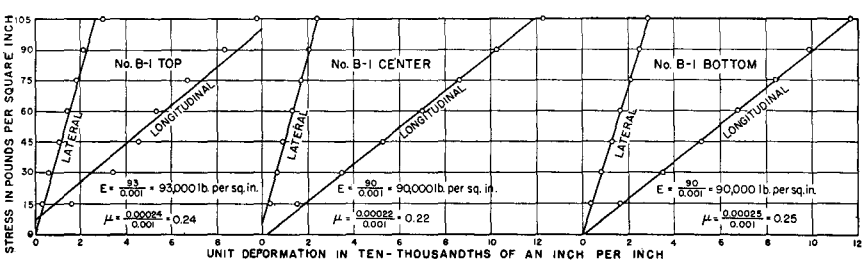

'Specimen No. B-1 taken from El. 1150 to El. 950. Two layers, joints vertical Composition: 2.4 lb. plaster, 1.2 lb. Celite, and 4.5 lb. water.

FIGURE 66—TEST OF CYLINDER TAKEN FROM MODEL

very little difference between the tests made in vertical and horizontal planes, which indicated that the material was isotropic.

A more conclusive test for isotropic properties could be made on a cube, where the modulus of elasticity could be measured on three axes. A 6-inch cube, comprising three layers of material, was cut out and tested in the laboratory hydraulic testing machine. Dial gages were attached directly to the faces of the cube, and load was applied through flat steel plates with a thin sheet of rubber between each plate and the specimen.

Results of the cube test indicated practically the same deformations

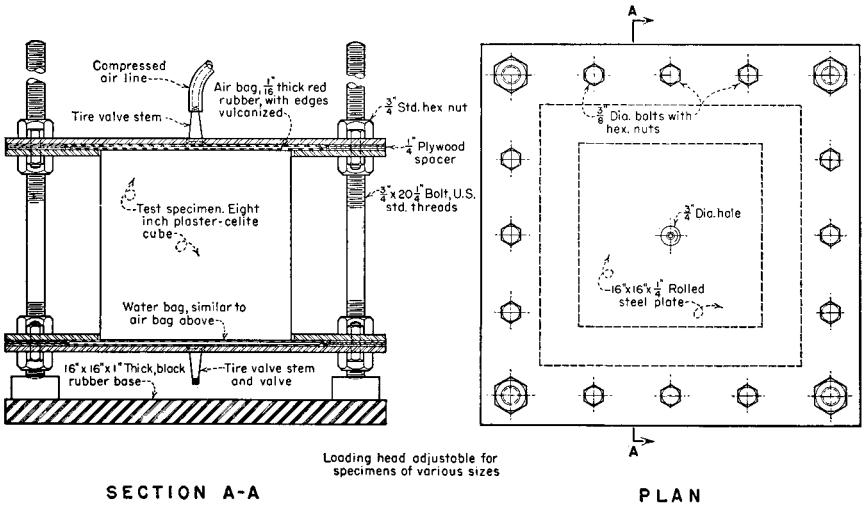

FIGURE 67—COMPRESSED-AIR LOADING MACHINE

on each axis; but the end restraint caused bulging of the specimen, and the gages did not record true deformations. By applying loads through steel plates, there was no assurance of uniform load distribution over the ends of the specimens. Although various thicknesses of rubber were used to distribute the load, bulging of the specimen could not be eliminated.

Lack of satisfactory results on the cube test made necessary development of loading apparatus which would produce uniform pressures over the ends of the specimen. A machine was built in which the load was applied by means of compressed air. This machine is shown on figure 67. The loading head consisted of two steel plates, separated by spacers, and a rubber bladder connected to a compressed-

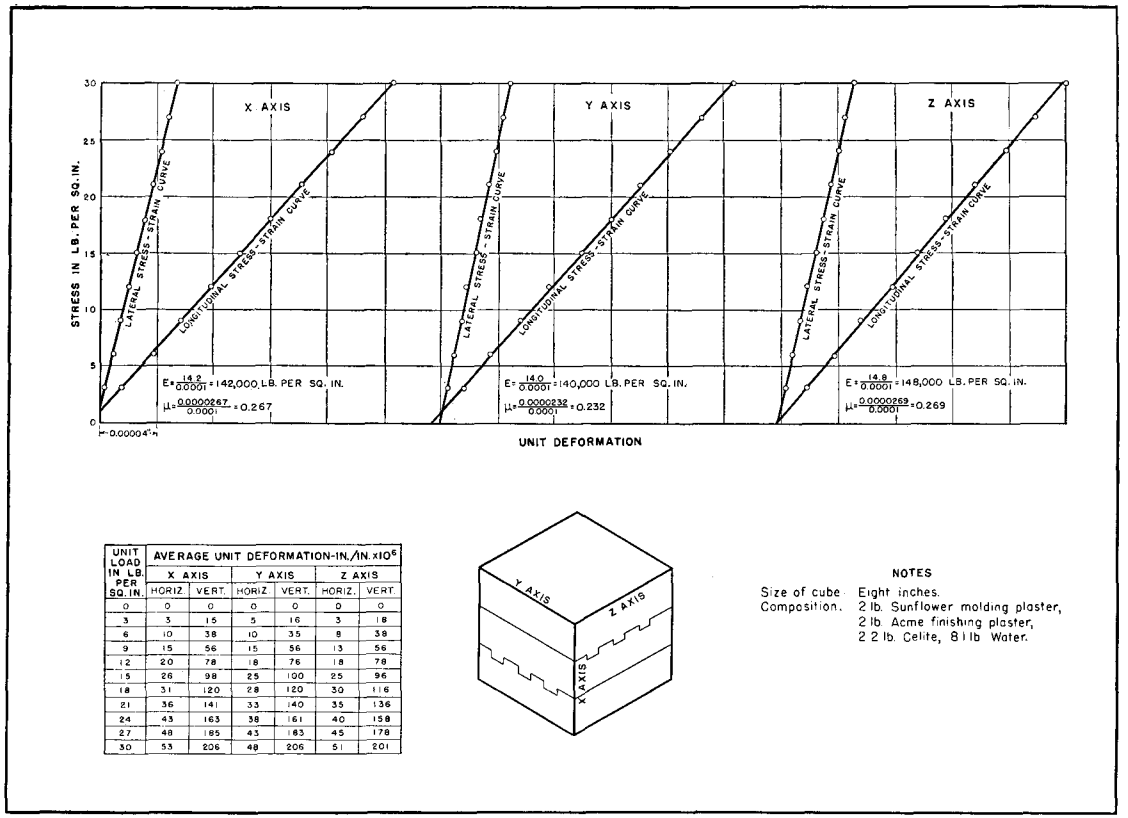

UNIT LOAD IN LB. PER SQ. IN.	AVERAGE UNIT DEFORMATION-IN./IN. X10⁶					
	X AXIS		Y AXIS		Z AXIS	
	HORIZ.	VERT.	HORIZ.	VERT.	HORIZ.	VERT.
0	0	0	0	0	0	0
3	3	15	5	16	3	18
6	10	38	10	35	8	38
9	15	56	15	56	13	56
12	20	78	18	76	18	78
15	26	98	25	100	25	96
18	31	120	28	120	30	116
21	36	141	33	140	35	136
24	43	163	38	161	40	158
27	48	185	43	183	45	178
30	53	206	48	206	51	201

NOTES

Size of cube: Eight inches.
Composition: 2 lb. Sunflower molding plaster, 2 lb. Acme finishing plaster, 2.2 lb. Celite, 8.1 lb. Water.

FIGURE 68—RESULTS OF TESTS FOR ISOTROPIC PROPERTIES

air supply. The bottom plate had a square hole in which the end of the specimen fitted. The reaction plate was identical, except that the bladder receiving the reaction was filled with water. This machine gave uniform pressures on the ends of the specimen and did not cause restraint.

Since the specimen taken from the dam was not suitable for further testing, three special cubes for additional tests were prepared. They were built up in three-inch layers, following the same procedure used in casting the model. Each layer was cast from a separate batch of material. After each cube was dry, it was dressed down to a perfect cube 8 inches in size. Typical results from the tests are shown on figure 68. All three specimens had small variations in moduli along the three axes, similar to those shown, but the variations were not on the same axes for the different specimens. It was, therefore, concluded that the variations were caused by experimental errors rather than by directional properties of the built-up specimens.

CHAPTER IV—PRELIMINARY TESTS OF PLASTER-CELITE MODEL

TESTING PROCEDURE

75. Loading the Model.—The method of loading the model of Boulder Dam was the same as the method used in testing previous models built by the Bureau of Reclamation. A rubber bag, shaped to fit the upstream face of the model, was made of heavy automobile inner-tube stock, see figure 69. The bag served as a container for the water or mercury during the application of triangular pressure loads at the upstream face of the model. The upstream form which had been used in casting the model was reshaped so that it would uniformly support the rubber bag when placed about three-fourths of an inch upstream from the model. The rubber bag was placed in the space between the model and the form and clamped to the top and bottom of the form so that it would not press against the model while empty. The form was carefully braced against the opposite side of the testing pit and against the concrete ceiling of the laboratory, so that it could

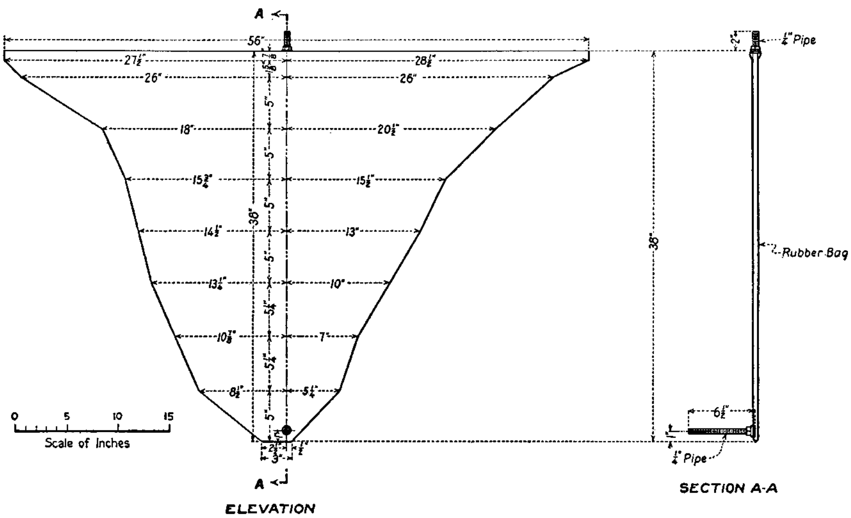

FIGURE 69—RUBBER BAG FOR LOADING MODEL

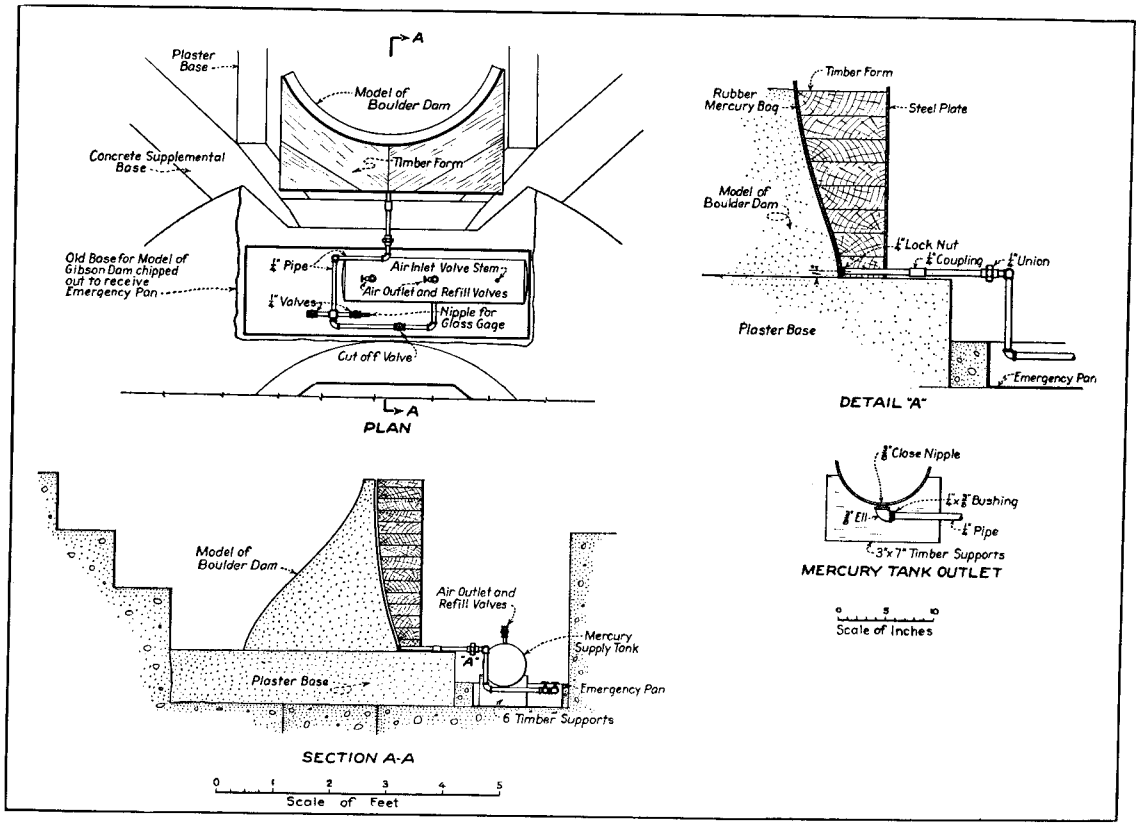

FIGURE 70—MERCURY SUPPLY TANK AND PIPING

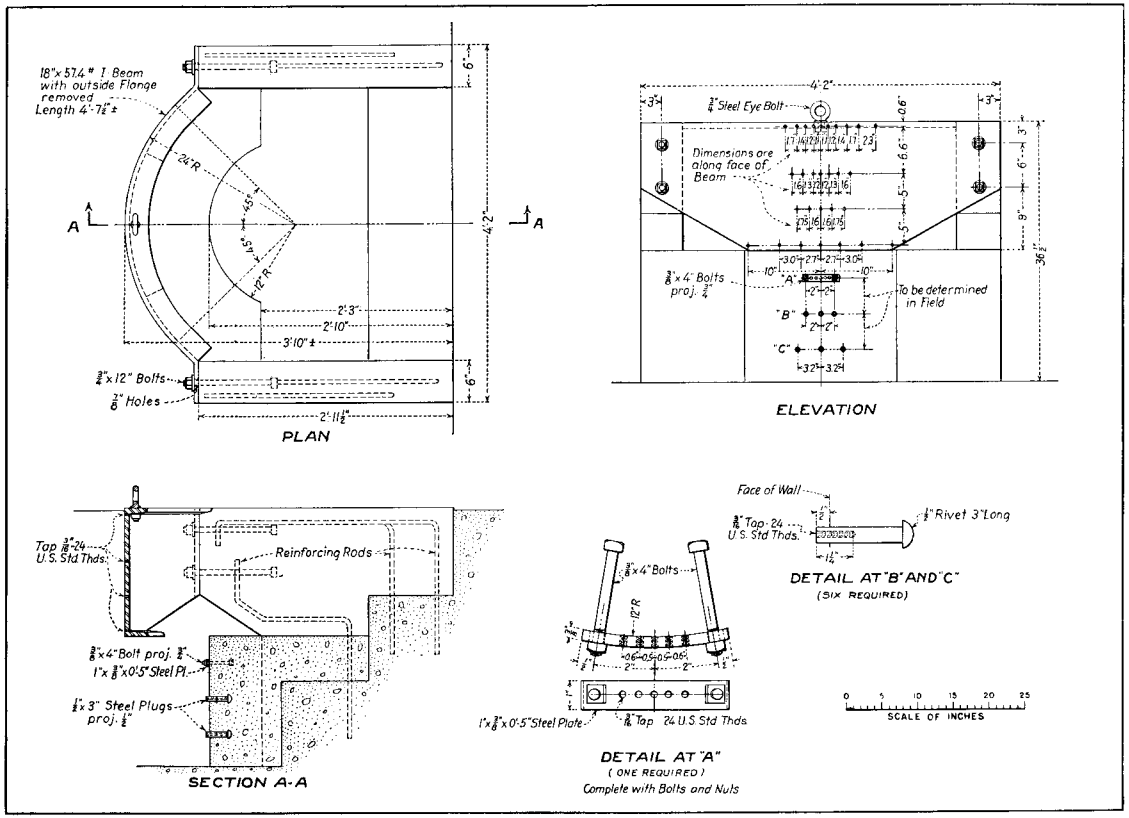

FIGURE 71—DETAILS OF INSTRUMENT STAND

not slide from its original position while supporting the reaction of the load on the model. The rubber bag was connected to the mercury supply tank by the piping system shown in figure 70. Water from the city mains could be used in loading the model, when desired. When mercury was used as the loading agent, water pressure was admitted to the top of the supply tank, forcing the mercury from the bottom of the tank into the rubber bag. A gage made of glass tubing served to show the elevation of the water or mercury surface inside the bag.

76. Conduct of Tests.—Invar steel rods were used for attaching gages to the model to reduce temperature effects as much as possible. For radial deflection tests, dial gages, mounted on radial rods, were rigidly attached to the face of the model. The dials were kept in alinement by similar rods, mounted on the reference base and held in flexible guides. The guides prevented lateral movements of the deflection rods but did not interfere with movement in the direction of the length of the rods. Figure 71 shows details of the instrument stand which served as a reference base. Figure 72 shows a typical arrangement of gages for radial deflection measurements. The dial gages used on the Boulder model were sensitive to 0.0001 of an inch

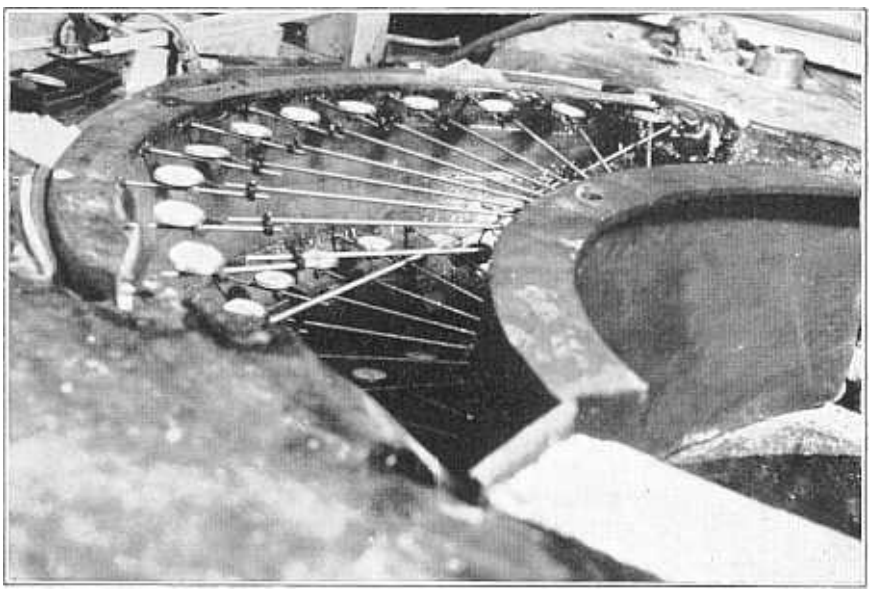

FIGURE 72—ARRANGEMENT OF GAGES FOR RADIAL DEFLECTION MEASUREMENTS

with a range of 0.023 inches. There was very little inertia to the moving parts of the gage, and by lightly tapping the deflection rods, the pointers of the gages would vibrate and come to rest at the correct reading. This process eliminated friction and any stress in the rods which actuated the dials. This was a valuable feature, especially where it was necessary to bend the deflection rods, or where the rods were quite long.

For all load-deflection tests, the procedure was as follows:

1. The dial gages were adjusted to an initial deflection, vibrated, and read.

2. The load was applied to the model and the gages vibrated and read again.

3. The load was removed and recovery readings made.

Differences between no-load readings and load readings gave deflections due to load. Differences between load and recovery readings gave the recovery of the model during removal of load.

77. **First Deflection Measurements.**—The first deflection tests were made on July 7, 1931. The purpose of this series of tests was to measure radial deflections of the model when loaded to elevation 1232 with water or mercury. The first three tests were made using water for the loading agent. In bracing the supporting form, insufficient clearance had been allowed between the upstream face of the model and the rubber bag. When the water load was applied, it was doubtful if the rubber bag was completely filled. The measured deflections were unusually small and the results were considered questionable. A mercury load was next applied. This load was sufficient to force the supporting form slightly upstream, loosening the wedges in the bracing. By adjusting the bracing, a film of mercury approximately one-fourth of an inch thick, was obtained in the rubber bag. The measured radial deflections were fairly satisfactory but contained several erratic readings.

78. **Movement of Unsupported Base.**—During the preliminary series of tests, a lack of symmetry was noticed in the deflection curves. As the model was nearly symmetrical in shape, a symmetrical deflection curve was expected. The deflection of the model at the Arizona abutment was materially greater than at the Nevada abutment. During the construction of the plaster-celite supplemental base and the model, cracking developed between the supplemental base and

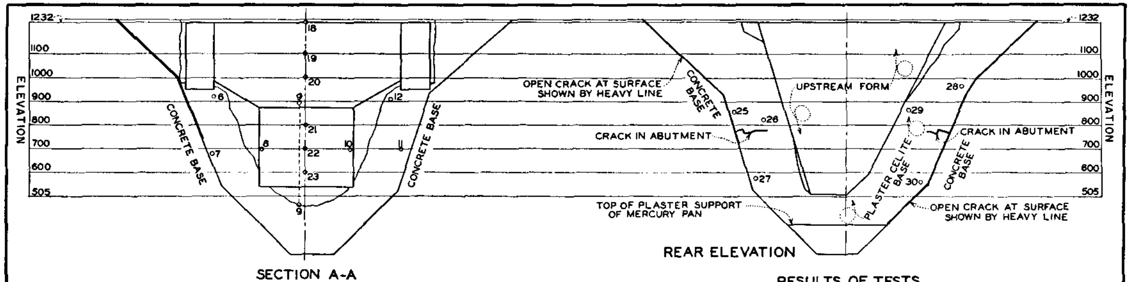

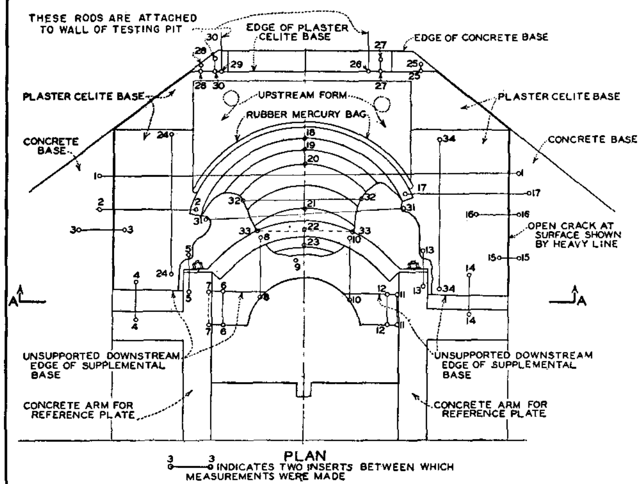

RESULTS OF TESTS

MERCURY AT EL. 1232 UNIT MEASUREMENT = .0001

MEAS.	TEST NO. 49A	TEST NO. 49 B	TEST NO. 50 A	TEST NO. 50 B	TEST NO. 51	TEST NO. 52	TEST NO. 53	TEST NO. 54	AVE
1	1.3	1.2	0.3	1.0	2.0	—	—	—	+1.2
2	-7.3	-7.5	-7.0	-7.6	-7.3	-7.6	-6.8	-6.7	-7.2
3	-6.0	-5.7	-6.2	-6.3	-6.2	-6.3	-5.2	-5.5	-5.9
4	-3.8	-4.3	-3.3	-3.5	-4.1	-4.0	-3.0	-3.6	-3.7
5	-7.6	-7.5	-7.4	-7.7	-9.7*	-12.2*	-6.3	-7.2	-7.3
6	-7.0	-6.5	-6.5	-6.3	-6.5	-6.2	-5.9	-6.3	-6.4
7	-2.0	-1.8	-1.8	-2.0	-2.0	-1.7	-1.8	-1.8	-1.9
8	-7.5	—	-7.0	-7.0	-7.2	-7.5	-7.0	-7.2	-7.2
9	1.7	1.7	2.0	2.0	2.0	1.7	1.9	1.9	+1.9
10	-13.8	-12.4	-12.5	-13.0	-12.9	-13.0	-12.6	-13.2	-12.9
11	-9.8	-9.5	-9.8	-9.8	-9.2	-9.7	-9.6	-9.8	-9.7
12	-17.2	-17.3	-17.0	-17.7	-16.8	-17.5	-17.0	-17.7	-17.3
13	-18.2	-17.5	-17.7	-18.2	-18.2	-18.0	-17.2	-17.9	-17.9
14	-8.5	-8.0	-8.2	-9.0	-8.3	-9.3	-8.8	-8.7	-8.6
15	-1.8	-1.6	-1.2	-1.8	-1.8	-1.4	-1.8	-2.0	-1.6
16	-1.1	-1.8	-1.5	-1.8	-1.2	-2.3	-1.4	-1.4	-1.5
17	-1.6	-2.0	-1.8	-1.2	-1.3	-1.2	-2.0	-2.0	-1.6
18	-56.6	-56.5	-56.2	-57.0	-56.3	-56.2	-55.8	-55.8	-56.3
19	-55.8	-56.0	-56.5	-56.2	-56.0	-56.8	-55.5	-56.0	-56.1
20	-44.8	-44.8	-45.5	-45.8	-45.5	-46.0	-45.0	-45.3	-45.3
21	-25.0	-24.6	-25.5	-24.5	-24.4	-24.5	-24.1	-24.2	-24.6
22	-14.2	-14.0	-14.5	-14.2	-14.0	-14.2	-13.9	-14.0	-14.1
23	-8.0	-7.0	-7.0	-8.2	-7.8	-8.2	-7.7	-7.7	-7.7
24	—	—	—	-1.5	-2.6	-2.6	-2.5	-2.6	-2.4
25	9.0*	16.0	16.7	16.5	15.3	15.5	15.6	15.5	+15.9
26	19.1	20.0	19.0	21.5	20.6	20.2	21.1	20.3	+20.2
27	15.8	14.9	14.0	6.8*	6.0*	6.7*	11.7	12.0	+12.0
28	6.2	6.0	6.2	6.3	6.3	6.7	6.2	6.6	+6.3
29	15.5	15.5	15.5	16.5	15.7	15.8	15.7	15.7	+15.7
30	4.6	4.2	5.2	5.0	5.0	5.0	5.0	5.0	+5.0
31	8.1	8.5	8.3	8.0	8.0	6.4	8.3	7.8	+7.9
32	9.2	9.5	9.0	8.5	9.0	8.7	9.2	10.8	+9.2
33	6.5	4.2	4.8	4.8	4.8	4.2	4.5	4.6	+4.8
34	—	—	—	—	—	-4.0	-2.5	-1.7	-2.4

\+ INDICATES LENGTHENING BETWEEN INSERTS
\- INDICATES SHORTENING BETWEEN INSERTS
*ERRATIC

MEASURMENTS 18 TO 23 INCLUSIVE ARE RADIAL DEFLECTION MEASUREMENTS AT CANTILEVER E
MERCURY BAG No. 1 USED IN THIS TEST
SUPPLEMENTAL BASE UNSUPPORTED AT DOWNSTREAM FACE OF DAM.

FIGURE 73—DEFORMATION OF BASE AS ORIGINALLY CONSTRUCTED

the concrete primary base. The positions of the cracks are shown in figure 73. It was believed that the cracks closed when the load was applied and opened when the load was removed. Consequently, an investigation of the action of the supplemental base and the open cracks was made.

Inserts were attached to the concrete primary base and to the supplemental base, using quick-setting plaster to fasten them in place as shown in figure 74. Invar steel rods, on which dial gages

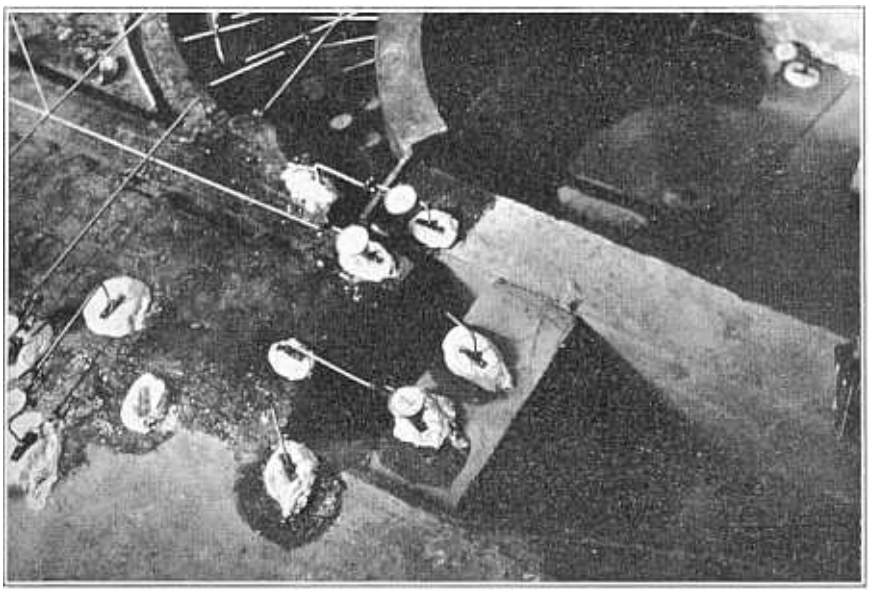

FIGURE 74—GAGES MOUNTED FOR MEASURING MOVEMENT OF BASE

were mounted, were attached to the inserts at the locations shown in figure 73, so that any movement of the base could be measured. When the model was loaded, the crack at the Nevada side of the base closed 0.000,59 inches at measurement 3, figure 73. The corresponding movement at the crack on the Arizona side showed a closure of 0.000,15 inches at measurement 16. The entire base, however, deflected downstream under load, as may be seen from measurements 4 to 8 and 10 to 14, inclusive. The largest deflections occurred at measurements 12 and 13 on the Arizona side of the canyon.

In casting the plaster-celite base against the concrete primary base, no dowels or keyways were used as a mechanical bond between

the two materials. Cracks developed in several places, either due to the drying of the plaster or to the different rates of expansion of plaster and concrete caused by temperature changes. The cracks between the two materials were undoubtedly affecting the deflection of the model under load. It was therefore decided to add supports of sand and quick-setting plaster to the supplemental base as shown in figure 75. The supports filled the small space at the downstream edge of the plaster-celite base, and transferred the load from the abutments to the concrete walls of the testing pit.

79. Deflection of Supported Base.—The effect of the addition of sand-plaster supports to the plaster-celite base is shown in figure 75. Downstream deflections of both the base and the model were lessened materially. The closing of the cracks was more uniform. Measurement 3 showed that the crack on the Nevada side closed 0.000,30 inches, and measurement 16 showed that the corresponding crack on the Arizona side closed 0.000,37 inches.

Measurements 25 to 30, inclusive, indicated that the upstream face of the supplemental base deflected downstream under load. However, no appreciable movement along the open cracks was discernible. Any sliding of the supplemental base along the crack would have been indicated by measurements 35 and 36. Measurement 35 showed a reading of zero and measurement 36 showed a reading of 0.000,01 of an inch.

Measurements 24 and 34 were of particular interest because they showed that the upstream side of the supplemental base was actually compressed toward the downstream support when the model was loaded. The downstream face of the supplemental base did not deflect under load as it was in direct contact with the fairly rigid sand-plaster support. Measurements 4, 14, 37, and 38 would show any deflection of the downstream edge of the plaster-celite base toward the sand-plaster support. The movement registered at each of these points was very small, being less than 0.0001 of an inch.

The addition of sand-plaster supports did not make a great deal of difference in the change of chord lengths at measurements 31, 32, and 33. With the sand-plaster supports added, these measurements were +0.000,73, +0.001,12, and +0.000,62 inches, respectively. The change in chord length at elevation 1200 should be corrected by the amount the cracks closed at measurements 3 and 16. After applying this correction, the change in chord length was +0.000,06 inches for the supported base. Measurements of the width of the crack opening

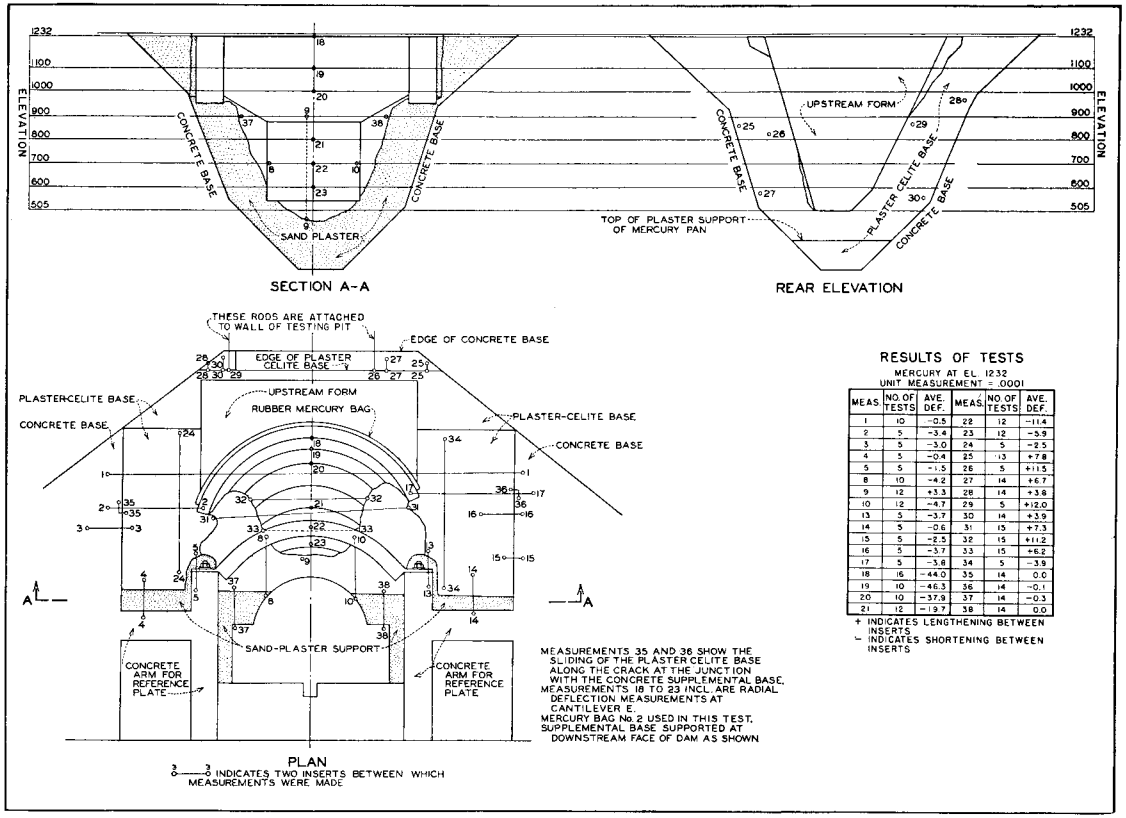

RESULTS OF TESTS

MERCURY AT EL. 1232

UNIT MEASUREMENT = .0001

MEAS.	NO. OF TESTS	AVE. DEF.	MEAS.	NO. OF TESTS	AVE. DEF.
1	10	−0.5	22	12	−11.4
2	5	−3.4	23	12	−5.9
3	5	−3.0	24	5	−2.5
4	5	−0.4	25	13	+7.8
5	5	−1.5	26	5	+11.5
8	10	−4.2	27	14	+6.7
9	12	+3.3	28	14	+3.8
10	12	−4.7	29	5	+12.0
13	5	−3.7	30	14	+3.9
14	5	−0.6	31	15	+7.3
15	5	−2.5	32	15	+11.2
16	5	−3.7	33	15	+6.2
17	5	−3.8	34	5	−3.9
18	16	−44.0	35	14	0.0
19	10	−46.3	36	14	−0.1
20	10	−37.9	37	14	−0.3
21	12	−19.7	38	14	0.0

+ INDICATES LENGTHENING BETWEEN INSERTS
− INDICATES SHORTENING BETWEEN INSERTS

FIGURE 75—DEFLECTION OF BASE AFTER ADDING DOWNSTREAM SUPPORTS

could not be made at other elevations where changes in chord lengths were measured.

After completion of the preliminary tests with the base of the model supported at the downstream end, it was concluded that the action of the model and foundation was satisfactory.

ALTERATIONS TO MODEL

80. New Mercury Bag.—The rubber mercury bag did not fit the upstream face satisfactorily, owing to shrinkage which took place during curing. It lacked sufficient height to reach to the top of the model on one side. By stretching, it could be made high enough; but in doing so, the width of the bag was decreased, leaving an uncovered area of about twenty square inches at the upstream face. The scant fit of the bag might have been a contributing cause of the unsymmetrical deflection. Consequently, a new mercury bag was obtained. This bag was made slightly higher than the first, so that it would fit without being stretched. The first loading bag was designated number 1 and the new bag, number 2. These designations are used on various drawings which appear in subsequent sections of this report.

81. Revision of Instrument Stand.—The instrument stand, which served as a reference pier for the radial deflection measurements, consisted of two parts; first, a concrete post, and, second, a steel plate supported by two concrete arms which were anchored to the wall of the testing pit, as shown in figure 71. The steel plate was a little too wide at the bottom edge to fit into the canyon. Notches had been cut in the canyon walls to permit the installation of the steel plate. It was feared that these notches might affect the deflection of the model. Accordingly, the steel plate was removed and rebent until it fit the canyon satisfactorily. Keyways were cut around the notches and the canyon walls rebuilt to their original form.

82. Loading Canyon Walls.—Up to this time mercury load had been applied to the upstream face of the model only. In actual conditions reservoir water pressure is exerted against the sides of the canyon as well as along the upstream face of the dam. It was not known what effect reservoir pressure on the walls of the canyon would have on the deflection of the dam. As this could be determined approximately by applying mercury pressure to the canyon walls, the loading apparatus was remodeled so as to permit the application of the desired pressures.

Two additional mercury bags were obtained which fit between the ends of the upstream form and the sides of the canyon. These are designated on the drawings as numbers 3 and 4. The sides of the canyon were somewhat irregular and did not make satisfactory supports of the mercury bags. Therefore, keyways were cut in the upstream canyon walls and an additional layer of plaster-celite poured against them, so as to eliminate warped surfaces. The three mercury bags were attached to the supply tank by a system of pipes and valves which permitted the application of pressure to the model or to the sides of the canyon as desired. The condition of the model, after the alterations to the canyon walls were completed, is shown in figure 76.

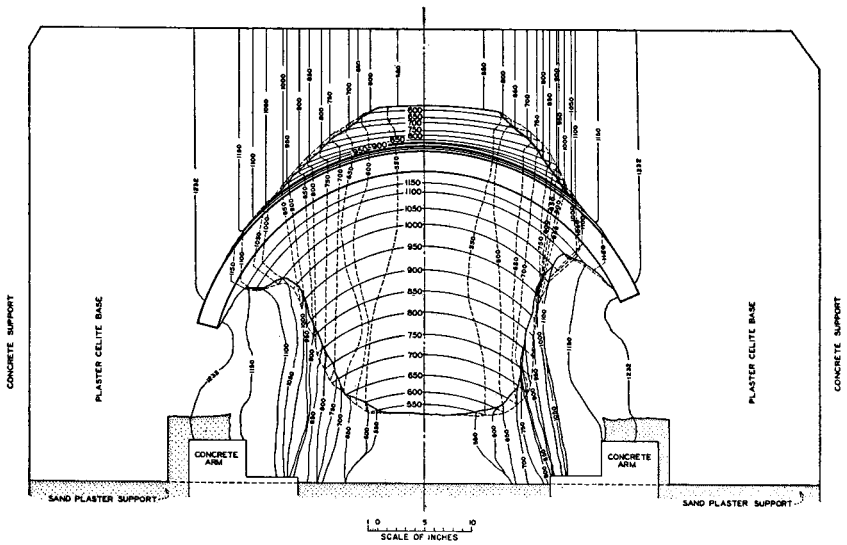

FIGURE 76—MODEL AFTER ALTERING CANYON WALLS

ADDITIONAL TESTS

83. Movement of Base.—Deformations of the foundation and abutments were measured in the first tests after installing the three mercury bags. The results of the tests are shown in figure 77. They may be compared with the tests made before and after adding the sand-plaster supports, see figures 74 and 75. Additional inserts were installed so that a more complete investigation of the action of the base could be made. Results of the measurements showed that the supplemental base was twisted by the pressures applied at the can-

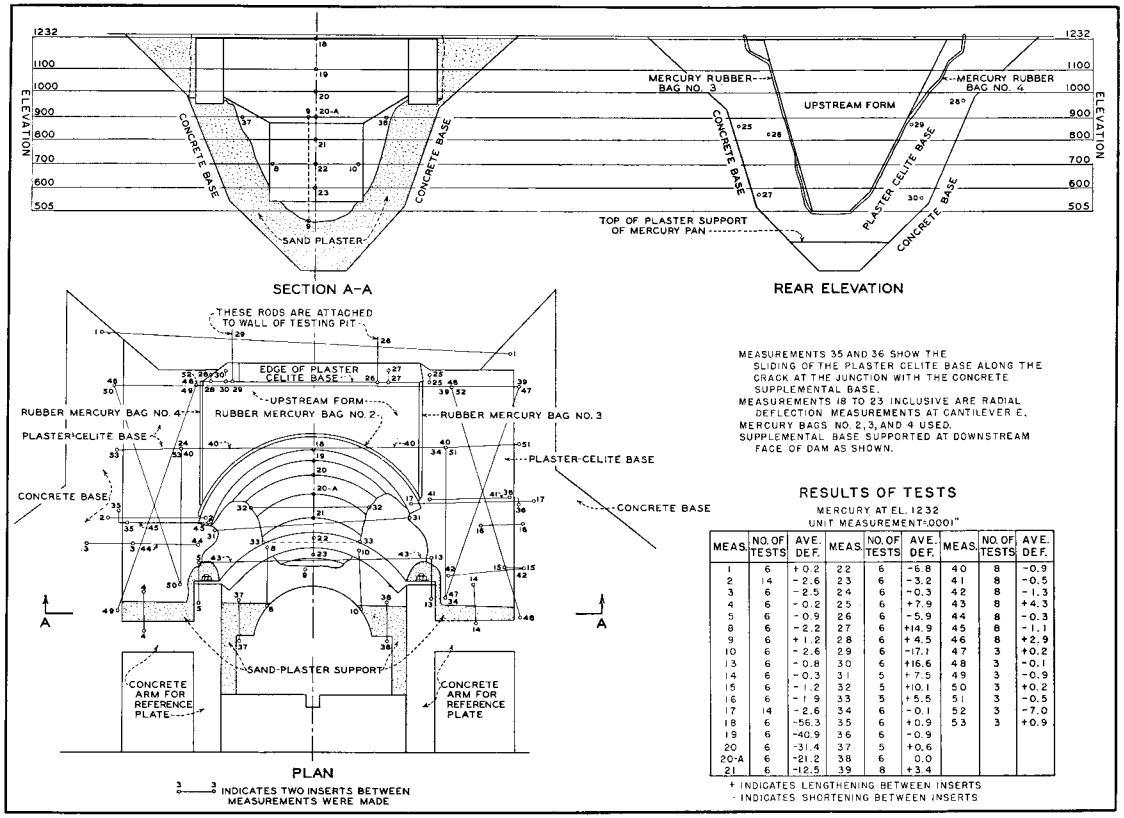

RESULTS OF TESTS

MERCURY AT EL. 1232
UNIT MEASUREMENT=.0001"

MEAS.	NO. OF TESTS	AVE. DEF.	MEAS.	NO. OF TESTS	AVE. DEF.	MEAS.	NO. OF TESTS	AVE. DEF.
1	6	+0.2	22	6	-6.8	40	8	-0.9
2	14	-2.6	23	6	-3.2	41	8	-0.5
3	6	-2.5	24	6	-0.3	42	8	-1.3
4	6	-0.2	25	6	+7.9	43	8	+4.3
5	6	-0.9	26	6	-5.9	44	8	-0.3
8	6	-2.2	27	6	+14.9	45	8	-1.1
9	6	+1.2	28	6	+4.5	46	8	+2.9
10	6	-2.6	29	6	-17.1	47	3	+0.2
13	6	-0.8	30	6	+16.6	48	3	-0.1
14	6	-0.3	31	5	+7.5	49	3	-0.9
15	6	-1.2	32	5	+10.1	50	3	+0.2
16	6	-1.9	33	5	+5.5	51	3	-0.5
17	14	-2.6	34	6	-0.1	52	3	-7.0
18	6	-56.3	35	6	+0.9	53	3	+0.9
19	6	-40.9	36	6	-0.9			
20	6	-31.4	37	5	+0.6			
20-A	6	-21.2	38	6	0.0			
21	6	-12.5	39	8	+3.4			

+ INDICATES LENGTHENING BETWEEN INSERTS
- INDICATES SHORTENING BETWEEN INSERTS

FIGURE 77—MOVEMENT OF FOUNDATION DUE TO MERCURY LOAD ON DAM AND CANYON WALLS

yon walls. The length of the canyon was relatively short. The application of pressure at the upstream end tended to spread the upstream part of the canyon and close the downstream part. The arch thrust at the lower elevations tended to spread the downstream part of the canyon. The result was that the pressure against the upstream canyon walls acted against the thrust of the arch and decreased the radial deflections at the lower elevations.

84. Tangential Deflection Measurements.—No attempts to measure tangential deflections had been made in testing the previous model dams built by the Bureau of Reclamation. As tangential deflection measurements were desired in the Boulder model investigations, considerable experimenting was necessary before suitable in-

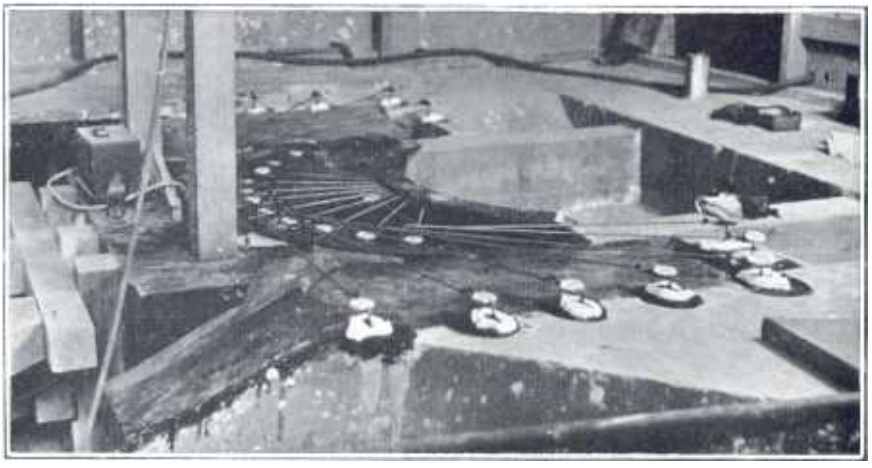

FIGURE 78—EQUIPMENT FOR MEASURING TANGENTIAL DEFLECTION OF TOP ARCH

stallations of measuring equipment could be made. Figures 78 and 79 show the installations finally devised for measuring tangential deflections.

At the top of the model, elevation 1242, invar steel deflection rods were attached in a tangential direction at the center line of the arch element and allowed to bear against dial gages mounted on the concrete abutment. At the lower elevations, dial gages were mounted on L-shaped invar rods, fastened to anchors on the downstream face of the model as shown in figure 79. They were set to record movement of the model in a tangential direction.

Theoretically, all tangential deflection measurements should have been made at the center lines of the arch elements. This could not be done at elevations below the top without boring holes in the model. The measurements were therefore made as close to the downstream face as the gages could be conveniently mounted. Distances from the downstream face to the gages varied from 1.1 to 1.6 inches. It was necessary to apply small corrections to the gage readings to obtain deflections at the downstream face.

85. Measurements of Twists and Strains.—While radial deflection measurements were in progress, some experiments in measuring

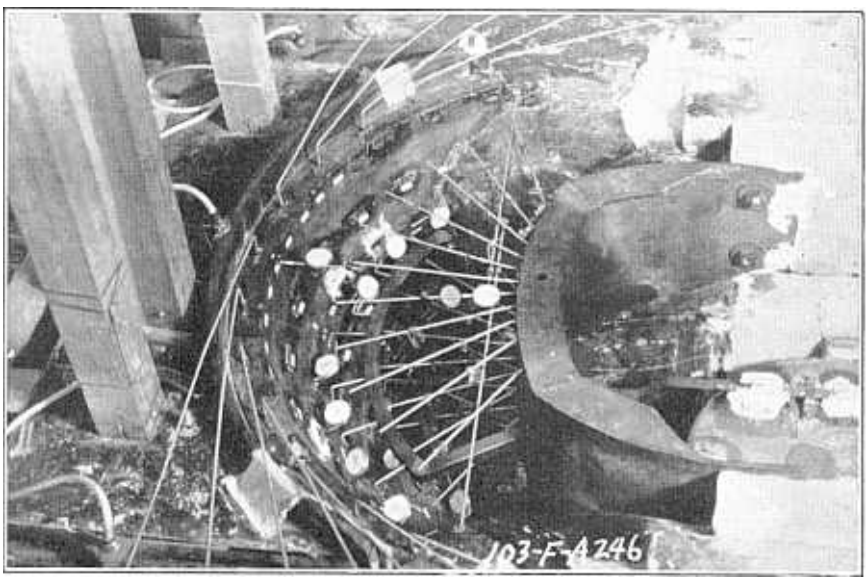

FIGURE 79—EQUIPMENT FOR MEASURING TANGENTIAL DEFLECTION AT DOWNSTREAM FACE

twist or slope deflections of the model were conducted. As angular changes of the slopes of the arch elements were very small, precise work was necessary to obtain measurements of reasonable accuracy. It was found that twist deflections could be measured by an optical lever system. Since difficulty was experienced in obtaining satisfactory images with mirrors available in the laboratory, optical flats to be used in place of mirrors were obtained.

Preliminary measurements of strain consisted in trying out avail-

able apparatus to determine its suitability for use in testing the Boulder model. No systematic measurements of strain were made at this time as it was felt that special equipment might have to be developed. The equipment finally adopted for measuring strains is discussed in chapter V.

86. Elastic Conditions of Model.—Investigations of materials had shown that the model material was highly elastic when dry. Care was exercised in constructing the model to reduce the moisture content to less than four per cent before applying protective coatings of shellac and varnish. The shellac and varnish coatings kept the moisture content constant during the testing period.

Radial deflection tests showed that the model was highly elastic. Recovery movements were usually about the same as load deflections. After taking no-load gage readings, ten to fifteen minutes were required to fill the mercury bags. Observations for load deflections usually required five to ten minutes. About twenty minutes were allowed for the mercury to drain out, after which recovery readings were taken. From the materials tests it was found that plastic flow would occur if the load was allowed to remain on the model for a considerable length of time. In order to reduce plastic flow to a minimum, dial gages were read as rapidly as possible and the load released before plastic flow of any consequence occurred. As the test program advanced, it was found that most consistent results were obtained after a few tests had been run. A small amount of flow occurred during the first few tests, after which fairly stable conditions were reached. This was shown by the recovery readings which were equal to the no-load readings after the first two or three tests were run. It was also observed that if tests were begun each half hour, gradually increasing deflections were obtained; while, if the tests were begun each hour, sufficient time for recovery was allowed so that uniform results were obtained.

Having demonstrated that satisfactory elastic action was obtained in the model, and having established a technique of testing, the detailed program of tests described in the following chapters was begun.

CHAPTER V—DEFLECTIONS, STRAINS, AND STRESSES

RADIAL DEFLECTIONS

87. Normal Load Tests.—As soon as the sand-plaster supports for the base were completed and the instrument stand remodeled, radial deflection tests were made, using the new mercury bag and applying mercury load to elevation 1232. A set of eleven tests, numbers 84 to 95, was found to be very consistent. The purpose of the tests was to obtain data for comparison with the results of a trial load analysis. Test number 85, which was virtually identical with the average for the group, was used for the actual comparison. Figures 80 and 81 show average results for the group of tests, and figure 82 shows radial arch deflections for test 85. These tests were run before the shape of the upstream end of the canyon was altered to provide for loading the canyon walls.

After the model was arranged for loading the canyon walls, the radial deflection tests were repeated. Observations were made with load on the model only and with combined loads on the model and canyon walls. Results of the tests are shown in figures 83 and 84. The deflection of the arch at elevation 1232 was characteristic of a long slender arch. At the abutments, the deflections were negative, a condition also observed on the Stevenson Creek test dam. No contraflexure was observed in the lower arches of the model, where the horizontal elements were relatively short and thick. Deflections observed between elevations 900 and 1100 were greater at the Arizona abutment than at the Nevada abutment, due to the fact that the Arizona sections of the horizontal arch elements were considerably longer at the upstream face than the Nevada sections.

An interesting observation was the effect of canyon wall loads on arch deflections. The canyon wall loads produced large increases in the deflections of the top arches and small decreases in the deflections of the lower arches. It is evident that the direct spreading effect of the canyon walls at the top would increase the downstream deflections of the upper arches. Apparently, the spreading effect near the bottom produced a slight rotation of the arch abutments,

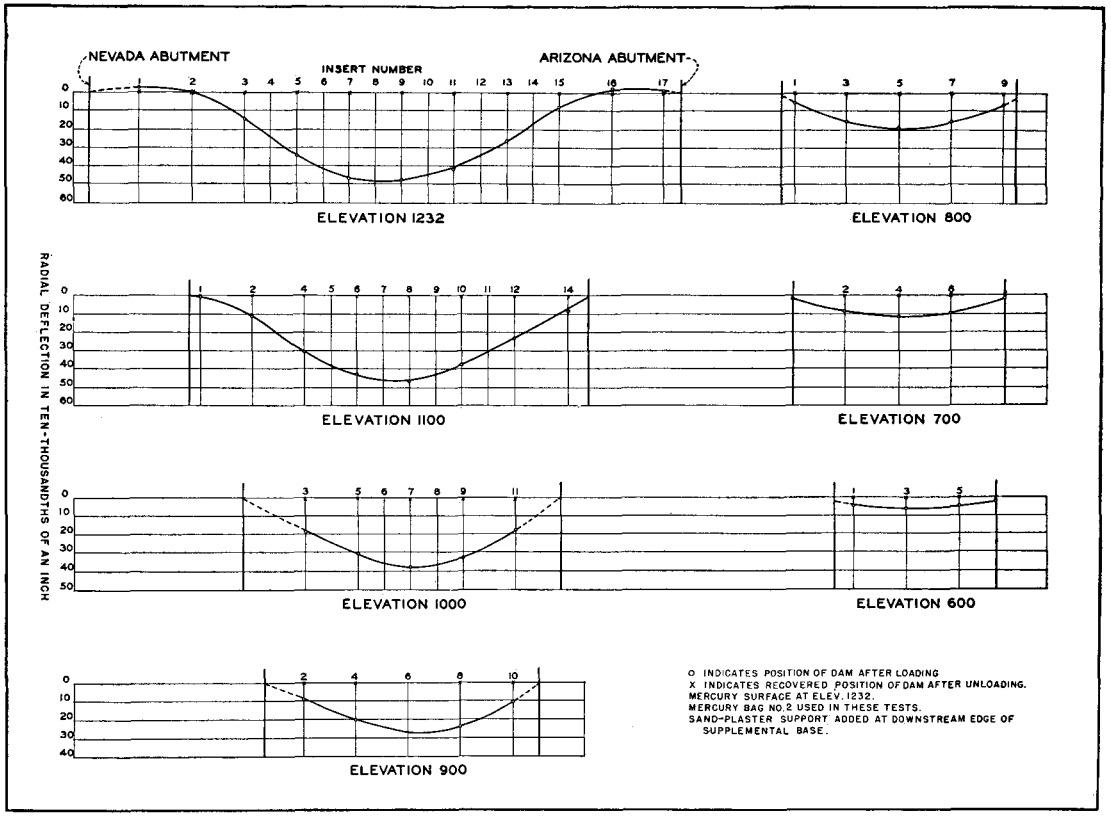

FIGURE 80—AVERAGE RADIAL DEFLECTIONS OF ARCH ELEMENTS, TESTS 84 TO 95

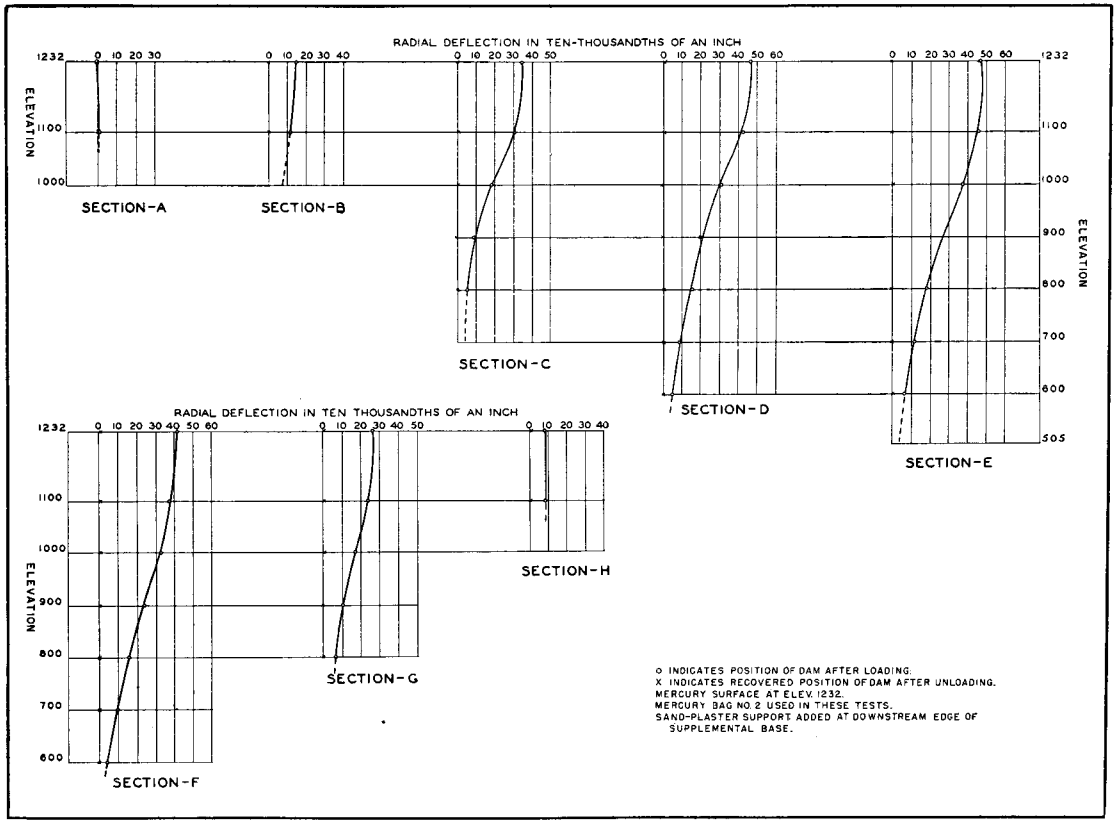

FIGURE 81—AVERAGE RADIAL DEFLECTIONS OF CANTILEVER ELEMENTS, TESTS 84 TO 95

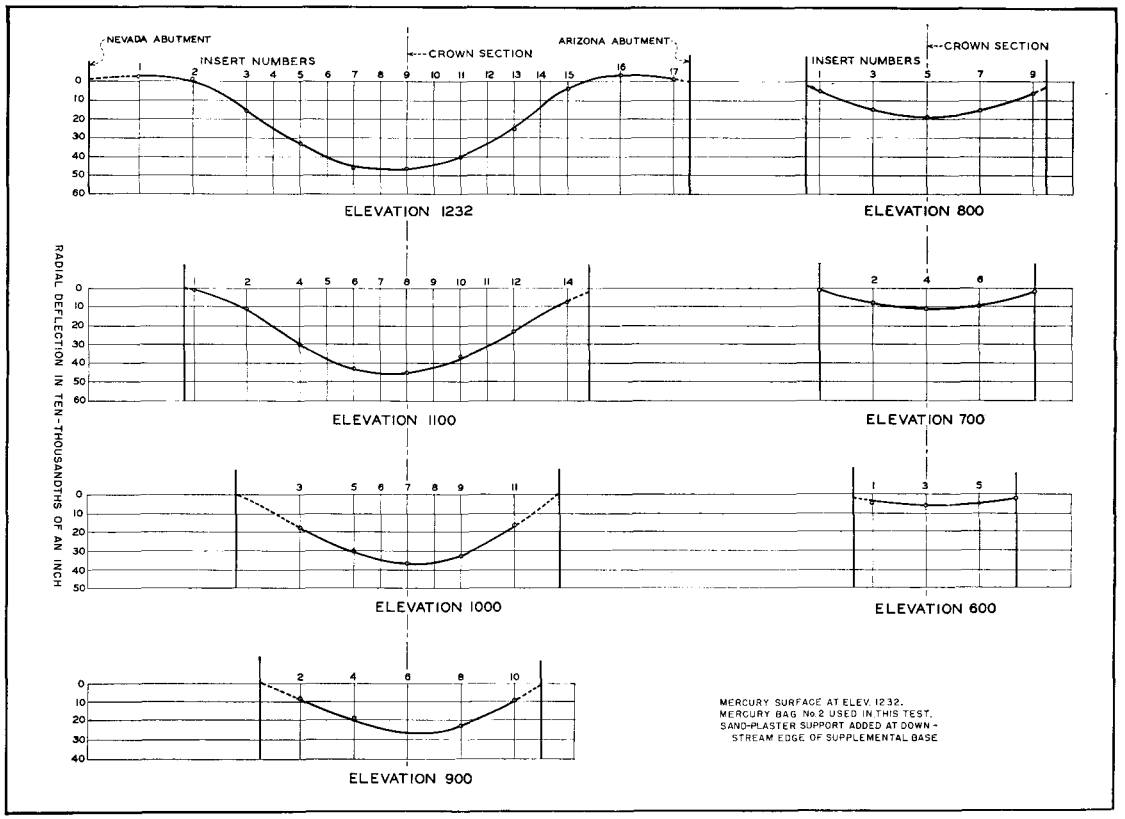

FIGURE 82—RADIAL DEFLECTIONS OF ARCH ELEMENTS, TEST 85

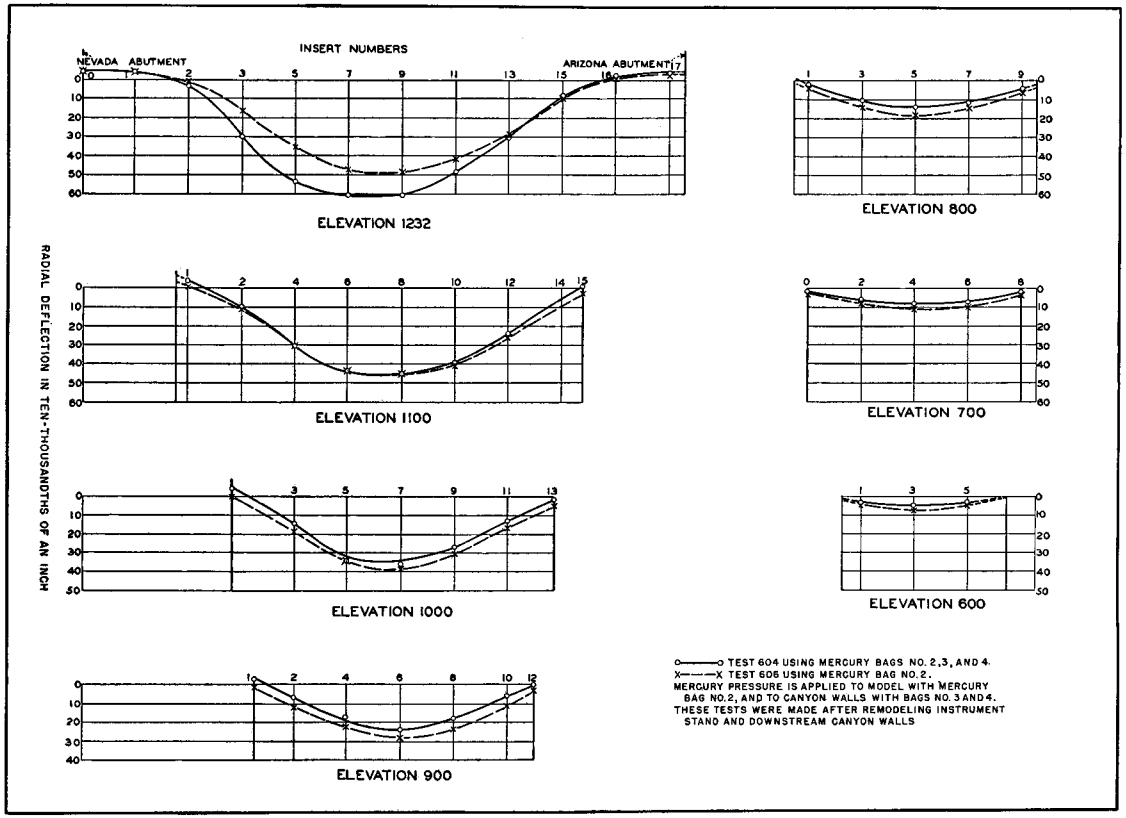

FIGURE 83—EFFECT OF CANYON WALL LOADS ON ARCH DEFLECTIONS, LOAD AT ELEVATION 1232

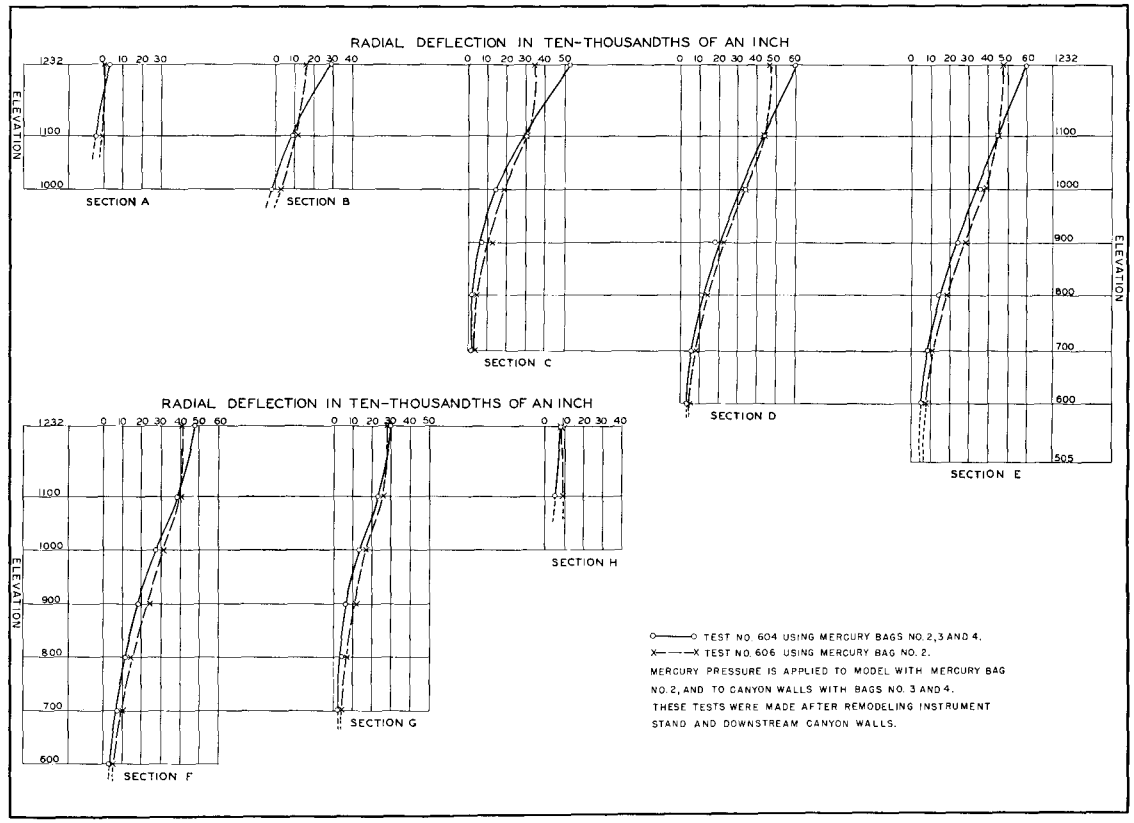

FIGURE 84—EFFECT OF CANYON WALL LOADS ON CANTILEVER DEFLECTIONS, LOAD AT ELEVATION 1232

causing reductions in deflection. The cantilever deflection curves show the stiffening effect of the upper arch elements. The resistance of the top arch produced negative loads on the cantilever elements, causing contraflexure in the cantilever deflection curves.

88. Partial Load and Overload Tests.—In conducting tests on the model, observations were begun with the load at elevation 1100 and increased by 50-foot increments to an overload at elevation 1400. Only results of minimum, normal, and maximum loads are presented in this report. Figures 85 and 86 show radial arch and cantilever deflections for loads at elevation 1100. Figures 87 and 88 show similar data for loads at elevation 1400. In all cases deflections are shown for both conditions of loading; that is, for loads at the upstream face of the model only, and for loads on the canyon walls as well as on the upstream face.

It should be noted that the difference between results with load on the model only, and combined load on the model and canyon walls, decreases as the depth of load increases. For load at elevation 1100, the canyon wall load doubled the radial deflection due to load on the model only, whereas, for load at 1400 the effect of canyon wall load was very slight. For load at elevation 1100 on the model only, it was observed that the deflection of the cantilever in the center portion of the model was greater at elevation 1100 than at 1232, indicating vertical tension in the upper portions of the cantilevers. This again was caused by the resistance of the top arch.

TANGENTIAL DEFLECTIONS

89. Methods of Making Tests.—In making tests for tangential deflections, dial gages were mounted to measure deflections of the top arch at the center line and deflections of the downstream face at elevations 800, 900, 1000, and 1100. The apparatus used in making tangential deflection measurements, shown in figure 79, required considerable space to adjust and operate. Consequently, it was not feasible to install gages for measuring tangential deflections below elevation 800.

The procedure used in making tangential deflection measurements was the same as in the radial deflection tests. It included tests for overload, normal load, and partial load conditions. Mercury load was first applied to the model and all gages read. Load was then applied to the canyon walls and the observations repeated. Overload

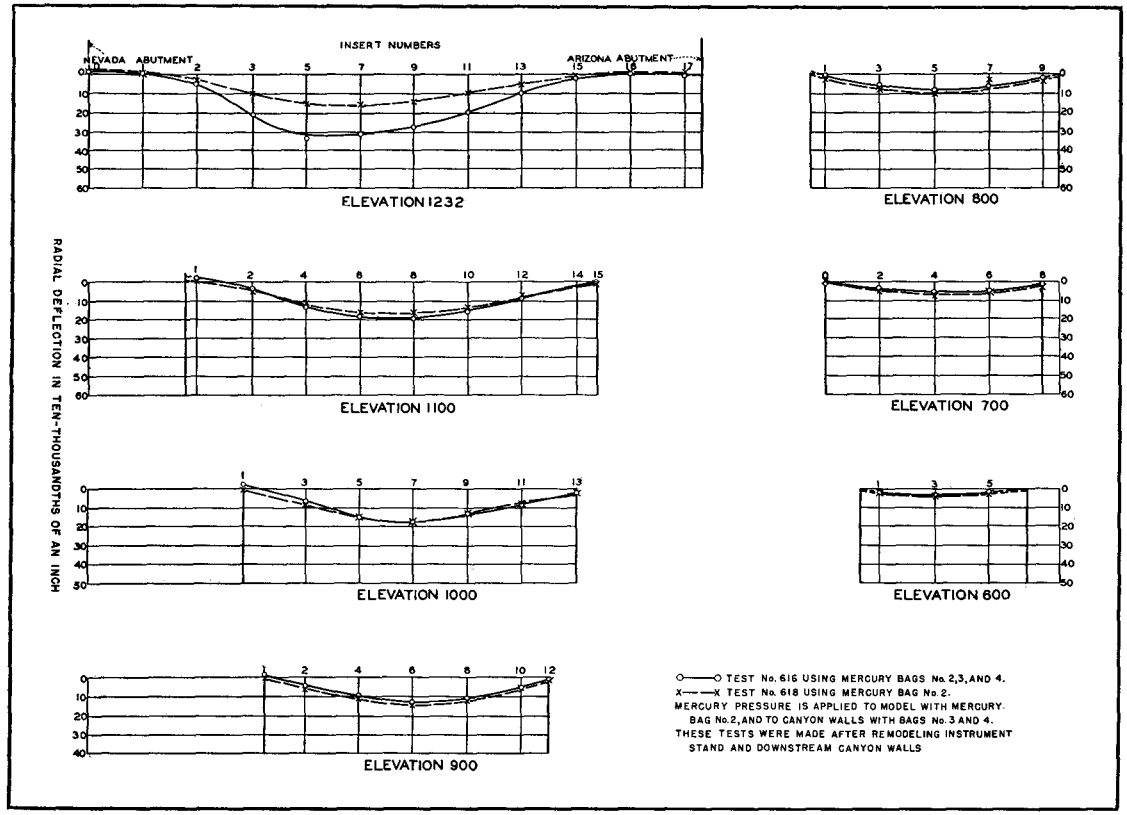

FIGURE 85—EFFECT OF CANYON WALL LOADS ON ARCH DEFLECTIONS, LOAD AT ELEVATION 1100

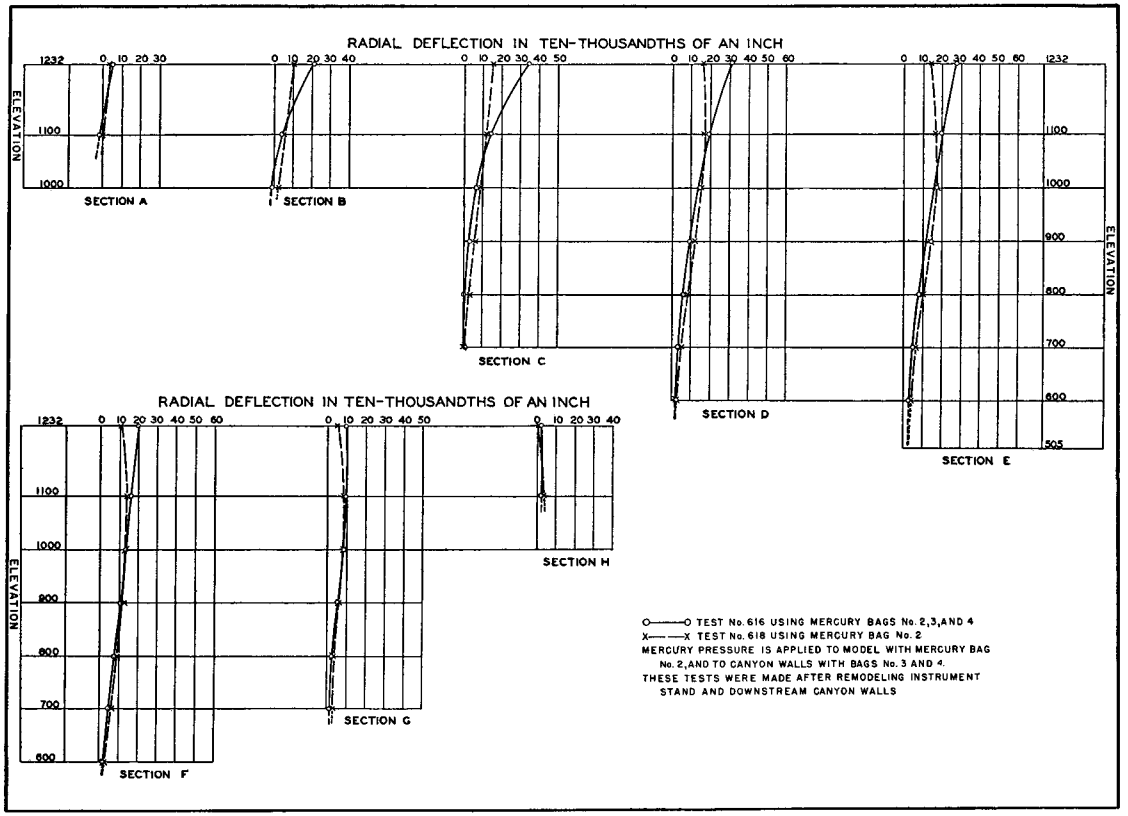

FIGURE 86—EFFECT OF CANYON WALL LOADS ON CANTILEVER DEFLECTIONS, LOAD AT ELEVATION 1100

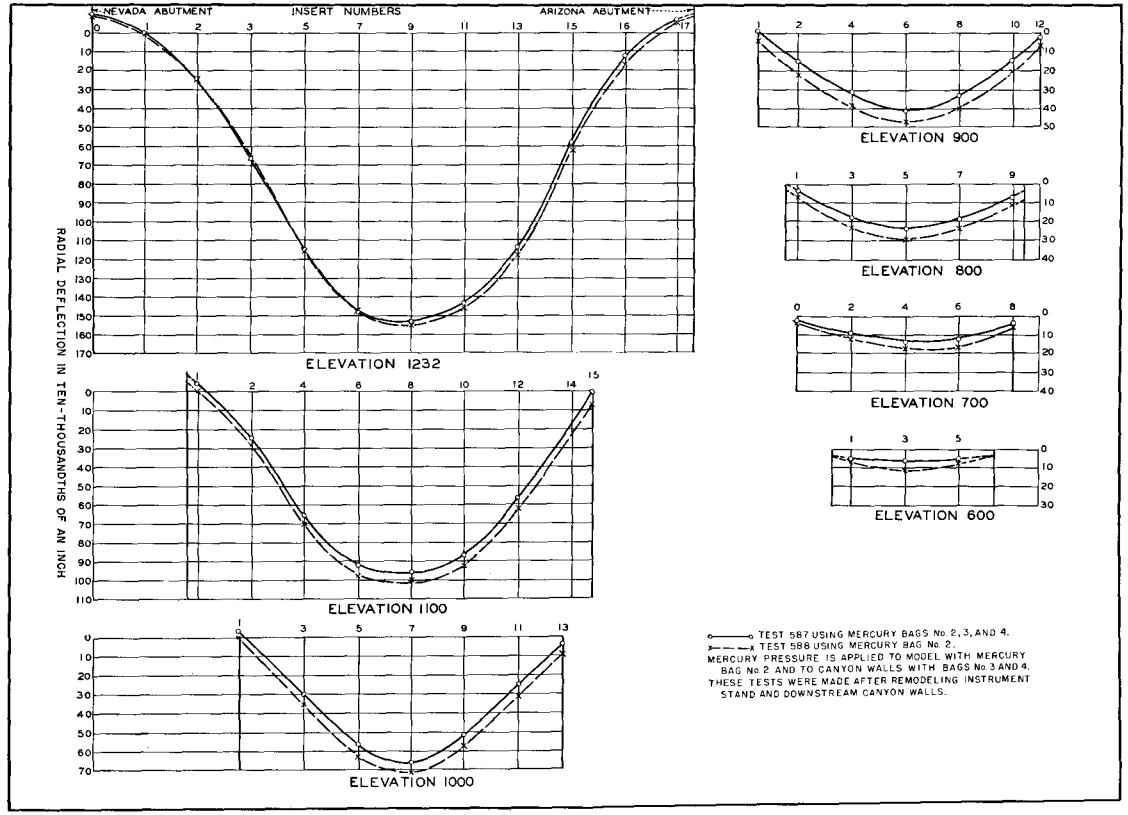

FIGURE 87—EFFECT OF CANYON WALL LOADS ON ARCH DEFLECTIONS, LOAD AT ELEVATION 1400

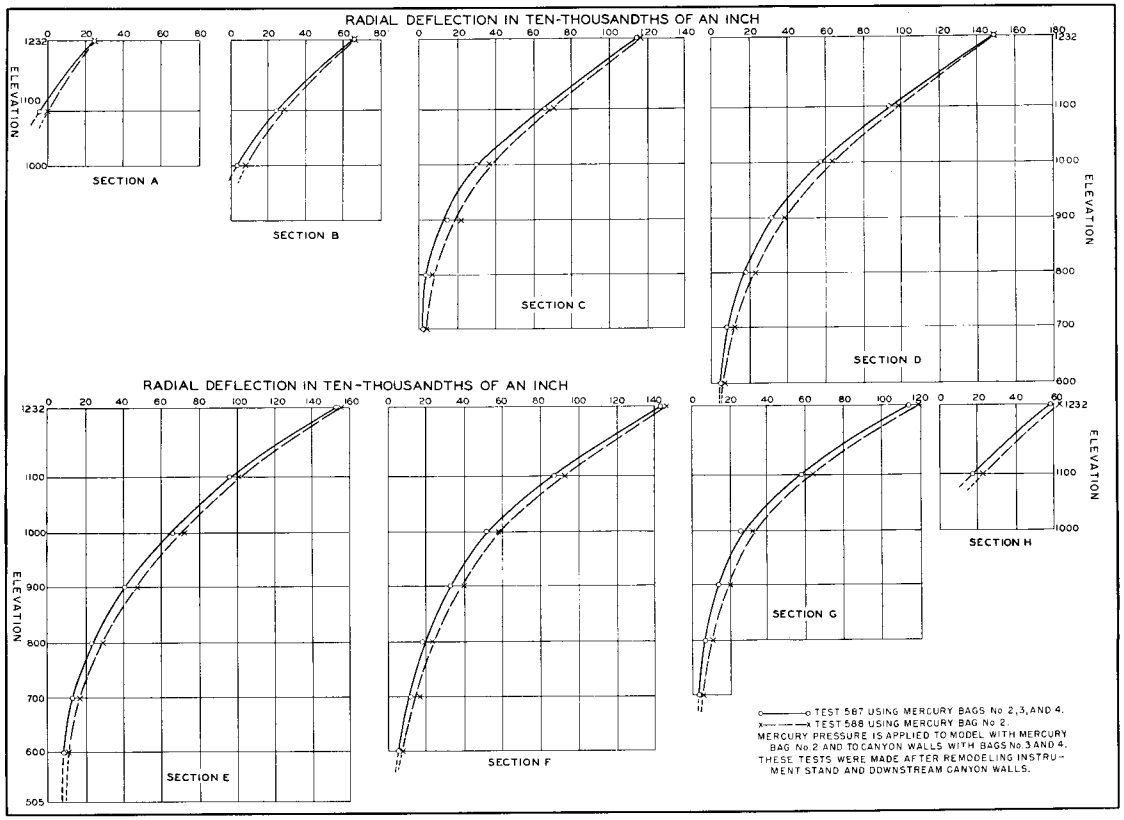

FIGURE 88—EFFECT OF CANYON WALL LOADS OF CANTILEVER DEFLECTIONS, LOAD AT ELEVATION 1400

tests were made with the surface of the mercury at elevations 1400, 1350, 1300, and 1250. Partial load tests were made with the surface of the mercury at elevations 1200, 1150, and 1100. When the surface of the mercury was below elevation 1100, tangential deflections were too small to measure satisfactorily.

90. Results of Tests.—There was but little difference in the results of tangential deflection tests for the two methods of loading. Generally, the tangential deflection was slightly greater when load was applied to the model alone. Results of tests made with the mercury surface at elevation 1400 are shown in figure 89. The maximum observed tangential deflection occured at elevation 1100 near the Arizona abutment and amounted to 0.0054 inches. On the Nevada side of the model, the deflection was somewhat smaller at this elevation, being 0.0048 inches.

The measured deflection curve of the arch element at elevation 1242 was characteristic of thin arches. The deflection was a maximum near the quarter points, and diminished toward the abutments. At lower elevations, where the arch elements were thicker, the maximum deflection occurred nearer the abutments.

Tangential deflections measured in normal load and partial load tests are shown in figures 90 and 91. The method of loading the model did not greatly affect the tangential deflection for normal load conditions. For partial loads some difference was noted, particularly when the mercury surface was at elevation 1100, see figure 91. The curves in figure 91 show that below elevation 1100 the tangential deflection was almost zero when the mercury pressure was applied to the model and to the canyon walls. By applying pressure to the model only, the deflection was increased considerably, the maximum deflection along the Arizona abutment being 0.0011 inches and along the Nevada abutment, 0.0008 inches. This observation confirms the previously mentioned conclusion that the canyon wall pressure caused a slight rotation of the abutments at the lower elevations.

SLOPE DEFLECTIONS

91. Apparatus.—Before making slope or angular deflection measurements of the model, it was necessary to develop a system for accurately measuring very small angular changes. After some experimenting, an optical lever system was developed which gave satis-

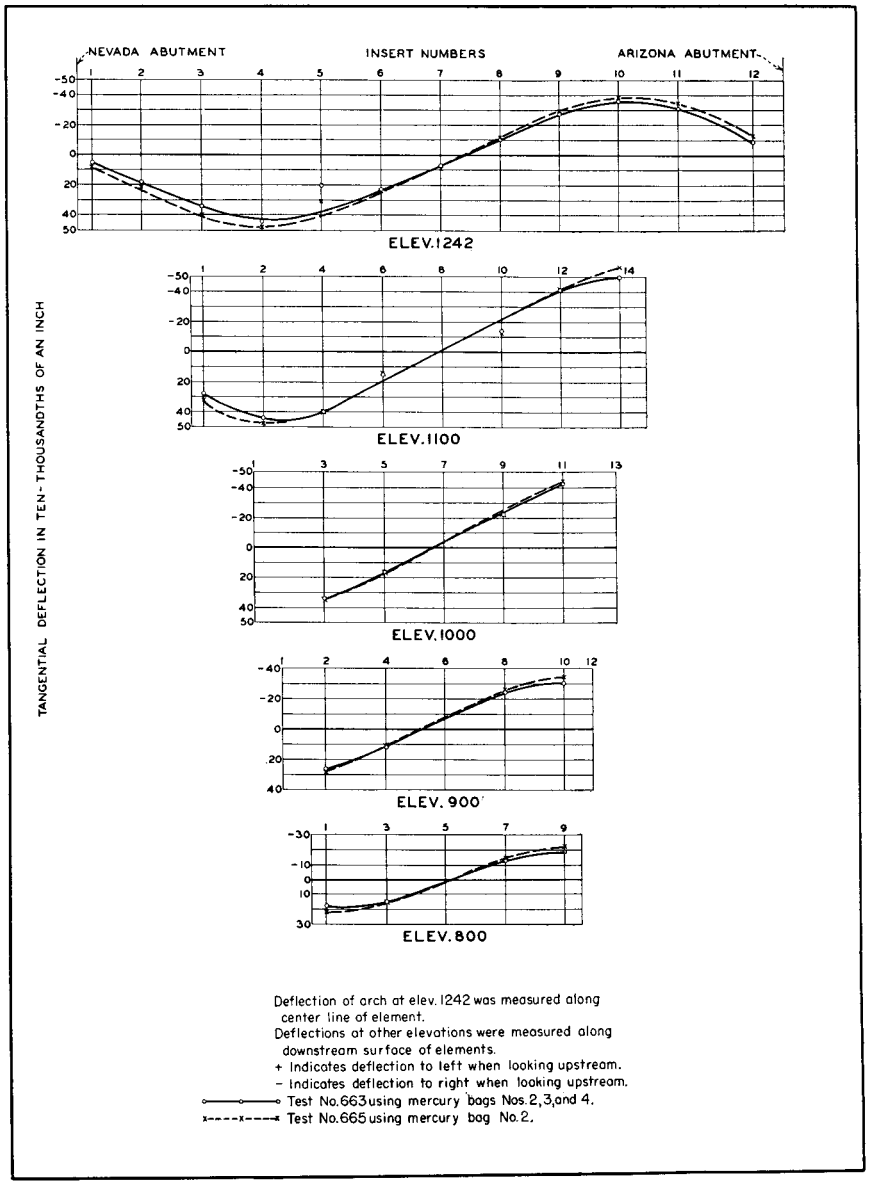

FIGURE 89—TANGENTIAL DEFLECTIONS OF ARCH ELEMENTS, LOAD AT ELEVATION 1400

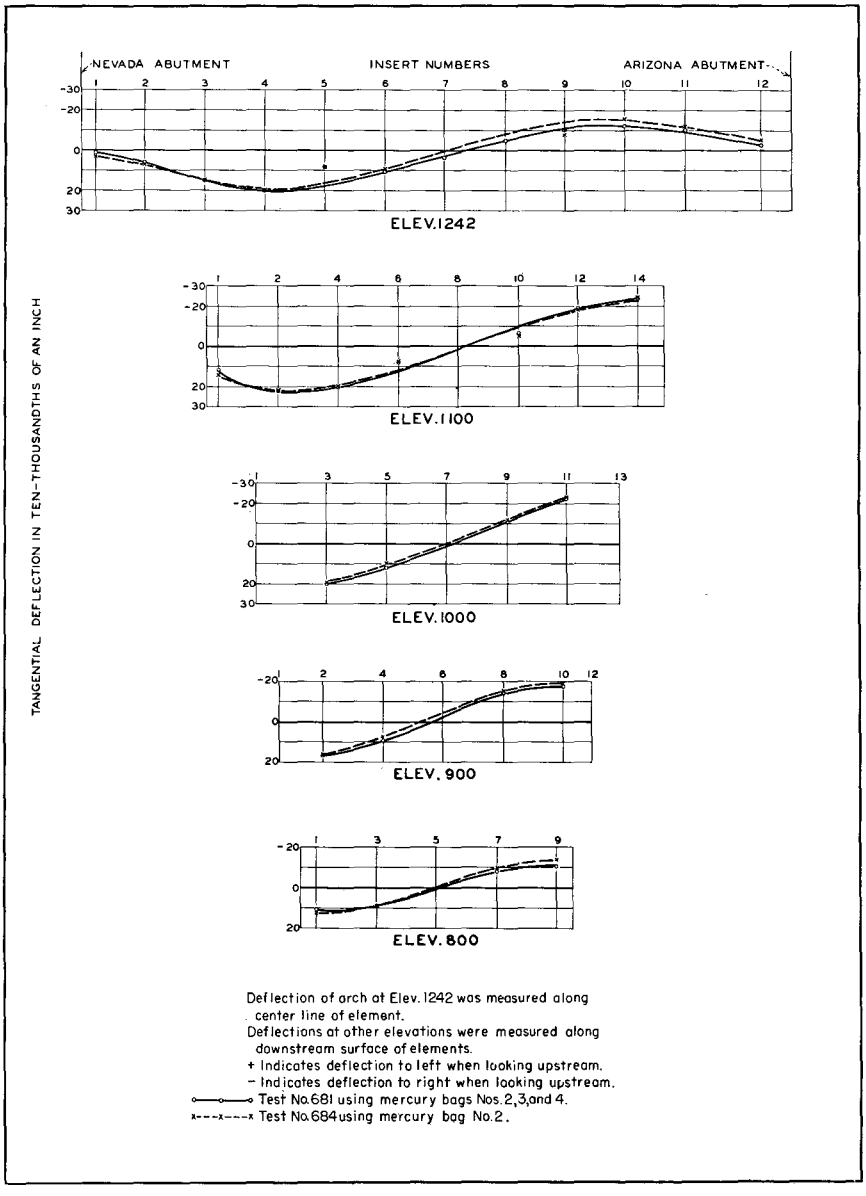

FIGURE 90—TANGENTIAL DEFLECTIONS OF ARCH ELEMENTS, LOAD AT ELEVATION 1232

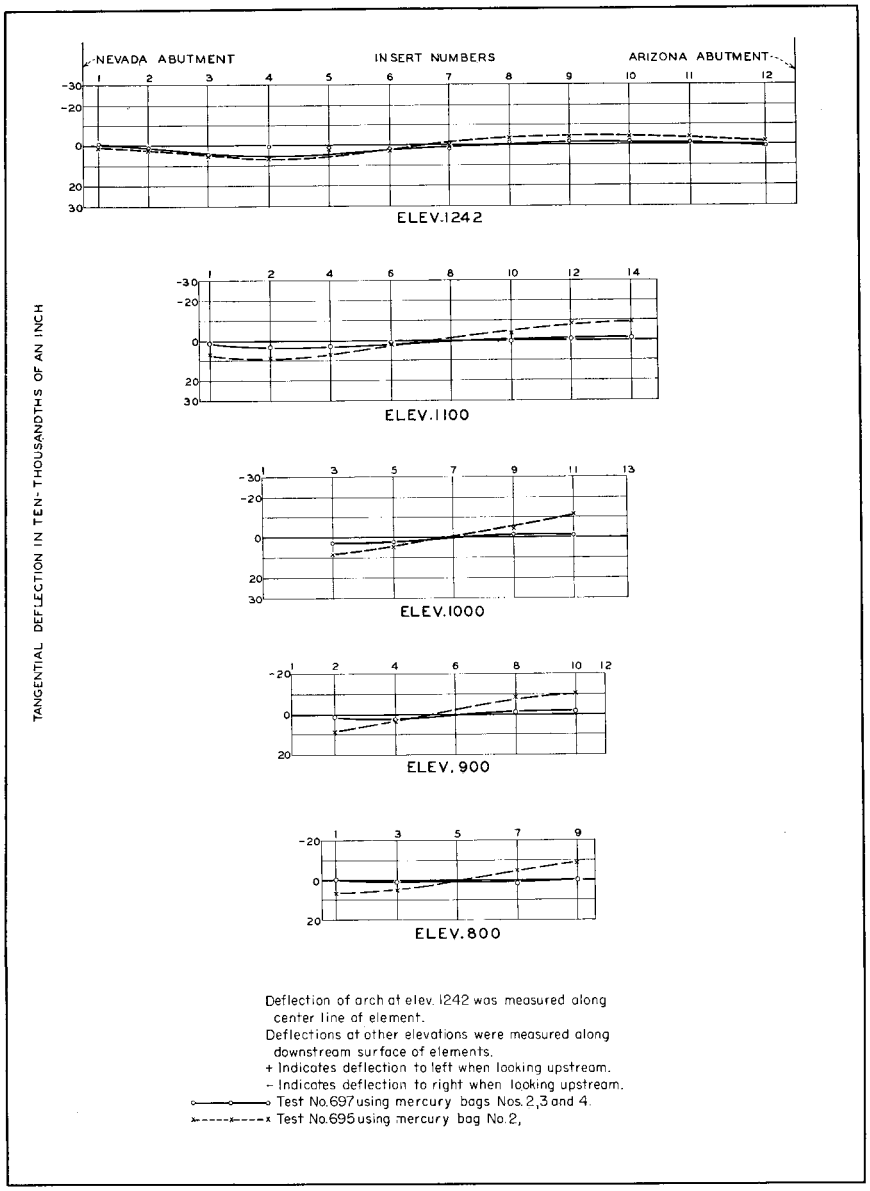

FIGURE 91—TANGENTAL DEFLECTIONS OF ARCH ELEMENTS, LOAD AT ELEVATION 1100

factory results. The apparatus consisted of an engineer's scale, a transit having a telescope of good quality, and mirrors having very flat surfaces.

The transit was mounted on a concrete pedestal in one corner of the testing room. A number 50 engineer's scale, having a white celluloid face, was clamped to the pedestal in front of the transit and perpendicular to its line of sight. Optical flats, ground to a tolerance of 0.000,003 inches, were obtained for use as mirrors. These were mounted on trunnions supported by a fork which was attached to inserts at the downstream face of the model.

92. **Principle of Operation.**—The principle of operation of the optical lever system used in these tests is based on the fact that the angle which an incident ray of light makes with the plane of a mirror is equal to the angle of the reflected ray. The incident ray was the line of sight from the telescope to the mirror, and the reflected ray was the reflection of the scale. Therefore, when the mirror rotated through a certain angle, the reflected ray was rotated through twice that angle, and the apparent movement of the image of the scale across the cross-hair of the telescope was equivalent to the tangent of twice the angle of rotation of the mirror.

Actually, the mirror rotated through an unknown angle about an unknown axis. The mirror registered only the component of the rotation about an axis in the plane of the mirror. Rotations about axes normal to the face of the mirror produced no apparent movement of the scale. Since the scale was in a horizontal position, the angle measured was the angle which had an axis within the plane of the mirror, the direction of the axis being normal to the direction of the scale. By an extension of the stem of the mirror, it was possible to mount the mirror so that the actual angle measured was about a vertical axis through the point of support. Due to the relatively small readings obtained, it was necessary to apply small corrections to the computed angles caused by the displacement of the mirror. Using a 50 scale, readings to the nearest 0.01 of an inch were possible. With a distance of 150 inches from the scale to the mirror, a sensitivity of $0.01/(150\times2)$, or 0.000,033 radians was obtained.

93. **Results of Tests.**—Results of slope deflection tests are shown in figures 92 to 94, inclusive. As in radial and tangential deflection tests, slope deflection measurements were made for overload, normal load, and partial load conditions for both methods of load applica-

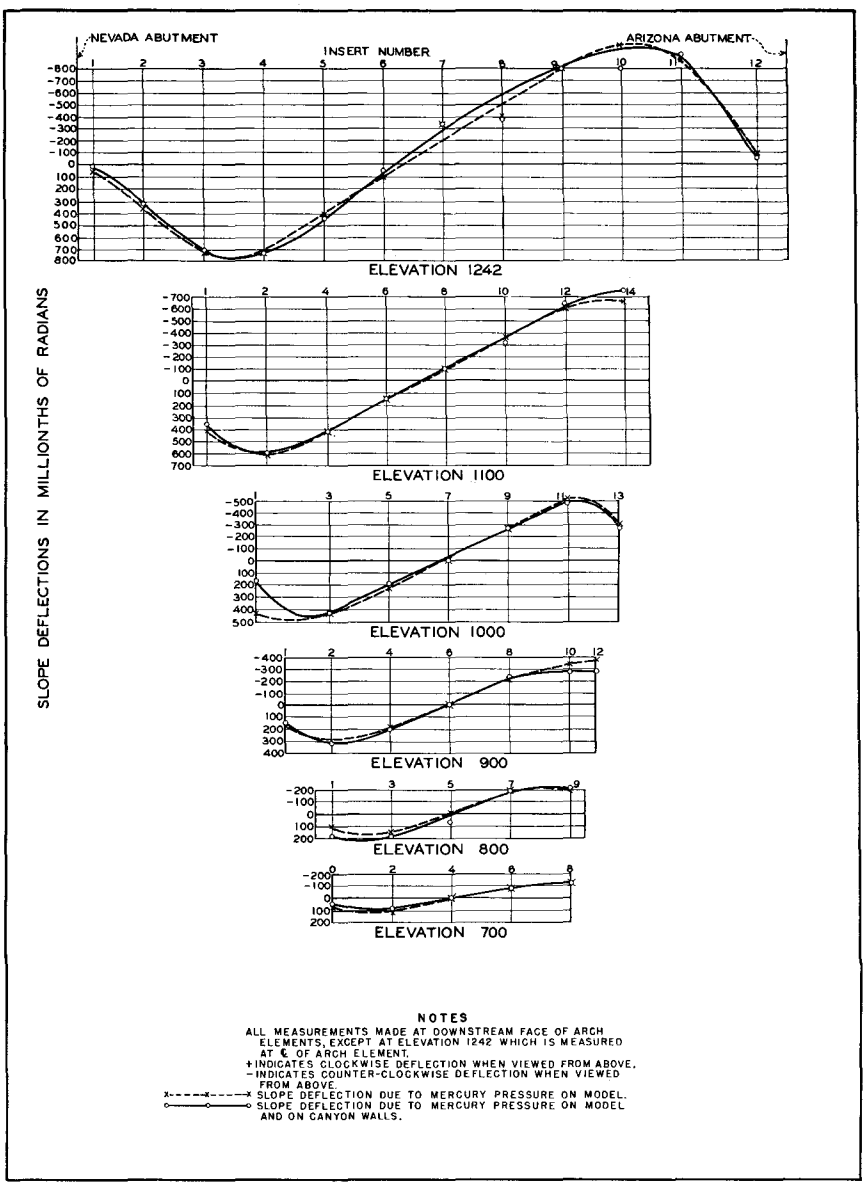

FIGURE 92—SLOPE DEFLECTIONS OF ARCH ELEMENTS, LOAD AT ELEVATION 1400

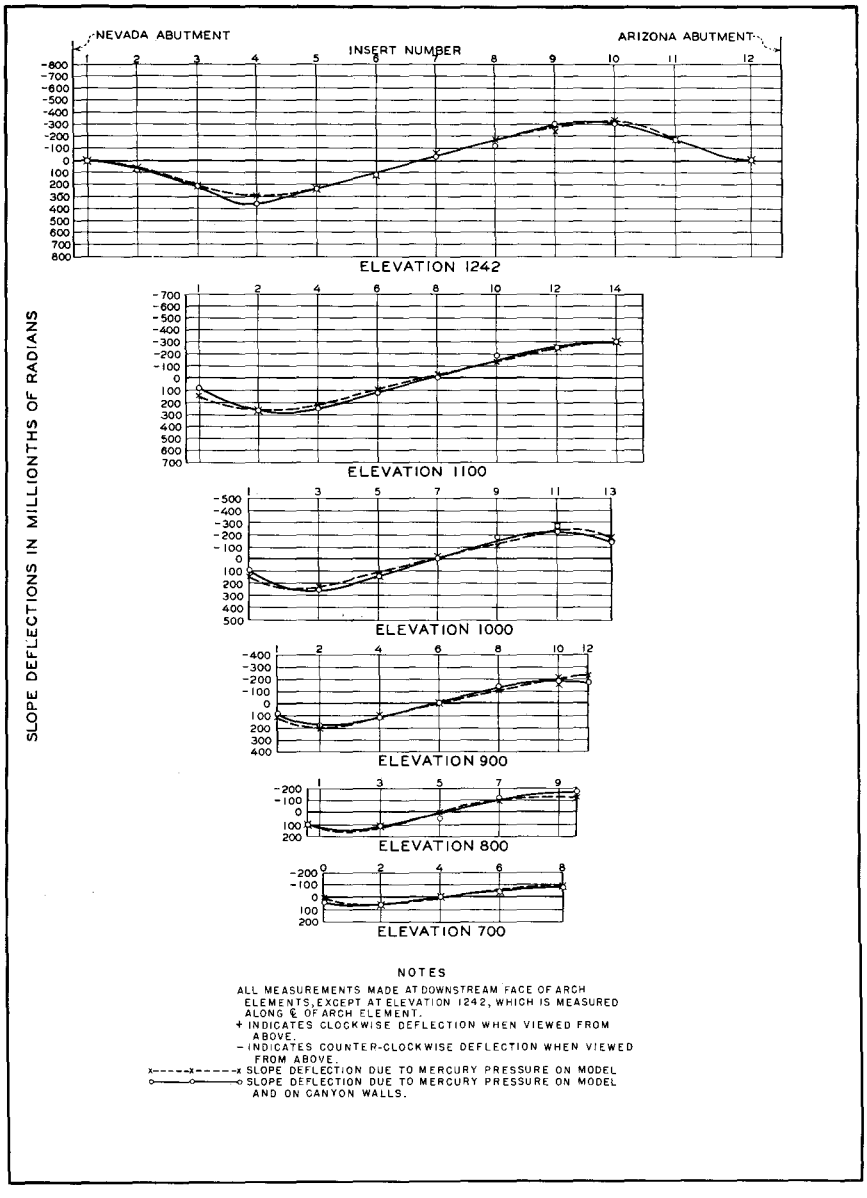

FIGURE 93—SLOPE DEFLECTIONS OF ARCH ELEMENTS, LOAD AT ELEVATION 1232

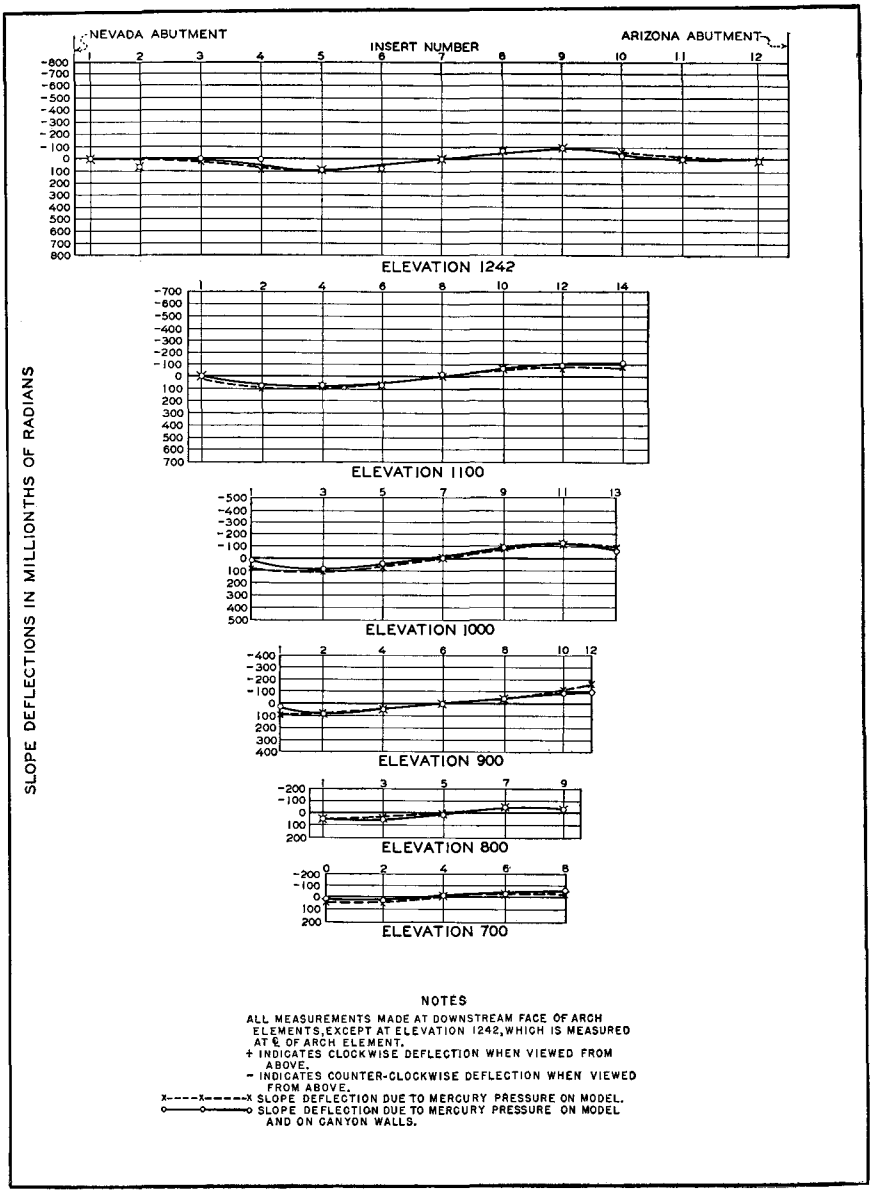

FIGURE 94—SLOPE DEFLECTIONS OF ARCH ELEMENTS, LOAD AT ELEVATION 1100

tion. Overload tests were made with the mercury surface at elevations 1400, 1350, 1300, and 1250; but results for overload at 1400 only are included in this report. The two methods of loading the model caused only small differences in deflection curves.

When the surface of the mercury load was at elevation 1232, the deflection curves were nearly symmertical, as shown in figure 93. The maximum deflection occurred at elevation 1242, at insert 4 on the Nevada side. At the corresponding point on the Arizona side, the deflection was only slightly smaller. The deflection decreased to zero at the abutments at this elevation. At lower elevations the deflections decreased, but were still measurable. Slope deflections for load at elevation 1100, given in figure 94, show the same general characteristics as the normal load tests. Maximum rotations at elevations 1242, 1100, and 1000 were practically the same.

The position of the line of zero slope on the downstream face of the model varied with the elevation of the mercury surface. For partial mercury loads, the line of zero slope was at approximately the center of the canyon. For normal and overload conditions the line of zero slope shifted slightly toward the Nevada side.

MATHEMATICAL BASIS FOR STRAIN MEASUREMENTS

94. Stress-Strain Relations.—Systematic measurements of strains were made at the downstream face of the model. Stresses were computed from the strain measurements, using stress-strain relations developed by the theory of elasticity. A summary of the development of these relations is presented.

The magnitude and direction of principal strains at a point may be found by using the relation between principal strains and a given strain.

$$\epsilon = \epsilon_x \cos^2 \theta + \epsilon_y \sin^2 \theta \qquad (1)$$

where

ϵ is the linear strain in the given direction.

ϵ_x is the algebraically maximum principal strain.

ϵ_y is the algebraically minimum principal strain.

θ is the angle between the direction of ϵ and the direction of ϵ_x, measured from ϵ to ϵ_x.

An alternate form for this equation is:

$$\epsilon = \tfrac{1}{2}(\epsilon_x + \epsilon_y) + \tfrac{1}{2}(\epsilon_x - \epsilon_y)\cos 2\theta \qquad (2)$$

The three quantities, ϵ_x, ϵ_y, and θ involved in the determination of principal strains at a point may be found by measuring linear strains along three or more gage lines of known directions intersecting at the point. These strain measurements also furnish data for computing arch and cantilever stresses as well as shearing stresses on horizontal and vertical planes.

95. Equations for Principal Strains.—Take the measured strain ϵ_H as the reference direction, and the measured strains ϵ_D and ϵ_V making angles of 45 and 90 degrees respectively with ϵ_H. Let θ be the angle from ϵ_H to ϵ_x. ϵ_D and ϵ_V then make angles of $(45 - \theta)$ and $(90 - \theta)$ degrees respectively with ϵ_x, measured from ϵ_x to ϵ_D and ϵ_V. Successive substitution of these angles in equation 2 gives:

$$\epsilon_H = \tfrac{1}{2}(\epsilon_x + \epsilon_y) + \tfrac{1}{2}(\epsilon_x - \epsilon_y)\cos 2\theta \qquad (3)$$

$$\epsilon_D = \tfrac{1}{2}(\epsilon_x + \epsilon_y) + \tfrac{1}{2}(\epsilon_x - \epsilon_y)\sin 2\theta \qquad (4)$$

$$\epsilon_V = \tfrac{1}{2}(\epsilon_x + \epsilon_y) - \tfrac{1}{2}(\epsilon_x - \epsilon_y)\cos 2\theta \qquad (5)$$

Equations 3, 4, and 5 reduce to:

$$\epsilon_x + \epsilon_y = \epsilon_H + \epsilon_V \qquad (6)$$

$$\epsilon_x - \epsilon_y = (\epsilon_H - \epsilon_V)\sec 2\theta \qquad (7)$$

$$\tan 2\theta = \frac{2\epsilon_D - \epsilon_H - \epsilon_V}{\epsilon_H - \epsilon_V} \qquad (8)$$

The magnitude and direction of principal strains may be readily obtained from equations 6, 7, and 8.

96. Stress-Strain Equations.—A stress σ_H acting on a vertical plane is accompanied by a horizontal strain ϵ_H whose magnitude is $\frac{\sigma_H}{E}$, and also by a vertical strain whose magnitude is $\frac{-\mu\sigma_H}{E}$. The factor μ denotes Poisson's ratio and the minus sign indicates that the sign of the transverse strain is opposite to that of the stress which produces it. In like manner a stress σ_V on a horizontal plane is accompanied by a vertical strain equal to $\frac{\sigma_V}{E}$ and a horizontal strain equal

to $\frac{-\mu\sigma_V}{E}$. The linear strains which accompany shear stresses are of the order of infinitesimals as long as the requirements imposed by elastic action and Hooke's law are met. If horizontal and vertical normal stresses and shear stresses occur simultaneously, the accompanying strains, by superposition, are:

$$\epsilon_H = \frac{\sigma_H}{E} - \frac{\mu\sigma_V}{E} \tag{9}$$

$$\epsilon_V = \frac{\sigma_V}{E} - \frac{\mu\sigma_H}{E} \tag{10}$$

The equations for stresses in terms of strains are:

$$\sigma_H = \frac{E}{1-\mu^2}(\epsilon_H + \mu\epsilon_V) \tag{11}$$

$$\sigma_V = \frac{E}{1-\mu^2}(\epsilon_V + \mu\epsilon_H) \tag{12}$$

The expression $\frac{E}{1-\mu^2}$ is often called the plate modulus and designated by the symbol E'. The foregoing equations were derived for stresses in a plane. Assuming that the curvature between adjacent inserts can be neglected, the equations are also applicable to surface stresses at the downstream face of the model. The horizontal and vertical designations for strain measurements were chosen for convenience in the computation of arch and cantilever strains and stresses, although in the case of the cantilever elements, the strains and stresses may be along inclined directions instead of vertical.

If reference directions in the foregoing analysis are taken to coincide with the directions of principal strains and stresses, equations giving principal stresses in terms of principal strains are obtained. These equations are:

$$\sigma_x = \frac{E}{1-\mu^2}(\epsilon_x + \mu\epsilon_y) \tag{13}$$

$$\sigma_y = \frac{E}{1-\mu^2}(\epsilon_y + \mu\epsilon_x) \tag{14}$$

The shear stress τ on a horizontal plane may be found by setting up the equation for equilibrium in the horizontal direction, using the forces acting on a small triangular wedge of unit thickness, bounded by a horizontal plane and by planes parallel to the directions of the

two principal stresses. If the side parallel to σ_y be denoted by dy, the side parallel to σ_x be denoted by dx, and the angle between the horizontal distances ds and dx be denoted by θ, then

$$\tau ds = \sigma_x \cos\theta\, dy - \sigma_y \sin\theta\, dx \qquad (15)$$

or

$$\tau = \frac{1}{2}(\sigma_x - \sigma_y) \sin 2\theta \qquad (16)$$

If the shearing modulus of elasticity, $\frac{E}{2(1+\mu)}$, is denoted by G, shearing stresses may be calculated directly from strain measurement by the relation:

$$\tau = (2\epsilon_D - \epsilon_H - \epsilon_V)G \qquad (17)$$

If a square of unit thickness be placed in the first quadrant with respect to the H and V axes, and the edges subjected to the normal stresses σ_H and σ_V, respectively, and to a shear stress τ_{HV}, then positive shear will be that which causes a lengthening of the positive diagonal of the square.

APPARATUS FOR STRAIN MEASUREMENTS

97. Strain Gages.—In constructing the model, small anchors had been cast in the downstream face for attaching invar steel rods required in making deflection measurements. It was desired to use these anchors in attaching apparatus for making strain measurements so as to avoid installing additional inserts at the downstream face.

Several types of hand-operated strain gages were available in the laboratory, but were unsuitable since they required additional inserts for mounting. Furthermore, the working space in front of the model was limited and it was difficult for an observer to reach the lower elevations with a strain gage. After some experimenting, it was found that by mounting dial gages, reading to 0.0001 of an inch, on short invar rods between pairs of existing anchors, strains at the downstream face could be readily measured. By this method strains could be measured in four desired directions over most of the downstream face. Since the upstream face was covered with the rubber mercury bag, no strain measurements could be made at upstream locations.

98. Mounting Strain Gages.—The method of mounting dial gages between pairs of anchors is shown in figure 95. Invar steel rods were cut to the proper lengths and threaded so they could be attached to plates which were fastened to the anchors with small screws. The dial gage was mounted on a rod attached to one anchor and allowed to bear against the polished end of the rod attached to the other anchor. Any deformation occurring between the two anchors was indicated by the change in the reading of the gage. The average unit strain could then be computed by dividing the gage reading by the gage length. Peak strains occurring in small areas were not obtainable with this system of measurements because of the relatively long gage lines.

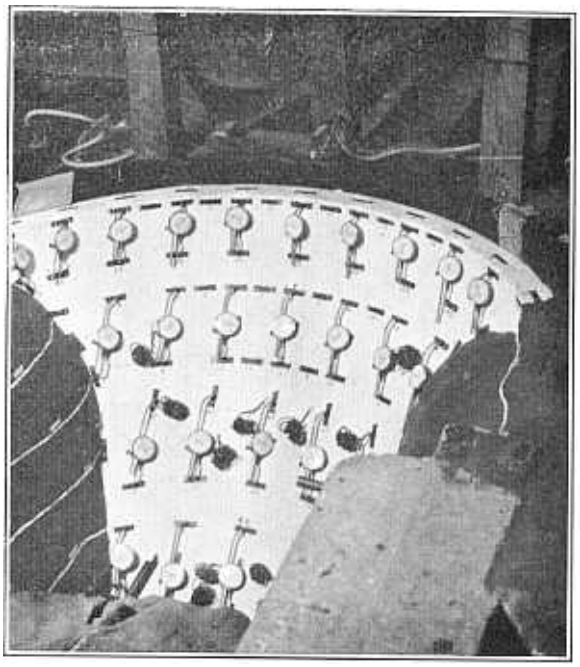

FIGURE 95—GAGES SET TO MEASURE CANTILEVER STRAINS

99. Gage Lines.—The usual arrangement for a set of strain measurements at a particular location included a square with gage lines forming the boundary and diagonal gage lines crossing at the center. A more ideal arrangement would have been for all gage lines to cross at a point, but with the existing arrangement of anchors, this was possible only in a few locations. However, by plotting smooth, continuous curves for each component of strain, the four components

required for computing stresses at a point were readily obtained. Special computations were necessary where gage lines made odd angles. Due to the curved face of the dam, gage lines were actually skewed at all locations except the center. Angles were measured with respect to the developed downstream face. In order to simplify the work, stresses were also plotted with respect to the developed face. Unit strains, however, were calculated with respect to actual lengths of gage lines.

Before calculating stresses from unit strains, the relationship between strain components at points where the gage lines intersected at 45-degree angles were checked by the equation

$$\epsilon_V + \epsilon_H = \epsilon_D + \epsilon_d \qquad (18)$$

Any discrepancies found were adjusted to make the strains fulfill the requirement of equation 18 before stresses were calculated.

RESULTS OF STRAIN MEASUREMENTS

100. Arch Strains.—Measured horizontal or arch strains for overload, normal, and partial load tests are shown in figures 96, 97, and 98. Two diagrams are shown in each figure, so that the effect of reservoir pressure on the canyon walls can be seen. Applying reservoir pressure to the canyon walls increased the arch strains slightly for overload conditions, as may be seen by referring to figure 96. At the Arizona abutment, between elevation 1100 and the top of the model, maximum compressive strains were increased from 400 to 425 millionths of an inch per inch. At cantilever section E, between elevations 800 and 900, maximum tensile strains were increased from 100 to 125 millionths of an inch per inch. Slight changes in position of strain contours were noted in other parts of the model, but the magnitudes of the strains were virtually unchanged.

Measured horizontal strains, with the mercury surface at elevation 1232, are shown in figure 97. As in the case of the overload tests, the effect of applying reservoir pressure to the canyon walls was to increase maximum strains. With the load applied to the model only, the maximum compressive strain of 175 millionths of an inch per inch occurred along the Arizona abutment between elevations 1100 and 1200. Applying reservoir pressure to the canyon walls increased this strain to 200 millionths of an inch per inch at the same location. The maximum tensile strain was the same for the two systems of loading, being 75 millionths of an inch per inch. When pressure was applied to the model only, the maximum tensile strain occurred be-

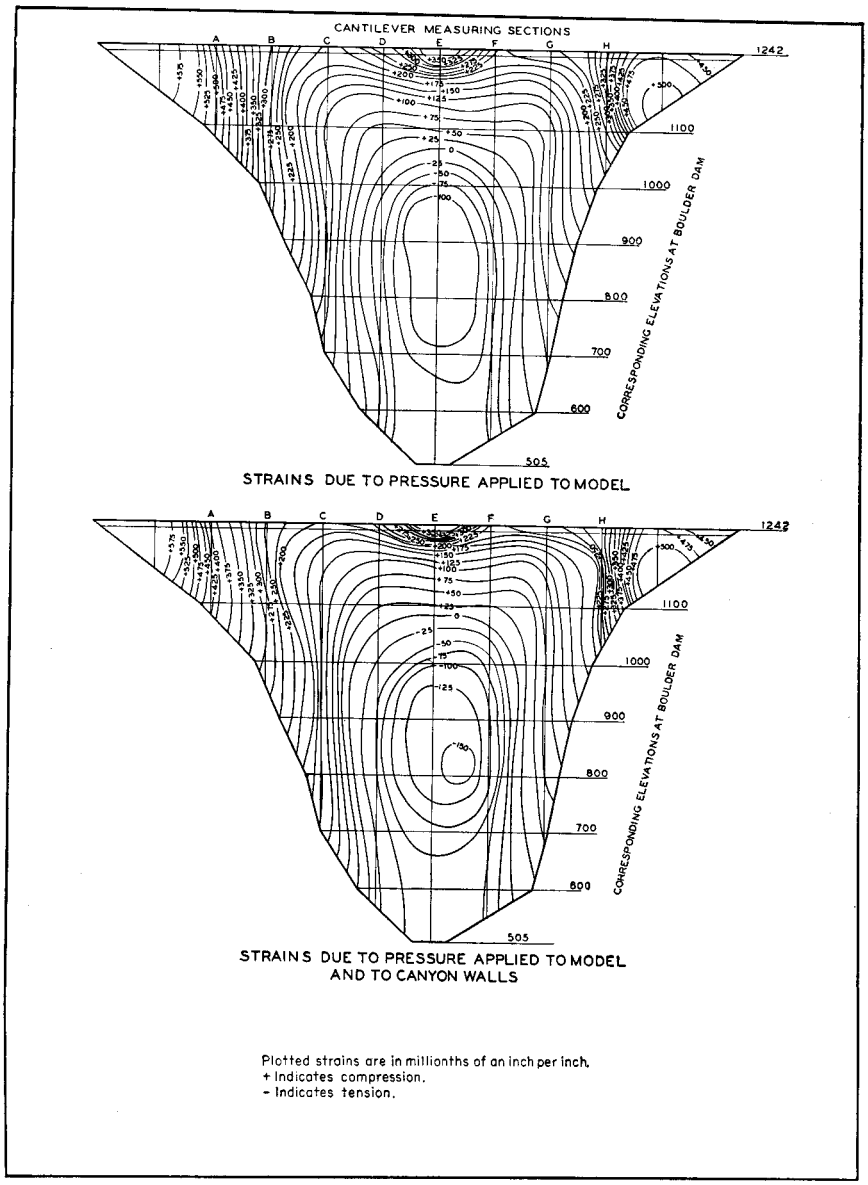

FIGURE 96—ARCH STRAINS AT DOWNSTREAM FACE, LOAD AT ELEVATION 1400

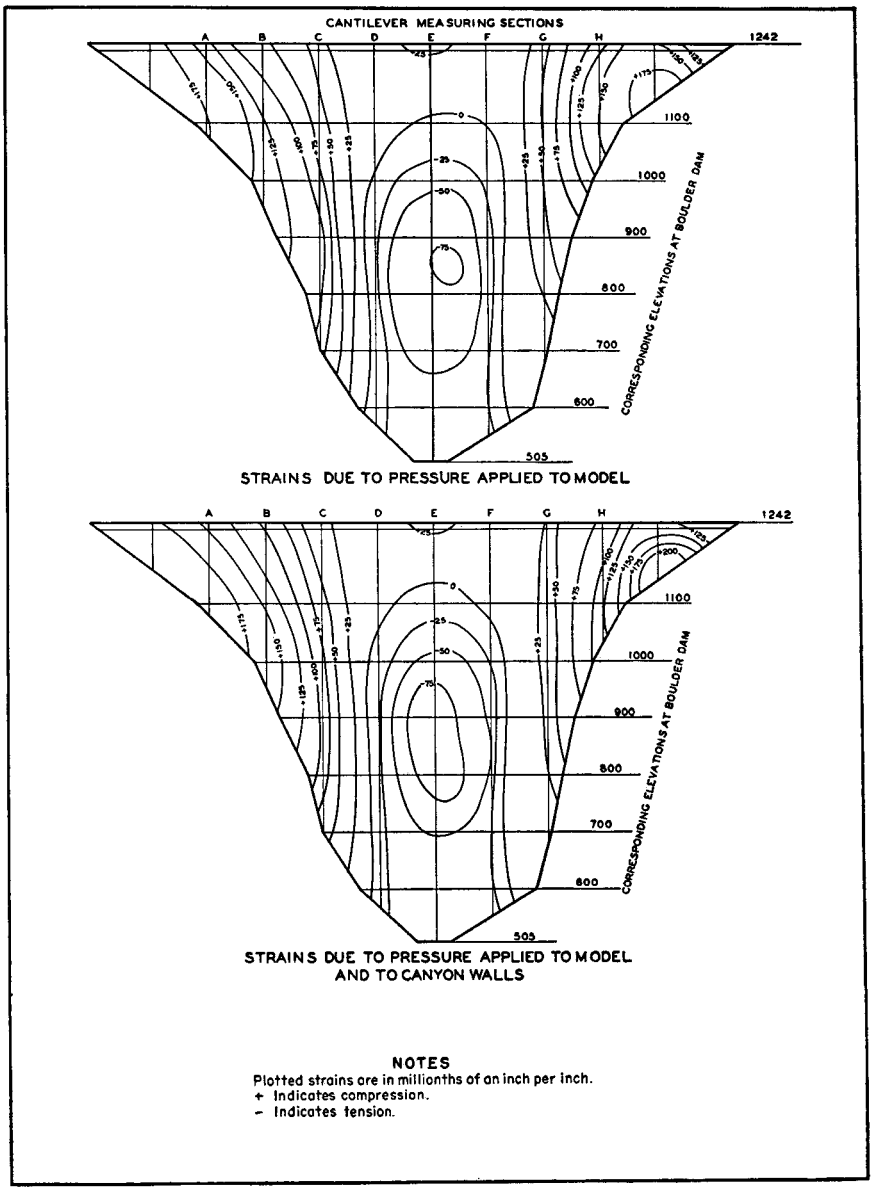

FIGURE 97—ARCH STRAINS AT DOWNSTREAM FACE, LOAD AT ELEVATION 1232

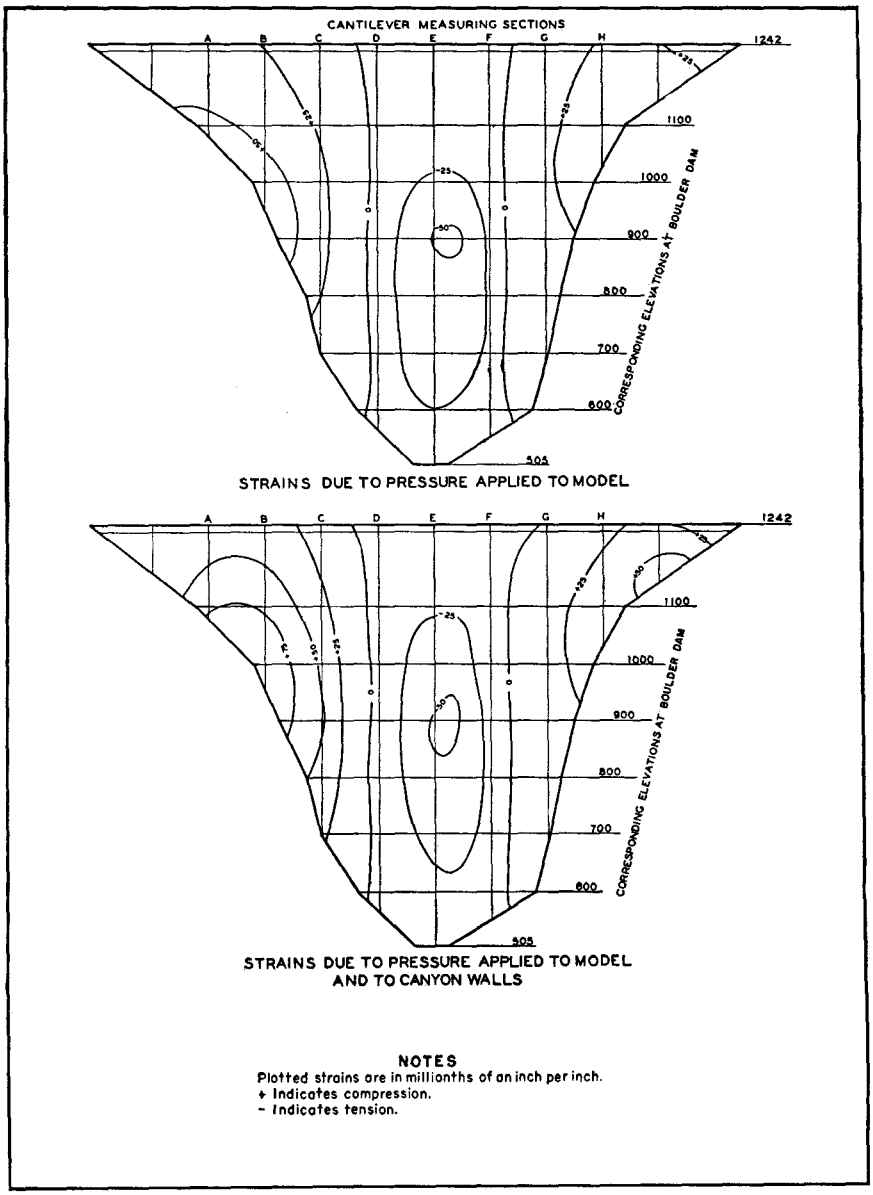

FIGURE 98—ARCH STRAINS AT DOWNSTREAM FACE, LOAD AT ELEVATION 1100

tween cantilever sections E and F and extended from elevation 825 to elevation 875. The area of the maximum tensile strain increased when the reservoir pressure was applied to the canyon walls. The area was almost symmetrical about cantilever section E. It was about five inches wide and extended from elevation 760 to elevation 960.

Horizontal strains with the mercury surface at elevation 1100 are shown in figure 98. The effect of reservoir pressure on the canyon walls was to increase maximum compressive strains slightly along the Arizona abutment between elevations 1125 and 1200, and along the Nevada abutment between elevations 875 and 1100. The distribution and magnitude of tensile strains were virtually unchanged by the two methods of loading.

101. Cantilever Strains.—Measured cantilever strains are shown in figures 99, 100, and 101. For the overload condition, shown in figure 99, effects of reservoir pressure on the canyon walls reduced the compressive strain from 100 to 75 millionths of an inch per inch at the base of the model adjacent to the canyon walls. The maximum compressive strain was 250 millionths of an inch per inch for both systems of loading. This strain was observed between elevations 1000 and 1100 near both abutments.

Cantilever strains observed with the mercury surface at elevation 1232 are shown in figure 100. Applying reservoir pressure to the canyon walls decreased the area of tensile strains at the top of the model slightly, and increased the area of maximum compressive strains between cantilever sections D and G and elevations 750 and 950. Strains for load at elevation 1100 were rather small and there was no great difference in either magnitude or distribution of strains caused by the two systems of loading.

102. Diagonal Strains.—Results of diagonal strain measurements are shown in table 2. Tabular values refer to gage lines on figure 102. These strains were used in the calculation of principal strains and stresses.

STRESSES COMPUTED FROM STRAINS

103. Arch Stresses.—Arch stresses computed from strain measurements are shown in figures 103, 104, and 105. The maximum compressive stress for load at elevation 1400 was 60 pounds per square

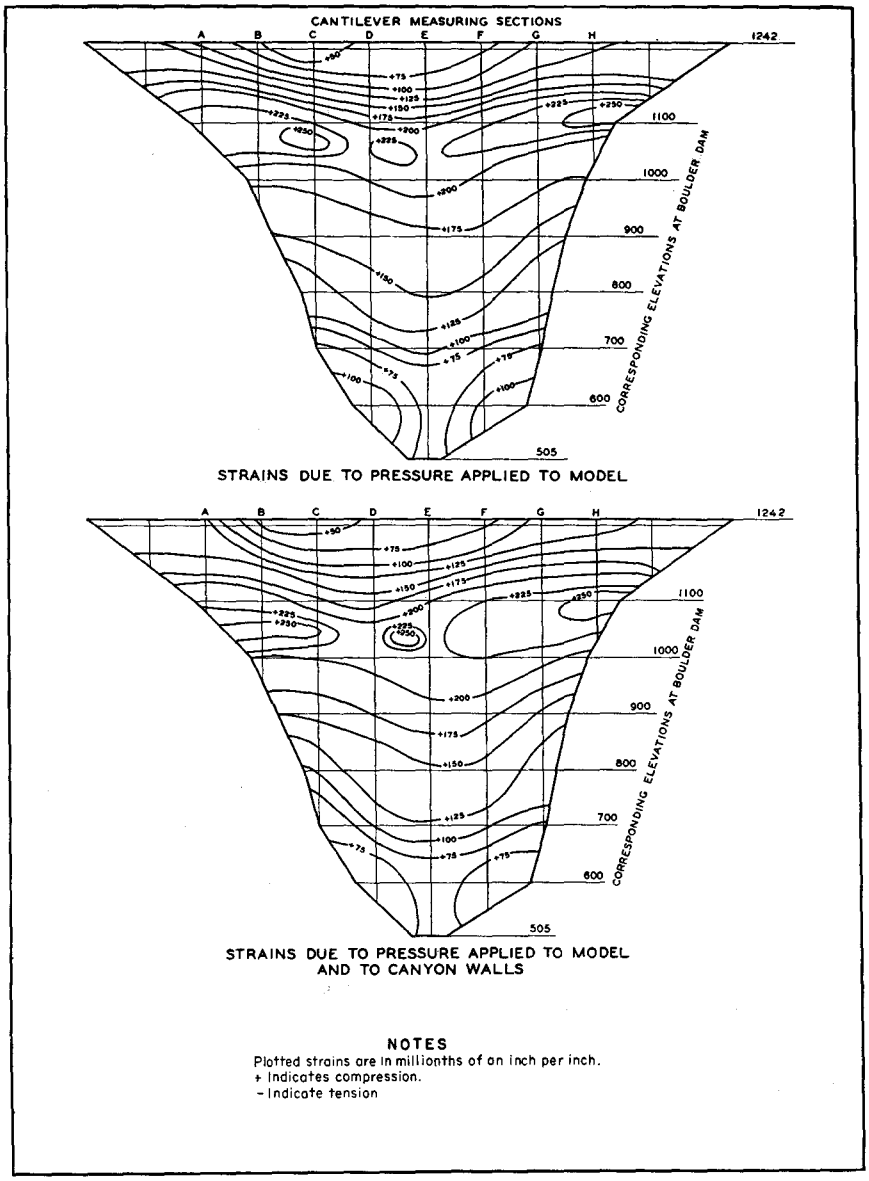

FIGURE 99—CANTILEVER STRAINS AT DOWNSTREAM FACE, LOAD AT ELEVATION 1400

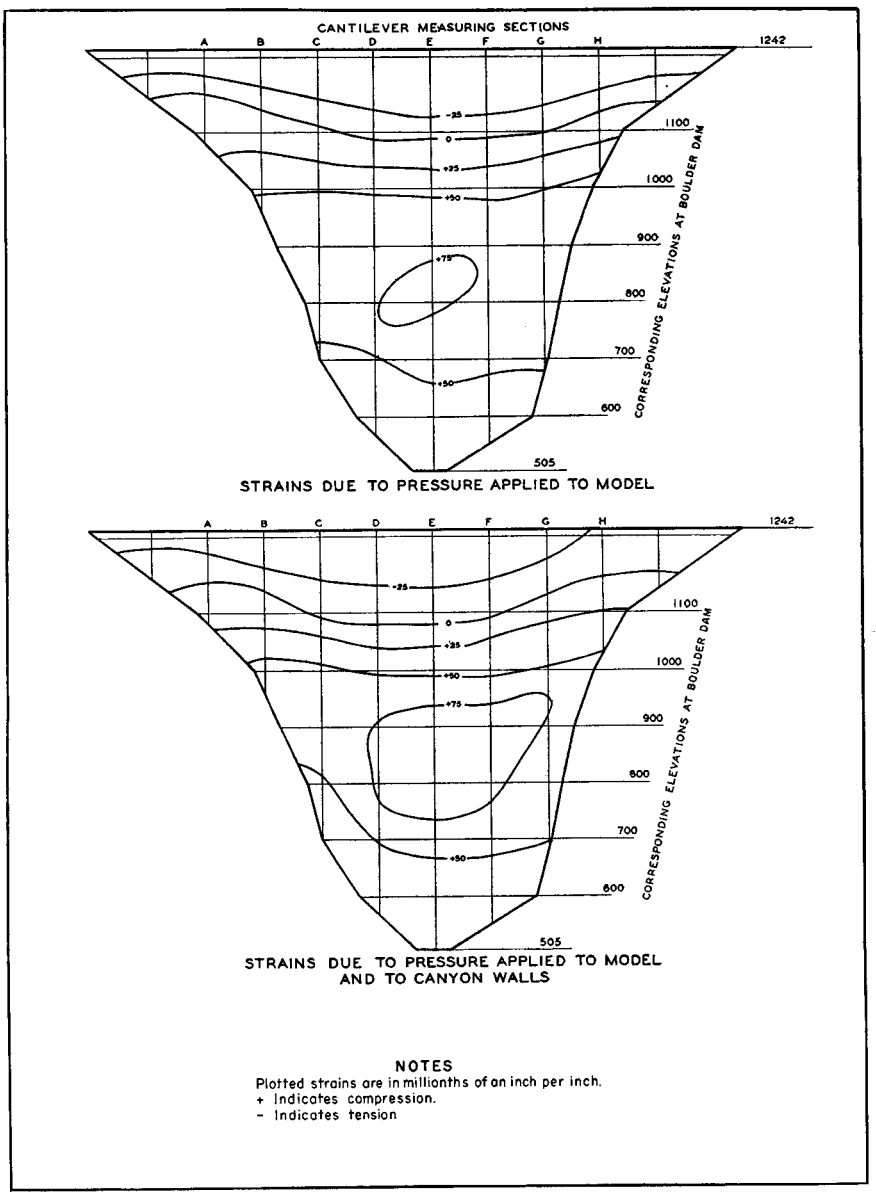

FIGURE 100—CANTILEVER STRAINS AT DOWNSTREAM FACE, LOAD AT ELEVATION 1232

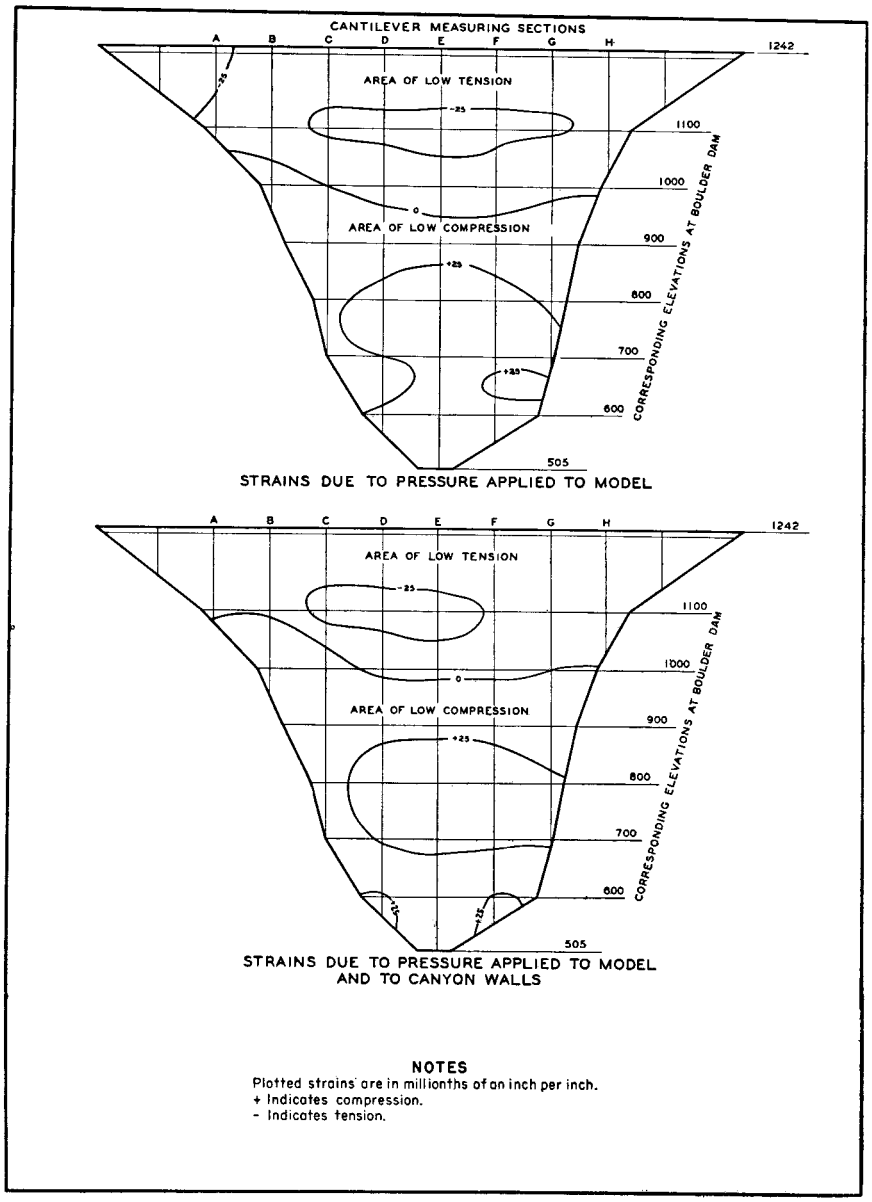

FIGURE 101—CANTILEVER STRAINS AT DOWNSTREAM FACE, LOAD AT ELEVATION 1100

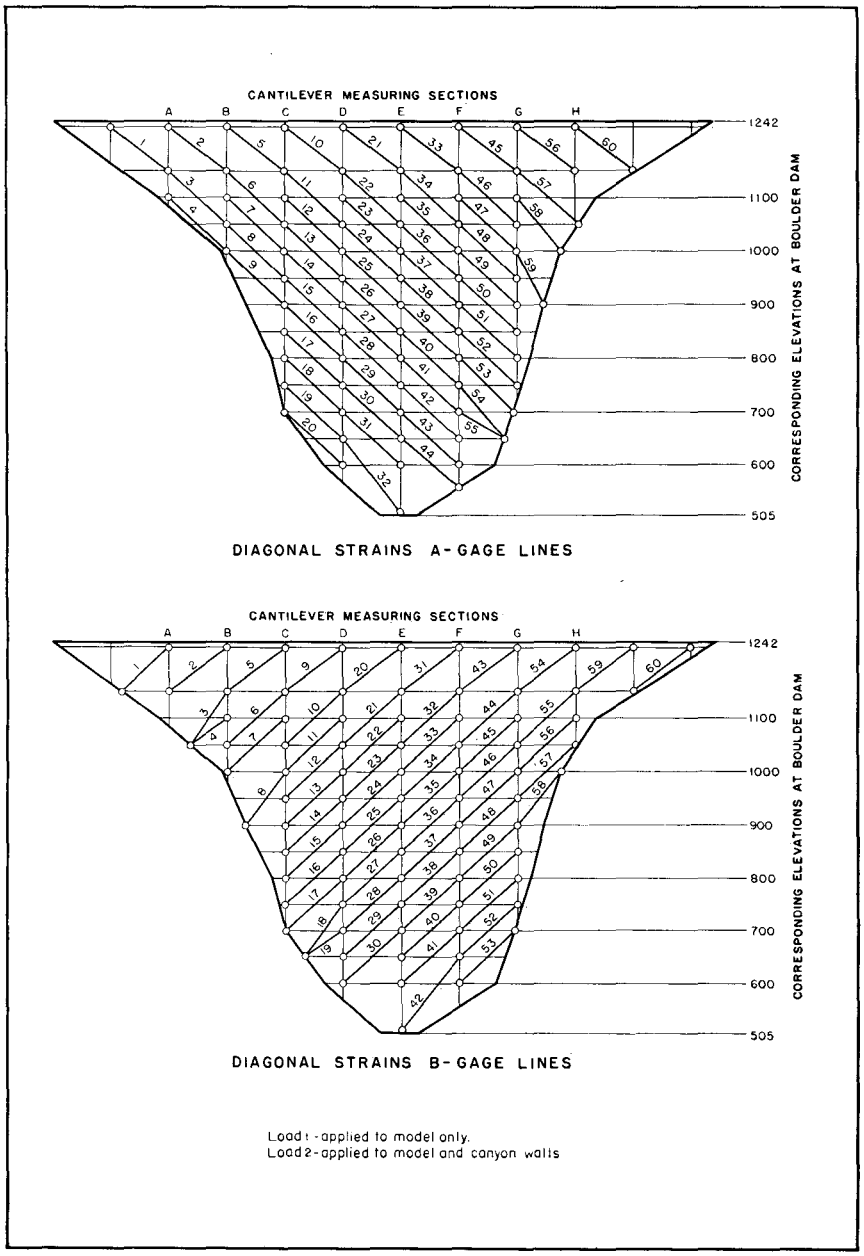

FIGURE 102—LOCATIONS OF DIAGONAL STRAIN-GAGE LINES

TABLE 2—DIAGONAL STRAINS AT DOWNSTREAM FACE

Gage Line No.	RESERVOIR MERCURY SURFACE AT EL. 1400				RESERVOIR MERCURY SURFACE AT EL. 1232				RESERVOIR MERCURY SURFACE AT EL. 1100			
	A-Gage Lines		B-Gage Lines		A-Gage Lines		B-Gage Lines		A-Gage Lines		B-Gage Lines	
	Load 1	Load 2	Load 1	Load 2	Load 1	Load 2	Load 1	Load 2	Load 1	Load 2	Load 1	Load 2
1	110.0	97.3	372.0	382.0	73.9	61.3	23.3	48.2	18.8	27.0	10.0	3.3
2	5.1	15.3	388.0	395.0	10.2	27.1	104.6	108.6	40.7	23.7	16.1	20.1
3	− 11.9	6.0	388.0	400.0	− 19.4	1.5	118.8	128.0	4.5	23.9	21.3	30.6
4	15.1	32.0	410.0	430.0	− 16.8	3.4	132.0	153.8	5.0	− 3.6	30.0	40.0
5	18.2	23.2	235.0	235.0	− 33.2	− 18.2	48.6	45.8	21.6	0.0	7.0	9.7
6	16.8	− 3.0	317.0	312.7	− 62.6	− 48.8	79.7	80.8	− 22.9	− 6.1	6.9	9.2
7	2.9	11.9	405.0	429.0	− 44.8	− 28.4	141.8	159.0	− 7.5	− 25.4	28.6	39.8
8	− 40.8	− 33.0	257.5	271.3	− 39.3	− 28.3	117.0	130.0	− 6.3	− 18.9	38.6	48.0
9	− 62.9	− 68.7	159.0	145.0	− 39.5	− 30.7	17.1	7.1	− 14.6	− 4.4	− 5.7	− 7.1
10	41.5	38.4	204.0	196.0	− 41.6	− 41.5	30.9	30.9	− 8.0	− 14.4	− 11.1	− 11.1
11	43.5	46.3	214.0	210.4	− 46.2	− 46.2	57.5	56.4	− 28.9	− 17.4	0.0	− 1.2
12	25.6	19.9	220.0	230.0	− 48.3	− 51.2	82.4	93.4	− 31.3	− 38.4	9.9	14.3
13	16.6	18.0	212.0	228.0	− 31.9	− 31.9	90.7	104.5	− 25.0	− 29.1	25.3	39.0
14	− 25.0	− 25.0	209.0	221.2	− 30.6	− 33.4	95.3	113.8	− 20.8	− 20.8	36.9	45.1
15	− 34.2	− 42.5	176.0	187.5	− 32.9	− 31.5	96.9	101.0	− 21.9	− 21.9	40.2	50.5
16	− 41.4	− 45.5	181.0	182.5	− 33.1	− 29.0	99.8	96.6	− 24.8	− 20.7	47.2	53.7
17	− 58.6	− 62.9	186.6	173.0	− 39.1	− 37.7	107.5	105.0	− 22.4	− 28.0	62.0	51.4
18	− 39.1	− 40.5	164.2	142.7	− 25.2	− 26.6	90.9	87.1	− 16.8	− 15.4	46.8	45.5
19	− 43.5	− 42.0	97.6	75.0	− 27.6	− 26.1	15.0	12.5	− 13.0	− 13.1	− 2.5	2.5
20	− 30.1	− 23.6	137.0	125.6	− 22.2	− 14.4	− 4.4	− 7.4	− 11.8	− 13.1	− 8.9	− 7.4
21	120.8	114.7	150.3	142.5	− 19.9	− 26.0	3.9	− 1.3	− 13.8	− 9.2	− 22.1	− 22.0
22	120.0	117.0	152.0	141.2	− 13.8	− 12.4	19.8	21.0	− 13.8	− 23.4	− 17.3	− 16.1
23	124.5	123.2	126.0	127.0	− 4.0	− 1.3	25.7	26.9	− 23.8	− 26.5	− 14.0	− 14.0
24	78.0	74.2	12.0	121.3	− 7.5	− 8.8	42.3	43.5	− 27.7	− 29.0	0.0	4.6
25	21.0	18.6	128.5	131.8	− 11.1	− 39.6	50.8	58.7	− 19.8	− 21.0	11.3	13.5
26	40.5	42.9	85.2	94.2	1.2	− 2.5	49.8	44.3	− 14.2	− 18.4	15.5	14.4
27	22.2	17.3	35.4	103.0	− 3.7	− 9.9	52.8	59.6	− 14.8	− 13.5	21.4	29.2
28	8.6	3.7	87.4	93.1	− 6.1	− 14.7	49.5	51.7	− 12.2	− 9.8	27.6	28.7
29	5.0	− 3.8	92.0	87.2	− 3.8	− 8.8	52.6	51.3	− 7.5	− 18.8	28.7	29.9
30	6.4	2.5	55.8	48.5	2.5	− 5.1	29.1	29.1	− 1.3	− 6.4	18.2	3.6

TABLE 2—DIAGONAL STRAINS AT DOWNSTREAM FACE—Continued

Gage Line No.	RESERVOIR MERCURY SURFACE AT EL. 1400				RESERVOIR MERCURY SURFACE AT EL. 1232				RESERVOIR MERCURY SURFACE AT EL. 1100			
	A-Gage Lines		B-Gage Lines		A-Gage Lines		B-Gage Lines		A-Gage Lines		B-Gage Lines	
	Load 1	Load 2	Load 1	Load 2	Load 1	Load 2	Load 1	Load 2	Load 1	Load 2	Load 1	Load 2
31	− 10.8	− 10.8	154.0	141.4	− 10.8	− 12.1	− 7.6	− 10.7	− 6.0	− 7.2	− 9.1	− 10.7
32	12.9	9.4	86.0	79.2	5.9	2.3	− 18.8	− 20.1	0.0	4.7	− 18.8	− 18.8
33	194.0	186.5	72.5	67.3	9.0	6.0	− 19.8	− 22.4	− 12.0	− 10.5	− 30.4	− 34.3
34	167.5	170.0	56.3	53.7	10.4	10.4	− 12.8	− 10.2	− 13.0	− 15.6	− 26.8	− 28.2
35	172.0	168.3	7.6	25.3	20.9	23.4	− 15.2	− 17.7	− 13.5	− 18.4	− 20.3	− 16.5
36	162.0	164.4	23.5	28.4	30.7	33.5	2.5	3.7	− 11.8	− 14.2	− 13.6	− 9.9
37	154.0	157.8	17.2	8.6	49.0	50.2	− 1.2	1.2	1.2	0.0	− 3.7	− 7.4
38	120.0	126.8	15.9	8.6	45.7	45.7	− 1.2	1.2	8.0	8.0	− 4.9	− 2.5
39	112.5	119.4	26.4	12.6	47.3	54.0	13.8	16.4	12.4	14.6	− 1.3	8.8
40	110.0	111.0	20.5	19.2	55.0	49.4	10.3	11.5	21.4	23.6	0.0	2.6
41	75.7	72.5	0.0	0.0	41.8	38.4	− 1.3	0.0	17.0	12.5	− 4.0	0.0
42	70.4	64.6	19.8	16.5	38.6	34.1	11.0	11.0	20.4	15.9	9.9	6.6
43	41.0	36.2	88.0	78.4	21.7	18.1	− 16.0	− 20.8	9.6	12.1	− 1.6	− 3.2
44	57.4	40.3	35.8	24.3	36.6	28.1	− 51.4	− 54.3	13.4	18.3	− 24.3	− 25.7
45	205.3	212.5	31.0	33.6	18.8	18.8	− 31.0	− 31.0	− 7.2	− 4.3	− 23.9	− 25.4
46	236.0	241.5	− 49.7	− 56.6	32.7	35.1	− 48.4	− 58.0	− 6.1	− 9.7	− 29.0	− 29.0
47	259.0	267.0	− 24.9	− 29.1	69.3	68.2	− 33.2	− 30.4	− 1.1	− 1.1	− 24.9	− 22.1
48	242.7	254.5	− 46.8	− 46.7	86.0	90.4	− 41.3	− 41.3	11.0	9.9	− 27.5	− 26.1
49	234.0	249.0	− 37.3	− 42.9	94.5	104.5	− 27.7	− 31.8	28.3	30.4	− 18.0	− 19.4
50	204.0	215.5	− 40.0	− 35.9	95.8	101.0	− 24.8	− 23.5	38.2	35.0	− 16.6	− 13.8
51	173.3	177.5	− 31.3	− 31.4	91.3	92.4	− 18.5	− 18.5	40.0	40.0	− 14.3	− 12.8
52	161.4	159.5	− 32.1	− 33.4	89.3	85.3	− 20.9	− 19.5	39.6	38.6	− 15.3	− 11.1
53	146.0	137.0	− 54.0	− 46.7	82.0	73.8	− 35.0	− 24.8	45.5	38.5	− 21.9	− 14.6
54	119.3	110.6	49.5	42.8	69.6	60.7	3.3	− 1.6	38.7	29.8	9.9	4.9
55	97.1	81.0	− 11.9	− 16.4	61.4	48.5	− 28.4	− 29.9	21.0	32.4	− 3.0	− 10.4
56	291.0	282.5	− 50.6	− 59.6	54.5	53.2	− 44.6	− 44.6	4.2	5.6	− 19.4	− 19.4
57	369.5	380.0	− 95.4	− 97.8	96.5	102.1	− 54.8	− 51.9	10.2	14.8	− 22.2	− 22.2
58	372.3	377.0	− 67.4	− 65.8	123.2	135.0	− 44.3	− 39.8	24.6	28.2	− 19.9	− 19.9
59	242.0	256.7	85.5	86.4	107.2	113.6	50.8	55.9	34.6	39.5	22.0	23.8
60	456.5	467.0	79.0	79.0	98.6	95.8	4.2	43.7	21.1	17.3	15.0	11.8

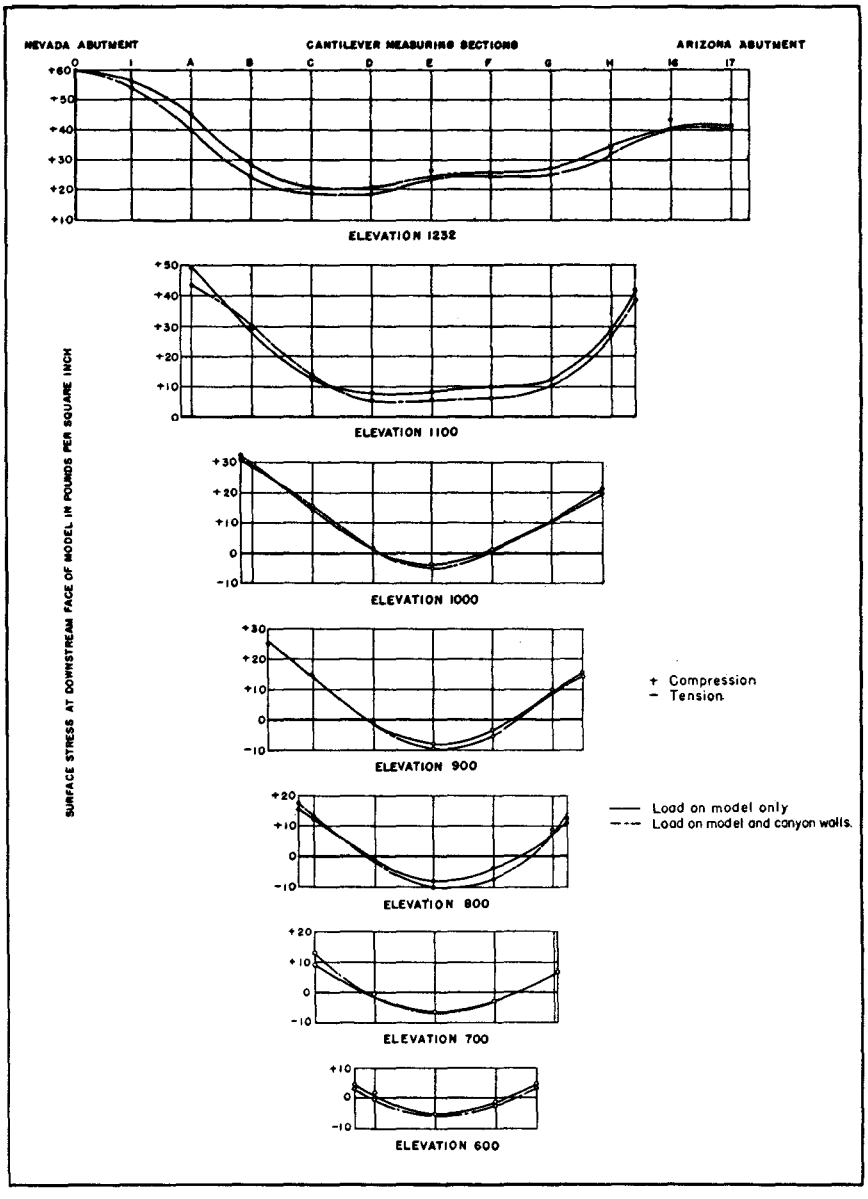

FIGURE 103—ARCH STRESSES AT DOWNSTREAM FACE, LOAD AT ELEVATION 1400

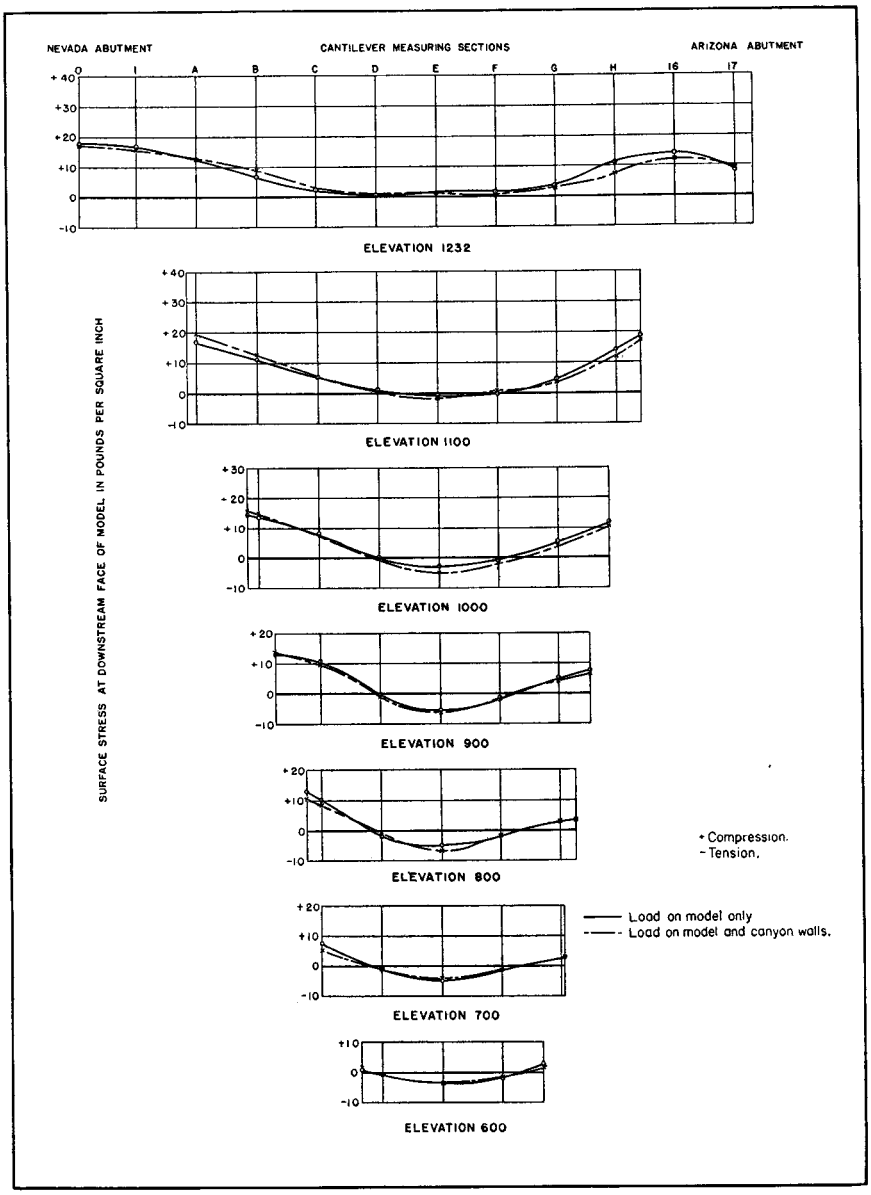

FIGURE 104—ARCH STRESSES AT DOWNSTREAM FACE, LOAD AT ELEVATION 1232

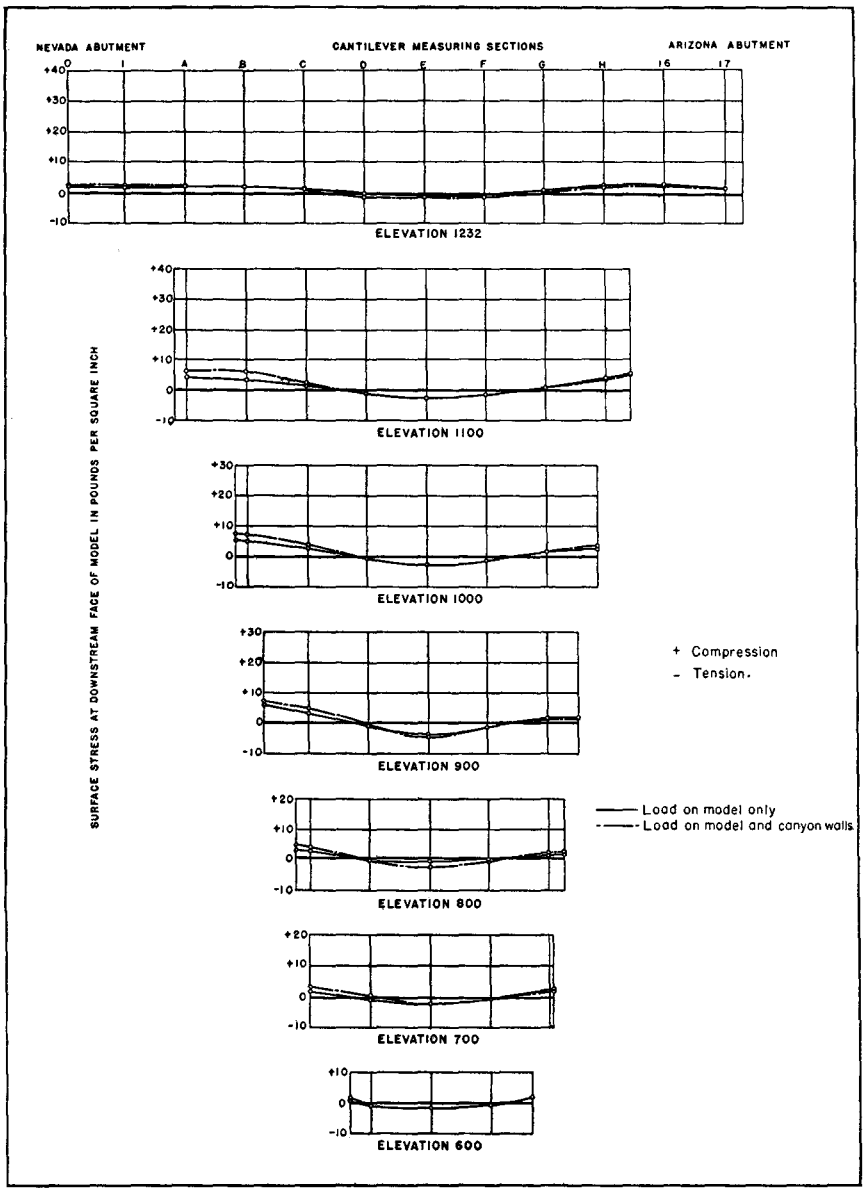

FIGURE 105—ARCH STRESSES AT DOWNSTREAM FACE, LOAD AT ELEVATION 1100

inch at elevation 1232, at the Nevada abutment, when pressure was applied to the model only. Applying reservoir pressure to the canyon walls reduced this stress slightly. The maximum tensile stress of ten pounds per square inch occurred at cantilever section E, between elevations 775 and 900, when reservoir pressure was applied to the canyon walls. When pressure was applied to the model only, this stress was reduced to eight pounds per square inch.

For load at elevation 1232, maximum compressive and tensile stresses occurred when the reservoir pressure was applied to the model and canyon walls. For this loading condition, a maximum compression of 20 pounds per square inch occurred along the Nevada abutment between elevations 1050 and 1150. A maximum tension, slightly greater than five pounds per square inch, occurred in an area about four inches wide between cantilever sections D and F and elevations 725 and 975. When load was applied to the model only, the stresses were slightly smaller.

With mercury surface at elevation 1100, there was very little difference between stresses resulting from the two methods of loading, see figure 105. By applying reservoir pressure to the canyon walls and the model, stresses along the Nevada abutment between elevations 825 and 1150 were increased slightly over those obtained by loading the model only.

104. Cantilever Stresses.—Cantilever stresses determined from strain measurements are shown in figures 106, 107, and 108. When loaded to elevation 1400, maximum compressive stresses of 30 pounds per square inch occurred at the abutments, at elevation 1100, with pressure applied to the model only. When reservoir pressure was applied to the canyon walls the maximum stress was reduced to 27.5 pounds per square inch at each abutment. When loaded to elevation 1232, the reservoir pressure on the canyon walls did not affect the stresses materially. Maximum compressive stresses for both methods of loading were nearly eight pounds per square inch. The maximum tensile stress was two pounds per square inch when pressure was applied to the model only, and about one pound per square inch when reservoir pressure was applied to the canyon walls.

When the mercury surface was at elevation 1100, cantilever stresses were relatively small. Reservoir pressure on the canyon walls had very little effect on the stress distribution. The maximum compressive stress was 2.5 pounds per square inch in the lower part of

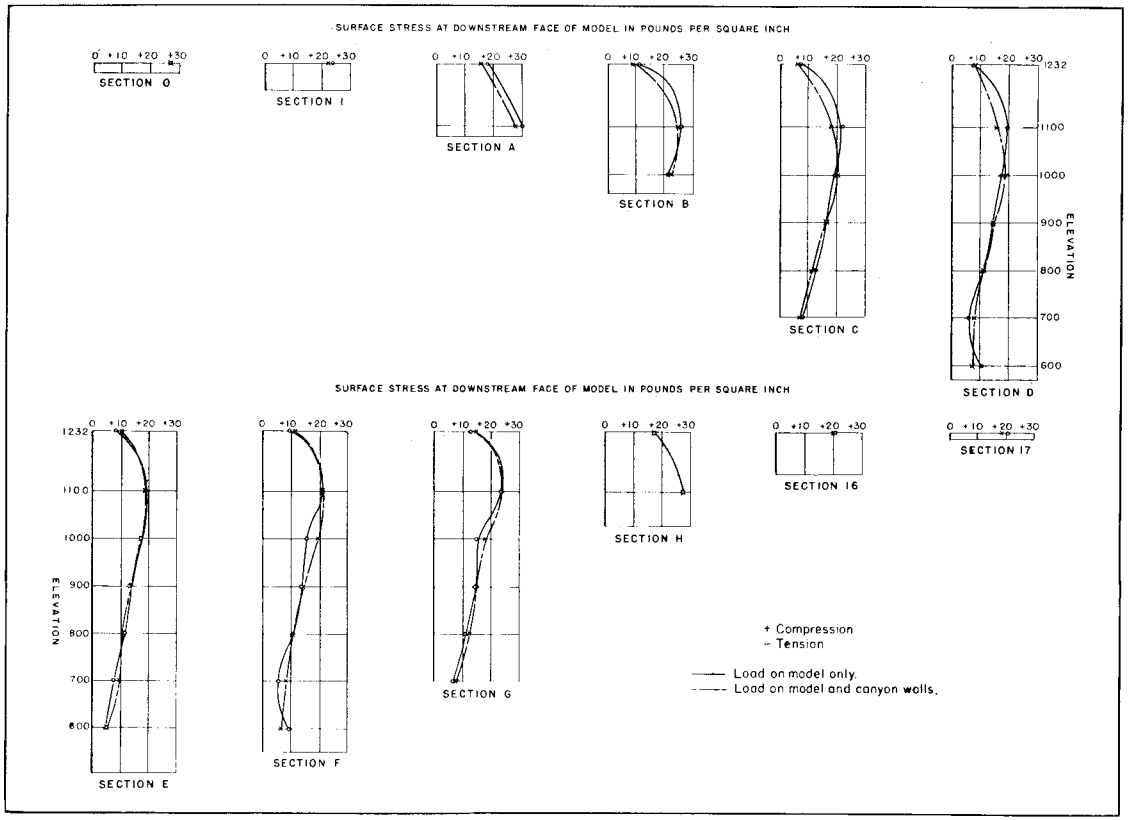

FIGURE 106—CANTILEVER STRESSES AT DOWNSTREAM FACE, LOAD AT ELEVATION 1400

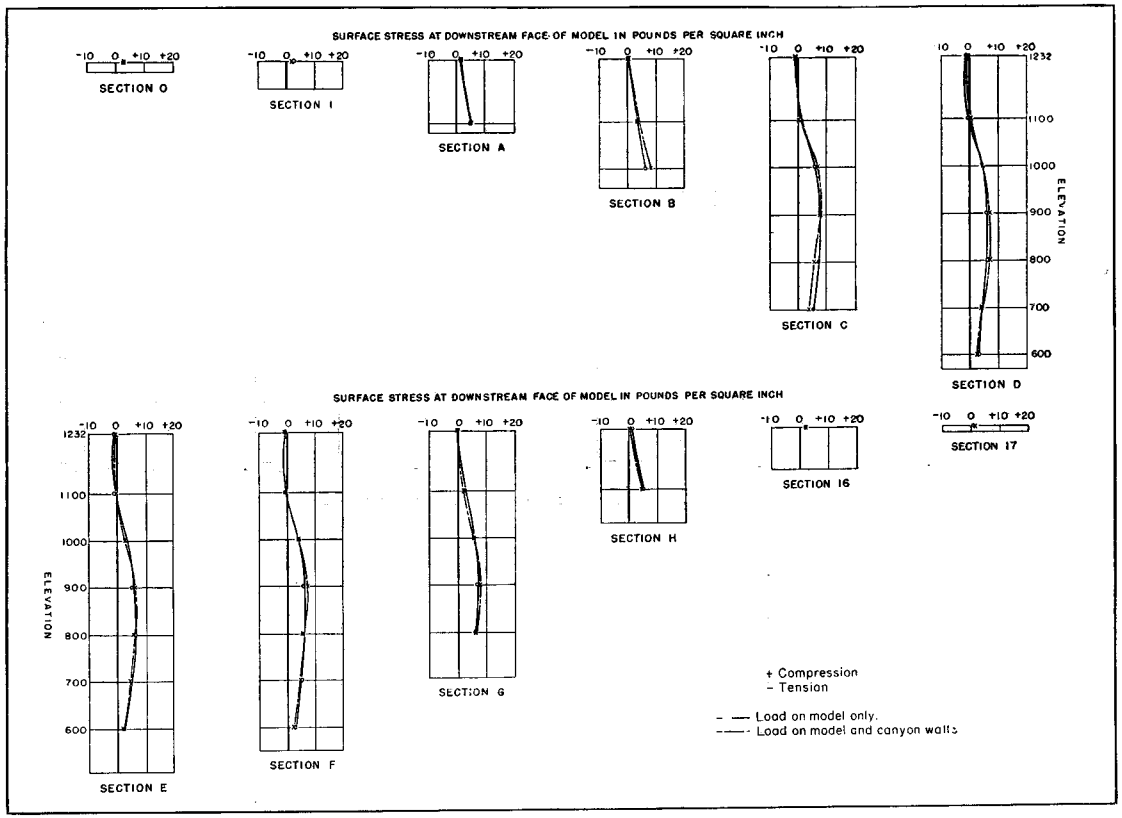

FIGURE 107—CANTILEVER STRESSES AT DOWNSTREAM FACE, LOAD AT ELEVATION 1232

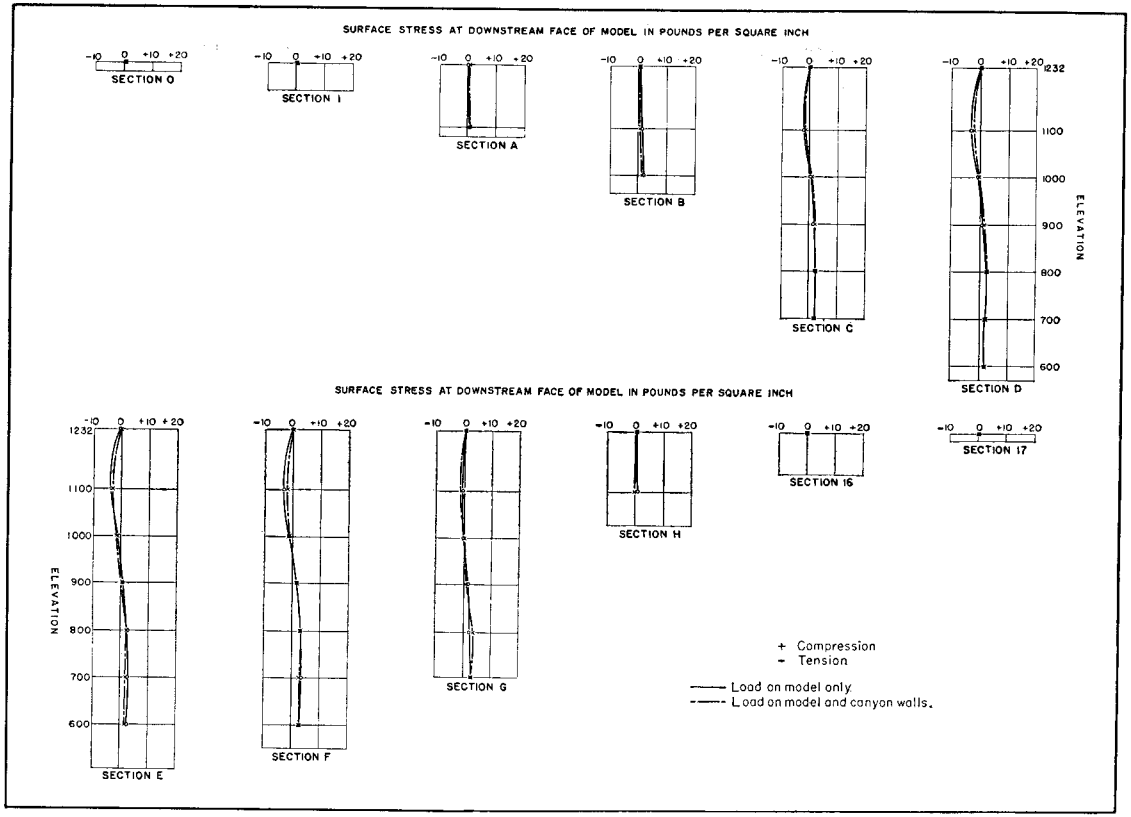

FIGURE 108—CANTILEVER STRESSES AT DOWNSTREAM FACE, LOAD AT ELEVATION 1100

the model. At elevation 1100 in the central part of the model, a maximum tensile stress of 2.5 pounds per square inch was found.

105. Horizontal Shearing Stresses.—Horizontal shearing stresses computed from strain measurements are shown in figures 109, 110, and 111. There was little difference in shearing stresses resulting from the two methods of loading. With reservoir load at elevation 1400, a maximum shearing stress of 23 pounds per square inch occurred at the Arizona abutment, at elevation 1100, when reservoir pressure was applied to the canyon walls. The reversal of shearing stresses at the abutments at elevation 1232, for load at elevation 1232, was due to contraflexure in the deflection of the model for that loading condition. The radial deflection of the arch element at elevation 1232 was upstream near the abutments, as shown in figure 82. At lower elevations this reversal of shearing stresses did not occur.

With the mercury surface at elevation 1100, shearing stresses were rather small, as shown in figure 111. Some reversal of stress occurred at the abutments at elevations 1232 and 1100.

106. Principal Stresses.—Principal stresses computed from strain measurements are shown in figures 112, 113, and 114. In figure 112, principal stresses for the overload condition are shown for the two methods of loading. Magnitudes of principal stresses were changed slightly due to the two methods of loading, but directions of stresses were virtually unchanged. A maximum compressive stress of 64.0 pounds per square inch occurred at elevation 1232 at the Nevada abutment. This stress was the same for both systems of loading. A maximum tensile stress of 10.3 pounds per square inch occurred at cantilever section E, elevation 800, when reservoir pressure was applied at the canyon walls. At the same location the maximum tension was 8.3 pounds per square inch when load was applied on the model only.

For load at elevation 1232, compressive stresses were largest along the abutments above elevation 800. The largest compressive stress along the Nevada abutment was 21.9 pounds per square inch. It occurred between elevations 900 and 1000 when pressure was applied at the canyon walls. The largest compressive stress along the Arizona abutment was 24.8 pounds per square inch at elevation 1100. The maximum tensile stresses occurred along cantilever section E. When pressure was applied at the canyon walls, a tensile stress of 6.5 pounds per square inch occurred at elevation 800. When pressure was applied

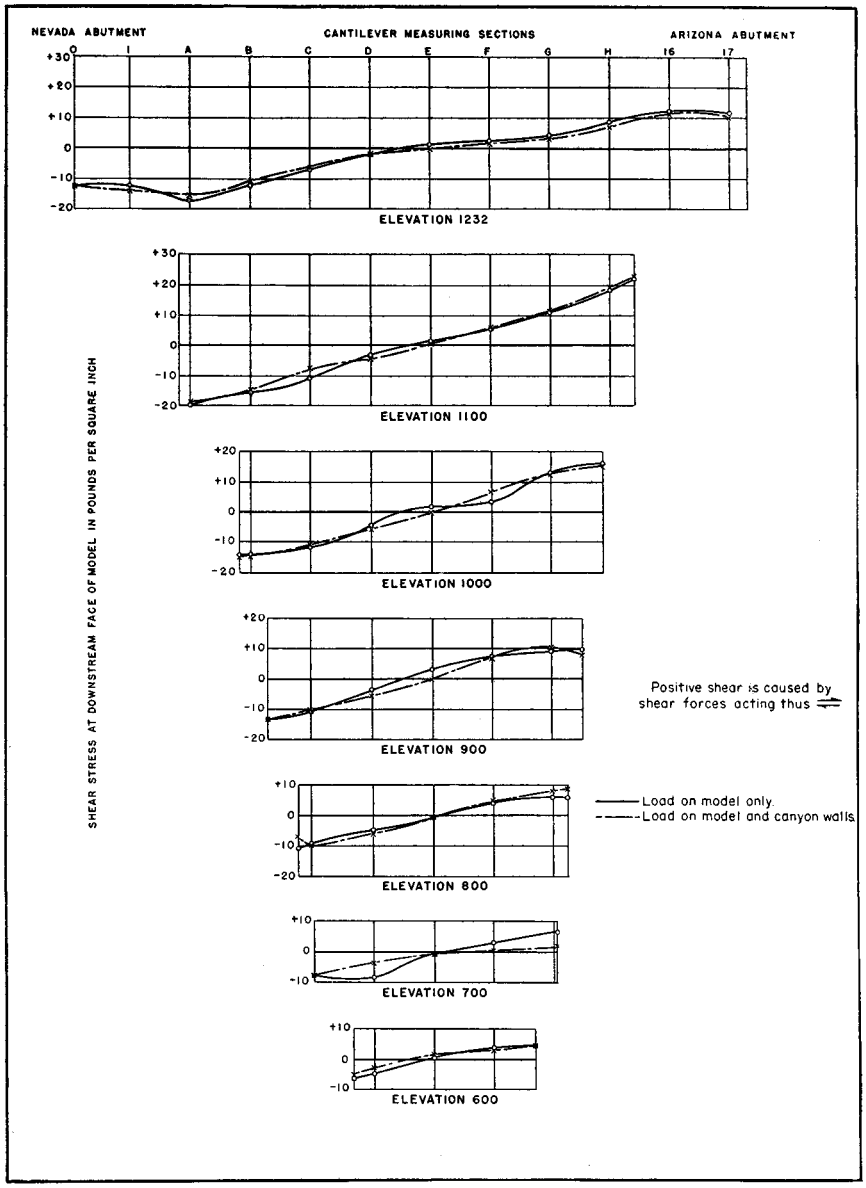

FIGURE 109—HORIZONTAL SHEARING STRESSES AT DOWNSTREAM FACE, LOAD AT ELEVATION 1400

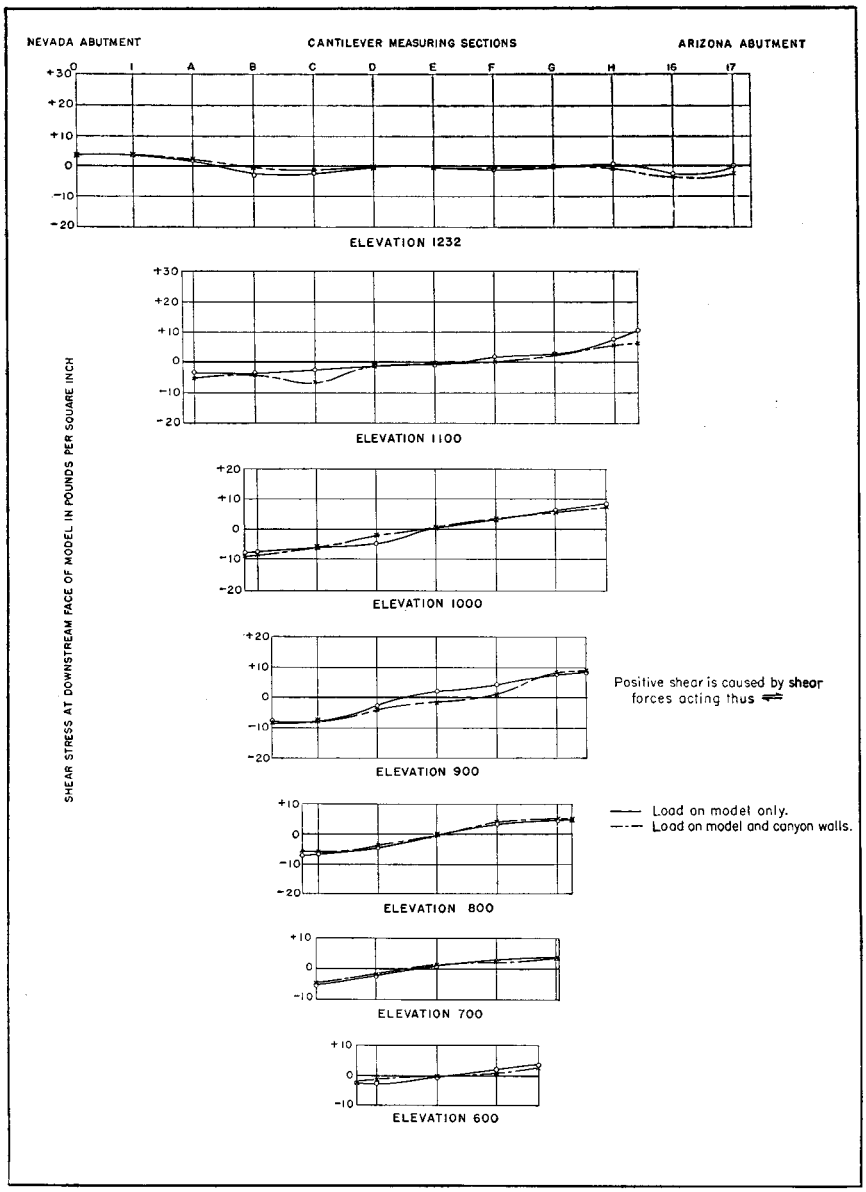

FIGURE 110—HORIZONTAL SHEARING STRESSES AT DOWNSTREAM FACE, LOAD AT ELEVATION 1232

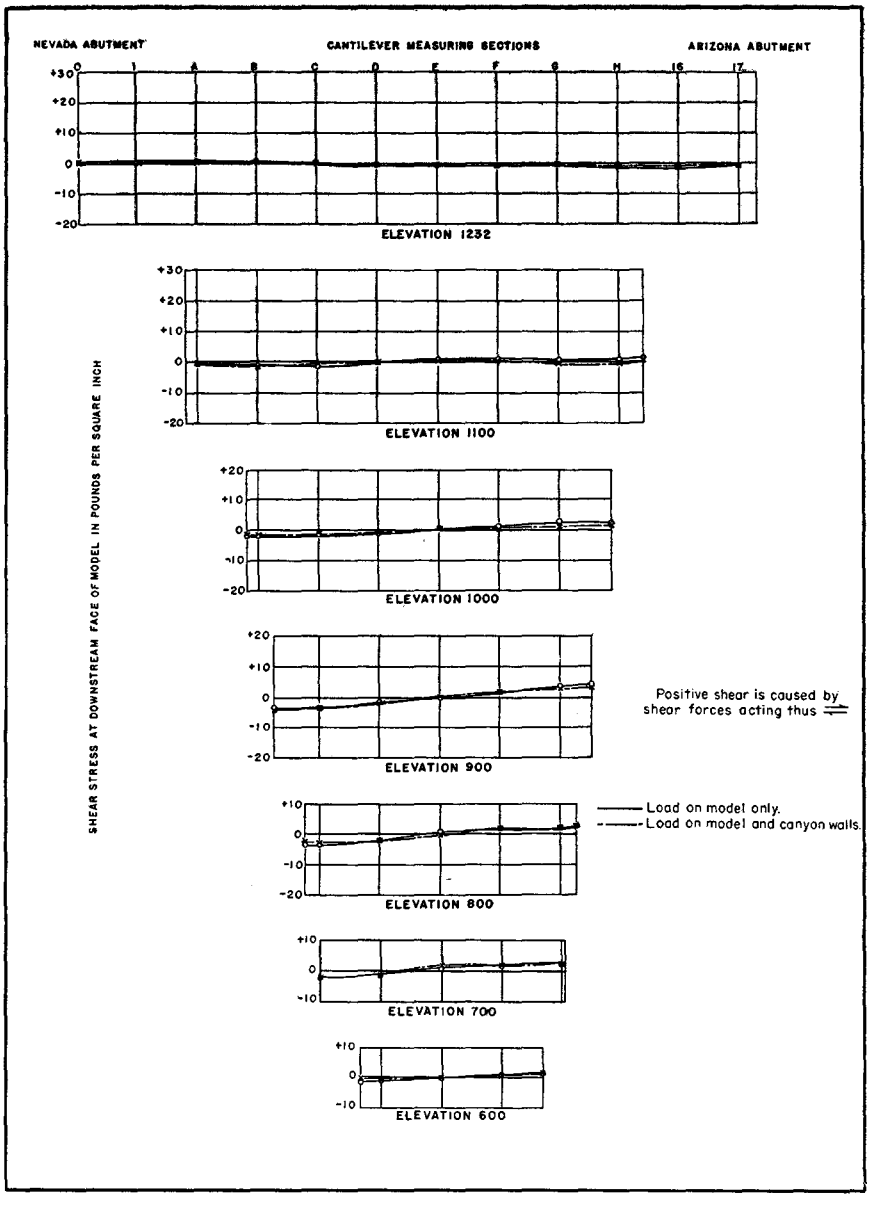

FIGURE 111—HORIZONTAL SHEARING STRESSES AT DOWNSTREAM FACE, LOAD AT ELEVATION 1100

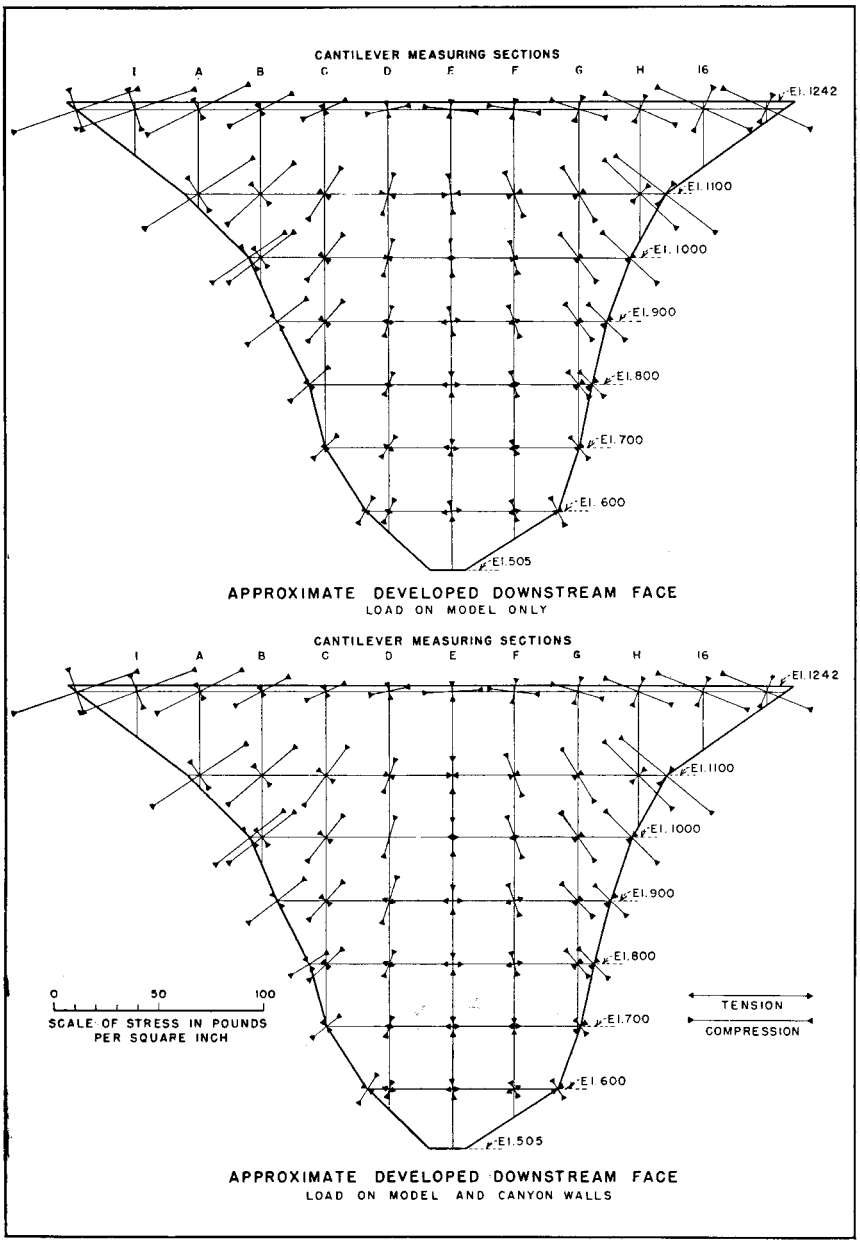

FIGURE 112—PRINCIPAL STRESSES AT DOWNSTREAM FACE, LOAD AT ELEVATION 1400

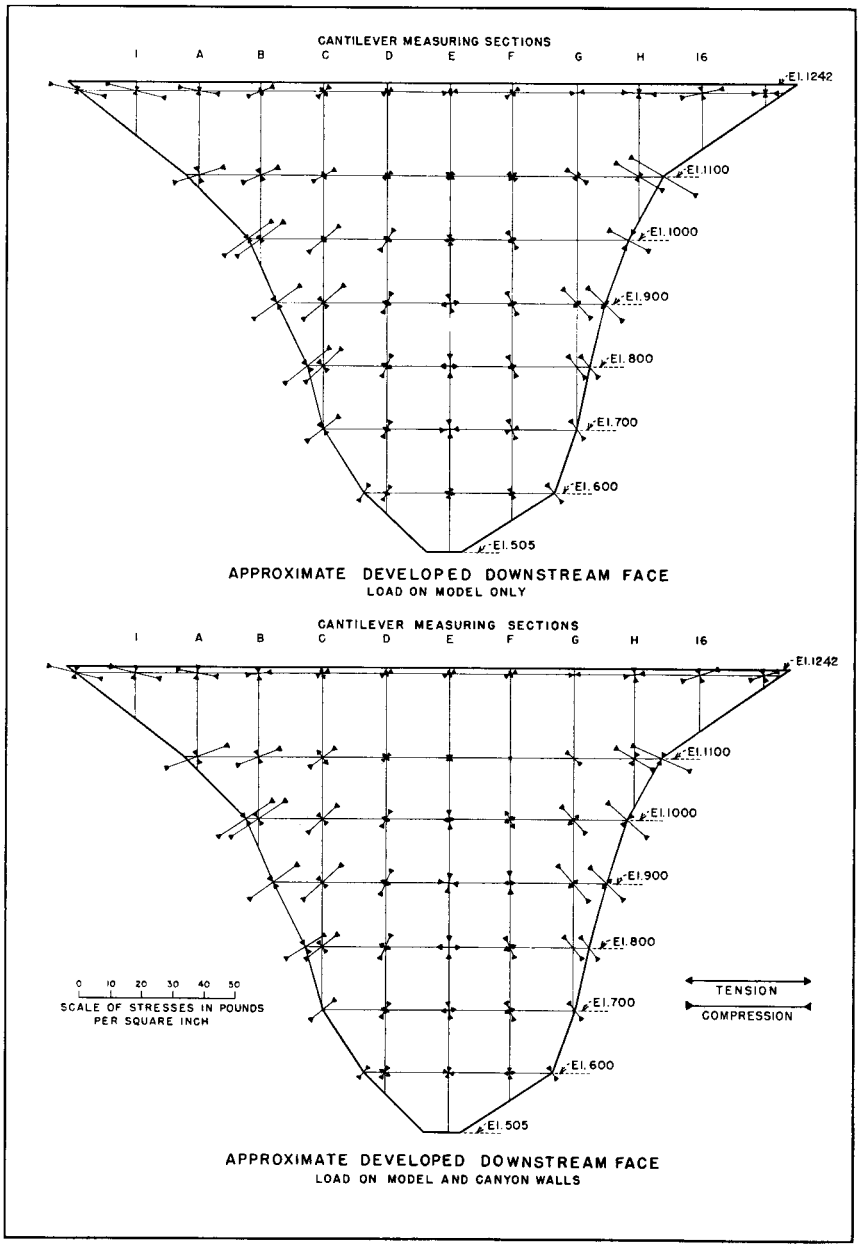

FIGURE 113—PRINCIPAL STRESSES AT DOWNSTREAM FACE, LOAD AT ELEVATION 1232

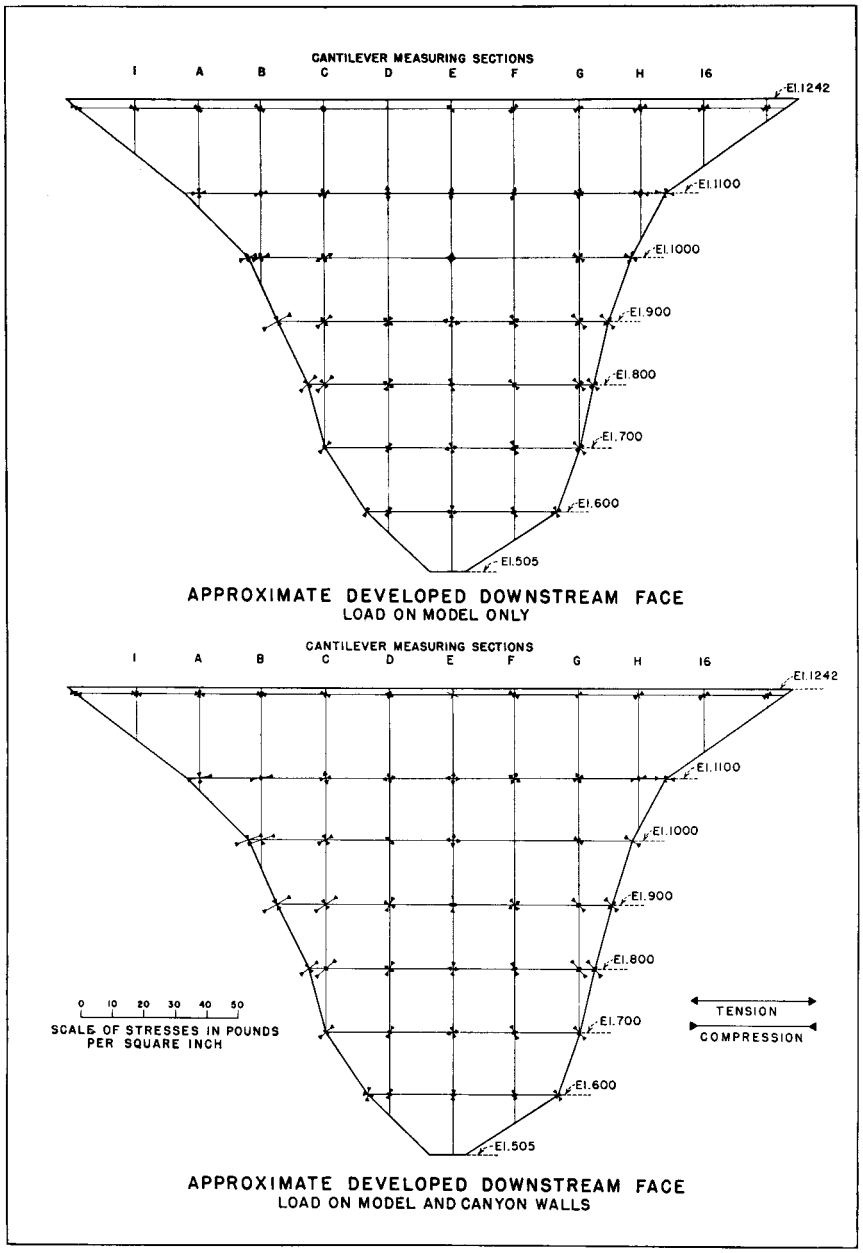

FIGURE 114—PRINCIPAL STRESSES AT DOWNSTREAM FACE, LOAD AT ELEVATION 1100

to the model only, a maximum tension of 5.3 pounds per square inch occurred at elevation 900.

The largest compressive stresses were nearly perpendicular to the abutments and occurred between elevations 900 and 1100. In the lower portion of the model, the directions were much steeper than in the upper portion, owing to the distribution of load by tangential shear. At elevation 1232, stresses near the abutments were inclined in directions more nearly horizontal than those occurring at lower elevations. For load at elevation 1100, stresses were negligible except along the abutments below elevation 1100.

CHAPTER VI—MISCELLANEOUS TESTS

SPECIAL DEFLECTION TESTS

107. Crown Cantilever Movements.—Radial and tangential measurements indicated that deformations occurred at the foundation and abutments. Such movements, combined with deformations of the model, caused vertical as well as horizontal movements at the cantilever elements. Tests were run to determine resultant movements at the crown cantilever, designated on the drawings as cantilever E.

The first tests were made with gages set to register movements in a vertical direction. The results of these tests are shown in figures 115, 116, and 117. Points above elevation 1000 rose above their original position while points below elevation 1000 deflected below their original position. The point at elevation 1100 showed a very small deflection in all tests. Deflections were plotted to an exaggerated scale from a section on the center line of the model.

By plotting vertical deflections and horizontal radial deflections from the same point, the position of the downstream face could be determined. The deflected position of each of the points fell on a smooth curve. The vertical deflection of the point at the top of the model was about one-sixth of the radial horizontal deflection when the mercury surface was at elevation 1400. When the mercury surface was at elevation 1232, the vertical deflection of the same point was about one-third the radial horizontal deflection, as shown in figure 116. For partial loads this ratio was still about one-third.

Deflection measurements normal to the face of the cantilever, also shown on figures 115, 116, and 117, were not as consistent nor as accurate as the vertical deflection measurements. The difficulty encountered in normal deflection tests was in setting gage rods in directions normal to the downstream face. If the directions of the invar rods deviated from the normal, the plotted points were in error and did not fall along a smooth curve. This accounts for the difference in the position of the downstream face as determined by vertical and normal measurements.

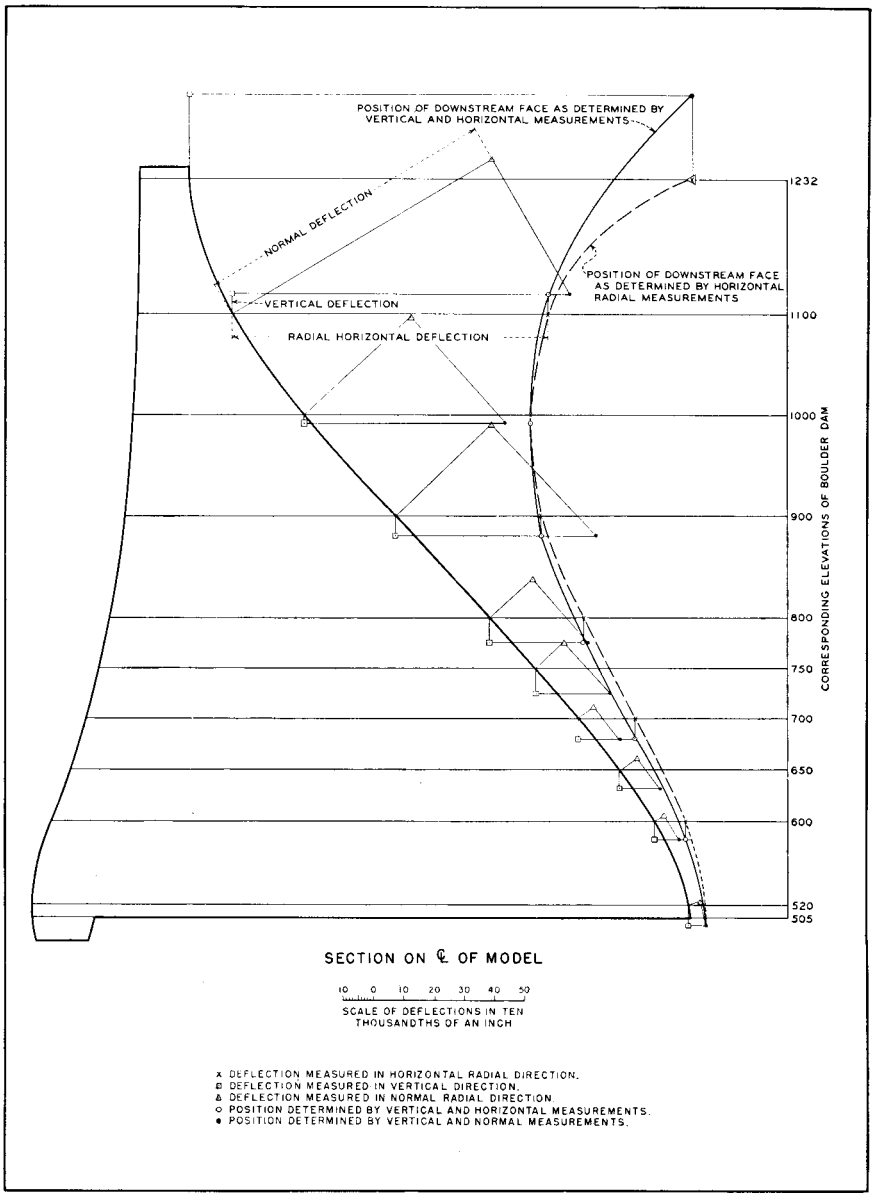

FIGURE 115—RESULTANT DEFLECTION OF CROWN CANTILEVER, LOAD AT ELEVATION 1400

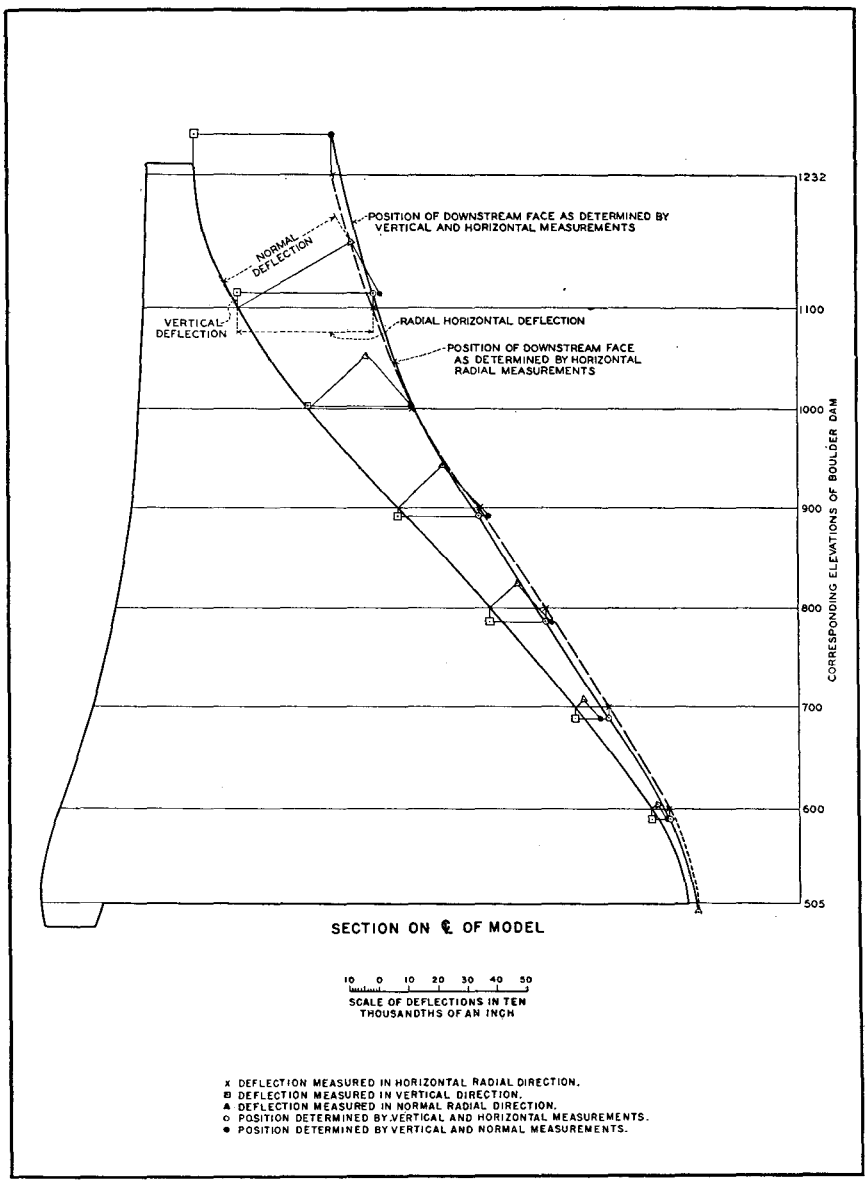

FIGURE 116—RESULTANT DEFLECTION OF CROWN CANTILEVER, LOAD AT ELEVATION 1232

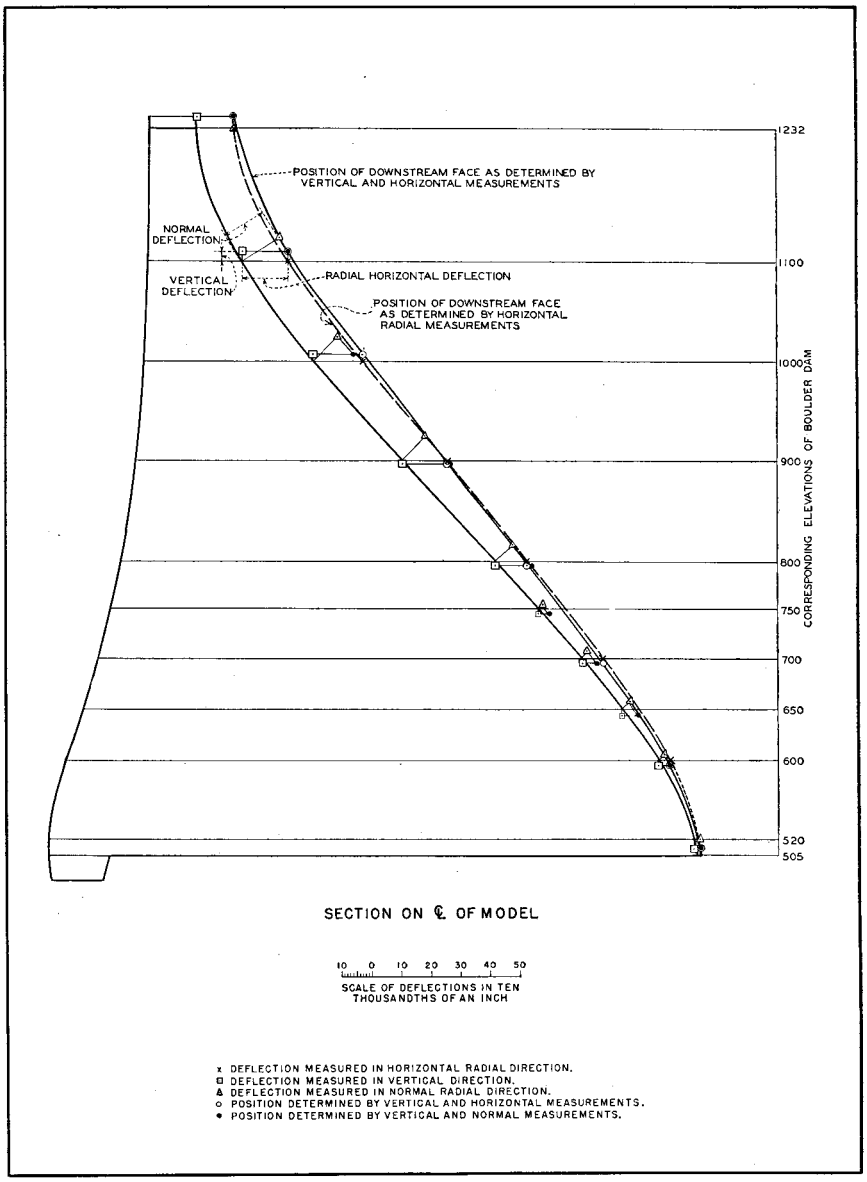

FIGURE 117—RESULTANT DEFLECTION OF CROWN CANTILEVER, LOAD AT ELEVATION 1100

At first appearance the tests might indicate that, because the upper points moved upward and the lower points downward, there must have been a lengthening of the face. Actually, the movement represents a rotation about some point within the model. In fact, the strain measurements showed that there was a slight shortening of the face.

108. Deflection of Interior.—In analyzing the model of Boulder Dam by the trial load method, radial deflections of the arch elements were calculated for center-line locations. In testing the model, radial deflections at the downstream face were measured. Since there were strains in the interior of the model, particularly at the lower elevations, it was decided to measure the radial deflections of the arch center lines.

Horizontal holes were drilled in the model to center-line locations, and invar rods with expansion ends anchored in place. The outer ends of the rods were supported by flexible couplings at the downstream face and were allowed to bear against dial gages reading to 0.0001 of an inch. The dial gages were attached to anchors on the downstream face of the model along cantilever section E. Any movement of the interior of the model at the point of anchorage with respect to the downstream face was registered on the gage. Locations of the measurements and results obtained are shown in figure 118.

At elevations 1100 and 1000 the squeezing of the model between the center line and the downstream face was small, even for overload conditions. At lower elevations the squeezing was as much as 0.0009 inches for overload conditions, and 0.0005 inches for normal load conditions. Applying mercury load to the canyon walls had very little effect on the squeezing of the model.

109. Cantilever Curvature at Downstream Face.—In preliminary designs for Boulder Dam the downstream face had considerable vertical curvature below elevation 700. This curvature evoked considerable discussion about its effect on the cantilever stress distribution. The objection to the curvature was that it tended to create tensile stresses in a direction normal to the curved downstream face. Consequently, tests were made to determine the magnitude of the tension.

The hole at F, figure 118, was drilled radially from elevation 600 at the downstream face of the crown cantilever. An invar rod, with an expansion end, was anchored in the hole. The end of the rod at the downstream face was supported with a flexible coupling and bore against a dial gage which was rigidly attached to the face of the model. No movement was registered on the gage, except when the

mercury surface was at elevation 1400, when a deflection of 0.000,02 inch was observed. This indicated an average tensile strain of 2.8 millionths of an inch per inch, corresponding to a stress of 0.28 pounds per square inch. This was the average stress over a gage length of 7.25 inches. The peak stress near the surface was undoubtedly greater, but a more refined system of measurements would have been required to determine it.

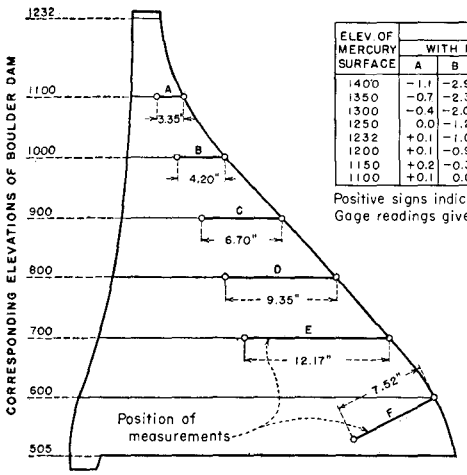

SECTION ON CENTER LINE OF CANTILEVER E

TABLE OF DEFLECTIONS

ELEV. OF MERCURY SURFACE	MEASUREMENTS											
	WITH MERCURY BAG NO. 2						WITH MERCURY BAGS NOS. 2-3-4					
	A	B	C	D	E	F	A	B	C	D	E	F
1400	−1.1	−2.9	−4.9	−9.2	−9.0	+0.2	−0.5	−3.1	−5.4	−9.1	−7.8	
1350	−0.7	−2.3	−4.3	−8.1	−8.2	0.0	−0.8	−2.7	−5.4	−8.2	−7.2	
1300	−0.4	−2.0	−3.8	−7.0	−7.3	0.0	−0.4	−2.0	−3.8	−7.3	−6.7	
1250	0.0	−1.2	−3.2	−6.2	−6.8	0.0	−0.2	−1.5	−3.4	−6.0	−5.7	
1232	+0.1	−1.0	−2.8	−5.2	−5.8	0.0	0.0	−1.2	−3.3	−5.4	−5.2	
1200	+0.1	−0.9	−2.3	−5.2	−5.8	0.0	0.0	−1.0	−2.8	−5.0	−4.8	
1150	+0.2	−0.3	−1.8	−4.1	−4.9	0.0	0.0	−0.7	−2.1	−4.1	−4.1	
1100	+0.1	0.0	−1.1	−3.3	−4.0	0.0	0.0	−0.3	−1.6	−3.3	−3.4	

Positive signs indicate lengthening; negative signs indicate shortening. Gage readings given in ten-thousandths of an inch.

Values in table are averages of two or more tests for each loading condition.
Load applied to model with mercury bag No. 2, and to canyon walls with bags Nos. 3 and 4.
Holes drilled in model to required depth and invar rods with expansion ends anchored in them.
Outside ends of rods supported by flexible couplings at downstream face and allowed to bear against "Last Word" gages.
Movement of interior of model at point of anchorage, with respect to downstream face, registered on the dial gages.

FIGURE 118—DEFLECTION OF INTERIOR OF CROWN CANTILEVER

FLOW TEST

110. Plastic Flow.—In making the tests of the model, some plastic flow occurred during the first two or three tests each day. After these tests had been made, the action of the model became elastic, and repeated measurements of strains or deflections agreed very closely. Apparently the movement of the model during the first test, after being idle for several hours, was partly plastic and partly elastic. Flow tests of cylinders had shown that the deformation increased rapidly when load was first applied, but became practically stationary after being under load for a few hours. Since only elastic deformations were desired in the deflection and strain measurements, tests in which some plastic flow had obviously occurred were always discarded. In order to determine the magnitude and rate of flow of the

model, a test was made under continuous load with mercury surface at elevation 1232.

111. Calibration of Instrument Stand.—As the flow test would require several days, temperature variations were expected. Although temperature changes in the testing room were relatively small and probably did not affect the model materially, they might be expected to affect the instrument stand which was equipped with a steel reference plate, as shown in figure 71. This plate was rigidly fastened to the concrete abutments, and any change of temperature caused it to deflect like a steel arch with fixed ends. To check the movement of the plate, a dial gage had been mounted on an invar rod, between the plate and the concrete pit, so that the movement of the plate could be measured. Since the usual test observations required less than an hour, the change in temperature was not sufficient to cause appreciable movement of the plate. However, in a test lasting several days some movement was probable.

A calibration of the steel plate of the instrument stand was therefore made for known changes in temperature. Mercurial thermometers were placed adjacent to the plate at a number of locations. The temperature was changed by opening the windows and shutting off the steam radiator. Temperatures were read at intervals, and positions of the model and instrument stand determined. From data thus obtained, curves were plotted showing movements of the plate caused by temperature changes.

112. Procedure.—The flow test was started on the morning of December 10, 1931. Dial gages and thermometers were read and the mercury load applied. When the mercury surface reached elevation 1232, the gages and thermometers were read again. Readings were made at intervals of 15 minutes during the first few hours of the test, then at 30-minute intervals during the remainder of the first day. As the rate of flow diminished, the interval between readings was increased. After eight days the model was unloaded and allowed to recover. Deflection readings were continued for four days. At the end of the fourth day the upper portion of the model had returned to its original position, but complete recovery had not taken place in the lower part.

In plotting the data from the plastic flow test, a number of minor discrepancies were encountered. Small variations of temperature and atmospheric conditions seemed to affect the model and the apparatus

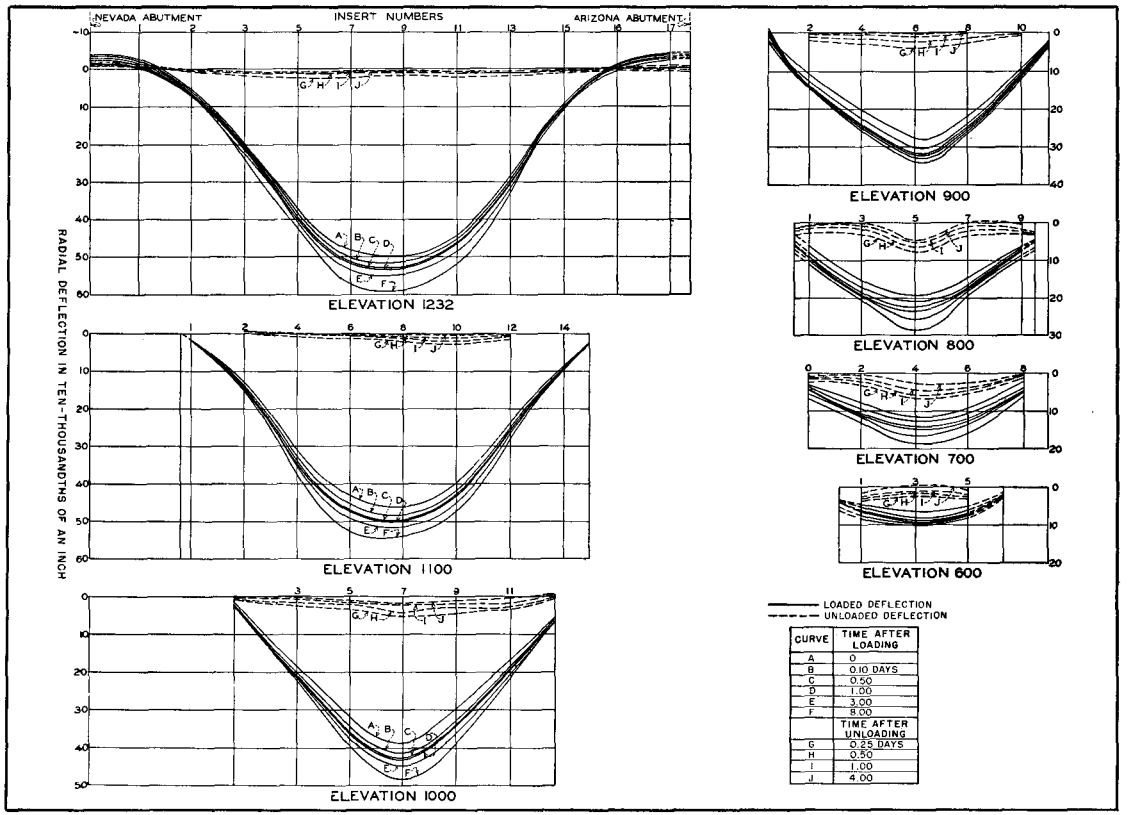

FIGURE 119—INCREASE IN ARCH DEFLECTIONS DUE TO FLOW, LOAD AT ELEVATION 1232

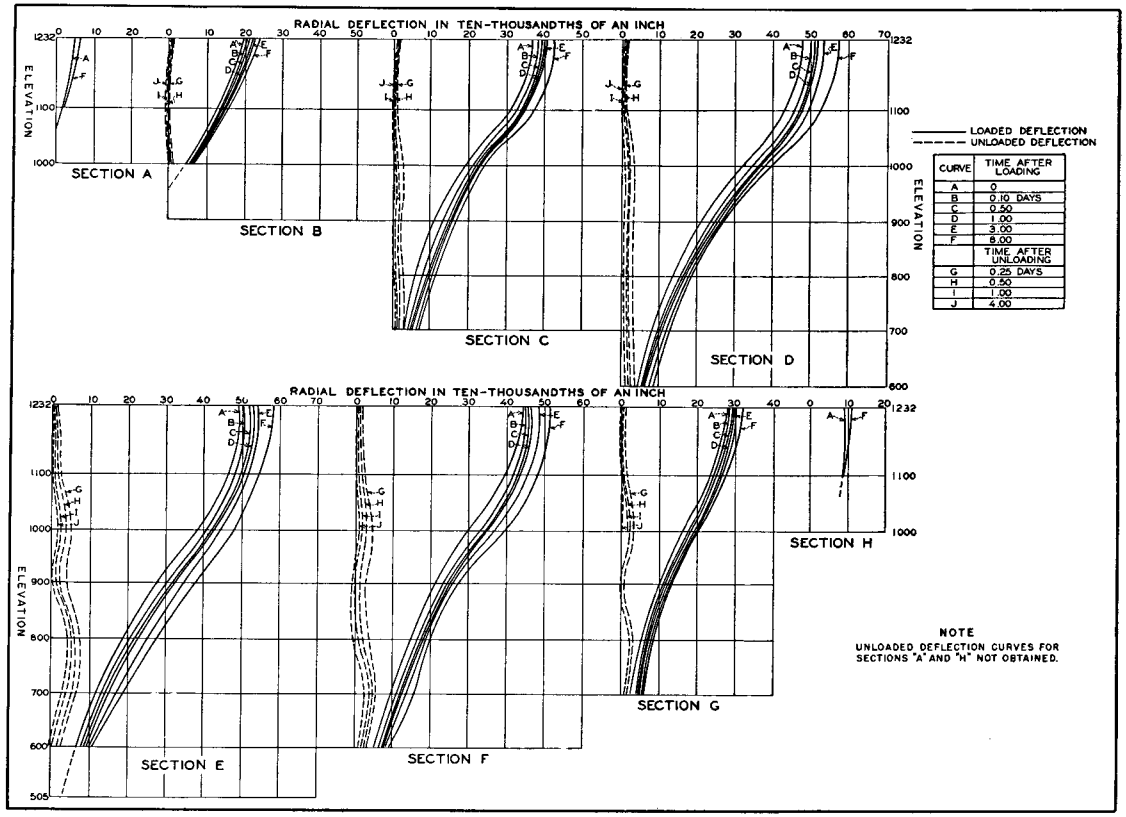

FIGURE 120—INCREASE IN CANTILEVER DEFLECTIONS DUE TO FLOW, LOAD AT ELEVATION 1232

more than had been anticipated. After correcting for the change of temperature of the steel plate, the observed points varied periodically. Observed deflections were greater in the morning than in the afternoon. These periodic variations were disregarded and smooth curves drawn through the general trend of the plotted points. Most of the variations occurred above elevation 900, where the measurements were made with reference to the steel plate of the instrument stand. Below elevation 900 the plotted points fell on smooth curves with practically no irregularities.

113. Results of Flow Test.—Results of the flow test are shown in figures 119 and 120. The maximum deflection at the top of the crown section, elevation 1232, increased from 0.004,92 inches to 0.005,35 inches in eight days. This increase was 8.75 per cent of the original deflection. After unloading, the upper part of the structure recovered almost to its original position in four days. At lower elevations the flow was greater in proportion to the original deflection, due to the higher stresses in the material. At insert 3, elevation 600, the original deflection increased from 0.000,65 inches to 0.001,00 inches, 53.9 per cent, in eight days. The lower part of the model did not recover so completely as the upper part in the period of time allotted to recovery. Although the increase in deflection observed during the test must have been principally due to flow, small proportions of the increase probably were caused by the cracking of the model, discussed in the following section.

114. Condition of Model.—As soon as the flow test was completed the upstream form and rubber bags were removed from the pit. A careful inspection of the upstream face was then made to determine if any cracks had formed. The results of the inspection are shown in figure 121. The model had cracked from the abutments nearly all the way around the upstream face. The width of the crack was small, but it showed definitely through the protective coat of shellac. There was also a small horizontal crack, about six inches long, at the Nevada abutment near elevation 1150. These cracks must have formed during the flow tests, as several inspections of the upstream face, prior to the beginning of the test, failed to reveal any indications of cracking.

The plaster-celite material had an ultimate strength in tension of about thirty pounds per square inch, about one-sixth of its ultimate strength in compression. The cracks along the abutments at the upstream edge may have affected the action of the structure as an

arch. After the model was dismantled, examination showed that the cracks around the abutments varied from one to one and one-half inches in depth. Some proportions of these depths probably were caused by tests made after the flow test was completed. The horizontal crack extended only through the surface coating of shellac. A close examination of the downstream face of the model failed to show any cracks, even in the area of known tensile stresses.

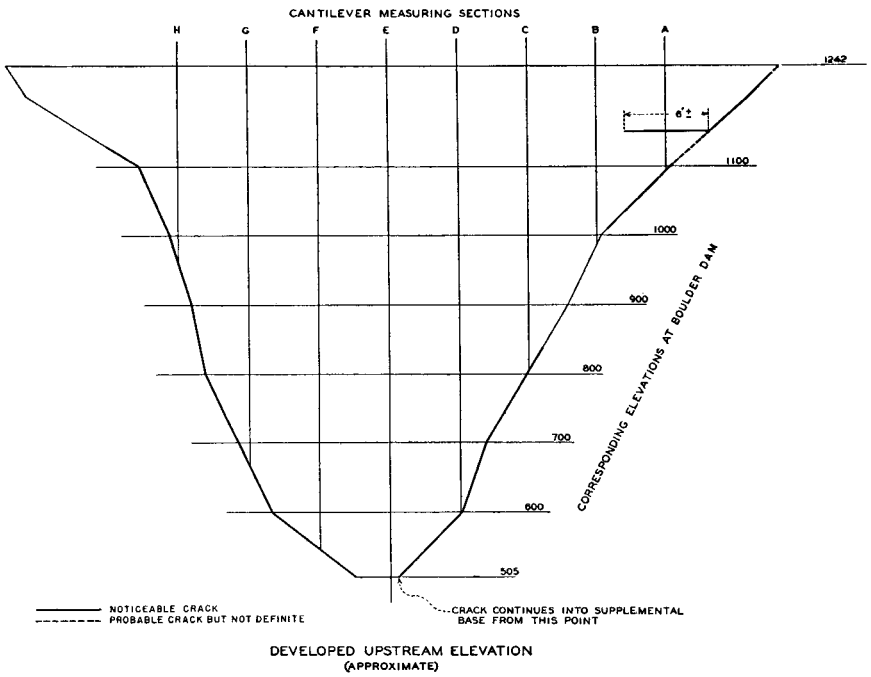

FIGURE 121—CRACKS AT UPSTREAM FACE ON COMPLETION OF FLOW TEST

115. Effect of Cracking.—Since cracking in the model reduced the effective section, an increase in radial deflection was expected. Accordingly, a series of radial deflection measurements was made to determine the effect of the cracks on the action of the model. The results of the measurements, plotted along the arch elements, are shown in figures 122, 123, and 124. They should be compared with the results obtained from former tests, made before any cracking occurred, see figures 87, 83, and 85, respectively. In the former tests, the model acted as an arch fixed at the abutments. By applying mer-

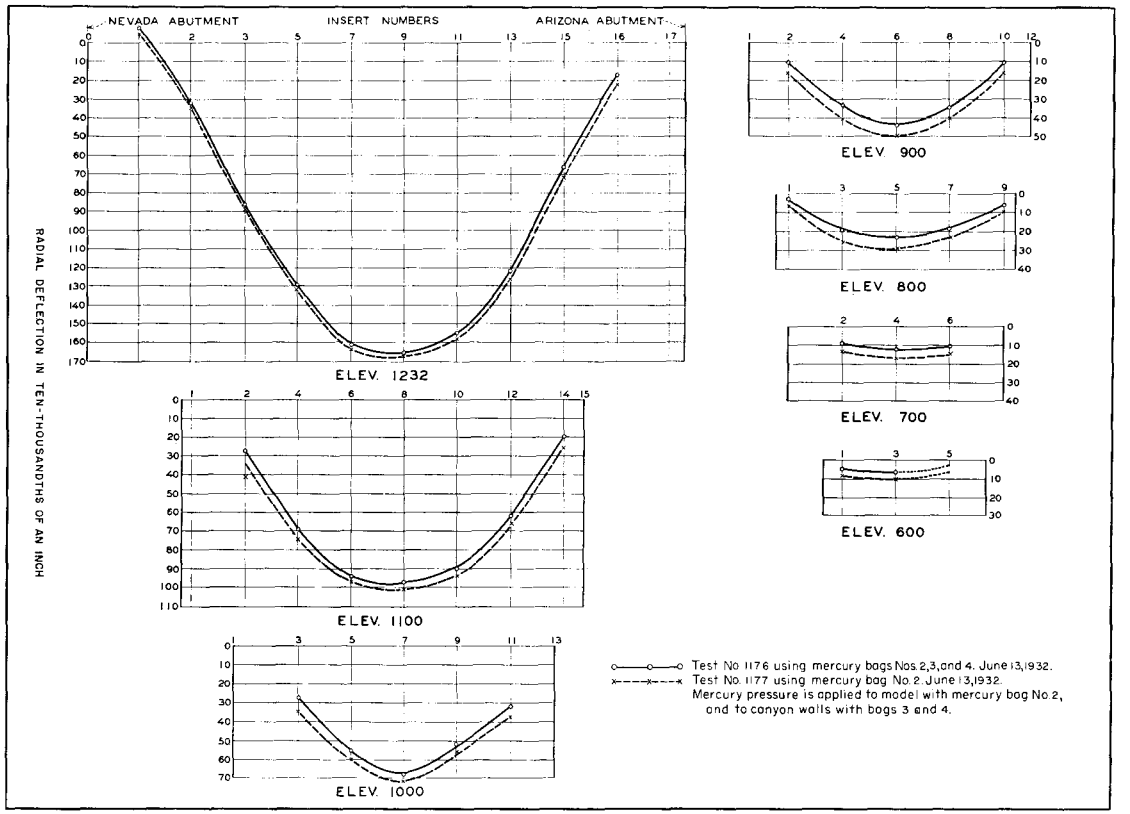

FIGURE 122—RADIAL DEFLECTIONS OF ARCH ELEMENTS AFTER CRACKING, LOAD AT ELEVATION 1400

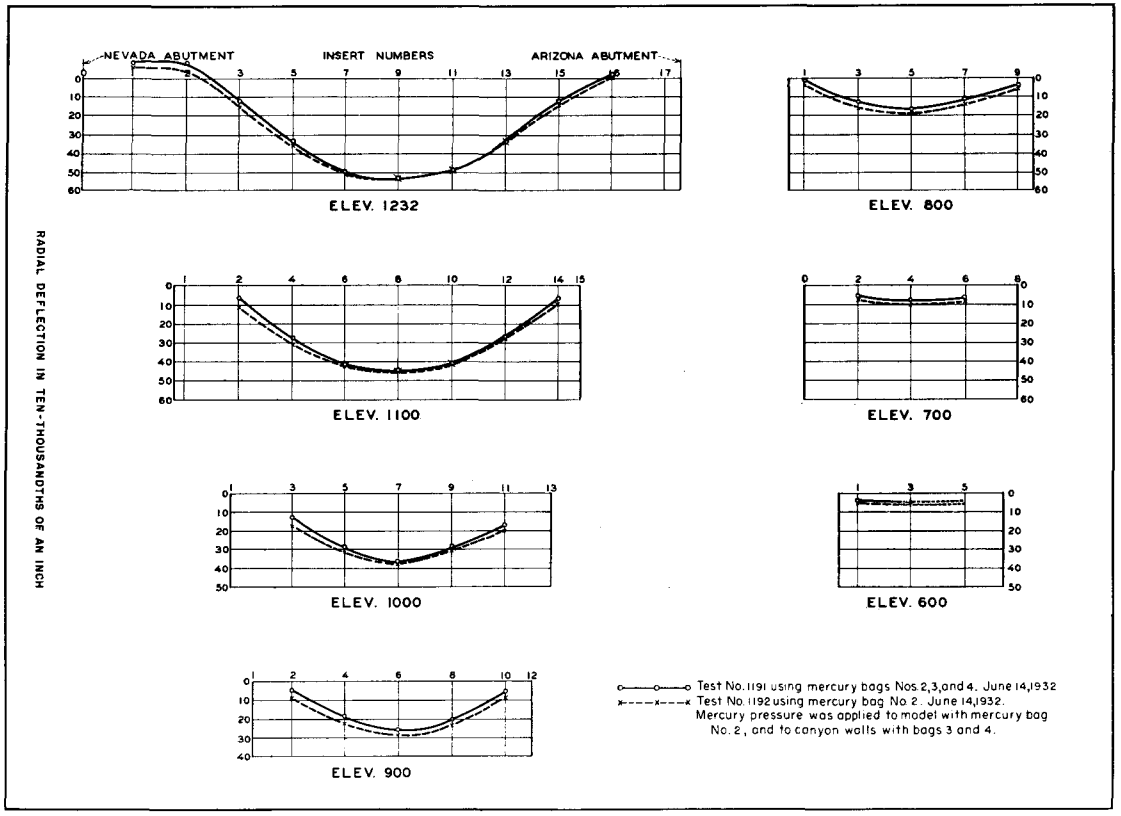

FIGURE 123—RADIAL DEFLECTIONS OF ARCH ELEMENTS AFTER CRACKING, LOAD AT ELEVATION 1232

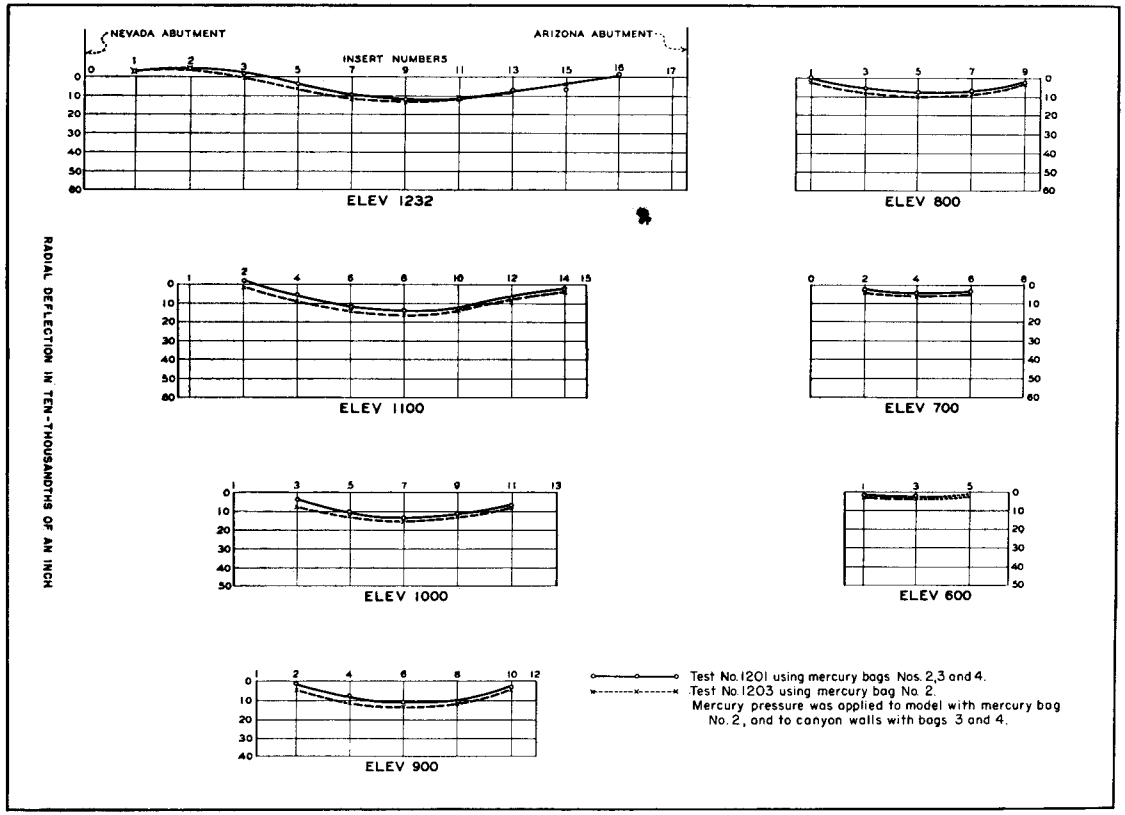

FIGURE 124—RADIAL DEFLECTIONS OF ARCH ELEMENTS AFTER CRACKING, LOAD AT ELEVATION 1100

cury pressure to the abutments, the deflection of the model was changed materially. After the model cracked at the abutments, it acted more like a hinged arch. It was more flexible, as shown by the increased downstream deflection at the crown and the increased upstream deflection of the upper arch elements at the abutments. Mercury pressure on the canyon walls had practically no effect on the deflection of the model after cracking.

The differences in deflection caused by the cracking of the model along the abutments at the upstream face are shown in table 3. In this tabulation, radial deflections of the model at insert 9, elevation 1232, before and after cracking, are listed for the two loading conditions and for partial, normal, and overloads of mercury.

TABLE 3—RADIAL DEFLECTIONS OF MODEL AT INSERT 9, ELEVATION 1232, SHOWING EFFECTS OF CRACKING

Elevation of Mercury Surface	Deflection Before Cracking*		Deflection After Cracking*	
	Pressure on Model	Pressure on Model and Canyon	Pressure on Model	Pressure on Model and Canyon
1400	155.0	152.8	168.8	165.8
1350	117.7	119.9	132.2	130.2
1300	83.5	86.2	99.0	95.5
1250	54.0	64.7	62.0	62.3
1232	48.0	60.2	52.5	53.0
1200	34.0	50.3	37.0	39.2
1150	22.8	41.0	22.0	22.1
1100	14.6	28.1	12.1	12.0

*Each unit represents 0.0001 inch.

TEMPERATURE TESTS

116. Purpose of Tests.—The arches which make up the top portion of Boulder Dam are comparatively slender and their action under temperature changes can be predicted. The lower arches, having a much larger area in contact with the abutments than exposed to the reservoir or atmosphere, have a more complex action. Temperatures a short distance within the rock abutments remain fairly uniform, which tends to maintain uniform temperatures along the contact with the dam. For a period of several years before the reservoir is filled, the upper portion of the dam will be exposed to the

atmosphere on both faces, while the lower part of the upstream face will be at the temperature of the reservoir water.

It was not feasible to duplicate on the model the actual conditions at the dam. It was possible, however, to expose both faces of the model to uniform temperatures, both higher and lower than actual conditions, and therefore to produce much higher temperature stresses. The purpose of the temperature tests on the model was to obtain distribution of temperature in the interior of the model for known temperatures at the faces, and to measure the model deflections caused by the imposed temperature conditions.

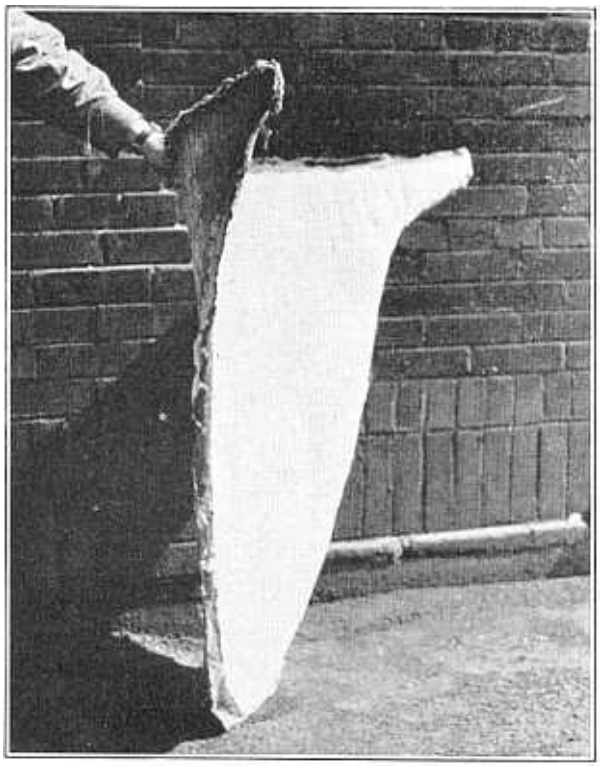

FIGURE 125—UPSTREAM PART OF MODEL JACKET

117. **Temperature Control.**—In making temperature tests of concrete models, water had been used as the medium for producing temperature changes. Water could not be used in temperature tests of the Boulder model, owing to the nature of the plaster-celite

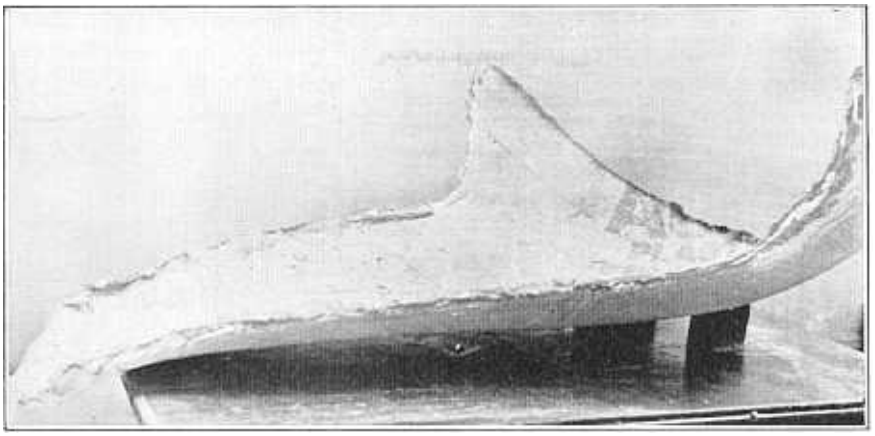

FIGURE 126—DOWNSTREAM PART OF MODEL JACKET

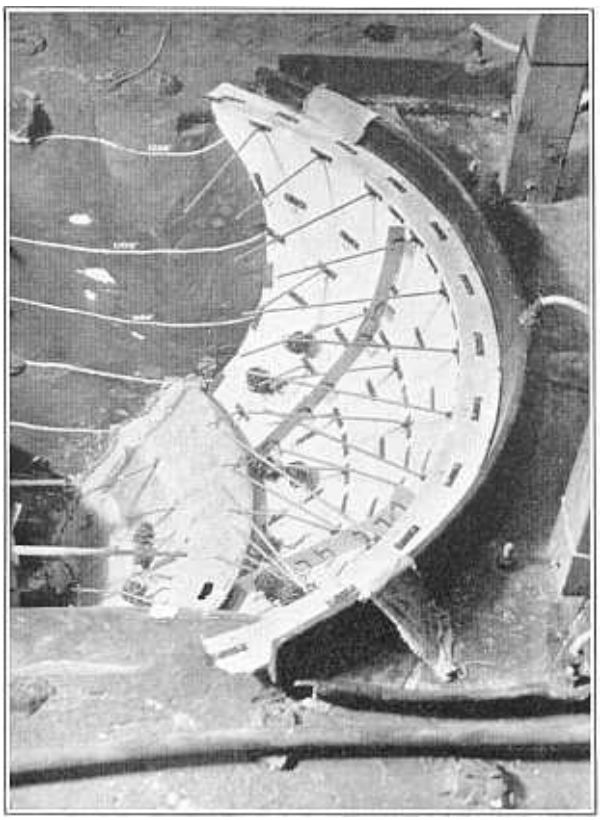

FIGURE 127—DOWNSTREAM PART OF JACKET BEING INSTALLED
Cardboard Vanes on Face are for Distributing Flow of Air

material. Frozen carbon dioxide, dry ice, was chosen for the cooling medium and warm air for the heating medium. This necessitated building a jacket around the model so that vapor from the dry ice could circulate along the model faces and not over the abutments. It was desired to keep the abutments at as near a constant temperature as possible.

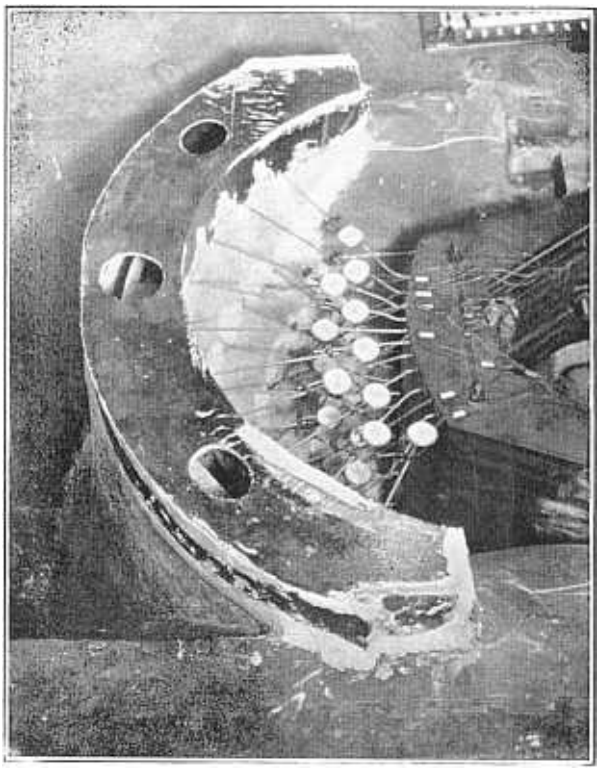

FIGURE 128—JACKET IN PLACE OVER MODEL

118. Construction of Jacket.—The jacket was made by casting plaster shells, one-fourth of an inch thick, over the forms used in casting the model. The shells were reinforced with burlap to prevent cracking. The two shells are shown in figures 125 and 126. In figure 127 the lower part of the downstream shell is shown as it was being installed one inch from the downstream face of the model A mixture of asbestos and building plaster was used for sealing the shells to the abutments. This mixture was rather soft and did not prevent the canyon walls from deforming. The holes in the top of

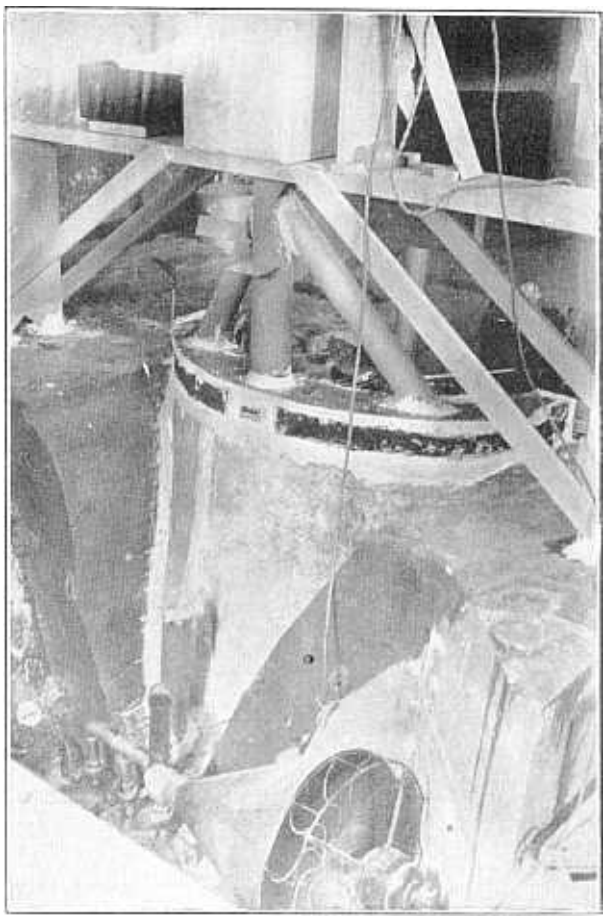

FIGURE 129—MODEL READY FOR TEMPERATURE TEST

the finished jacket, shown in figure 128, were for attaching flues through which vapor could be circulated. Deflection rods extended through small holes in the jacket. These were sealed with cotton, which prevented escape of air but did not affect movements of the rods. Apparatus for cooling the model is shown in figure 129. Carbon dioxide was placed in the container on the support above the model, and an electric fan forced the vapor into the manifold attached to the top of the jacket. Dampers were placed in the branches of the manifold for the purpose of equalizing the flow of vapor inside the jacket. After the vapor passed over the faces of the model it was allowed to exhaust into the open air. The fan shown in the bottom

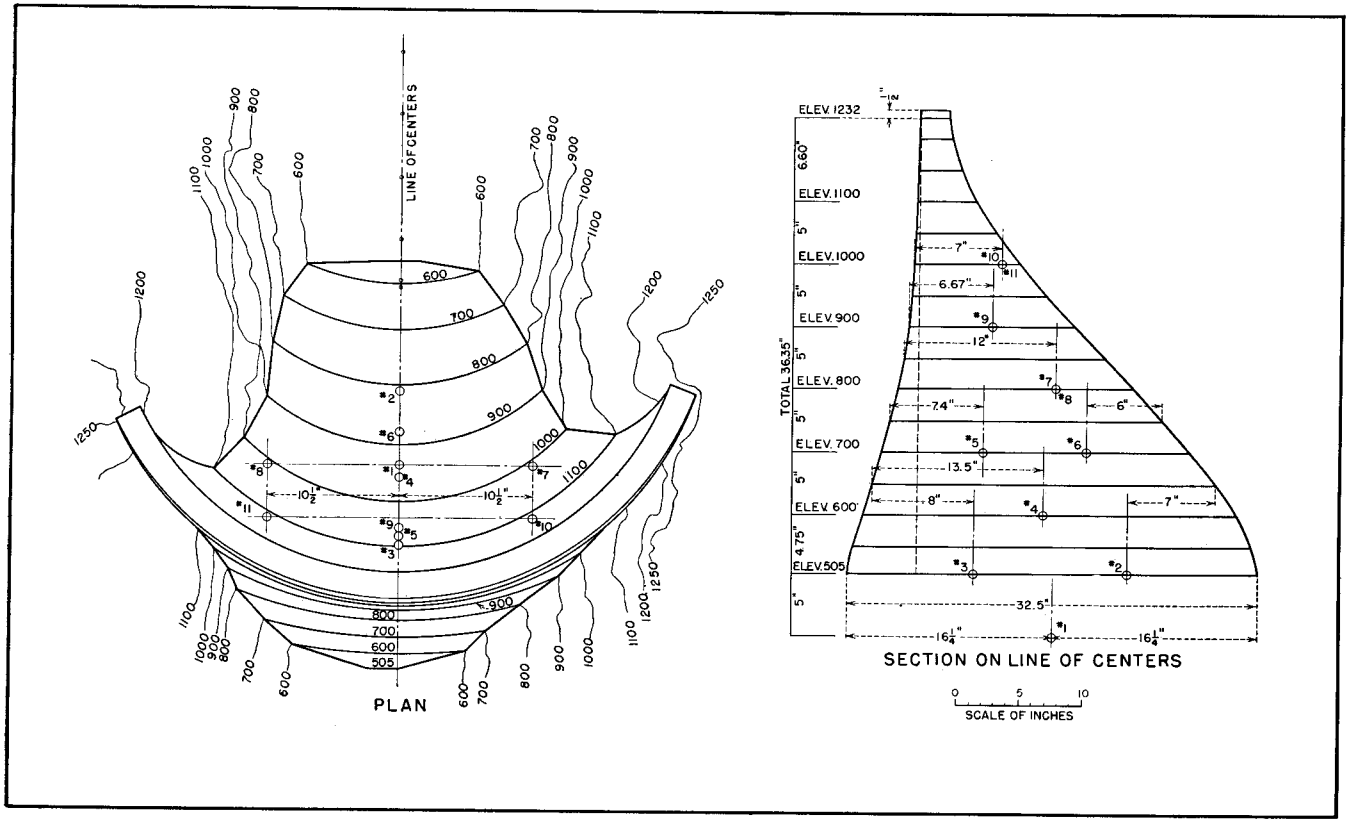

FIGURE 130—LOCATIONS OF THERMOCOUPLES

of figure 129 circulated air at room temperature through a ventilating system in the supplemental base.

119. Equipment.—Temperatures at different locations in the model were measured with thermocouples and mercurial thermometers. The locations of the thermocouples, which were installed while constructing the model, are shown in figure 130. The potentiometer and equipment used in measuring temperatures are shown in figure 131. Cold junctions of the thermocouples were placed in the thermos jug which was filled with melting ice. Next to the thermos jug in figure 131 is the thermocouple switchboard. The standard cell, potentiometer, and storage battery are in the center of the figure, while the galvanometer is in the extreme left. This apparatus was borrowed from the Physics Department of the University of Colorado. Measurements of temperature by thermocouples were supplemented by 15 mercurial thermometers. The locations of the thermometers are shown in figure 132.

The steel plate of the instrument stand was removed and one built of laminated wood installed. This was done because wood is much less susceptible to temperature changes than steel.

120. Cooling Test.—The method of procedure adopted for the cooling test was as follows:

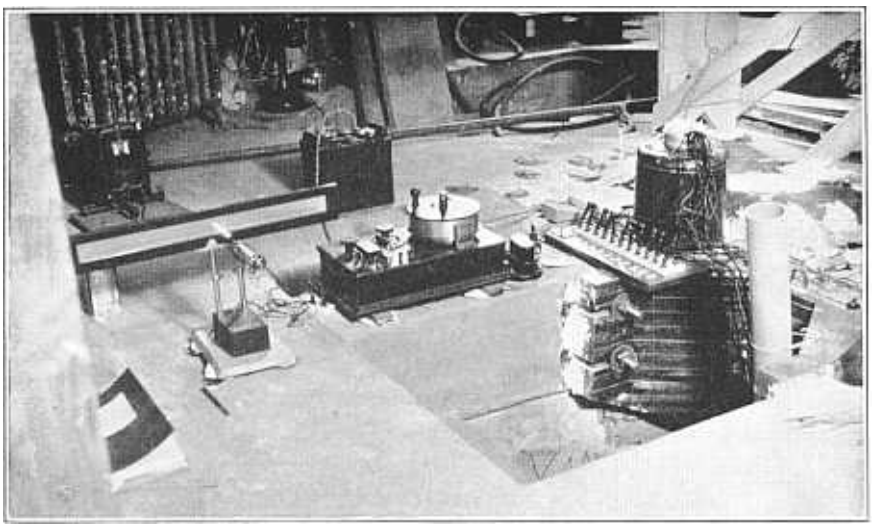

FIGURE 131—TEMPERATURE MEASURING APPARATUS

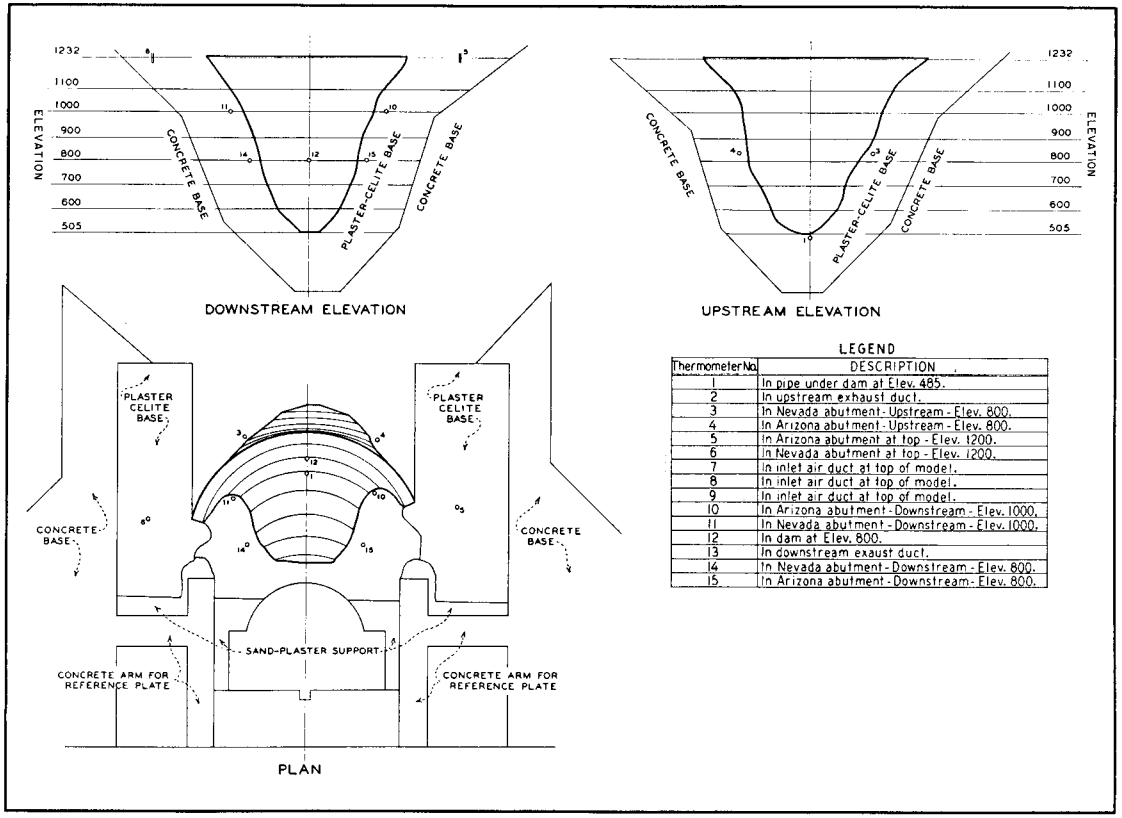

LEGEND

Thermometer No.	DESCRIPTION
1	In pipe under dam at Elev. 485.
2	In upstream exhaust duct.
3	In Nevada abutment - Upstream - Elev. 800.
4	In Arizona abutment - Upstream - Elev. 800.
5	In Arizona abutment at top - Elev. 1200.
6	In Nevada abutment at top - Elev. 1200.
7	In inlet air duct at top of model.
8	In inlet air duct at top of model.
9	In inlet air duct at top of model.
10	In Arizona abutment - Downstream - Elev. 1000.
11	In Nevada abutment - Downstream - Elev. 1000.
12	In dam at Elev. 800.
13	In downstream exaust duct.
14	In Nevada abutment - Downstream - Elev. 800.
15	In Arizona abutment - Downstream - Elev. 800.

FIGURE 132—LOCATIONS OF THERMOMETERS

1. The model was brought to a stable condition of temperature and radial movement by circulating air at room temperature through the jacket system.

2. The model was cooled to as low a temperature as possible by circulating carbon dioxide vapor through the system.

3. The model was returned to the approximate starting conditions of temperature and position by circulating air at room temperature.

Observations of temperature and radial deflection were made at frequent intervals, so that the action of the model could be studied. The test was commenced on the morning of June 23, 1932. Air at room temperature was circulated through the system until stable conditions were reached. At 10:40 a. m., June 23, the temperature and position of the model being fairly stable, carbon dioxide was placed in the cooling system. Cooling by carbon dioxide was then continued until the model temperature had been lowered as much as possible.

121. Results of Cooling Test.—The average temperature of the model at the beginning of the test was about 68 degrees Fahrenheit. The material of which the model was made had fairly good insulating qualities. Consequently, considerable time was required to cool the model to a stable temperature. Graphs showing the temperature range as determined by the thermocouples and thermometers are shown in figures 133 and 134. All temperatures are in degrees Fahrenheit.

It is obvious that in a structure such as Boulder Dam, the upper portion of the structure, which is relatively thin, will respond more quickly to a change in outside temperature than the lower portion. The lowest temperature reached during the cooling test was indicated by thermocouple 10, where a temperature of 40 degrees, giving a drop of 28 degrees, was observed. Thermocouple 1, which was located in the supplemental base underneath the dam, indicated a drop in temperature of only 6 degrees. This was the smallest change noted.

Temperature observations were made hourly during the early part of the test and at intervals of about two hours after the temperature changes became less rapid. At the end of one week the model became stationary with respect to temperature and position. The conduction of heat from the abutments into the model was equal to the radiation of heat from the model into the carbon dioxide vapor, so that the temperature of the model became stationary. The average

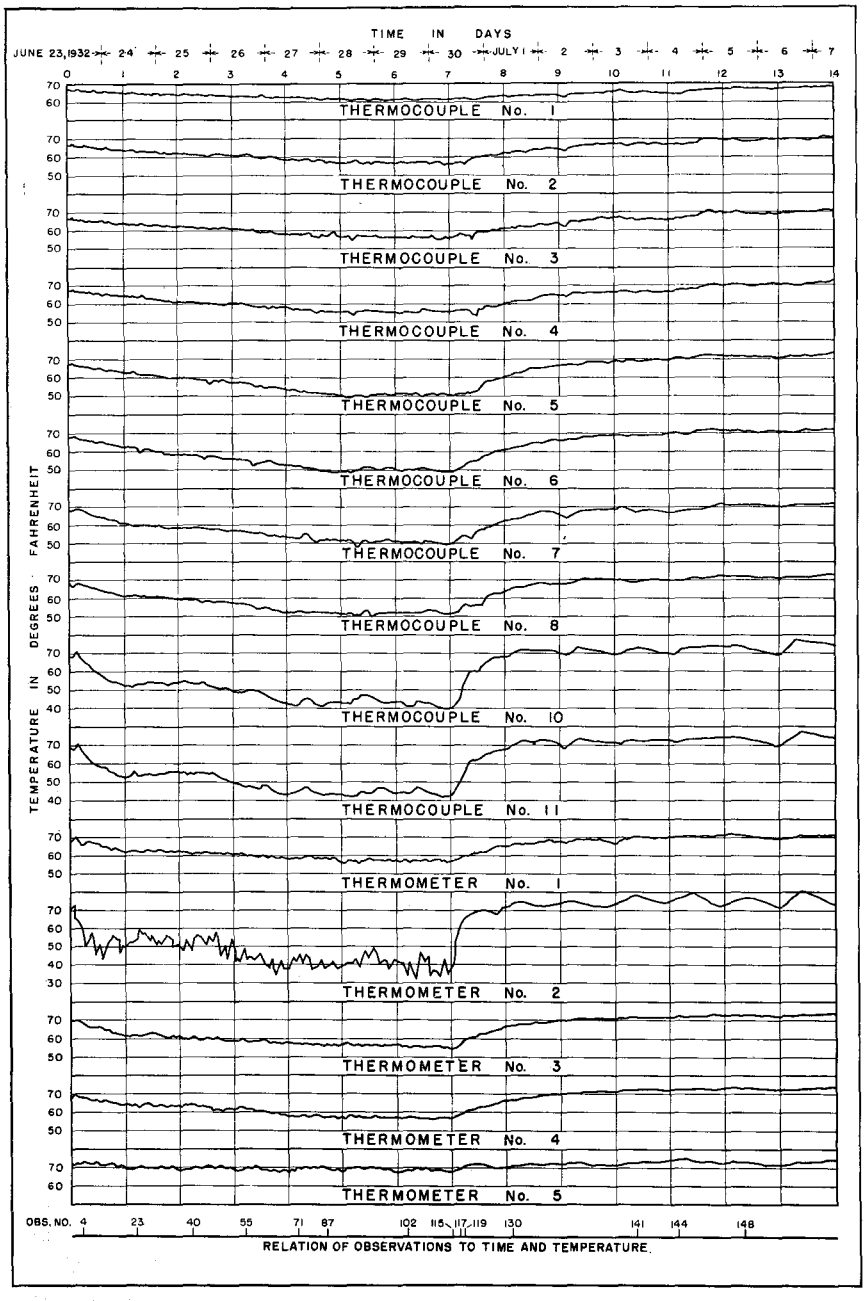

FIGURE 133—TEMPERATURE RECORD DURING COOLING TEST
For Locations of Thermocouples and Thermometers see Figures 130 and 132

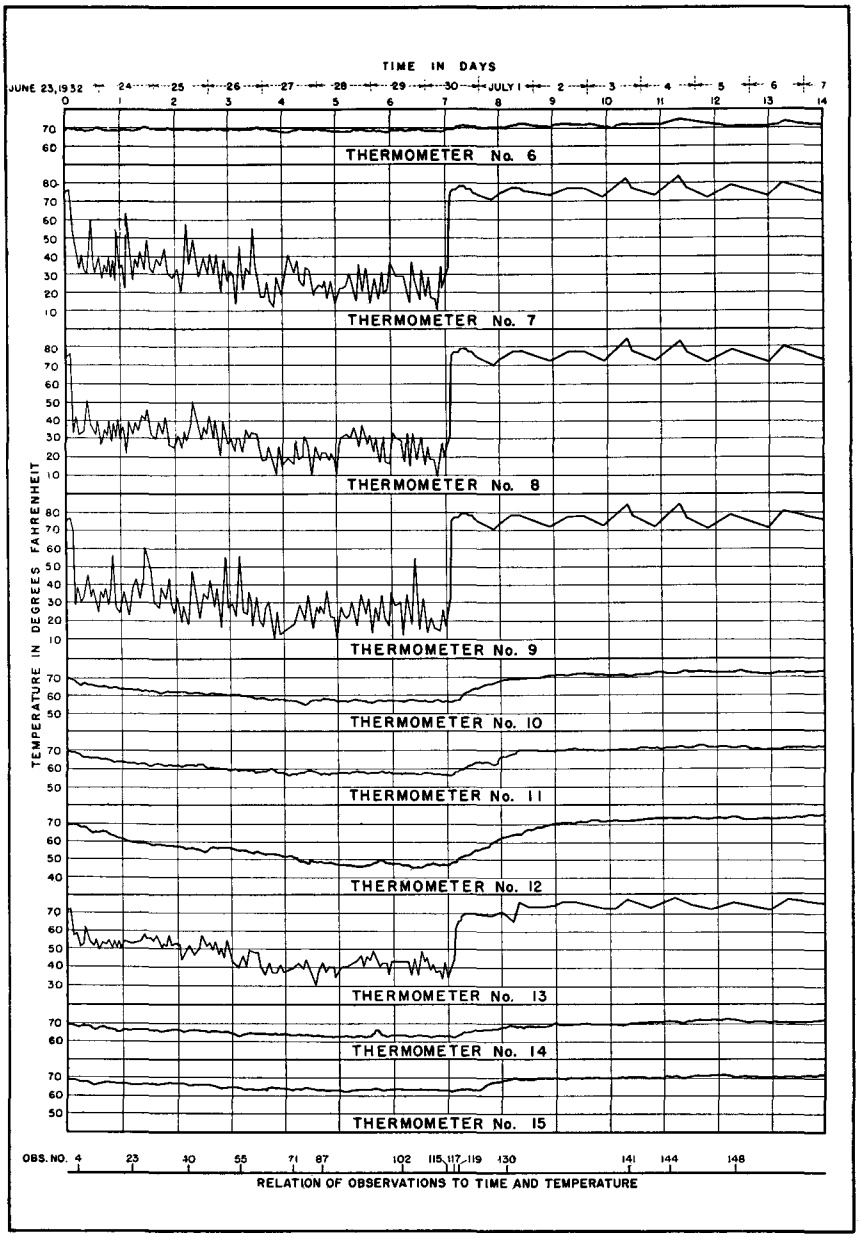

FIGURE 134—TEMPERATURE RECORD DURING COOLING TEST (CONTINUED)

For Locations of Thermometers see Figure 132

decrease in temperature was about twenty degrees when the model had reached its coolest condition.

Radial deflections caused by the lowering of the temperature are shown in figures 135 and 136. Deflections measured at the lower elevations showed the effect of the high coefficient of expansion of the material, 0.000,001 of an inch per inch per degree Fahrenheit. Deflection measurements were made at the downstream face of the model instead of at the center line of the arch elements. The shrinkage of the model at the surface, below elevation 800, was greater than the downstream deflection at the center line. Consequently, the net movement of the downstream face below elevation 800 was upstream.

The dry ice was removed from the cooling system on June 30, 1932. Air at room temperature was circulated until the model returned approximately to its original temperature and position. This required about one week. Deflection curves observed during this period are shown in figures 137 and 138. The final observed position of the model is shown by deflection curves numbered 148. At elevations 800 and 1100 some deformation still remained in the model. This deformation was probably the result of flow under the severe stresses caused by the cooling operations.

122. Heating Test.—Before starting the heating test, the dial gages were removed and cleaned, the tray which held the dry ice was removed, and the fan in the ice box was reversed so as to draw air from the top of the jacket. Two 550-watt electric heating elements were used to furnish heat, which was admitted to the system through openings in the bottom of the jacket. The warm air was drawn upward over both faces of the model.

The method of procedure adopted for the test was essentially the same as in the cooling test, except that the temperature of the model was increased instead of lowered. In detail the procedure was the same as the cooling test described in section 120. A temperature of 125 degrees was the maximum to which the plaster-celite material could be exposed without danger of dehydrating the plaster.

Heat was admitted to the system July 11, 1932, and applied for one week. At the end of that time the model was fairly stationary as regards position and temperature. The range of temperature during this period is shown in figures 139 and 140. In the lower elevations of the model the temperature increased from 70 to 100 degrees. At 10:15 p. m., July 11, electric power was turned off at the plant and

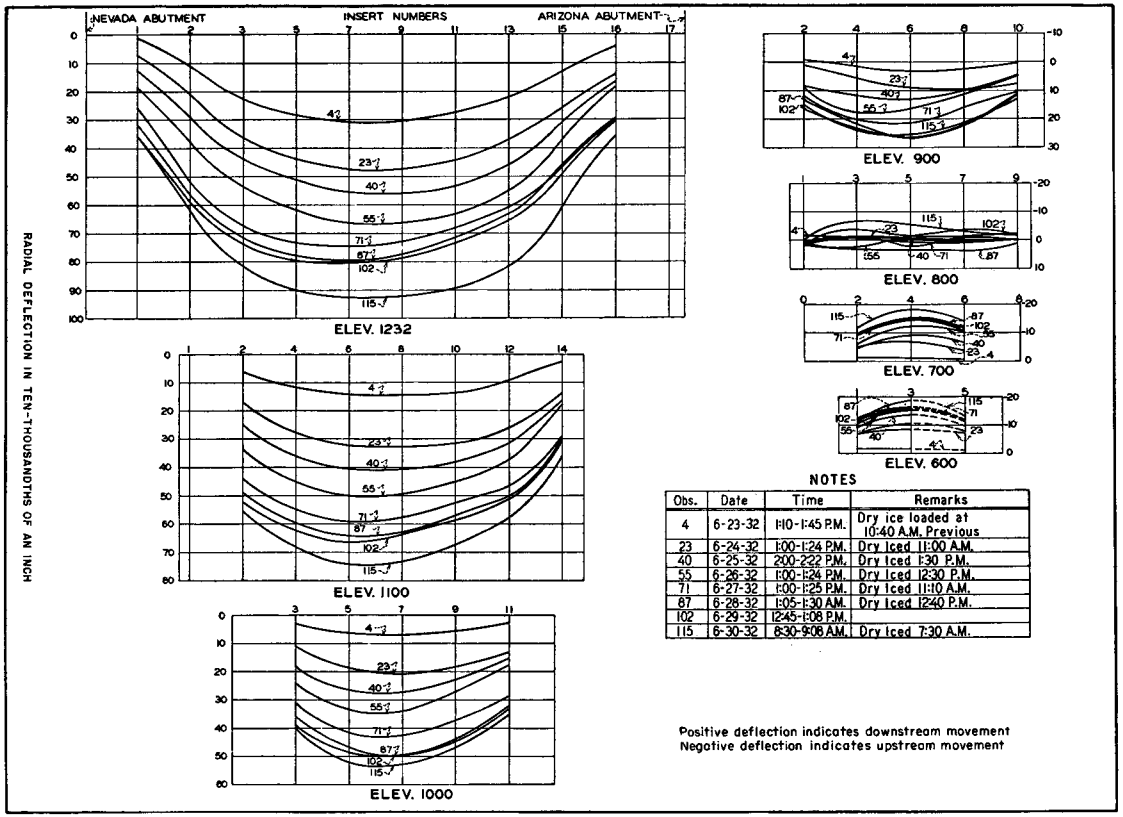

FIGURE 135—RADIAL DEFLECTIONS OF ARCH ELEMENTS DUE TO COOLING

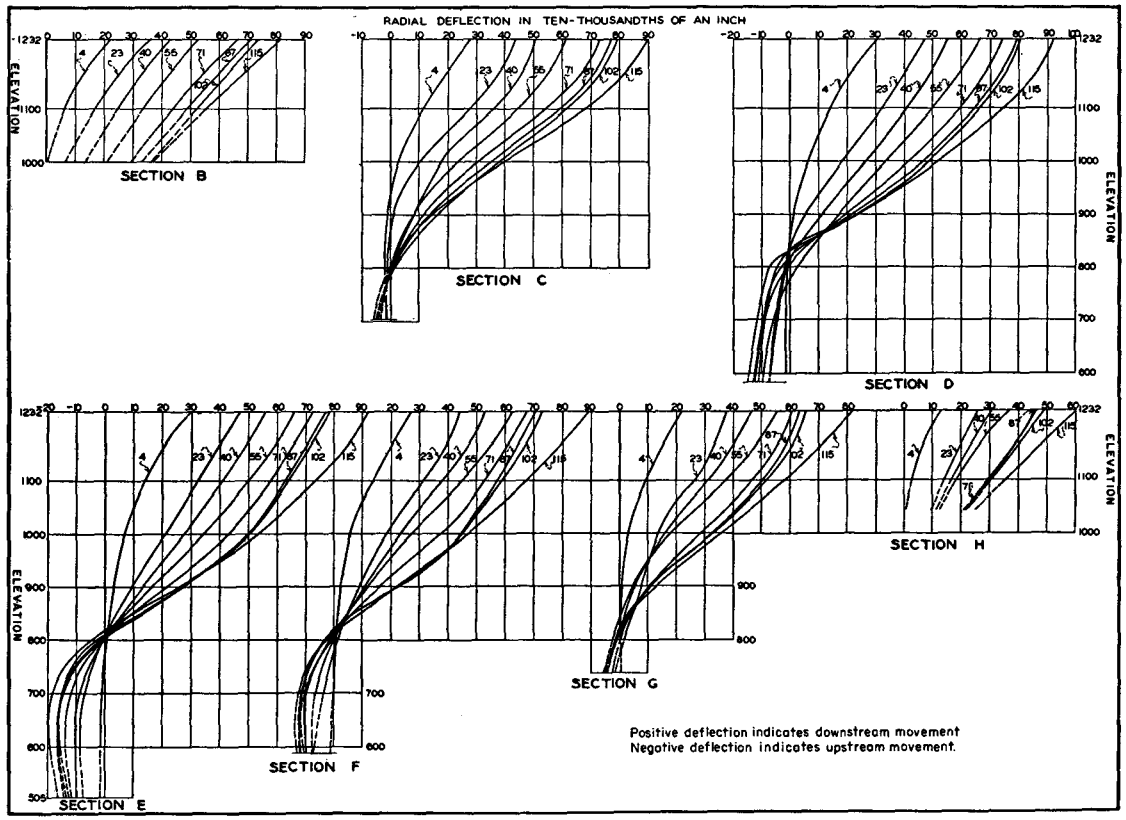

FIGURE 136—RADIAL DEFLECTIONS OF CANTILEVER ELEMENTS DUE TO COOLING

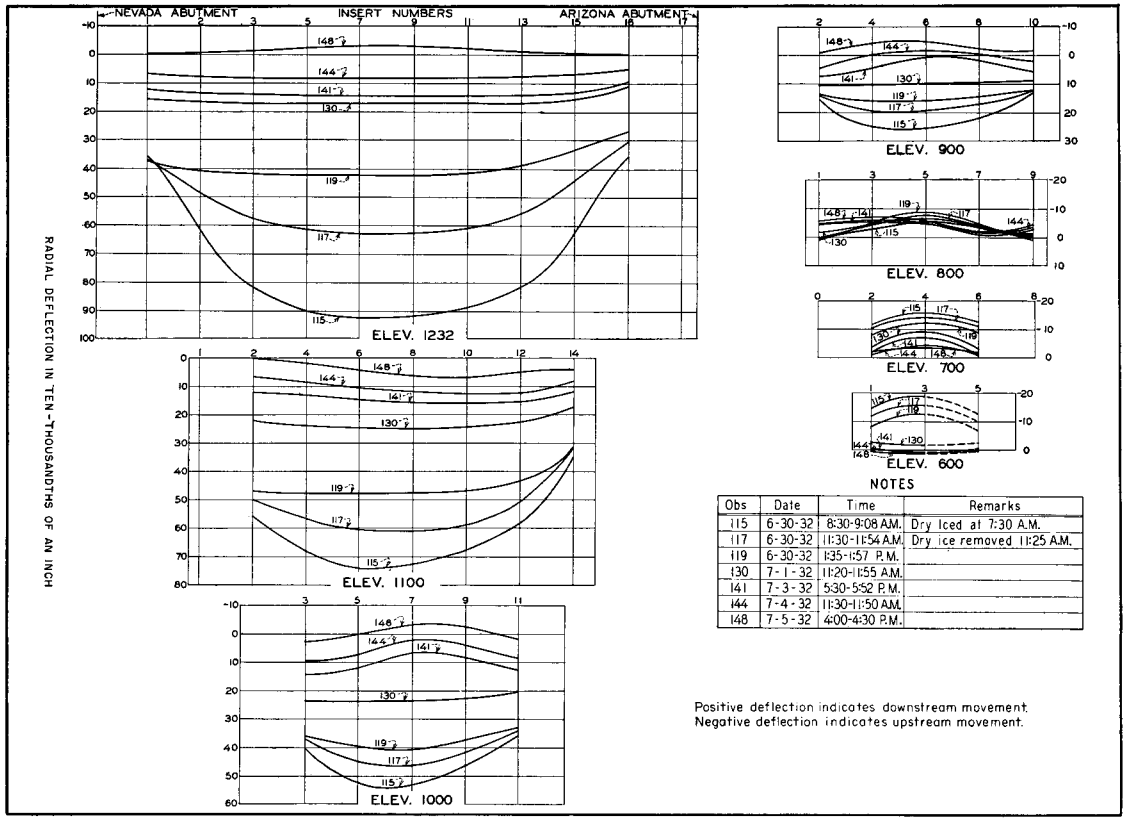

Obs	Date	Time	Remarks
115	6-30-32	8:30-9:08 A.M.	Dry Iced at 7:30 A.M.
117	6-30-32	11:30-11:54 A.M.	Dry Ice removed 11:25 A.M.
119	6-30-32	1:35-1:57 P.M.	
130	7-1-32	11:20-11:55 A.M.	
141	7-3-32	5:30-5:52 P.M.	
144	7-4-32	11:30-11:50 A.M.	
148	7-5-32	4:00-4:30 P.M.	

FIGURE 137—RADIAL DEFLECTIONS OF ARCH ELEMENTS SHOWING RECOVERY FROM COOLING

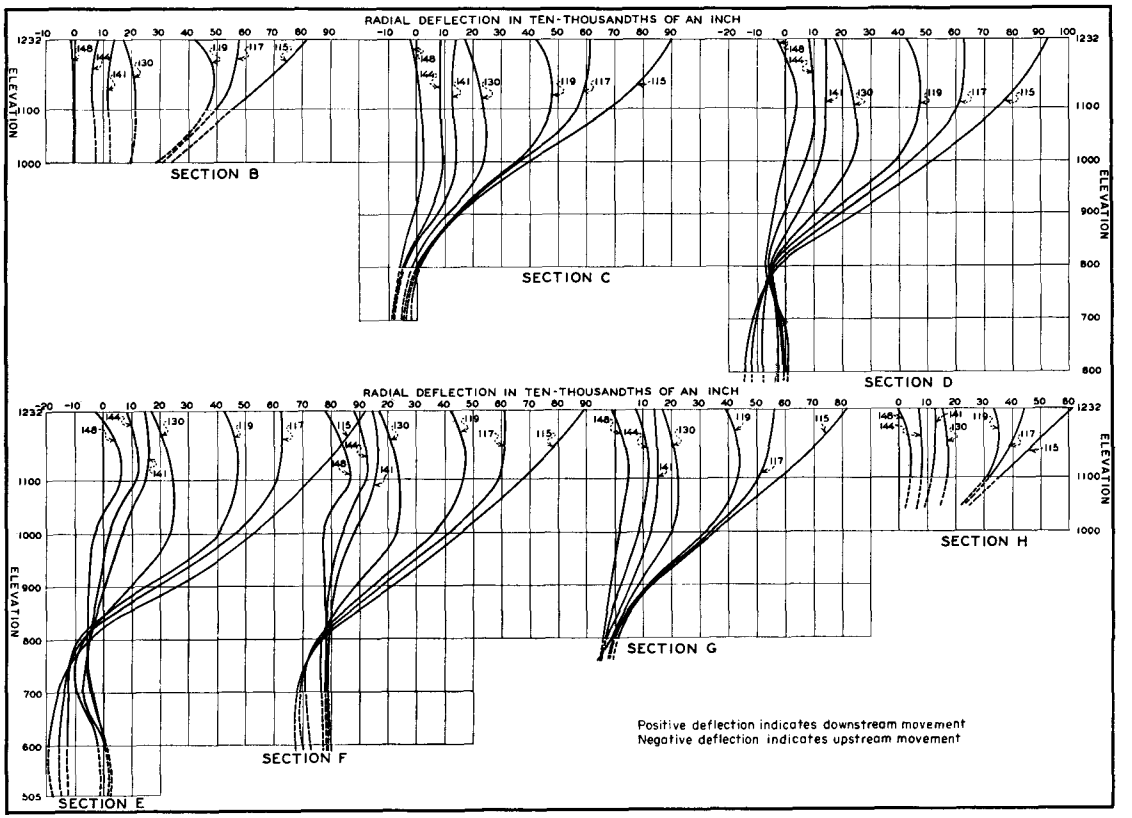

FIGURE 138—RADIAL DEFLECTIONS OF CANTILEVER ELEMENTS SHOWING RECOVERY FROM COOLING

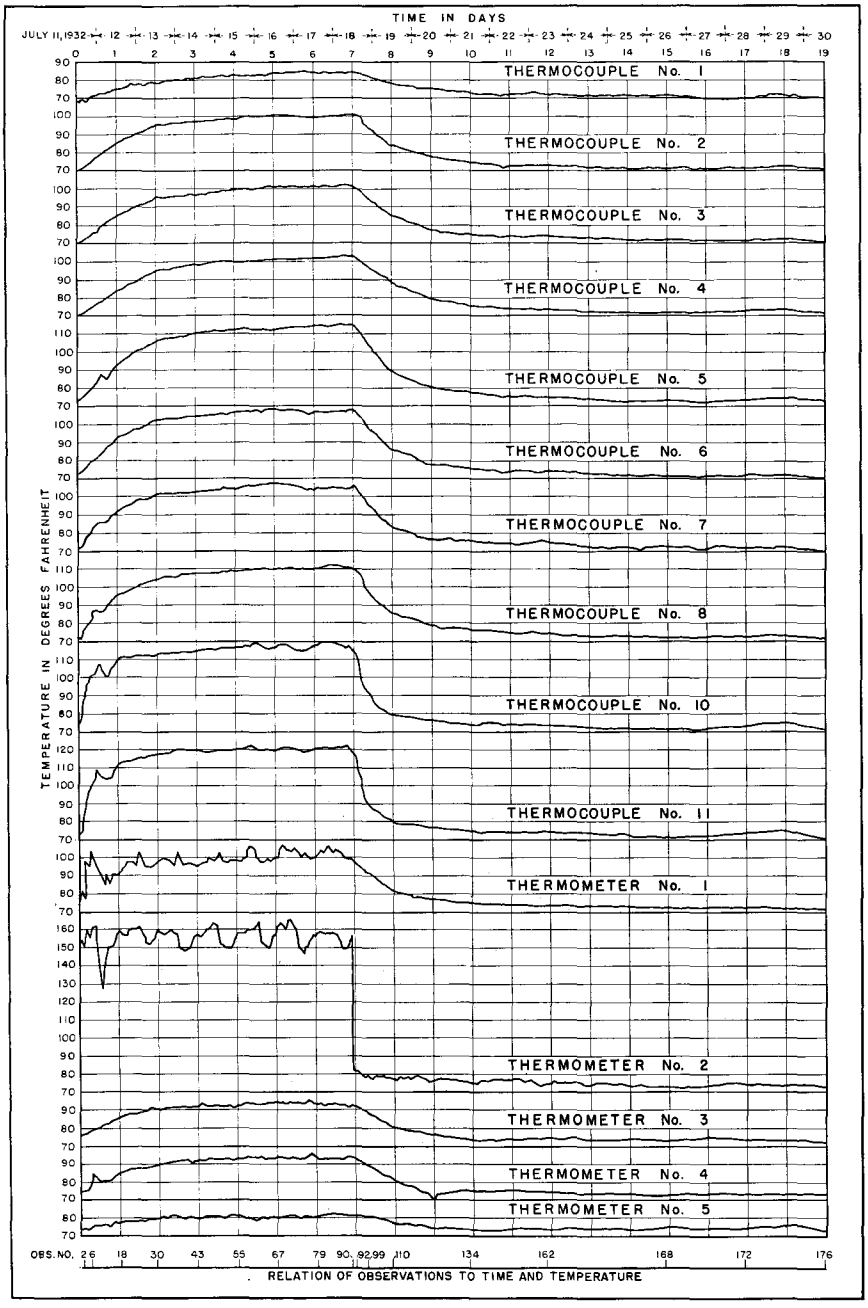

FIGURE 139—TEMPERATURE RECORD DURING HEATING TEST

For Locations of Thermocouples and Thermometers see Figures 130 and 132

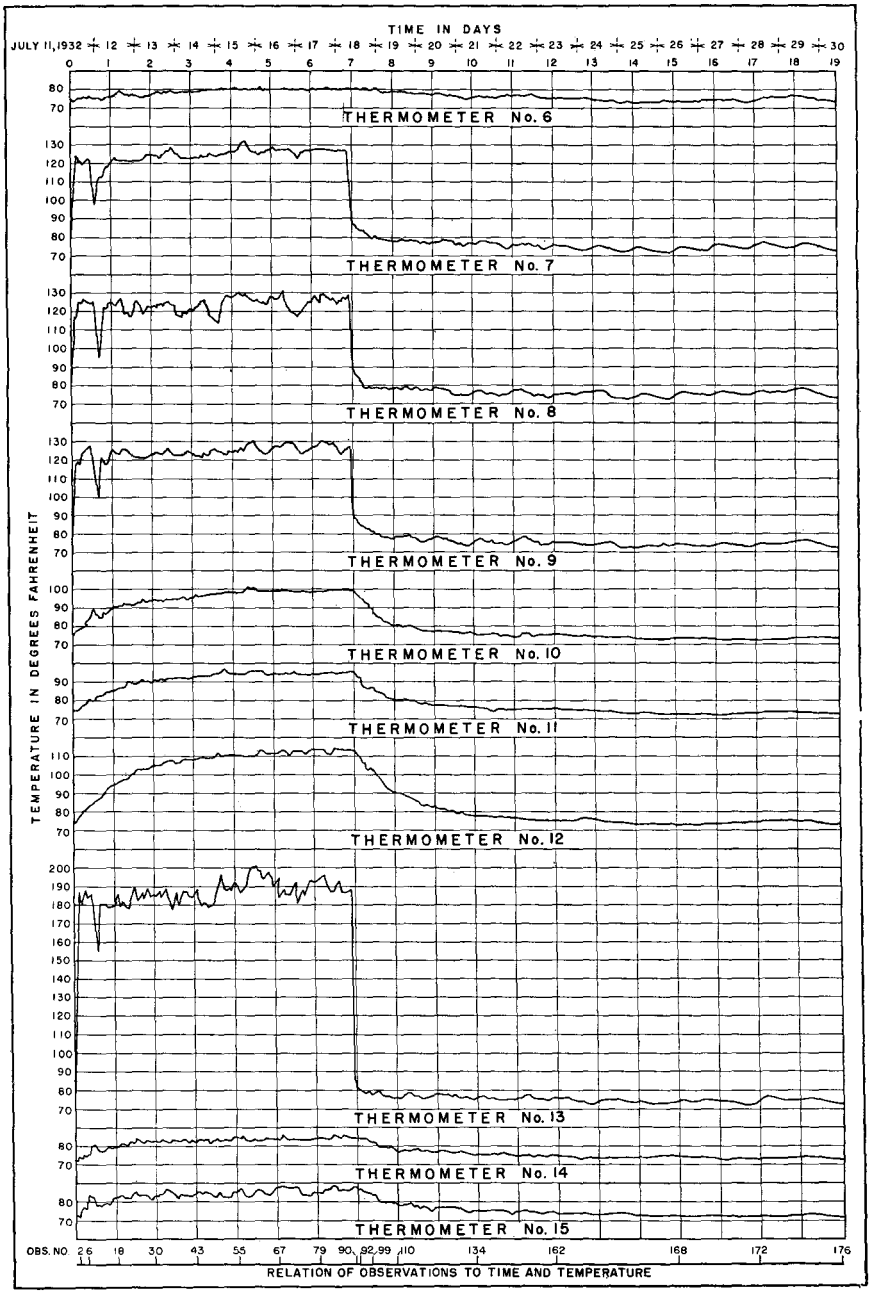

FIGURE 140—TEMPERATURE RECORD DURING HEATING TEST (CONTINUED)

For Locations of Thermometers see Figure 132

remained off for two hours. This accounts for the irregularities in the temperature graphs shown in figures 139 and 140.

123. Results of Heating Test.—Radial deflections of the model during the heating test and recovery are shown in figures 141 to 144. The deflection curves contained more erratic points than were encountered in the cooling test. This was due to the fact that the dial gages were mounted so that upstream deflections were recorded as negative movements on the gages. The dial gages did not register negative movements as satisfactorily as positive movements, particularly when the measurement was about one hundred dial divisions, because of the changing tension in the springs of the gages. Frequently, the gages above elevation 800 went out of range and had to be reset, which involved some errors.

The heat was turned off on the morning of July 18. After 12 days the model had returned approximately to its original position and temperature. The mean temperature of the air had risen during the three weeks devoted to the test so that the model temperature at the completion of the test was slightly higher than at the beginning.

The upper part of the model, where arch elements were relatively thin, deflected upstream due to expansion of the arch rings. Below elevation 800, where the model was relatively thick, the expansion of the heated model caused the measured deflections to be downstream in direction. These deflections were opposite to those measured in the cooling test.

124. Condition of Model.—After completion of the temperature tests the jacket was removed and both faces of the model carefully inspected for cracks. The crack around the upstream face at the foundation and abutments, originally started in the flow tests, apparently had been extended by the temperature tests. Additional cracks on both faces of the dam were also observed. It was found later, after the model was dismantled, that these additional cracks were almost entirely on the surface, due, probably, to the brittle film of shellac and varnish being more affected by temperature than the plastercelite. The abutment cracks were about 1½ inches deep at the top and decreased to about 1 inch deep at the base. There was no way of determining what proportions of these depths were caused by the plastic flow test and by the temperature tests.

125. Effect of Cracking.—Radial deflection measurements were next made to determine the effect of the additional cracking on the

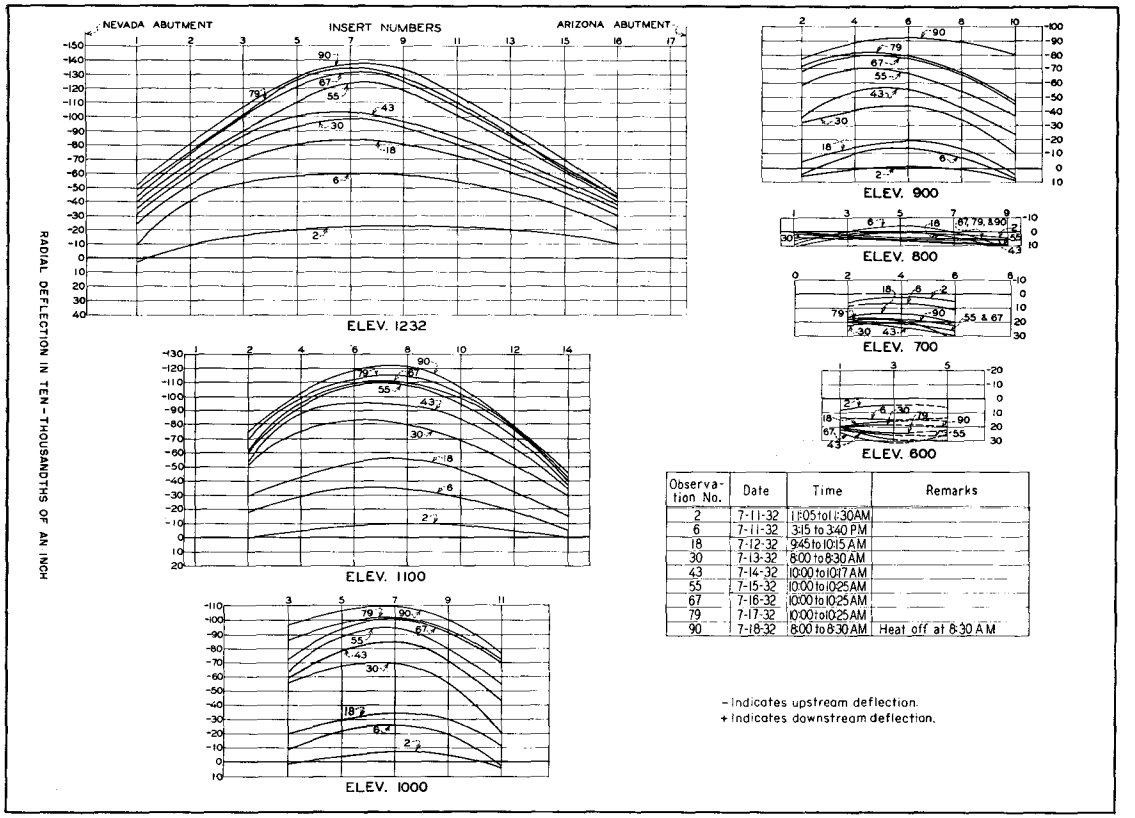

Observation No.	Date	Time	Remarks
2	7-11-32	11:05 to 11:30 AM	
6	7-11-32	3:15 to 3:40 PM	
18	7-12-32	9:45 to 10:15 AM	
30	7-13-32	8:00 to 8:30 AM	
43	7-14-32	10:00 to 10:17 AM	
55	7-15-32	10:00 to 10:25 AM	
67	7-16-32	10:00 to 10:25 AM	
79	7-17-32	10:00 to 10:25 AM	
90	7-18-32	8:00 to 8:30 AM	Heat off at 8:30 A.M.

FIGURE 141—RADIAL DEFLECTIONS OF ARCH ELEMENTS DUE TO HEATING

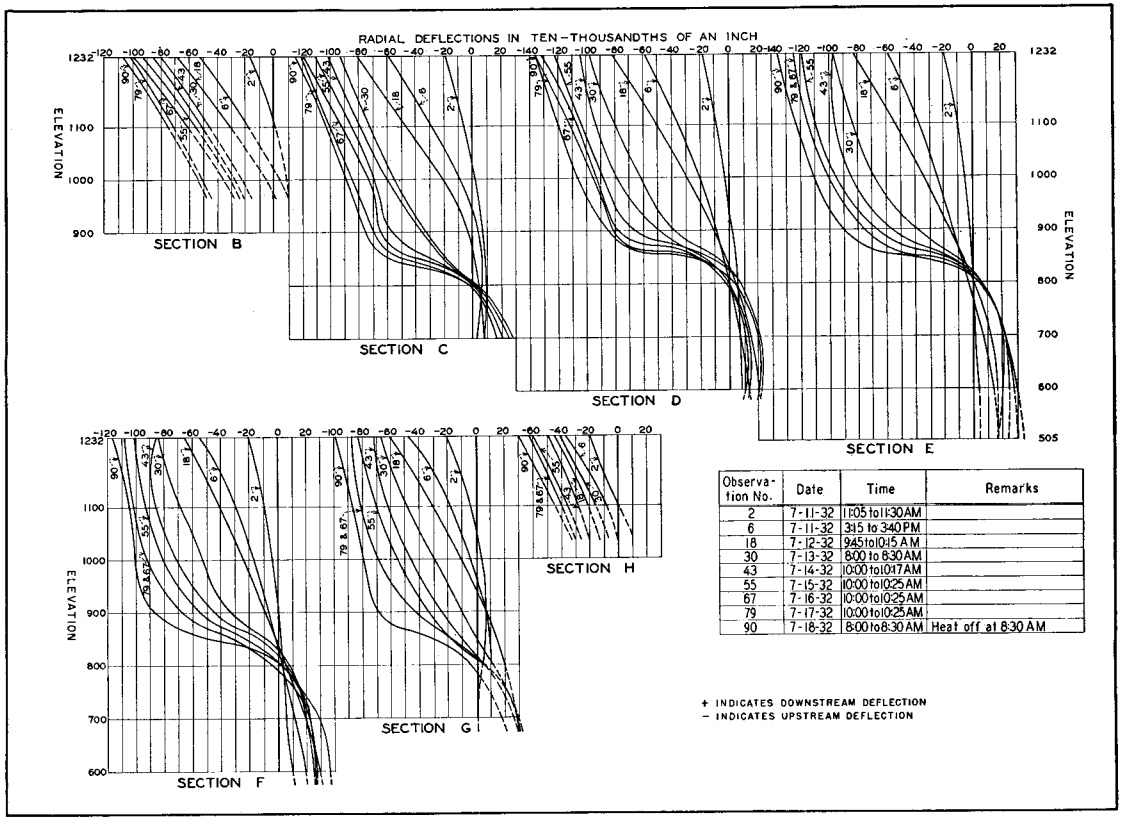

Observation No.	Date	Time	Remarks
2	7-11-32	11:05 to 11:30 AM	
6	7-11-32	3:15 to 3:40 PM	
18	7-12-32	9:45 to 10:15 A.M.	
30	7-13-32	8:00 to 8:30 AM	
43	7-14-32	10:00 to 10:17 AM	
55	7-15-32	10:00 to 10:25 AM	
67	7-16-32	10:00 to 10:25 AM	
79	7-17-32	10:00 to 10:25 AM	
90	7-18-32	8:00 to 8:30 AM	Heat off at 8:30 AM

FIGURE 142—RADIAL DEFLECTIONS OF CANTILEVER ELEMENTS DUE TO HEATING

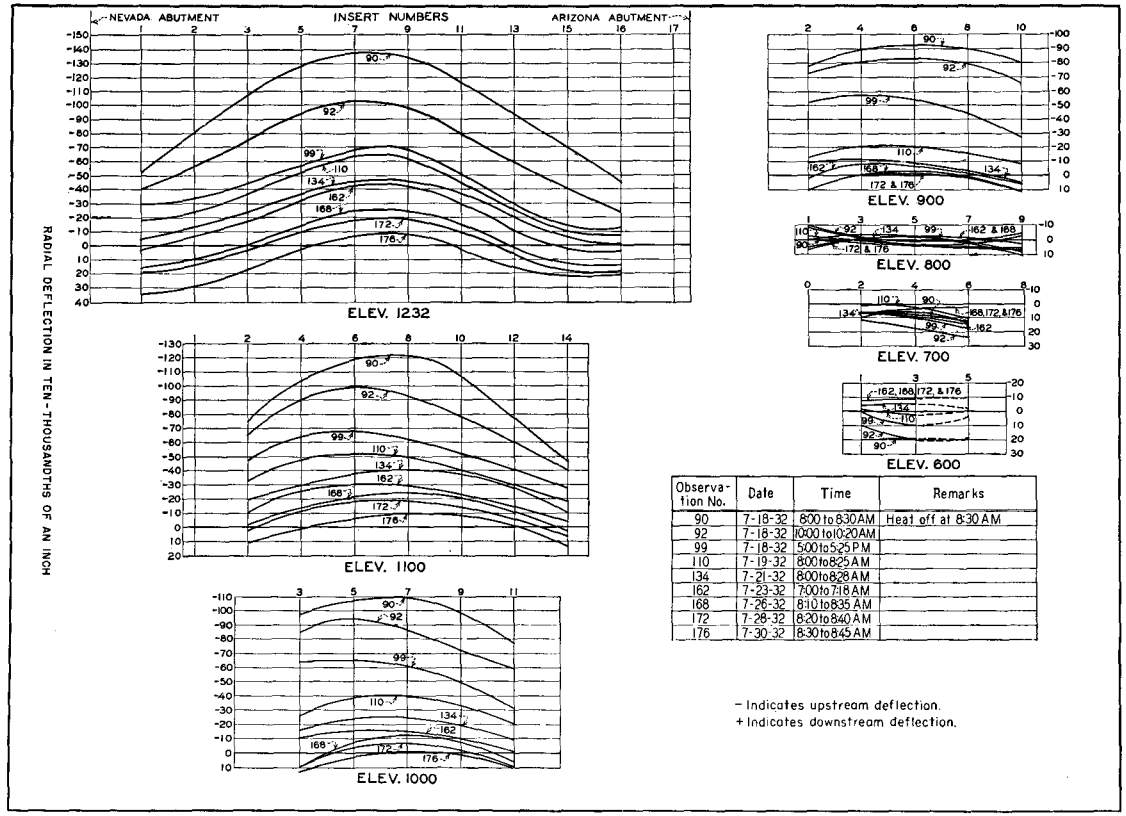

Observation No.	Date	Time	Remarks
90	7-18-32	8:00 to 8:30 AM	Heat off at 8:30 AM
92	7-18-32	10:00 to 10:20 AM	
99	7-18-32	5:00 to 5:25 P.M.	
110	7-19-32	8:00 to 8:25 A.M.	
134	7-21-32	8:00 to 8:28 A.M.	
162	7-23-32	7:00 to 7:18 A.M.	
168	7-26-32	8:10 to 8:35 A.M.	
172	7-28-32	8:20 to 8:40 A.M.	
176	7-30-32	8:30 to 8:45 A.M.	

− Indicates upstream deflection.
+ Indicates downstream deflection.

FIGURE 143—RADIAL DEFLECTIONS OF ARCH ELEMENTS SHOWING RECOVERY FROM HEATING

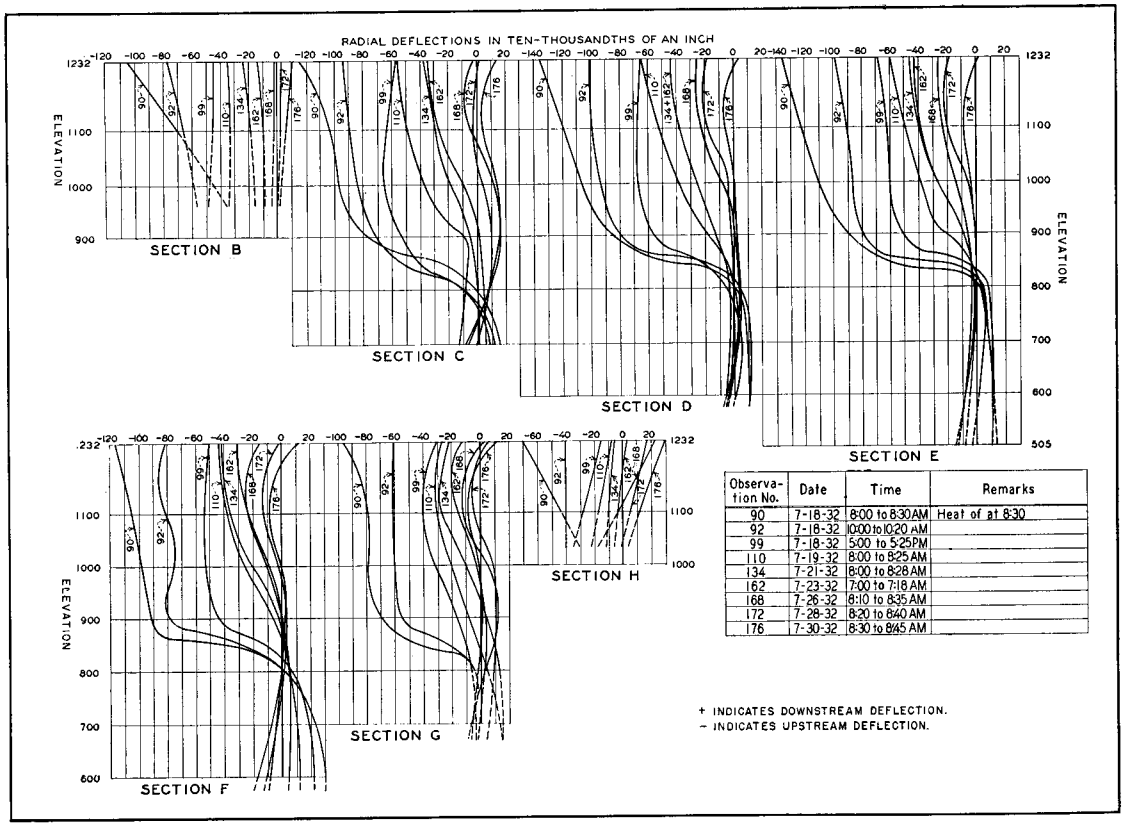

Observation No.	Date	Time	Remarks
90	7-18-32	8:00 to 8:30 AM	Heat of at 8:30
92	7-18-32	10:00 to 10:20 AM	
99	7-18-32	5:00 to 5:25 PM	
110	7-19-32	8:00 to 8:25 AM	
134	7-21-32	8:00 to 8:28 AM	
162	7-23-32	7:00 to 7:18 AM	
168	7-26-32	8:10 to 8:35 AM	
172	7-28-32	8:20 to 8:40 AM	
176	7-30-32	8:30 to 8:45 AM	

FIGURE 144—RADIAL DEFLECTIONS OF CANTILEVER ELEMENTS SHOWING RECOVERY FROM HEATING

flexibility of the arch. Downstream deflections at the crown increased about eight per cent for the overload conditions and about five per cent for load at elevation 1232. The differences were less for partial loads. The increase in deflection changed the shape of the deflection curves only slightly from those shown in figures 122 to 124. Applying mercury pressure to the canyon walls had practically no effect on the radial deflections. Frequently, the two deflection curves coincided, particularly at elevation 1100.

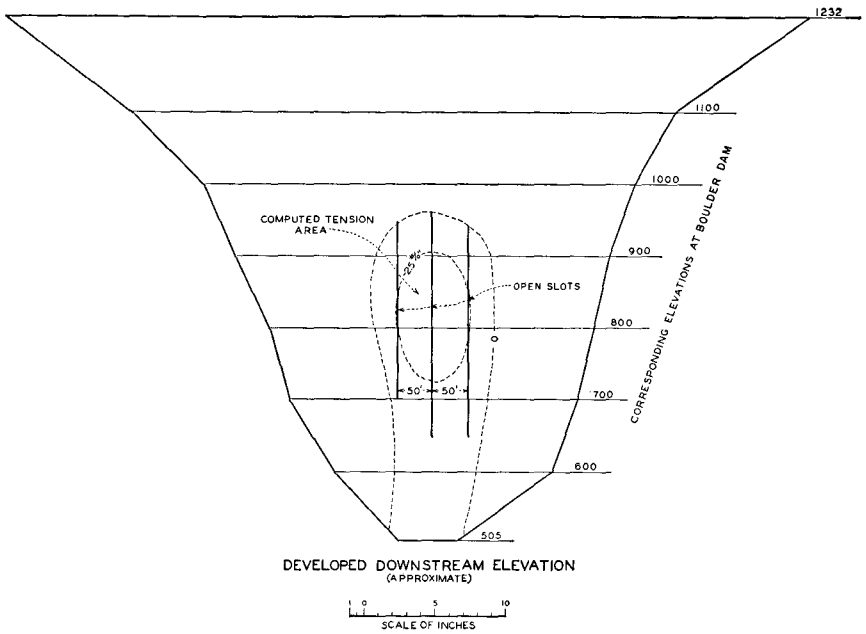

FIGURE 145—LOCATION OF SLOTS IN TENSION AREA

TENSION AT DOWNSTREAM FACE

126. Slots in Tension Area.—The strain measurements showed a zone of tension in the arch elements at the downstream face of the model. Since Boulder Dam was built in blocks, separated by joints, the development of similar stresses in the dam would probably result in the opening of vertical radial joints in the tension area. To obtain a similar condition in the model, vertical slots were sawed into the downstream face at the locations of the joints, as shown in figure 145.

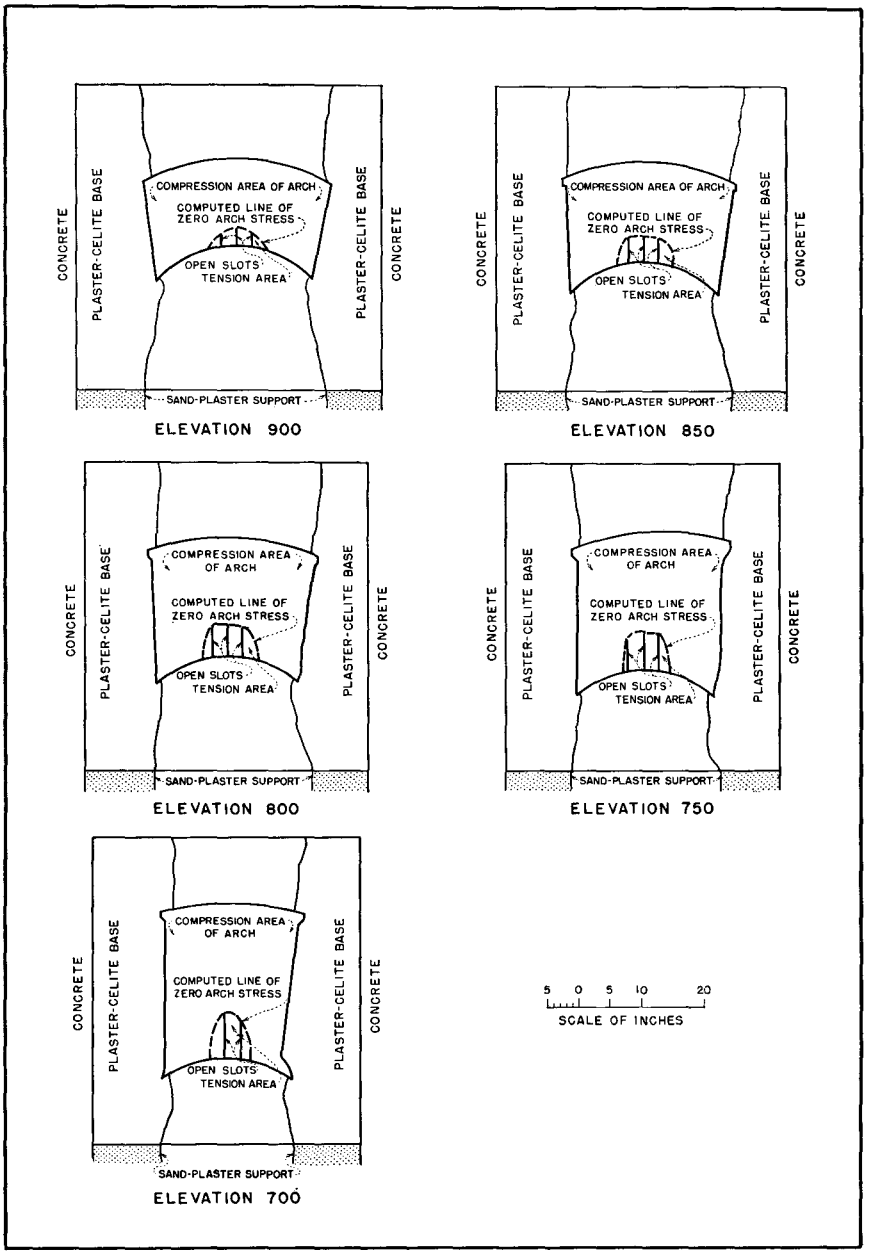

FIGURE 146—DEPTHS OF SLOTS IN TENSION AREA

TABLE 4—RADIAL DEFLECTIONS AT INSERT 9, ELEVATION 1232, SHOWING EFFECT OF SLOTS IN DOWNSTREAM FACE*

Elevation of Mercury Surface	Deflection Before Cracking		Deflection After Cracking		Deflection With Slots	
	Pressure on Model	Pressure on Model and Canyon	Pressure on Model	Pressure on Model and Canyon	Pressure on Model	Pressure on Model and Canyon
1400	155.0	152.8	177.5	174.5	174.6	173.2
1350	117.7	119.9	139.4	137.6	140.0	142.6
1300	83.5	86.2	103.0	101.0	99.8	98.0
1250	54.0	64.7	66.0	60.5	66.2	63.4
1232	48.0	60.2	55.0	52.2	54.4	51.5
1200	34.0	50.3	39.5	36.9	39.8	36.1
1150	22.8	41.0	23.0	22.1	22.3	21.4
1100	14.6	28.1	14.0	12.8	15.0	12.2

*One unit of deflection equals 0.0001 inch.

The limits of tension stresses in the model, due to a mercury load, were calculated from stresses determined by a trial load analysis. Using computed stresses at the faces and assuming a straight line variation of stress between the faces, tension areas in the arch elements were computed as shown in figure 146. Depths of the slots sawed into the downstream face were determined from the data shown in figure 146.

127. **Radial Deflections.**—After the slots were cut in the model a series of radial deflection tests were run. It was found that relieving tension by cutting slots had very little effect on radial deflections. Apparently, at these elevations, the load was carried by arch thrust and cantilever bending; and cutting the slots did not appreciably alter the arch thrust in the uncracked portion and had virtually no effect on the cantilever loads. In table 4, observed deflections at the top of the crown cantilever are compared with original deflections and with deflections after cracking at the abutments.

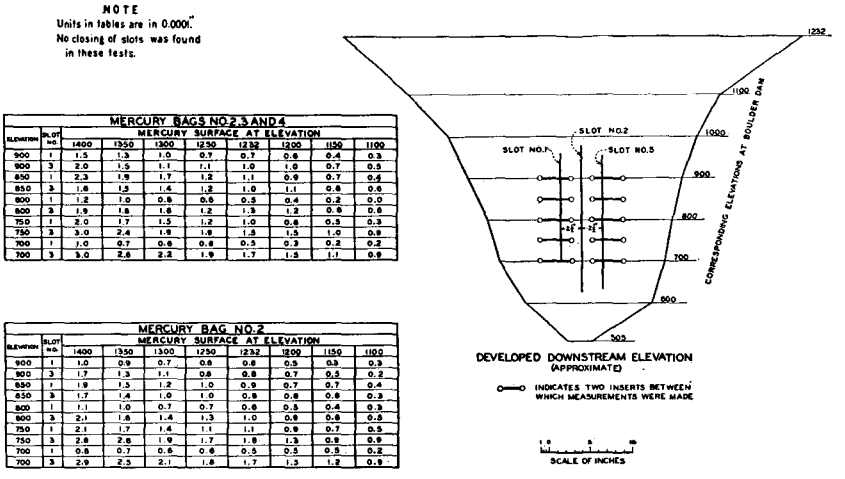

FIGURE 147—OPENING OF SLOTS 1 AND 3

128. **Slot Openings Due to Load.**—Additional inserts were set in the downstream face of the model, so that dial gages could be mounted to register changes in the width of the slots. Two sets of measurements were made as shown in figures 147 and 148. A maximum increase of 0.001,27 inches in width occurred at slot 2, which coin-

cided with cantilever section E. This increase was measured at elevation 850, with the mercury surface at elevation 1400 and with pressure applied to both the model and the canyon walls. For the same conditions of loading, with the mercury surface at elevation 1232, the spreading was 0.0008 inches. The opening and closing of the slots was elastic, since the recovery on unloading was nearly always 100 per cent. No closing of the slots during loading was observed in these tests.

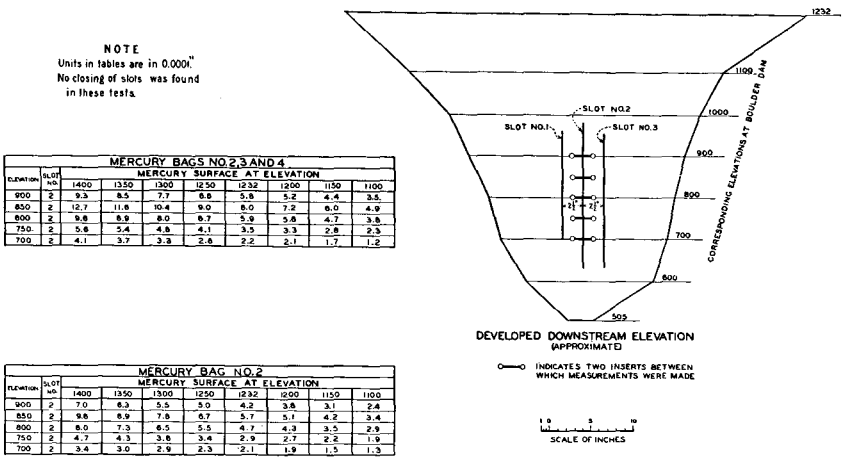

FIGURE 148—OPENING OF SLOT 2

129. Slot Openings Due to Flow.—A study of the action of the open slots under sustained load was made. Slot 2 always had a greater increase in width while being loaded than slots 1 or 3. For this reason, as many dial gages as possible were mounted across this slot for measurements under sustained load. Gages were mounted across slot 2 at elevations 700, 800, 850, and 900, and across slots 1 and 3 at elevation 750. Gages were also set to register radial deflections at all other inserts which were not used for measuring changes in width of slots.

The radial deflection measurements indicated that the model was more flexible and considerably weaker, due to cracking and repeated loading and unloading. The amount of radial flow in previous tests had caused permanent set at points of high stress.

The action of the open slots under sustained load is of considerable interest. The first few observations indicated that the change in width was negligible in most cases, with a slight tendency

to close as shown in figure 149. After an interval of one day all three slots had opened. They continued to open for about four days, after which the width remained practically constant.

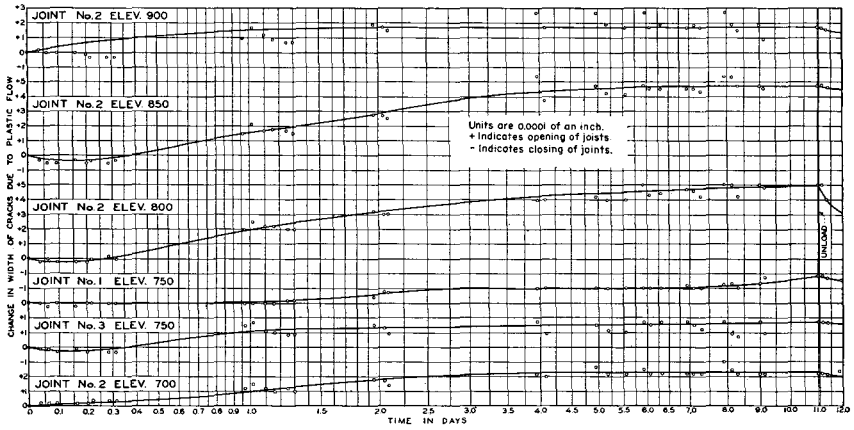

FIGURE 149—CHANGE IN SLOT OPENING DUE TO FLOW

CHAPTER VII—TRIAL LOAD ANALYSIS OF MODEL

INTRODUCTION

130. General.—The trial load method of analyzing arch dams is described in detail in another bulletin of the Boulder Canyon reports.[12] Only a brief description, showing the application of the method to the analysis of the plaster model, is presented herein. For the purpose of the analysis, the model was replaced by two systems of elements, a system of vertical cantilevers and a system of horizontal arches. The mercury load was divided between the arches and cantilevers, and equal and opposite tangential and twist loads were applied to the two systems until geometrical continuity was established throughout the structure. The required loads were determined gradually, by trial, until calculated deflections and rotations in the two systems were equal at all conjugate points. Since this satisfied the conditions of continuity, stresses and strains due to the applied loads were then calculated for both systems of elements. Seven arches and nine cantilevers, spaced at approximately equal intervals throughout the model, were used in the analysis.

The mercury load at the upstream face of the model produced movements in radial and tangential directions, and rotations in horizontal planes. These movements and rotations were considered in the radial, tangential, and twist adjustments, respectively. In the radial adjustment, the mercury load was divided between the arches and cantilevers in such a way as to produce radial continuity in the two systems of elements. In the tangential adjustment, equal and opposite internal tangential loads were introduced in such a way as to restore tangential continuity. In the twist adjustment, equal and opposite internal twist loads were introduced in such a way as to produce the same rotations in the arches and cantilevers.

---

[12] "Trial Load Method of Analyzing Arch Dams," Bull. 1, Part V—Technical Investigations, Boulder Canyon Project Final Reports, 1938.

131. Data and Assumptions.—The principal structural data and assumptions made for the analysis are listed as follows:

1. Scale of the model, 1:240.
2. Elevation of mercury surface, 1232.
3. Density of mercury, 13.6.
4. Modulus of elasticity of plaster-celite in tension and compression, 90,000 pounds per square inch.
5. Modulus of elasticity of plaster-celite in shear, 37,500 pounds per square inch.
6. Normal stresses vary as a straight line from the upstream to the downstream face of the model.
7. Cantilever stresses at the faces of the model act parallel to the slopes of the faces.

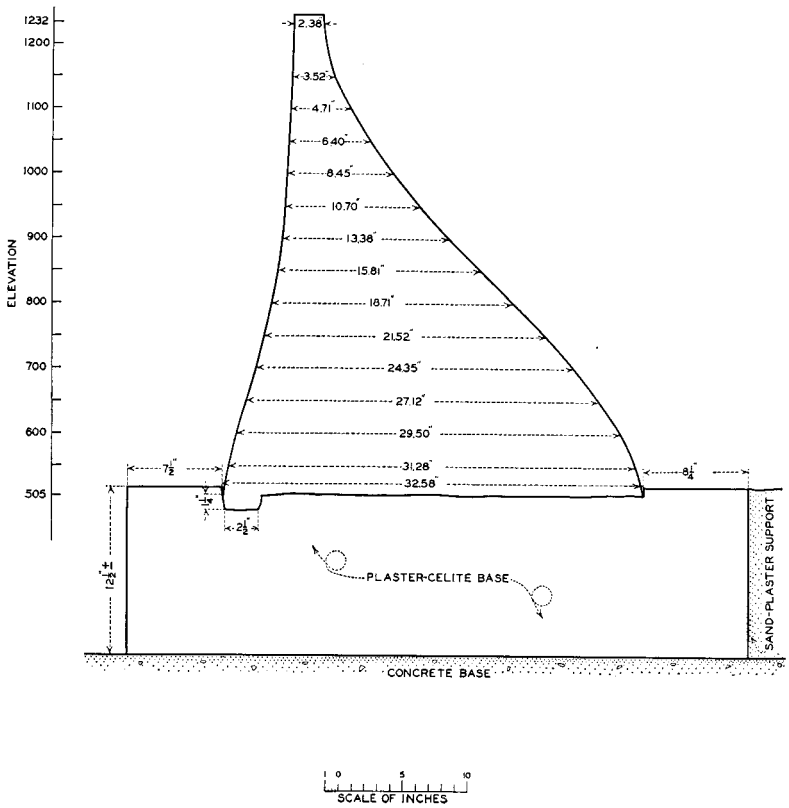

FIGURE 150—CANTILEVER SECTION E

8. The foundation deformation was adjusted to conform to the model measurements.

9. The concrete support around the plaster-celite base and the sand-plaster support at the downstream side of the plaster-celite base were considered to be rigid.

132. Cantilever Elements.—Cantilever elements were assumed to be one inch wide at the axis of the model and to have radial sides that converged from the upstream face to the downstream face. They were elastic units, set on elastic bases, and resisted shear and bending in radial directions, shear in tangential and vertical directions, and torsion in horizontal and vertical planes. Cantilever section E, as constructed, is shown in figure 150.

The mercury load on the upstream face of the model was divided into vertical and horizontal components and the vertical components assigned to the cantilevers. Horizontal components were divided and applied to the arches and cantilevers, using unit radial pattern loads. Unit loads on the cantilevers were triangular in shape and varied from one pound per square inch pressure at a given arch elevation to zero pressure at the arch elevations directly above and below, see figure 151-a. This made it possible to supply any horizontal load that varied as a straight line between the elevations of the sample arches used in the analysis. Shears, moments, and deflections were computed for each of the unit pattern loads to provide data for use in the following steps of the analysis.

Equal and opposite tangential forces, one set acting on the arches and the other on the cantilevers, were necessary to produce equal tangential deflections in the two systems. In the application of tangential forces, it was also found convenient to use a triangular unit load system. Unit tangential loads applied to the cantilevers were similar to the unit radial loads except that they represented tangential shearing forces applied at the center lines instead of radial forces applied at the upstream face, see figure 151-b.

Equal and opposite twisting moments, one set applied to the arches and the other to the cantilevers, were required to make angular rotations of the arches coincide with the rotations of the cantilevers. As in the case of the tangential loads, it was found convenient to use a triangular unit load system. Unit cantilever twist loads, representing twisting moments applied to the cantilevers, are shown in figure 151-c.

Radial cantilever loads deflected the cantilevers in radial direc-

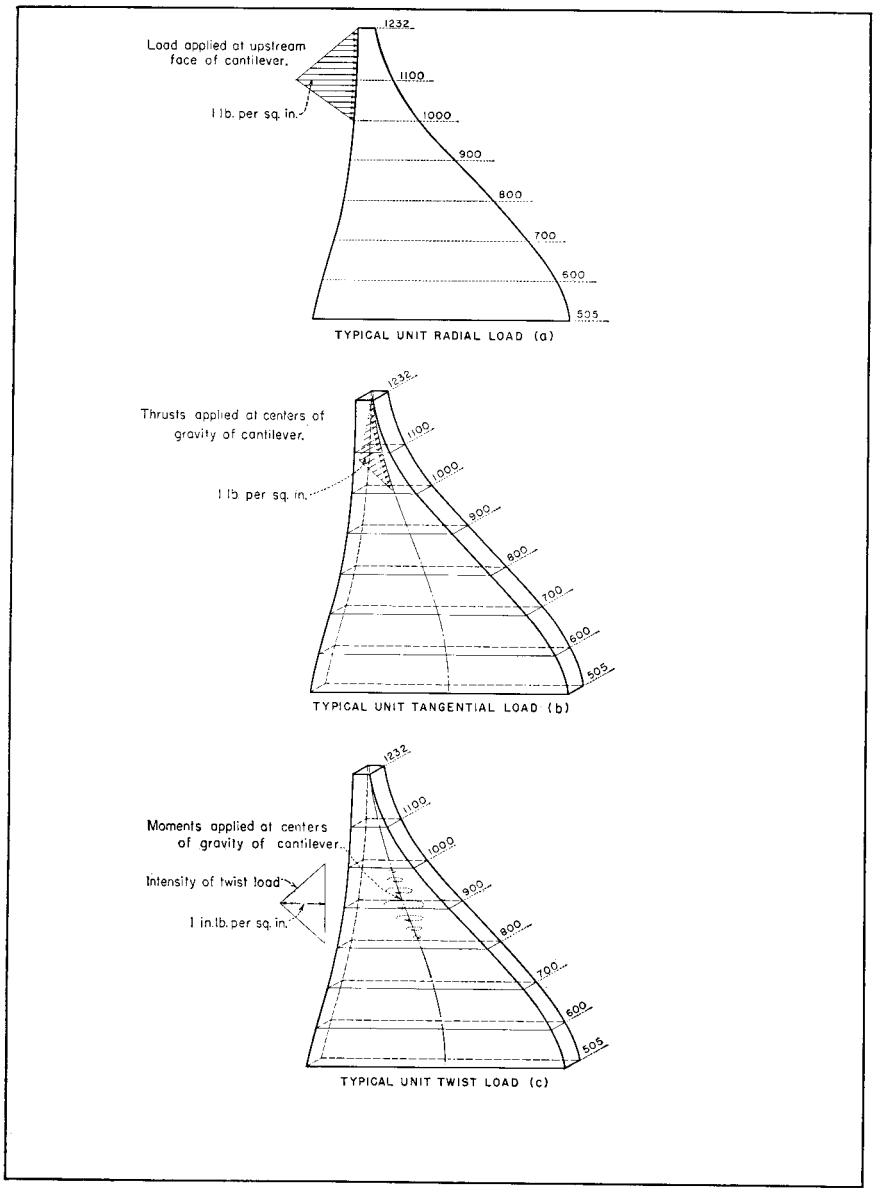

FIGURE 151—TYPICAL UNIT CANTILEVER LOADS

tions only, but tangential loads produced tangential deflections and also rotations in horizontal planes. These rotations existed because the center lines of the cantilevers were not vertical. Tangential thrusts applied near the top of a cantilever produced twisting moments in horizontal planes at all lower elevations. Twist loads not only rotated the cantilevers, but also deflected them radially. These radial deflections appeared because the rates of change of the applied twisting moments along the arch center lines produced rates of change of bending moments in the cantilevers.

Deflections were computed for unit radial, tangential, and twist loads. These were tabulated so they could be used easily in the trial load adjustments. The tabulations simplified the problem of estimating the amounts of loads to be applied to the arches and cantilevers. After the loads had been determined by the adjustments, stresses in the cantilevers were calculated by ordinary stress formulas.

133. Arch Elements.—Horizontal arch elements were circular and of constant radial thickness. They were assumed to be one inch high and to have horizontal top and bottom faces. Abutments of the arches were radial at the top elevations, half radial at elevations 1100 and 1000, and gradually approached directions parallel to the canyon walls at the lower elevations. The arch elements were statically indeterminate, set on elastic abutments, and were assumed to resist moments, thrusts, and shears in horizontal planes. Calculations for arch elements included effects of irregular abutments and a lack of symmetry between the crown cantilever and the arch crowns.

Unit pattern loads were used in applying horizontal mercury loads to the arch elements. Radial pattern loads included a uniform load over an entire arch, and triangular loads varying from a maximum pressure at the abutment to zero pressure at the quarter points, see figure 152-a. With these unit loads it was possible to apply any load to an arch that varied as a straight line between quarter points. Uniform loads, with one pound per square inch radial pressure at the upstream face, and triangular loads, with one pound per square inch radial pressure at the abutment, were computed for all arches used in the analysis.

Tangential thrust loads, applied at arch center lines, were required for the tangential adjustment of deflections. Unit loads, needed to build up tangential loading, consisted of triangular loads varying from one pound per square inch tangential thrust at each abutment to zero thrust at the different quarter points, as shown in figure 152-b.

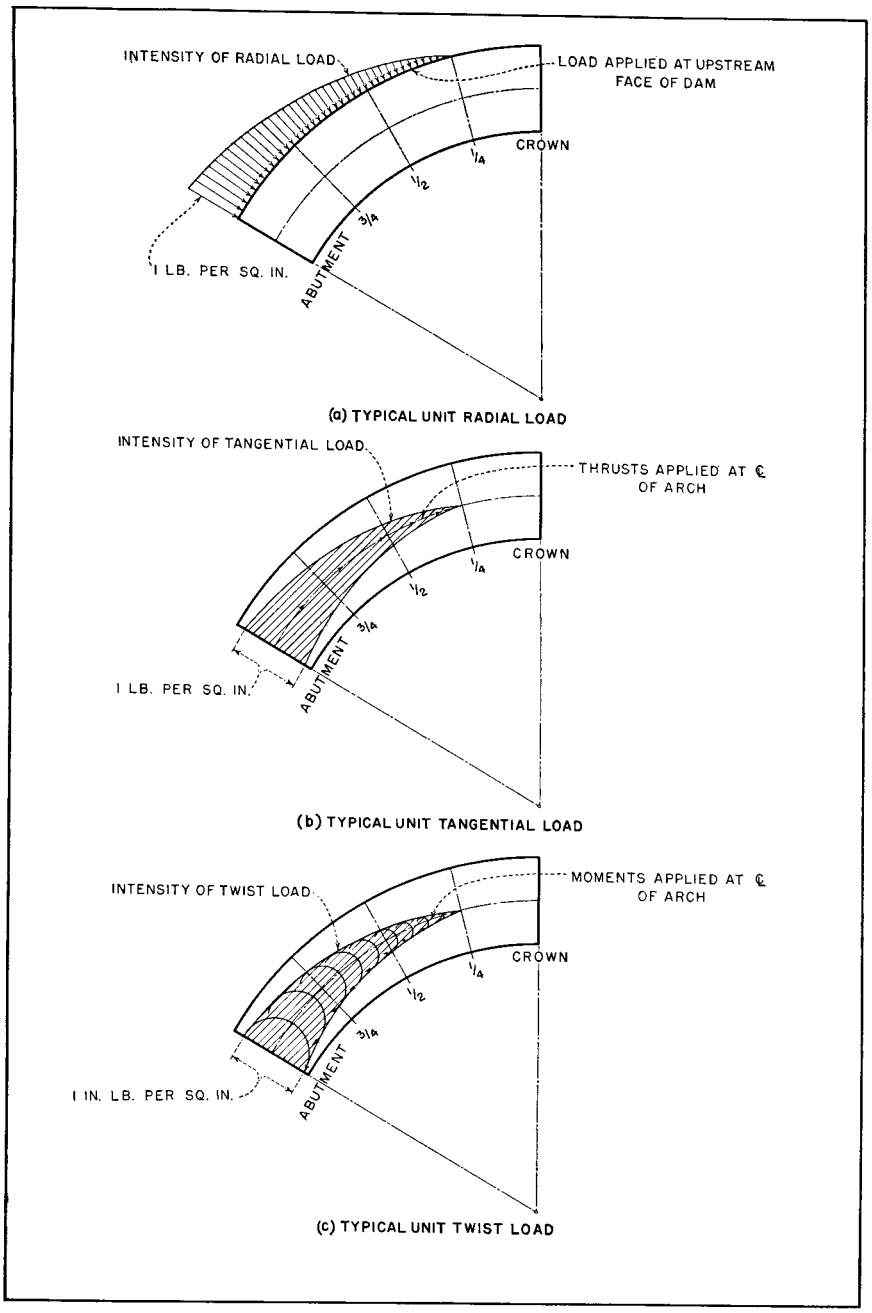

FIGURE 152—TYPICAL UNIT ARCH LOADS

Besides radial and tangential loads, twist loads were required for the purpose of establishing equal rotations in the arches and cantilevers at conjugate points. Unit twist loads were also triangular in shape. They varied from a moment of one inch-pound per square inch at an arch abutment to zero moment at the quarter points, as illustrated in figure 152-c.

Concentrated loads at the arch abutments were introduced for the purpose of transferring cantilever shears, thrusts, and moments from the cantilever foundations to the arch abutments. In this way forces were conveniently transferred between the two systems at abutment locations. Concentrated radial, tangential, and twist loads were a radial shear of one pound, a tangential shear of one pound, and a moment of one inch-pound, respectively.

As only part of the unit arch loads were necessary for the adjustments, the loads needed were calculated as the adjustments were made. Deflections due to required unit arch loads were tabulated, so they could easily be used in the deflection adjustments. After the proper arch loads had been determined by the trial load method, arch stresses were calculated by ordinary stress formulas.

RADIAL ADJUSTMENT

134. Procedure.—The radial adjustment was the first step in the analysis of the model by the trial load method. Figure 153 shows the adjustment at the arch elements, including the division of mercury load between the two systems and the final adjusted radial deflections of the arches and cantilevers. The positions indicated on the drawing apply to the developed center lines of the arches. Locations of arch quarter points and cantilevers are also shown. The plotted points, representing calculated movements of the arches and cantilevers for the final distribution of mercury load, show that a very satisfactory agreement of radial deflections was obtained at all conjugate points.

As previously mentioned, concentrated loads were introduced at the arch abutments for the purpose of maintaining equilibrium and continuity. Figure 154 shows that the center-line width of a cantilever resting on the end of an arch element of unit height is equal to $tan\ \psi$. As the assumed unit cantilever used in the analysis was one inch wide at the axis, the radial shear at the base of a cantilever was multiplied by the factor $\frac{R_{axis}}{R_{center\ line}} tan\ \psi$ to give the correct amount

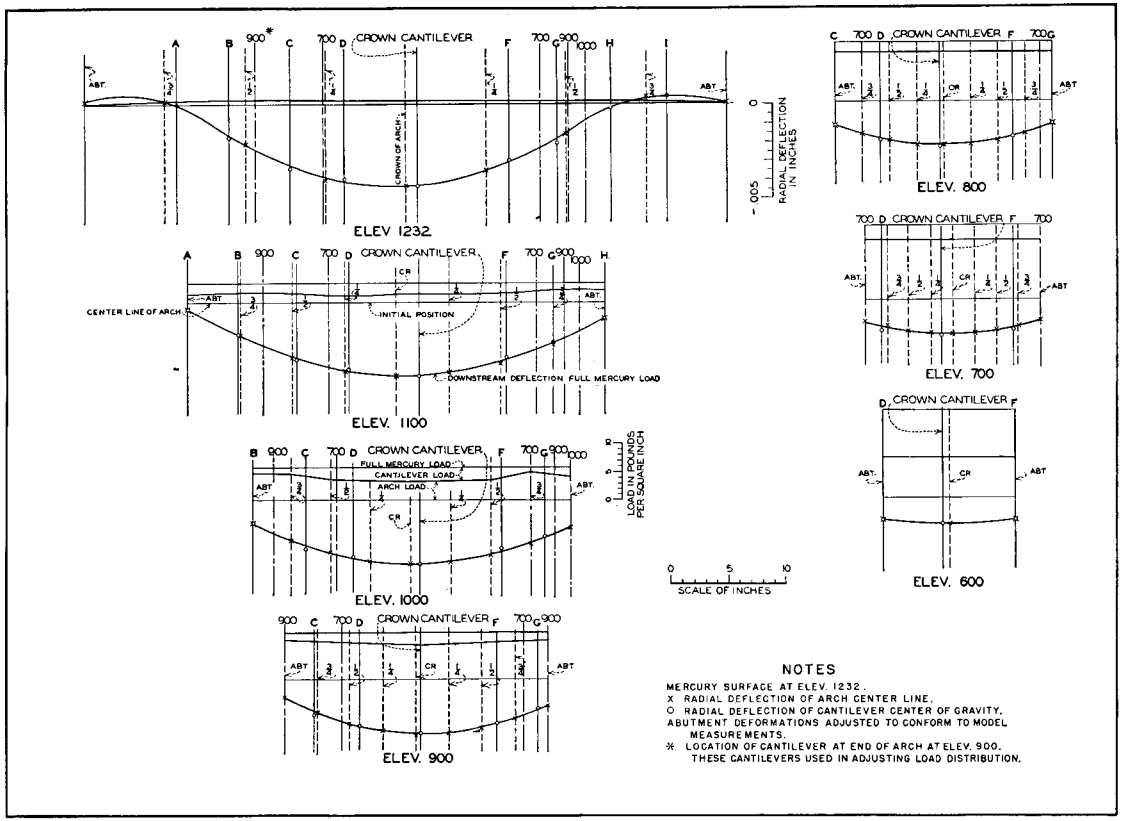

FIGURE 153—RADIAL ADJUSTMENT AT ARCH ELEMENTS

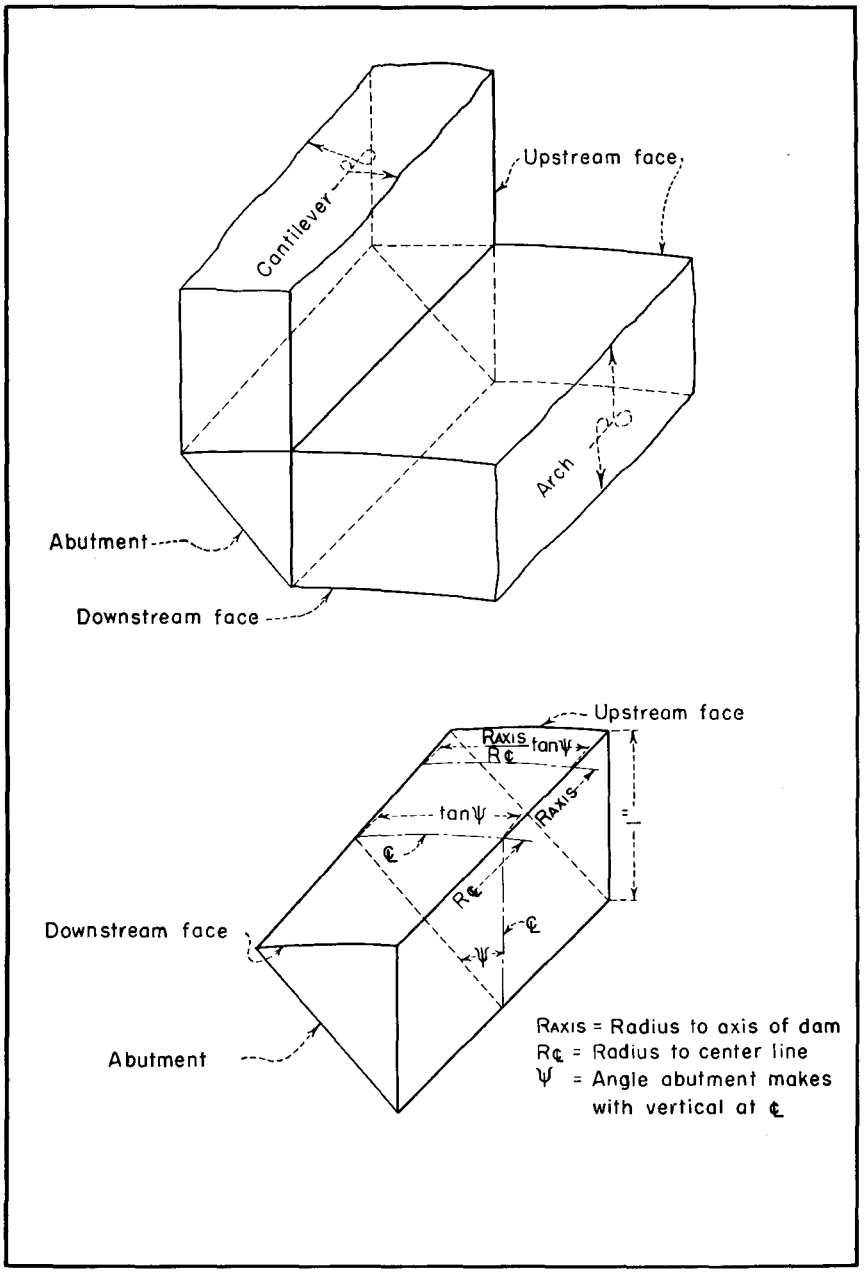

FIGURE 154—CONTACT OF ARCH AND CANTILEVER AT ABUTMENT

of concentrated radial load which should be applied to an arch of one-inch height. For the same reason tangential shears and twisting moments at the cantilever foundations were corrected by the factor $\frac{R_{axis}}{R_{center\ line}} \tan \psi$, to determine concentrated tangential and twist loads for the arches. Since the base of each cantilever, except the crown, rested on the end of an arch, the abutment deflection of the arch was added algebraically to the cantilever deflections.

135. Distribution of Load.—For the first estimate of load distribution, crown cantilever deflections were adjusted to crown deflections of the arches. In this step only uniform and concentrated loads were used on the arch elements. After the crown cantilever was adjusted, deflections of other arch and cantilever points were computed and plotted on an adjustment sheet in the same manner as the final deflections shown in figure 153. By comparing preliminary deflections, additional loads were estimated and applied to the structure until the calculated arch and cantilever deflections were approximately the same at all conjugate points. After several trials the deflections were brought into close agreement, thereby completing the first stage of the radial adjustment. Since the subsequent twist and tangential adjustments caused radial arch and cantilever movements, radial readjustments were required to restore continuity. Altogether ten radial adjustments and readjustments were made before arriving at the final deflections shown in figure 153.

As different trial loads were applied to the two systems, it was necessary to have the sum of the arch and cantilever loads equal to the horizontal mercury load at each point. This was done by plotting the arch load and also the total mercury load on each of the developed center lines of the arches. The difference between the arch load and the total load represented the cantilever load.

The radial adjustment constituted the most important step in the trial load analysis. Although twist and tangential adjustments were required, they were of secondary importance compared with the radial adjustment. The reason for this was that the radial movements were much greater than the tangential or angular movements.

TANGENTIAL ADJUSTMENT

136. Tangential Arch Deflections.—After radial deflections due to radial loads had been adjusted, the tangential adjustment was made.

Results of the tangential adjustment at the arch elements are shown in figure 155. This drawing gives initial positions and final tangential displacements of the arch center lines; also, amounts of tangential loads required for the adjustment. Positive tangential loads and movements shown in figure 155 act toward the right abutment. Negative loads and movements act toward the left abutment. Following this convention, it is seen that tangential displacements are toward the left abutment in the left part of the model and toward the right abutment in the right part of the model. Tangential loads applied to the arches are away from the left abutment in the left part of the model, and away from the right abutment in the right part of the model. The right abutment is the end of the arch on the observer's right when looking upstream.

An analysis of the effects of the radial adjustment showed that the radial loads deflected the arch center lines in tangential directions as well as in radial directions. Therefore conjugate points of the two systems were out of agreement in tangential directions. These initial tangential arch movements were computed by combining tangential deflections of the unit loads used in the first stage of the radial adjustment. Since the base of each cantilever moved with the abutment of the corresponding arch, the initial deflection of the cantilever equalled the movement of the arch abutment.

137. Tangential Shear Loads.—Equal and opposite tangential shear loads, one on the arch and the other on the cantilever, were introduced to remove relative tangential deflections. Required amounts of the loads were estimated and applied to the two systems. As in the radial adjustment, it was expedient to use unit arch and cantilever loads in determining tangential loads and deflections. For the purpose of simplifying the estimate of the first tangential loads to apply to the structure, only cantilevers B and C were investigated. After these elements were brought into approximate agreement with the arches by trial tangential loads, tangential deflections of other arch and cantilever points were computed. The relative tangential deflections of all points were then compared and additional loads estimated until tangential deflections were approximately the same at all conjugate points. A close agreement of deflections was secured after several trials, thus completing the first stage of the tangential adjustment.

Subsequent readjustments of tangential deflections were required because twist adjustment and radial readjustment loads deflected the

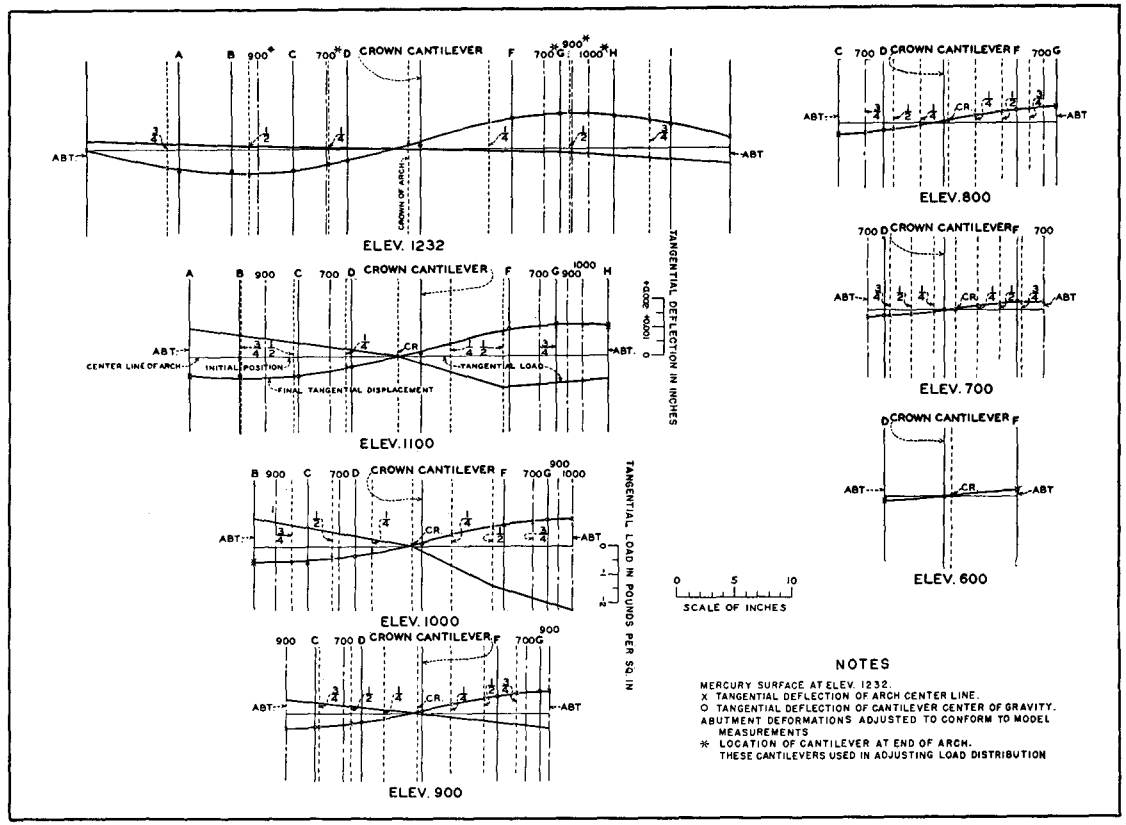

FIGURE 155—TANGENTIAL ADJUSTMENT AT ARCH ELEMENTS

arches tangentially. Nevertheless, the adjustments converged rapidly and only four sets of trial loads were required to produce the close agreement shown in figure 155. Satisfactory adjustment was obtained by applying tangential loads to the top four elevations only, no loads being required at elevations 600, 700, and 800.

It was necessary at all stages of the adjustment to keep tangential loads equal and opposite at all points in the two systems. To insure that this condition was satisfied, arch loads were plotted on developed center lines and amounts of unit loads for the cantilevers determined from the arch load diagrams.

Tangential loads and deflections were small compared with radial loads and deflections. This indicated that tangential loads had a comparatively small effect on the total movements of the model. However, the tangential loads had a considerable effect on arch stresses, since they changed the arch thrusts without causing appreciable movement in the structure.

TWIST ADJUSTMENT

138. Twist Loads.—Rotations of arch and cantilever elements about vertical axes were considered in the twist adjustment. Figure 156 shows the twist loads and final adjusted rotations, or twist deflections. Rotations are designated as twist deflections to make them comparable with radial and tangential deflections. The final rotations were clockwise in the left part of the model and counterclockwise in the right part, viewed from above. The twisting moments applied to the arches were in the opposite direction and opposite to the cantilever twisting moment loads.

Radial and tangential loads from previous adjustments rotated the arches, and tangential loads rotated the cantilevers. The rotations, or twist deflections, of the arches were calculated by combining twist deflections of all unit loads used in the first stages of the radial and tangential adjustments. In the same manner, twist deflections of the cantilevers were calculated by adding rotations due to applied unit tangential loads and combining them with abutment rotations of the corresponding arches. Resulting relative rotations were removed by introducing equal and opposite twist loads which acted on the arches and cantilevers. The required amounts of the twist loads were estimated and gradually adjusted by trial. As in the preceding adjustments, it was found expedient to use unit arch and cantilever loads in the application of successive trial loads.

139. Procedure.—The first set of trial twist loads applied to the model gave approximate deflection agreements at arch and cantilever intersections at cantilevers C and G. Successive sets of trial loads were applied until the deflection agreements were close enough at all cantilevers to complete the first stage of the adjustment. Since subsequent radial and tangential readjustments rotated the arches and cantilevers, twist readjustments were made for the purpose of restoring agreement between the twist deflections. After the required readjustments had been completed, the resulting loads and deflections were drawn on the adjustment sheet, see figure 156.

Twist loads caused radial and tangential deflections in the arches and radial deflections in the cantilevers. The cantilever deflections appeared because the rates of change of the applied twisting moments along the arch center lines produced rates of change of bending moments in the cantilevers. It was found that resulting bending moments were relatively large and amounted to approximately twenty-five per cent of the moments due to radial loads. The following steps show the procedure used in calculating these deflections:

1. Twisting moments were computed for all cantilevers at all arch elevations.

2. Twisting moments were differentiated along arch center lines. This gave rates of change of twisting moments along arch center lines which were equal to rates of change of radial bending moments in the cantilevers.

3. Rates of change of radial bending moments were integrated from the top of each cantilever to the lower elevations, giving bending moments in the cantilevers.

4. A double integration of the M/EI curve from the base of each cantilever gave cantilever deflections.

The twist adjustment indicated that twist resistance stiffened the structure considerably, thereby reducing deflections and stresses in the structure. Although effects of twist were greater than effects of tangential movements, they were still relatively small when compared with the results of the radial adjustment.

140. Additional Adjustments.—After the first stage of the twist adjustment had been completed, there remained secondary movements which had not been considered. These were radial deflections due to tangential and twist loads and tangential deflections due to twist loads. The secondary radial movements were considered in the first

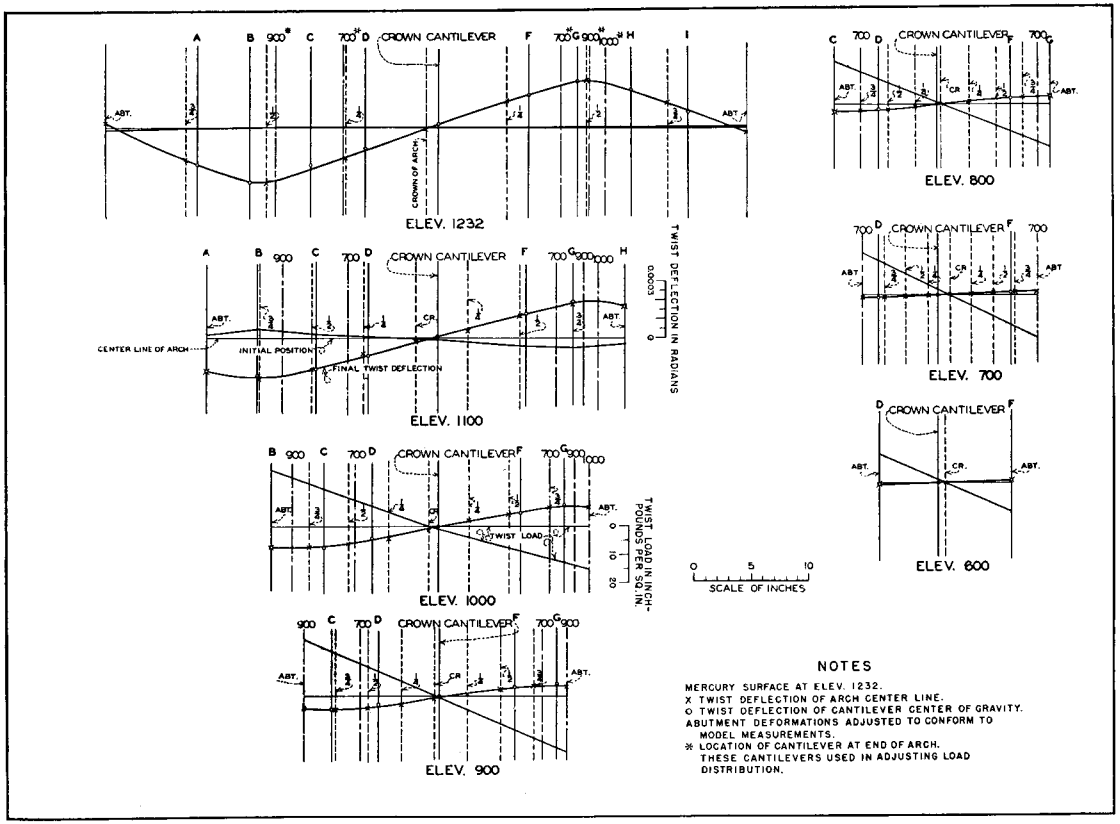

FIGURE 156—TWIST ADJUSTMENT AT ARCH ELEMENTS

radial readjustment. This required additional radial loads, causing new tangential and twist movements. Next, the first tangential readjustment was made to correct discrepancies caused by twist loads and radial adjustment loads. Likewise, a twist readjustment and subsequent radial, tangential, and twist readjustments were required, since each readjustment produced movements which had to be considered in the following readjustments. However, the effects converged rapidly. After a few readjustments, the secondary movements became so small that they did not change the adjustments by appreciable amounts.

The complete analysis, including all adjustments and readjustments required ten radial, four tangential, and four twist load trials. These adjustments determined the total movements of the model, also the distribution of the different types of loads. With this information, arch and cantilever stresses were calculated by usual stress formulas.

RESULTS OF ANALYSIS

141. Stresses and Deflections.—The most important results of the analysis are shown in figure 157. In this drawing, arch and cantilever stresses are shown on the developed profile at the axis of the model. Final radial loads and deflections are shown at the assumed cantilever elements. Cantilever deflection curves show deflections due to the weight of the plaster-celite material, deflections due to the plaster-celite material plus vertical components of the mercury load on the upstream face, and deflections due to weight of the model plus vertical and horizontal components of the mercury load.

142. Comparison with Experimental Stresses.—Arch stresses determined by the trial load analysis are compared with those determined from the model measurements in figure 158. The agreement was very close at the lower elevations, but some differences occurred along the abutments above elevation 1000. The greatest differences occurred at elevation 1232 at the abutments.

The discrepancies in stress were due to inadequacies in both analytical and experimental procedures. In the first place, formulas for abutment deformations and accompanying stresses had been developed on the assumption that the foundation was infinite in extent. Actually, the model had a supplemental base of highly elastic plaster-celite material, about twelve inches thick, supported by a compara-

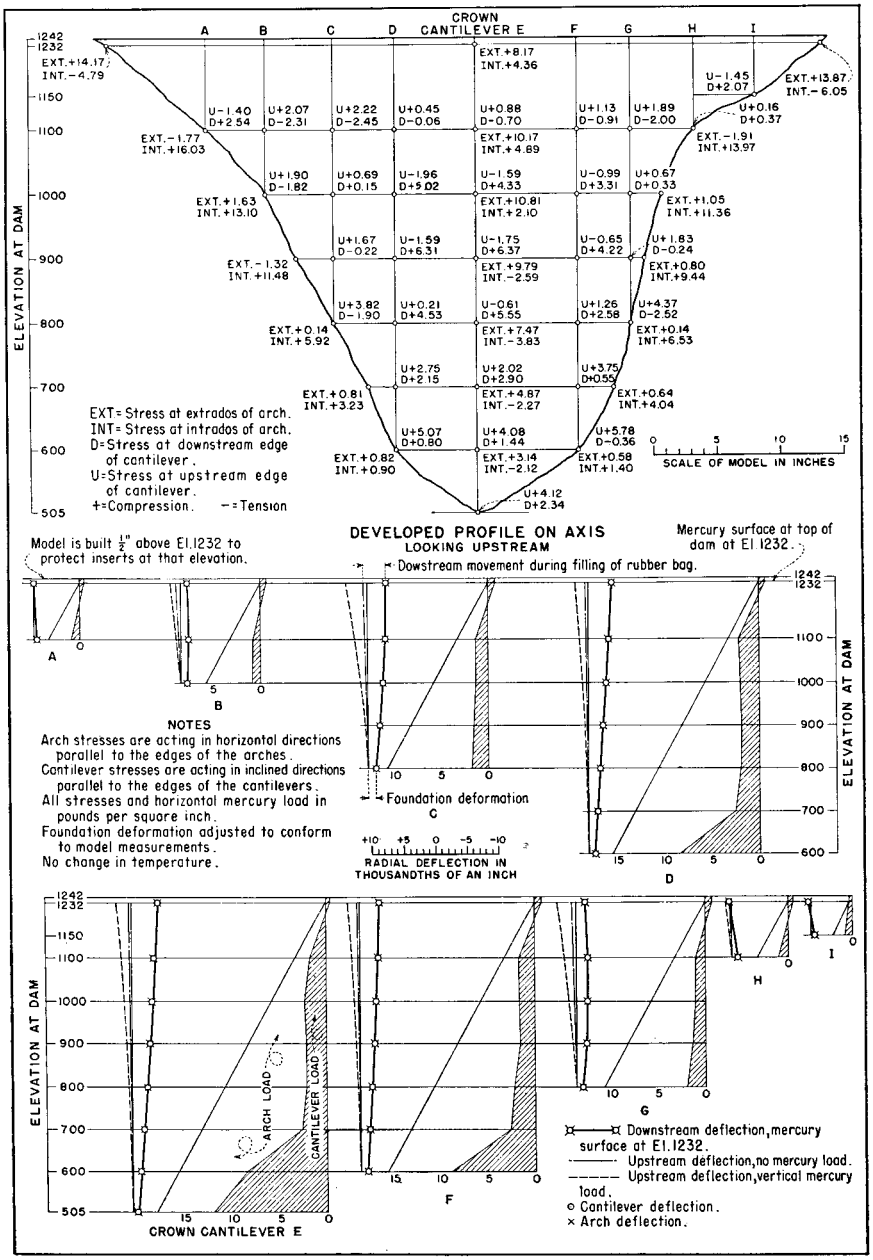

FIGURE 157—RESULTS OF TRIAL LOAD ANALYSIS

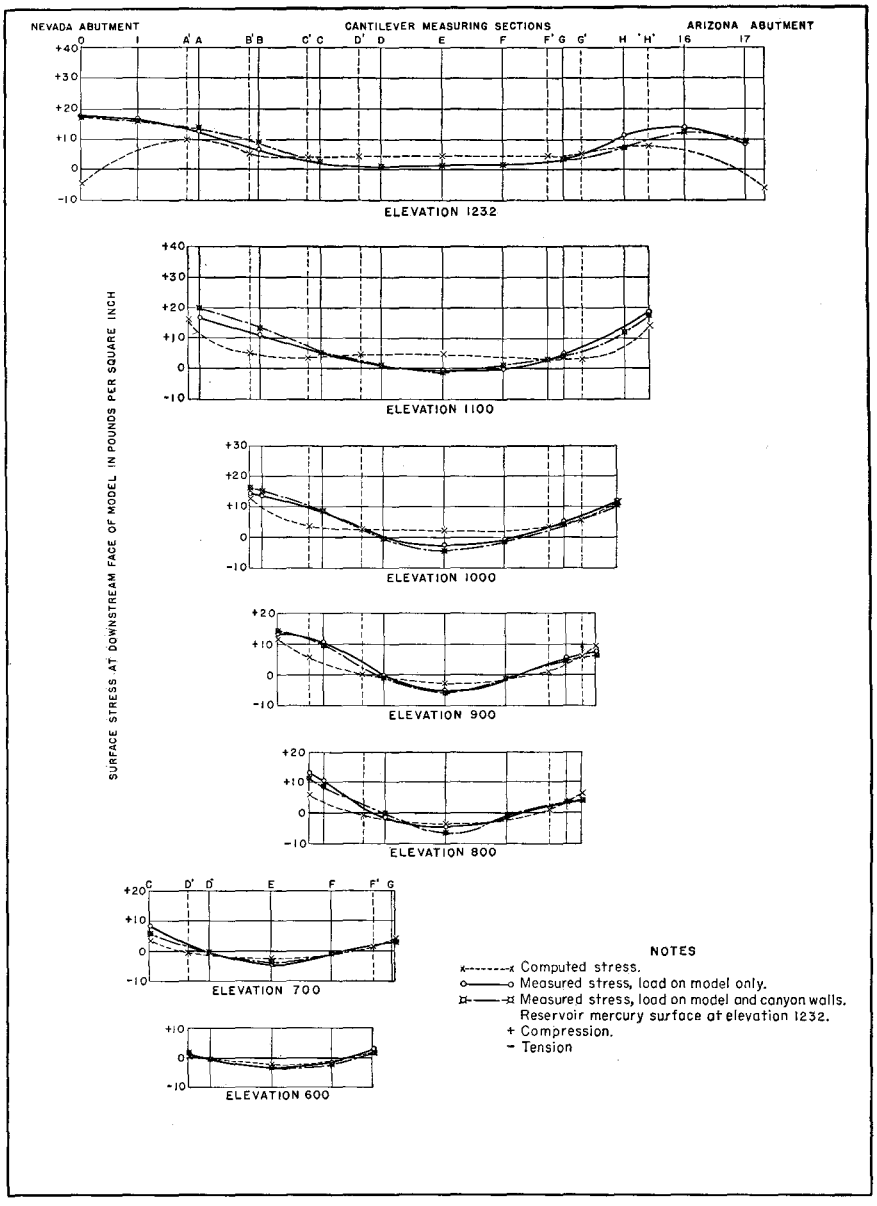

FIGURE 158—COMPARISON OF EXPERIMENTAL AND COMPUTED ARCH STRESSES

tively rigid concrete primary base. It was therefore necessary to use some approximation in determining abutment deformation. In the second place, strain measurements along the abutments would have been more accurate if more sensitive measuring apparatus had been available. A more sensitive type of strain gage, operating over a gage length of 0.25 or 0.50 inches, was needed.

Figure 159 shows lines of equal arch stress plotted on the developed downstream face of the model. Stresses determined from strain measurements were slightly greater than those determined from the analysis. At the time strains were measured, over 800 tests had been made, and some small cracks in the model may have developed along the upstream abutments. The occurrence of cracks at such locations would be accompanied by increases in stress at the downstream face, as shown in figure 159. The width of the tension area was about the same for the two sets of stresses shown in the figure. However, the height of the tension area was somewhat greater in the case of the stresses determined from the model measurements. Along the abutments between elevations 900 and 1150, analytical stresses were more concentrated than experimental stresses, although the latter were slightly greater in magnitude.

Cantilever stresses determined analytically are compared with experimental stresses in figure 160. In the central part of the model where stresses were not affected by the abutments, the agreement was very close, as shown by the curves at cantilever sections D′, E′, and F′. Along the abutments, stresses at sections B′, C′, and G′ showed considerable variation. This variation is also shown by the lines of equal stress at the downstream face in figure 161. In the experimental stresses, the tension area occurred between cantilever sections C′ and G′ above elevation 1075. Analytically, the tension area extended to both abutments. This was due to the inadequacy of the mathematical method in computing deformations and accompanying stresses for abutment conditions in the model.

An inspection of the load-distribution diagrams in figure 157 shows that the proportions of load carried by arch action were considerably greater than those carried by cantilever action. Arch stresses were therefore materially greater than cantilever stresses. The agreement between analytical and experimental stresses was very close for the higher stresses. Discrepancies found between the two sets of stresses were in regions of low stress. Consequently, the agreement of arch stresses was better than the agreement of cantilever stresses.

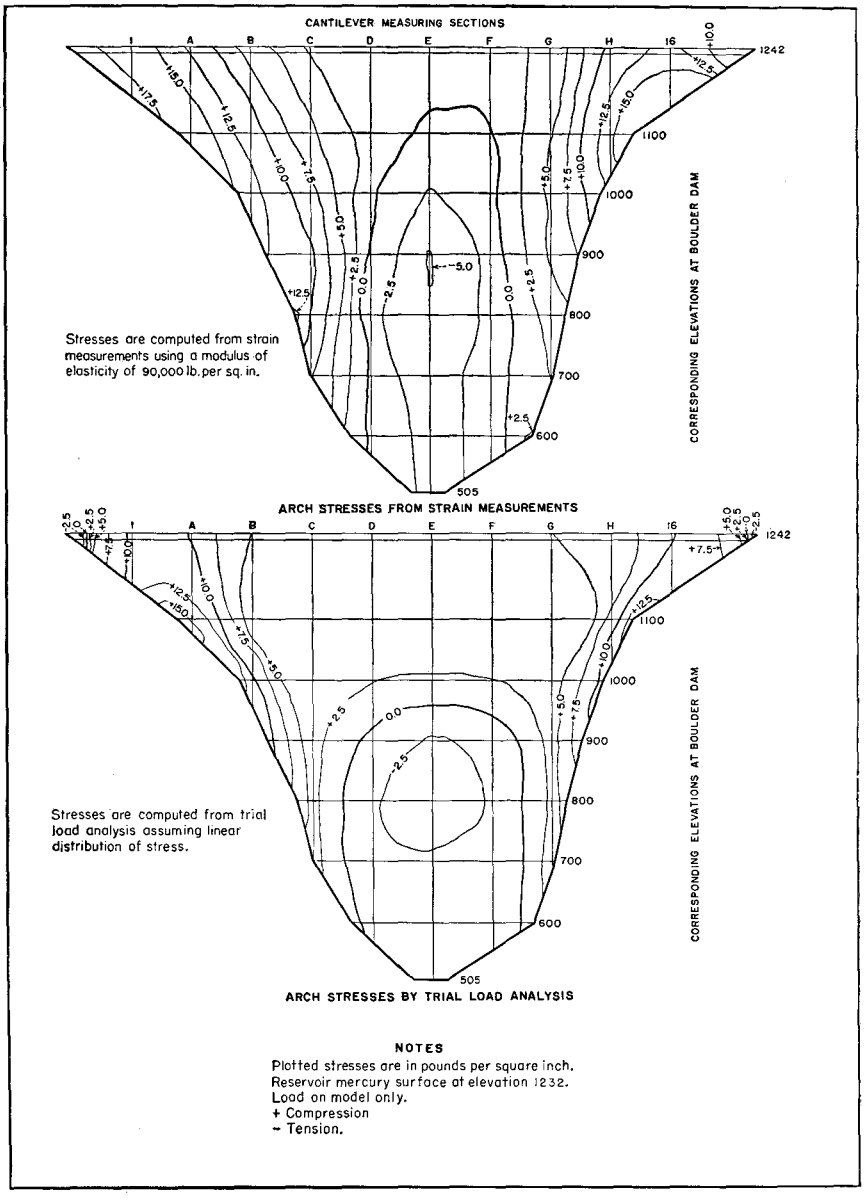

FIGURE 159—COMPARISON OF LINES OF EQUAL ARCH STRESS

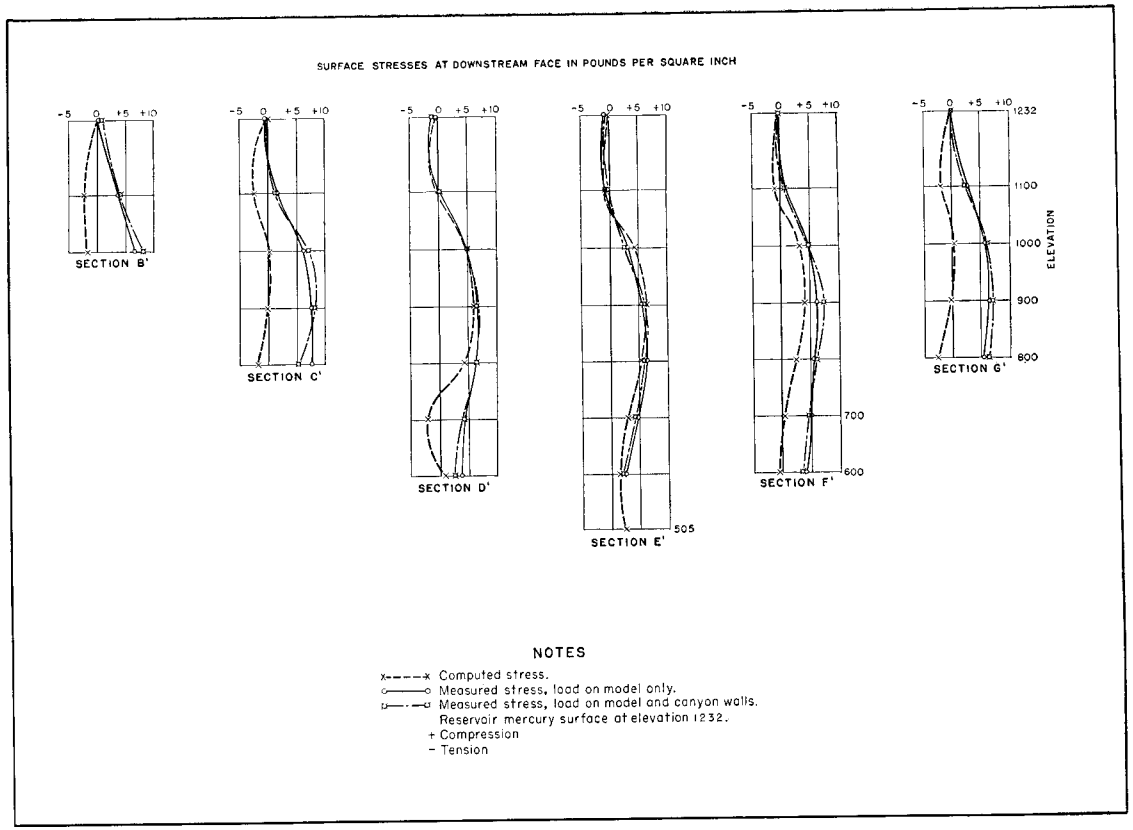

FIGURE 160—EXPERIMENTAL AND COMPUTED CANTILEVER STRESSES

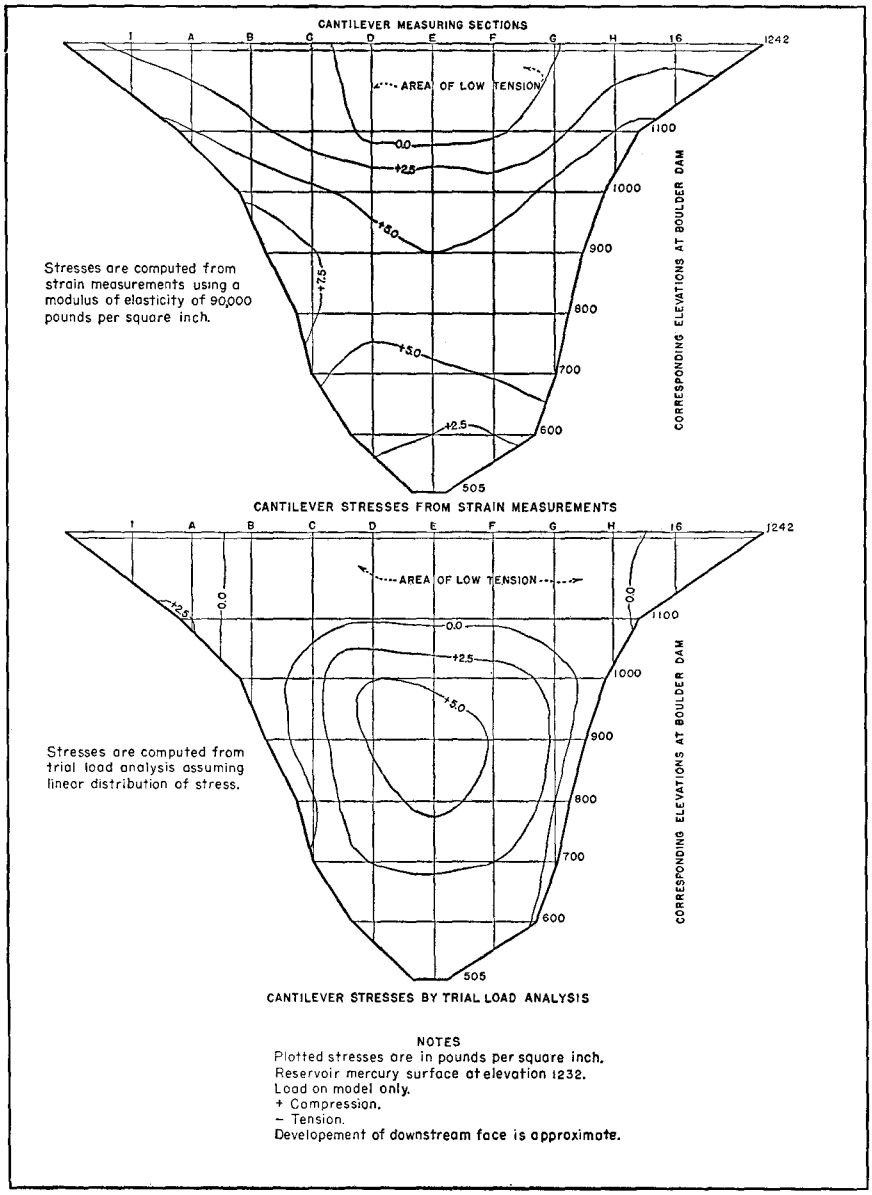

FIGURE 161—COMPARISON OF LINES OF EQUAL CANTILEVER STRESS

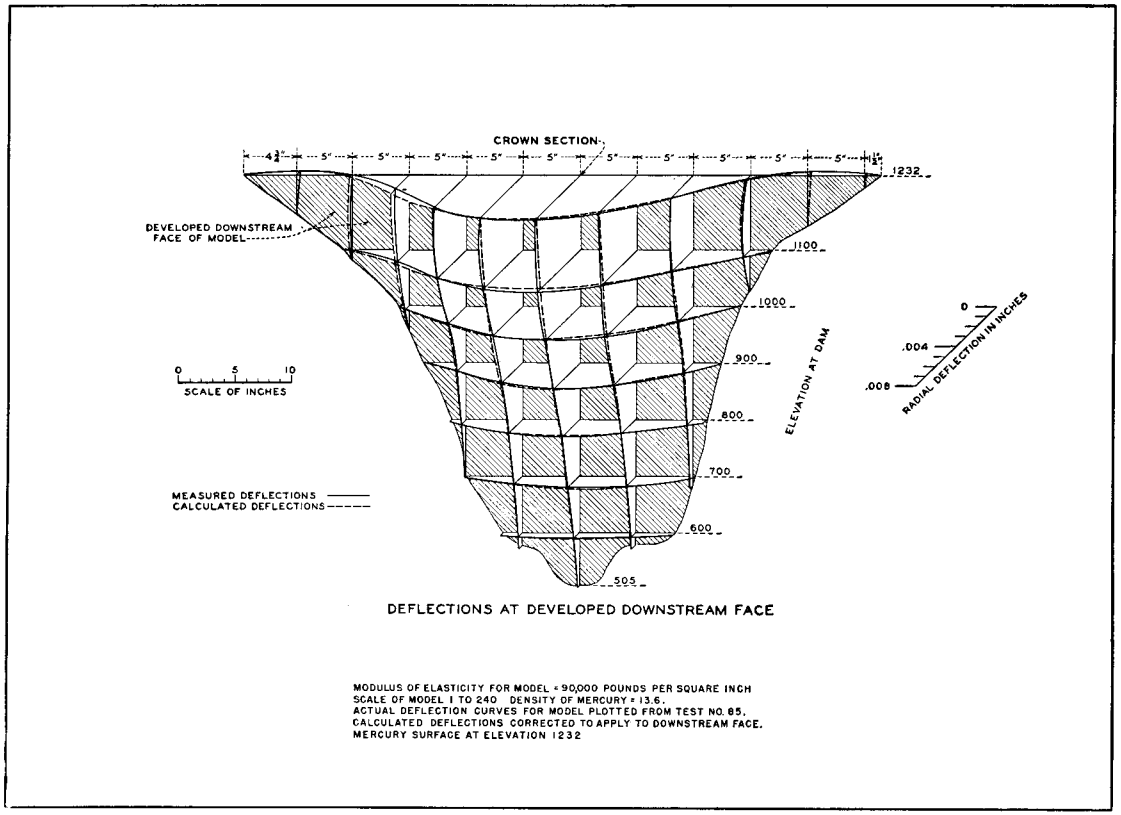

FIGURE 162—COMPARISON OF COMPUTED AND MEASURED DEFLECTIONS

143. Comparison with Measured Deflections.—The comparison of deflections calculated by the trial load method with those measured on the model, given in figure 162, shows a remarkably close agreement. The small discrepancies which appear at some locations may be partly due to differences between actual thicknesses of the model and uniform thicknesses assumed at the different elevations considered in the trial load analysis. The differences between calculated and measured deflections probably would have been less if more sample arches and cantilevers had been used in the analysis. Nevertheless, sufficient elements were investigated to give an adequate solution. The unusually close agreement of calculated and measured deflections at all locations at the downstream face, shown by the curves in figure 162, constitutes a very satisfactory check on the accuracy of the trial load method of analysis.

CHAPTER VIII—INVESTIGATION OF RUBBER-LITHARGE MATERIAL

144. Introduction.—After completing the test program on the plaster model of Boulder Dam, the test results, together with further analytical studies, indicated that an improvement in stress distribution could be obtained by adding arch fillets at the downstream face. A new model incorporating these changes in design was then proposed. The rubber-litharge compound developed by the Aluminum Corporation of America was selected for building the new model, and 20 tons of this material was ordered from the Republic Rubber Company of Youngstown, Ohio.

When the rubber-litharge arrived at the laboratory, preliminary investigations of the physical properties of the material were immediately made. The tests indicated different elastic properties along different axes, showing that the material was anisotropic. Consequently, mathematical studies of the stress-strain relations of anisotropic materials were made in order to interpret properly the results of the tests and to aid in developing testing procedures.

STRESS-STRAIN RELATIONS

145. Characteristics of Material.—In the process of manufacture, the rubber-litharge compound acquired different elastic properties in different directions. The blocks or sheets into which the rubber was molded may be considered to have three mutually perpendicular axes of elasticity. In the following discussions, these reference axes are assumed to be parallel to the edges of the blocks. The rubber blocks were similar in their elastic properties to a block of wood cut from the outer portion of a tree in such a way that two faces are perpendicular to the direction of the wood fibers, two faces intersect the rings of growth at right angles, and two faces are tangent to the rings of growth. The structure of such a material is different in the three directions and has a different modulus of elasticity in each di-

rection. Tests show that such materials have three shear moduli and six Poisson's ratios, two for each axis.

The rubber-litharge compound presented an additional difficulty in that it was not possible, as in the case of the wood block, to determine the direction of the three axes by inspection. Some of the blocks were smooth, apparently having been cured against the steel face of a press; others showed cloth prints, probably caused by curing against a cloth-covered press; others, which were originally too thick, had been dressed with a sanding machine and showed the marks of the sander. There was no difficulty in recognizing the axis perpendicular to the thickness of the block, but the other two axes could only be distinguished by determining the modulus of elasticity in each tranverse direction. In order to follow a logical procedure in investigating the physical properties of the material, the mathematical development described in the following sections was used as a basis for the test program.

146. Notation.—The notation used in subsequent formulas and discussions is as follows:

X, Y, Z = coordinates of three mutually perpendicular axes.

ϵ_x = strain in the x direction.

ϵ_y = strain in the y direction.

ϵ_z = strain in the z direction.

γ_{xy} = change in angle between the x and y axes.

γ_{yz} = change in angle between the y and z axes.

γ_{zx} = change in angle between the z and x axes.

σ = direct stress.

τ = shear stress.

μ = Poisson's ratio.

E = modulus of elasticity.

K = volume modulus.

A, B, C, F, G, H = elastic coefficients.

L, M, N = shearing moduli of elasticity in the directions of the pairs of axes y, z; x, z; and x, y, respectively.

147. Elastic Symmetry.—The report on tests of similar material, made by the Aluminum Company of America,[13] indicated that the material had three planes of elastic symmetry which were mutually perpendicular. These planes were parallel to the faces of the material, which was molded in blocks. The strain energy function for a material with three planes of symmetry is:[14]

$$2W = A\epsilon_x^2 + B\epsilon_y^2 + C\epsilon_z^2 + 2F\epsilon_y\epsilon_z + 2G\epsilon_z\epsilon_x + 2H\epsilon_x\epsilon_y + L\gamma_{yz}^2 + M\gamma_{zx}^2 + N\gamma_{xy}^2 \qquad (19)$$

Stresses in terms of strains are:

$$\sigma_x = A\epsilon_x + H\epsilon_y + G\epsilon_z \qquad (20)$$

$$\sigma_y = H\epsilon_x + B\epsilon_y + F\epsilon_z \qquad (21)$$

$$\sigma_z = G\epsilon_x + F\epsilon_y + C\epsilon_z \qquad (22)$$

$$\tau_{yz} = L\gamma_{yz} \qquad (23)$$

$$\tau_{zx} = M\gamma_{zx} \qquad (24)$$

$$\tau_{xy} = N\gamma_{xy} \qquad (25)$$

Young's modulus for each of the three principal directions is given by the following equations:

$$\frac{\Delta}{E_x} = BC - F^2 \qquad (26)$$

$$\frac{\Delta}{E_y} = CA - G^2 \qquad (27)$$

$$\frac{\Delta}{E_z} = AB - H^2 \qquad (28)$$

---

[13]Templin, R. L., and R. G. Sturm, "Methods for Determining the Physical Properties of Certain Rubber Compounds at Low Stresses," Proc. Am. Soc. Test. Mats., Vol. 31, Part II, p. 882, 1931.

[14]Love, A. E. H., "Mathematical Theory of Elasticity," 4th Ed., 1927, pp. 106-107 and pp. 160-162, Cambridge University Press, London.

where the value of Δ is given by the determinant:

$$\Delta = \begin{vmatrix} A & H & G \\ H & B & F \\ G & F & C \end{vmatrix}$$

In terms of the coefficients, the values of Poisson's ratio may be expressed by the following equations:

$$\mu_{xy} = \frac{CH - FG}{BC - F^2} \tag{29}$$

$$\mu_{xz} = \frac{BG - FH}{BC - F^2} \tag{30}$$

$$\mu_{yx} = \frac{CH - FG}{AC - G^2} \tag{31}$$

$$\mu_{yz} = \frac{AF - GH}{AC - G^2} \tag{32}$$

$$\mu_{zx} = \frac{BG - FH}{AB - H^2} \tag{33}$$

$$\mu_{zy} = \frac{AF - GH}{AB - H^2} \tag{34}$$

where μ_{xy} is the ratio of the extension in the y direction to the contraction in the x direction produced by a compressive load acting in the x direction. By this definition, the sign of μ is always negative.

Three other coefficients related to Poisson's ratio may be defined as follows:

$$\frac{\Delta}{F_x} = AF - GH \tag{35}$$

$$\frac{\Delta}{F_y} = BG - HF \tag{36}$$

$$\frac{\Delta}{F_z} = CH - FG \tag{37}$$

These coefficients may be determined experimentally from the relations:

$$\frac{1}{F_x} = \frac{\mu_{yz}}{E_y} = \frac{\mu_{zy}}{E_z} \tag{38}$$

$$\frac{1}{F_y} = \frac{\mu_{zx}}{E_z} = \frac{\mu_{xz}}{E_x} \tag{39}$$

$$\frac{1}{F_z} = \frac{\mu_{xy}}{E_x} = \frac{\mu_{yx}}{E_y} \tag{40}$$

It should be noted that since the sign of μ is negative, the sign of F_x, F_y, and F_z must also be negative.

Strains may be expressed in terms of stresses by means of these coefficients as follows:

$$\epsilon_x = \frac{\sigma_x}{E_x} - \frac{\sigma_y}{F_z} - \frac{\sigma_z}{F_y} \tag{41}$$

$$\epsilon_y = \frac{\sigma_y}{E_y} - \frac{\sigma_z}{F_x} - \frac{\sigma_x}{F_z} \tag{42}$$

$$\epsilon_z = \frac{\sigma_z}{E_z} - \frac{\sigma_x}{F_y} - \frac{\sigma_y}{F_x} \tag{43}$$

148. Elastic Constants.—Nine constants of the material may be determined experimentally; namely, three values of Young's modulus and six values of Poisson's ratio. Since these may be expressed in terms of the coefficients A, B, C, F, G, and H, it is evident that three relations must exist between them. These relations, obtained from equations 38, 39, and 40 are

$$E_y\mu_{zy} = E_z\mu_{yz} \tag{44}$$

$$E_z\mu_{xz} = E_x\mu_{zx} \tag{45}$$

$$E_x\mu_{yx} = E_y\mu_{xy} \tag{46}$$

A relation which involves the different Poisson's ratios only may be obtained from the product of the above equations as follows:

$$\mu_{zy}\mu_{xz}\mu_{yx} = \mu_{yz}\mu_{zx}\mu_{xy} \qquad (47)$$

The coefficients L, M, and N, as stated in section 146, represent shearing moduli of elasticity in the directions of the pairs of axes y,z; x,z; and x,y, respectively. By torsion tests on specimens of circular cross section, average values of the two shearing moduli in the plane normal to the axis of the specimen may be determined. If test specimens are built up with the different planes of symmetry normal to the axis of the cylinder, as shown on figures 176 and 177, averages of the shearing moduli on the x, y, and z planes may be obtained experimentally. Each shearing modulus so obtained is independent of the others.

149. Volume Modulus.—The volume modulus of elasticity for an anisotropic material is given by the equation:

$$\frac{1}{K} = \frac{1}{E_x} + \frac{1}{E_y} + \frac{1}{E_z} - \frac{2}{F_x} - \frac{2}{F_y} - \frac{2}{F_z} \qquad (48)$$

where K is the volume modulus. Equations 38, 39, and 40 show that each value of F is a function of two separate values of μ and E. Since the experimentally determined values of μ and E in these equations were not identical, the average values of these quantities were used to compute K. If all values of μ and E are averaged, the expression for K becomes the same as that for an isotropic material:

$$K = \frac{E}{3(1-2\mu)} \qquad (49)$$

It is evident from the above equation that when μ equals 0.50, K becomes infinite. If μ is slightly greater than 0.50, K will have a large negative value; and conversely, if μ is slightly smaller than 0.50, K will have a large positive value. Small experimental errors in determining μ will, therefore, greatly influence the value of K computed from equation 48. According to Karl Pearson and St. Venant,[15] negative values of the volume modulus of elasticity are not impossible in the case of anisotropic materials. This would mean that the material would increase in volume when subjected to pressure.

150. Axis of Symmetry.—Preliminary tests on the material indicated that the lowest modulus of elasticity was obtained in the di-

[15]Todhunter, Isaac, and Karl Pearson, "A History of the Theory of Elasticity," 1893, pp. 110 and 208. Cambridge University Press, London.

rection normal to the thickness of the sheets. It was not possible to determine, by inspection, the transverse directions of the sheet to which the other two reference axes corresponded. Since the sheets were laid horizontally in building the model, it may be expected that half of the sheets had their transverse reference axes turned in one direction, and the other half in the direction at right angles. For such a condition, the material may be expected to act as if it were isotropic in the transverse direction of the sheets. The reference axis normal to the sheet is then the axis of symmetry.

151. Isotropic Conditions in Two Directions.—If the axis of symmetry is taken as the z axis, the strain energy function is

$$2W = A(\epsilon_x^2 + \epsilon_y^2) + C\epsilon_z^2 + 2F(\epsilon_y + \epsilon_x)\epsilon_z + 2(A - 2N)\epsilon_x\epsilon_y + L(\gamma^2_{yz} + \gamma^2_{zx}) + N\gamma^2_{xy} \qquad (50)$$

Stresses in terms of strains are:

$$\sigma_x = A\epsilon_x + (A - 2N)\epsilon_y + F\epsilon_z \qquad (51)$$

$$\sigma_y = (A - 2N)\epsilon_x + A\epsilon_y + F\epsilon_z \qquad (52)$$

$$\sigma_z = F\epsilon_x + F\epsilon_y + C\epsilon_z \qquad (53)$$

$$\tau_{yz} = L\gamma_{yz} \qquad (54)$$

$$\tau_{zx} = L\gamma_{zx} \qquad (55)$$

$$\tau_{xy} = N\gamma_{xy} \qquad (56)$$

The elastic constants may be expressed in terms of coefficients by the following relations:

$$\frac{\Delta}{E_x} = \frac{\Delta}{E_y} = AC - F^2 \qquad (57)$$

$$\frac{\Delta}{E_z} = 4AN - 4N^2 \qquad (58)$$

$$\mu_{xy} = \mu_{yx} = \frac{AC - 2CN - F^2}{AC - F^2} \qquad (59)$$

$$\mu_{xz} = \mu_{yz} = \frac{2FN}{AC - F^2} \qquad (60)$$

$$\mu_{zx} = \mu_{zy} = \frac{2FN}{4AN - 4N^2} \qquad (61)$$

$$\frac{\Delta}{F_x} = \frac{\Delta}{F_y} = 2FN \tag{62}$$

$$\frac{\Delta}{F_z} = AC - 2CN - F^2 \tag{63}$$

where Δ is the determinant:

$$\Delta = \begin{vmatrix} A & (A-2N) & F \\ (A-2N) & A & F \\ F & F & C \end{vmatrix}$$

or $$\Delta = 4N(AC - CN - F^2) \tag{64}$$

Values of F_x, F_y, and F_z may be obtained from experimentally determined values of μ and E by the relations:

$$\frac{1}{F_x} = \frac{1}{F_y} = \frac{\mu_{xz}}{E_x} = \frac{\mu_{zx}}{E_z} \tag{65}$$

$$\frac{1}{F_z} = \frac{\mu_{xy}}{E_x} \tag{66}$$

From equation 65, the relation between the experimentally determined constants is

$$E_x\mu_{zx} = E_z\mu_{xz} \tag{67}$$

A second relation may be obtained from equations 57, 63, and 64; namely,

$$\frac{\Delta}{2N} = 2AC - 2CN - 2F^2 = \frac{\Delta}{E_x} + \frac{\Delta}{F_z}$$

whence

$$G_z = \frac{E_x}{2(1+\mu_{xy})} \tag{68}$$

where the symbol G_z for the shear modulus is used in place of N. This is the same as the relation which holds for an isotropic material.

The volume modulus of elasticity is given by the equation,

$$\frac{1}{K} = \frac{2}{E_x} + \frac{1}{E_z} - \frac{4}{F_x} - \frac{2}{F_z} \qquad (69)$$

ELASTICITY TESTS

152. Specimens.—Three types of specimens were made and tested. The first type, specimens A, B, and C, were rectangular prisms, approximately 6 by 6 by 12 inches in dimension. They were made by cementing together twelve 6 by 6 by 1-inch blocks and grinding the faces of the prisms to plane surfaces. Specimen A was made from blocks cut from a single 24 by 24 by 1-inch sheet. A small arrow was marked on each block before the sheet was cut, and the specimen was built up with the arrows all turned in the same direction, so that the assembled specimen had the same directional properties as the individual blocks. This specimen was made to determine the elastic properties in the direction of its three principal axes.

Specimen B was made from blocks cut from a single sheet, but the arrows on alternate blocks were turned at right angles to each other. This specimen was made to determine whether the rubber, under such conditions of assembly, behaved as an isotropic material in one plane.

Specimen C was made from a group of 6 by 6 by 1-inch slabs selected at random from the stock pile. No regular arrangement of the transverse axes of the individual blocks was made since these axes could not be identified. This specimen was, therefore, representative of the material as it was assembled in the model.

The second type of specimen, D and E, consisted of circular cylinders, three inches in diameter and about 12 inches long. Specimen D was made of 12 circular disks, 3 inches in diameter and 1 inch thick, cemented together without regard to the directions of the transverse axes, and turned to a true circular section in a lathe. This specimen was tested in tension, compression, and torsion. Specimen E had a middle section 7 inches long turned from 3 sheets cemented together, with the joints parallel to the axis of the specimen. The reference axes of the three sheets were parallel. At each end was a section 3 inches long with transverse joints for use in gripping the specimen.

The third type of specimen was used to find the modulus of elas-

ticity of the material in flexure. Specimen F was a rectangular prism, 3 by 3 by 16 inches in size, made by cementing together three strips cut from a 24 by 24 by 1-inch slab. It was tested on a 15-inch span, with the cemented joints vertical.

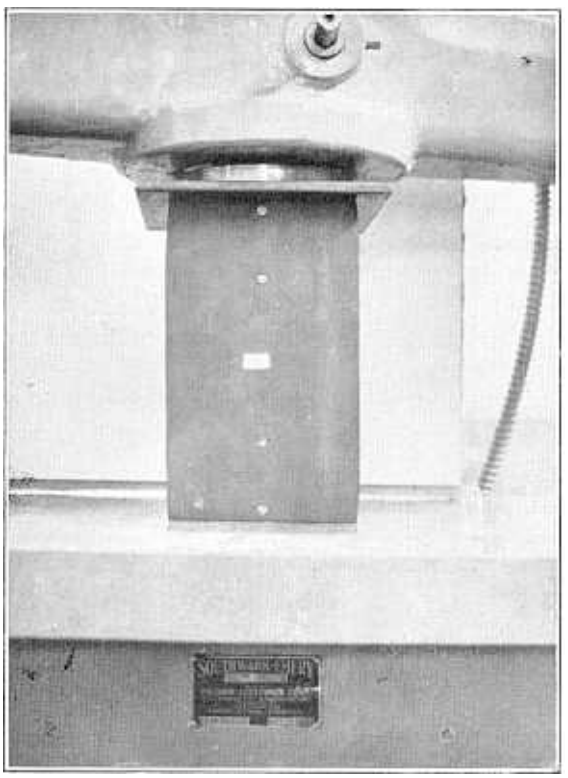

FIGURE 163—COMPRESSION TEST OF RUBBER-LITHARGE PRISM SHOWING END RESTRAINT

153. **End Conditions.**—The 6 by 6 by 12-inch prisms were tested in compression, using a hydraulic testing machine equipped with a dial graduated in 20-pound divisions over a 10,000-pound range. In testing such a soft material, relatively large strains were produced by small loads. Considerable bulging of the specimen occurred, as shown in figure 163. This resulted in a complex strain condition near the ends of the specimen, due to friction between the material and the bearing plates through which the load was applied. The bulging in the middle and the restraint at the ends was eliminated by greasing the ends of the specimen with cup grease. The same specimen, with

the ends greased, is shown in figure 164. No bulging occurred when the load was applied. Therefore, bearing surfaces of the specimen were greased in all subsequent compression tests.

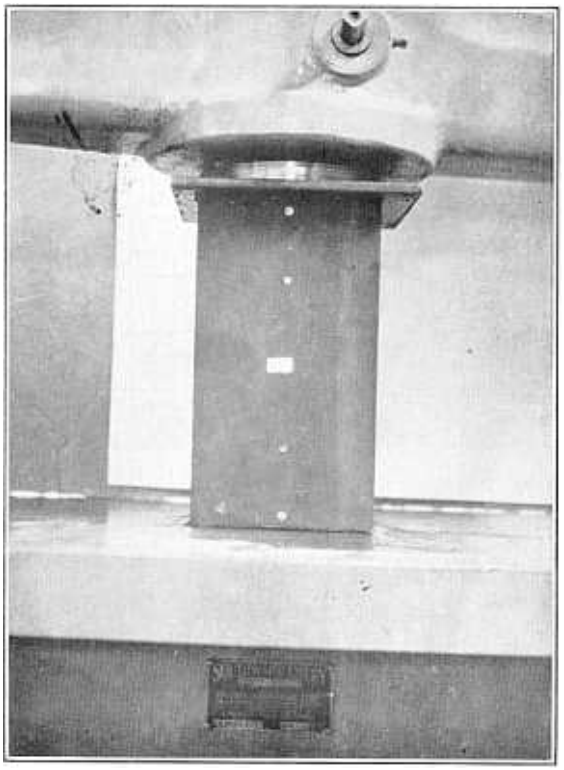

FIGURE 164—COMPRESSION TEST OF RUBBER-LITHARGE PRISM WITH ENDS GREASED

154. Compression Tests.—In testing specimens A, B, and C, loads were applied in increments of 400 pounds in the direction of the short axes of the specimens, and 200 pounds in the direction of the long axes. This made the unit stress increments in the specimen slightly less than six pounds per square inch. Longitudinal deformations of the specimen were determined by measuring changes in length between the base of the testing machine and reference marks at each of the four corners of the block at the upper end of the specimen, using a steel scale graduated in hundredths of an inch. Lateral deformations were measured with calipers, between gage points made by cementing small

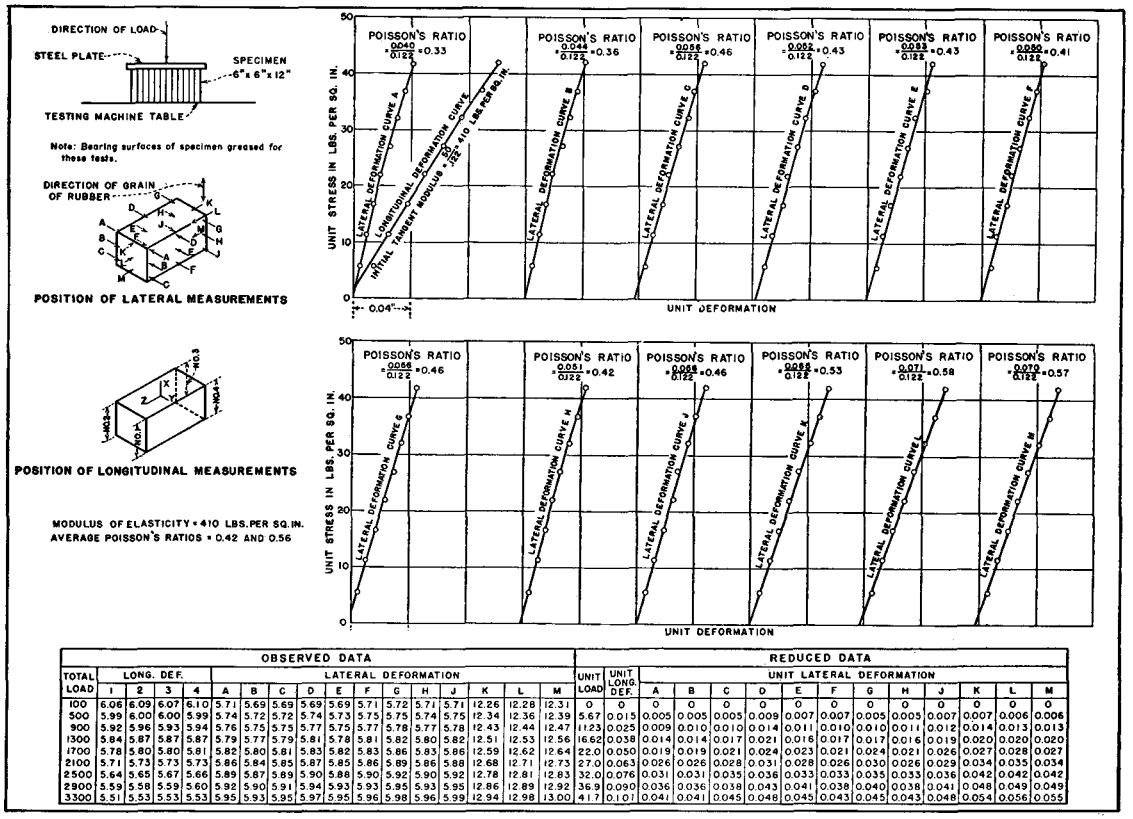

OBSERVED DATA																	REDUCED DATA														
TOTAL LOAD	LONG. DEF.				LATERAL DEFORMATION												UNIT LOAD	UNIT LONG. DEF.	UNIT LATERAL DEFORMATION												
	1	2	3	4	A	B	C	D	E	F	G	H	J	K	L	M			A	B	C	D	E	F	G	H	J	K	L	M
100	6.06	6.09	6.07	6.10	5.71	5.69	5.69	5.69	5.69	5.71	5.72	5.71	5.71	12.26	12.28	12.31	0	0	0	0	0	0	0	0	0	0	0	0	0	0	0
500	5.99	6.00	6.00	5.99	5.74	5.72	5.72	5.74	5.73	5.75	5.75	5.74	5.75	12.34	12.36	12.39	5.67	0.015	0.005	0.005	0.005	0.009	0.007	0.007	0.005	0.005	0.007	0.007	0.006	0.006
900	5.92	5.96	5.93	5.94	5.76	5.75	5.75	5.77	5.75	5.77	5.78	5.77	5.78	12.43	12.44	12.47	11.23	0.025	0.009	0.010	0.010	0.014	0.011	0.010	0.010	0.011	0.012	0.014	0.013	0.013
1300	5.84	5.87	5.87	5.87	5.79	5.77	5.79	5.81	5.78	5.81	5.82	5.80	5.82	12.51	12.53	12.56	16.62	0.038	0.014	0.014	0.017	0.021	0.016	0.017	0.017	0.016	0.019	0.020	0.020	0.020
1700	5.78	5.80	5.80	5.81	5.82	5.80	5.81	5.83	5.82	5.83	5.86	5.83	5.86	12.59	12.62	12.64	22.0	0.050	0.019	0.019	0.021	0.024	0.023	0.021	0.024	0.021	0.026	0.027	0.028	0.027
2100	5.71	5.73	5.73	5.73	5.86	5.84	5.85	5.87	5.85	5.86	5.89	5.86	5.88	12.68	12.71	12.73	27.0	0.063	0.026	0.026	0.028	0.031	0.028	0.026	0.030	0.026	0.029	0.034	0.035	0.034
2500	5.64	5.65	5.67	5.66	5.89	5.87	5.89	5.90	5.88	5.90	5.92	5.90	5.92	12.78	12.81	12.83	32.0	0.076	0.031	0.031	0.035	0.036	0.033	0.033	0.035	0.033	0.036	0.042	0.042	0.042
2900	5.59	5.58	5.59	5.60	5.92	5.90	5.91	5.94	5.93	5.93	5.95	5.93	5.95	12.86	12.89	12.92	36.9	0.090	0.036	0.036	0.038	0.043	0.041	0.038	0.040	0.038	0.041	0.048	0.049	0.049
3300	5.51	5.53	5.53	5.53	5.95	5.93	5.95	5.97	5.95	5.96	5.98	5.96	5.99	12.94	12.98	13.00	41.7	0.101	0.041	0.041	0.045	0.048	0.045	0.043	0.045	0.043	0.048	0.054	0.056	0.055

FIGURE 165—COMPRESSION TEST OF SPECIMEN A LOADED IN *X* DIRECTION

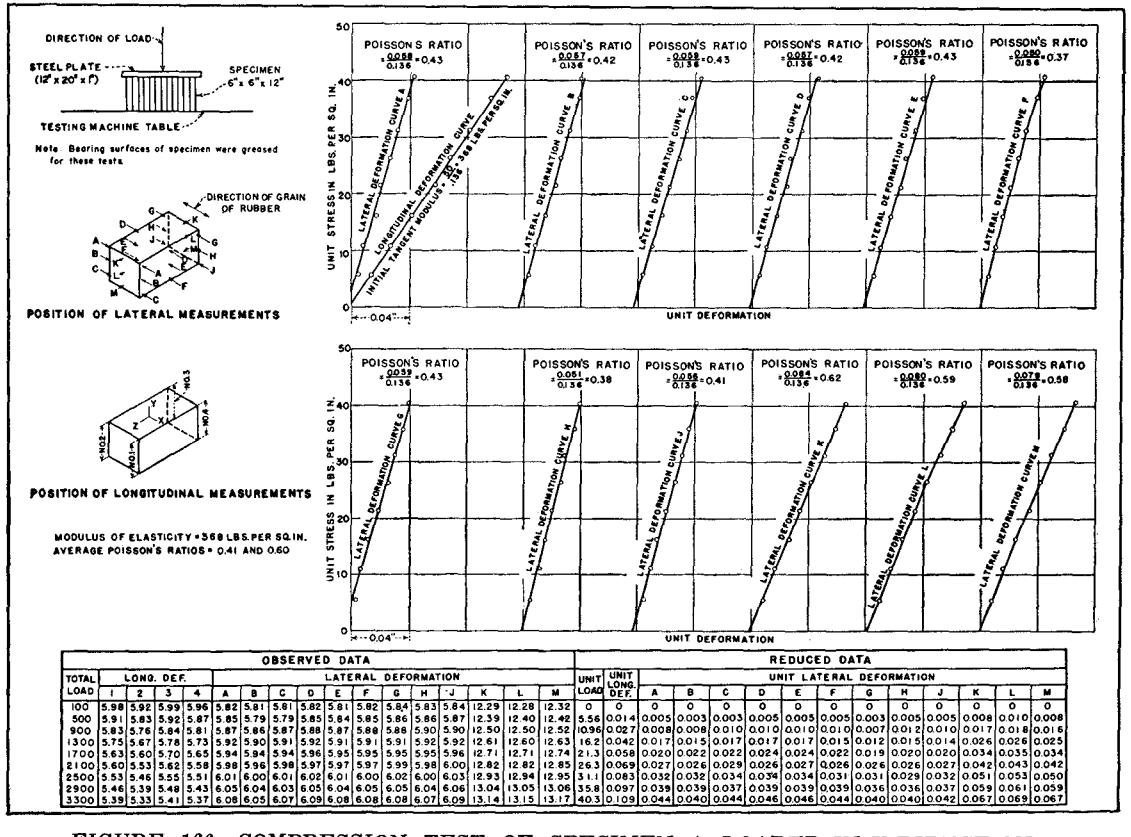

OBSERVED DATA																	REDUCED DATA														
TOTAL LOAD	LONG. DEF.				LATERAL DEFORMATION												UNIT LOAD	UNIT LONG. DEF.	UNIT LATERAL DEFORMATION												
	1	2	3	4	A	B	C	D	E	F	G	H	J	K	L	M			A	B	C	D	E	F	G	H	J	K	L	M
100	5.98	5.92	5.99	5.96	5.82	5.81	5.81	5.82	5.81	5.82	5.84	5.83	5.84	12.29	12.28	12.32	0	0	0	0	0	0	0	0	0	0	0	0	0	0	0
500	5.91	5.83	5.92	5.87	5.85	5.79	5.79	5.85	5.84	5.85	5.86	5.86	5.87	12.39	12.40	12.42	5.56	0.014	0.005	0.003	0.003	0.005	0.005	0.005	0.003	0.005	0.005	0.008	0.010	0.008
900	5.83	5.76	5.84	5.81	5.87	5.86	5.87	5.88	5.87	5.88	5.88	5.90	5.90	12.50	12.50	12.52	10.96	0.027	0.008	0.008	0.010	0.010	0.010	0.010	0.007	0.012	0.010	0.017	0.018	0.016
1300	5.75	5.67	5.78	5.73	5.92	5.90	5.91	5.92	5.91	5.91	5.91	5.92	5.92	12.60	12.60	12.63	16.2	0.042	0.017	0.015	0.017	0.017	0.017	0.015	0.012	0.015	0.014	0.026	0.026	0.025
1700	5.63	5.60	5.70	5.65	5.94	5.94	5.94	5.96	5.95	5.95	5.95	5.95	5.96	12.71	12.71	12.74	21.3	0.058	0.020	0.022	0.022	0.024	0.024	0.022	0.019	0.020	0.020	0.034	0.035	0.034
2100	5.60	5.53	5.62	5.58	5.98	5.96	5.98	5.97	5.97	5.97	5.99	5.98	6.00	12.82	12.82	12.85	26.3	0.069	0.027	0.026	0.029	0.026	0.027	0.026	0.026	0.026	0.027	0.042	0.043	0.042
2500	5.53	5.46	5.55	5.51	6.01	6.00	6.01	6.02	6.01	6.00	6.02	6.00	6.03	12.93	12.94	12.95	31.1	0.083	0.032	0.032	0.034	0.034	0.034	0.031	0.031	0.029	0.032	0.051	0.053	0.050
2900	5.46	5.39	5.48	5.43	6.05	6.04	6.03	6.05	6.04	6.05	6.05	6.04	6.06	13.04	13.05	13.06	35.8	0.097	0.039	0.039	0.037	0.039	0.039	0.039	0.036	0.036	0.037	0.059	0.061	0.059
3300	5.39	5.33	5.41	5.37	6.08	6.05	6.07	6.09	6.08	6.08	6.08	6.07	6.09	13.14	13.15	13.17	40.3	0.109	0.044	0.040	0.044	0.046	0.046	0.044	0.040	0.040	0.042	0.067	0.069	0.067

FIGURE 166—COMPRESSION TEST OF SPECIMEN A LOADED IN *Y* DIRECTION

steel plates to opposite points on the lateral faces of the specimen. Nine such sets of gage points were provided on the 6 by 12-inch faces of specimens A and B, and three sets on the rest of the faces of A and B and on all faces of specimen C. The results of the tests are shown in figures 165 to 173, inclusive.

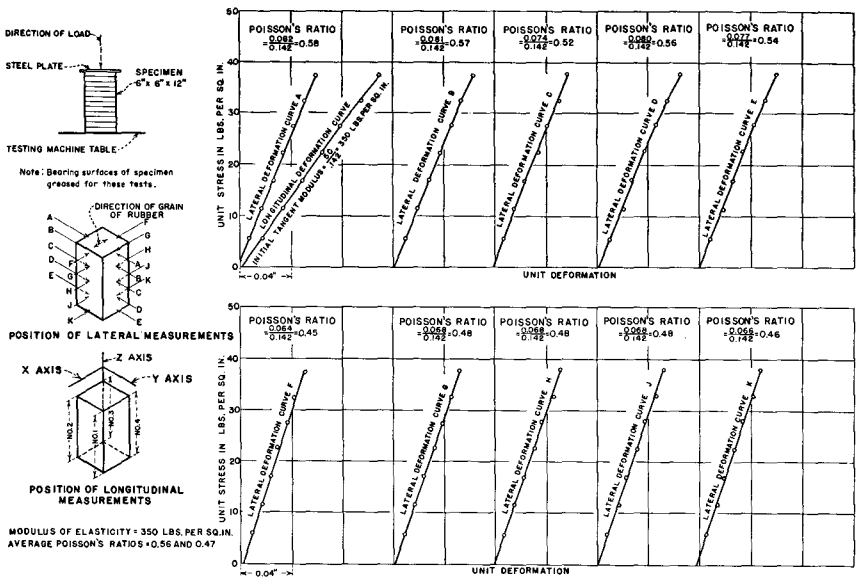

TOTAL LOAD	OBSERVED DATA: LONG. DEF. 1	2	3	4	LATERAL DEFORMATION A	B	C	D	E	F	G	H	J	K	UNIT LOAD	UNIT LONG. DEF.	REDUCED DATA: UNIT LATERAL DEFORMATION A	B	C	D	E	F	G	H	J	K
400 Lb.	11.95	11.95	11.98	12.00	5.85	5.86	5.90	5.90	5.96	5.90	5.91	5.92	5.91	5.95	0	0	0	0	0	0	0	0	0	0	0	0
600 "	11.74	11.77	11.74	11.79	5.89	5.92	5.94	5.96	6.01	5.95	5.96	5.96	5.95	5.98	5.85	0.018	0.007	0.010	0.007	0.010	0.009	0.009	0.009	0.007	0.007	0.005
800 "	11.54	11.56	11.60	11.60	5.95	5.97	5.99	6.02	6.07	6.00	6.01	6.01	6.01	6.03	11.50	0.034	0.017	0.019	0.015	0.021	0.019	0.017	0.017	0.015	0.017	0.014
1000 "	11.36	11.37	11.42	11.42	6.01	6.03	6.04	6.06	6.11	6.04	6.05	6.05	6.04	6.06	17.00	0.050	0.027	0.029	0.024	0.027	0.028	0.024	0.024	0.022	0.022	0.019
1200 "	11.19	11.20	11.25	11.25	6.05	6.08	6.10	6.12	6.16	6.07	6.10	6.10	6.09	6.11	22.30	0.065	0.034	0.037	0.034	0.037	0.034	0.029	0.032	0.031	0.031	0.027
1400 "	11.02	11.04	11.09	11.09	6.10	6.13	6.14	6.17	6.21	6.12	6.14	6.13	6.13	6.15	27.43	0.079	0.042	0.046	0.041	0.046	0.042	0.037	0.039	0.036	0.037	0.034
1600 "	10.85	10.86	10.90	10.90	6.15	6.18	6.20	6.23	6.27	6.15	6.18	6.19	6.18	6.20	32.40	0.096	0.051	0.054	0.05	0.055	0.052	0.042	0.046	0.046	0.046	0.042
1800 "	10.69	10.71	10.70	10.75	6.21	6.24	6.24	6.29	6.32	6.20	6.22	6.22	6.22	6.23	37.20	0.110	0.060	0.064	0.057	0.065	0.060	0.05	0.052	0.051	0.052	0.047

FIGURE 167—COMPRESSION TEST OF SPECIMEN A LOADED IN *Z* DIRECTION

155. Tension Tests.—Specimens D and E were tested in tension, using the machine developed for plaster-celite specimens, see figure 46. Flat-headed tacks, with small conical holes in their heads, were driven in opposite sides of the specimen, 5.3 inches apart, and cemented in place. These served as gage points for measuring longitudinal deformations. Strains were measured with a pair of sharp-pointed dividers and a micrometer caliper. Small steel plates were cemented to the specimen for lateral gage points, and lateral deformations measured with a micrometer caliper. The load was applied in three-

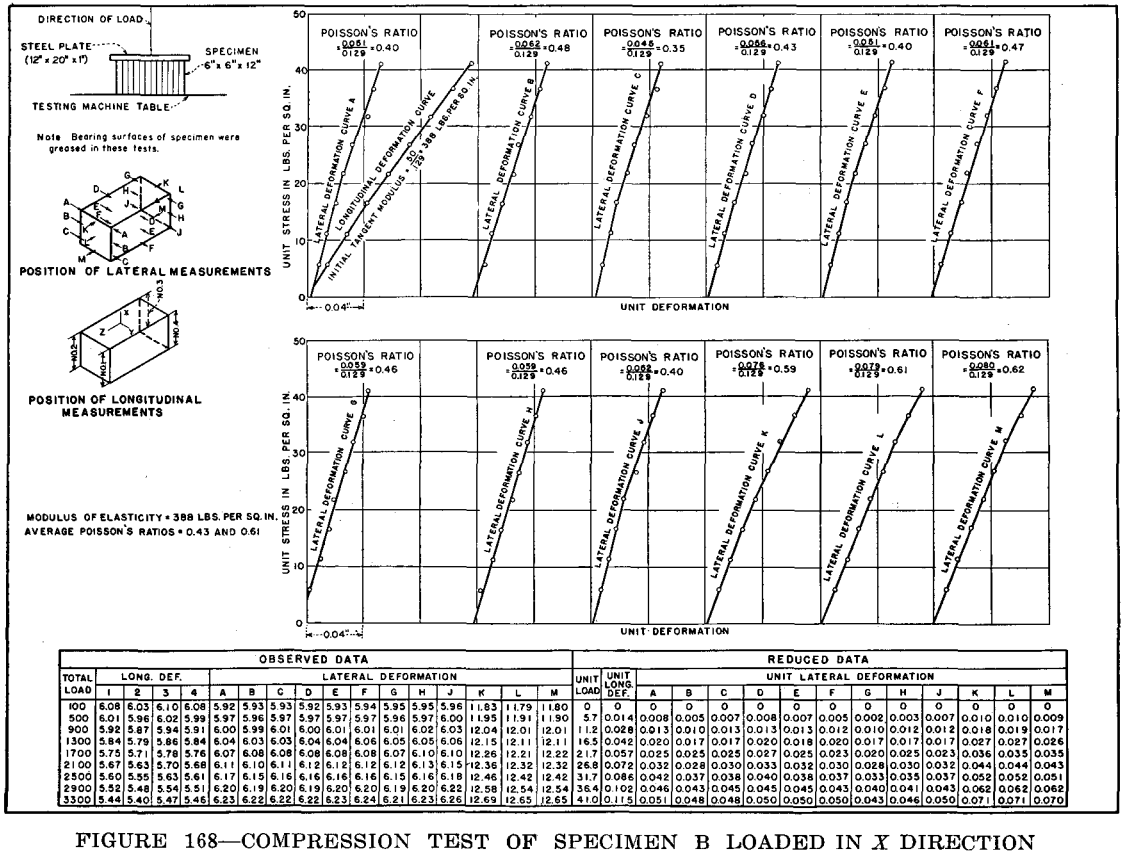

OBSERVED DATA															REDUCED DATA											
TOTAL LOAD	LONG. DEF.				LATERAL DEFORMATION										UNIT LOAD	UNIT LONG. DEF.	UNIT LATERAL DEFORMATION										
	1	2	3	4	A	B	C	D	E	F	G	H	J	K	L	M			A	B	C	D	E	F	G	H	J	K	L	M
100	6.08	6.03	6.10	6.08	5.92	5.93	5.93	5.92	5.93	5.94	5.95	5.95	5.96	11.83	11.79	11.80	0	0	0	0	0	0	0	0	0	0	0	0	0	0
500	6.01	5.96	6.02	5.99	5.97	5.96	5.97	5.97	5.97	5.96	5.97	6.00	11.95	11.91	11.90	5.7	0.014	0.008	0.005	0.007	0.008	0.007	0.005	0.002	0.003	0.007	0.010	0.010	0.009
900	5.92	5.87	5.94	5.91	6.00	5.99	6.01	6.00	6.01	6.01	6.01	6.02	6.03	12.04	12.01	12.01	11.2	0.028	0.013	0.010	0.013	0.013	0.013	0.012	0.010	0.012	0.012	0.018	0.019	0.017
1300	5.84	5.79	5.86	5.84	6.04	6.03	6.03	6.04	6.04	6.06	6.05	6.05	6.06	12.15	12.11	12.11	16.5	0.042	0.020	0.017	0.017	0.020	0.018	0.020	0.017	0.017	0.017	0.027	0.027	0.026
1700	5.75	5.71	5.78	5.76	6.07	6.08	6.08	6.08	6.08	6.08	6.07	6.10	6.10	12.26	12.21	12.22	21.7	0.057	0.025	0.025	0.025	0.027	0.025	0.023	0.020	0.025	0.023	0.036	0.035	0.035
2100	5.67	5.63	5.70	5.68	6.11	6.10	6.11	6.12	6.12	6.12	6.12	6.13	6.15	12.36	12.32	12.32	26.8	0.072	0.032	0.028	0.030	0.033	0.032	0.030	0.028	0.030	0.032	0.044	0.044	0.043
2500	5.60	5.55	5.63	5.61	6.17	6.15	6.16	6.16	6.16	6.16	6.15	6.16	6.18	12.46	12.42	12.42	31.7	0.086	0.042	0.037	0.038	0.040	0.038	0.037	0.033	0.035	0.037	0.052	0.052	0.051
2900	5.52	5.48	5.54	5.51	6.20	6.19	6.20	6.19	6.20	6.20	6.19	6.20	6.22	12.58	12.54	12.54	36.4	0.102	0.046	0.043	0.045	0.045	0.045	0.043	0.040	0.041	0.043	0.062	0.062	0.062
3300	5.44	5.40	5.47	5.46	6.23	6.22	6.22	6.22	6.23	6.24	6.21	6.23	6.26	12.69	12.65	12.65	41.0	0.115	0.051	0.048	0.048	0.050	0.050	0.050	0.043	0.046	0.050	0.071	0.071	0.070

FIGURE 168—COMPRESSION TEST OF SPECIMEN B LOADED IN *X* DIRECTION

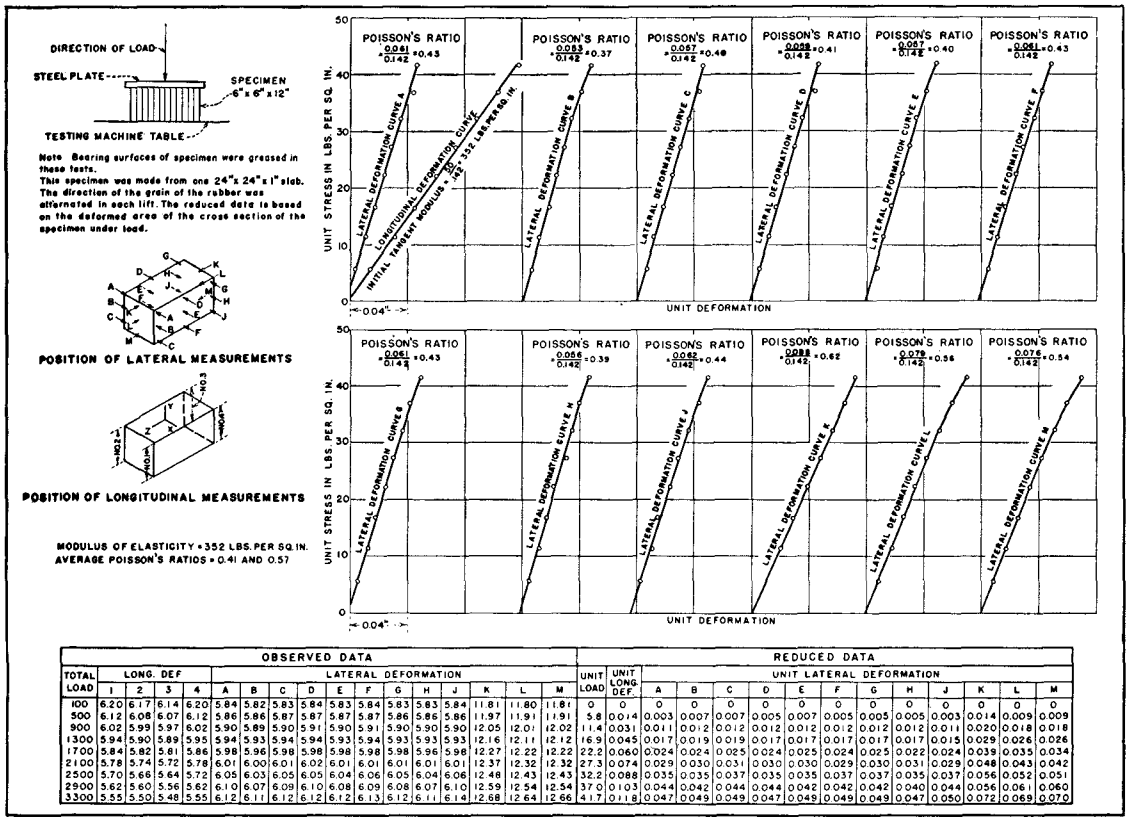

OBSERVED DATA																	REDUCED DATA														
TOTAL LOAD	LONG. DEF				LATERAL DEFORMATION												UNIT LOAD	UNIT LONG. DEF.	UNIT LATERAL DEFORMATION												
	1	2	3	4	A	B	C	D	E	F	G	H	J	K	L	M			A	B	C	D	E	F	G	H	J	K	L	M
100	6.20	6.17	6.14	6.20	5.84	5.82	5.83	5.84	5.83	5.84	5.83	5.83	5.84	11.81	11.80	11.81	0	0	0	0	0	0	0	0	0	0	0	0	0	0	0
500	6.12	6.08	6.07	6.12	5.86	5.86	5.87	5.87	5.87	5.87	5.86	5.86	5.86	11.97	11.91	11.91	5.8	0.014	0.003	0.007	0.007	0.005	0.007	0.005	0.005	0.005	0.003	0.014	0.009	0.009
900	6.02	5.99	5.97	6.02	5.90	5.89	5.90	5.91	5.90	5.91	5.90	5.90	5.90	12.05	12.01	12.02	11.4	0.031	0.011	0.012	0.012	0.012	0.012	0.012	0.012	0.012	0.011	0.020	0.018	0.018
1300	5.94	5.90	5.89	5.95	5.94	5.93	5.94	5.94	5.93	5.94	5.93	5.93	5.93	12.16	12.11	12.12	16.9	0.045	0.017	0.019	0.019	0.017	0.017	0.017	0.017	0.017	0.015	0.029	0.026	0.026
1700	5.84	5.82	5.81	5.86	5.98	5.96	5.98	5.98	5.98	5.98	5.98	5.96	5.98	12.27	12.22	12.22	22.2	0.060	0.024	0.024	0.025	0.024	0.025	0.024	0.025	0.022	0.024	0.039	0.035	0.034
2100	5.78	5.74	5.72	5.78	6.01	6.00	6.01	6.02	6.01	6.01	6.01	6.01	6.01	12.37	12.32	12.32	27.3	0.074	0.029	0.030	0.031	0.030	0.030	0.029	0.030	0.031	0.029	0.048	0.043	0.042
2500	5.70	5.66	5.64	5.72	6.05	6.03	6.05	6.05	6.04	6.06	6.05	6.04	6.06	12.48	12.43	12.43	32.2	0.088	0.035	0.035	0.037	0.035	0.035	0.037	0.037	0.035	0.037	0.056	0.052	0.051
2900	5.62	5.60	5.56	5.62	6.10	6.07	6.09	6.10	6.08	6.09	6.08	6.07	6.10	12.59	12.54	12.54	37.0	0.103	0.044	0.042	0.044	0.044	0.042	0.042	0.042	0.040	0.044	0.056	0.061	0.060
3300	5.55	5.50	5.48	5.55	6.12	6.11	6.12	6.12	6.12	6.13	6.12	6.11	6.14	12.68	12.64	12.66	41.7	0.118	0.047	0.049	0.049	0.047	0.048	0.049	0.049	0.047	0.050	0.072	0.069	0.070

FIGURE 169—COMPRESSION TEST OF SPECIMEN B LOADED IN *Y* DIRECTION

pound increments. These specimens were also tested in compression and the results of both tests are shown in figures 174 and 175.

156. Torsion and Flexure Tests.—Specimens D and E were tested in torsion in the machine shown in figure 50. The load was applied in increments of one pound, causing a unit shearing stress of 1.12 pounds per square inch at the outside fiber of the specimen. Deformation measurements were made by measuring distances between reference points of the troptometer. The results of the torsion tests are shown in figures 176 and 177.

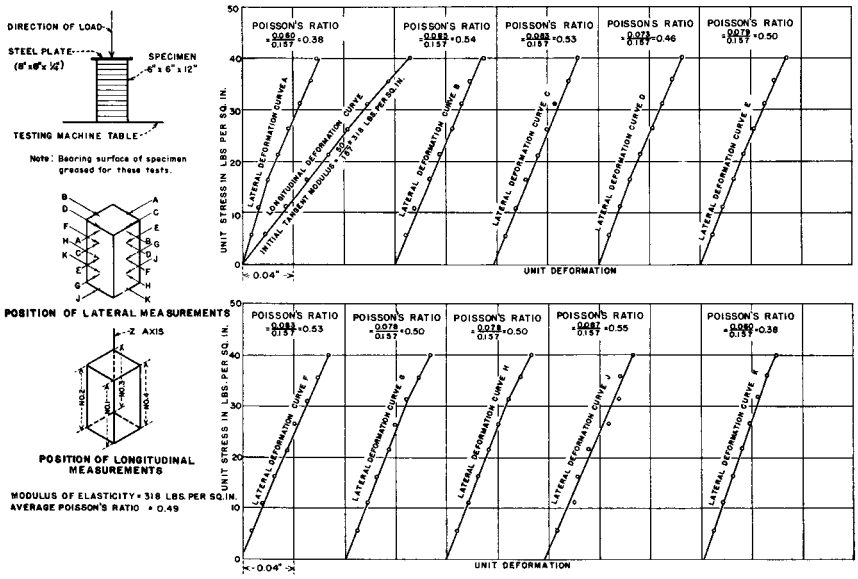

TOTAL LOAD	OBSERVED DATA: LONG. DEF. 1	2	3	4	LATERAL DEFORMATION A	B	C	D	E	F	G	H	J	K	UNIT LOAD	UNIT LONG DEF.	REDUCED DATA: UNIT LATERAL DEFORMATION A	B	C	D	E	F	G	H	J	K
100 Lb	11.72	11.83	11.79	11.68	6.01	6.02	6.04	6.00	6.02	6.04	6.00	6.01	5.94	6.01	0	0	0	0	0	0	0	0	0	0	0	0
300 "	11.51	11.62	11.58	11.47	6.05	6.07	6.08	6.05	6.08	6.08	6.06	6.06	5.98	6.07	5.6	0.018	0.007	0.008	0.007	0.008	0.010	0.007	0.010	0.008	0.007	0.010
500 "	11.32	11.45	11.41	11.30	6.08	6.11	6.13	6.10	6.13	6.13	6.11	6.11	6.06	6.11	11.0	0.034	0.012	0.015	0.015	0.017	0.018	0.015	0.018	0.017	0.020	0.017
700 "	11.13	11.26	11.22	11.11	6.13	6.16	6.18	6.15	6.18	6.19	6.15	6.16	6.08	6.16	16.3	0.051	0.020	0.027	0.023	0.025	0.027	0.025	0.025	0.025	0.023	0.025
900 "	10.95	11.07	11.03	10.92	6.18	6.23	6.23	6.20	6.23	6.25	6.21	6.21	6.13	6.20	21.4	0.068	0.028	0.035	0.032	0.033	0.035	0.035	0.035	0.033	0.032	0.032
1100 "	10.73	10.90	10.89	10.75	6.23	6.29	6.28	6.26	6.28	6.30	6.24	6.26	6.23	6.24	26.3	0.083	0.036	0.045	0.040	0.043	0.043	0.043	0.040	0.041	0.048	0.038
1300 "	10.62	10.74	10.69	10.58	6.28	6.34	6.32	6.31	6.33	6.35	6.30	6.31	6.28	6.29	31.0	0.099	0.045	0.053	0.046	0.051	0.051	0.051	0.049	0.049	0.056	0.046
1500 "	10.44	10.56	10.53	10.40	6.34	6.38	6.39	6.36	6.38	6.40	6.36	6.37	6.28	6.34	35.6	0.118	0.054	0.059	0.057	0.059	0.059	0.059	0.059	0.059	0.056	0.052
1700 "	10.28	10.40	10.36	10.25	6.37	6.45	6.43	6.41	6.44	6.45	6.41	6.42	6.35	6.38	40.0	0.132	0.059	0.070	0.064	0.067	0.069	0.067	0.067	0.067	0.067	0.060

FIGURE 170—COMPRESSION TEST OF SPECIMEN B LOADED IN *Z* DIRECTION

Specimen F was tested in flexure as a simply supported beam on a 15-inch span. As the beam was very flexible, the load was applied at the center in increments of 200 grams. Deflections at the center were measured with a dial gage reading to one-thousandth of an inch. Results of the flexural test are given in figure 178.

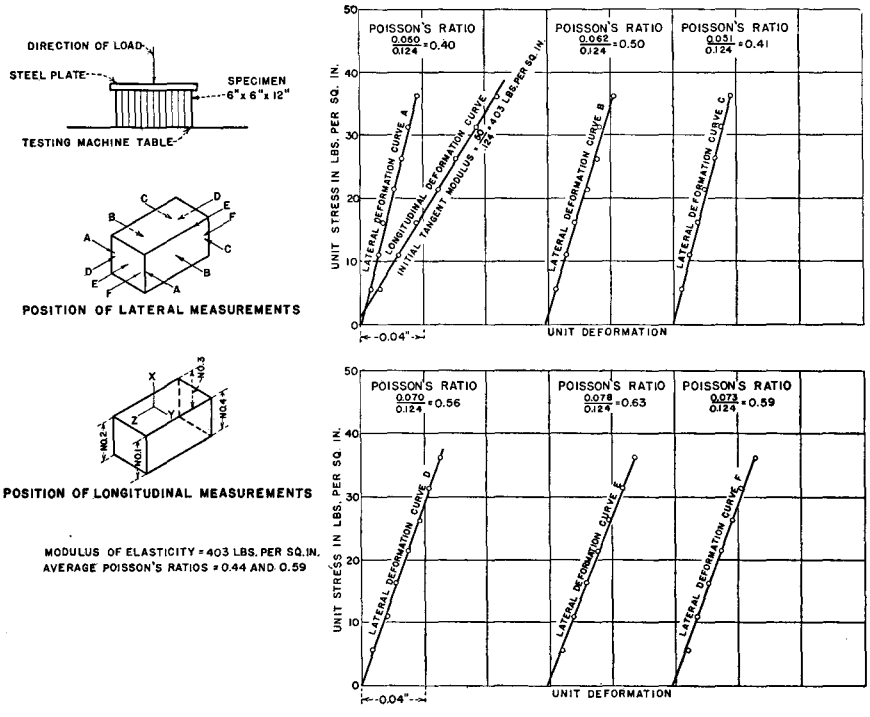

TOTAL LOAD	OBSERVED DATA: LONGITUDINAL DEF. 1	2	3	4	LATERAL DEFORMATION A	B	C	D	E	F	UNIT LOAD	UNIT LONG. DEF.	REDUCED DATA: LATERAL DEFORMATION A	B	C	D	E	F
100 Lb.	6.20	6.18	6.14	6.18	6.02	6.03	6.03	12.20	12.22	12.21	0	0	0	0	0	0	0	0
500	6.13	6.11	6.07	6.10	6.06	6.06	6.06	12.28	12.31	12.30	5.6	0.013	0.007	0.005	0.005	0.007	0.008	0.008
900	6.07	6.04	5.98	6.03	6.09	6.10	6.09	12.39	12.40	12.38	11.0	0.025	0.012	0.012	0.010	0.015	0.016	0.014
1300	5.98	5.97	5.92	5.96	6.11	6.13	6.12	12.47	12.50	12.47	16.3	0.037	0.015	0.017	0.015	0.022	0.023	0.021
1700	5.92	5.89	5.84	5.88	6.15	6.18	6.15	12.56	12.59	12.56	21.5	0.051	0.022	0.025	0.020	0.030	0.030	0.029
2100	5.84	5.82	5.77	5.81	6.19	6.22	6.19	12.65	12.69	12.65	26.4	0.063	0.028	0.032	0.027	0.037	0.038	0.036
2500	5.78	5.75	5.70	5.74	6.21	6.25	6.21	12.74	12.78	12.73	31.4	0.076	0.032	0.033	0.030	0.044	0.046	0.042
2900	5.70	5.68	5.63	5.66	6.25	6.28	6.25	12.83	12.88	12.84	36.2	0.089	0.038	0.042	0.037	0.051	0.054	0.051

FIGURE 171—COMPRESSION TEST OF SPECIMEN C LOADED IN X DIRECTION

ELASTICITY DATA

157. Elastic Constants.—Elastic constants of the material, obtained graphically from the test data and based on original dimensions of the specimens, are given in table 5. The z axis is perpendicular to the thickness of the slabs, while the x axis is in the direction of the greatest modulus of elasticity. The first subscript in the symbols for Poisson's ratio indicates the direction of the longitudinal strain. The second subscript indicates the direction of the lateral strain. Thus, μ_{xy} is the ratio of the lateral strain in the y direction to the strain in the x direction when a load is applied to the speci-

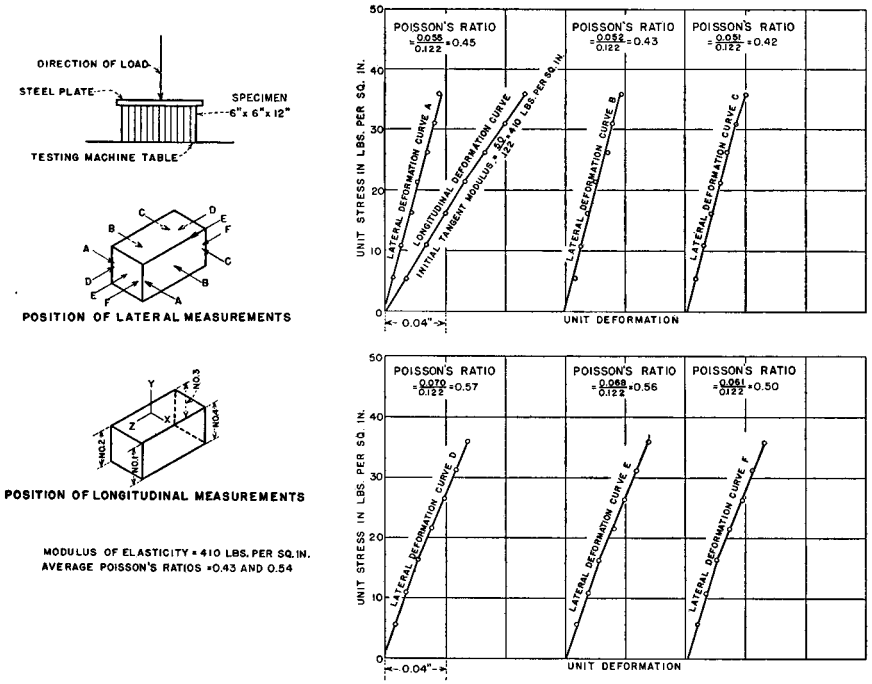

OBSERVED DATA											REDUCED DATA							
TOTAL LOAD	LONGITUDINAL DEF.				LATERAL DEFORMATION						UNIT LOAD	UNIT LONG. DEF.	LATERAL DEFORMATION					
	1	2	3	4	A	B	C	D	E	F			A	B	C	D	E	F
100 Lb.	6.23	6.20	6.20	6.25	6.00	6.01	6.00	12.21	12.21	12.20	0	0	0	0	0	0	0	0
500 "	6.15	6.13	6.12	6.16	6.03	6.05	6.04	12.29	12.31	12.29	5.5	0.014	0.005	0.007	0.007	0.007	0.008	0.008
900 "	6.08	6.05	6.04	6.09	6.06	6.07	6.07	12.38	12.40	12.37	10.9	0.027	0.010	0.010	0.012	0.014	0.015	0.014
1300 "	6.00	5.97	5.97	6.02	6.10	6.10	6.10	12.48	12.48	12.46	16.2	0.040	0.017	0.015	0.017	0.022	0.022	0.021
1700 "	5.93	5.89	5.89	5.94	6.13	6.13	6.14	12.59	12.60	12.57	21.3	0.053	0.021	0.020	0.023	0.031	0.032	0.030
2100 "	5.85	5.82	5.82	5.87	6.17	6.18	6.17	12.69	12.69	12.67	26.2	0.067	0.028	0.028	0.028	0.039	0.039	0.038
2500 "	5.77	5.75	5.74	5.80	6.20	6.20	6.21	12.79	12.79	12.75	31.0	0.080	0.033	0.031	0.035	0.047	0.047	0.045
2900 "	5.70	5.68	5.68	5.73	6.22	6.24	6.24	12.89	12.89	12.86	35.8	0.093	0.036	0.038	0.040	0.055	0.055	0.053

FIGURE 172—COMPRESSION TEST OF SPECIMEN C LOADED IN Y DIRECTION

men parallel to the x axis. It should be emphasized that the elastic constants given in table 5, being based on original dimensions, are usually different from those given on figures 165 to 178, which were based on actual dimensions.

158. Changes in Dimension.—For a material which deforms greatly under small loads, the usual method of computing unit stress, by dividing the total load by the original cross-sectional area, gives rise to considerable error. Error is also involved in computing the unit strain by dividing the deformation by the original length of the specimen.

In the compression tests of specimens A, B, and C, the cross-

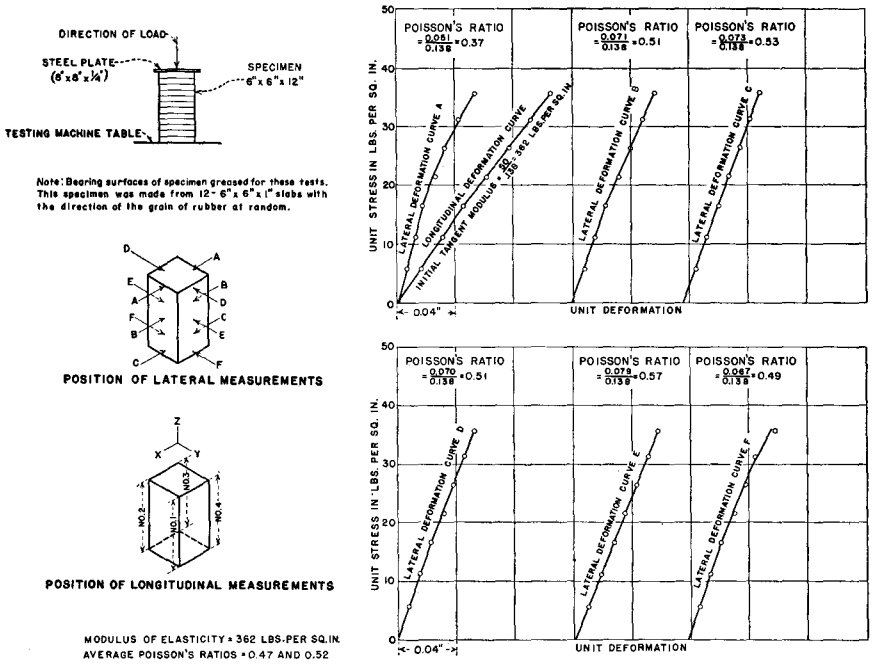

TOTAL LOAD	OBSERVED DATA: LONGITUDINAL DEF. 1	2	3	4	LATERAL DEFORMATION A	B	C	D	E	F	REDUCED DATA: UNIT LOAD	UNIT LONG DEF.	LATERAL DEFORMATION A	B	C	D	E	F
100 Lb	11.62	11.59	11.57	11.62	6.05	6.05	6.07	6.03	6.02	6.04	0	0	0	0	0	0	0	0
300 "	11.42	11.39	11.37	11.42	6.09	6.10	6.10	6.07	6.08	6.08	5.6	0.017	0.007	0.008	0.005	0.007	0.010	0.007
500 "	11.23	11.21	11.20	11.25	6.13	6.14	6.14	6.12	6.13	6.12	11.1	0.032	0.013	0.015	0.012	0.015	0.019	0.014
700 "	11.08	11.05	11.04	11.08	6.16	6.19	6.19	6.17	6.19	6.16	16.4	0.046	0.018	0.023	0.020	0.023	0.028	0.021
900 "	10.88	10.88	10.85	10.90	6.21	6.24	6.23	6.22	6.23	6.22	21.5	0.062	0.027	0.032	0.027	0.032	0.035	0.030
1100 "	10.72	10.69	10.68	10.69	6.25	6.29	6.28	6.26	6.28	6.27	26.4	0.078	0.033	0.040	0.035	0.038	0.043	0.038
1300 "	10.56	10.53	10.52	10.57	6.31	6.34	6.32	6.31	6.33	6.31	31.2	0.092	0.043	0.048	0.041	0.046	0.051	0.045
1500 "	10.41	10.37	10.36	10.42	6.38	6.39	6.36	6.35	6.37	6.39	35.8	0.106	0.054	0.056	0.048	0.053	0.056	0.058

FIGURE 173—COMPRESSION TEST OF SPECIMEN C LOADED IN Z DIRECTION

sectional area of the specimen at a stress of 40 pounds per square inch was about ten per cent greater than the area of the specimen under no load, so that discrepancies might be expected in values of stress and strain computed by usual methods. To reduce the discrepancies, stresses were computed by dividing each value of the load by the corresponding area of cross-section. Similarly, strains were obtained by dividing each deformation by the mean of the initial and final length for the particular strain observation. Stress-strain and lateral deformation curves, shown on figures 165 to 173, were determined by this method.

159. Plotting Test Data.—In plotting test data, measurements of longitudinal deformations at the four corners of the block were

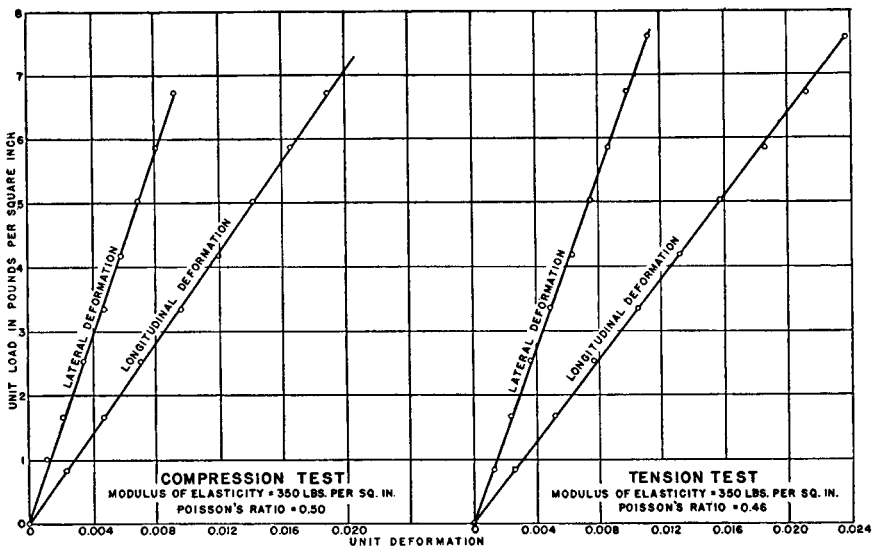

COMPRESSION						TENSION					
TOTAL LOAD	UNIT LOAD	AVER. LONG. DEF.	UNIT LONG. DEF.	AVER LAT. DEF.	UNIT LAT. DEF.	TOTAL LOAD	UNIT LOAD	AVER LONG DEF	UNIT LONG DEF	AVER LAT DEF	UNIT LAT. DEF.
0	0	0	0	0	0	0	0	0	0	0	0
6	0.84	0.0194	0.0024	0 0033	0.0011	6	0 84	0 0210	0 0026	0 0040	0.0013
12	1.68	0.0384	0.0048	0.0072	0.0023	12	1 68	0.0423	0 0052	0.0075	0.0024
18	2.52	0.0573	0.0072	0.0113	0.0035	18	2 52	0 0619	0.0077	0 0115	0 0036
24	3.36	0.0776	0.0097	0.0155	0.0049	24	3.36	0.0852	0.0105	0 0155	0 0049
30	4.20	0.0960	0.0120	0.0190	0 0060	30	4 20	0 1057	0 0132	0 0198	0.0063
36	5.04	0.1139	0.0142	0 0225	0 0070	36	5 04	0 1274	0 0158	0.0237	0.0075
42	5.88	0 1331	0.0166	0.0260	0 0081	42	5 88	0. 1503	0.0186	0.0275	0.0087
48	6.72	0.1518	0.0190	0.0297	0 0093	48	6.72	0. 1716	0 0212	0 0313	0.0099
						54	7 56	0. 1928	0.0238	0.0360	0 0113

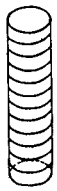

TEST SPECIMEN

FIGURE 174—RESULTS OF TESTS ON SPECIMEN D

averaged for each increment of applied load, and the average values plotted as shown in the upper left-hand diagram of figure 165. A curve was then drawn through the plotted points and the initial tangent modulus of elasticity determined from the curve. In the case of lateral deformations, separate measurements made along each axis of the block were not averaged before plotting. Instead, results of measurements along each gage line were plotted on a separate diagram, a curve drawn through the plotted points, and Poisson's ratio determined for each gage line, as shown in figure 165. The different values of Poisson's ratio obtained for a given axis of the block were then averaged and the average value recorded at the left of the diagrams. Thus figure 165 shows two average values of Poisson's ratio, one for each direction at right angles to the applied load.

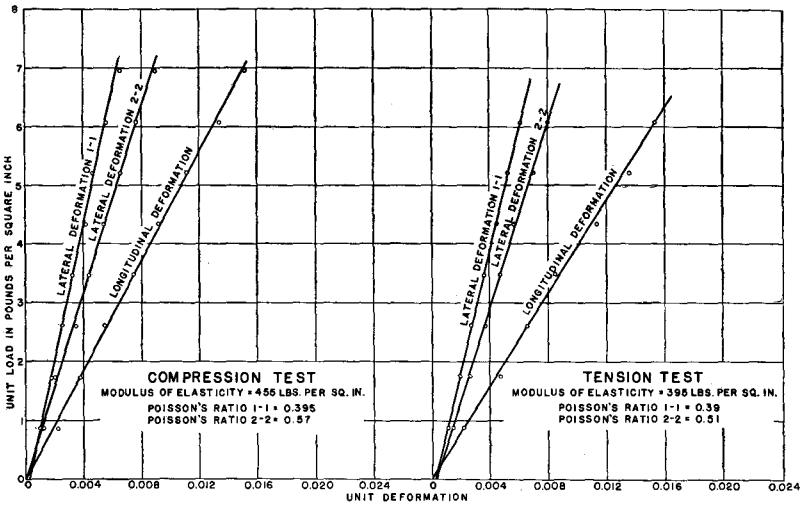

COMPRESSION								TENSION							
TOTAL LOAD	UNIT LOAD	AVER. LONG. DEF.	UNIT LONG. DEF.	AVER. LAT. DEF. 1-1	UNIT LAT. DEF. 1-1	AVER. LAT. DEF. 2-2	UNIT LAT. DEF. 2-2	TOTAL LOAD	UNIT LOAD	AVER. LONG. DEF.	UNIT LONG DEF.	AVER. LAT. DEF. 1-1	UNIT LAT. DEF. 1-1	AVER. LAT. DEF. 2-2	UNIT LAT. DEF. 2-2
0	0	0	0	0	0	0	0	0	0	0	0	0	0	0	0
6	0.87	0.0118	0.0022	0.0030	0.0010	0.0037	0.0012	6	0.87	0.0114	0.0021	0.0030	0.0010	0.0043	0.0014
12	1.74	0.0201	0.0038	0.0055	0.0018	0.0062	0.0020	12	1.74	0.0249	0.0047	0.0060	0.0019	0.0080	0.0026
18	2.61	0.0290	0.0055	0.0080	0.0026	0.0110	0.0035	18	2.61	0.0353	0.0066	0.0083	0.0027	0.0117	0.0037
24	3.48	0.0396	0.0075	0.0102	0.0033	0.0137	0.0044	24	3.48	0.0466	0.0085	0.0113	0.0036	0.0147	0.0047
30	4.35	0.0487	0.0092	0.0132	0.0042	0.0170	0.0054	30	4.35	0.0607	0.0114	0.0140	0.0045	0.0180	0.0057
36	5.22	0.0592	0.0112	0.0147	0.0047	0.0207	0.0066	36	5.22	0.0727	0.0136	0.0167	0.0053	0.0220	0.0070
42	6.09	0.0706	0.0134	0.0175	0.0056	0.0240	0.0077	42	6.09	0.0820	0.0154	0.0190	0.0061	0.0250	0.0080
48	6.96	0.0806	0.0152	0.0207	0.0066	0.0280	0.0090								

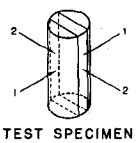

TEST SPECIMEN

FIGURE 175—RESULTS OF TESTS ON SPECIMEN E

If the separate measurements of lateral deformation along each axis of the block had been averaged for each load increment before plotting, the resulting curves would have been smoother than the individual curves shown in the figures. In this case Poisson's ratios, determined from the curves, would have represented average values for the different axes of the block. The latter method was used in computing the elastic constants, based on actual dimensions of the loaded specimens, given in table 6. The values given in table 6 are sometimes slightly different from those shown on the figures, due to the different methods of determination. For example, in figure 165 the modulus of elasticity of specimen A is 410 pounds per square inch and the average values of Poisson's ratio 0.42 and 0.56, whereas in table 6, the corresponding values are 420 pounds per square inch, 0.47 and 0.58, respectively. Although the differences are small, the quantities in table 6 more nearly satisfy the stress-strain equations.

TABLE 5—ELASTIC CONSTANTS BASED ON ORIGINAL DIMENSIONS

Specimen	Direction of Slabs	Test	Modulus of Elasticity Lb. per Sq. In.				Poisson's Ratio					
			E or G	E_x	E_y	E_z	μ_{xy}	μ_{xz}	μ_{yx}	μ_{yz}	μ_{zx}	μ_{zy}
		Compression										
A	Parallel			475	430	395	0.48	0.60	0.43	0.68	0.47	0.57
B	Alternate			430	430	370	0.46	0.65	0.47	0.68	0.55	0.53
C	Random			460	435	390	0.46	0.61	0.42	0.64	0.51	0.58
D	Random					350					0.50	0.50
E	Parallel			455			0.40	0.57				
		Tension										
D	Random					315					0.46	0.46
E	Parallel			395			0.39	0.51				
		Torsion										
D	Random		120									
E	Parallel		135									
		Flexure										
F	Parallel		405									

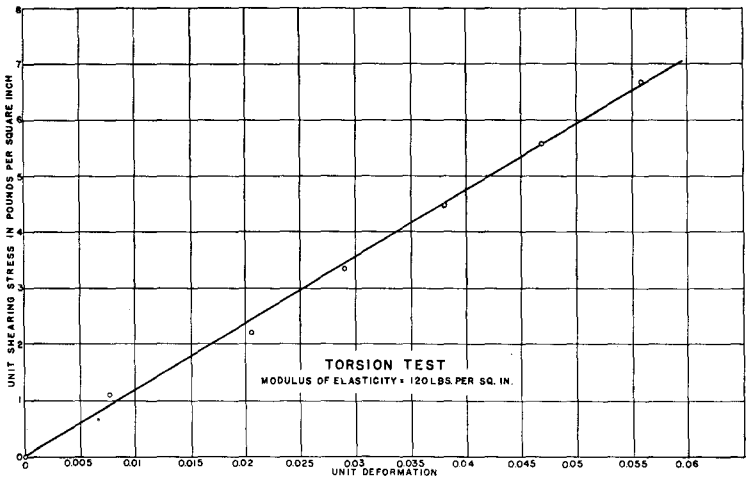

APPLIED LOAD POUNDS	UNIT SHEARING STRESS POUNDS PER SQ. IN.	AVERAGE TOTAL DEF.	AVERAGE UNIT DEF
0	0	0	0
1	1.12	0.16	0.0078
2	2.23	0.43	0.0209
3	3.35	0.58	0.0282
4	4.46	0.80	0.0389
5	5.58	0.98	0.0476
6	6.70	1.17	0.0569

Unit shearing stress $S_s = \frac{Ta}{J} = \frac{12P}{\pi a^3} = 1.116P$

Unit shearing strain $\delta_s = \frac{ae}{RL} = \frac{1.51e}{5.44 \times 5.71} = 0.0486e$

T = Applied torque
P = Applied load
a = Radius of specimen
e = Total observed deflection of troptometer
R = Lever arm of troptometer
L = Gage length of specimen

TEST SPECIMEN

FIGURE 176—TORSION TEST ON SPECIMEN D

TABLE 6—ELASTIC CONSTANTS BASED ON ACTUAL DIMENSIONS

Compression Specimen	Direction of Slabs	Modulus of Elasticity*			Poisson's Ratio					
		E_x	E_y	E_z	μ_{xy}	μ_{xz}	μ_{yx}	μ_{yz}	μ_{zx}	μ_{zy}
A	Parallel	420	355	340	0.47	0.58	0.40	0.62	0.47	0.55
B	Alternate	350	340	320	0.42	0.58	0.41	0.58	0.54	0.54
C	Random	400	375	335	0.42	0.56	0.42	0.58	0.50	0.53

*Pounds per Square Inch.

160. Consistency of Results.—Nine elastic constants were determined in the compression tests of specimens A, B, and C. According to the theory of elasticity, only six are independent. Consequently, there must be three necessary relations between the nine constants. These relations are expressed by equations 44, 45, and 46, and in an alternate form by equation 47.

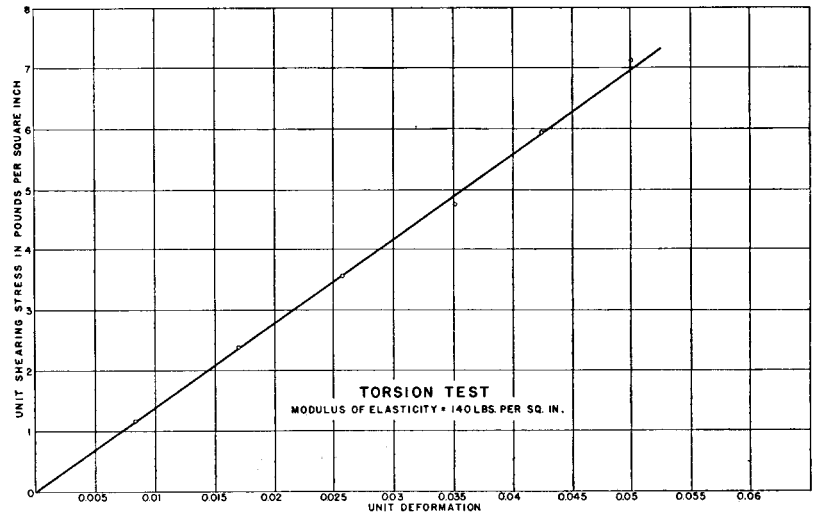

APPLIED LOAD POUNDS	UNIT SHEARING STRESS POUNDS PER SQ. IN.	AVERAGE TOTAL DEF.	AVERAGE UNIT DEF.
0	0	0	0
1	1.185	0.177	0.0084
2	2.370	0.360	0.0171
3	3.555	0.540	0.0257
4	4.740	0.737	0.0351
5	5.925	0.893	0.0425
6	7.11	1.053	0.0501

NOTES

Unit shearing stress $S_s = \frac{Ta}{J} = \frac{12P}{\pi a^3} = 1.185P$

Unit shearing strain $\delta_s = \frac{ae}{RL} = \frac{1.48e}{5.38 \times 5.78} = 0.0476e$

T = Applied torque
P = Applied load
a = Radius of specimen
e = Total observed deflection of troptometer
R = Lever arm of troptometer
L = Gage length of specimen

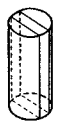

TEST SPECIMEN

FIGURE 177—TORSION TEST ON SPECIMEN E

The exactness with which theoretical relations are satisfied by experimentally determined constants furnishes an indication of the consistency of the experimental work. Results obtained by substi-

TABLE 7—CONSISTENCY OF TEST RESULTS DETERMINED BY EQUATIONS 44 TO 46, INCLUSIVE*

Specimen	Original Dimensions		Actual Dimensions	
	Mean	Maximum	Mean	Maximum
A	6	10	3	8
B	5	10	1	2
C	2	4	5	7

*Tabular quantities are percentages, as explained in the text.

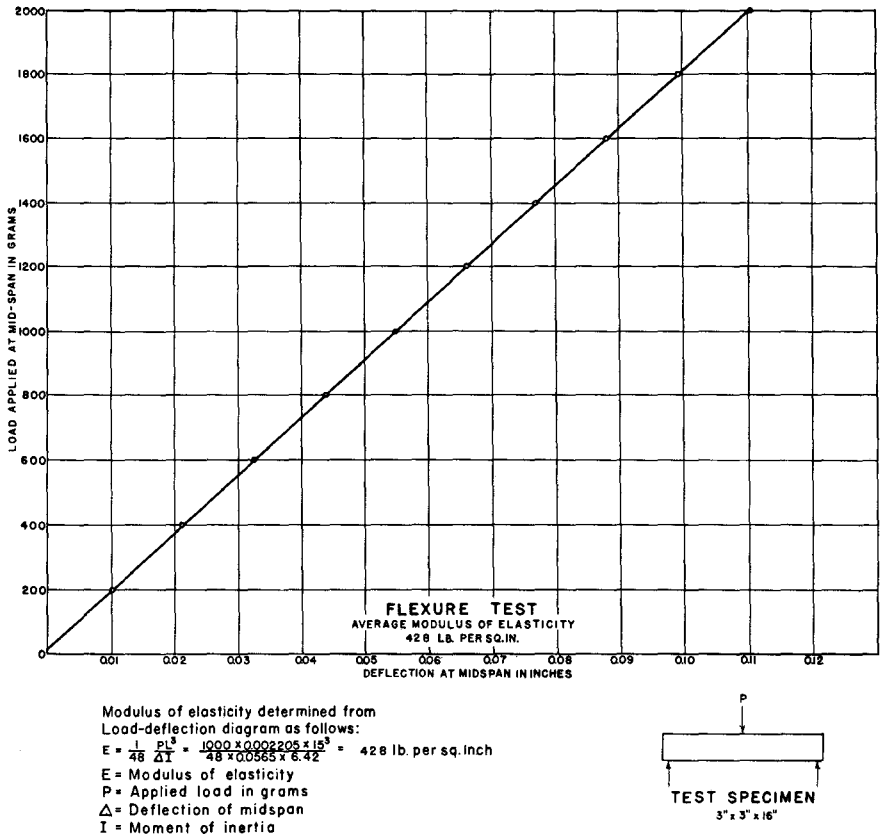

FIGURE 178—FLEXURE TEST ON SPECIMEN F

tuting the values of the elastic constants found for specimens A, B, and C, in the theoretical equations, are summarized in table 7. The amount by which the larger of the two sides of the equation exceeded the smaller was expressed as a percentage of the smaller. Values of maximum and average variations are given in the table for three relations of equations 44 to 46, inclusive. Computations were made for elastic constants based on original dimensions, as given in table 5, and for those based on actual dimensions, as given in table 6.

161. Computed Volume Modulus.—Values of the volume modulus of elasticity, as computed by equation 48, are given in table 8. As explained in section 149, the large negative values are the result of Poisson's ratios slightly larger than 0.50.

TABLE 8—VOLUME MODULUS OF ELASTICITY

Specimen	Original Dimensions	Actual Dimensions
A	−1,890	− 4,170
B	−1,200	− 4,540
C	−1,890	−25,000

162. Discussion of Results.—The determination of the proper value of the modulus of elasticity to use in analyzing test data obtained on the model was complicated by the following causes:

1. There were some variations in the elastic properties of the material due to variations in curing different batches at the manufacturing plant.

2. The modulus of elasticity differed in different directions and there was no way of determining how the transverse axes of the different slabs were oriented in the model.

3. Two sets of values for elastic constants were obtained for specimens A, B, and C, depending on whether original or actual dimensions were used in computing stresses and strains.

The effect of variation in the material was minimized by building up a specimen from sheets selected at random. This was done in the case of specimen C. The uncertainty as to direction of the transverse elastic axes was also taken into account in specimen C, due to the method of assembling the block. Effects of differences in elastic properties along different axes were averaged in specimen B, where horizontal directions of blocks cut from the same slab were alternated in building the specimen. Values of E_x and E_y were the same for specimen B, indicating that the specimen was isotropic in the transverse plane. There was a difference of about six per cent in these values for specimen C. For specimen A, which had the reference axes parallel, E_x, computed on the basis of actual dimensions, was 18 per cent larger than E_y. When average values of E_x and E_y were computed for the three specimens, they were found to be consistent.

Whether elastic constants, computed on the basis of original dimensions or those based on actual dimensions, should be used in analyzing the model is problematical. First of all, it is certain that some error is involved in the determination of at least one set of values, due to the assumption that the stress-strain curve was a

straight line. Since the change from original to actual dimensions involved a correction of the second degree, if one stress-strain curve was a straight line, the other must have had a small curvature.

An isotropic material cannot increase in volume under uniform pressure. Consequently, the maximum value which Poisson's ratio can have for an isotropic material is 0.50. For this condition the volume modulus is infinite. If these restrictions are assumed to hold for the anisotropic rubber-litharge material, they are best satisfied by the values of Poisson's ratio based on actual dimensions. These have an average for the three specimens of 0.510 as compared with an average of 0.544 for the values based on original areas. The values computed for the volume modulus, as given in table 8, also favor the constants based on actual dimensions, since the computed volume modulus more nearly approaches infinity.

Two specimens, D and E, were tested in compression under small values of load, so that the effect of using actual dimensions in determining the elastic constants was small. These tests gave values of moduli slightly larger than the values found for specimens A, B, and C, based on actual dimensions.

The moduli of elasticity in tension for specimens D and E were found to be about 90 per cent of the corresponding compression moduli. If actual dimensions were used in computing values of stress and strain, the tension moduli would be increased and the compression moduli decreased, so that the values would be very nearly equal.

The modulus of elasticity in shear for specimen D, with transverse joints, satisfied very closely the relation of equation 68, namely, that the shear modulus should be one-third of the tension or compression modulus when Poisson's ratio equals 0.50. The modulus of elasticity in flexure is subject to a small correction for the effect of shear stress.

In the analysis of the model, it was important that the ratio of the modulus of elasticity in the vertical or z direction to that in the transverse direction be determined as closely as possible. This ratio was approximately $\frac{7}{8}$, with very little variation in the specimens tested.

163. Conclusions.—In view of the test results and the foregoing discussions, the following values of the elastic moduli are considered

to be the average for the rubber-litharge material used in building the model.

Stress Condition		Modulus of Elasticity, lb. per sq. in.
Tension and compression:	Vertical	343
	Transverse	389
Shear:	Vertical	120

The average value of Poisson's ratio is considered to be 0.50.

THERMAL EXPANSION

164. Specimens and Apparatus.—Determination of the coefficient of thermal expansion was made by using 3 by 4 by 24-inch beams, built up from strips three inches wide, cut from one 24 by 24 by 1-inch slab. The apparatus was the same as that used in determining the coefficient of thermal expansion of soft plaster beams, illustrated in figures 64 and 65. Small steel bearing plates were cemented to the ends of the beam for use in the measurements. Changes in length were measured with two dial gages reading to one ten-thousandth of an inch. The gages were supported by the steel yoke and rested against the steel plates on the ends of the specimen. Changes in length of the specimen were determined by comparing observations made on the specimen with those made on a reference bar kept at constant temperature.

165. Determination of Coefficient.—Two sets of tests were made. In the first set the beam was cooled from an initial temperature of 75 degrees Fahrenheit. In the second set the beam was heated from a temperature of 75 degrees. The rubber-litharge beam was so soft that there was considerable difficulty in placing it in the measuring yoke so that it would be unrestrained. Finally, the beam was placed on a greased plank so that it would be free to expand or contract, and the yoke placed over it.

The results of the tests of thermal expansion showed that the coefficient was not a linear function of temperature. In considering a temperature test of the model, it was evident that the value of the coefficient would depend on the range of temperature change. The initial temperature of the model would probably be the same as the atmospheric temperature in the testing room, which usually was

about 75 degrees. If the model were cooled to 35 degrees, the coefficient of expansion to be used in analyzing the results would be 0.000,065 inches per inch per degree Fahrenheit. If the model were heated to a temperature of 100 degrees, the coefficient of expansion would be 0.000,078 inches per inch per degree Fahrenheit. The temperature tests of the model are described in chapter XII.

CHAPTER IX—CONSTRUCTION OF RUBBER-LITHARGE MODEL

MODEL BASE

166. Reconstruction of Testing Pit.—The rubber-litharge model was constructed in the pit where the previous models had been tested. In order to accommodate the new model, considerable reconstruction was necessary. First the concrete base and abutments for the plaster-celite model were removed. As the height of the new model was greater than the depth of the pit, it was necessary to add heavy concrete curbs along the tops of the sides. Concrete cross-walls, joining the ends of the curbs, completed the model enclosure. The shape of the inside of the pit was determined by the requirements for the rubber supplemental base. The reconstructed testing pit is shown in figure 179.

167. Boundary of Supplemental Base.—Some uncertainties had arisen concerning boundary conditions of the bases of previous models. Methods of analyses have been developed for the deformation of the foundation and abutments of dams, based on the assumption that the rock is homogeneous, isotropic, and infinite in extent. Although such conditions never exist at actual dams, it was considered desirable to make the supplemental base of the rubber-litharge model somewhat thicker than the supplemental base of the plaster-celite model. Consequently, a minimum thickness of two feet was assumed for the supplemental base, with a minimum extension of two feet upstream and downstream from the base of the model. This was twice the minimum thickness used for the plaster-celite model. For the scale selected, the thickness of the supplemental rubber-litharge base was one-half the height of the model. Figure 180 shows the design of the reconstructed testing pit, rubber-litharge model, and supplemental base.

168. Reservoir.—The upstream cross-wall of the testing pit enclosed a space upstream from the dam to provide a reservoir. Drain

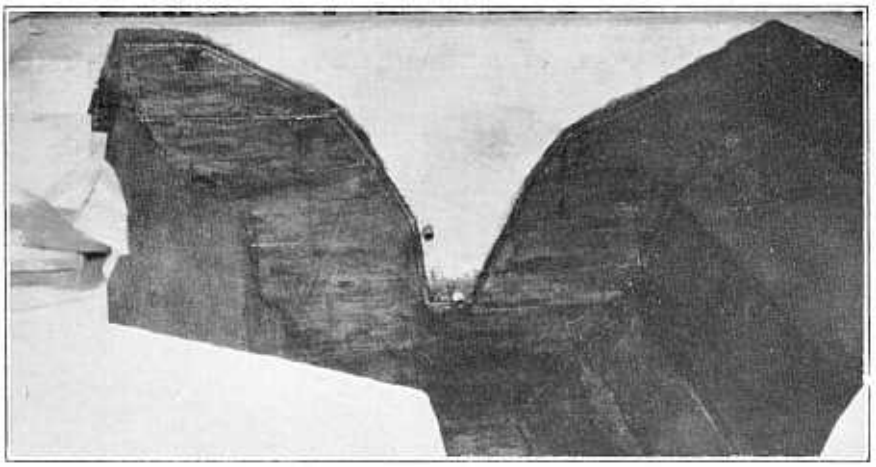

FIGURE 179—RECONSTRUCTED TESTING PIT

and overflow pipes were provided as shown on figure 180, and suitable valves were installed to control the reservoir water surface. A drain pipe was laid in the bottom of the pit to carry discharged water to the sump at the downstream end of the pit. The original sump was enlarged and connected to a larger sump, outside the pit, where a pump was installed for emptying the sump and filling the supply tank. The supply tank, located in the basement adjacent to the testing room, had a capacity of about forty cubic feet. A gas heater was attached to the supply tank, for controlling the temperature of the water. Two 1½-inch diameter pipe lines were laid from the supply tank to the reservoir, so that the reservoir could be quickly filled.

169. Laying Rubber-Litharge Slabs.—The method of building the supplemental base is shown in figure 181. The rubber-litharge slabs were not exactly uniform in thickness. Consequently, considerable fitting was necessary before a layer could be cemented in place. The usual procedure was to fit the slabs for an entire layer before cementing. This included trimming the slabs along the edges of the layer and grinding off excess thickness where necessary. The slabs were cut and trimmed with a band saw. A jet of water was allowed to impinge on the saw blade, just above the rubber, to prevent the blade from binding. The saw was equipped with a device for tilting the table, so that bevel cuts could be made as required. A motor-driven sanding drum was used in grinding the slabs to the proper thickness.

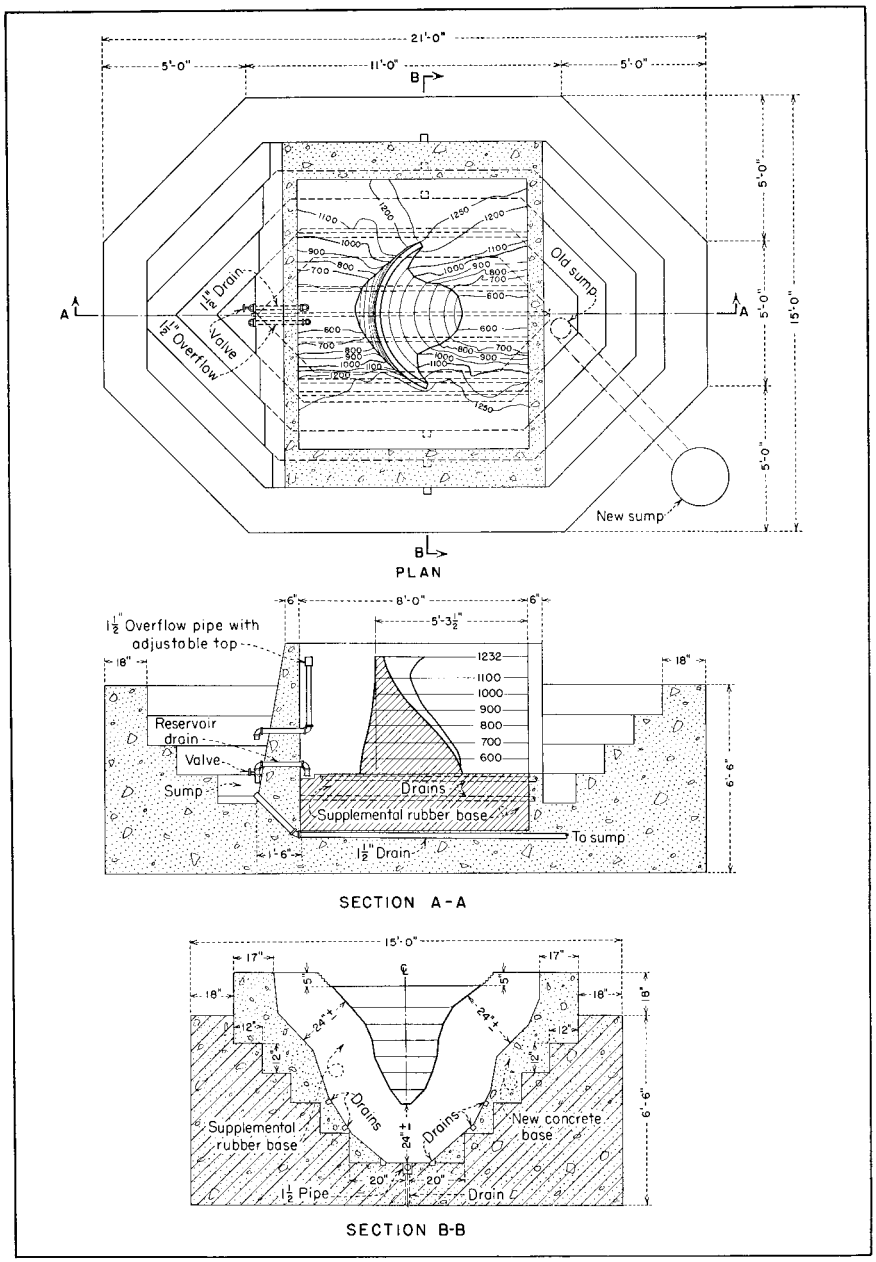

FIGURE 180—TESTING PIT, RUBBER-LITHARGE MODEL, AND SUPPLEMENTAL BASE

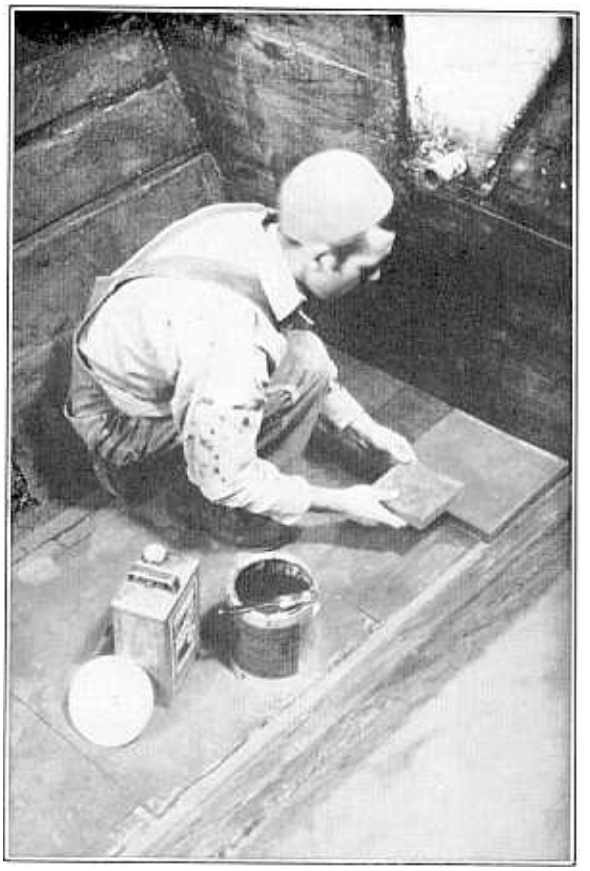

FIGURE 181—CONSTRUCTING THE SUPPLEMENTAL BASE

As soon as the slabs for a layer had been fitted, each was carefully cleaned with benzol. Rubber cement was then applied to the bottom faces and edges of the slabs and the slabs placed in position. The cement caused the slabs to shrink slightly while the cement was wet, but the rubber regained its normal volume as soon as the cement dried. The shrinkage of the slabs caused the vertical joints to open slightly. As soon as the cement was thoroughly dry, the joints were closed by hammering until a tight fit was obtained. The joint between the rubber slabs and the concrete support was filled with quick-setting building plaster to complete the layer. The supplemental base, built to elevation 505, is shown in figure 182.

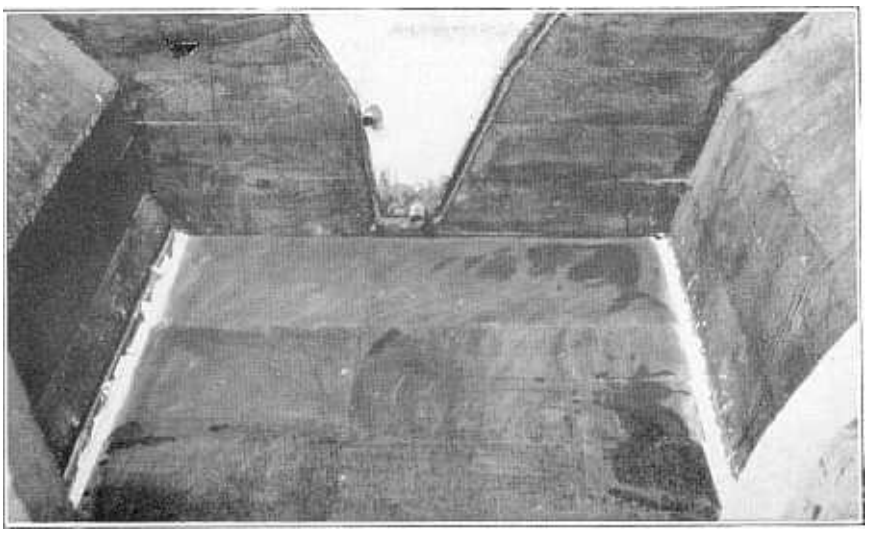

FIGURE 182—SUPPLEMENTAL BASE BUILT TO ELEVATION 505

NSTRUCTION OF MODE

170. Plans for Model.—Plans for the model were made from the design drawings for Boulder Dam, changing all dimensions to conform to the scale of the model. Figure 183 shows the plan of the dam, study 37, and figure 184 shows thicknesses and radii at the crown cantilever, reduced to the scale of the model. Figure 185 shows the abutment excavation lines at the dam.

A contour map of the dam and adjacent canyon, on a scale of 1 to 180, was drawn on wallboard; and lines for the abutment excavation were added by transference from figure 185. The adopted scale of 1 to 180 made one inch on the model correspond to 15 feet on the dam. In constructing the model, slabs having a thickness of one inch were used, so that each layer had a thickness corresponding to 15 feet on the dam. This facilitated the laying out of the patterns for the model and the topography of the canyon. When completed, the top of the model was at elevation 1236 or about one-fourth of an inch higher than the scale requirement.

In placing each layer, the arch element of the model was cut out from patterns and cemented first. The abutments and canyon topography were next placed. This procedure insured a tight fit of the model against the abutments. Any variation in the width of the

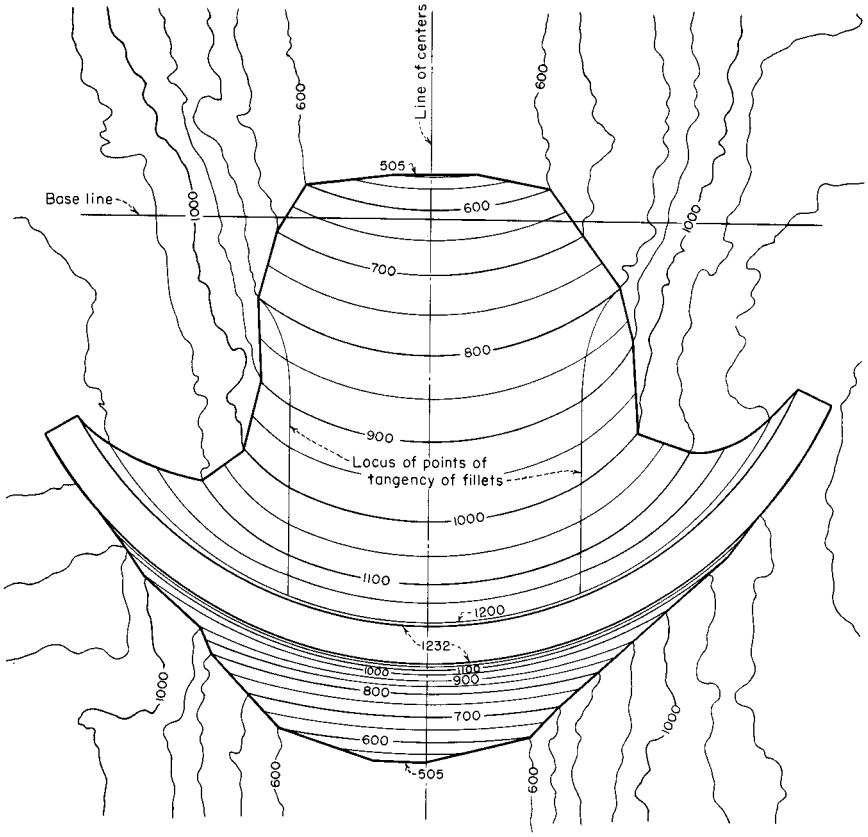

FIGURE 183—PLAN OF BOULDER DAM, STUDY 37

vertical joints was allowed to accumulate at the joint between the rubber and the concrete, and the space filled with quick-setting building plaster, as in the construction of the model base.

171. Installation of Apparatus.—Tests of the plaster-celite model of Boulder Dam had shown that radial deflections were greater at the arch center lines than at the downstream face. In the case of the rubber-litharge model, greater differences were expected, because of the large value of Poisson's ratio. To measure deflections at the arch center lines and at the upstream face, invar steel rods were anchored in the model at elevations 595, 700, and 915, as shown in figure 186. Grooves, with sufficient clearance to prevent binding of the rubber on the deflection rods, were cut in the top of the slabs after placing.

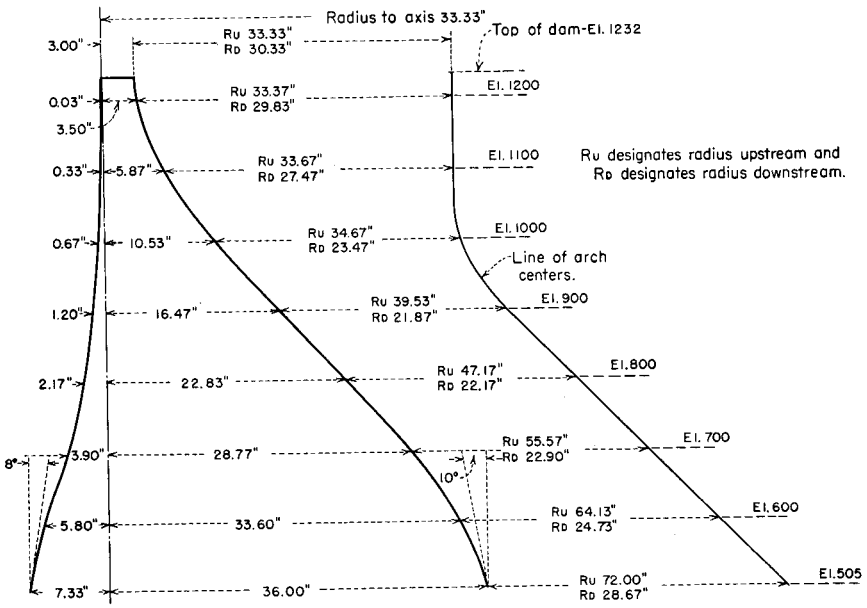

FIGURE 184—DIMENSIONS OF MODEL AT CROWN SECTION

The rods were then inserted, and the grooves filled with cup grease. A piece of thin paper was placed over the slot and the next layer of the model added.

In planning the experimental program, a test to determine the effect of temperature was included. Temperature changes had been satisfactorily determined with thermocouples and a potentiometer in the plaster-celite model tests. As a similar set of measurements was desired for the rubber model, nineteen thermocouples were placed in the model and adjacent foundation. The thermocouples consisted of two wires, one of copper, the other constantan, each about twelve feet long. The ends of each pair were soldered together and one connection was embedded in the model at the point where the temperature measurement was desired. The wires were placed in spaghetti tubing for insulation.

172. **Waterproofing the Upstream Face.**—As soon as the model was completed, the entire upstream face was carefully cleaned and covered with uncured gum rubber to prevent uplift pressure from occurring within the model. This type of rubber had no elastic properties, so the action of the model was not affected by the waterproof

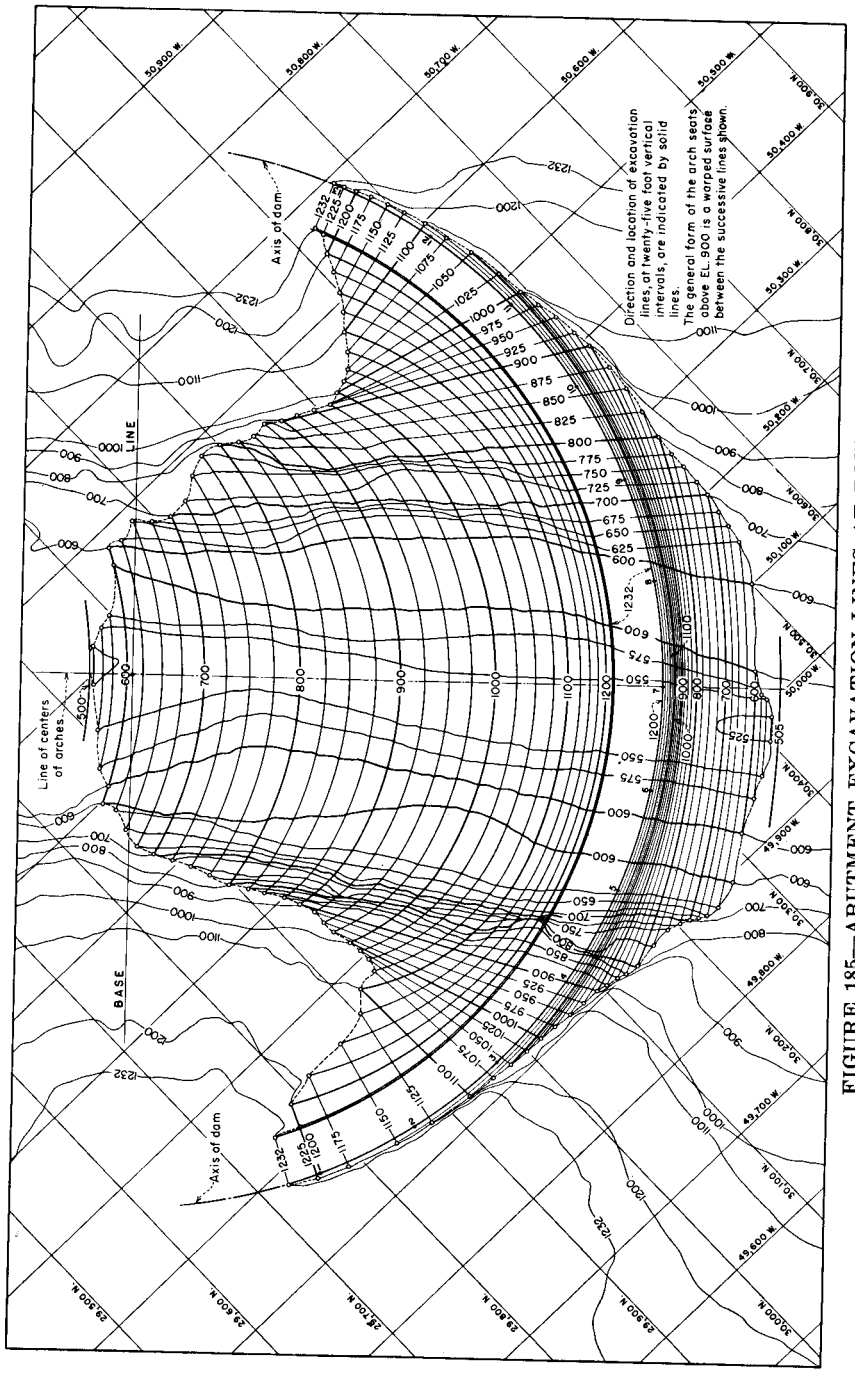

FIGURE 185—ABUTMENT EXCAVATION LINES AT BOULDER DAM

FIGURE 186—MODEL AND CANYON BUILT TO ELEVATION 595
Rods in Place for Measuring Downstream Movement of Upstream Face and Center Line

membrane. The edges of the gum rubber sheet were sealed with asphaltic putty at the junction of the upstream face and the abutments. Figure 187 shows the completed rubber-litharge model.

Tests of the reservoir upon completion of the model revealed a few small leaks through the abutments. These were sealed by painting the entire reservoir with several coats of rubber cement. The junction of the supplemental base and the concrete was sealed with a strip of inner tube rubber, which was caulked into a groove in the concrete wall and cemented to the rubber base. All seams and joints that might possibly leak were coated with asphaltic putty.

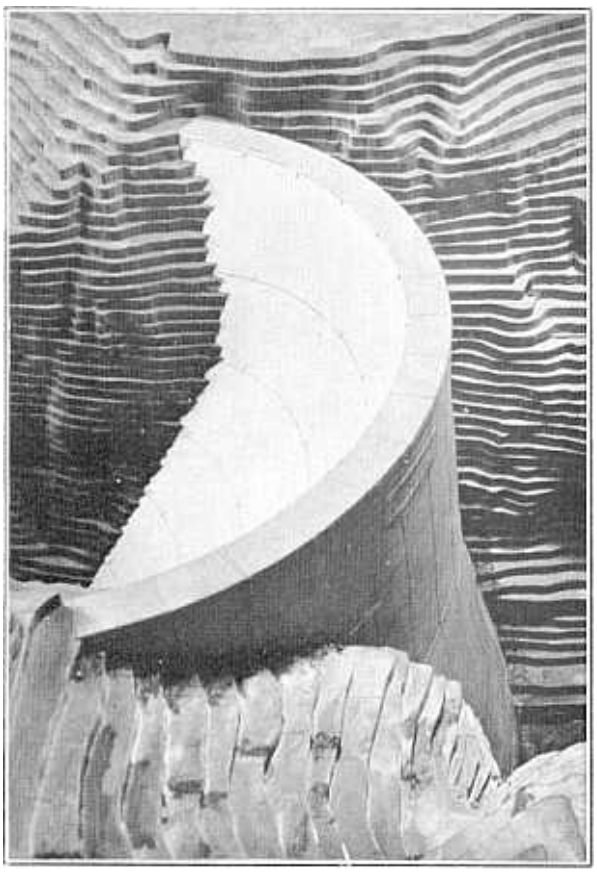

FIGURE 187—THE COMPLETED RUBBER-LITHARGE MODEL

173. **Reference Structure.**—After completing the model, the structure shown in figure 188 was constructed for reference use during the progress of the testing work. Since temperature changes in the reference piers and steel instrument stands of other models had introduced small errors, an effort was made to reduce such errors by using laminated wood construction. The reference structure consisted of two parts, a beam fifteen feet long by twelve inches square and a laminated wood instrument stand. The beam was built of 2 by 12-inch planks which had been thoroughly seasoned. The planks were bolted together and fastened to the curb which supported the supplemental base, as shown in figure 188. The detachable reference pier, for supporting instruments, was made of 1 by 8-inch planks, glued and bolted together. This stand was used to support micrometers, gages, and other apparatus used in measuring deflections.

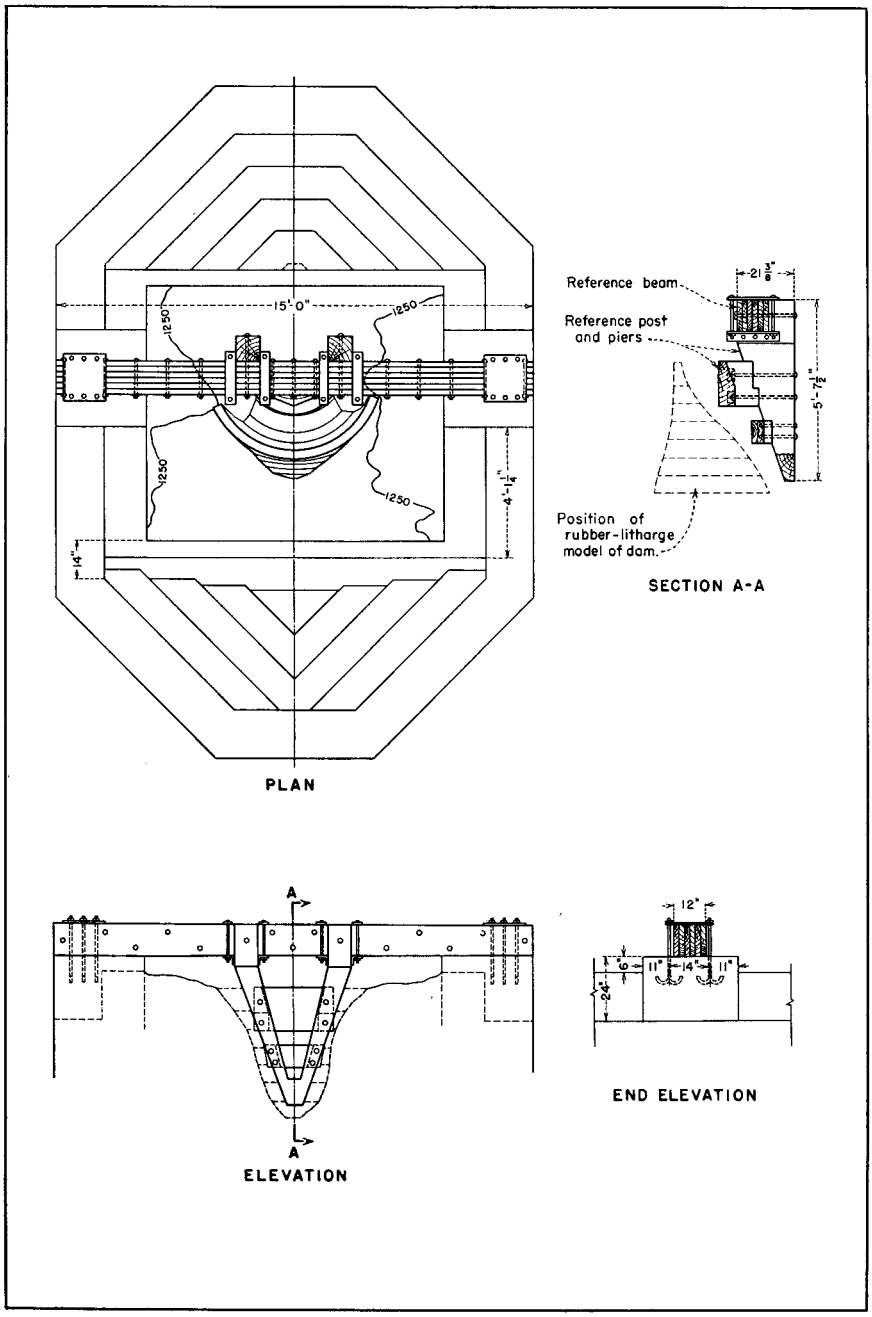

FIGURE 188—REFERENCE STRUCTURE FOR DEFLECTION MEASUREMENTS

CHAPTER X—DEFLECTION MEASUREMENTS

RADIAL DEFLECTION TESTS

174. Apparatus.—The general layout of apparatus for measuring radial deflections was similar to that used in the plaster-celite model tests. Inserts were set in the downstream face for measuring deflections of cantilever and arch elements at the locations shown in figure 189. Inserts consisted of specially made aluminum tacks with spherical heads which were forced into the rubber at the points of measurement. Invar steel rods were fastened to the laminated wood reference pier and alined so that dial gages could be mounted in directions radial to the axis of the model. Gages were set to bear against the inserts in the downstream face.

Owing to the low modulus of elasticity of the rubber-litharge material, this model was more flexible than any model previously tested. Radial deflections were much greater than the range of available dial gages which measured to one ten-thousandth of an inch. It was therefore necessary to procure additional dial gages which had a range of 0.25 inches and measured to one-thousandth of an inch.

Figure 190 shows a typical arrangement of gages for radial deflection measurements. The top row of gages are set to measure deflections at the downstream face. The two pairs of gages at the center and lower part of the model are set to measure radial movements of the rods anchored at the center line and at the upstream face. As there were not sufficient gages available to measure deflections at all inserts at one time, it was necessary to make a large number of tests to complete the deflection measurements.

175. Test Procedure.—The method of making radial deflection tests was as follows. Initial readings of the gages were made with the reservoir empty. Temperatures of the air, model, and reservoir water were also noted. As the coefficient of linear expansion of the rubber-litharge material was rather high, about ten times that of concrete, an effort was made to have the three temperatures the same. The temperature of the water in the supply tank was regulated by

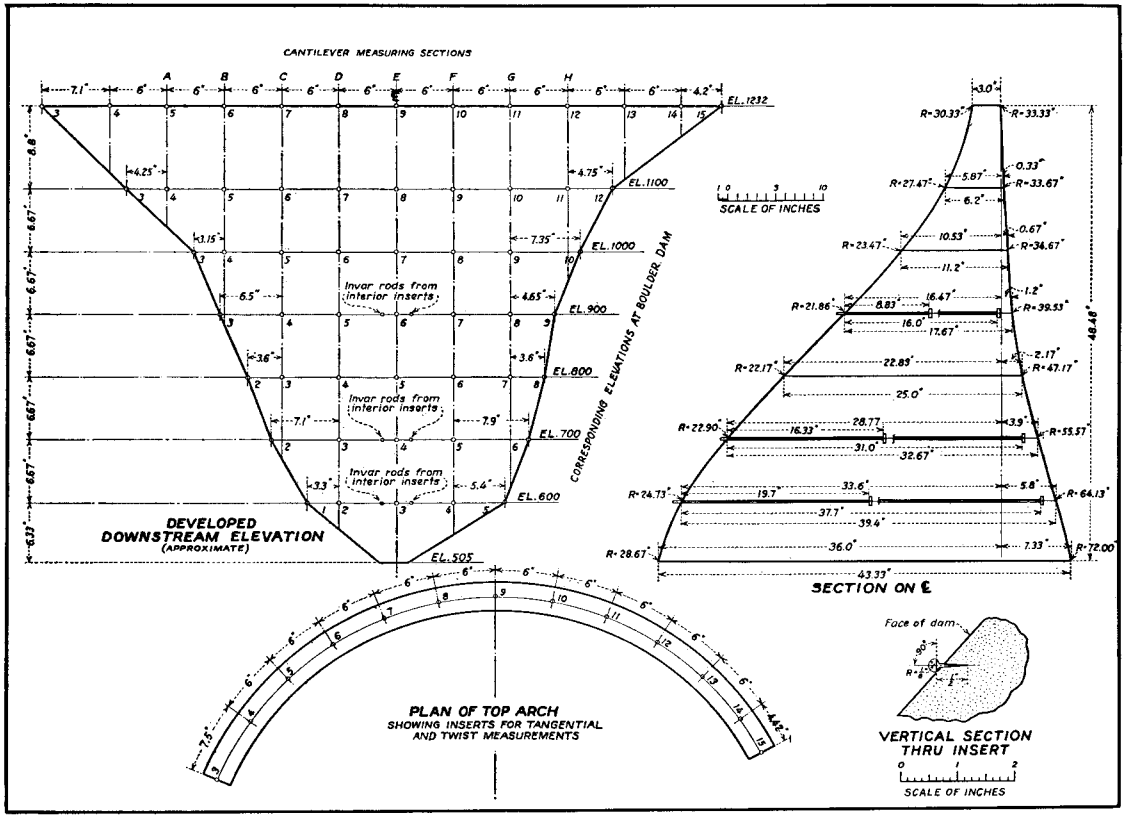

FIGURE 189—INSERTS FOR DEFLECTION MEASUREMENTS

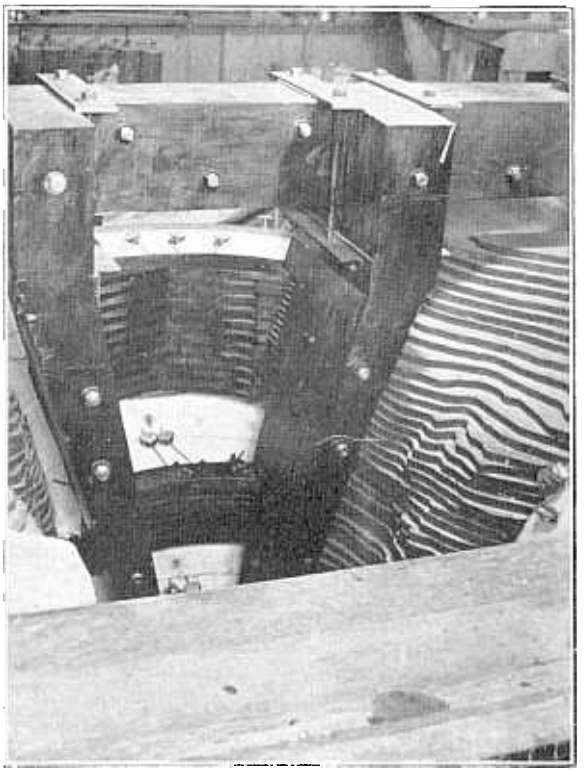

FIGURE 190—TYPICAL ARRANGEMENT OF GAGES FOR RADIAL DEFLECTION MEASUREMENTS

using a gas water heater attached to the tank, or by adding cold water from the city supply. Water was allowed to flow by gravity from the supply tank to the reservoir. It required about twenty minutes to fill the reservoir to elevation 1232. Hook gages were used to determine the water surface elevation. Gages at the downstream face of the model were read and the reservoir allowed to drain. The water drained into a sump and was then pumped back into the supply tank. Thirty to forty-five minutes were usually allowed for the model to return to its initial position.

Deflection measurements were made for full load and for a range of partial loads. For partial loads, observations were made with the reservoir surface at elevations 900, 950, 1000, 1050, 1100, 1150, and 1200.

176. Full Load Deflections.—Results of radial deflection tests made with the reservoir surface at elevation 1232 are shown in figures 191 and 192. In general, the deflection curves were similar to those obtained in the tests of the plaster-celite model. As shown in figure 191, the arch element at elevation 1232 deflected upstream at the abutments about the same as in the plaster-celite model. The maximum upstream deflection of 0.006 inches occurred at the Nevada abutment. The maximum downstream deflection of 0.166 inches occurred at the crown of the top arch. At elevation 1100 the deflection of the arch at the Arizona abutment was greater than at the Nevada abutment. Deflections were 0.015 inches and zero at these respective locations. A similar condition existed at elevation 1000 where the deflection was 0.022 inches at the Arizona abutment, and 0.011 inches at the Nevada abutment. This lack of symmetry in deflections at the abutments was also found in the tests of the plaster-celite model.

Between elevations 900 and 600, appreciable deflections occurred at both abutments. As the arch elements were relatively thick in this part of the model, the opportunity for bending was small. Deflections at the abutments were primarily due to shear. Owing to the greater depth and extent of the foundation, abutment deflections were relatively larger than in the tests of the plaster-celite model. In the lower elevations of the model, the deflections at the abutments were large in proportion to the deflections at the crown section. At elevation 700, the deflection was 0.024 inches at the abutments and 0.039 inches at the crown. Deflections at elevation 600 were 0.024 inches, 0.028 inches, and 0.020 inches at the Arizona abutment, crown, and Nevada abutment, respectively.

Radial deflections of cantilever elements are shown in figure 192. As in the case of the arch abutments, there was considerable deflection at the foundations of the cantilever sections. Due to the flexibility of the rubber-litharge material, the restraining effect of negative loads on the cantilevers, caused by the upper arches, was not pronounced.

177. Squeezing of Model.—Considerable differences between the deflections of the upstream and downstream faces of the model were noted. The rods for measuring deflections at the upstream face and at the arch center lines were located as closely as possible to cantilever section E. The results of these measurements for the full water load are shown on the deflection curve for cantilever E in figure 192. The deflection of the model at elevation 600 at the upstream

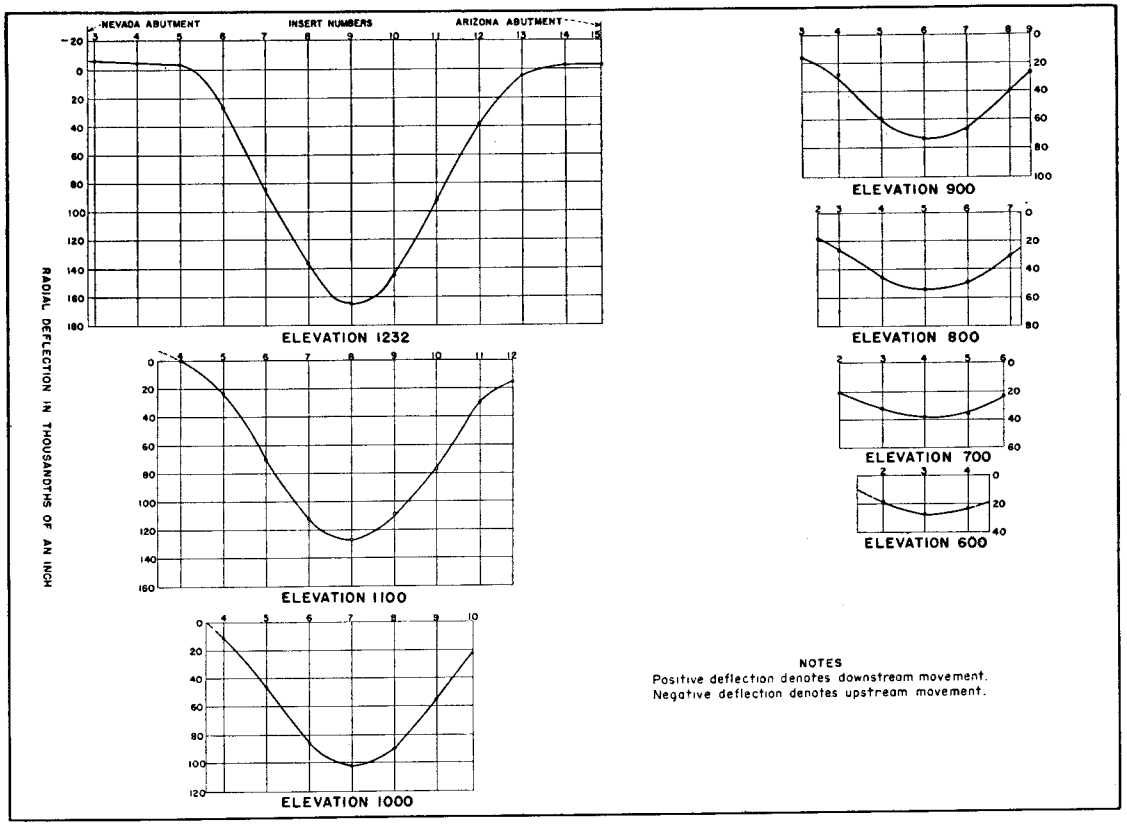

FIGURE 191—RADIAL DEFLECTIONS OF ARCH ELEMENTS, LOAD AT ELEVATION 1232

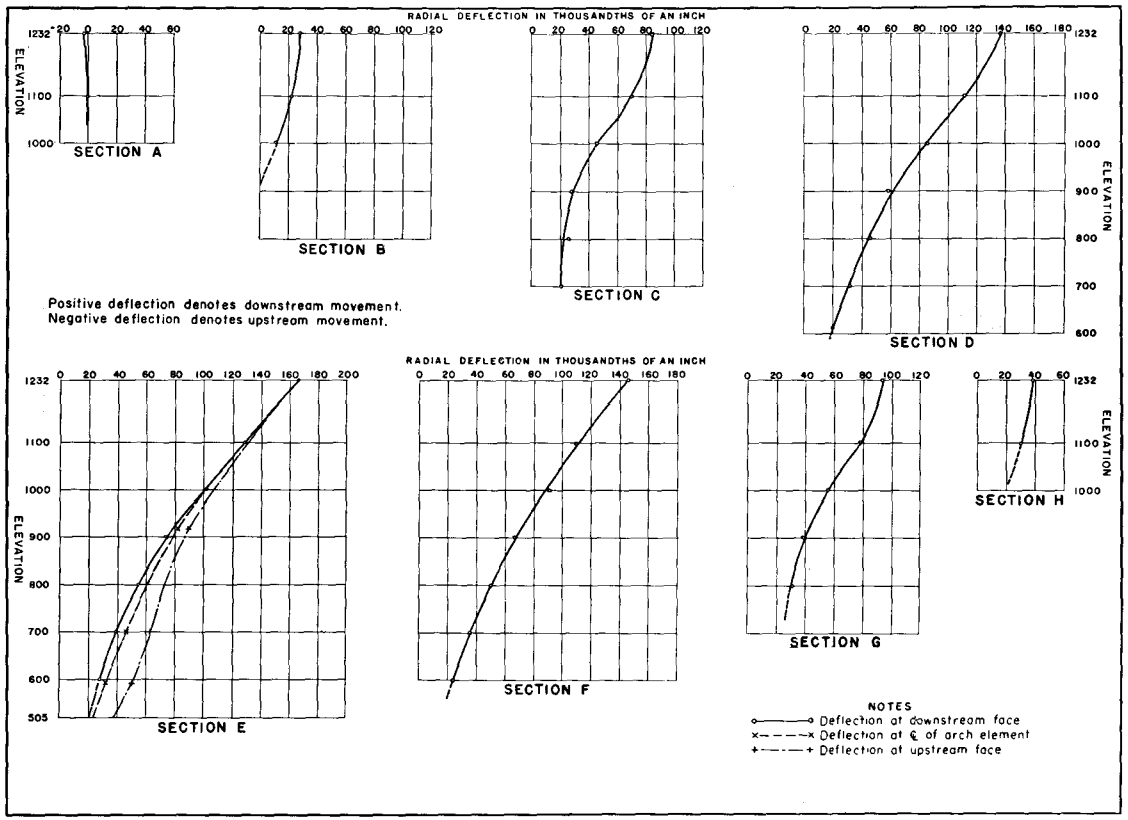

FIGURE 192—RADIAL DEFLECTIONS OF CANTILEVER ELEMENTS, LOAD AT ELEVATION 1232

face was about twice the deflection at the downstream face. At the higher elevations the differences were smaller. Differences between deflections at the arch center lines and the downstream face were relatively small, indicating that most of the squeezing of the model occurred between the upstream face and the arch center lines.

178. Partial Load Deflections.—Radial deflection measurements were made for partial load conditions with the reservoir water surface varying at 50-foot increments between elevations 900 and 1200. Results of partial load tests were very similar to those obtained in the tests of the plaster-celite model. When the reservoir water surface was above elevation 1100, the maximum deflection occurred at elevation 1232. With the reservoir water surface at elevation 1100 or lower, the maximum deflection occurred below the top of the model, indicating the presence of vertical tensile strains at the downstream face. Table 9 gives deflection data for loads at elevations 1232, 1100, and 1000.

179. Consistency of Repeated Tests.—The radial deflection tests showed that the model was highly elastic if load was applied for short intervals of time. Variations between repeated tests, performed under the same conditions, were always small. Table 10 contains measured deflections of cantilever section E, obtained in several different tests. The tabulations show that the observations agreed very closely. Recovery after unloading was very consistent if a sufficient interval of time was allowed in each test. The small discrepancies which sometimes occurred were usually traceable to a change in temperature, insufficient time for recovery, or some local cause such as a gage sticking or working loose on its support.

The model flowed appreciably under sustained loads. As flow was not desired in deflection tests, the reservoir was filled as rapidly as possible and the measurements made before appreciable flow occurred. Zero readings of the gages could be recorded, the model loaded, and load deflections measured in about half an hour. Draining the reservoir required only ten or fifteen minutes, so that the entire test could be completed in less than an hour.

TANGENTIAL DEFLECTION TESTS

180. Installation of Micrometers.—For measuring tangential deflections of the model, it was planned to use dial gages, mounted on

TABLE 9—RADIAL DEFLECTIONS FOR FULL AND PARTIAL LOADS

Elev.	Insert No.	Deflections, Reservoir Water Surface Elevation 1232	1100	1000
1232	3	−6	−4	−2
	4	−5	−3	−2
	5	−3	−6	−3
	6	28	0	−1
	7	85	14	3
	8	137	30	9
	9	166	38	12
	10	146	31	9
	11	93	16	5
	12	39	3	1
	13	5	−3	−2
	14	−3	−4	−2
	15	−3	−2	0
1100	4	0	−1	−1
	5	22	6	3
	6	70	21	7
	7	112	36	12
	8	128	42	15
	9	109	36	12
	10	77	23	7
	11	30	7	2
	12	15	3	−1
1000	4	11	4	2
	5	46	20	9
	6	86	38	17
	7	103	45	21
	8	91	42	19
	9	56	24	11
	10	22	10	2
900	3	16	7	4
	4	28	15	8
	5	59	30	16
	6	74	39	21
	7	67	35	19
	8	39	20	11
	9	27	12	5

Elev.	Insert No.	Deflections, Reservoir Water Surface Elevation 1232	1100	1000
800	2	18	10	6
	3	26	16	9
	4	46	25	17
	5	55	33	20
	6	50	29	17
	7	31	18	10
700	2	21	14	9
	3	32	20	12
	4	39	23	14
	5	36	22	14
	6	24	15	9
600	2	20	14	8
	3	28	19	12
	4	24	16	11

Deflections at Interior Points

Upstream Face

El.	915	90	47	24
El.	700	64	43	30
El.	595	50	37	28

Arch Center Line

El.	915	82	42	22
El.	700	47	31	21
El.	595	32	22	16

NOTES

The unit of measurement is 0.001 of an inch.
Positive values denote downstream deflection.
Negative values denote upstream deflection.
For location of inserts, see figure 189.

invar rods, similar to those used for measuring radial deflections. Some difficulty was encountered in mounting the gages so that local strains would not occur around the inserts. By using micrometer screws which measured to 0.001 of an inch this difficulty was avoided. As the available micrometers were of much lighter weight than the gages and contained no springs to actuate their movement, they

TABLE 10—RADIAL DEFLECTIONS OF CANTILEVER SECTION E
(Thousandths of an Inch)

Elevation	Test Number and Date						
	98 4-28-33	99 4-28-33	100 4-28-33	123 4-28-33	124 5-4-33	125 5-4-33	996 10-7-33
1232	166	166	166	166	167	169	163
1100	127	129	128	129	129	130	126
1000	102	102	101	101	101	102	.....
900	75	75	75	74	73	74	76
800	55	55	56	55	55	55	54
700	39	38	38	38	38	38	40
608	28	28	28	28	28	28	29

proved very satisfactory. The general arrangement of apparatus is shown in figure 193.

The micrometers were mounted in a tangential direction on invar steel rods. Brass pins, having polished pointed heads, were bent to an L shape and forced into the rubber at points where measurements were desired. The micrometers were adjusted to bear against the pointed heads of the pins. Contact was determined by a 2-volt electric circuit which caused a flashlight bulb to glow. This system was very satisfactory, as repeated readings checked within 0.001 of an inch. The micrometers were mounted about one-half inch from the downstream face of the model; so it was necessary to apply small corrections to the observed readings to obtain deflections at the face of the model.

181. Procedure.—The method of testing was similar to that used in making radial deflection tests. Zero readings were made with the reservoir empty. The reservoir was filled and readings made for the loaded condition. The reservoir was then emptied and a period of about thirty minutes allowed for recovery. Usually the micrometers were set to measure the tangential deflection of one arch element at a time, so that the test could be completed before appreciable flow occurred in the model.

FIGURE 193 APPARA 'S FOR MEASURING 'ANGENTIAL DEFLECTIONS AT ELEVATION 1 2

182. Full Load Deflections.—Tangential deflection measurements, made with the reservoir water surface at elevation 1232, are shown in figure 194. The symmetry of the deflection curves obtained at the different elevations was remarkable. The line of zero deflection coincided with cantilever section E, except at elevations 1232 and 800. At elevation 1232, the point of zero deflection was about three-fourths of an inch toward the Nevada abutment from section E, and at elevation 800, it was about one inch toward the Arizona abutment from section E. Tangential deflection curves reached their maximum values near the quarter points of the arch elements, except below elevation 800 where arch elements were relatively thick. Below elevation 800, maximum tangential deflections occurred at the abutments.

'he argest angential deflection, 0.057 inches, occurred at ele

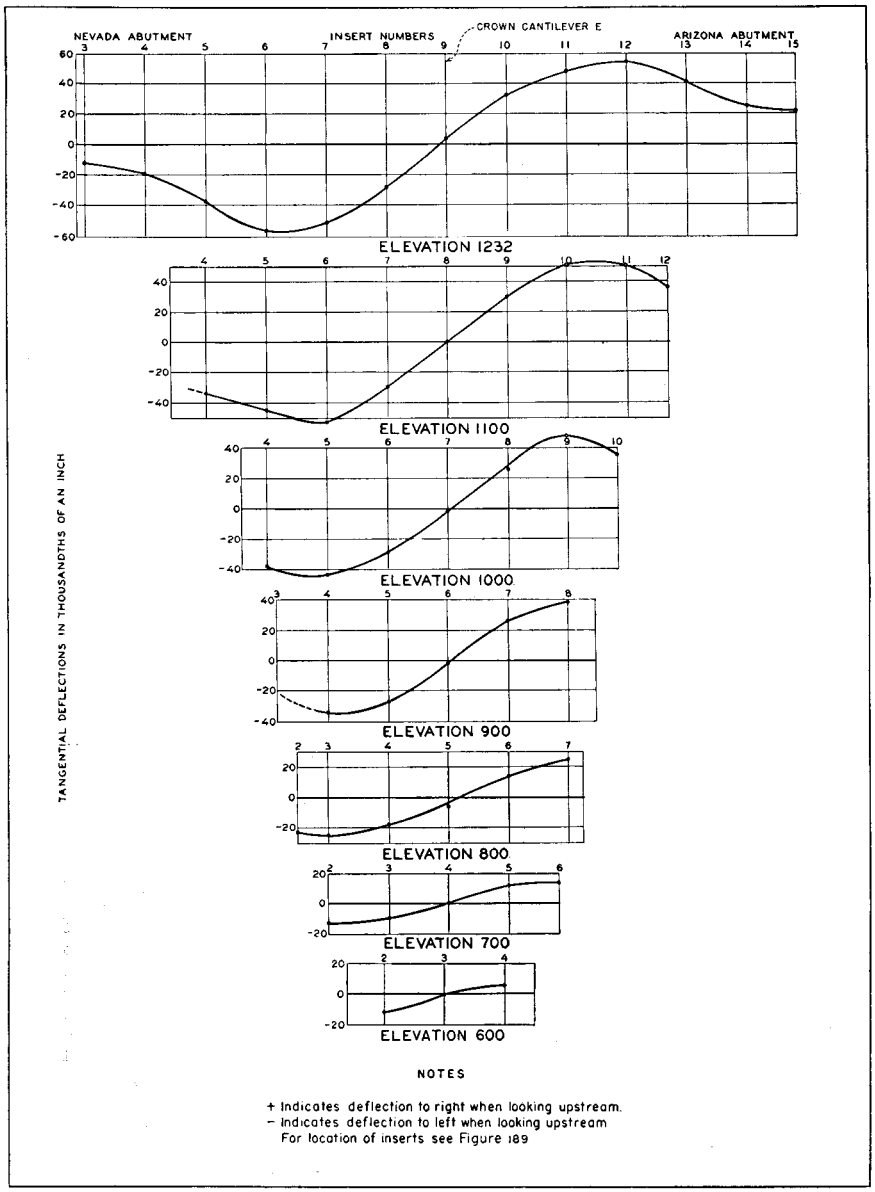

FIGURE 194—TANGENTIAL DEFLECTIONS OF ARCH ELEMENTS, LOAD AT ELEVATION 1232

vation 1232, insert 6, on the Nevada side of the model. The corresponding deflection at the same elevation on the Arizona side, insert 12, was 0.054 inches. At elevation 1100 the maximum deflections were slightly smaller, being 0.053 inches on the Nevada side and 0.052 inches on the Arizona side.

183. Partial Load Deflections.—In general, partial load deflection curves were similar to those shown for full loads, except that the tangential movements were smaller. With the reservoir water surface at elevation 1000 or lower, most of the tangential movement occurred below elevation 1000. Tangential deflections in the upper part of the model were practically negligible. Data from observations of tangential deflections during full and partial loads are given in table 11.

TABLE 11—TANGENTIAL DEFLECTIONS FOR FULL AND PARTIAL LOADS

Elev.	Insert No.	Deflections, Reservoir Water Surface Elevation		
		1232	1100	1000
1232	3	−12	− 6	− 2
	4	−19	− 6	− 3
	5	−37	− 9	− 3
	6	−57	−16	− 5
	7	−52	−15	− 5
	8	−28	−10	− 3
	9	3	0	0
	10	32	9	2
	11	47	14	6
	12	54	15	5
	13	40	11	4
	14	25	8	4
	15	22	7	3
1100	4	−34	−13	− 5
	5	−45	−16	− 5
	6	−53	−20	− 7
	7	−30	−10	− 3
	8	0	1	0
	9	29	11	4
	10	51	19	6
	11	50	19	6
	12	36	12	7
1000	4	−38	−16	− 8
	5	−44	−18	− 7
	6	−30	−13	− 5
	7	− 2	− 1	− 1
	8	27	12	6
	9	48	22	10
	10	35	16	7
900	4	−34	−20	−12
	5	−28	−11	− 7
	6	− 2	0	0
	7	27	12	6
	8	39	21	11
800	2	−22	−12	− 7
	3	−25	−15	− 9
	4	−18	−11	− 6
	5	− 5	− 2	− 2
	6	14	8	5
	7	25	15	8
700	2	−13	−11	− 5
	3	−10	− 6	− 3
	4	0	1	0
	5	12	11	5
	6	14	9	5
600	2	−12	− 7	− 4
	3	− 1	2	− 1
	4	5	4	3

The unit of measurement is 0.001 of an inch.

Positive values indicate deflection to right when looking upstream.

Negative values indicate deflection to left when looking upstream.

For location of inserts, see figure 189.

SLOPE DEFLECTION TESTS

184. Apparatus.—Since slope deflections of the arch elements were relatively small, a precise system of measuring angular changes in the order of one one-hundred-thousandth of a radian was necessary. The optical lever system, developed for the plaster-celite model tests, was used for the slope deflection measurements on the rubber-litharge model, see section 91.

Small optical flats, one and one-half inches in diameter, were used as mirrors for the optical lever system. These were much lighter in weight than those previously used. They were mounted in an aluminum frame with trunnions supported by an adjustable yoke. The yoke was attached to the rubber with small wood screws which were coated with rubber cement before placing. With this system of support, an optical flat could be set in any desired direction. In order to obtain sufficient length of radius for the optical lever system, transits were mounted on concrete pedestals outside the building, in line with a window and the model.

185. Procedure.—In making observations for slope deflections, the transit and mirror were set so that the telescope could be focused on the reflection of the scale in the mirror. The scale reading was noted by the observer and the reservoir filled to the desired elevation. As the model deflected under load, the optical flat rotated slightly, due to the angular or twist deflection. This rotation could be noted by the change of the scale reading. The amount of rotation could then be computed after correcting for the radial and tangential deflection of the model at the insert at which the mirror was mounted. Since it was not possible to move the transit during an observation, two instruments were used in this series of tests. Measurements were made at the 48 inserts shown in figure 189. In filling the reservoir, the water surface was held at four different elevations long enough to make an observation at each elevation. The reservoir was then lowered to the same elevations and check readings made.

186. Full Load Deflections.—Slope deflections measured with the reservoir water surface at elevation 1232 are shown in figure 195. With the exception of the slight irregularity at the Nevada abutment, elevation 900, the curves were symmetrical about cantilever section E. Maximum deflections of 0.0089 radians occurred at stations 7 and 11 at the top of the model. Slope deflections were materially smaller

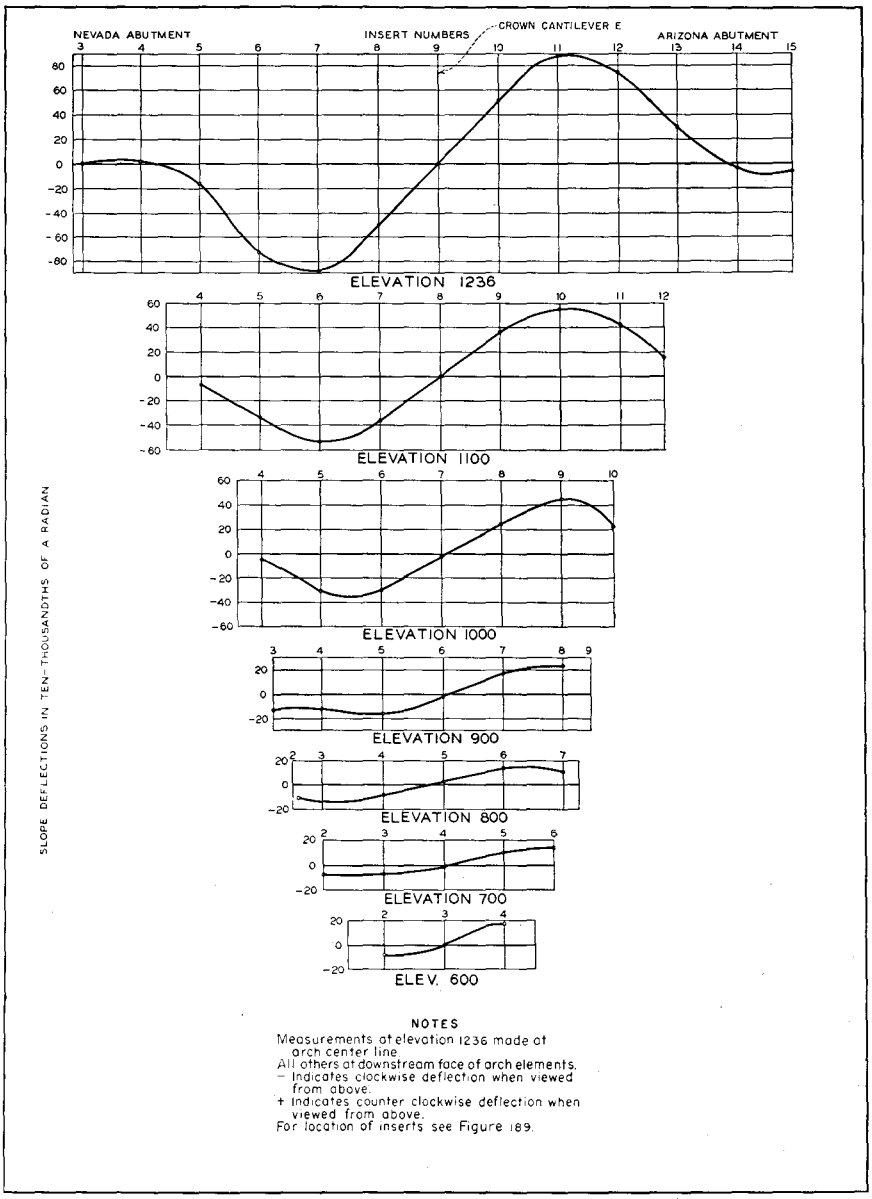

FIGURE 195—SLOPE DEFLECTIONS OF ARCH ELEMENTS, LOAD AT ELEVATION 1232

at the lower elevations where the arch lengths were shorter and the thicknesses greater.

The slope deflection curves were consistent with the radial deflection curves shown in figure 191. The radial deflection was upstream at both abutments at elevation 1232. The slope changed from counterclockwise at the Nevada abutment, when viewed from above, to clockwise as the radial deflection changed to downstream in the Nevada half of the arch. At the Arizona abutment the slope was clockwise at the end of the model where the deflection was upstream. As the radial deflection became downstream the direction of the slope changed. The maximum radial deflection of the arch at elevation 1232 occurred at insert 9. At this point the slope of the neutral axis of the model was zero, and the measured slope deflection was zero.

187. Partial Load Deflections.—Measurements of slope deflections during partial loads were made with the reservoir water surface varying at 50-foot intervals from elevation 900 to elevation 1200. The deflection curves were similar to those shown for the full load tests, except that the movements were smaller. Table 12 gives slope deflections measured at the different inserts during tests with the reservoir water surface at elevations 1000, 1100, and 1232.

VERTICAL DEFLECTION TESTS

188. Effect of Squeezing.—In making deflection measurements at cantilever sections, it was noticed that considerable vertical movement occurred at both upstream and downstream faces of the model. The vertical movement was the result of squeezing that took place in the model when water load was applied. The horizontal radial deflection of the upstream face was greater than that of the downstream face; and, since it is difficult to compress compounds of soft rubber, due to their high Poisson's ratio, the model deflected in the direction of least restraint when the reservoir was filled. The result was that vertical deflections were observed at both faces of the model. Tests were next made in which vertical deflections of the model were measured.

189. Apparatus.—Invar steel rods were attached to the upstream face along horizontal arch elements below the top of the model, and were alined so that vertical deflections were registered on dial gages reading to 0.001 of an inch. Micrometers were mounted in vertical

TABLE 12—SLOPE DEFLECTIONS FOR FULL AND PARTIAL LOADS

Elevation	Insert No.	Angle of Deflection in Radians — Reservoir Water Surface Elevation 1232	1100	1000
1236	3	0.000109	0.000016	−0.000021
	4	0.000333	0.000313	0.000090
	5	−0.001823	−0.000025	−0.000041
	6	−0.007195	−0.001662	−0.000527
	7	−0.008926	−0.002602	−0.000747
	8	−0.005023	−0.001840	−0.000596
	9	0.000031	−0.000103	−0.000051
	10	0.005363	0.001675	0.000502
	11	0.008886	0.002609	0.000852
	12	0.007578	0.001767	0.000529
	13	0.002903	0.000364	0.000145
	14	−0.000373	−0.000184	−0.000092
	15	−0.000694	−0.000288	−0.000114
1100	4	−0.000709	−0.000355	−0.000179
	5	−0.003275	−0.001245	−0.000442
	6	−0.005528	−0.002213	−0.000771
	7	−0.003673	−0.001637	−0.000613
	8	−0.000317	−0.000313	−0.000130
	9	0.003657	0.001457	0.000573
	10	0.005614	0.002178	0.000786
	11	0.004247	0.001450	0.000519
	12	0.001571	0.000683	0.000311
1000	4	−0.000387	−0.000302	−0.000205
	5	−0.002997	−0.001554	−0.000779
	6	−0.002989	−0.001519	−0.000723
	7	−0.000130	−0.000311	−0.000207
	8	0.002294	0.001134	0.000567
	9	0.004568	0.002021	0.000931
	10	0.002321	0.001190	0.000525
900	3	−0.001161	−0.000810	−0.000540
	4	−0.001188	−0.000870	−0.000606
	5	−0.001587	−0.001064	−0.000686
	6	−0.000428	−0.000136	−0.000055
	7	0.001682	0.000926	0.000531
	8	0.002496	0.001625	0.000991
800	3	−0.000968	−0.000708	−0.000512
	4	−0.000847	−0.000614	−0.000450
	5	0.000279	0.000094	0.000019
	6	0.001402	0.000898	0.000618
	7	0.001116	0.000926	0.000677
700	2	−0.000699	−0.000577	−0.000465
	3	−0.000717	−0.000573	−0.000401
	4	−0.000142	−0.000116	−0.000056
	5	0.000961	0.000670	0.000452
	6	0.001410	0.000977	0.000722
600	2	−0.000762	−0.000560	−0.000413
	3	−0.000146	−0.000037	−0.000002
	4	0.001725	0.001141	0.000744

All measurements made at downstream face of arch element except at El. 1236 where measurements were made along center line of arch element.

Positive values indicate counterclockwise deflection when viewed from above.

Negative values indicate clockwise deflection when viewed from above.

directions at the downstream edges of the arch elements and at the top arch at the upstream face. The arrangement of apparatus for measuring vertical deflections at the top arch is shown in figure 196. Contacts of the micrometers were determined by an electric circuit, as in preceding tests. Dial gages were installed for measuring vertical deflections at the crown cantilever, as shown in figure 197.

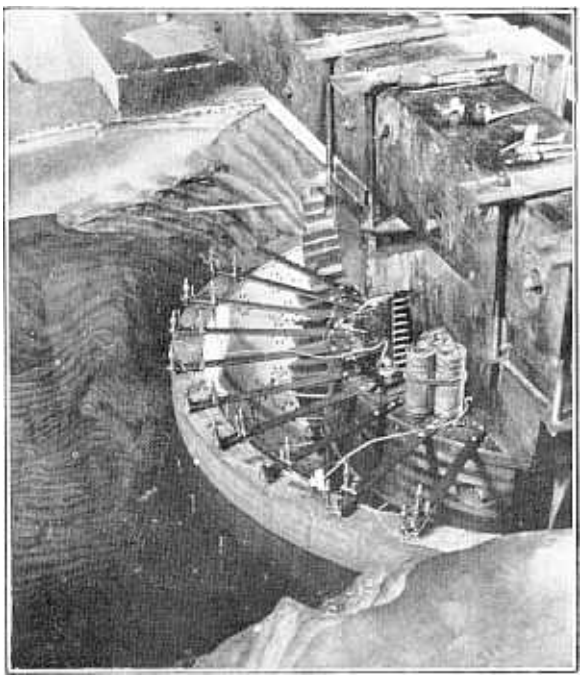

FIGURE 196—MICROMETERS FOR MEASURING VERTICAL DEFLECTIONS OF TOP ARCH

190. Results.—Vertical deflections of the arch elements during full load are shown in figure 198. A comparison of full load and partial load deflections is given in table 13. Vertical deflections of arch elements were consistent with horizontal radial deflections. In the central portion of the model, where the radial deflection was downstream, bending in the cantilever section caused the upstream edge of the model to deflect higher than the downstream edge. At the abutments of the upper part of the model, where the radial deflection was upstream, bending of the cantilever elements caused the downstream edge of the model to deflect higher than the upstream edge.

During full load tests, vertical deflections at the top of the model

were about 40 per cent of the horizontal radial deflections at the upstream side and about 25 per cent of the radial deflections at the downstream side. For partial reservoir loads, ratios of vertical deflections to horizontal radial deflections were slightly higher. Such conditions appear to be abnormal and probably occur only in models made of soft materials having a high Poisson's ratio.

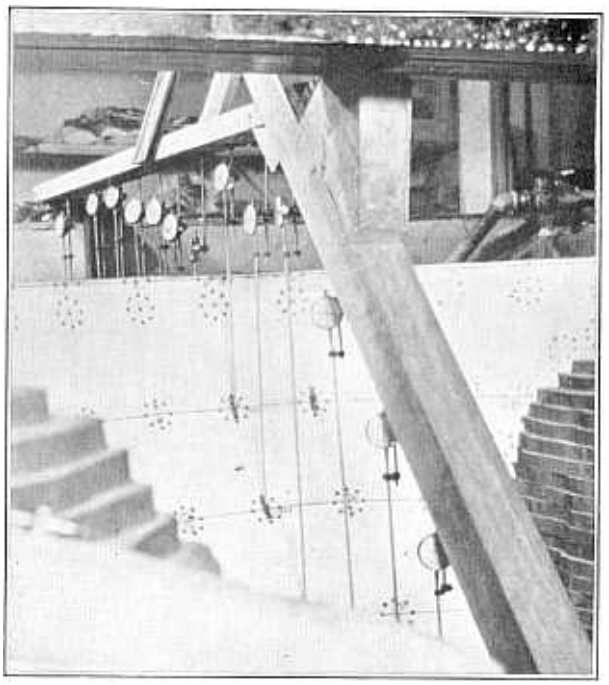

FIGURE 197—DIAL GAGES FOR MEASURING VERTICAL DEFLECTIONS AT THE CROWN CANTILEVER

Figure 199 shows results of vertical deflection measurements at the crown cantilever, also results of horizontal and normal deflection measurements at the same section, measured movements being plotted on an exaggerated scale in all cases. The deflection diagrams show the effect of squeezing between the upstream and downstream faces of the model. Downstream movements were greater at the upstream face than at the downstream face. The greatest vertical movement occurred at the upstream edge of the top of the section. The vertical deflection measurements showed a slight rising of the supplemental base downstream from the model, and a relatively greater lowering

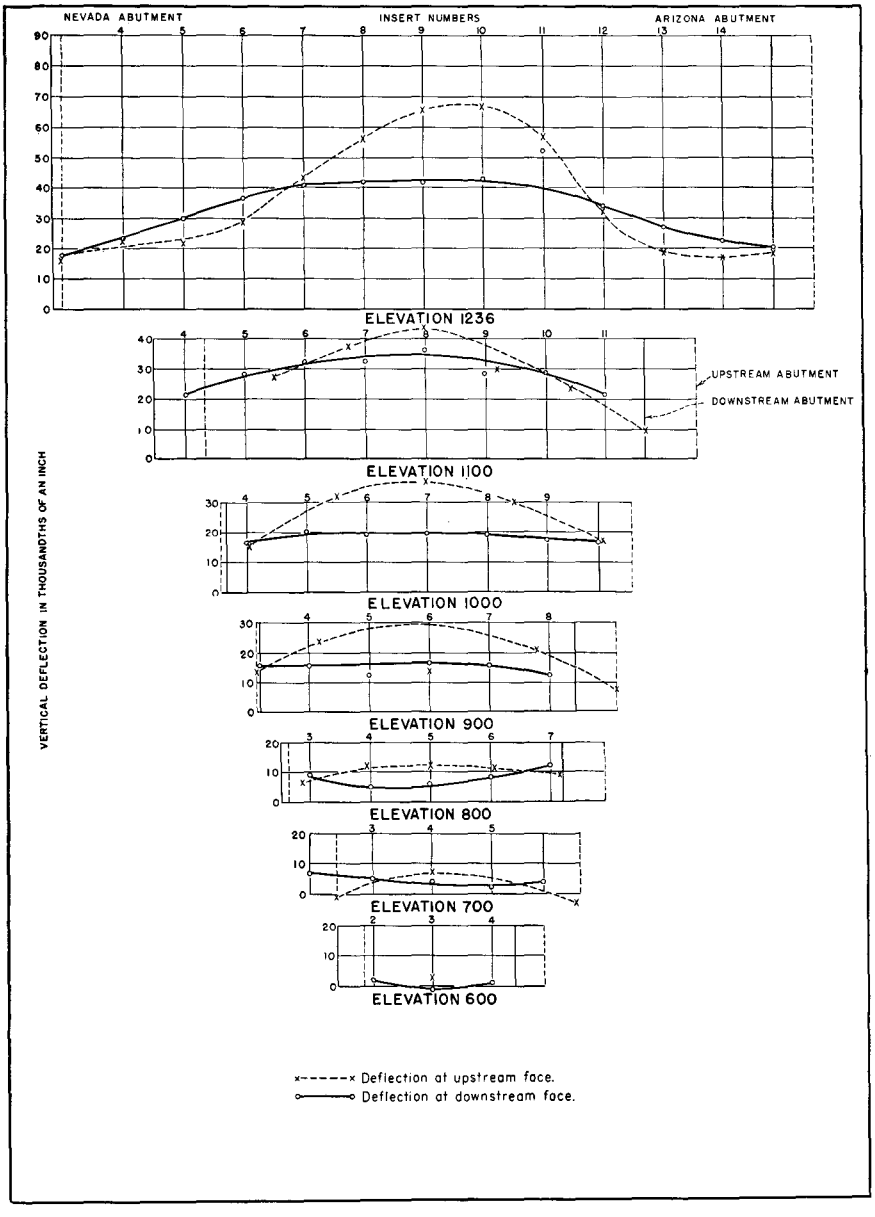

FIGURE 198—VERTICAL DEFLECTIONS OF ARCH ELEMENTS, LOAD AT ELEVATION 1232

TABLE 13—VERTICAL DEFLECTIONS OF ARCH ELEMENTS
(In Thousandths of an Inch)

Elevation	Insert No.	Reservoir Water Surface Elevation					
		1232		1100		1000	
		U.S.*	D.S.*	U.S.	D.S.	U.S.	D.S.
1236	3	18	18	9	10	5	5
	4	21	24	10	12	7	7
	5	23	30	11	14	7	8
	6	29	37	13	16	7	9
	7	43	41	16	17	7	9
	8	56	42	19	17	8	8
	9	66	43	21	17	8	8
	10	67	42	20	17	8	8
	11	47	40	15	17	7	9
	12	32	34	12	15	7	9
	13	20	27	11	13	6	8
	14	19	23	11	13	7	7
	15	18	20	11	12	7	7
1100	4	....	21	....	14	....	8
	5	....	27	....	17	....	8
	6	31	31	11	19	6	9
	7	39	34	13	19	6	10
	8	43	35	14	18	6	10
	9	37	33	12	18	5	9
	10	28	28	10	17	4	9
	11	18	21	8	15	4	8
1000	4	15	17	7	14	4	9
	5	27	19	10	15	5	13
	6	35	20	12	17	5	14
	7	36	20	13	17	6	15
	8	33	19	12	16	6	14
	9	25	18	10	14	5	12
	10	18	17	8	12	5	9
900	A**	13	15	7	11	4	8
	4	22	15	8	12	3	10
	5	27	16	9	14	2	11
	6	29	16	9	14	1	12
	7	25	15	8	13	1	11
	8	18	12	6	12	2	9
	A**	7	....	4	....	3	....
800	3	7	9	2	8	1	7
	4	11	5	4	10	0	7
	5	12	5	5	11	0	7
	6	11	8	4	10	0	7
	7	9	12	2	9	1	9
700	A**	−1	7	−4	7	−4	4
	3	4	5	−1	6	−2	6
	4	7	3	1	6	−1	6
	5	5	3	0	5	−1	6
	6	−3	4	−1	4	−2	5
600	2	....	2	....	3	....	3
	3	3	−1	4	2	3	2
	4	....	1	....	3	....	2

*U.S. indicates Upstream face. D.S. indicates Downstream face.
**A indicates Abutment.
For location of inserts, see figure 189.

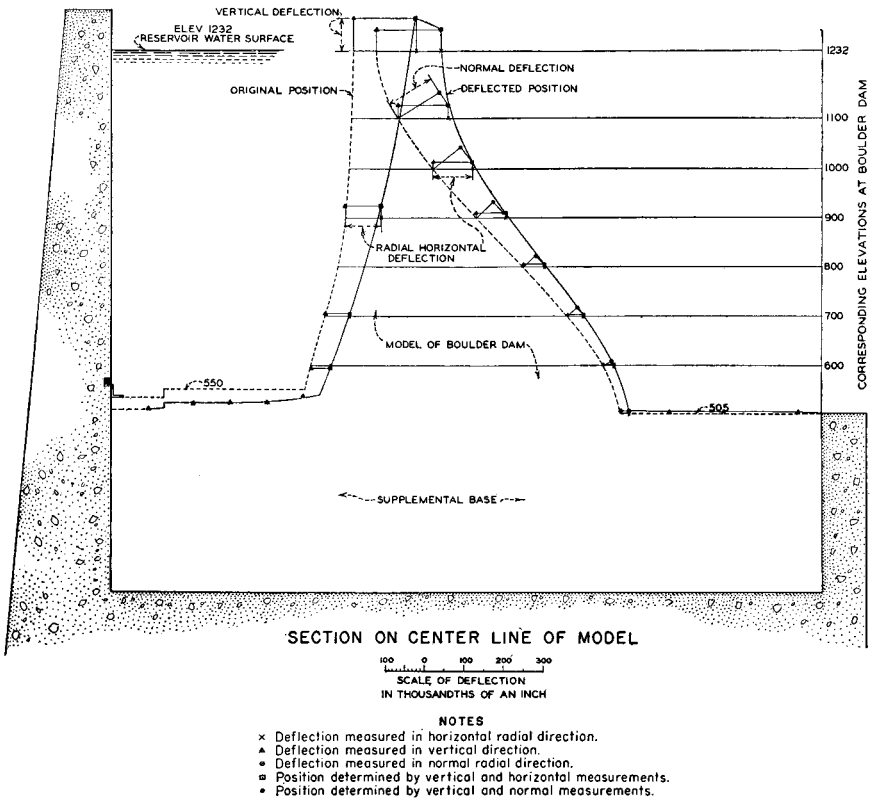

FIGURE 199—RESULTANT DEFLECTION OF CROWN CANTILEVER

of the supplemental base upstream from the model. The latter deformation was caused by the reservoir weight.

CANYON MOVEMENTS

191. Downstream Movements.—Horizontal deflection rods were attached at the junction of the downstream face with the canyon walls. The rods were set parallel to the line of arch centers, so that downstream movements of the canyon could be measured. A typical arrangement of the apparatus is shown in figure 200. Gages were mounted on the concrete curb at the downstream end of the test pit. Observations were made with the reservoir water surface at elevation 1232 and at vertical intervals of 50 feet between elevations 900 and 1200. Results of the measurements are shown in figure 201.

With the reservoir water surface at elevation 1232, the maximum movement on the Arizona side occurred at elevation 1100 and amounted to 0.0340 inches. At elevation 900 the movement was slightly smaller, being 0.0334 inches. On the Nevada side the maximum movement occurred at elevation 900 and amounted to 0.0245 inches. At elevation 1100 the deflection corresponding to the maximum on the Arizona side was only 0.0200 inches.

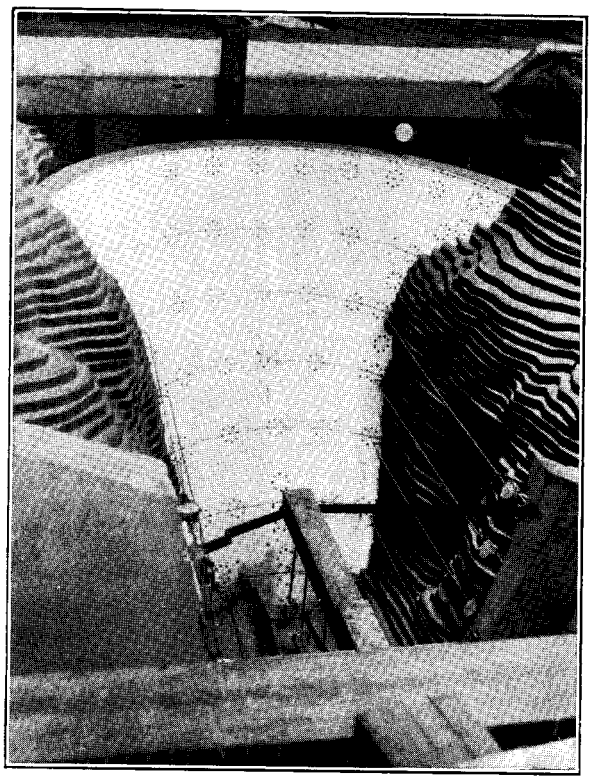

FIGURE 200—MEASUREMENT OF DOWNSTREAM MOVEMENTS AT ABUTMENTS

Maximum movements when the reservoir was partially full occurred at lower elevations than for full load conditions. Magnitudes of the deflections are shown in the table in figure 201. When the reservoir water surface was at elevations 950 and 900, deflections were very small.

The data in figure 201 show that full load deflections on the Arizona side of the canyon were about one-third larger than on the

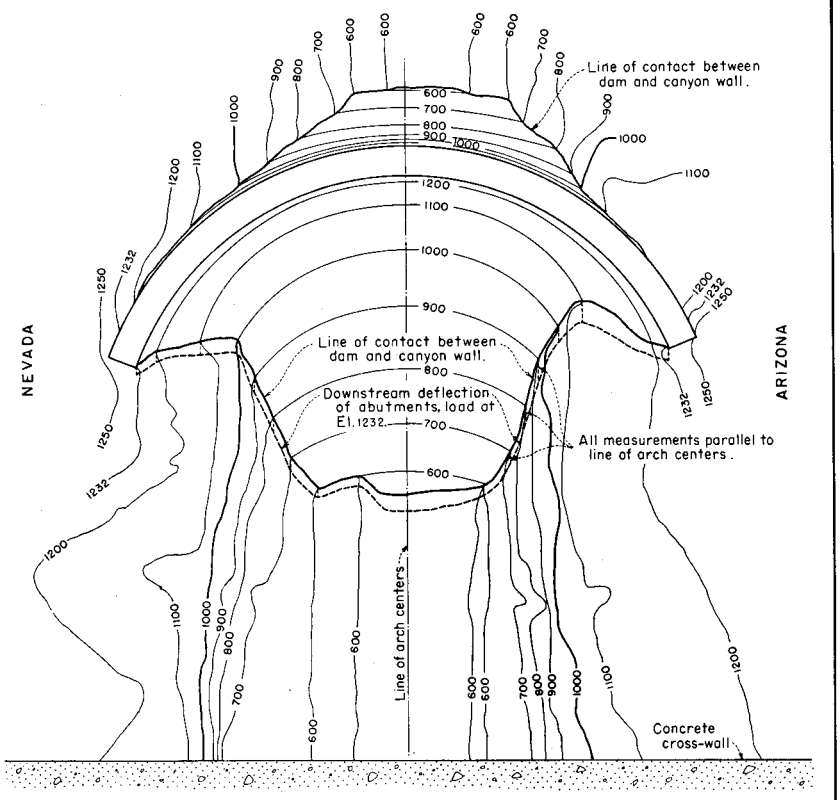

NEVADA ABUTMENT

ELEV. OF POINT OF MEASUREMENT	ELEVATION OF RESERVOIR WATER SURFACE					
	1232	1200	1150	1100	1050	1000
	DEFLECTIONS					
1232	100	90	60	40	30	20
1100	200	170	120	80	60	50
1000	206	177	128	97	72	50
900	245	217	170	135	98	71
800	232	205	167	135	103	80
700	221	192	163	135	106	83
600	131	122	92	69	70	72

ARIZONA ABUTMENT

ELEV. OF POINT OF MEASUREMENT	ELEVATION OF RESERVOIR WATER SURFACE					
	1232	1200	1150	1100	1050	1000
	DEFLECTIONS					
1232	180	130	90	60	40	20
1100	340	270	180	120	70	50
1000	254	290	210	148	101	67
900	334	284	222	165	124	90
800	253	221	180	142	119	90
715	200	171	148	118	92	70
600	150	140	121	90	80	63

Deflections in ten-thousandths of an inch.

FIGURE 201—DOWNSTREAM MOVEMENTS AT ABUTMENTS

Nevada side. The differences between the movements on the two sides of the canyon decreased with the lowering of the reservoir water surface. The lack of symmetry of the measurements was consistent with the radial deflection measurements which showed larger deflections on the Arizona side of the canyon. The difference was largely due to the lack of symmetry in the structure, the upstream portions of the arch elements being longer on the Arizona side.

192. Spreading of Reservoir Walls. — Measurements of the spreading of the reservoir walls were difficult, since it was necessary to make all observations under water. A vertical post was placed between the concrete cross-wall and the 12 by 12-inch beam which supported the reference pier. The post was located at the intersection of the line of centers and the upstream gage line, as shown in figure 202. Horizontal measurements of the movement of each canyon wall with reference to the vertical post were made at elevations 600, 800, and 1000. As in other deflection tests, dial gages and invar rods were used for the measurements. It was necessary, however, to pro-

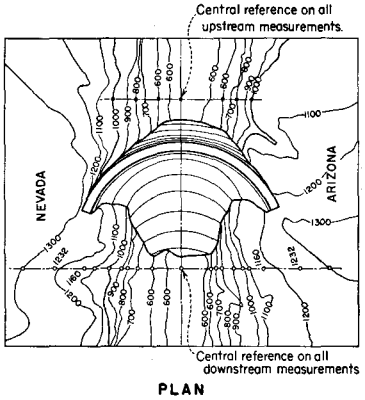

PLAN

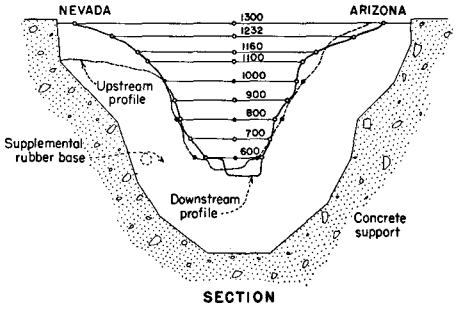

SECTION

NOTES

o——o Position of measurement at downstream canyon walls.

•——• Position of measurement at upstream canyon walls.

The unit of measurement is 0.0001 of an inch.

In the table of deflections, positive values indicate lengthening between measuring points, and negative values indicate shortening between measuring points.

A possible error of approximately 10 percent may have been introduced due to submerging the gages.

TABLE OF DEFLECTIONS

DOWNSTREAM CANYON WALLS

WATER SURFACE ELEVATION	ARIZONA GAGE LOCATIONS									NEVADA GAGE LOCATIONS								
	1300	1232	1160	1100	1000	900	800	700	600	1300	1232	1160	1100	1000	900	800	700	600
900	6	10	5	6	3	0	1	3	3	2	6	9	11	7	7	2	1	4
950	12	18	13	8	7	1	6	6	5	4	11	11	8	7	1	1	0	-6
1000	13	20	13	11	7	2	3	7	8	4	15	15	15	9	7	-2	-4	8
1050	19	26	23	16	8	1	0	5	6	6	20	20	18	7	1	-4	-7	0
1100	23	30	24	20	10	1	-2	4	6	6	25	25	24	9	0	-4	-11	-2
1150	32	40	33	24	8	-2	-7	4	5	9	31	23	27	8	-2	-5	-11	-7
1200	43	50	33	25	5	-8	-11	3	4	13	45	46	38	12	-3	-4	-12	-11
1232	49	58	40	25	3	-14	-14	2	0	16	50	53	42	9	-6	-6	-13	-16
UPSTREAM CANYON WALLS																		
950					12		93		78					10		101		128
1000					50		139		109					25		116		132
1050					67		154		103					48		158		157
1100					103		194		137					74		154		157
1150					100		190		120					117		212		187
1200					127		219		149					142		220		197
1232					115		209		137					170		268		207

FIGURE 202—MEASUREMENTS OF SPREADING OF RESERVOIR WALLS

tect the gages from water by covering them with a membrane of thin rubber. When a gage was mounted with its face upward, the dial could easily be read through the water with a pair of low-power field glasses.

A table of measured deflections is shown in figure 202. With the reservoir water surface above elevation 1100, movements were greater at the Nevada abutment than at the Arizona abutment, due to lack of symmetry. The maximum full load deflection was 0.0266 inches and occurred at elevation 800 on the Nevada side. The corresponding movement on the Arizona side was 0.0209 inches. With the water surface at elevation 1100, the deflection on the Arizona side at elevation 800 was 0.0194 inches, as compared with 0.0154 inches on the Nevada side. The measurements may contain small errors due to the use of dial gages covered with rubber membranes, located under water.

193. Spreading of Downstream Walls.—Measurements of the spreading of the canyon walls downstream from the model were made along the gage line shown in figure 202. A vertical post was also used as a central reference for these measurements, so that displacements of each side of the canyon could be obtained. Measurements were made between elevations 600 and 1300. The section of the canyon where the measurements were made was more symmetrical than the section in the reservoir. Consequently the deflections were more symmetrical. When the reservoir was full the maximum spreading was 0.0058 inches at elevation 1232 on the Arizona side. The corresponding measurement on the Nevada side was 0.0050 inches. Below elevation 900, the spreading was negative, apparently due to the effect of Poisson's ratio. The negative movements of the canyon walls below elevation 900 decreased as the reservoir water surface was lowered. Measurements made at elevation 1300 showed that the spreading of the canyon above the top of the model was greater on the Arizona side than on the Nevada side.

194. Changes in Chord Lengths.—Changes in chord lengths were measured at the downstream face of the model, at elevations 1232 and at 100-foot intervals between elevations 1100 and 600. The installation of equipment for measuring changes in chord lengths is shown in figure 203. Invar steel rods were fastened to the abutments at the ends of each arch element, with pivot mountings, and held together by flexible couplings. A dial gage was mounted on one bar so that it would register the relative movement of the other bar. By using

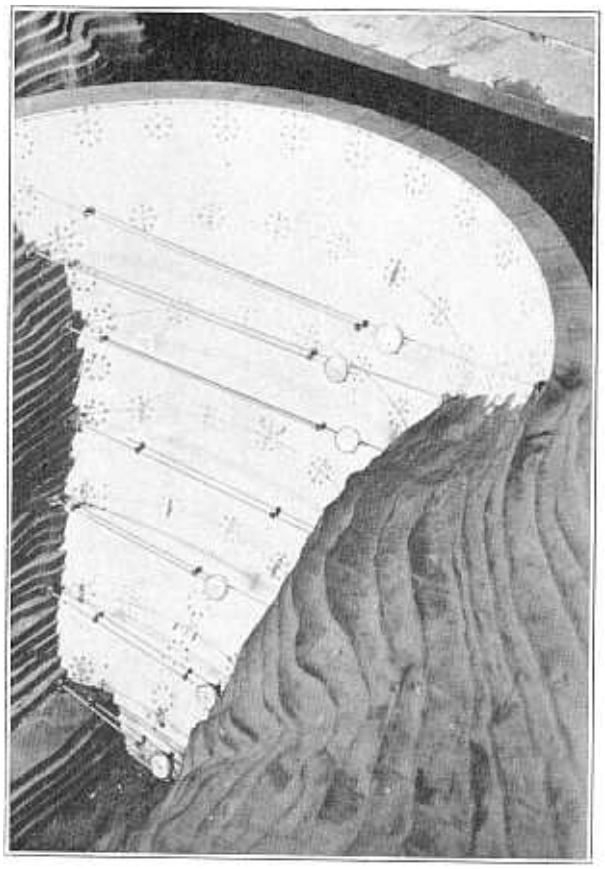

FIGURE 203—MEASURING CHANGES OF CHORD LENGTH

this system of mounting, bending of the bars due to the deflection of the model while under load was eliminated.

Results of the measurements of changes in chord lengths are shown in figure 204. The chords increased in length in all tests. The maximum increase of 0.0143 inches occurred at elevation 1232, with the model under full water load. At elevations 1100 and 1000 the deflections were only slightly smaller, being 0.0135 and 0.0102 inches, respectively.

195. Resultant Movement of Model.—The resultant horizontal movement of the model was determined by combining data obtained from the radial, tangential, and foundation deflection tests. Figure

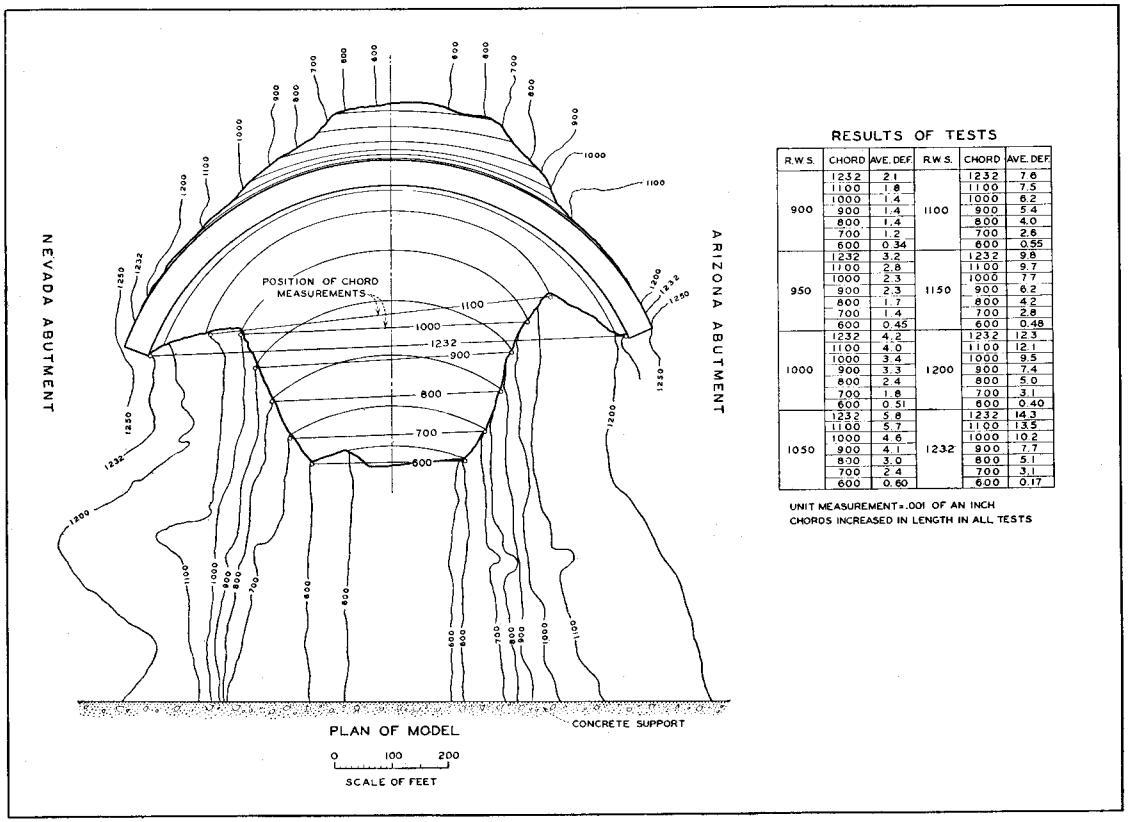

RESULTS OF TESTS

R.W.S.	CHORD	AVE. DEF.	R.W.S.	CHORD	AVE. DEF.
900	1232	2.1	1100	1232	7.6
	1100	1.8		1100	7.5
	1000	1.4		1000	6.2
	900	1.4		900	5.4
	800	1.4		800	4.0
	700	1.2		700	2.6
	600	0.34		600	0.55
950	1232	3.2	1150	1232	9.8
	1100	2.8		1100	9.7
	1000	2.3		1000	7.7
	900	2.3		900	6.2
	800	1.7		800	4.2
	700	1.4		700	2.8
	600	0.45		600	0.48
1000	1232	4.2	1200	1232	12.3
	1100	4.0		1100	12.1
	1000	3.4		1000	9.5
	900	3.3		900	7.4
	800	2.4		800	5.0
	700	1.8		700	3.1
	600	0.51		600	0.40
1050	1232	5.8	1232	1232	14.3
	1100	5.7		1100	13.5
	1000	4.6		1000	10.2
	900	4.1		900	7.7
	800	3.0		800	5.1
	700	2.4		700	3.1
	600	0.60		600	0.17

UNIT MEASUREMENT=.001 OF AN INCH
CHORDS INCREASED IN LENGTH IN ALL TESTS

FIGURE 204—TESTS FOR CHANGES IN CHORD LENGTH

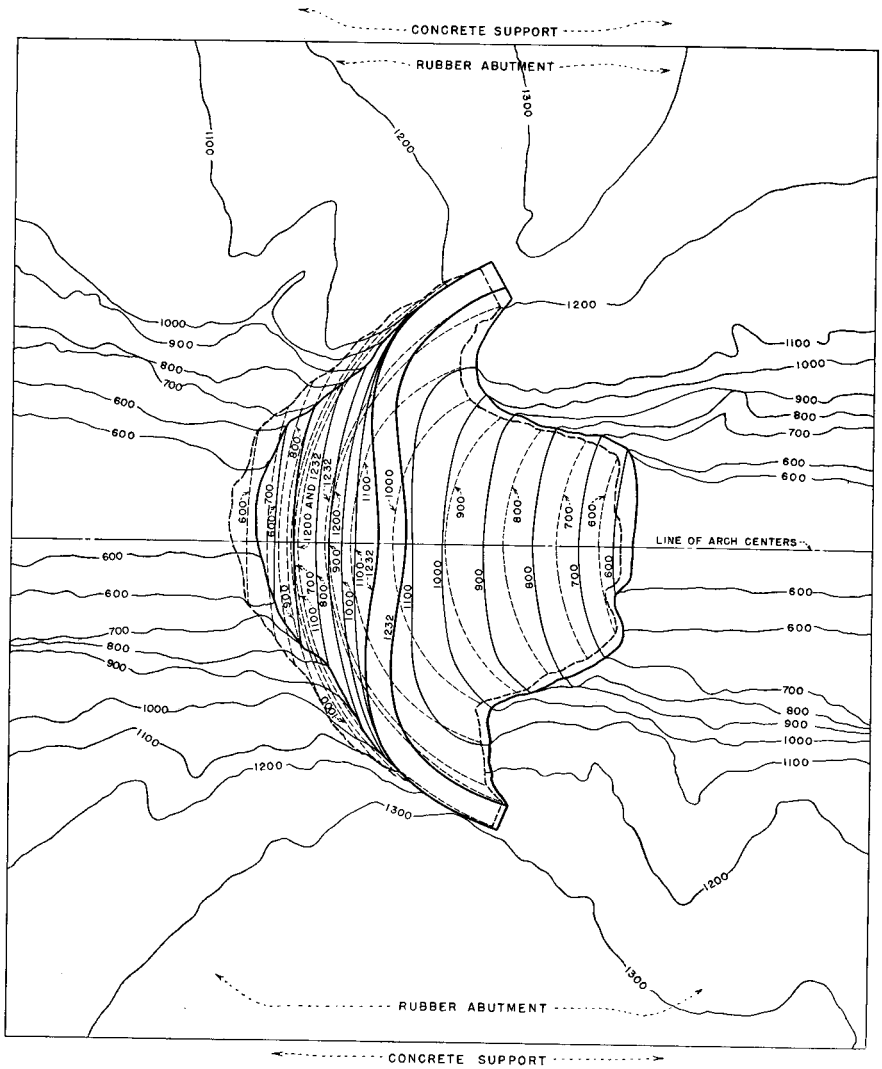

FIGURE 205—RESULTANT HORIZONTAL MOVEMENT OF MODEL

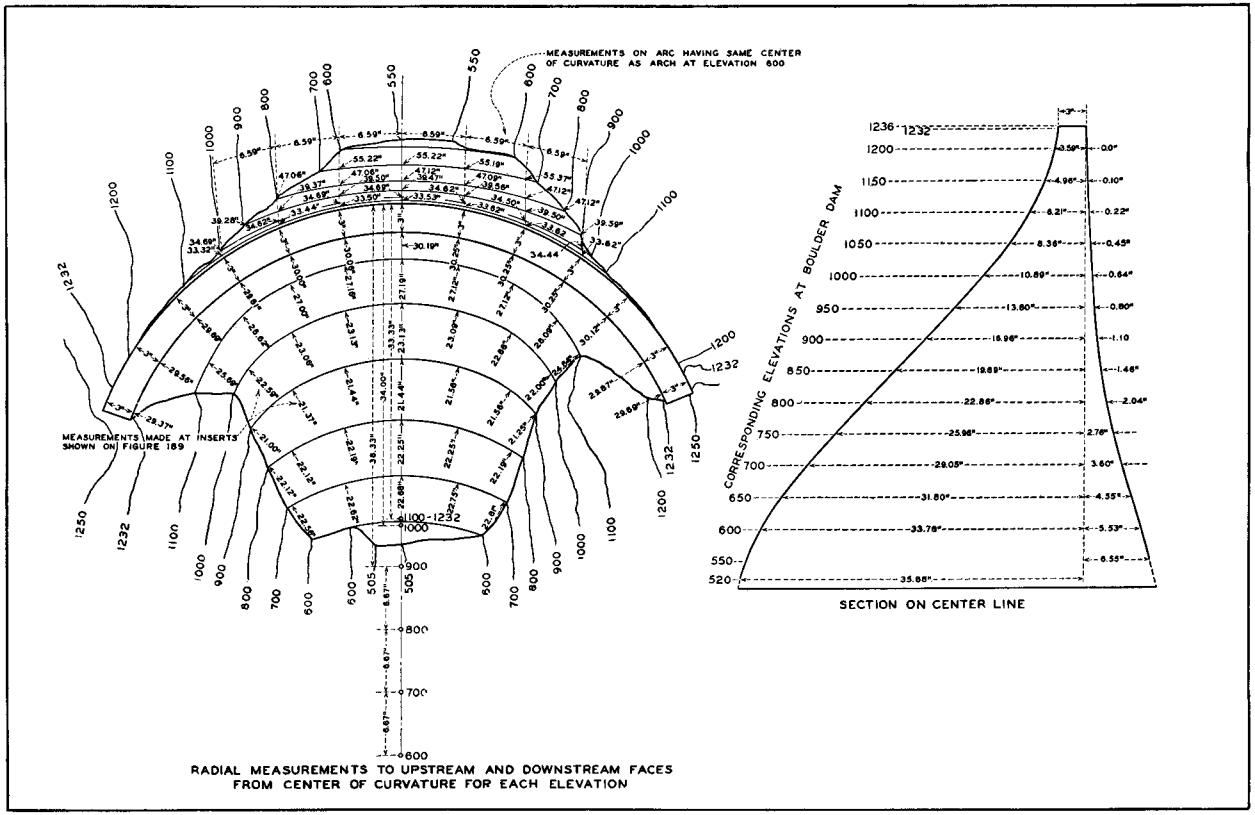

FIGURE 206—DIMENSIONS OF MODEL AFTER COMPLETION OF 700 TESTS

205 shows the results of the calculations. Some interpolation was necessary in combining the data, since all components of movement were not measured at each point. In plotting the movements, only those measured at the model dam were used, foundation movements remote from the dam being neglected. The squeezing of the material between the faces of the model is quite apparent from the figure.

196. Changes in Shape of Model.—The shape of the model changed gradually, due to flow and to cumulative effects of repeated loadings. The changes occurred slowly and were hardly noticeable between tests. However, after a period of four months, when about seven hundred tests had been completed, it was realized that the shape of the model had changed considerably. The model was carefully measured and the results are shown in figure 206. A comparison with original dimensions may be made by referring to figure 184. Appreciable proportions of the changes probably represent flow caused by the weight of the material.

The greatest change in the shape of the model occurred above elevation 900. The thickness of the model along cantilever section E increased about three-tenths of an inch. The arch had been carefully alined while being built, and the position of each piece of rubber was checked before being cemented in place. After seven hundred tests had been made on the model, the arch elements were no longer circular as constructed, but varied considerably. The downstream radius of the top of the model was originally 30.33 inches. After deforming, the distance from the original center to the downstream face varied from 29.37 to 30.25 inches.

CHAPTER XI—STRAINS AND STRESSES

197. General.—It was realized at the beginning of the tests that the stress and strain distribution would be considerably different from that obtained in a model with a lower Poisson's ratio. The squeezing effects observed in the deflection tests showed that the top of the model moved upward at both faces, causing vertical tensile strains. This, however, does not necessarily indicate vertical tensile stresses if the horizontal strain was compressive. From equation 12, section 96, it is evident that σ_V is a compressive stress if μ is 0.50, ϵ_V is a tensile strain, and ϵ_H is a compressive strain more than twice as large as ϵ_V.

Methods of computing strains and stresses from experimental measurements were developed in chapter V. The same methods were followed in analyzing data obtained on the rubber model. A large number of detailed strain diagrams were prepared as intermediate steps in calculating stresses, in the same manner as in the plaster-celite tests. Since these were important only as an aid in compiling final results, detail strain diagrams are not included in this chapter.

APPARATUS

198. Gages at Upstream Face.—The use of water for the loading medium permitted the measurement of strains at the upstream face, a testing operation which was not possible on the plaster-celite model. For this purpose, specially designed gages, which could operate under water, were constructed. The gages were essentially the same as those developed by the Aluminum Company of America, except for a change in gage length.[16]

The general assembly of the gages is shown in figure 207, where three gages are mounted on horizontal, vertical, and diagonal gage lines. Details of the vertical strain gage are shown in figures 208 and 209. The other gages were similar, except for the shape of the

[16]Karpov, A. V., and R. L. Templin, "Building and Testing an Arch Dam Model," Civil Engineering, Jan., 1932, pp. 11-16.

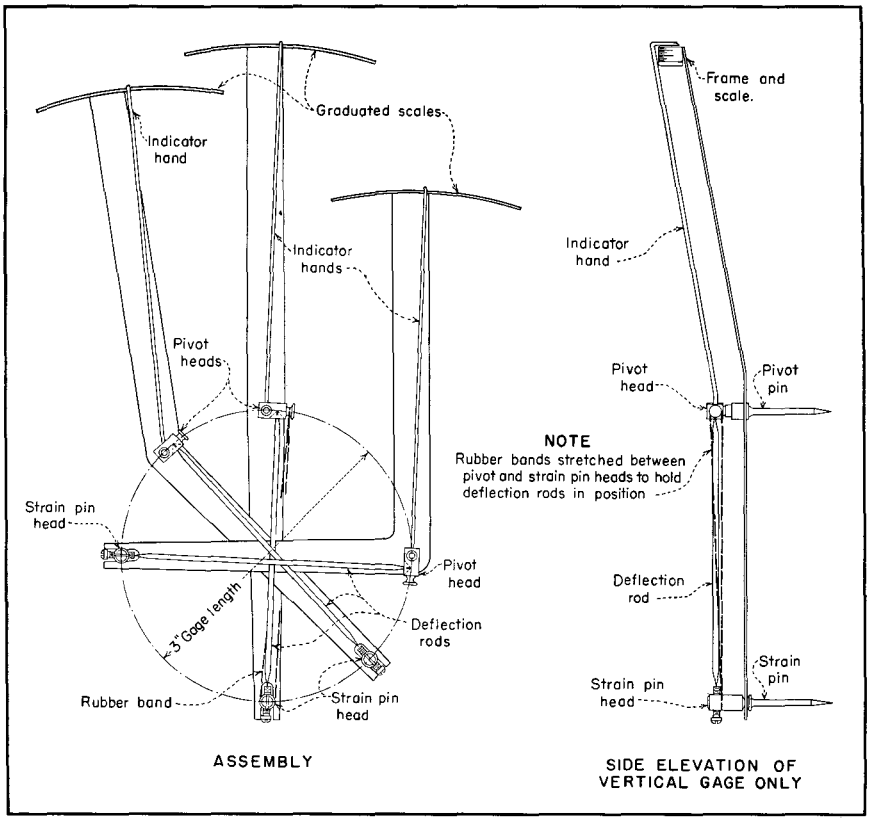

FIGURE 207—STRAIN GAGES FOR UPSTREAM FACE

gage frame. The gage consisted of a lever and fulcrum attached to the face of the model by pins. Relative movements between pairs of pins were registered by pointers on graduated scales. The movement of the pins was magnified approximately thirty times by the pointer. The gages were constructed of aluminum with jewel bearings at the pivot pins. Since it was impossible to obtain identical dimensions in constructing the gages, each gage was calibrated separately, against a ten-thousandth micrometer on a special calibration jig.

The apparatus was designed so that an assembly of three gages could be mounted on a rosette, making angles of 0, 90, and 135 degrees with the horizontal. A jig with holes drilled at proper locations was used to set the pins in the face of the model. When assembled on the model, very thin rubber bands were stretched between the strain

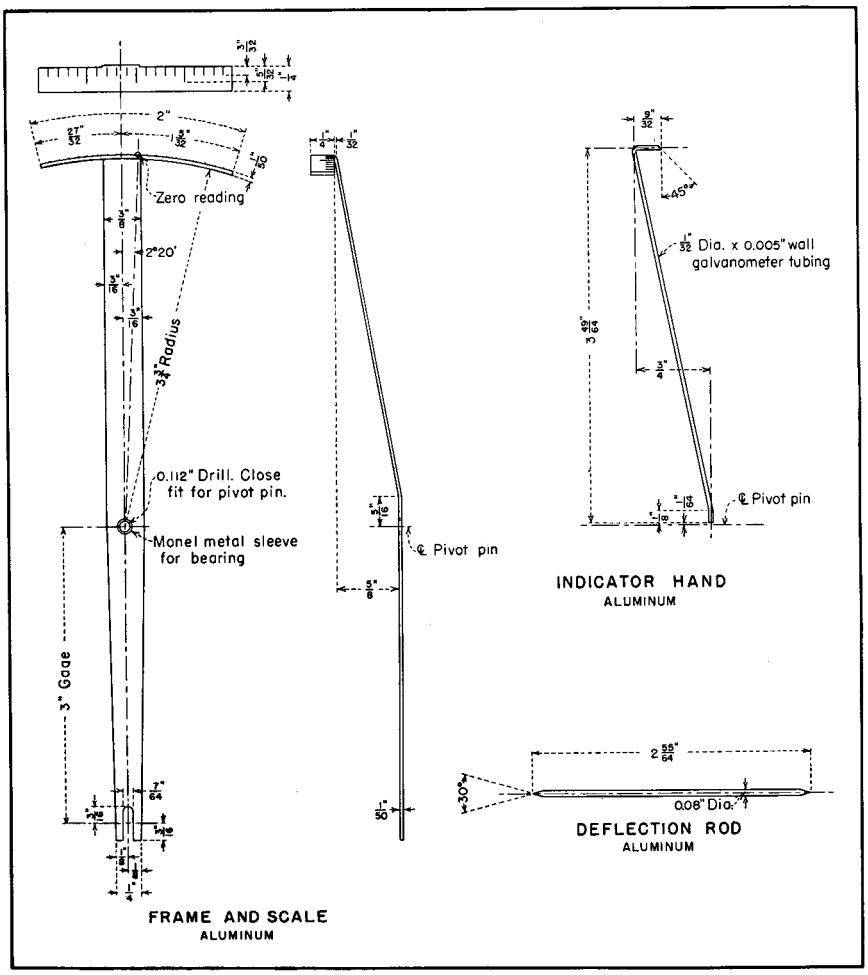

FIGURE 208—FRAME DETAILS FOR VERTICAL STRAIN GAGE

pins and pivot heads to maintain a slight pressure on the deflection rods. Figure 210 shows gages assembled on the face of the model.

As constructed, the pins which actuated the gages were all the same length, requiring different depths of penetration in the model to obtain proper clearance between different gages. In conducting the tests it was observed that the pins having the deepest setting gave the most consistent results. Gages having the least penetration were affected by friction which caused erratic readings. At a number of points it was necessary to repeat the tests, using single gages with

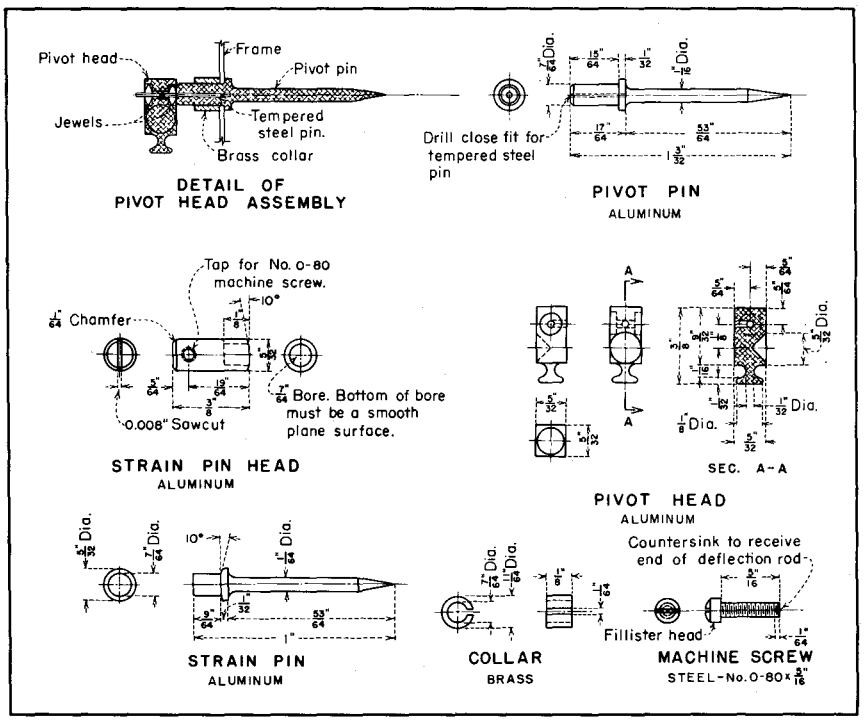

FIGURE 209—PIN DETAILS FOR VERTICAL STRAIN GAGE

pins set to maximum depth. The water used for loading was very clear and it was possible to read gages at any location on the upstream face with a pair of low-power field glasses.

199. Gages at Downstream Face.—Strains at the downstream face of the model were measured with the gage shown in figure 211, which was developed for measuring surface strains in soft rubber. It consisted of a dial gage mounted on a steel frame. At one end of the frame was a fixed arm with a pointed end, and at the other was a movable arm with a pointed end. The plunger of the dial bore against a smooth area on the upper end of the movable arm. The dial spring was balanced by a light-weight rubber band, so that virtually no force was exerted on the strain pins. To make a strain observation, points of the arms of the gage were set in countersunk holes in the heads of tacks, driven in the rubber to form rosettes, as shown in figure 212. The tacks were set with a template so that the gage lines intersected in a point. The lever arm of the gage had a two to one ratio so that

average unit strains over 2-inch gage lengths could be read directly on the dial. Two gages were assembled, carefully calibrated, and adjusted to 0.0001 of an inch so that unit strains could be read exactly, thereby eliminating mathematical computations or corrections.

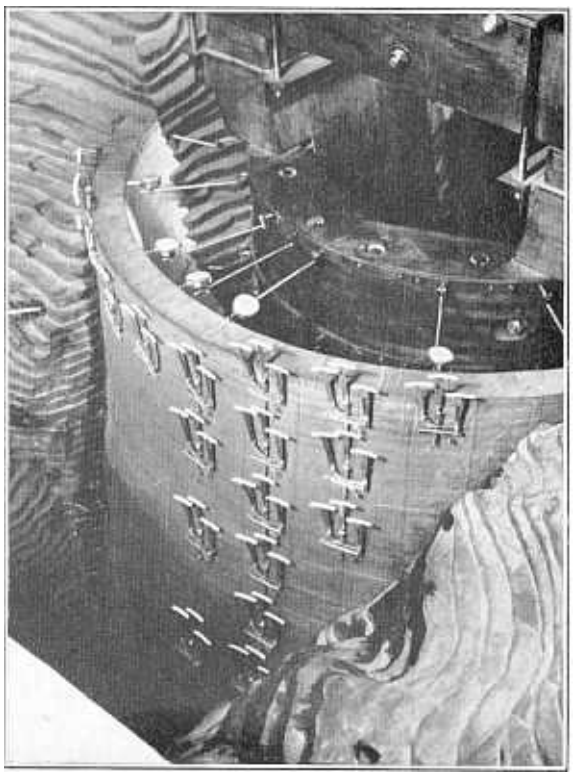

FIGURE 210—STRAIN GAGES MOUNTED ON UPSTREAM FACE

200. Directions of Measurements.—Sufficient data for computing principal strains and stresses could be obtained by making strain measurements along any three gage lines intersecting at a point. In order to simplify computations of stresses from strains and to take advantage of a number of arithmetical checks in the computations, the gage lines at the downstream face were set horizontal, vertical, and at 45 and 135-degree diagonal directions. At the upstream face, the 45-degree diagonal strains were omitted from the water load measurements because of the difficulty involved in setting up four gages at the same location. When strains are measured along four gage lines

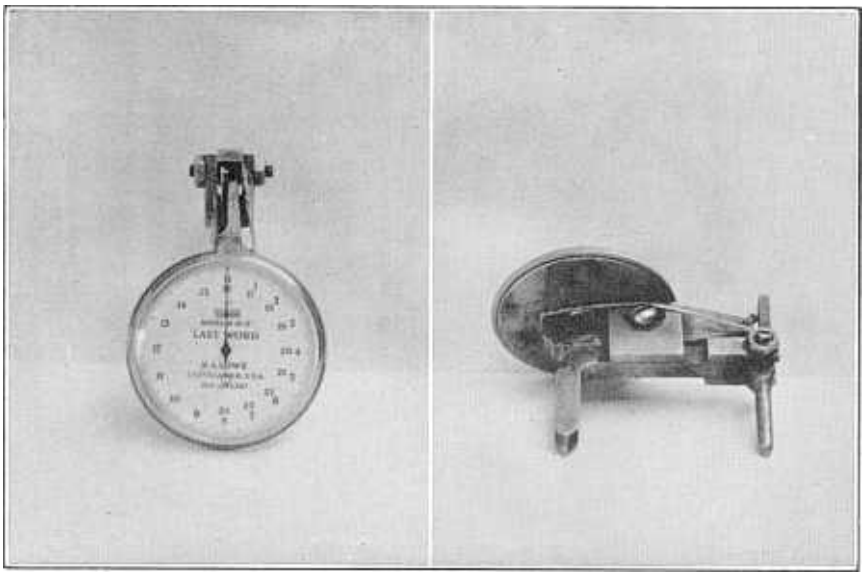

FIGURE 211—HAND-OPERATED STRAIN GAGE

intersecting at a point, a valuable check on the accuracy of the measurements is obtained from the relation that the sum of the strains measured along any two perpendicular gage lines is a constant.

WATER LOAD CONDITIONS

201. Water Load Strains.—Strains due to water load were measured on the upstream and downstream faces at locations shown in figures 213 and 214. Rosettes on the downstream face show gage lines used with the dial strain gage. Rosettes on the upstream face show four gage lines, only three of which were used during the water load tests. The fourth gage line was added later, for use in the dead load strain measurements.

In conducting tests, zero gage readings were made on both faces with the reservoir empty. Temperatures of model and canyon walls were determined by mercurial thermometers placed at convenient locations. The temperature of the water in the supply tank was regulated until it was the same as the average temperature of the canyon and model. The reservoir was then filled and full load readings made. Since dead load strains remained constant, changes in gage readings represented strains due to water load only. Because of the high

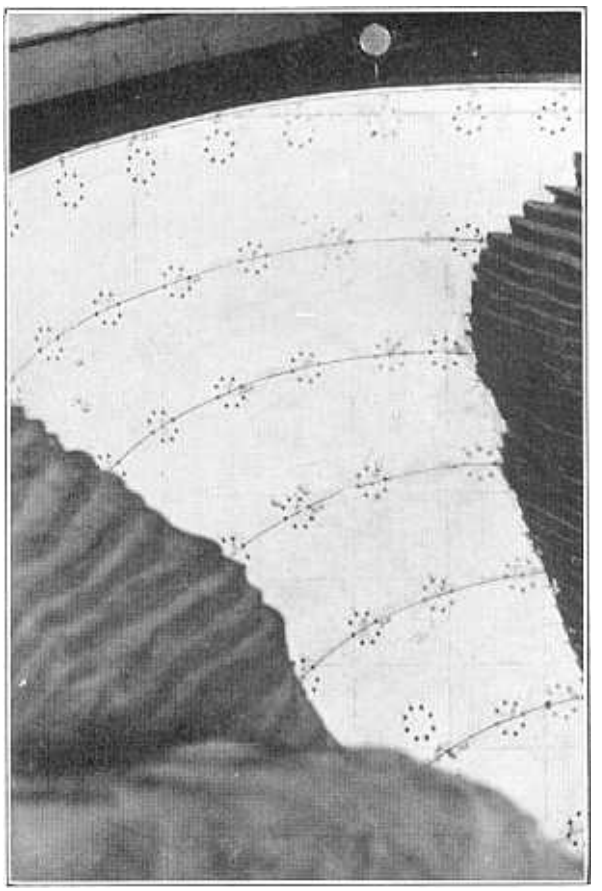

FIGURE 212—STRAIN GAGE ROSETTES ON DOWNSTREAM FACE

Poisson's ratio, definite conclusions could not be drawn from the strain measurements until they had been converted to stresses.

202. Arch Stresses.—Arch stresses at extrados and intrados locations, due to full water load, are shown in figure 215. Stresses were largely compressive, except for a small area below elevation 1200 at the center of the downstream face. Tension probably occurred at the upstream face along the abutments, but the width of the tension area was probably small, since strain measurements on a 3-inch gage length did not show tension. The maximum compression shown on the curves was 1.48 pounds per square inch. This stress occurred at the downstream face at cantilever section B, elevation 1100, and also

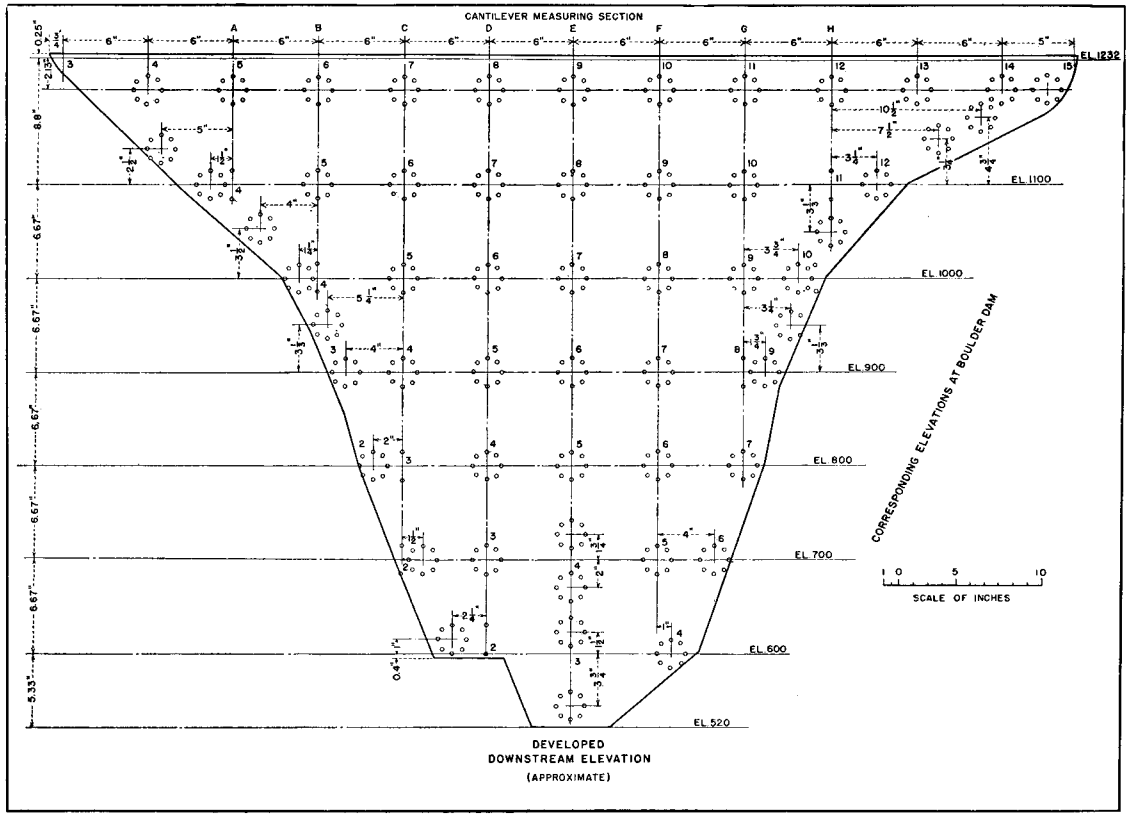

FIGURE 213—LOCATIONS OF ROSETTES ON DOWNSTREAM FACE

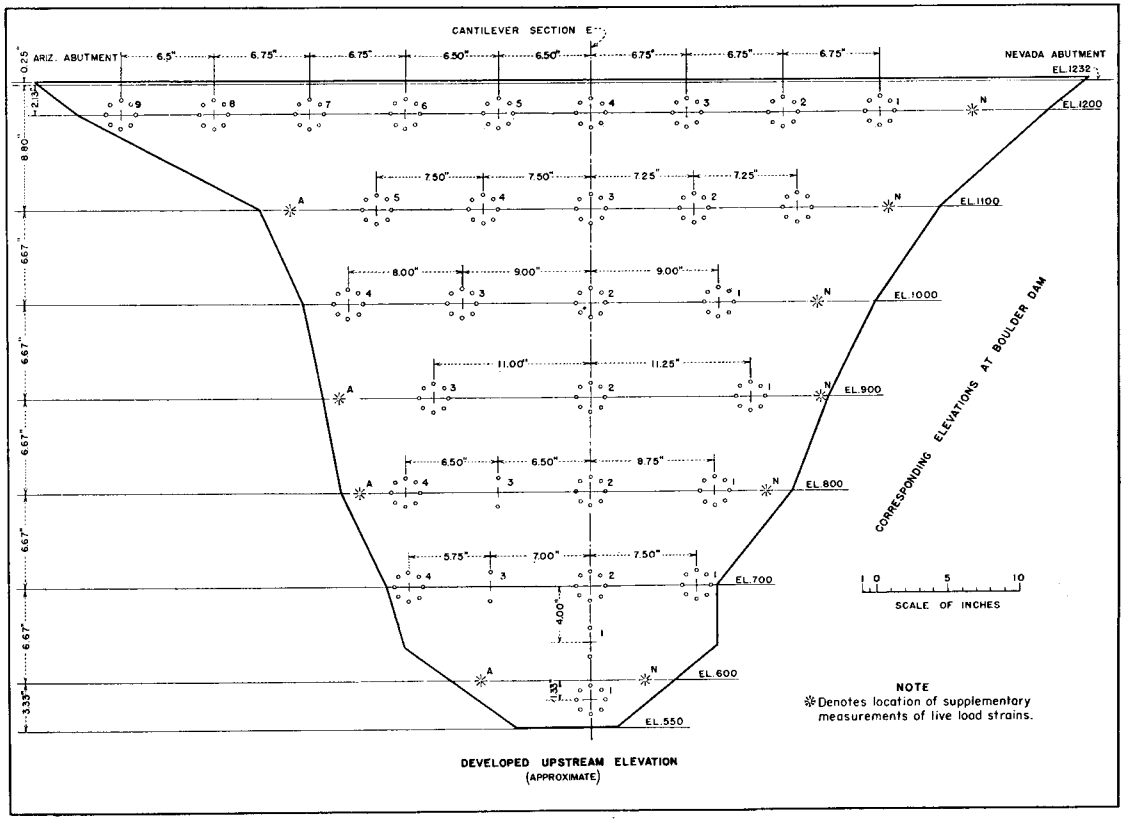

FIGURE 214—LOCATIONS OF ROSETTES ON UPSTREAM FACE

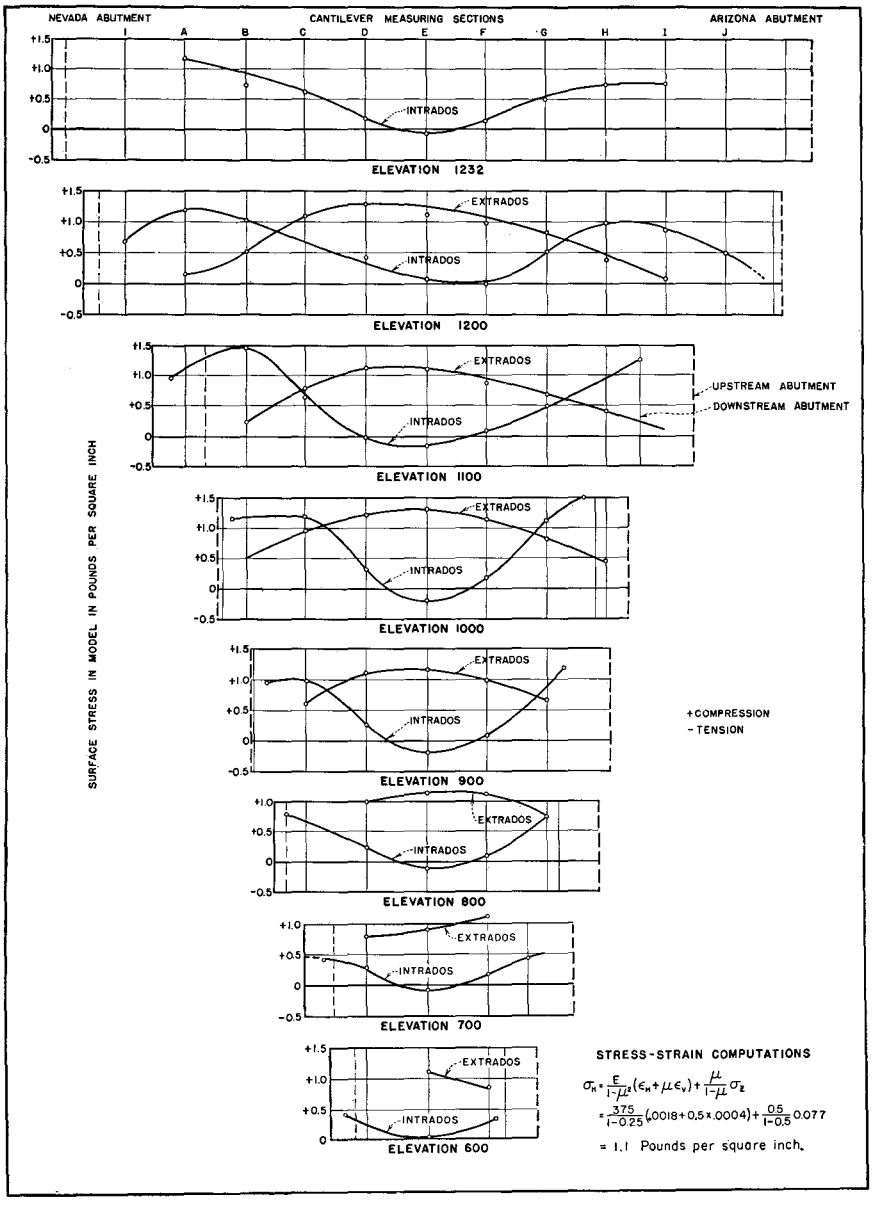

FIGURE 215—ARCH STRESSES, LOAD AT ELEVATION 1232

between sections G and H at elevation 1000. At elevation 1050 at the Arizona abutment, a peak stress of 1.78 pounds per square inch was found. This stress occurred in the region of maximum stress shown by the plaster model tests.

The effect of adding fillets at the downstream face is shown in figure 215. Compressive stresses which occur at the abutment ends of the intrados curves were reduced considerably. At the elevations of the fillets, arch stresses were larger at distances of two to eight inches from the abutments than at the abutments.

203. Cantilever Stresses.—Cantilever stresses at the upstream and downstream faces, due to full water load, are shown in figure 216. These were considerably smaller than the arch stresses, the maximum being only 0.62 pounds per square inch. The maximum stress occurred at the Arizona abutment at elevation 1050. Below elevation 1000 both upstream and downstream stresses were compression. Tension occurred above elevation 1100 at the downstream face.

An abnormal condition of stress existed in the upper part of the model between sections E and F. Strain measurements showed that tensile cantilever strains existed at both faces of the model when the water load was applied. This was due to the fact that the soft rubber compound deforms at constant volume. When stresses were computed from strains, including the effect of Poisson's ratio, most of the tension disappeared. This was because the compressive arch strains were much larger than the cantilever strains. However, between sections E and F and above elevation 1100, vertical tensile stresses were found at both faces of the model. This condition is abnormal and would not occur in a dam made of concrete.

204. Horizontal Shear.—Horizontal shearing strains and stresses at extrados and intrados locations, due to full water load, are shown in figure 217. These stresses were relatively small, being less than 0.4 pound per square inch. With the exception of some variation at elevations 900 and 1000, where the fillets were of maximum thickness, shearing stress curves at the upstream and downstream faces were similar. This shows the consistency of the strain measurements made with two radically different types of strain gages.

205. Principal Stresses.—Principal stresses at the upstream and downstream faces of the model, due to full water load, are shown in figure 218. Stresses at the upstream face are shown in the upper diagram, and stresses at the downstream face in the lower diagram.

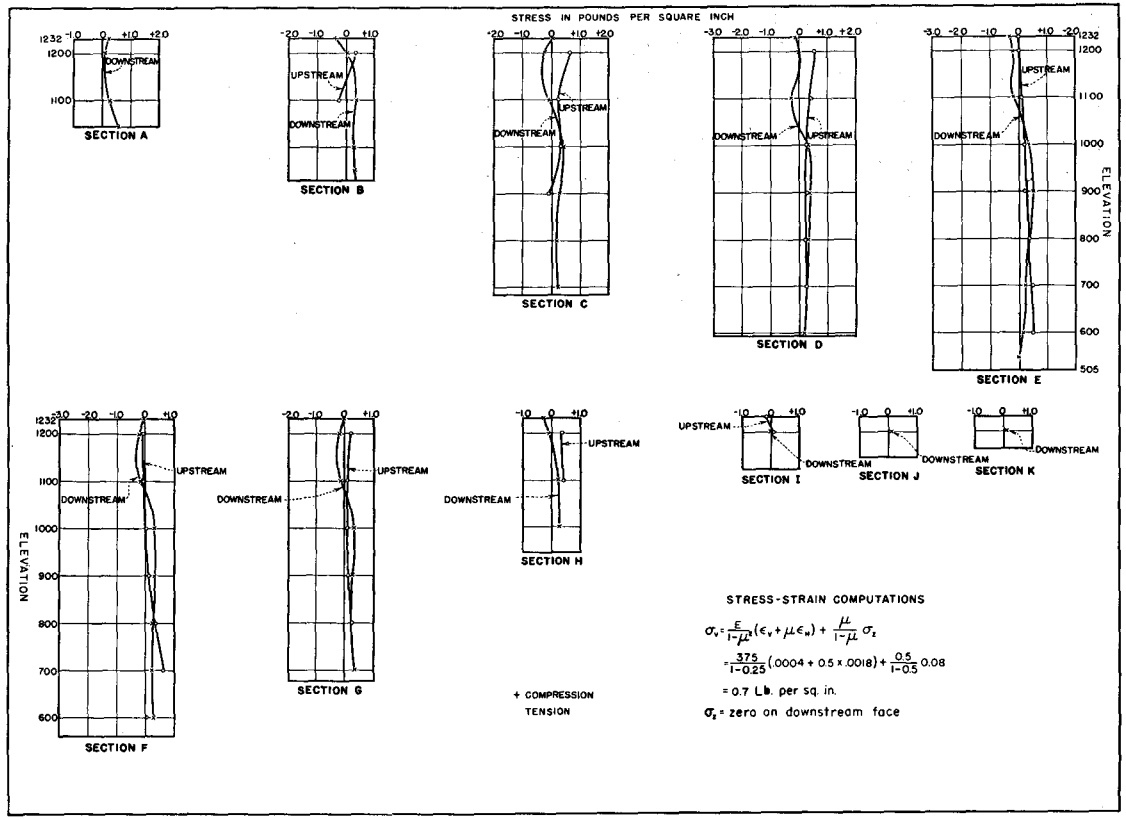

FIGURE 216—CANTILEVER STRESSES, LOAD AT ELEVATION 1232

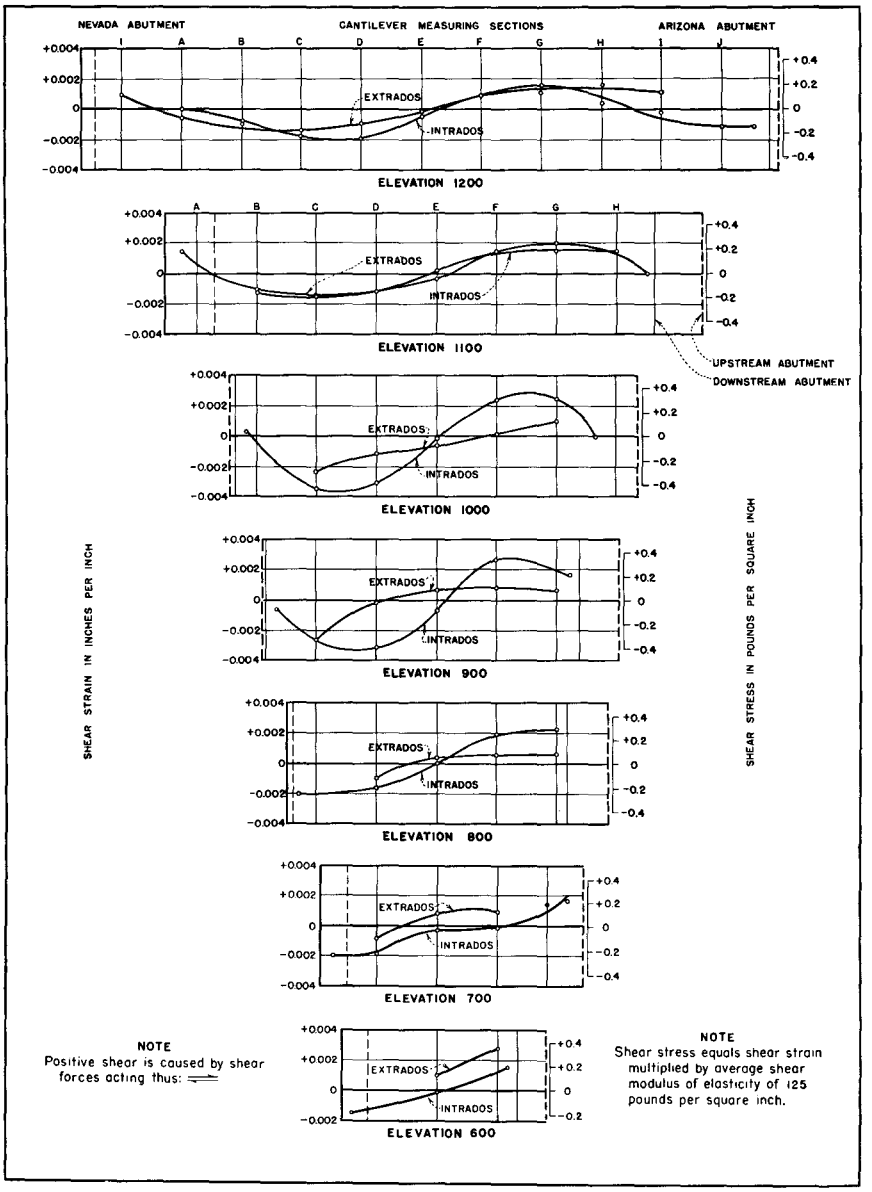

FIGURE 217—HORIZONTAL SHEARING STRAINS AND STRESSES, LOAD AT ELEVATION 1232

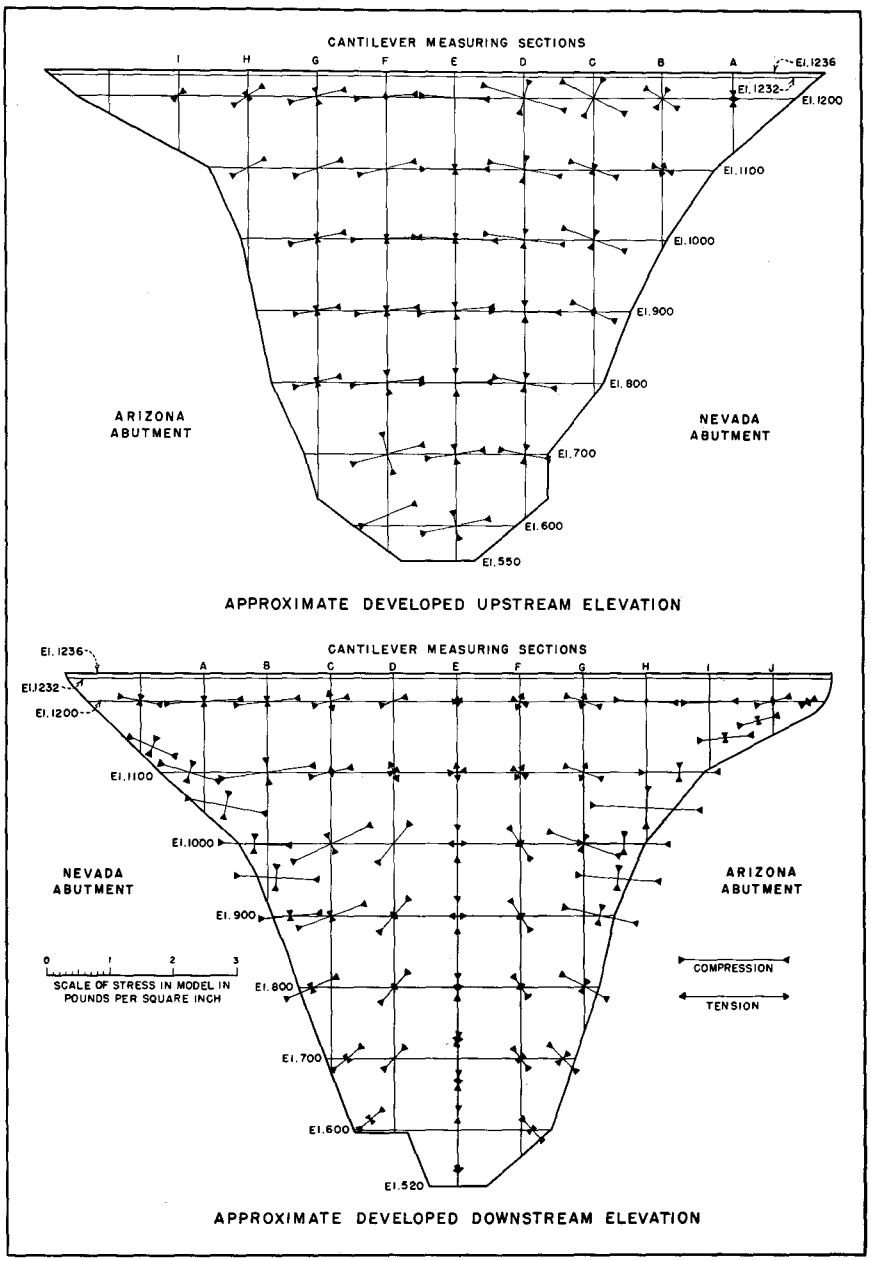

FIGURE 218—PRINCIPAL STRESSES DUE TO WATER LOAD

Considering the upstream face, major principal stresses were nearly horizontal at the central sections. All major principal stresses were compression, as were most of the minor principal stresses. Tension occurred as a minor principal stress at section F, elevation 1200. Major principal stresses calculated from strain measurements nearest the abutments were inclined approximately normal to the abutments. Minor principal stresses were compression, except along the Nevada abutment at elevations 900, 1100, and 1200. It is possible that some unmeasured tension existed as a minor principal stress nearer the abutments. The maximum principal stress of 1.33 pounds per square inch was approximately horizontal at elevation 1000.

Principal stresses at the downstream face, given in the lower diagram of figure 218, show the effect of adding fillets at the ends of the intrados curves. In the case of a circular arch under normal load, stresses at the downstream face are relatively high compressions along the abutments and relatively low compressions or tensions at the crown. The general effect of adding fillets was to reduce the arch stresses at the abutments, thus causing some changes in the directions of principal stresses.

Below elevation 800, where the arch is circular, major principal stresses along the abutments at the downstream face were compression. The general direction of the stresses was almost normal to the abutment lines. Above elevation 800, where fillets were added, slopes of the principal stresses were changed until the major principal stresses were almost horizontal. This condition prevailed along both abutments between elevations 950 and 1100. Above elevation 1100, slopes were inclined still further until the major principal stresses made acute angles with the abutments.

The downstream face of Boulder Dam cannot be developed exactly because of its warped shape. Consequently, the developed downstream elevation shown in the lower diagram of figure 218 is approximate. The diagram contains considerable distortion along the abutments, particularly in the region of the fillets, so that the directions of principal stress are somewhat exaggerated.

Tension occurred as a minor principal stress in the central part of the downstream face. Such stresses were nearly horizontal below elevation 1100. Above elevation 1100, tension occurred in diagonal directions between sections G and H. The maximum tension, which occurred at section D, elevation 1100, was only 0.35 pounds per square inch.

DEAD LOAD CONDITIONS

206. Strain Measurements.—In building the model and canyon, many uncertainties arose in connection with the strains and stresses, due to the weight of the structure. It was necessary to build the model and canyon in continuous layers from abutment to abutment, because of the relatively large deformations in the soft rubber caused by its own weight. Strains in the model were affected by the deformation of the canyon walls, since it was not practical to build the walls first and then put in the model. The measurement of dead load strains was therefore postponed until all other tests had been completed. Dead load strains were measured as the model was removed from the testing pit.

Dead load strains were measured with the dial gage shown in figure 211. Locations of rosettes for strain measurements are shown in figures 213 and 214. The rosettes were located at the intersections of the arch and cantilever elements, as far as possible. Additional measurements were made along the abutments at the downstream face and at points halfway between the cantilever sections on the lower part of the upstream face.

The procedure in making dead-load strain measurements was as follows: An observer took zero readings on all rosettes on both faces. These readings were checked by a second observer who repeated the observations. A layer of rubber one inch in thickness, corresponding to a height of 15 feet on the dam, was then carefully removed from the top of the model and readings on all rosettes repeated and checked. This procedure was continued until the entire model was removed from the canyon.

Curves were plotted to show the magnitude of strains due to dead load above the center of each rosette. As no observations could be made when the rubber containing a rosette was removed, the curve was extended until it reached the elevation of the center of the rosette. Values obtained in this way, reversed as to tension and compression, gave dead load strains at the rosettes. From these strains dead load stresses at each arch element were calculated.

207. Dead Load Stresses.—Arch stresses due to dead load are shown in figure 219. Stresses at the downstream face were largely compression, although some tension occurred at the abutments. Tension stresses were relatively small and did not exceed 0.5 pounds per square inch, except at the Arizona abutment at elevation 1000 where

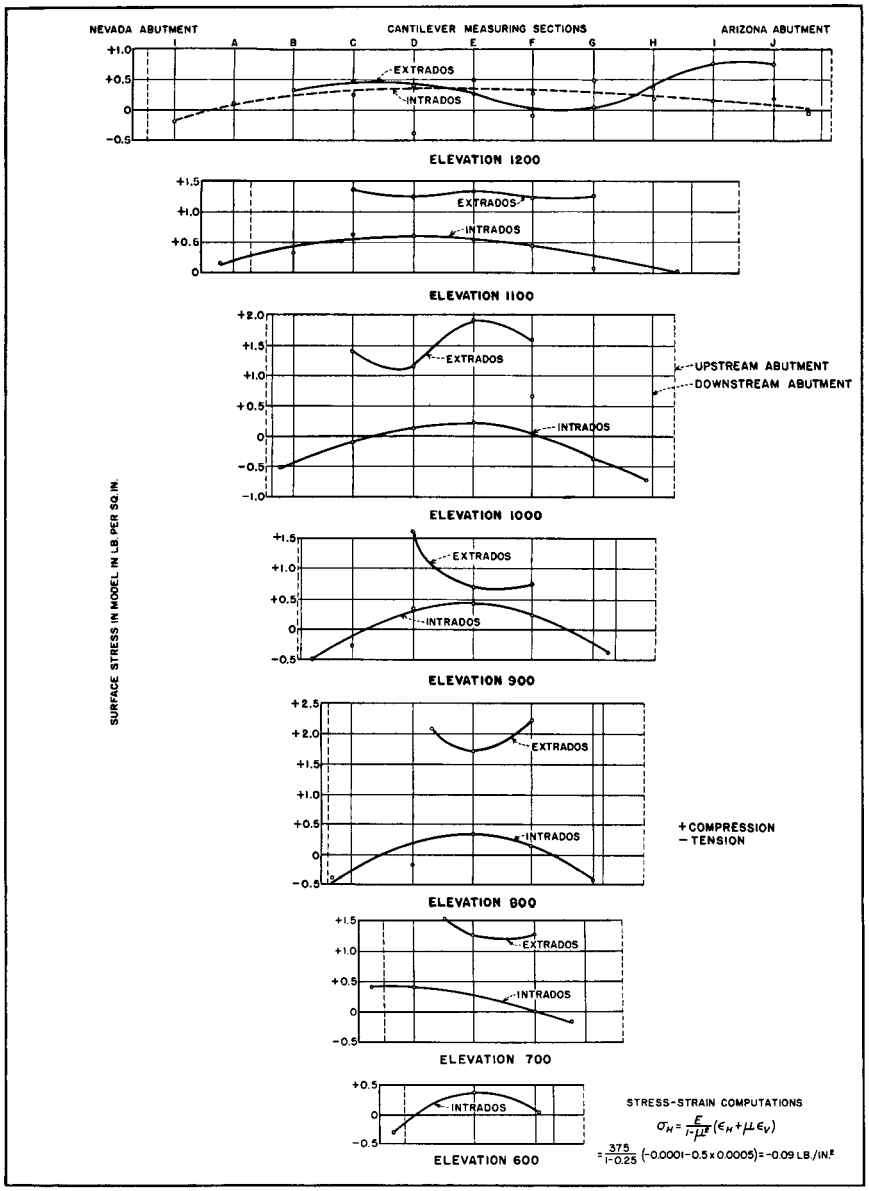

FIGURE 219—DEAD LOAD ARCH STRESSES

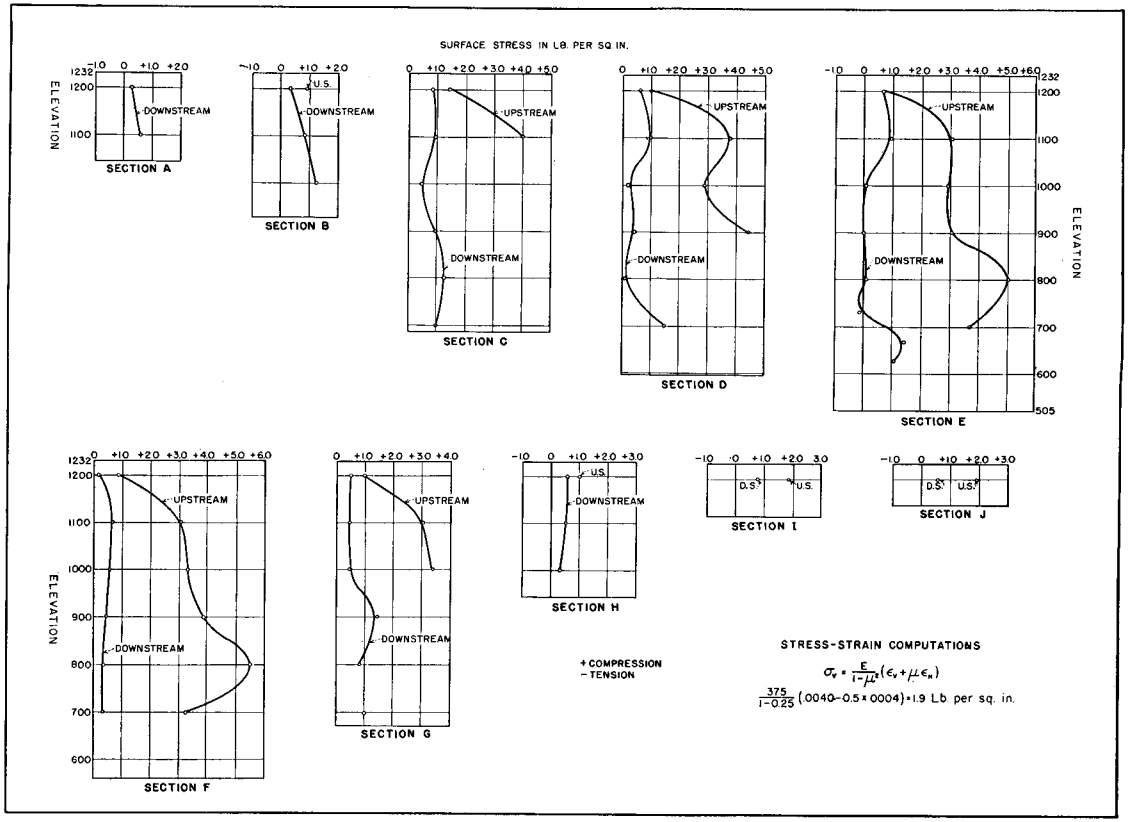

FIGURE 220—DEAD LOAD CANTILEVER STRESSES

0.75 pounds per square inch was found. At the upstream face, arch stresses were materially larger. Between elevations 700 and 1000 they were about two pounds per square inch, the peak stress of 2.3 pounds per square inch occurring at cantilever section F, elevation 800. No tension due to dead load was found at the upstream face.

Cantilever stresses due to dead load are shown in figure 220. At the downstream face, cantilever stresses were small. At section E, the stress was almost zero between elevations 800 and 1000, with a negligible amount of tension between elevations 700 and 800. At section G, elevation 900, the stress at the downstream face reached its maximum value of 1.5 pounds per square inch. At the upstream face, cantilever stresses were considerably larger. Stresses between three and five pounds per square inch occurred between sections C and G. The peak stress occurred at section F, elevation 800, and was 5.5 pounds per square inch.

Horizontal shearing strains and stresses due to dead load are shown in figure 221. Since shear stress is equal to shear strain multiplied by the average shearing modulus of elasticity, one set of curves shows both strains and stresses. Two scales are provided so that either the strain or the stress can be read from the curves as desired. In the upper elevations of the model, shearing stresses were small. In the lower part, where the model was thicker, shearing stresses were larger and fairly symmetrical. The maximum shearing stress was 1.0 pound per square inch and occurred at the Nevada abutment at elevation 600.

Principal stresses due to dead load are shown in figure 222. At the upstream face, major principal stresses were almost vertical. Major principal stresses and all except one of the minor stresses were compression. A negligible amount of tension occurred at cantilever section F, elevation 1200. At this elevation the stresses were so small that their values hardly exceeded the limits of accuracy of the strain gages. Below elevation 1100, the stresses increased in magnitude toward the lower part of the model. The largest principal stress, 5.85 pounds per square inch, occurred at section E, elevation 580.

Principal stresses at the downstream face were much smaller than at the upstream face. Considerable tension was found along both abutments. The maximum tension of 1.38 pounds per square inch occurred at the Nevada abutment near elevation 600. The maximum compression, 1.63 pounds per square inch, occurred near the Nevada abutment at elevation 700.

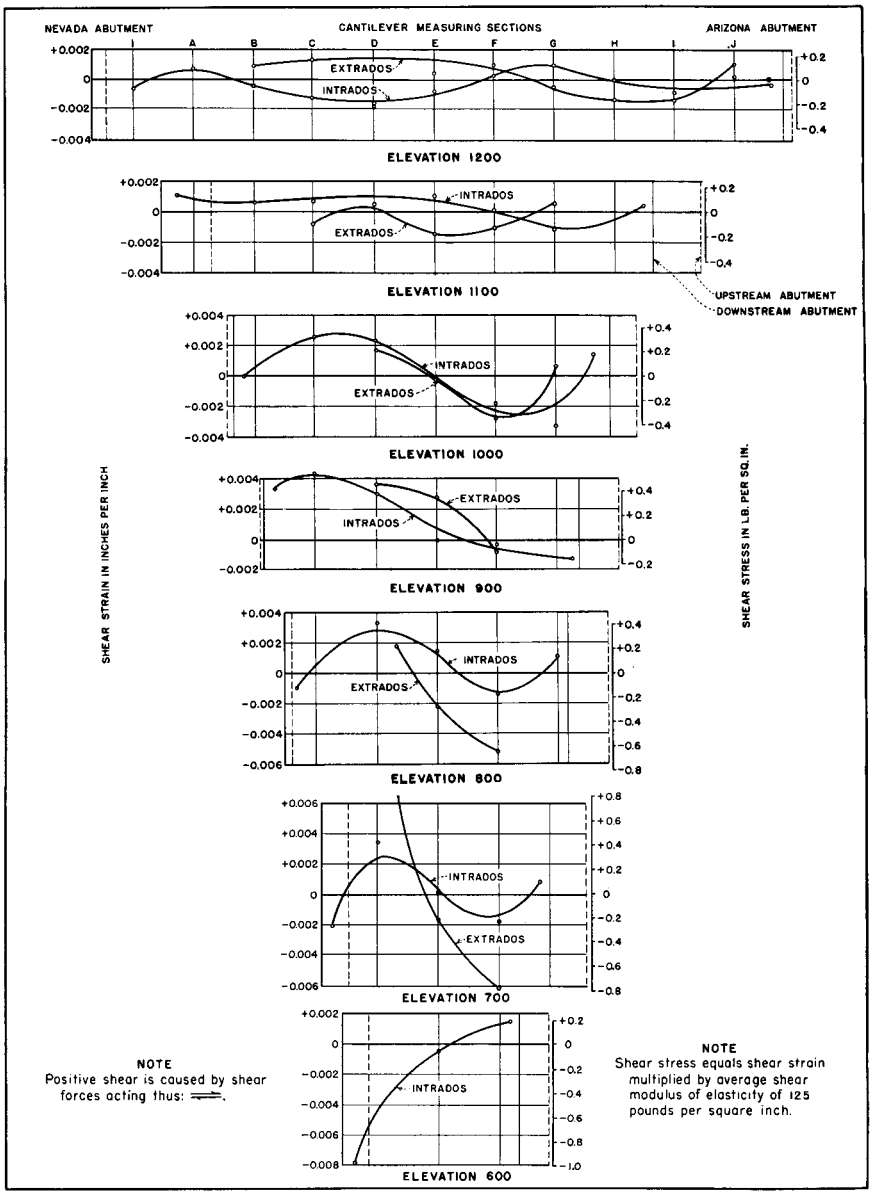

FIGURE 221—DEAD LOAD HORIZONTAL SHEARING STRAINS AND STRESSES

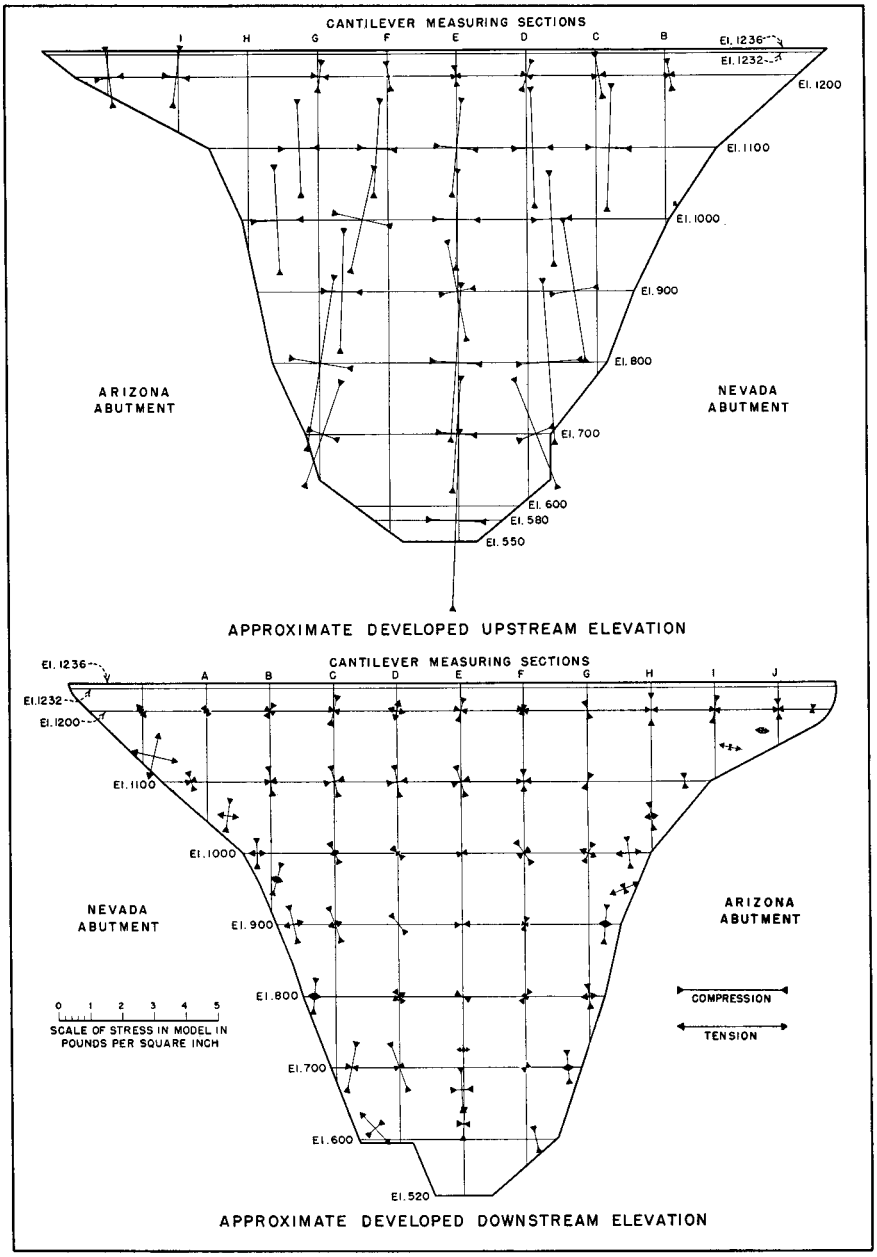

FIGURE 222—PRINCIPAL STRESSES DUE TO DEAD LOAD

COMBINED LOAD CONDITIONS

208. Combining Strains.—To obtain actual horizontal, vertical, and shearing stresses in the model during the application of reservoir load, dead and live load stresses were added at the different locations when strains were measured. Since directions of principal stresses varied during different load conditions, these stresses could not be added directly. It was necessary to combine original strain readings and to compute magnitudes and directions of principal stresses from the combined values.

209. Arch Stresses.—Arch stresses due to combined loads, weight plus full reservoir pressure, are shown in figure 223. When the two sets of stresses were combined, the most important result was the elimination of tension from the arch elements. Some tension may have existed along the abutments at the upstream face, beyond the region of measured strain; but all tension at the downstream face was eliminated. The weight of the model caused it to deflect upstream, thereby producing horizontal tension along the downstream abutments and horizontal compression in the central portion of the downstream face, see figure 219. The water load produced stresses of an opposite nature; compression occurred along the abutments at the downstream face with tension in the central portion. When the two sets of stresses were combined, compressive stresses predominated. In the central part of the downstream face, the stresses had no magnitude at elevations 1000 and 1200, and were small at elevations 600, 700, and 800. The largest arch stress for the combined load was 3.1 pounds per square inch. This stress occurred at elevation 800, at the upstream face near the Arizona abutment.

210. Cantilever Stresses.—Cantilever stresses due to combined loads are shown in figure 224. Cantilever stresses at the upstream face of the model were from three to five times as large as those at the downstream face. The largest stress, 5.5 pounds per square inch, occurred at elevation 800 between sections D and G at the upstream face. Stresses at the downstream face were approximately uniform in magnitude, being about one pound per square inch. Some variation in the downstream stress occurred at cantilever D, below elevation 800. This condition did not occur at other cantilever sections.

No tension of any consequence was found after the stresses were combined. Dead load cantilever stresses were compression, except for

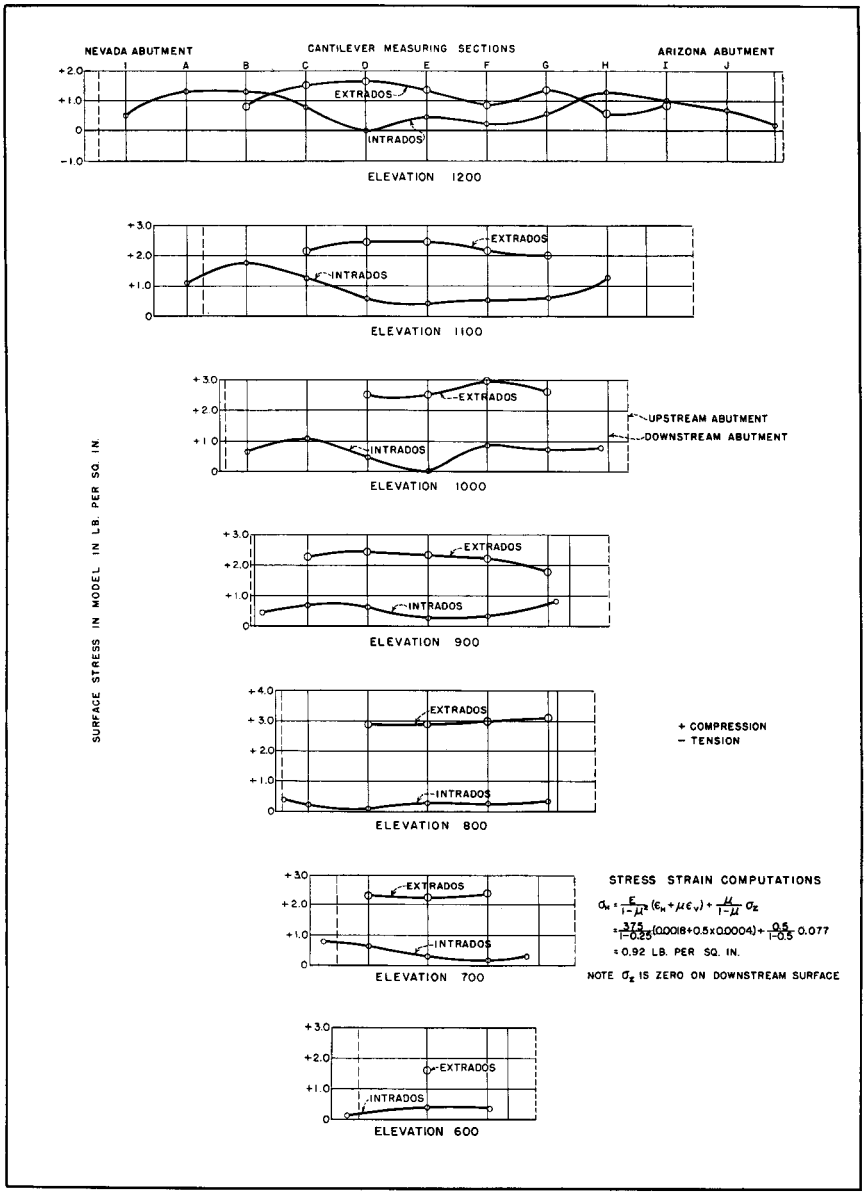

FIGURE 223—ARCH STRESSES, DEAD LOAD COMBINED WITH FULL RESERVOIR LOAD

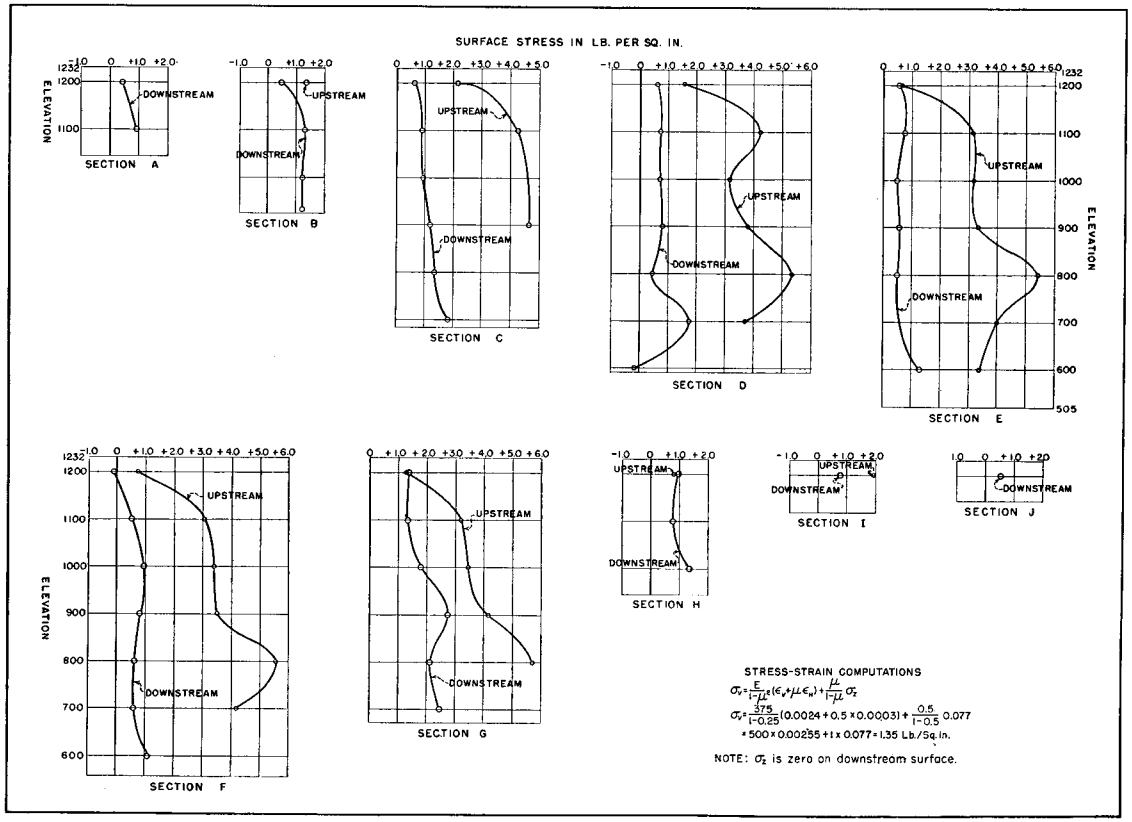

FIGURE 224—CANTILEVER STRESSES, DEAD LOAD COMBINED WITH FULL RESERVOIR LOAD

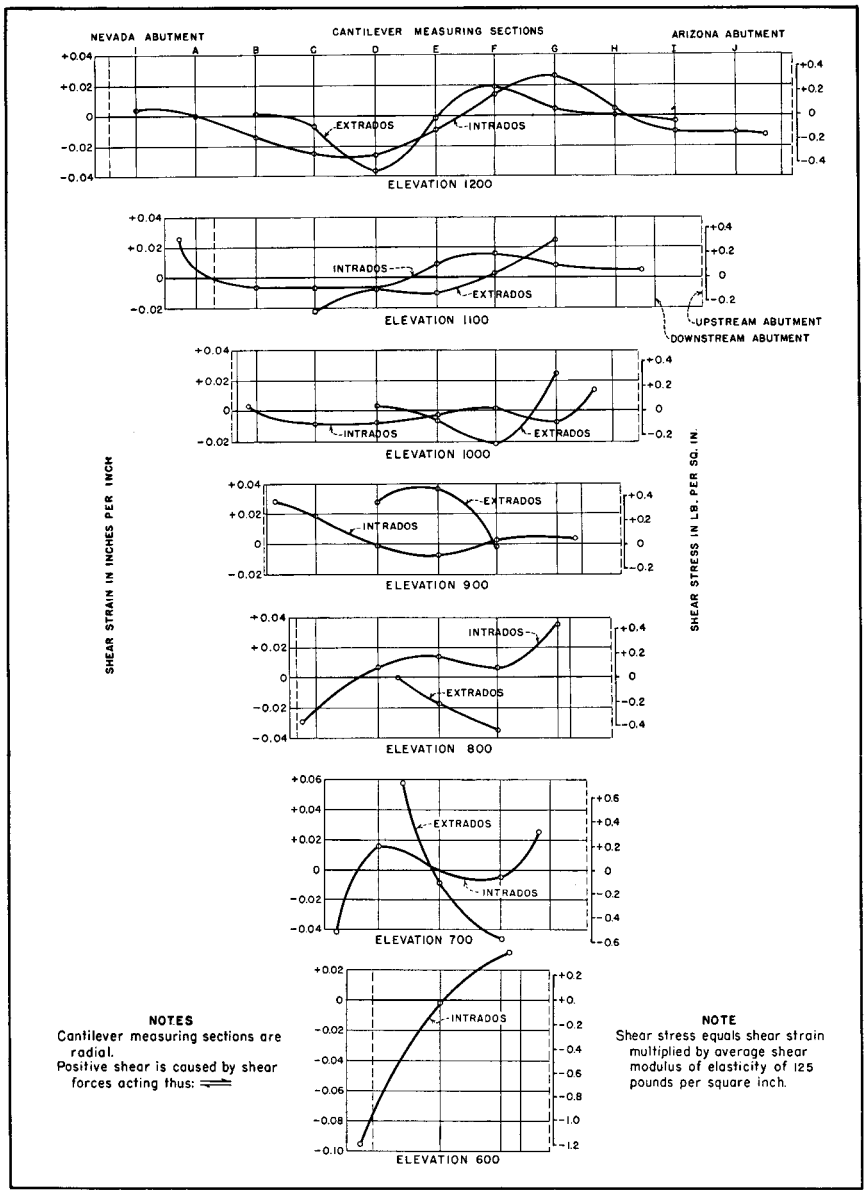

FIGURE 225—HORIZONTAL SHEARING STRESSES, DEAD LOAD COMBINED WITH FULL RESERVOIR LOAD

a small area at the downstream face between elevations 700 and 900. Small tensile stresses existed in the upper elevations of the model on both faces as a result of applying water load. When the two stresses were combined, most of the tensile stresses were offset by the larger compressive stresses, only a negligible amount of tension remaining at sections D and F.

211. **Horizontal Shear.**—Horizontal shearing strains and stresses are shown in figure 225. In the upper part of the model, where the structure was relatively thin, shearing stresses were small, being less than 0.4 pounds per square inch. The maximum shearing stress was 1.20 pounds per square inch. This stress occurred at the downstream face at elevation 600 at the Nevada abutment.

212. **Principal Stresses.**—Principal stresses at the upstream face, due to combined loading, are shown in the upper diagram of figure 226. The major principal stresses due to dead load were approximately vertical while those due to water load were roughly horizontal. The effect of dead load on the stresses was much greater than the effect of water load. Consequently, major principal stresses were almost vertical in direction. The largest major stress occurred at elevation 580, cantilever section E, and was 6.12 pounds per square inch. No tension occurred as a minor stress.

Principal stresses at the downstream face, due to combined loading, are shown in the lower diagram of figure 226. The stresses were larger along the abutments than in the central part of the downstream face. Directions of principal stresses along the abutments, in the regions of fillets between elevations 800 and 1100, are slightly distorted in the diagram, owing to the method of development. The maximum compression occurred at elevation 700 near the Nevada abutment and was 2.04 pounds per square inch. The maximum tension, which occurred as a minor principal stress, was 1.23 pounds per square inch. This stress occurred at elevation 600 near the Nevada abutment. Tensile stresses at the downstream face always occurred as minor principal stresses and were small in magnitude.

It must be remembered that the method of obtaining dead load stresses did not conform with the construction procedure; also that the effect of this lack of conformity was increased by the high Poisson's ratio of the rubber. Had the canyon been constructed before building the model, stresses obtained by removing the model would

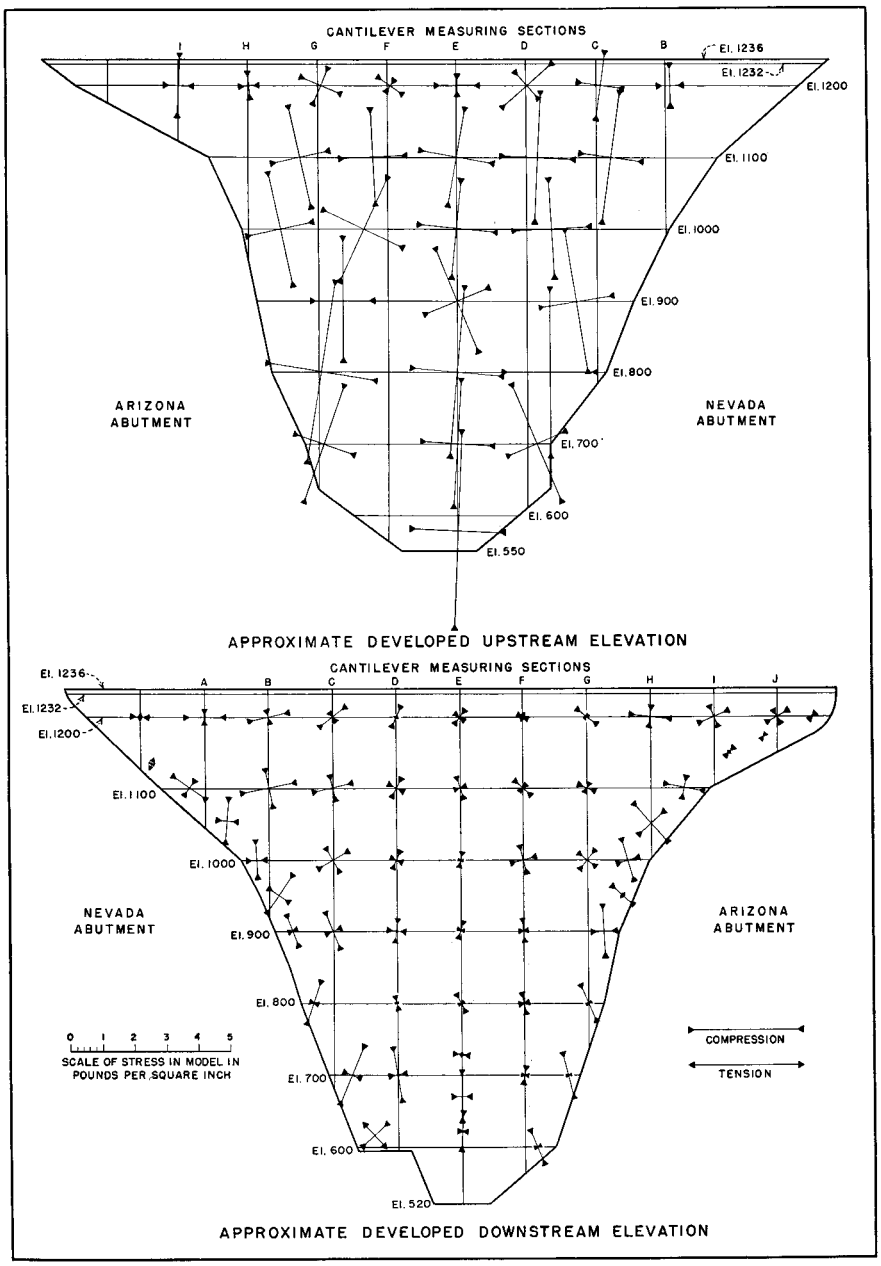

FIGURE 226—PRINCIPAL STRESSES DUE TO DEAD AND LIVE LOADS

have been fairly similar to those occurring in the prototype. Since the dam and canyon walls were built as a unit, and the dam removed separately, the expansion of the canyon walls after a portion of the model was removed caused squeezing in the lower portions of the model. Such squeezing undoubtedly had some effect on the measured strains. This effect appears in the horizontal stress components shown in figure 222.

CHAPTER XII—FLOW AND TEMPERATURE TESTS

FLOW TEST

213. Effect of Flow.—In tests of previous models it was noticed that when load remained on the model for a considerable length of time, deflections were increased due to flow. Flow tests had been made on the concrete model of the Stevenson Creek test dam and the plaster-celite model of Boulder Dam. The rubber-litharge material was so different from concrete and plaster-celite that it was believed a sustained load would cause the material to flow appreciably. A gradual change of shape due to repeated loadings was mentioned in chapter X.

The effect of flow on a model of an arch dam is usually most noticeable in changes of radial deflection. Tangential and twist deflections undoubtedly change slightly, but since the initial magnitudes of these deflections are small, it is not feasible to measure the small changes due to flow. The same condition prevails in the strains. Flow probably causes a slight redistribution of strain which would require very precise instruments to measure. A test was therefore made to determine only the effect of flow on the radial deflections of the model.

214. Method of Making Flow Test.—The flow test was similar to the radial deflection tests, except that the water load was allowed to remain on the model for an extended period of time. As the model deflected the reservoir water surface became lower, and it was necessary to add water to the reservoir to maintain the proper surface elevation. The water in the reservoir cooled slightly during the test; so it was necessary to add warm water to maintain the proper temperature. This was usually done each morning.

Radial deflection measurements were made with micrometers and dial gages reading to 0.001 of an inch. The micrometers and gages were set to measure radial movements at the inserts shown in figure 189. An initial reading with the model unloaded was made at 8:15

a. m., October 9, 1933. The reservoir was filled and radial deflection measurements made immediately, before flow of any consequence occurred. These observations were repeated at intervals of one-half hour during the first day and at greater intervals during succeeding days. Differences between readings at any time during the test and the first set of readings, made with the reservoir full, constituted the deflections due to flow.

Curves were plotted showing flow at individual inserts. At the beginning of the test, slight irregularities in deflections were noticed. These irregularities were apparently due to small variations of temperature. At the lower elevations, where the arch was thicker, such irregularities were not encountered. A small periodic variation occurred daily above elevation 700.

The model became practically stationary at the end of the tenth day of observation, and it was planned to unload the model on the fourteenth day of the test. However, on the fourteenth day the deflection began to increase rapidly. Unloading was therefore postponed for a few days. During this time, the deflection increased rapidly until the twenty-third day, when the model was unloaded.

The cause of the increase in deflection could not be seen at the time of the test. Later, when the model was being dismantled, the cause was discovered. The rubber cement in the horizontal joint at elevation 580 had failed near the Arizona abutment at the upstream face. About three hundred square inches of the cemented joint had opened. This made the cantilever elements more flexible and caused the rapid increase in deflection.

After the load was removed, observations for radial deflections were continued, so that the amount of recovery could be observed. Very little recovery occurred after the model had been unloaded two days. The remaining deflection was due to the open joint and plastic flow. The proportion of the deflection due to each factor could not be determined.

215. Results of Test.—Radial deflections of arch elements are shown in figures 227 and 228. In general, flow tended to increase the radial deflection. This increase was very consistent below elevation 1000. At the upper elevations of the model, particularly at elevation 1232, some irregularities were encountered, owing to the reversal of directions of movement. At the abutments the model deflected upstream while at the crown the deflection was downstream. The initial upstream deflection was small and the increase due to flow

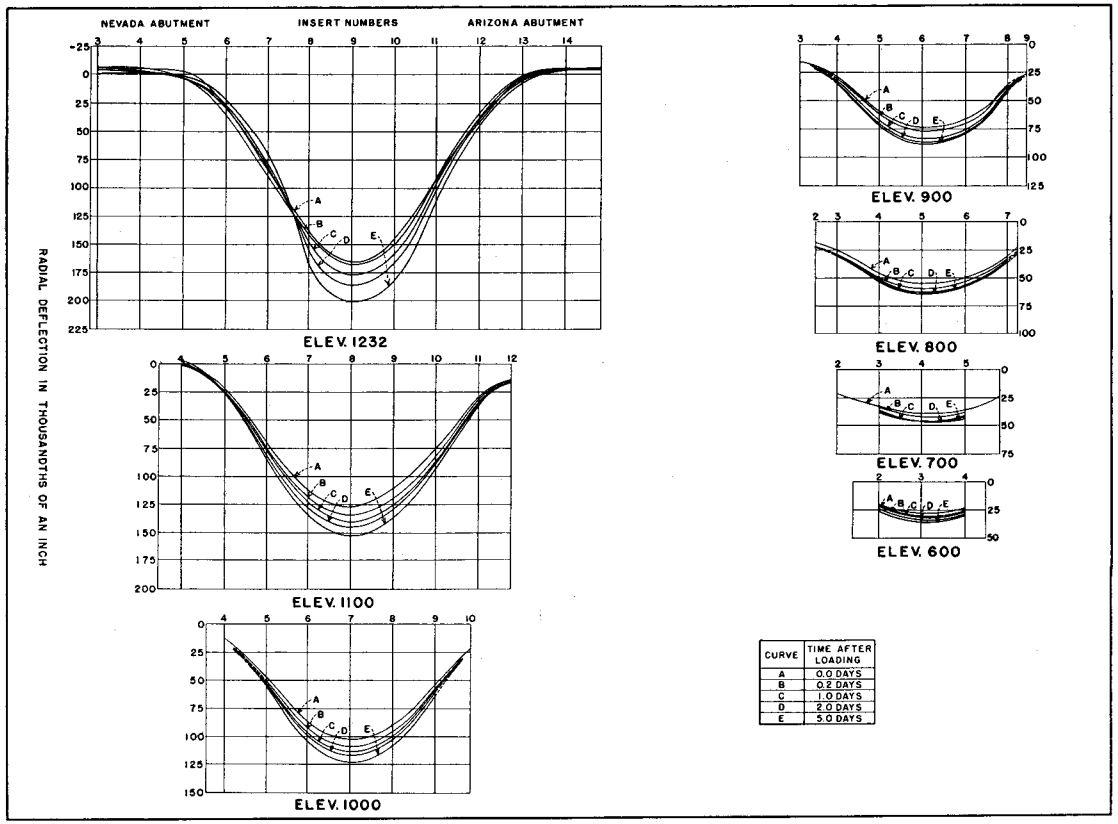

FIGURE 227—RADIAL ARCH DEFLECTIONS DUE TO FLOW

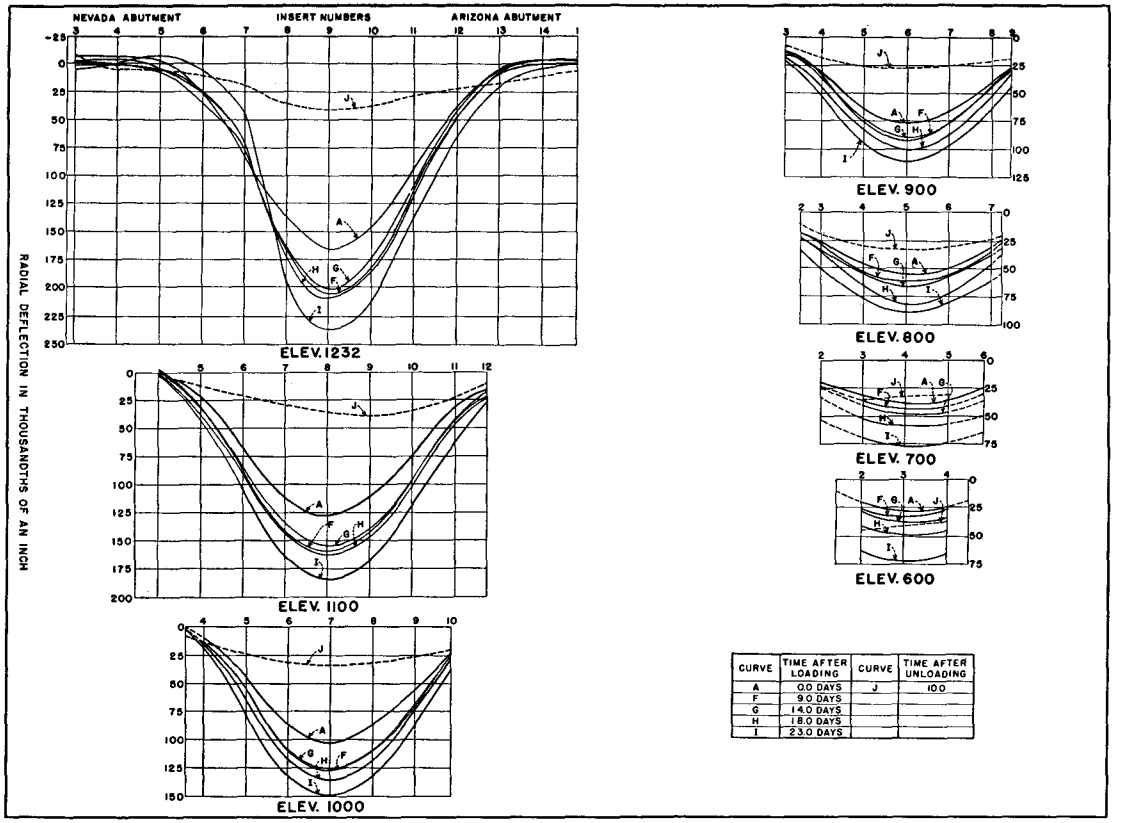

FIGURE 228—RADIAL ARCH DEFLECTIONS DUE TO FLOW AND RECOVERY

was less than the minor fluctuations caused by temperature changes. The results of observation G, made on the fourteenth day of the test, were assumed to represent flow. The results of the later observations were complicated by the failure of the rubber cement at elevation 580.

The radial deflection due to flow was consistent above elevation 700. It varied from 20.0 per cent at elevation 800 to 23.1 per cent at elevation 700. At elevation 600, the flow amounted to 35.6 per cent of the original radial deflection. This was rather large compared with the flow at higher elevations, and may have been due to the beginning of failure at elevation 580.

The effect of the failure of the joint was to increase the flexibility of the structure. At elevation 1232 the initial deflection at the crown of the arch was 0.166 inches. At the end of 14 days, flow increased this deflection to 0.202 inches. At the end of 23 days, the combined effects of the open joint and flow increased the deflection to 0.238 inches. At elevation 600, the effect was relatively greater. The initial deflection was 0.028 inches; at the end of fourteen days, the deflection was 0.038 inches; and at the end of 23 days it had increased to 0.073 inches.

At the end of the twenty-third day, the model was unloaded and allowed to recover. For 1.5 days after unloading, the model recovered rapidly. After that it became practically stationary. Observations made ten days after unloading showed that the model lacked 0.027 to 0.041 inches from recovering to its initial position. The deflection curves, designated by J in figure 228, show the final position of the model on the completion of the test.

216. Condition of Model.—After the model had been unloaded for two weeks, a radial deflection test was made to determine the effect of the open joint on the action of the model. The results of the test are shown in figure 229, where radial deflections after failure of the joint are compared with those obtained from previous tests. The differences between the two sets of deflections were relatively small. During the two weeks that the model remained idle, the weight of the material caused the joint to close and the rubber cement apparently reunited the two layers. In the investigation of properties of various brands of rubber cements, it was found that the cement used in building the model would allow surfaces to readhere after being torn apart, if no dust or dirt entered the joint while it was open. In the case of the torn joint, the upstream edge was covered with an uncured sheet of crude rubber which prevented the entrance of foreign

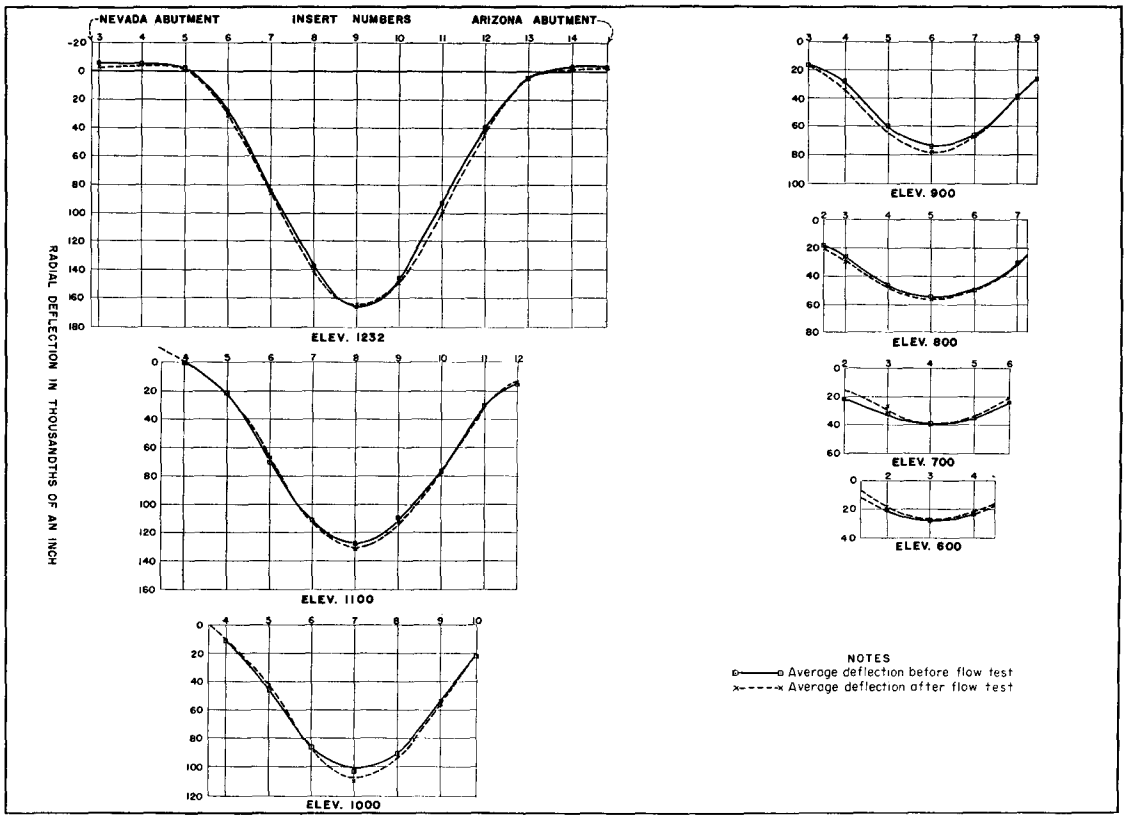

FIGURE 229—RADIAL ARCH DEFLECTIONS BEFORE AND AFTER FLOW TEST

matter, so that the conditions for readhesion were ideal. The torn joint developed sufficient strength after the idle period to permit the application of full load without causing much change from previously measured deflections.

TEMPERATURE TEST

217. Purpose of Test.—Temperature changes in arch dams produce deformations and stresses which may be of considerable magnitude. Temperature changes occur in a dam with the reservoir empty, partially full, or full. If the reservoir is empty, both faces of the dam are exposed to atmospheric temperature changes. If the reservoir is full, the upstream face is subject to water temperature changes, while the downstream face is subject to atmospheric temperature changes. In investigating temperature effects in arch dams by means of models, tests had been made on the concrete model of Gibson Dam[17] and the plaster-celite model of Boulder Dam. In both tests, effects of a decrease and an increase of temperature on unloaded models were investigated. When cold water is impounded behind a dam which is relatively warm, the upstream face cools rapidly while the downstream face remains at nearly constant temperature for a period of time depending on the thickness of the cross-section. This condition, which causes shrinkage at the upstream face, was investigated in the temperature test of the rubber-litharge model.

218. Procedure.—The procedure adopted for the temperature test was as follows:

1. The model was brought to stable conditions of temperature and radial movement by allowing it to remain unloaded in a room of fairly uniform temperature for a period of ten days.

2. The reservoir was filled with water at air temperature and a complete set of temperature and radial deflection measurements made.

3. The temperature of the reservoir water was lowered by adding chipped ice and the deflection and temperature conditions of the model observed at convenient intervals until stable conditions were reached.

---

[17] "Arch Dam Investigation, Report by Committee," Vol. II, pp. 292-325, Engineering Foundation, May, 1934.

4. The model was returned to its original temperature by adding warm water to the reservoir.

5. The reservoir was drained and the model allowed to return to its original position as it recovered from the deformation due to load and flow.

During the construction of the model, thermocouples had been placed at the locations shown in figure 230. Apparatus for obtaining temperature readings from thermocouples was the same as in the temperature tests of the plaster-celite model.

Stable conditions were reached at 10:00 a. m., November 27, 1933. The reservoir was filled with water at air temperature and observations for temperature and deflection made. Ice was added to the reservoir water and observations repeated at intervals of approximately three hours for four days, when stationary conditions of temperature and deflection were again reached. The ice was removed from the reservoir and warm water added until the temperature of the water had returned to normal. Observations for temperature and deflection were continued for eight days. At the end of this period, the temperature of the model was approximately the same as the initial temperature. The reservoir was drained and observations for deflections continued during a six-day period. At the end of this time the model had recovered from flow due to water load until it was almost at its initial position. The observations were then terminated.

219. Initial Temperature Conditions.—All temperatures in the test are expressed in degrees Fahrenheit. Temperatures existing in the model at the beginning of the test varied from 68.0 to 69.9 degrees, see table 14. The minimum occurred at elevation 505, at thermocouple 3, located 12.8 inches from the upstream face. The maximum occurred at elevation 505 at thermocouple 2, 14.5 inches from the downstream face; also at elevation 1125 at thermocouples 16, 17, and 19. The model was slightly cooler below elevation 700 than in the thinner portions of the model above that elevation.

220. Conditions at End of One Day.—At the end of one day with ice in the reservoir, the temperature of the model had been lowered considerably, as shown in the third column of table 14. The temperature of the upper part of the model had been reduced about twenty degrees. Near the upstream face, at elevation 600, a temperature change of about 10 degrees was found. In the central part of the

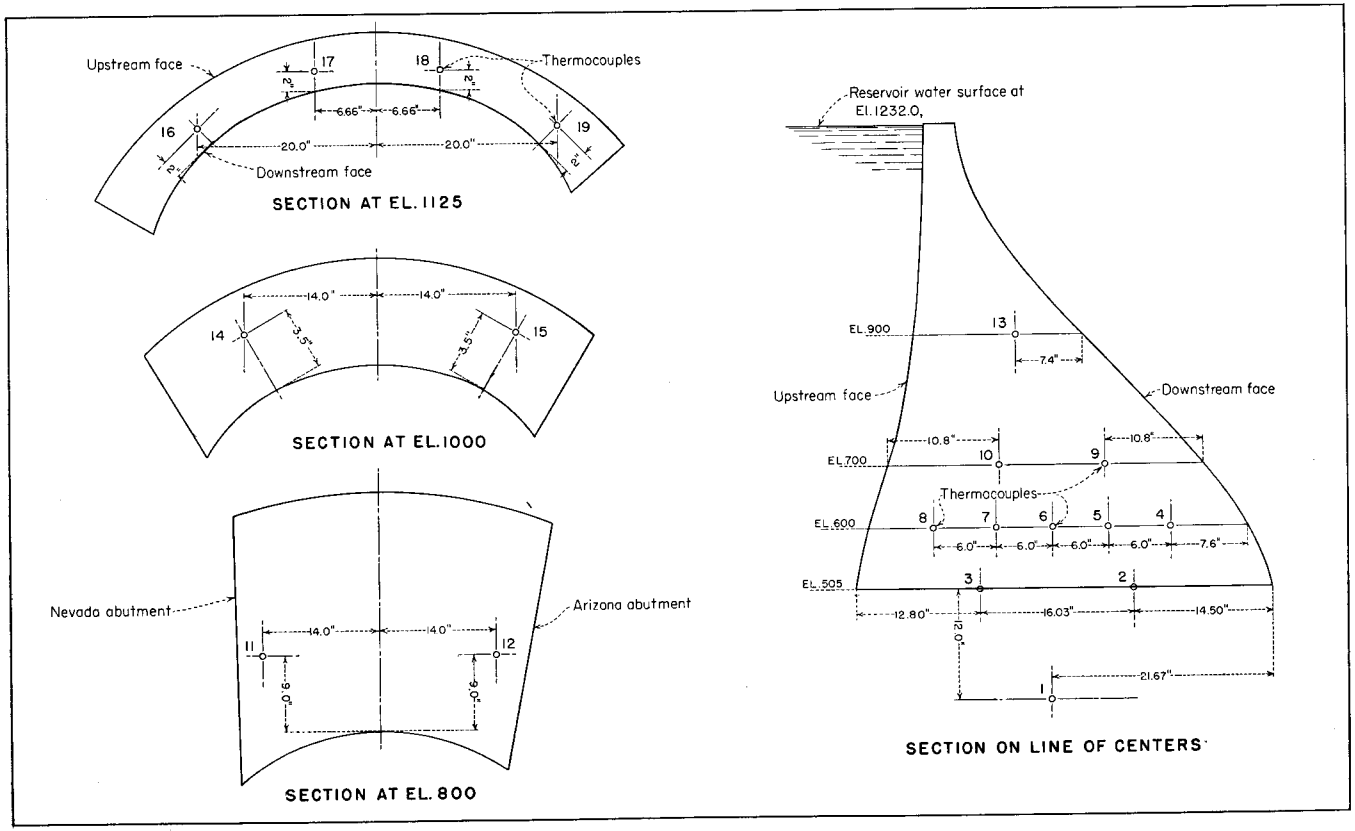

FIGURE 230—LOCATIONS OF THERMOCOUPLES

TABLE 14—TEMPERATURES IN MODEL

Thermocouple No.	Initial Temperature Deg. F.	Temperature at End of			
		1st day	2nd day	4th day	12th day
2	69.9	67.3	68.5	68.5	67.3
3	68.0	66.7	64.5	61.4	65.5
4	68.1	67.5	66.3	63.5	66.1
5	68.4	67.5	67.4	64.8	65.7
6	68.4	68.1	66.6	63.2	65.7
7	68.2	66.0	63.2	58.3	65.9
8	68.2	59.0	55.3	51.7	66.3
9	68.8	68.0	66.1	61.2	66.1
10	69.1	64.6	59.7	55.1	66.6
11	68.8	67.6	64.2	59.2	66.7
12	69.1	66.8	63.8	57.8	66.2
13	69.5	65.6	57.8	53.4	68.2
14	69.5	51.5	47.9	47.2	68.7
15	69.5	50.7	47.2	45.5	68.7
16	69.9	52.8	50.7	48.9	68.2
17	69.9	48.0	47.0	45.6	68.0
18	69.5	47.4	46.6	45.2	68.2
19	69.9	50.6	49.0	46.3	68.3

model and near the downstream face, there was less change in temperature.

The effect of cooling the material in the upper part of the model and at the entire upstream face was to deflect the model upstream. Radial deflections of the arch elements at the beginning of the test and at the end of one day are shown in figure 231. At insert 9, elevation 1232, the initial radial deflection was 0.166 inches. Cooling the model for one day reduced this deflection to 0.097 inches. At the abutments, a similar upstream movement was noted. At insert 5, elevation 1232, the deflection changed from —0.002 inches to —0.028 inches; and at insert 13 at the opposite end of the arch element, the change in deflection was from 0.007 inches to —0.045 inches. At lower elevations, deflections were less but a general upstream movement was observed.

Cantilever deflection curves in figure 232 show a pronounced upstream movement at the top. Vertical shrinkage of the cantilever, causing upstream movement, was more effective than the horizontal shrinkage of the arches, which normally causes downstream move-

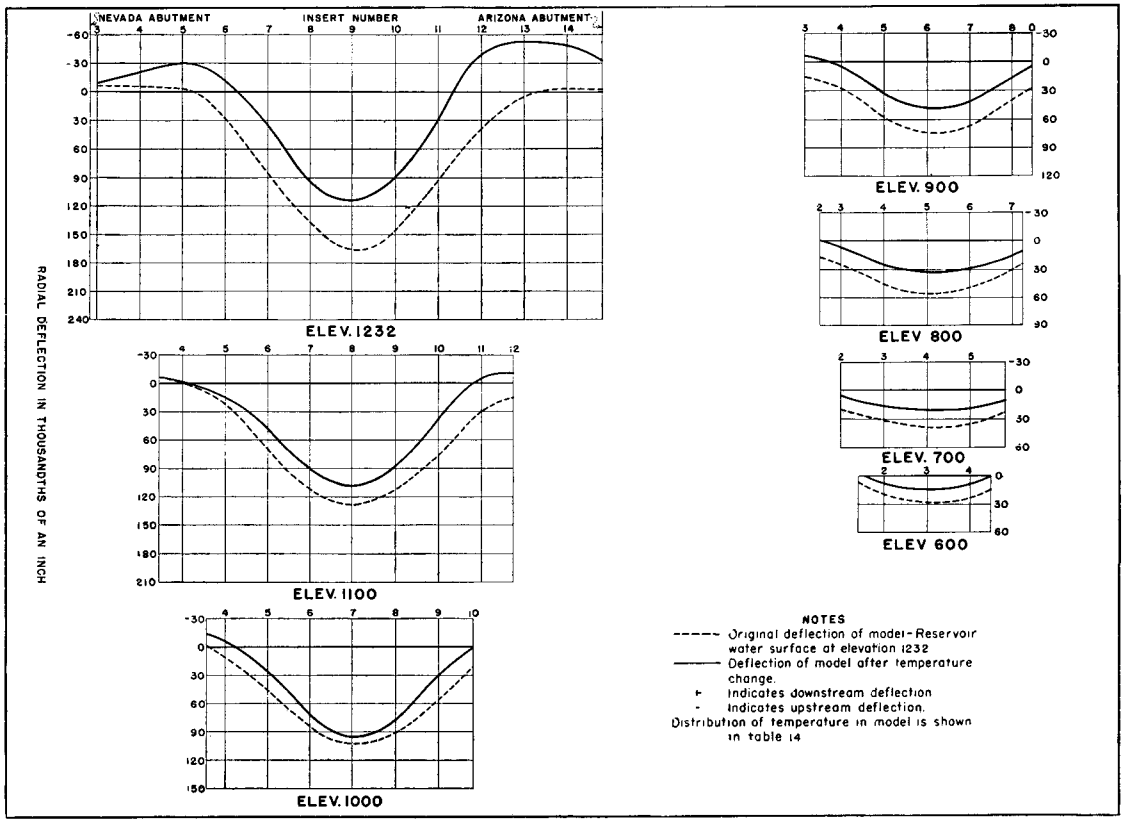

FIGURE 231—RADIAL DEFLECTIONS OF ARCHES AT END OF ONE DAY

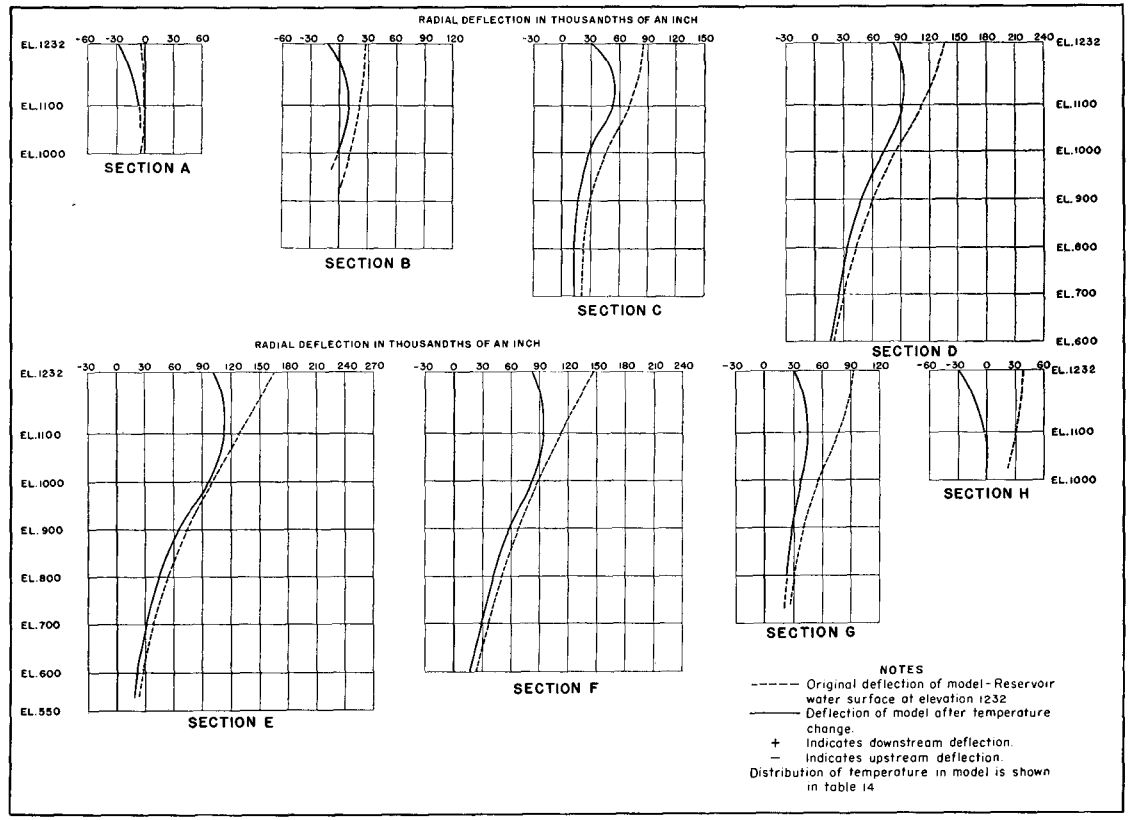

FIGURE 232—RADIAL DEFLECTIONS OF CANTILEVERS AT END OF ONE DAY

ment. The upstream movement of the lower portion of the cantilevers was fairly uniform.

221. Conditions at End of Two Days.—Temperatures existing in the model at the end of two days are shown in the fourth column of table 14. At elevation 1125 the average temperature was 48.3 degrees, a decrease of 21.5 degrees from the initial temperature. A general decrease in temperature had occurred in the upstream half of the model below elevation 900. At the base of the section on line of centers, the temperature was 64.5 degrees at thermocouple 3, a decrease of 3.5 degrees.

At that time, flow of the rubber-litharge material was beginning to affect the deflection of the model. A slight increase in radial deflection occurred at the crown section of the arch element at elevation 1232, as shown in figure 233. Below elevation 1000 the arch elements continued to deflect upstream as the decreasing temperature caused the model to shrink.

Deflections of the cantilever elements at the end of two days are shown in figure 234. The effect of vertical shrinkage of the upstream face was similar to that of the first day of observation.

222. Conditions at End of Four Days.—The temperature distribution in the model at the end of the fourth day is shown in the fifth column of table 14. At that time, model temperatures had become almost stationary. Since the minimum temperature of the reservoir water was 32 degrees, further cooling of the model was impossible. At elevation 1125, the average temperature was 44.5 degrees, a decrease of 25.3 degrees from the initial temperature. Temperatures of about fifty degrees existed in the lower part of the model near the upstream face. At elevation 505, the temperature at thermocouple 2, located 14.5 inches from the downstream face, was 68.5 degrees, a decrease of 1.4 degrees from the initial temperature of the test.

Radial deflections of the arch elements are shown in figure 235. Above elevation 900, deflections continued to increase due to flow of the rubber-litharge compound. At elevations 1000 and 1100, crown deflections were almost the same as the initial deflections; but along the abutments there was some variation. At elevations 600 and 700, deflections continued to decrease due to shrinkage.

Deflections of the cantilever elements are shown in figure 236. Temperatures at thermocouples 13, 14, and 15 indicated that cooling had become effective at the downstream face. The resulting shrinkage

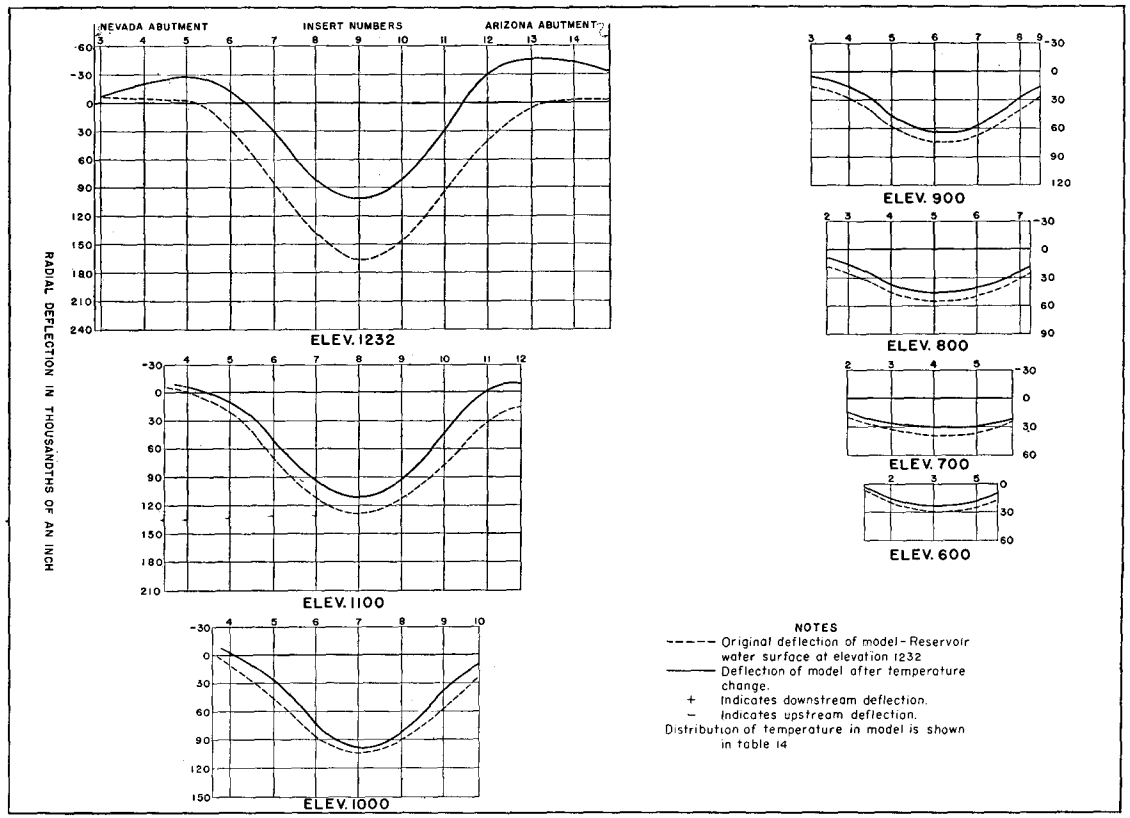

FIGURE 233—RADIAL DEFLECTIONS OF ARCHES, END OF TWO DAYS

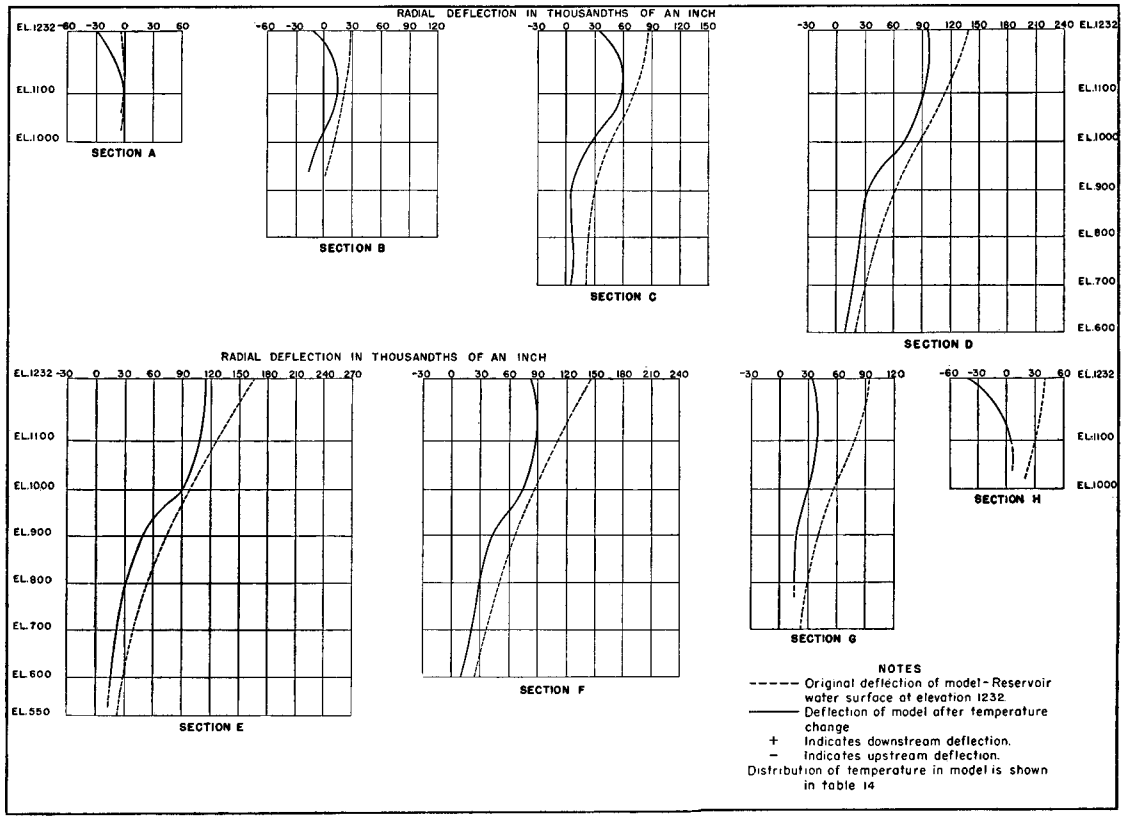

FIGURE 234—RADIAL DEFLECTIONS OF CANTILEVERS, END OF TWO DAYS

caused downstream deflections at elevations 1000 and 1100 in cantilevers D and E. Deflections at sections A and H showed the effect of abutment deformation.

At that time the model had become practically stationary in temperature distribution and position. A very slow increase in deflection was occurring due to flow. As there was no possibility of obtaining greater deformation with reservoir water having a temperature of 32 degrees, the ice was removed and warm water added until the reservoir temperature reached 68 degrees.

223. Conditions at End of Twelve Days.—At the end of twelve days the temperature of the model had risen until it was within about two degrees of the original temperature. Observed temperatures at that time are shown in the last column of table 14. The greatest variation from the original temperature occurred between elevations 600 and 700, where an average temperature of 66 degrees existed, 2.2 degrees lower than the initial temperature.

Deflections of the arch elements at the end of twelve days are shown in figure 237. At elevation 600 the deflection was slightly less than the initial deflection. This was to be expected as the temperature of the model was less than the initial temperature at that elevation. At elevation 700 the deflection was almost the same as the initial deflection. Above elevation 700, a general decrease in deflection occurred. The difference in deflection in the upper part of the model was largely due to flow. The maximum deflection at the top of the model was 0.202 inches. In the flow test the corresponding deflection, after being unloaded for 12 days, was 0.205 inches. The close agreement of these two deflections indicated that the joint which was torn apart during the flow test had knit together satisfactorily.

The reservoir was drained and the model allowed to recover. Observations for temperature and deflection were continued for four days. At the end of that period the average temperature was 68 degrees, which lacked one degree of being the initial temperature. The corresponding deflections are shown in figure 238. The recovery from the flow at the end of four days was very good, since the position of the model was almost the same as the initial position before filling the reservoir.

224. Conclusions.—The results of the temperature test indicate that the effect of cooling the upstream face of an arch dam is to cause an upstream deflection. If the reservoir is full at the time of

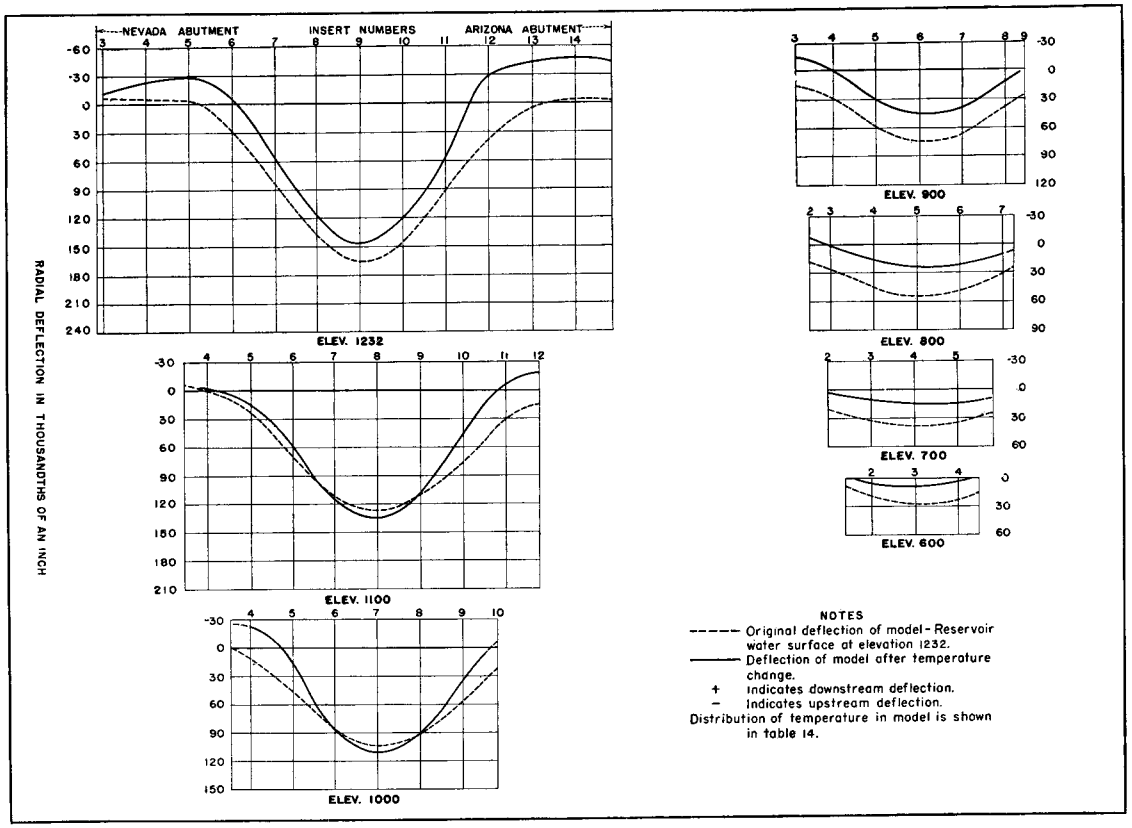

FIGURE 235—RADIAL DEFLECTIONS OF ARCHES AT END OF FOUR DAYS

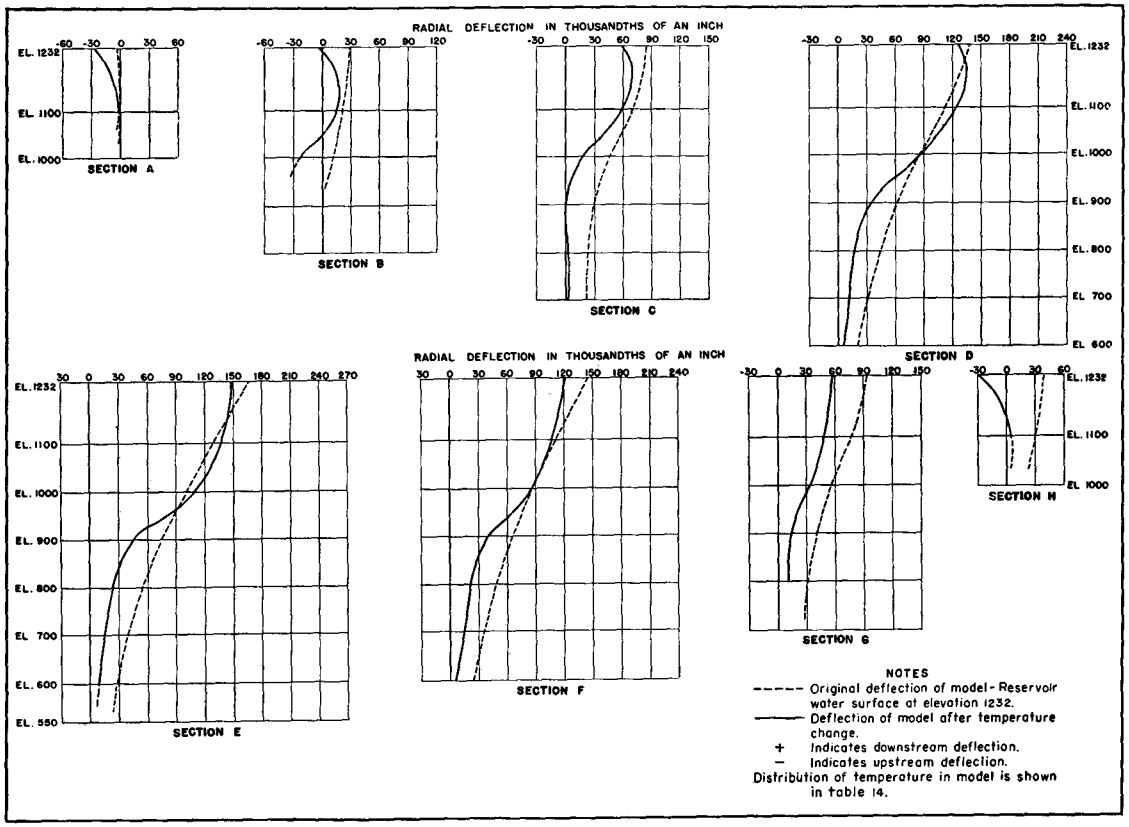

FIGURE 236—RADIAL DEFLECTIONS OF CANTILEVERS AT END OF FOUR DAYS

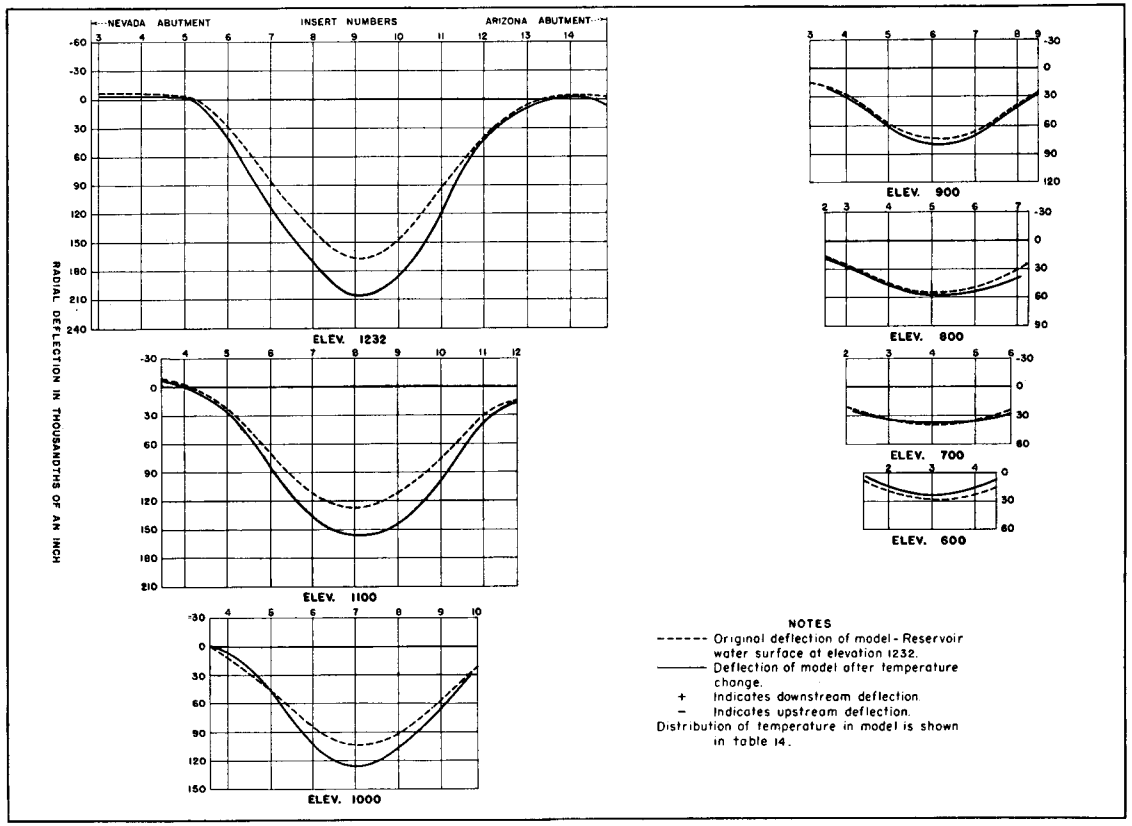

FIGURE 237—RADIAL DEFLECTIONS OF ARCHES AT END OF TWELVE DAYS

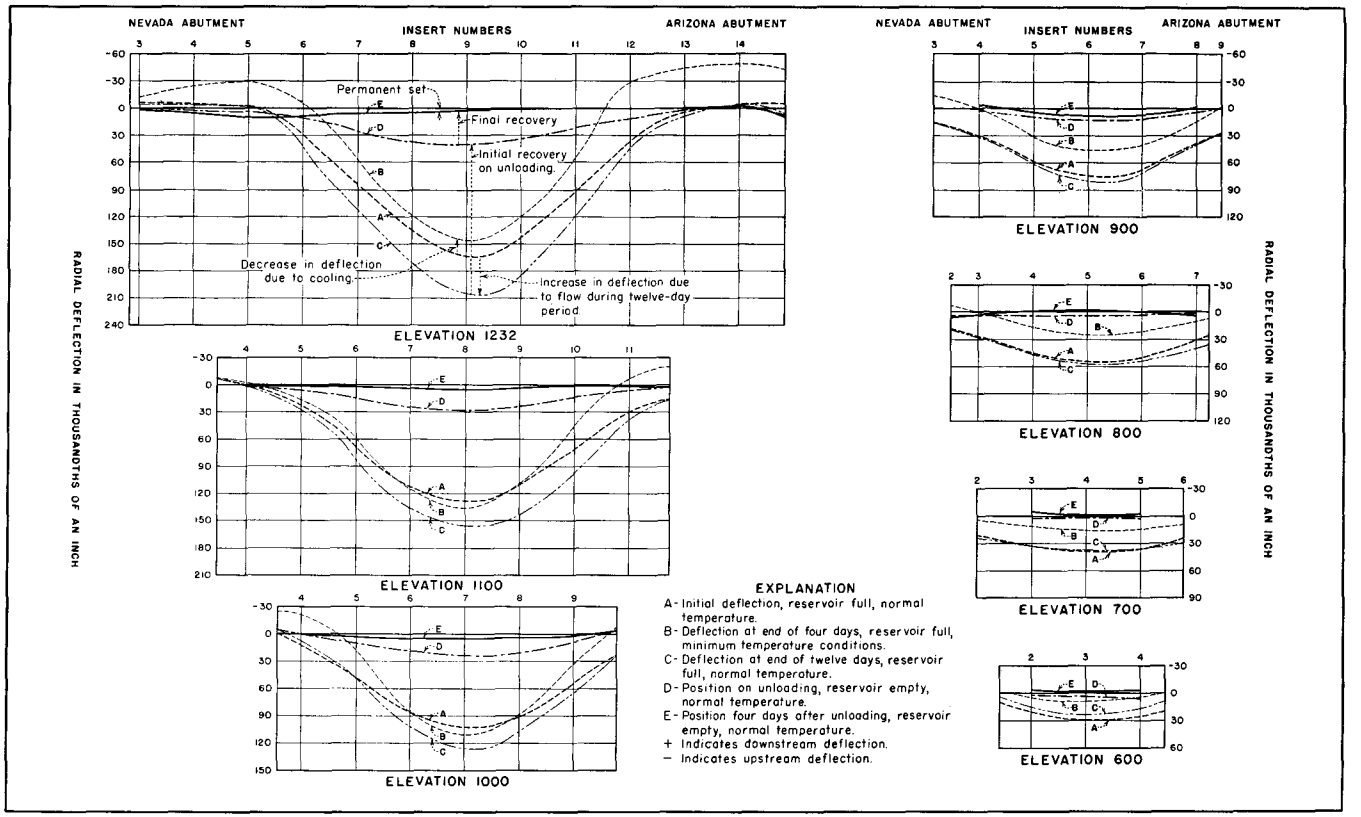

FIGURE 238—DEFLECTIONS SHOWING RECOVERY FROM TEMPERATURE TEST

cooling, a general reduction of the maximum deflection occurs. This is opposite from the effect of a uniform cooling of an arch dam which results in a downstream deflection. The difference is due largely to the vertical shrinkage of the upstream face of the cantilevers. The large upstream movement near the abutments, as shown on the arch deflection curves, indicates that shrinkage of the canyon walls may have been responsible for a portion of the upstream movement. The canyon walls, being continuous with the model and exposed to the same reservoir temperature conditions, tended to pull the model upstream.

CHAPTER XIII—TRIAL LOAD ANALYSIS OF RUBBER-LITHARGE MODEL

225. General.—A brief description of the trial load method was given in chapter VII, in discussing the analysis of the plaster-celite model. This chapter presents the application of the method to the rubber-litharge model with certain additions required to fit the peculiar properties of the model material. The most important additional consideration was the vertical movement, a feature not required in previous analyses.

Similar to the plaster-celite model analysis, seven sample arches and nine cantilevers were selected for consideration as representative structural elements. Elastic properties, determined in the materials investigations, were used with proper consideration of the differences in vertical and horizontal planes.

PROCEDURE

226. Data and Assumptions.—The principal items of structural data, together with the assumptions made for the purpose of the analysis, are listed as follows:

1. Scale of model, 1 to 180.
2. Reservoir water surface at elevation 1232.
3. Unit weight of water, 62.5 pounds per cubic foot.
4. Unit weight of rubber-litharge material, 150 pounds per cubic foot.
5. Average modulus of elasticity of rubber-litharge material for tension and compression in the cantilevers, 343 pounds per square inch.
6. Average modulus of elasticity of rubber-litharge material for tension and compression in the arches, 389 pounds per square inch.
7. Average modulus of elasticity of rubber-litharge material for shear in the cantilevers, 114.33 pounds per square inch.

8. Average modulus of elasticity of rubber-litharge material for shear in the arches, 129.67 pounds per square inch.

9. Average value of Poisson's ratio, 0.5.

10. Normal arch and cantilever stresses vary as a straight line from the upstream to the downstream face of the model.

11. Foundation movements made to conform to the model measurements.

12. The concrete pit assumed to be rigid.

13. The rubber-litharge material assumed to remain in contact with the concrete of the testing pit at all locations.

Note that values of the shearing modulus of elasticity for arches and cantilevers are slightly different from experimentally determined values. It was necessary to use the above values in order to maintain mathematical compatibility in the stress-strain relations.

227. Cantilever Elements.—Vertical cantilever elements were assumed to be one inch wide at the axis of the dam and to have radial sides, converging from the upstream face to the downstream face. The cantilevers were elastic units, set on elastic bases. They resisted radial forces applied at the upstream faces, tangential and vertical forces applied at the center lines, and horizontal and vertical moments applied at the center lines. Tabulations of unit radial, tangential, and twist loads were made for cantilever elements as described in section 132. Equal and opposite sets of vertical forces acting on arches and cantilevers were required to make vertical arch movements agree with vertical cantilever movements. In these considerations it was found convenient to use triangular loads at the center lines.

Figure 239 shows a plan of the arches and cantilevers used in the analysis. Due to changes in direction of radial lines at different elevations, the cantilevers were warped slightly. Consequently, radial cantilever loads caused not only radial deflections but also slight tangential, angular, and vertical movements.

Figure 151, chapter VII, shows typical unit radial, tangential, and twist loads applied to the cantilever of the plaster-celite model. Figure 240-a shows the additional unit vertical loads applied to the cantilevers of the rubber-litharge model.

228. Arch Elements.—The horizontal arch elements shown on figure 239 were assumed to be one inch high and to have horizontal

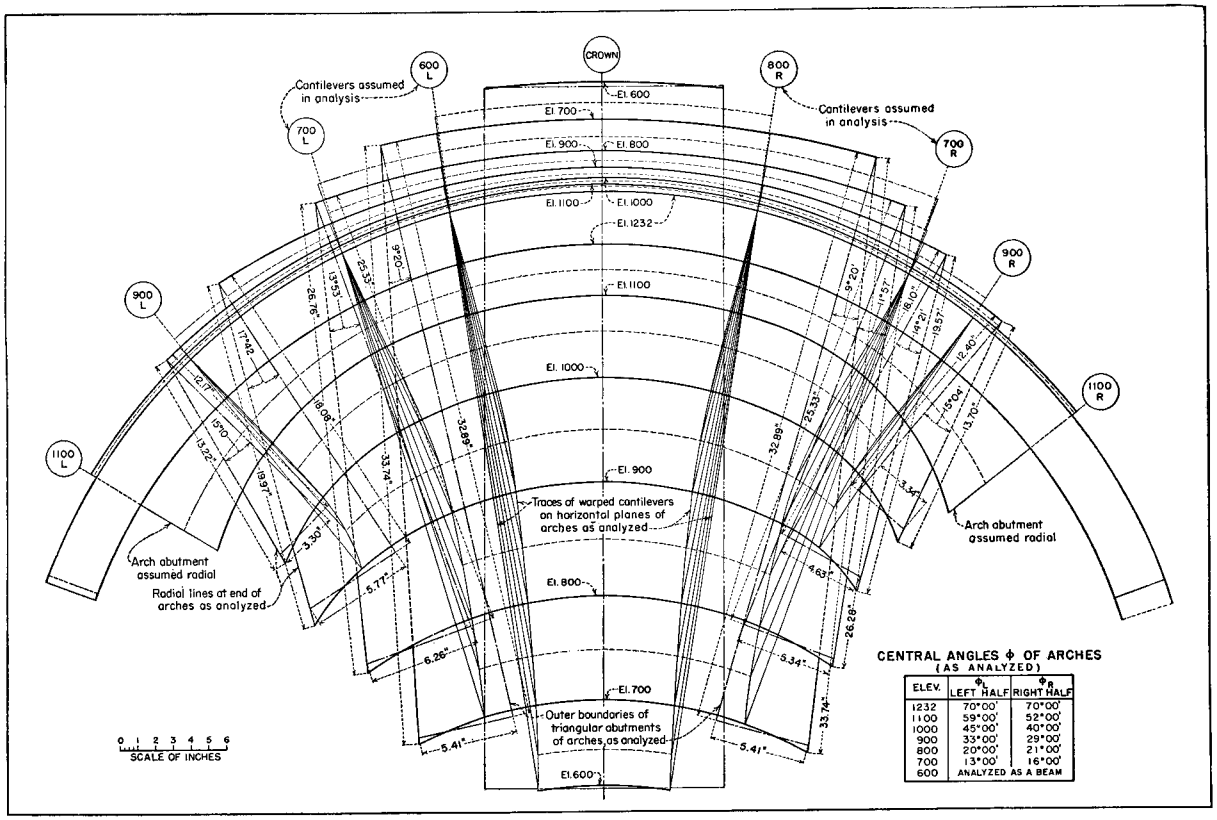

FIGURE 239—PLAN OF MODEL SHOWING ARCHES AND CANTILEVERS

top and bottom faces. The extrados of each arch was circular. The intrados followed a three-centered curve in which the central part had the same center as the extrados. The abutments of the arches were radial at the top elevations and gradually changed to lines that were closely parallel to the canyon walls at the lower elevations. The abutment lines of the arches, as they were constructed and analyzed, are shown on figure 239. At elevation 600, the arch was shaped more like a rectangle than an arch, so it was analyzed as a rectangular beam.

Calculations for arch elements considered effects of irregular abutments, thickening of arches due to fillets, and lack of symmetry between the crown cantilever and the arch crowns. Calculations of

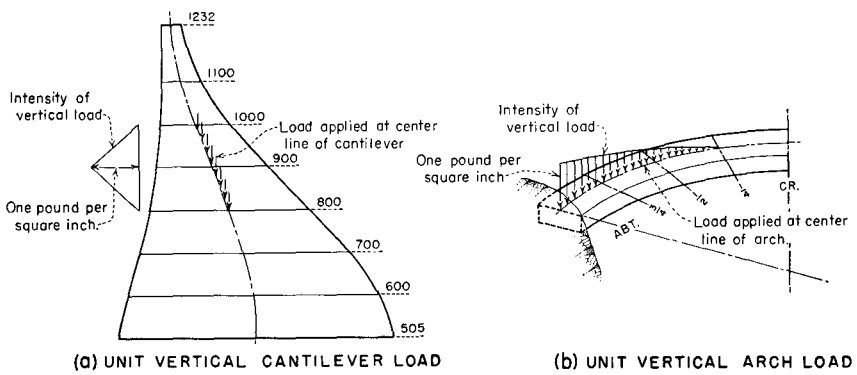

FIGURE 240—UNIT VERTICAL LOADS

deflections caused by unit radial, tangential, and twist loads were made in the same manner as described in section 133, chapter VII. These unit loads are shown in figure 152.

Besides the radial, tangential, and twist loads, vertical loads were required to make the vertical arch deflections agree with the vertical cantilever deflections. The required unit loads included a uniform load of one pound per square inch vertical shear, and triangular loads which varied from one pound per square inch vertical shear at the abutment to zero shear at the different arch quarter points, as shown on figure 240-b. Other features of the arch calculations were the same as described in section 133.

ADJUSTMENTS

229. Radial Adjustment.—The radial adjustment was the first step in the analysis. Figure 241 shows the final adjustment for the arch elements, including the division of water load as well as the adjusted deflections of the arches and cantilevers. The initial positions indicated on the drawings are the developed center lines of the arches. Locations of arch quarter points and intersections of the cantilevers with the arch center lines are also indicated on the diagrams. Deflections were measured from these points.

The horizontal component of the water load was divided into two parts, both radial, one acting on the arches and the other on the cantilevers. The vertical component of the water load was assigned to the cantilevers, and the resulting cantilever deflections combined with the deflections caused by the horizontal water load assigned to the cantilevers, before adjusting with the arch deflections.

Details of the application of concentrated loads at the abutments to maintain continuity were presented in section 134. Subsequent readjustments of radial deflections were necessary because loads introduced in the tangential, twist, and vertical adjustments, in addition to effects of Poisson's ratio, caused radial arch and cantilever movements. Altogether, thirteen trial adjustments and readjustments were made before arriving at the final loads and deflections shown on figure 241.

The radial adjustment constituted the principal step in the trial load analysis. Although tangential, twist, and vertical adjustments were required, they were of secondary importance compared with the radial adjustment. Radial movements were much greater than tangential, angular, and vertical movements. Poisson's ratio had considerable effect on radial deflections because of its high value.

230. Tangential Adjustment.—After radial deflections due to radial loads were adjusted, tangential movements were considered in the tangential adjustment. Figure 242 shows the initial position and final tangential displacements of arch center lines, also the tangential loads required for the adjustment. Positive tangential loads and movements act toward the right abutment; negative loads and movements act toward the left abutment.

The first stage of the radial adjustment showed that radial arch loads caused larger tangential movements of the arch center lines than radial cantilever loads. Consequently, conjugate points of the

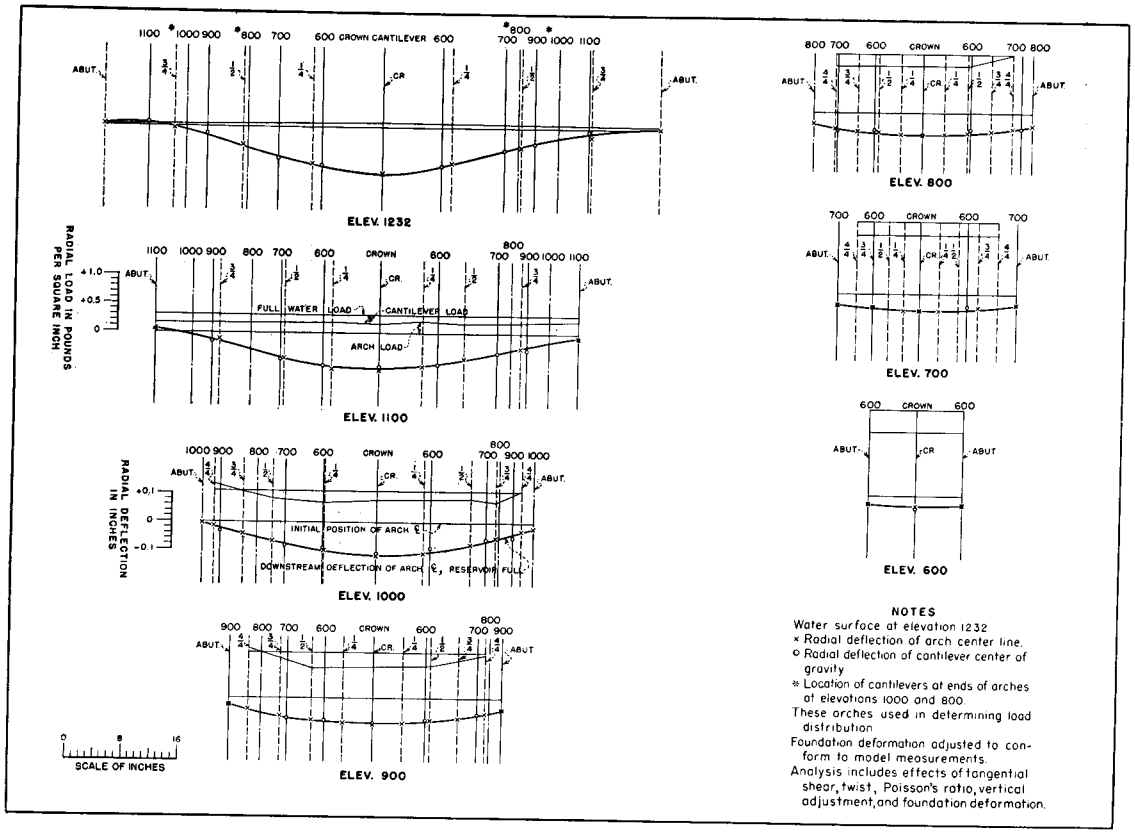

FIGURE 241—FINAL RADIAL ADJUSTMENT AT ARCH ELEMENTS

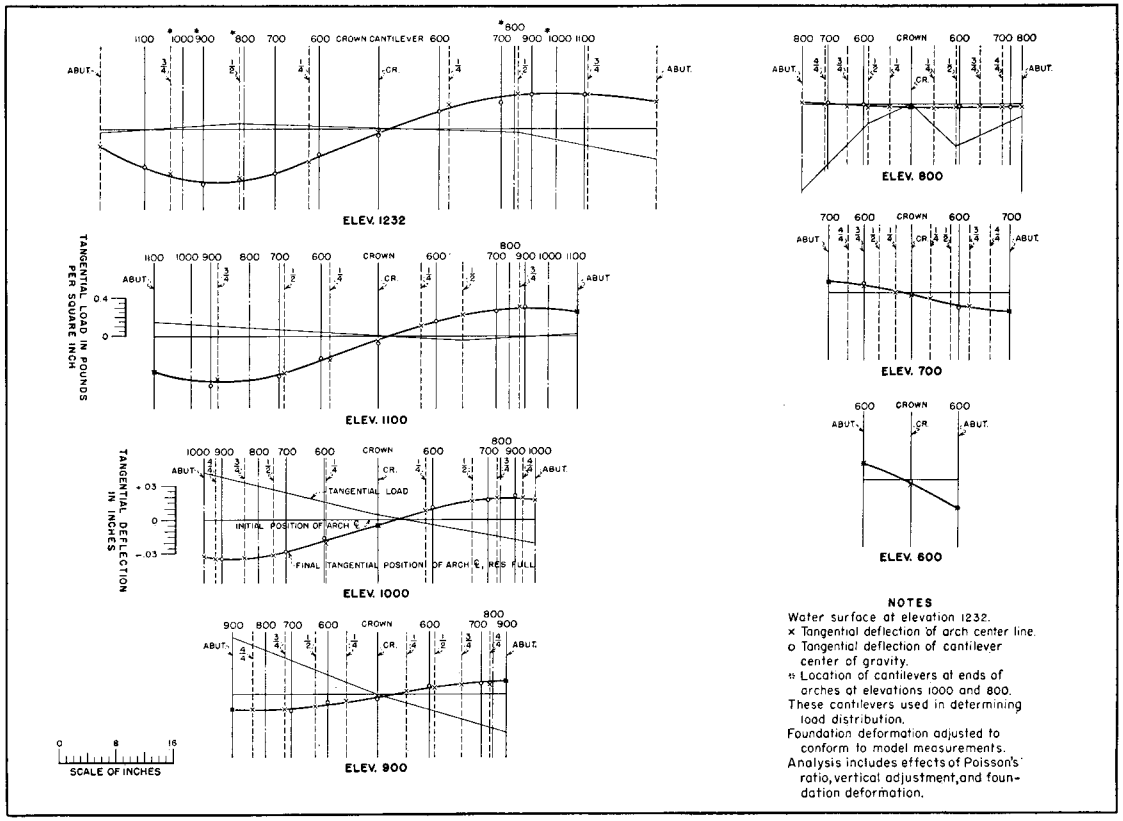

FIGURE 242—FINAL TANGENTIAL ADJUSTMENT AT ARCH ELEMENTS

two systems were out of agreement in tangential directions. For the purpose of simplifying the estimate of tangential loads required to bring arches and cantilevers into agreement, two cantilevers, 700 and 900, were investigated first. Relative tangential deflections of all points were then compared and an estimate made of the additional loads necessary to produce approximately the same deflections at conjugate points. After several trials, close agreement was obtained.

Subsequent readjustments of tangential deflections were required, since twist adjustment loads, radial readjustment loads, vertical loads, and effects of Poisson's ratio produced additional tangential movements. A total of twelve sets of trial tangential loads were required for the first stage and subsequent readjustments to obtain the resulting loads and deflections shown on figure 242.

231. **Twist Adjustment.**—Radial loads on the arches produced angular movements about vertical axes while radial loads on cantilevers produced very little rotation about vertical axes. To bring the conjugate points of the two systems into tangential agreement, further rotations of the arches and cantilevers were introduced. The first trial adjustment was made between the arches and cantilevers 900 and 700. From this adjustment a fairly close estimate was made of the loads required for the remainder of the structure. Since the vertical adjustment, radial and tangential readjustments, and the effects of Poisson's ratio all produced additional angular movements in the arches and cantilevers, subsequent twist readjustments were made to restore angular agreement. Figure 243 shows the loads and movements after the twist readjustments were completed.

232. **Vertical Adjustment.**—Before the rubber-litharge model of Boulder Dam was tested, vertical movements in a dam had not been seriously considered. Since appreciable vertical deflections occurred in the rubber-litharge model, these movements were measured at sufficient points to determine vertical deflection curves. The trial load analysis was, therefore, extended for the purpose of considering vertical loads and deflections.

Results of the vertical adjustment at the arch elements are given in figure 244. The diagrams show initial and final vertical displacements, also vertical loads required for the adjustment. Positive deflections are upward and positive vertical loads act in a downward direction on the arches. Figure 244 shows that the model was deflected vertically in an upward direction, except at elevation 600 where the

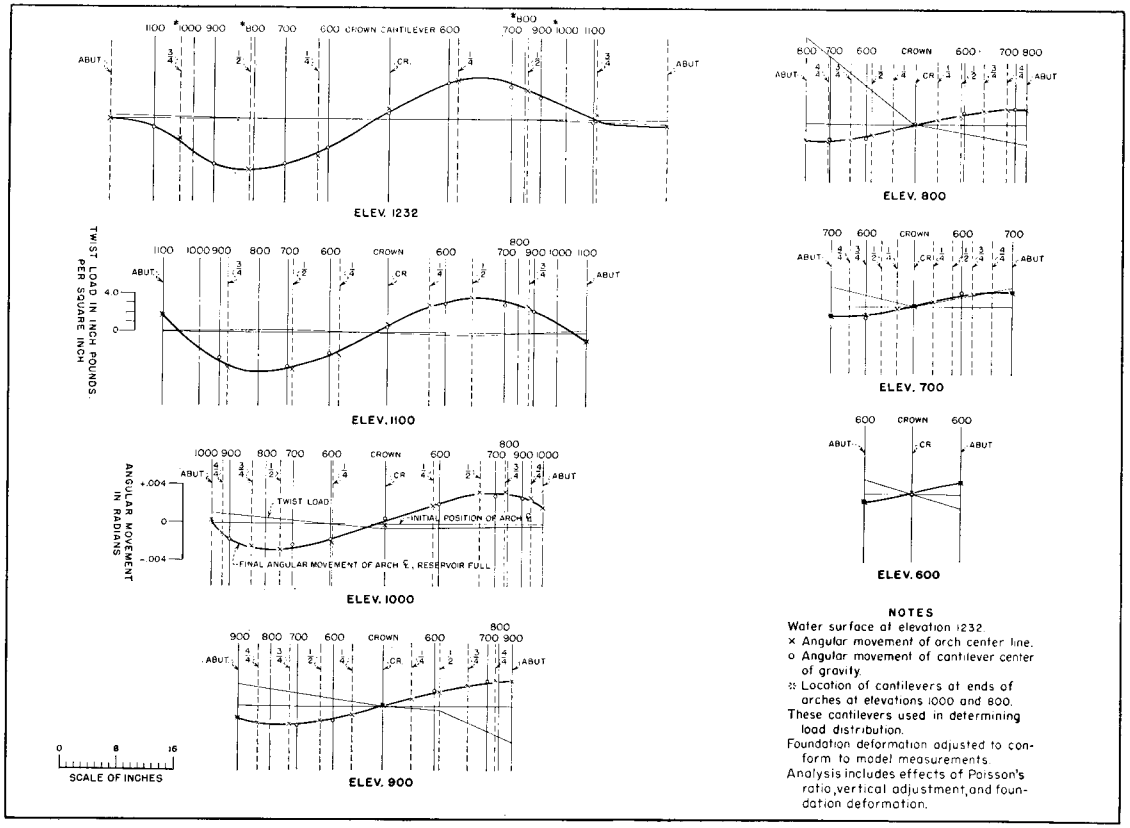

FIGURE 243—FINAL TWIST ADJUSTMENT AT ARCH ELEMENTS

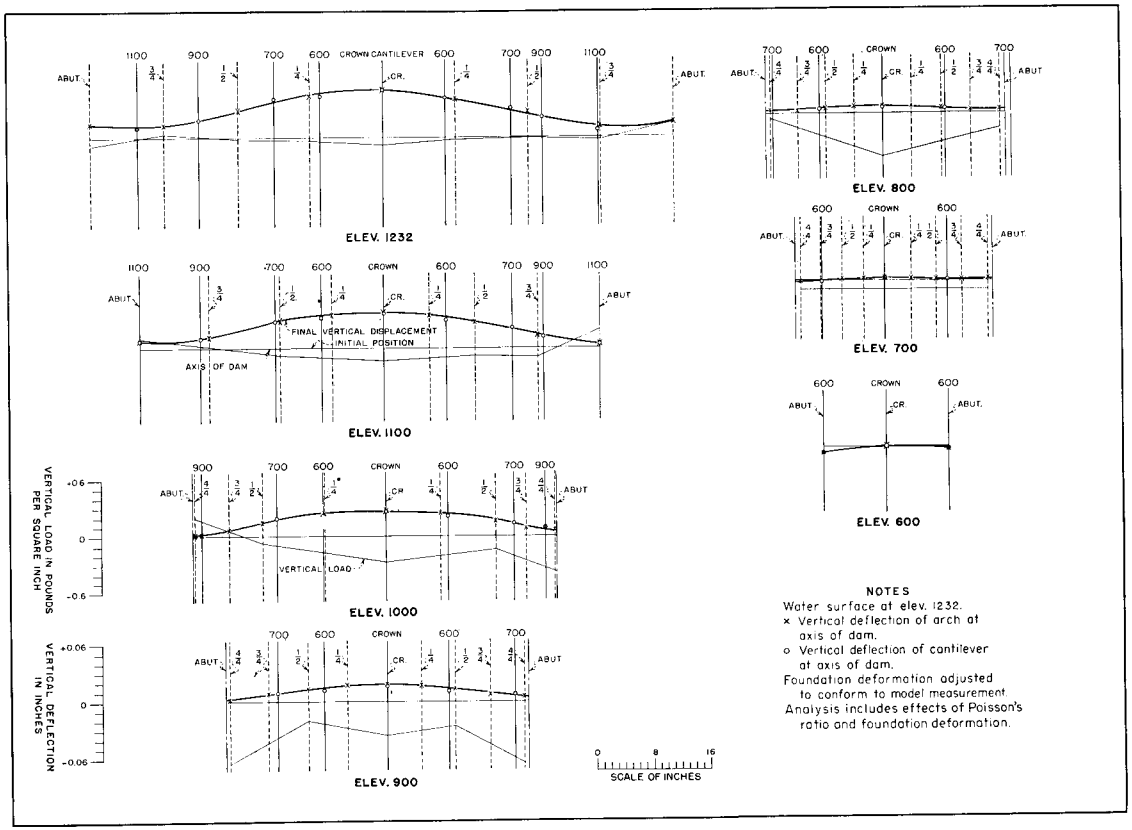

FIGURE 244—FINAL VERTICAL ADJUSTMENT AT ARCH ELEMENTS

deflection was downward. In general, the loads on the arches acted in an upward direction.

An analysis of the effects of radial, tangential, and twist adjustments showed that the arches and cantilevers moved in vertical directions. The major reason for the vertical movements was the effect of Poisson's ratio on the cantilevers. If the cantilever is visualized with the water pressure acting on its upstream face and the arch stresses acting on its sides, it is evident that Poisson's ratio causes vertical movements.

Equal and opposite vertical loads, one set on the arches and the other on the cantilevers, were introduced to remove relative vertical deflections. Required amounts of loads were estimated and gradually adjusted by trial. As in other adjustments, it was expedient to use unit arch and cantilever loads. In the first estimate of vertical loads, crown cantilever deflections were adjusted to the crown deflections of the arches. After the crown cantilever was adjusted, deflections of other arch and cantilever points were computed. All vertical deflections were then compared and additional loads estimated until conjugate points of the two systems were relatively close together. After five successive trials, a satisfactory deflection agreement was obtained, thus completing the first stage of the vertical adjustment.

The vertical loads caused radial, tangential, and angular movements in the arches and cantilevers. These movements were considered in subsequent readjustments. However, it was found that additional radial, tangential, and twist loads, used to correct for movements due to vertical loads, were not of sufficient magnitude to produce significant additional vertical deflections. Therefore, subsequent vertical readjustments were not required. Although vertical deflections were rather large, vertical adjustment loads produced only small radial, tangential, and angular movements. The major effect of vertical loads was to increase cantilever stresses at the upstream face. The loads caused only minor changes in normal arch stresses.

233. Sequence of Adjustments. — Movements not considered prior to the completion of the first stage of the twist adjustment were radial deflections due to tangential and twist loads, and tangential deflections due to twist loads. These radial movements, considered in the first radial readjustment, introduced additional radial loads, causing new tangential and twist movements. Next, the first tangential readjustment was made to correct for discrepancies caused by

twist loads and the first radial readjustment loads. Likewise, a twist readjustment and subsequent radial, tangential, and twist readjustments were required because each readjustment produced movements that had to be considered in the following readjustments. The effects converged rapidly. After a few radial, tangential, and twist readjustments, they became so small that they did not change the other adjustments by appreciable amounts.

The next step in the analysis was to determine the effect of Poisson's ratio in the radial, tangential, and twist adjustments. Poisson's ratio produced movements in the arches and cantilevers. Consequently, additional loads were introduced to restore continuity throughout the structure. The procedure of adjustments and readjustments was the same as described above.

Next, vertical movements due to Poisson's ratio were considered in the vertical adjustment. The resulting vertical loads caused radial, tangential, and angular movements that were considered in subsequent readjustments. However, effects of additional vertical loads were small, and only one set of readjustments was required.

The complete analysis, including all adjustments and readjustments, required thirteen radial, twelve tangential, twelve twist, and five vertical sets of trial loads. These adjustments determined the total movements of the model, also the amount and distribution of the different loads. With this information, arch and cantilever stresses were calculated by the usual stress formulas.

RESULTS OF ANALYSIS

234. Computed Stresses.—Computed arch and cantilever stresses are shown on the developed profile in the upper part of figure 245. Final radial loads and deflections at the assumed cantilever elements are shown in the lower diagrams.

Arch stresses are given for extrados and intrados locations at crown and abutment sections. The maximum compression in the arches occurred at the extrados of the arch at elevation 600 and amounted to 3.15 pounds per square inch. The maximum tension occurred at the extrados at the left abutment of the arch at elevation 1100 and amounted to 1.24 pounds per square inch.

Cantilever stresses are given for upstream and downstream faces at all arch elevations. Cantilever stresses were smaller than arch stresses, because the moments of the vertical and horizontal loads

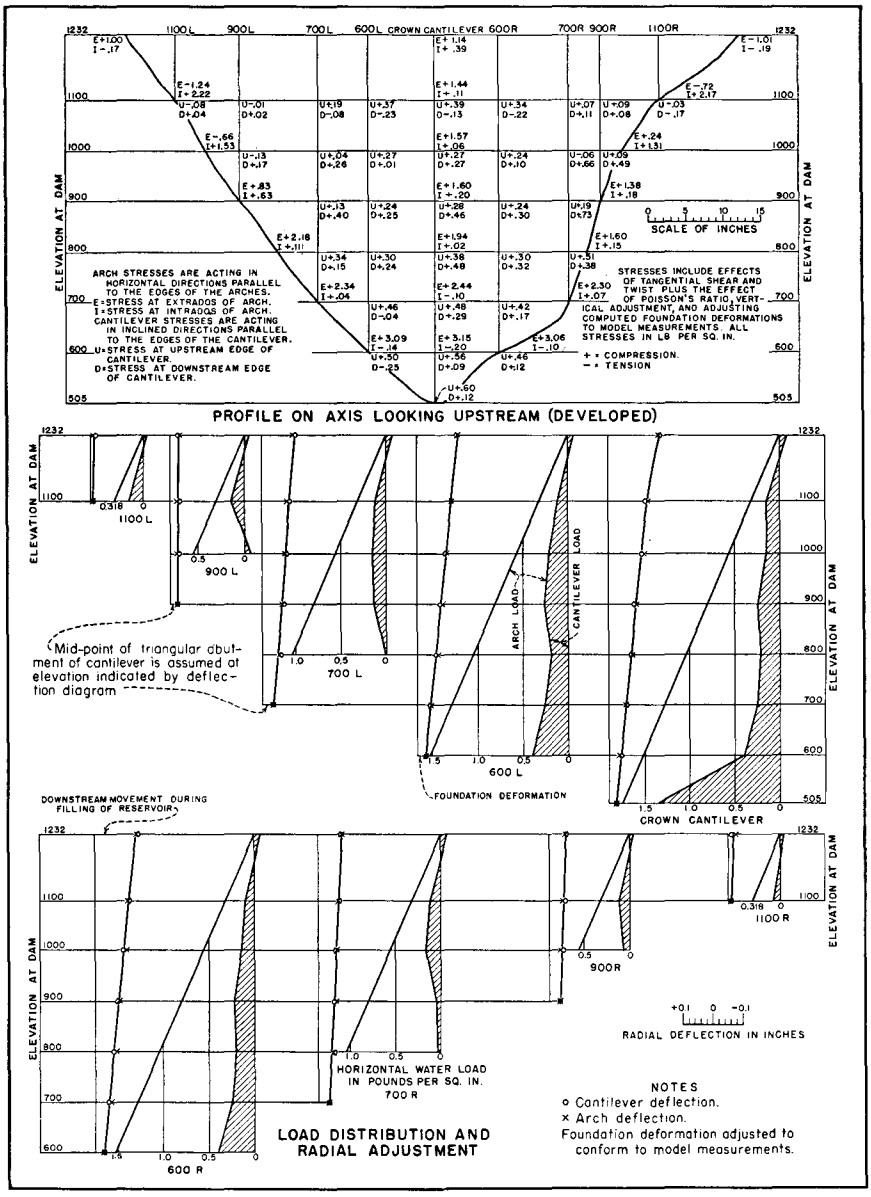

FIGURE 245—RESULTS OF TRIAL LOAD ANALYSIS

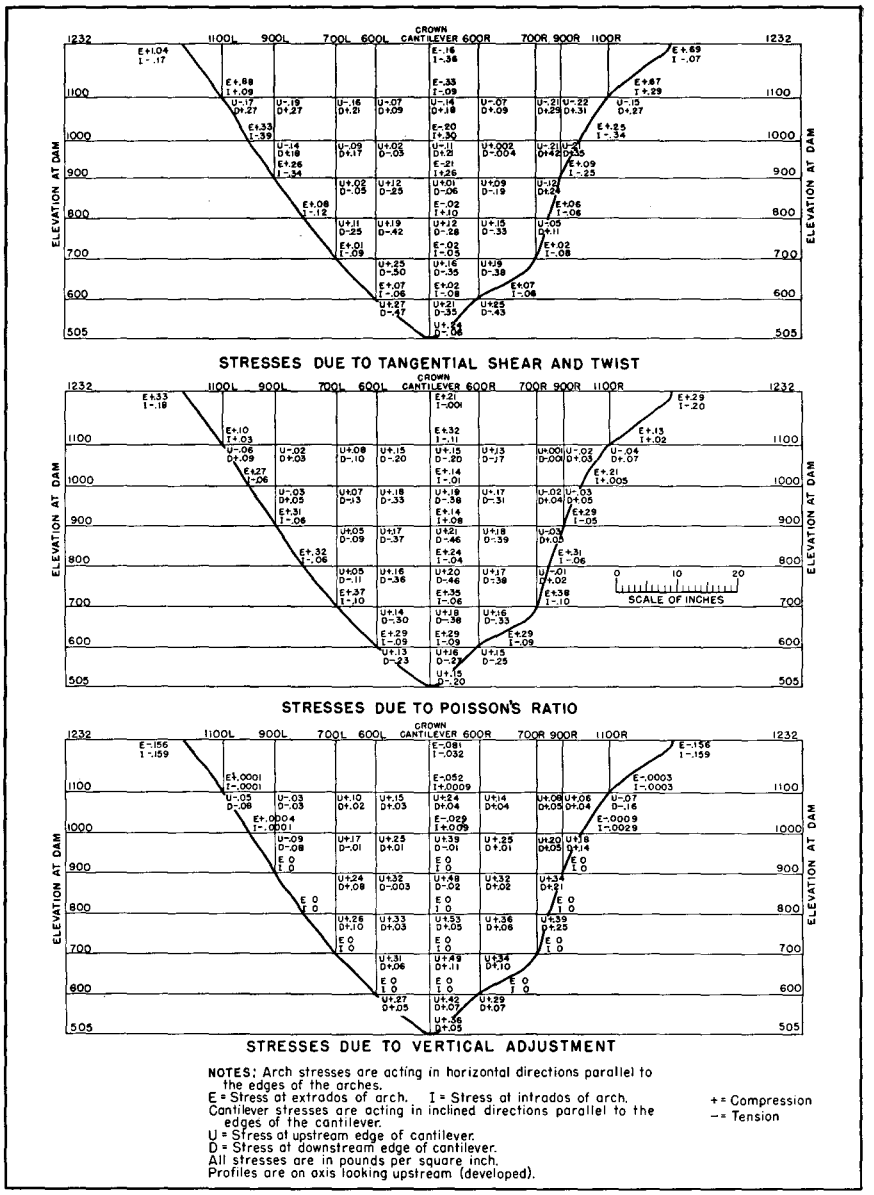

NOTES: Arch stresses are acting in horizontal directions parallel to the edges of the arches.
E = Stress at extrados of arch. I = Stress at intrados of arch.
Cantilever stresses are acting in inclined directions parallel to the edges of the cantilever.
U = Stress at upstream edge of cantilever.
D = Stress at downstream edge of cantilever.
All stresses are in pounds per square inch.
Profiles are on axis looking upstream (developed).

+ = Compression
− = Tension

FIGURE 246—ARCH AND CANTILEVER STRESSES

tended to balance each other. A maximum cantilever compression of 0.73 pounds per square inch occurred at the downstream face of cantilever 700-R at elevation 900. A maximum tension of 0.25 pounds per square inch occurred at the downstream face of cantilever 600-L at elevation 600. All cantilever stresses shown in the figure are acting in inclined directions parallel to the edges of the cantilevers.

The load distribution diagrams indicate that the greater part of the water load was carried by arch action; also that the load on each arch was fairly uniform. The load carried by cantilever action was a maximum at the base of the crown cantilever, and varied to a negative load at the top of the model. The negative load developed because the top arches resisted downstream cantilever movements.

Figure 246 shows changes in arch and cantilever stresses due to tangential shear and twist, Poisson's ratio, and vertical adjustment. Tangential shear and twist action changed both arch and cantilever stresses considerably. In general, tangential shear and twist effects reduced arch stresses at the intrados of the abutments and the extrados of the crowns. In the cantilevers, upstream stresses were increased at the lower elevations and decreased at the upper elevations. Downstream cantilever stresses were decreased in the lower part of the model and increased in the upper part.

Poisson's ratio effects did not change stresses as much as did tangential shear and twist. Nevertheless, the changes were appreciable. The effect of Poisson's ratio would be much less in a concrete dam where the ratio is approximately 0.20 instead of 0.50. The vertical adjustment changed arch stresses only slightly; and, in general, increased cantilever stresses.

235. Experimental and Analytical Stresses.—A comparison of experimentally determined arch stresses at the upstream face of the model, with those obtained in the trial load analysis, is shown in figure 247. Strain measurements could not be made at the upstream face at elevation 1232, where stresses were computed, as there was not sufficient space for mounting strain gages. However, the stress curve determined from strain measurements at elevation 1200 has the same general shape as the computed curve at elevation 1232. At elevations 1100 and 1000, the agreement between the two sets of stresses is satisfactory. At lower elevations, where the model was thicker, the two stress curves are somewhat farther apart, the analytical stresses being larger than the stresses determined from strains. Discrepancies between the two sets of stresses were probably due to effects of

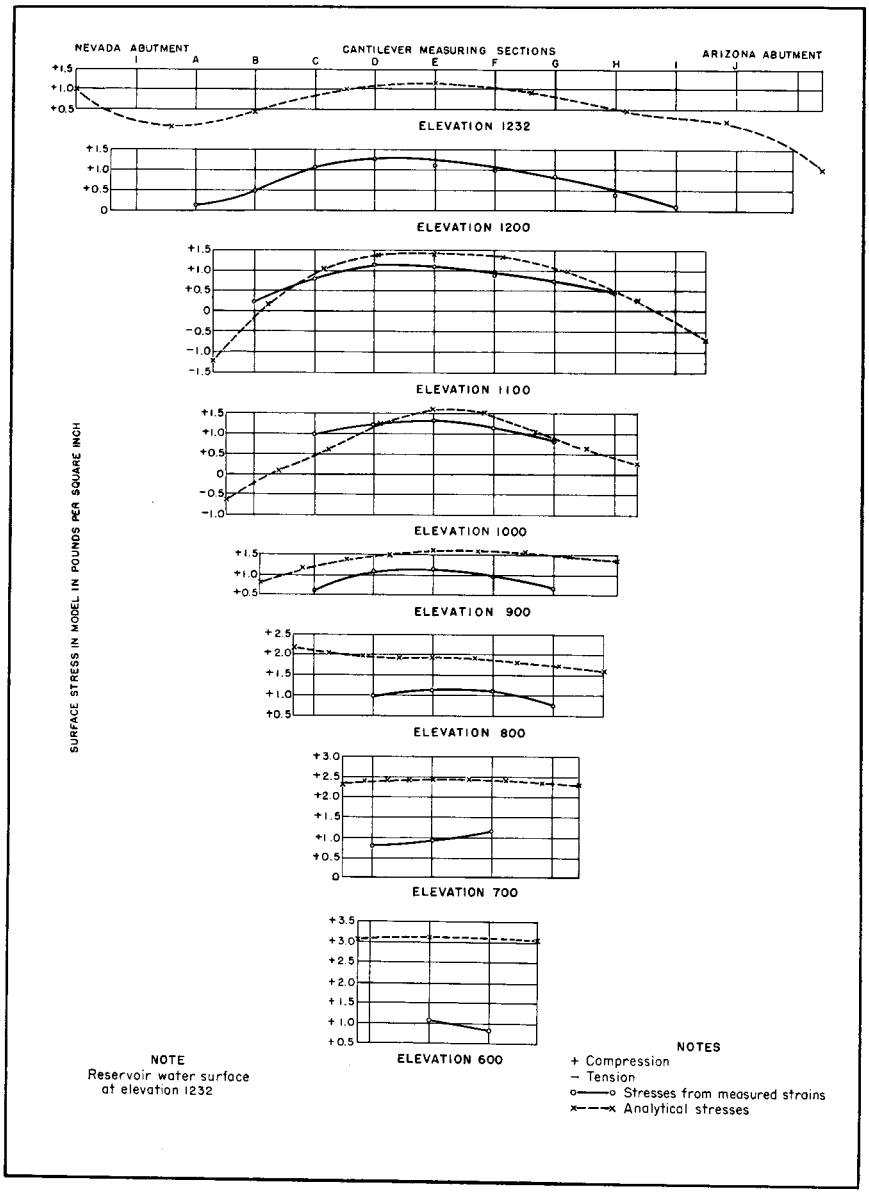

FIGURE 247—EXPERIMENTAL AND ANALYTICAL ARCH STRESSES AT UPSTREAM FACE

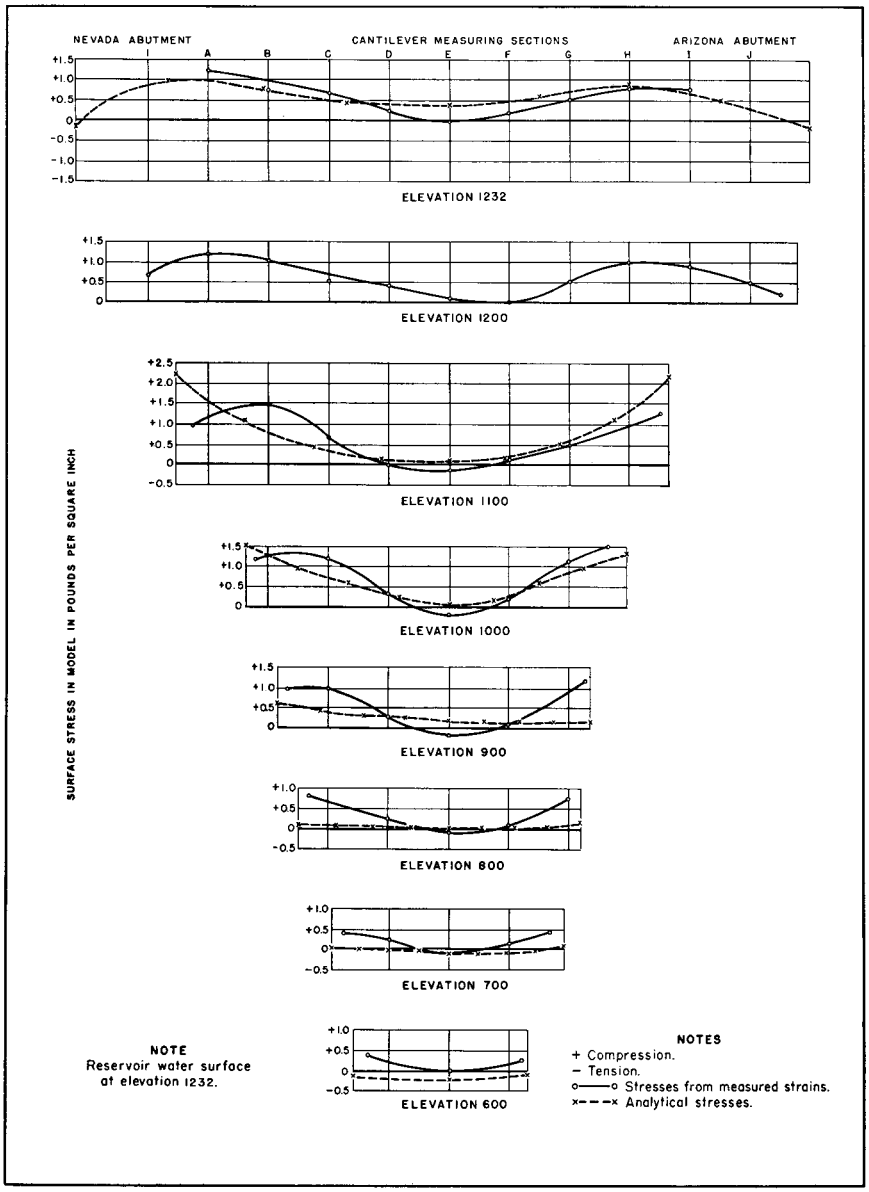

FIGURE 248—EXPERIMENTAL AND ANALYTICAL ARCH STRESSES AT DOWNSTREAM FACE

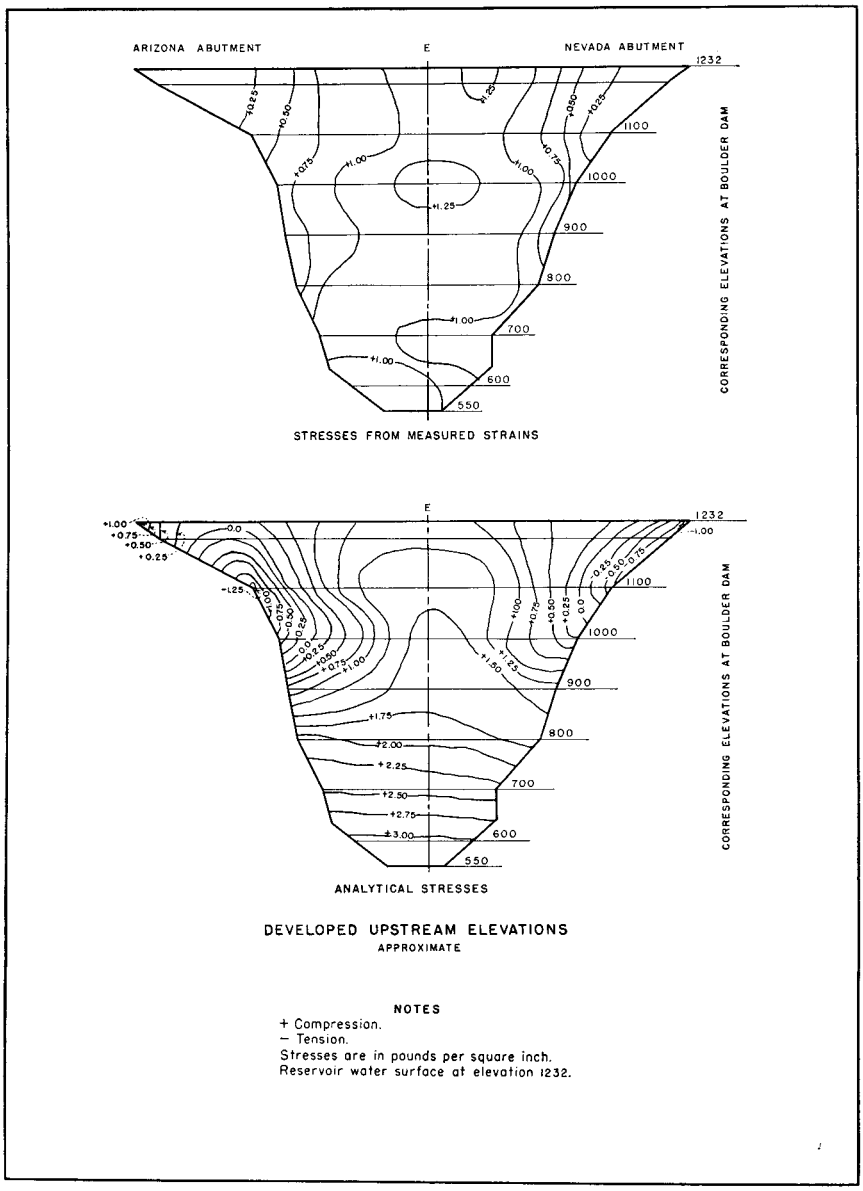

FIGURE 249—LINES OF EQUAL ARCH STRESS AT UPSTREAM FACE

Poisson's ratio, the proximity of the canyon walls, and the fact that the arch thicknesses were considerably greater than the arch lengths.

Arch stresses at the downstream face, determined by experimental and analytical methods, are compared in figure 248. With the exception of some variation along the abutments, the two sets of stresses show a good agreement above elevation 700. At elevation 600, experimental stresses were compressive at the abutments and decreased to zero at the crown, while analytical stresses were tensile from abutment to abutment. However, both stresses were small at all locations along the arch, and the greatest difference between the two was about one-half pound per square inch.

Lines of equal arch stress at the upstream face, determined experimentally and analytically, are compared in figure 249. It should be remembered that strains on the upstream face were measured over 3-inch gage lengths, so that the measurements indicated average strains over the 3-inch lengths. Consequently, stresses computed from the measurements do not show complete stress variations. The greatest differences occurred below elevation 700 where the model was relatively thick.

A similar comparison of stresses at the downstream face is shown in figure 250. The agreement between the two sets of stresses was much better, since the strains were measured with a more accurate instrument having a shorter gage length than was used at the upstream face. The line of zero stress, determined experimentally, extended from elevation 1200 to the base of the model. The corresponding line, determined analytically, crossed the downstream face between elevations 690 and 790. Both methods indicated a concentration of stress along the abutments between elevations 900 and 1100.

Cantilever stresses at the upstream face are compared in figure 251. In the central part of the model, the agreement was satisfactory, but some discrepancies occurred near the abutments. A similar comparison of cantilever stresses at the downstream face is shown in figure 252. The agreement between the two sets of stresses was close, the greatest discrepancy being about one-half pound per square inch.

Lines of equal cantilever stress at the upstream and downstream faces are shown in figures 253 and 254. Magnitudes of maximum tensile and compressive stresses agreed closely in both figures. Some variations occurred in locations of lines of zero stress between areas of tension and compression.

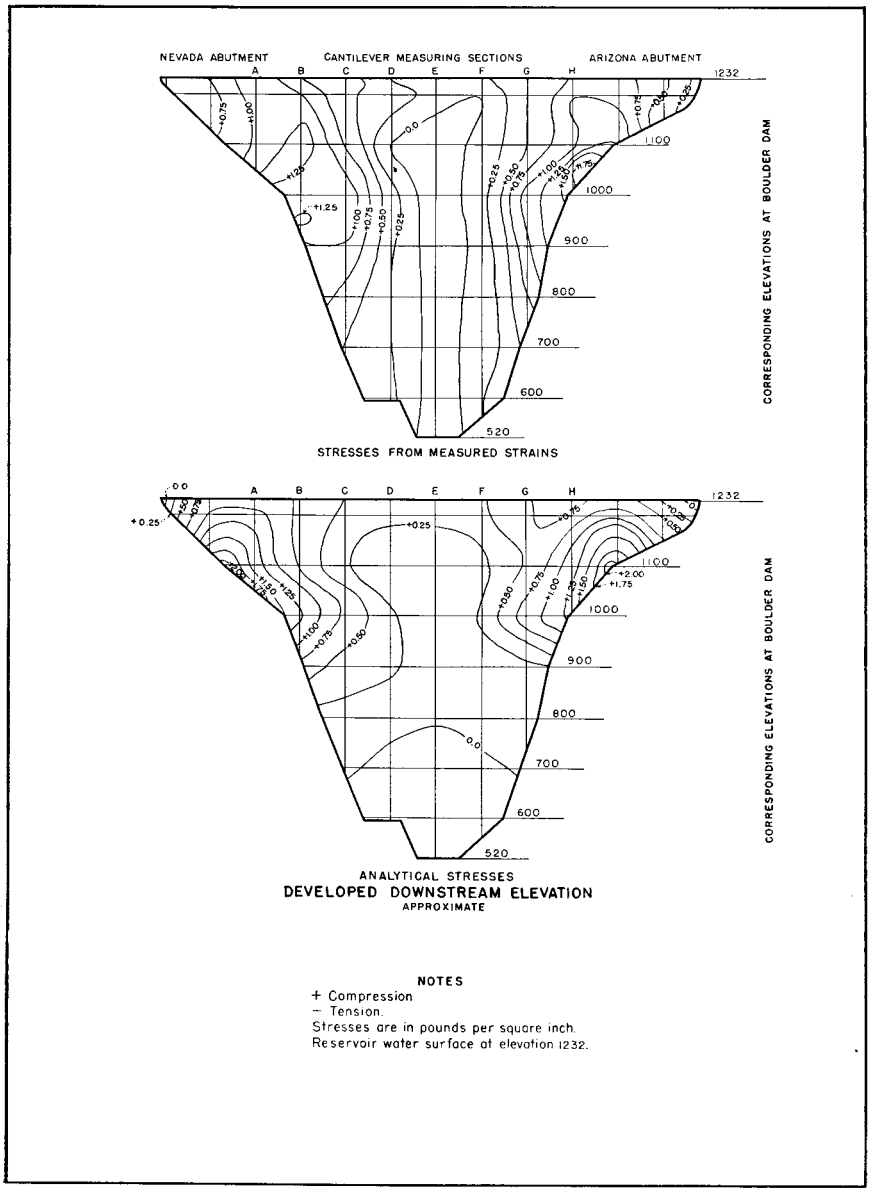

FIGURE 250—LINES OF EQUAL ARCH STRESS AT DOWNSTREAM FACE

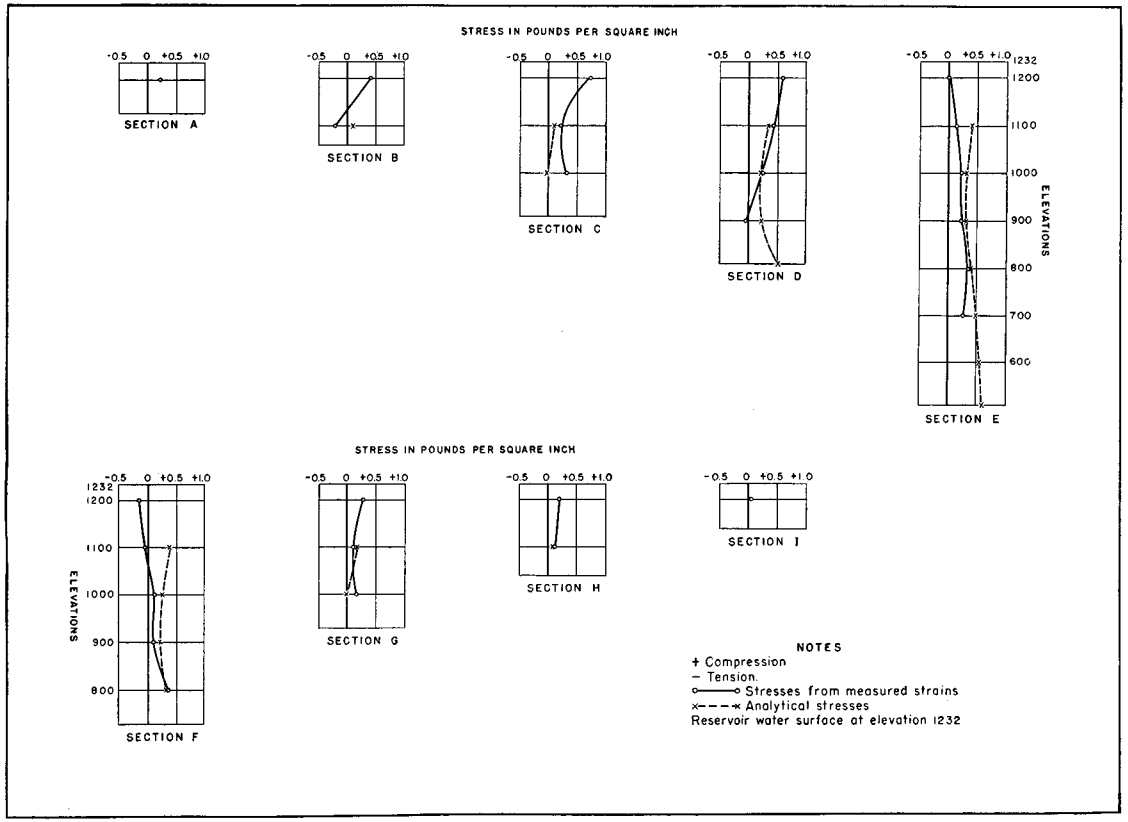

FIGURE 251—EXPERIMENTAL AND ANALYTICAL CANTILEVER STRESSES AT UPSTREAM FACE

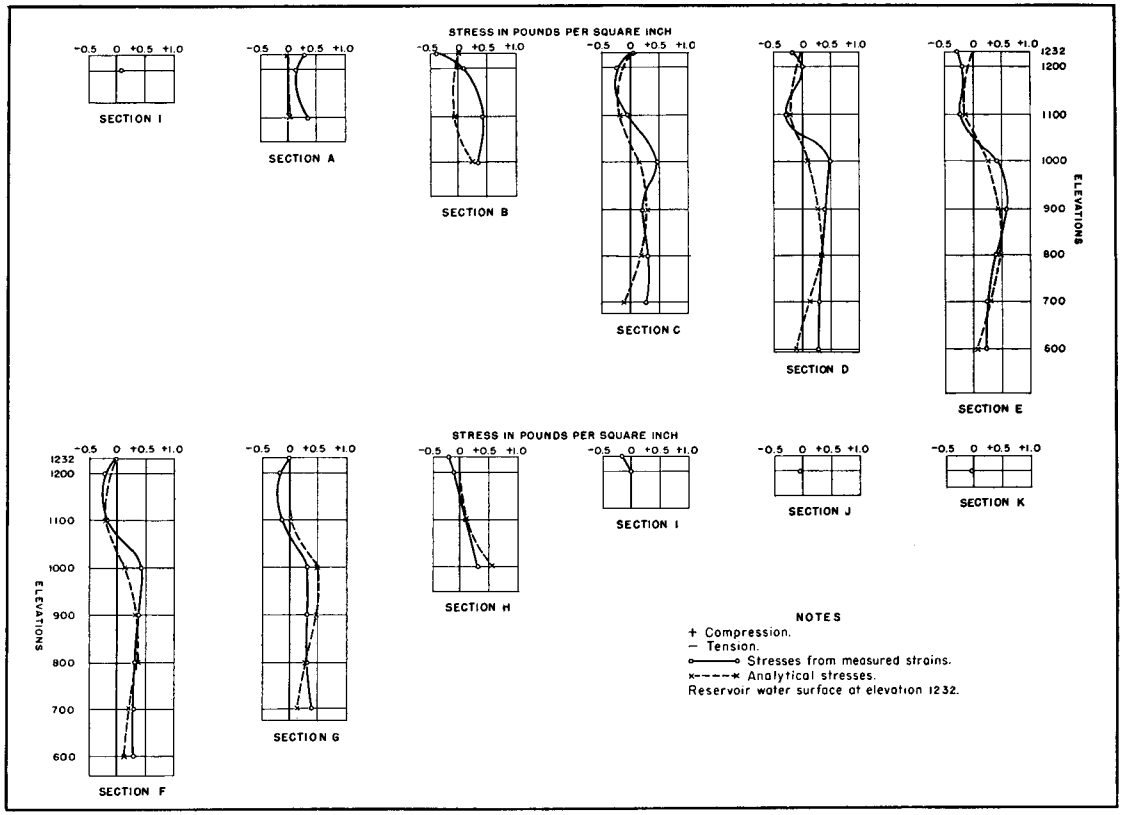

FIGURE 252—EXPERIMENTAL AND ANALYTICAL CANTILEVER STRESSES AT DOWNSTREAM FACE

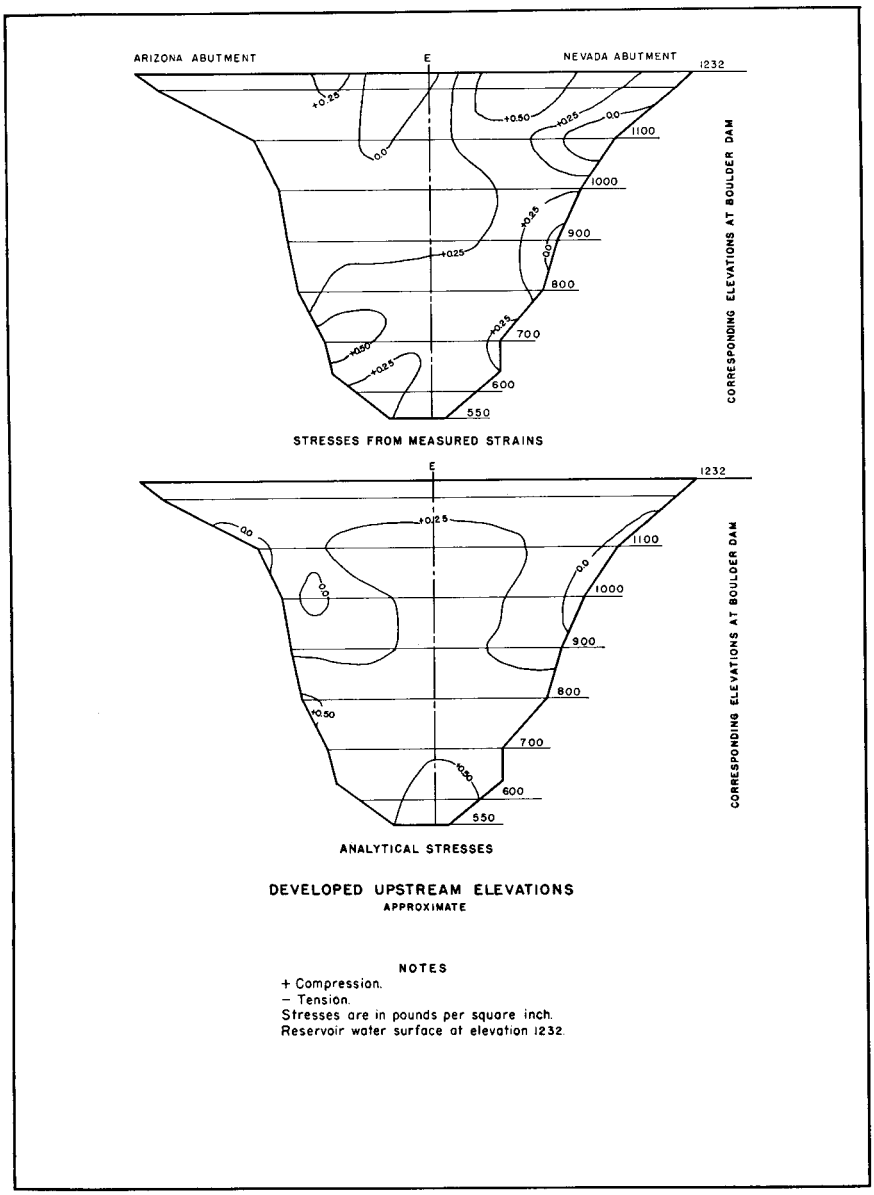

FIGURE 253—LINES OF EQUAL CANTILEVER STRESS AT UPSTREAM FACE

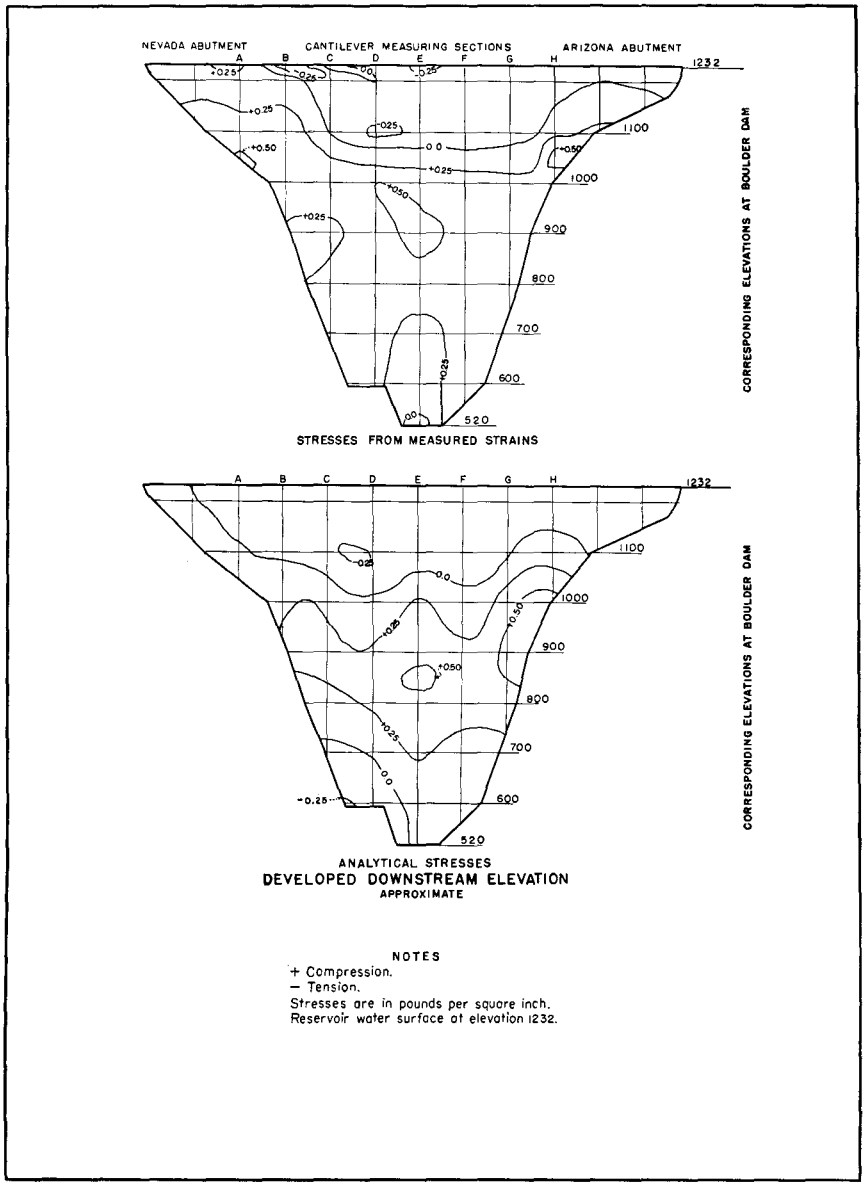

FIGURE 254—LINES OF EQUAL CANTILEVER STRESS AT DOWNSTREAM FACE

236. Comparison of Deflections.—Comparisons of movements calculated by the trial load method with those measured on the model are shown in figures 255 to 258, inclusive. The comparison of radial deflections indicates a satisfactory agreement between the two sets of deflections. The tangential deflections, angular movements, and vertical deflections did not agree as well with the measured values; but, with the exception of the angular movements near the top of the model, the agreement was fairly satisfactory. The probable reasons for the discrepancies were:

1. Variations between actual thicknesses of the model and values assumed in the analysis.

2. The rubber-litharge base was not securely bonded to the concrete base.

3. The modulus of elasticity and Poisson's ratio in the vertical direction were different from those in radial and tangential directions.

4. The correction of calculated movements at the center lines to apply to the downstream face could only be approximated.

The calculated movements would have been slightly more accurate if more arches and cantilevers had been used in the analysis. However, the results indicated that the elements investigated were sufficient to give a satisfactory solution.

237. Conclusions.—In the trial load analysis it was necessary to assume that the rubber-litharge compound was a homogeneous material, isotropic in the horizontal plane. Tests of the material gave three different moduli of elasticity in three mutually perpendicular directions, and two different Poisson's ratios for each direction. The only attempt that could be made to fit these conditions was to use different moduli of elasticity for the arches and cantilevers. It was necessary to assume in the analysis that the foundation was continuous. Since the rubber-litharge supplemental base was not securely bonded to the concrete support, movements may have occurred at the contact between the two materials. These movements probably caused deflections in the model that could not be accounted for in the trial load analysis.

It is believed that the discrepancies between calculated and measured data were due to the characteristics of the model rather than to the trial load analysis. Consideration should be given to the fact that agreements of stress in regions of high stress were much

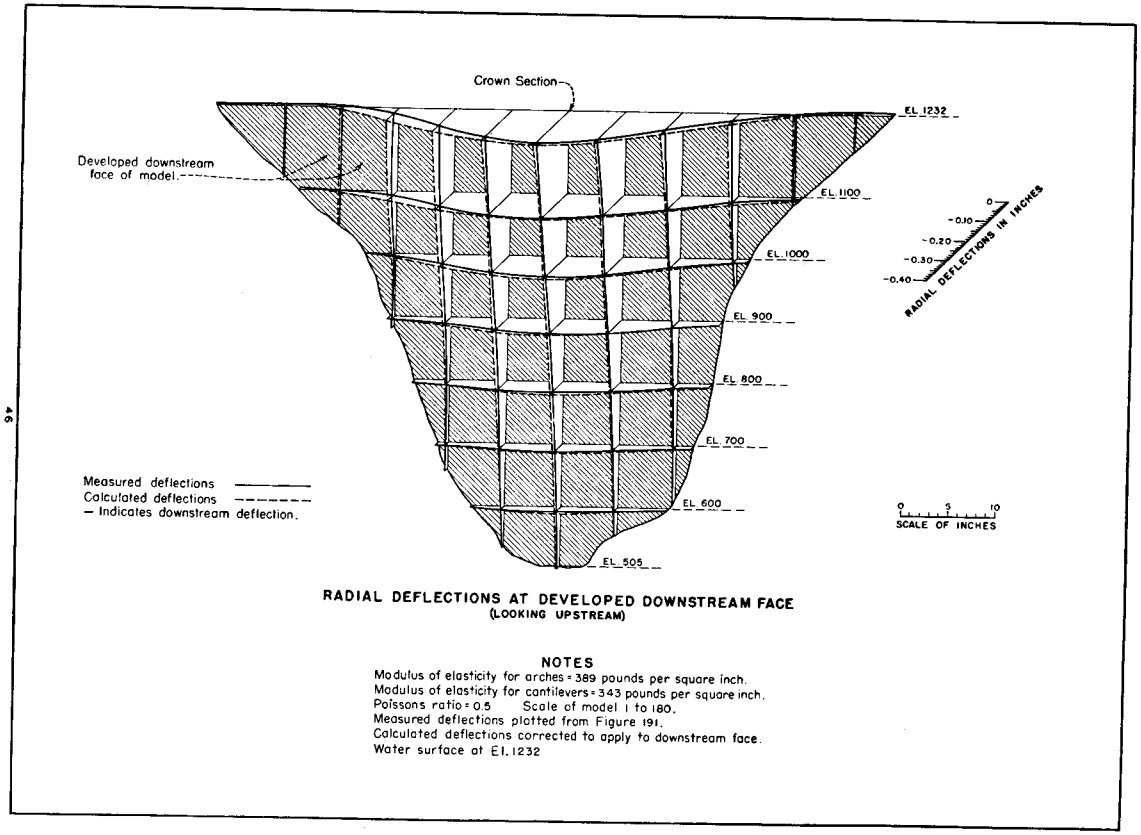

FIGURE 255—COMPUTED AND MEASURED RADIAL DEFLECTIONS

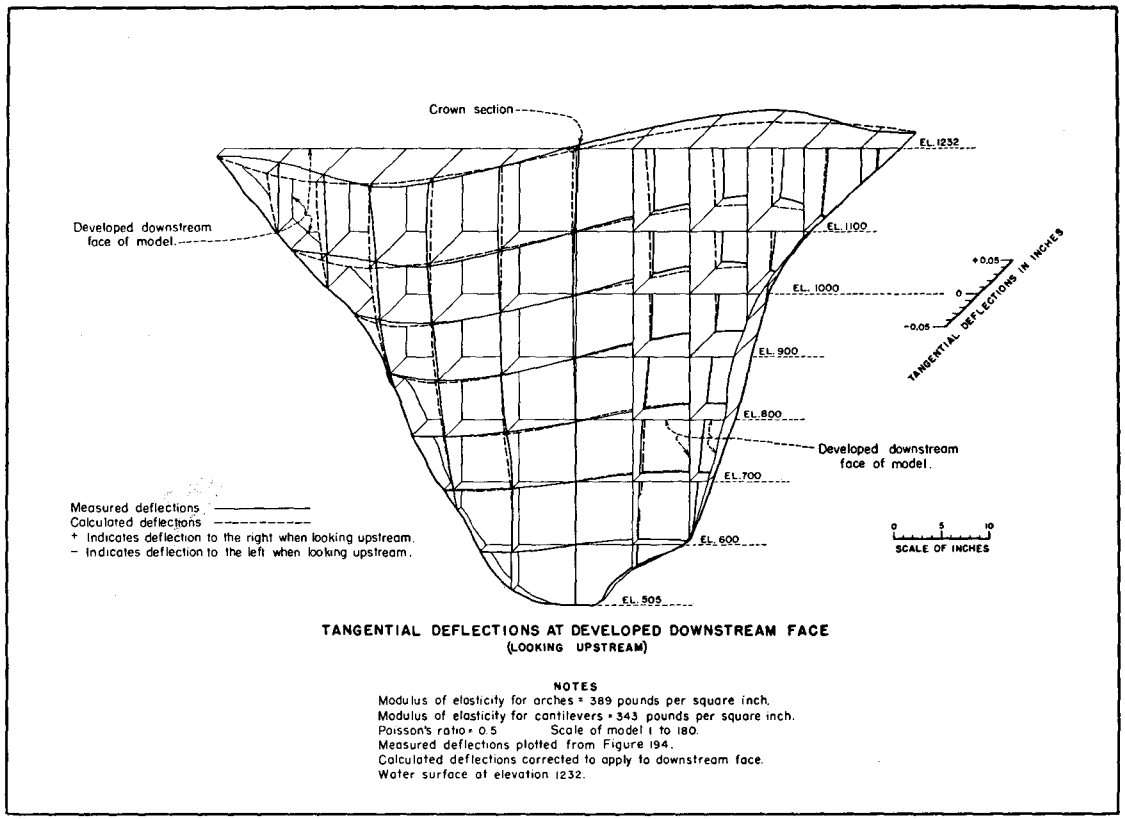

FIGURE 256—COMPUTED AND MEASURED TANGENTIAL DEFLECTIONS

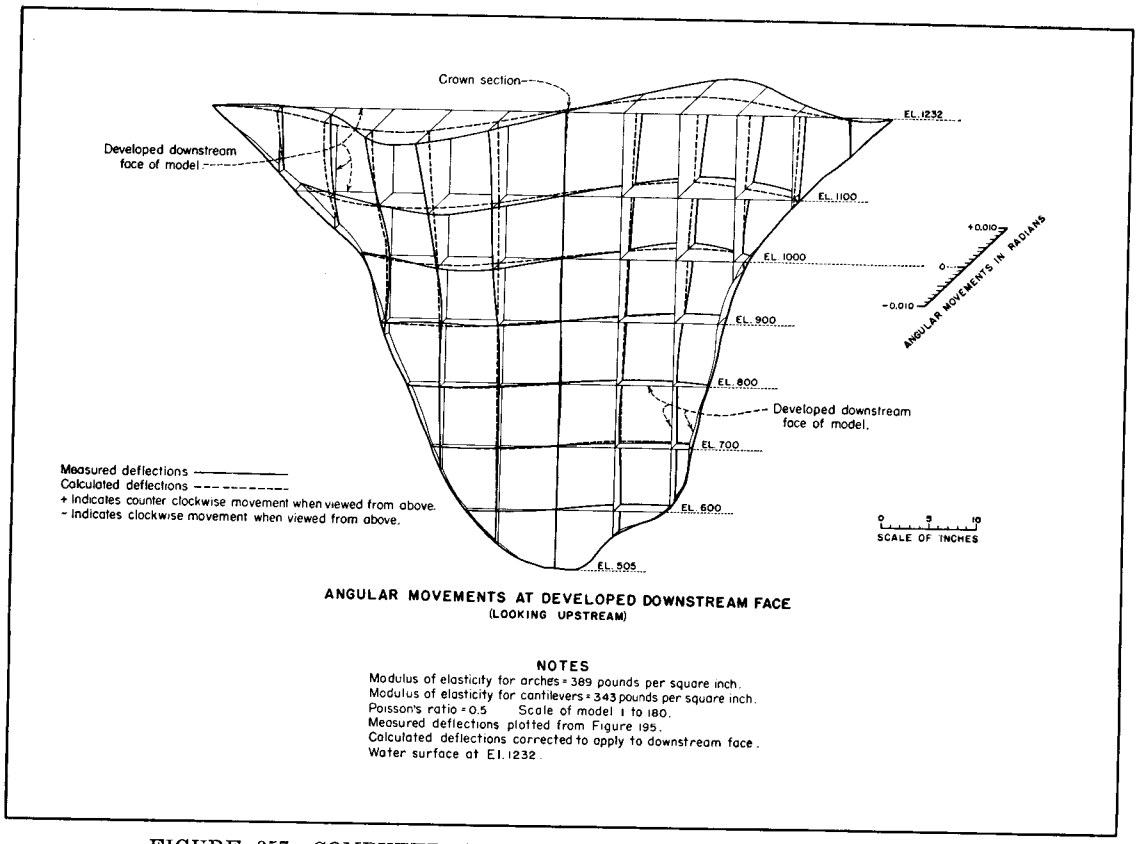

FIGURE 257—COMPUTED AND MEASURED ANGULAR MOVEMENTS

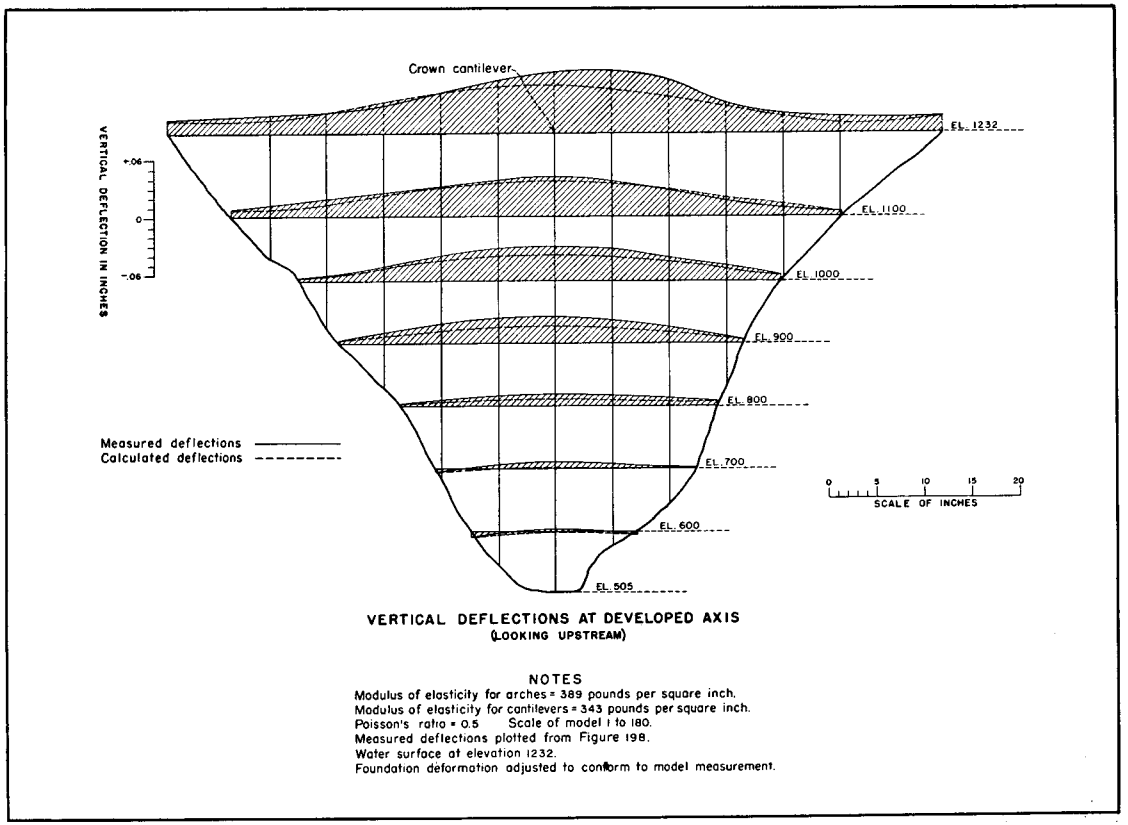

FIGURE 258—COMPUTED AND MEASURED VERTICAL DEFLECTIONS

closer than in regions of low stress. In general, agreements of observed and computed deflections were closer than agreements of stress.

Referring to the trial load analyses of the plaster-celite model, the reader will observe that a better agreement with experimental results was obtained. It is therefore concluded that the results of the plaster-celite model tests represent more closely the action of a concrete dam than do the results of the rubber-litharge model tests.

LIST OF BULLETINS

The following list shows tentative titles of final reports on the Boulder Canyon Project now being prepared for publication. Titles and prices of printed reports now ready for distribution are also included. Appropriate announcements will be made in engineering periodicals as additional bulletins become available.

PART I—INTRODUCTORY

General Description of Project
History of Project
Legal and Financial Problems

PART II—HYDROLOGY

Stream Flow and Reservoir Operation
Lower Basin Utilization
Upper Basin Utilization

PART III—PREPARATORY EXAMINATIONS AND CONSTRUCTION

Geologic Investigations
Surveys and Preliminary Construction
(Topographic surveys, highways, railways, power lines, substations, and Boulder City).

PART IV—DESIGN AND CONSTRUCTION

General Features
Boulder Dam
Diversion Structures and Spillways
Intake Towers and Outlet Works
Concrete Manufacture, Handling, and Control
Penstocks and Outlet Pipes
Hydraulic Valves and Gates
Handling Facilities
(Cableway, cranes, and other permanent handling facilities).
Power Plant Building
Generating, Transforming, and Switching Equipment
Turbines, Governors, and Mechanical Auxiliaries
Control, Communication, and Electrical Auxiliaries
Imperial Dam and Desilting Works
All-American Canal and Canal Structures

LIST OF BULLETINS—(Continued)

PART V—TECHNICAL INVESTIGATIONS

Trial Load Method of Analyzing Arch Dams*	(paper, $1.50; cloth, $2.00)
Slab Analogy Experiments*	(paper, $1.00; cloth, $1.50)
Model Tests of Boulder Dam*	(paper, $1.50; cloth, $2.00)
Stress Studies for Boulder Dam*	(paper, $1.50; cloth, $2.00)
Penstock Analysis and Stiffener Design	
Model Tests of Arch and Cantilever Elements	
Research Measurements at Dam	

PART VI—HYDRAULIC INVESTIGATIONS

Model Studies of Spillways*	(paper, $1.00; cloth, $1.50)
Model Studies of Penstocks and Outlet Works*	(paper, $1.00; cloth, $1.50)
Studies of Crests for Overfall Dams	
Model Studies of Imperial Dam and Desilting Works	
Model Studies of All-American Canal Structures	
Silt Movement in Colorado River	

PART VII—CEMENT AND CONCRETE INVESTIGATIONS

Thermal Properties of Concrete
Investigation of Portland Cements
Cooling of Concrete Dams
Mass Concrete Investigations
Contraction Joint Grouting
Volume Changes in Mass Concrete
(Largely Investigations at Owyhee Dam, Owyhee Project, Oregon).

*For Sale at Offices of the Bureau of Reclamation in Denver, Colo., and Washington, D. C.

The Bradford-Robinson Ptg. Co., Denver, Colo. 7-5-39 3000